Tokuda et al. BMC Research Notes 2014, 7:780
http://www.biomedcentral.com/1756-0500/7/780

BMC Research Notes

RESEARCH ARTICLE Open Access

The defect of SFRP2 modulates an influx of extracellular calcium in B lymphocytes

Yuichi Tokuda†, Masami Tanaka†, Tomohito Yagi† and Kei Tashiro*

Abstract

Background: In the Wnt pathway, the secreted frizzled-related protein 2 (SFRP2) is thought to act as one of the several competitive inhibitors of Wnt. However, the precise role of SFRP2 is still poorly understood especially in B lymphocytes. Here, we investigated the function of SFRP2, comparing the SFRP2 defective as well as normal B lymphocytes in mice.

Results: We demonstrated that calcium influx from extracellular to intracellular space in splenic B cells was clearly affected by the defect of SFRP2. In addition, the phosphorylation of phospholipase Cγ2 was observed to be reduced in SFRP2 defective splenic B cells with B cell receptor stimulation.

Conclusions: SFRP2 is suggested to modulate the influx from extracellular calcium in the B cell receptor signaling pathway.

Keywords: SFRP2, PLCγ2, Calcium influx, B cell receptor signaling

Background

The Wnt pathway is one of the important signal mechanisms related to cell differentiation in embryogenesis, hematopoiesis, and carcinogenesis [1]. It is mainly divided into three categories as Wnt/β-catenin, Wnt/planar cell polarity, and Wnt/calcium pathway [2-5]. In particular, the Wnt/β-catenin pathway, which also termed as "canonical pathway", has been investigated extensively and well understood, comparing to other pathways termed as "noncanonical pathway" [6,7].

The Wnt protein is one of the extracellular ligands binding to the family of Frizzled receptors associated with several receptor-related proteins. Also, the Wnt pathways are regulated with activators or inhibitors [8]. Especially, the secreted frizzled-related protein 2 (SFRP2) (also known as SDF5 [9]) is a competitive inhibitor to act as antagonist of the Wnt pathway [10,11].

During embryogenesis, where Wnt signaling is involved, the defect of *Sfrp2* causes brachysyndactyly in mice [12]. Our previous research also showed that the dysfunction of SFRP2 protein yields a phenotype of preaxial synpolydactyly and syndactyly [13]. Moreover, SFRP2 has reported to be hypermethylated in the prostate cancer [14], gastric cancer [15], and colorectal cancer [16], and to suppress bone formation in multiple myeloma cells [17]. On the other hand, the Wnt is known to maintain hematopoietic stem cells (HSCs) in the bone marrow (BM) niche under the both canonical [18] and noncanonical pathways [6], and various Wnt antagonists such as SFRP2 are suggested to play a role in the regulation of HSCs. In the Wnt pathways of hematopoiesis, SFRP2 as secreted protein is suggested to inhibit the Wnt pathway and maintain the quiescent of HSCs in mice [19]. SFRP2 is also known to be expressed in osteoblasts in BM and related to the proliferation of HSCs [20]. However, the function of SFRP2 on immune system is still unclear, especially in the calcium signaling of B lymphocytes.

Here, we demonstrated that SFRP2 modulates the calcium signal transduction associated with activation cascade in downstream of B cell receptor (BCR) signaling pathway.

Methods

Mice

Mice of wild-type (*Sfrp2*$^{+/+}$) C57BL/6 and of *Sfrp2*-defective strains (*Sfrp2*$^{-/-}$) were bred under the specific pathogen-free (SPF) conditions as described in our previous study [13]. In this study, all mice were examined at 10-12 weeks of age. Reproducibility of data was confirmed by repeating each experiment at least more

* Correspondence: tashiro@koto.kpu-m.ac.jp
†Equal contributors
Department of Genomic Medical Sciences, Kyoto Prefectural University of Medicine, 465 kajii-cho, Kawaramachi-Hirokoji, Kamigyo-ku, Kyoto 602-8566, Japan

than three pairs of *Sfrp2*$^{+/+}$ and *Sfrp2*$^{-/-}$. All procedures in mouse experiments followed the guidelines and were approved by the Kyoto Prefectural University of Medicine Animal Care and Use Committee.

Cell preparation

The cell suspensions were obtained from the BM and spleen samples. After the elimination of red blood cells, the cells in the BM or spleen were suspended in phosphate buffered saline (PBS) with 3% fetal bovine serum. For the western blotting, the splenic B cells were purified by negative isolation using Dynabeads® Mouse CD43 (Untouched™ B Cells) (Invitrogen, Carlsbad, CA, USA) according to the manufacturer's protocol.

Cell differentiation analysis

BM cells were stained by the monoclonal antibodies against the surface markers as follows: FITC-conjugated anti-IgM (II/41), anti-CD43 (S7) and APC-conjugated anti-CD45R/B220 (RA3-6B2; anti-B220). Splenocytes were similarly stained by the monoclonal antibodies as follows: FITC-conjugated anti-CD21/CD35 (7G6), PE-Cy7-conjugated anti-IgM (R6–60.2), anti-B220 antibody (BD Pharmingen, San Diego, CA, USA) and PE-conjugated anti-CD23 (B3B4) antibody (eBioscience, San Diego, CA, USA). All flow cytometry (FACS) experiments were performed by BD FACS Canto II and BD FACSDiva software version 6.1.3 (BD Biosciences, San Jose, CA, USA) according to the manufacturer's protocol. The analysis was performed using the FlowJo software (Tree Star, San Carlos, CA, USA).

Calcium influx analysis

Cell suspensions of splenocytes were incubated at 37°C for 45 min with Fluo 4-AM (Fluo4; Dojindo, Kumamoto, Japan) and Fura Red™ AM (Fura Red; Invitrogen), which final concentrations were 3 μM and 6 μM, respectively. After stained with anti-B220, the cells were resuspended in calcium-free Hank's balanced salt solution (HBSS/Ca^{-}). Intracellular calcium levels were assessed by the ratio of the intensities of Fluo4/Fura Red [21], which the ratios were averaged for every 10 sec. In the experiments, anti-mouse IgM $F(ab')_2$ fragments (anti-IgM; final concentration 10 μg/ml in HBSS/Ca^{-}, Jackson Immunoresearch, West Grove, PA, USA) and ethylene glycol bis(2-aminoethyl)-N,N,N',N'-tetraacetic acid (EGTA; final concentration 0.5 mM in HBSS/Ca^{-}), and calcium (Ca; $CaCl_2$ final concentration 1.26 mM in HBSS/Ca^{-}) were applied. These experiments were replicated at least three times.

Endoplasmic reticulum (ER) analysis

The splenocytes were incubated at 37°C in 5% CO_2 for 45 min in PBS (Mg^{+}, Ca^{+}) and 1 μM ER-Tracker™ Green dye (glibenclamide BODIPY® FL, ER-Tracker; Molecular Probes, Invitrogen) to evaluate the ER abundance [22]. After staining with anti-B220 for 10 min, the cells were resuspended in PBS (Mg^{+}, Ca^{+}) for FACS analysis.

Reverse Transcription Polymerase Chain Reaction (RT-PCR)

RT-PCR experiments were performed with Multiple Tissue cDNA (MTC) panels of Mouse (Clontech Laboratories, CA, USA) and *Sfrp2*$^{+/+}$ and *Sfrp2*$^{-/-}$ samples, which were from only *Sfrp2*$^{+/+}$ and both mouse for SFRP2 and β-catenin tests, respectively. The cDNAs from *Sfrp2*$^{+/+}$ and *Sfrp2*$^{-/-}$ mouse samples were synthesized in 20 μl products with 200 ng total RNA from splenic B and BM cells and Super Script II (Invitrogen) according to the manufacturer's protocol. In the PCR process, each cDNA in appropriate mixture was amplified with each specific primer pair, and their details were described in Additional files 1 and 2.

Protein phosphorylation assay by FACS

The phosphorylation assay of proteins was measured by FACS with BD™ Phosflow technology (BD Biosciences) according to the manufacturer's instructions. The stimulations for splenic B cells were examined by anti-IgM antibody (final concentration 10 μg/ml; Jackson Immuno research) or lipopolysaccharide (LPS, final concentration 20 μg/ml; Sigma-Aldrich, San Francisco, CA, USA) in time course of 0, 5, 10, and 15 min. In the case of IgM stimulation, the antibody set of Alexa Fluor® 488 Mouse ERK1/2 (pT202/pY204) (Erk1/2) and PE Mouse anti-Syk (pY348) (Syk) was applied to detect the phosphorylated proteins. In the case of LPS stimulation, Erk1/2 and PE Mouse p38 MAPK (pT180/pY182) (P38) (BD™ Phosflow, BD Biosciences) were examined. These antibodies with anti-B220 were stained for splenic B cells for 30 min in Phosflow experiment process.

Western blotting

The purified splenic B cells were stimulated by anti-IgM (10 μg/ml, Jackson) in HBSS with calcium. The samples were evaluated by antibodies from Antibody Sampler Kits (Cell Signaling Technology, Inc. (CST), Danvers, MA, USA) as follows: anti-phospho-Syk (Tyr525/526), anti-Syk, anti-phospho-Lyn (Tyr507), anti-Lyn, anti-phospho-Btk (Tyr223), anti-Btk, anti-phospho-CD19 (Tyr531), and anti-CD19 from B Cell Signaling Antibody Sampler Kit; anti-phospho-PLCγ2 (Tyr1217), anti-phospho-PLCγ2 (Tyr759), and anti-PLCγ2 antibody from PLCγ Antibody Sampler Kit; anti-phospho-SAPK/JNK (Thr183/Tyr185), and anti-phospho-ATF-2 (Thr71) from Phospho-SAPK/JNK Pathway Antibody Sampler Kit. Moreover, anti-NFAT1, anti-NFAT2, and β-actin antibody (CST) were also applied. These antibodies were detected with anti-rabbit IgG-HRP (CST) as secondary antibody. The signals were detected with the ECL Prime or ECL Plus

Western Blotting Detection System (GE Healthcare UK Ltd., Buckinghamshire, UK) according to the manufacturer's protocol. In addition, the Can Get Signal Immunoreaction Enhancer Solution (Toyobo Co., Ltd, Osaka, Japan) was applied if necessary. The results of western blots were analyzed by ImageJ software (http://imagej.nih.gov/ij/index.html).

Statistical analysis

In order to prepare the FACS data for statistical analysis, Office Excel and Visual C++ (Microsoft, Redmond, Washington, USA) were used. We employed R software (http://www.R-project.org/) to perform the statistical analysis including *t*–test in each FACS data and draw the graphs. In the histograms, error bars indicate standard

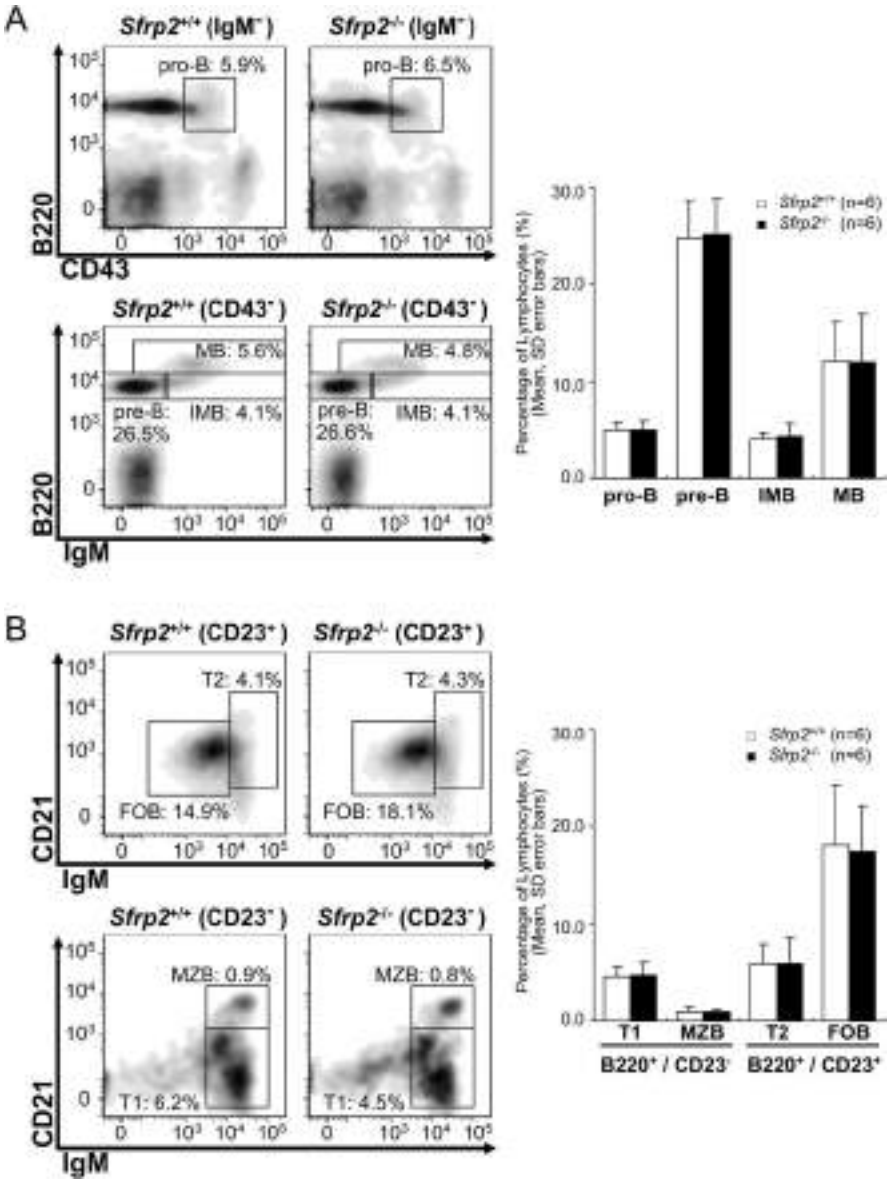

Figure 1 Comparison of BM and splenic B cell differentiation. The cells in the BM or spleen were assessed with each surface marker. The representative FACS plots are demonstrated by FlowJo. **(A)** The results of BM are indicated for B cell differentiation stages of pro-B, pre-B, immature B (IMB), and mature B (MB) cells. The histograms indicate the means and SD of the 6 littermates with same gender pairs for these cell stages. No statistical significant difference between *Sfrp2*$^{+/+}$ and *Sfrp2*$^{-/-}$ in these cell stages was observed by Student's *t*-tests. **(B)** The results of splenic B cells for transitional type 1 (T1), marginal zone B (MZB), transitional type 2 (T2), and follicular B (FOB) cells are indicated. The histograms indicate the means and SD of the 6 gender-matched littermates. In splenic B cells, there was no statistical significant difference between *Sfrp2*$^{+/+}$ and *Sfrp2*$^{-/-}$ by Student's *t*-tests.

deviation with mean. In addition, the R package of "exactRankTests" was used for Wilcoxon tests.

Results

Cell differentiation

In order to evaluate the differences in B cell differentiation, BM and splenic B cells obtained from *Sfrp2*$^{+/+}$ and *Sfrp2*$^{-/-}$ mice were assessed by FACS analysis. No change in B cell differentiation was observed between *Sfrp2*$^{+/+}$ and *Sfrp2*$^{-/-}$ mice by the statistical analysis (Figure 1).

Calcium influx

The differences of calcium signal transduction between *Sfrp2*$^{+/+}$ and *Sfrp2*$^{-/-}$ splenic B cells were evaluated by FACS. No significant difference of intracellular calcium levels was observed with anti-IgM stimulation under the calcium free condition (open arrows in Figure 2). After the addition of extracellular calcium (dotted arrows in Figure 2), intracellular calcium levels rapidly increased because of the influx of extracellular calcium after anti-IgM stimulation. Once reaching the peak, intracellular calcium levels were then gradually decreased with the statistical significant difference between *Sfrp2*$^{+/+}$ and *Sfrp2*$^{-/-}$ splenic B cells (Figure 2A). However, the difference of intracellular calcium levels between *Sfrp2*$^{+/+}$ and *Sfrp2*$^{-/-}$ splenic B cells rapidly disappeared after the removal of extracellular calcium by EGTA (filled arrow in Figure 2B).

ER abundance analysis

ER abundance in splenic B cells was evaluated with ER-Tracker. The results showed that there was no statistical significant difference for ER abundance between the *Sfrp2*$^{+/+}$ and *Sfrp2*$^{-/-}$ splenic B cells (Figure 3).

SFRP2 and β-catenin expression

The expression of SFRP2 studied by RT-PCR was high in BM, but very low in spleen/splenic B cells (Additional file 1). On the other hand, the expression of β-catenin was clearly noted in spleen similar to other tissues, as well as in *Sfrp2*$^{+/+}$ and *Sfrp2*$^{-/-}$ splenocytes (Additional file 2A and B). However, phosphorylated β-catenin was barely detectable in BM or spleen tissues by Western blotting (Additional file 2C).

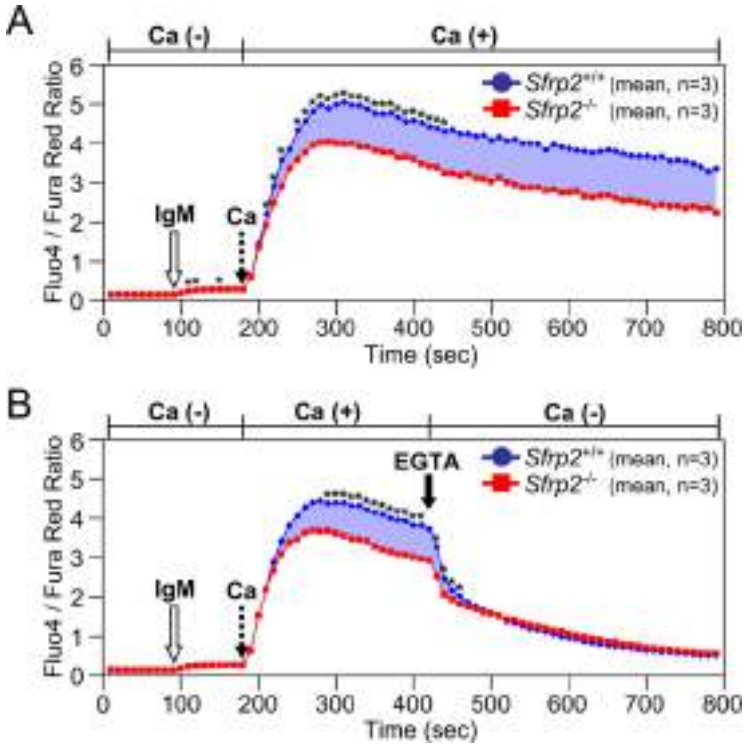

Figure 2 Calcium influx of splenic B cell. The calcium influx in splenic B cells was examined by FACS. The *Sfrp2*$^{+/+}$ and *Sfrp2*$^{-/-}$ splenic B cells were derived from 3 littermates with same gender pair and assessed after gated with anti-B220. The means of 3 replicates are plotted by the blue circles (*Sfrp2*$^{+/+}$) and red squares (*Sfrp2*$^{-/-}$). The black asterisks indicate the statistical significance by paired *t*-test in each time point. Blue shaded regions indicate the differences of intensity ratios between *Sfrp2*$^{+/+}$ and *Sfrp2*$^{-/-}$ splenic B cells. **(A)** After 1.5 min acquisition of signals, the cells were stimulated with anti-IgM (IgM; open arrow). Furthermore, the cells were treated with calcium at 3 min (dotted arrow). **(B)** Following the similar process, the cells were then incubated with EGTA at 7 min (filled arrow).

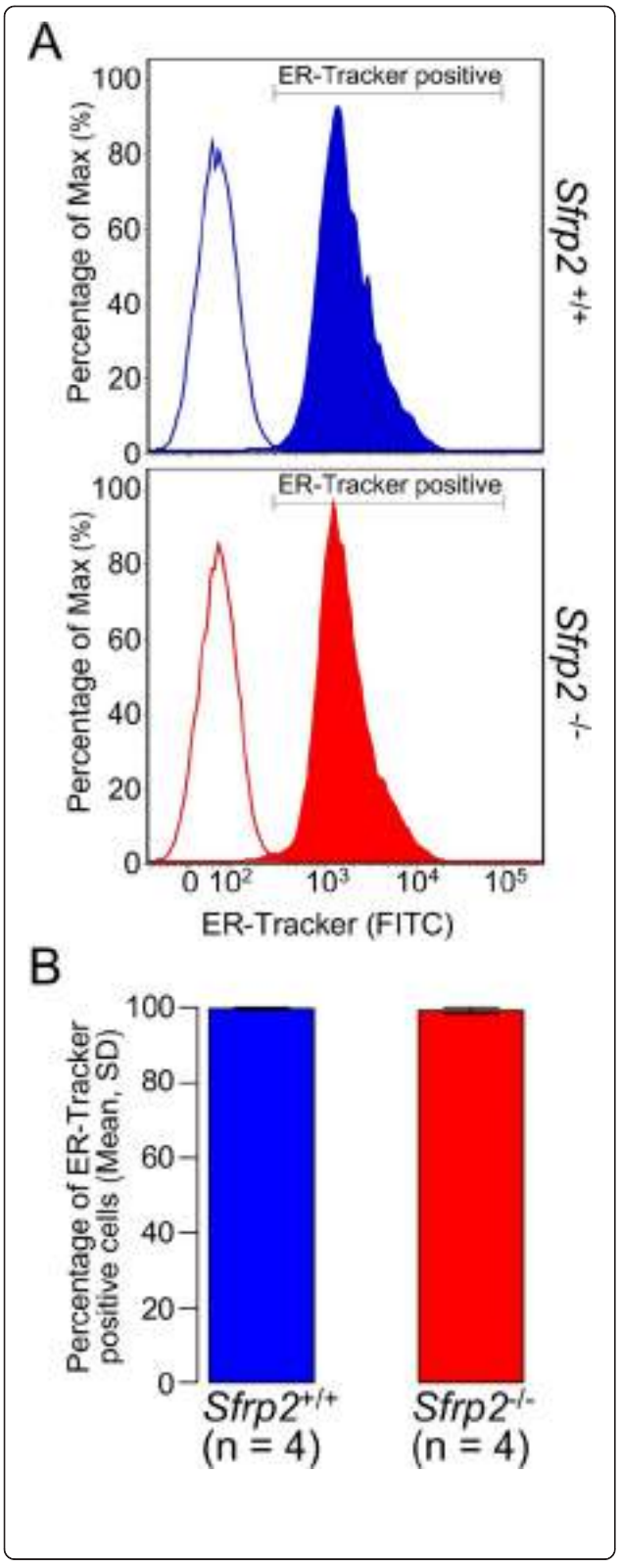

Figure 3 ER abundance of splenic B cell. (A) The representative results of ER abundance in splenic B cells gated with anti-B220 are displayed by using FlowJo. Upper (blue) and lower (red) plots are represented as the percentages of the max of the ER-Tracker signals in splenic B cell of *Sfrp2*$^{+/+}$ and *Sfrp2*$^{-/-}$, respectively. The filled areas indicate ER-Tracker stained B cells and the line areas indicate the intensity of non-stained samples. **(B)** The histograms indicate the means and SD of the 4 littermate pairs for the percentage of ER-Tracker positive cells. No statistical significant difference in ER abundance between *Sfrp2*$^{+/+}$ and *Sfrp2*$^{-/-}$ splenic B cells was observed by Student's *t*-tests.

Western blotting analysis on phosphorylated protein

Before western blots analysis, we first tested each phosphorylation of Erk1/2, P38, and Syk in *Sfrp2*$^{+/+}$ and *Sfrp2*$^{-/-}$ splenic B cells with use of FACS (Additional file 3). Results showed that there was no significant phosphorylation difference between *Sfrp2*$^{+/+}$ and *Sfrp2*$^{-/-}$ when stimulated with either IgM or LPS. Therefore, we examined phosphorylation status of the proteins involved in the BCR signaling pathway with use of western blotting for purified splenic B cells. The purity of splenic B cells was about 98.6% in lymphocytes confirmed by FACS analysis (data not shown).

The phosphorylation of Syk, Lyn, Btk, CD19, and PLCγ2, which is the important downstream effectors of BCR signaling pathway, were assessed comparing with the total amount of each protein. In the western blot analysis, no difference between *Sfrp2*$^{+/+}$ and *Sfrp2*$^{-/-}$ splenic B cells was observed in the time-course experiments after BCR stimulation with anti-IgM (0, 1, 5, 20, and 60 min) (Figure 4A). However, in the Tyr1217 site of PLCγ2, the signals of *Sfrp2*$^{-/-}$ splenic B cells decreased after 5 min stimulation compared with *Sfrp2*$^{+/+}$ samples (Figure 4B). By contrast, no significant difference was observed in the phosphorylation of PLCγ2 at Tyr759 in this study. Accordingly, the defect of *Sfrp2* was considered to affect the phosphorylation of PLCγ2 at Tyr1217 but not Tyr759 in the BCR signaling pathway.

In addition, NFAT1 and NFAT2 were investigated as downstream components of PLCγ2 in the BCR signaling (Figure 4C). Because there was no difference in these proteins between *Sfrp2*$^{+/+}$ and *Sfrp2*$^{-/-}$, the defect of *Sfrp2* was considered not to play a role in the downstream of PLCγ2. Also, in the downstream of calcium signaling cascade related to BCR signaling pathway, no significant difference of phosphorylation in JNK and ATF-2 was found between *Sfrp2*$^{+/+}$ and *Sfrp2*$^{-/-}$ splenic B cells (Figure 4D).

Discussion

In this study, we investigated B lymphocytes in mice affected by the defect of *Sfrp2*, and this defect did not yield the remarkable influence on the early differentiation of B cells (Figure 1). Therefore, we further examined mature B cells in spleen about the influence of the defect of *Sfrp2* in intracellular signal transduction in detail.

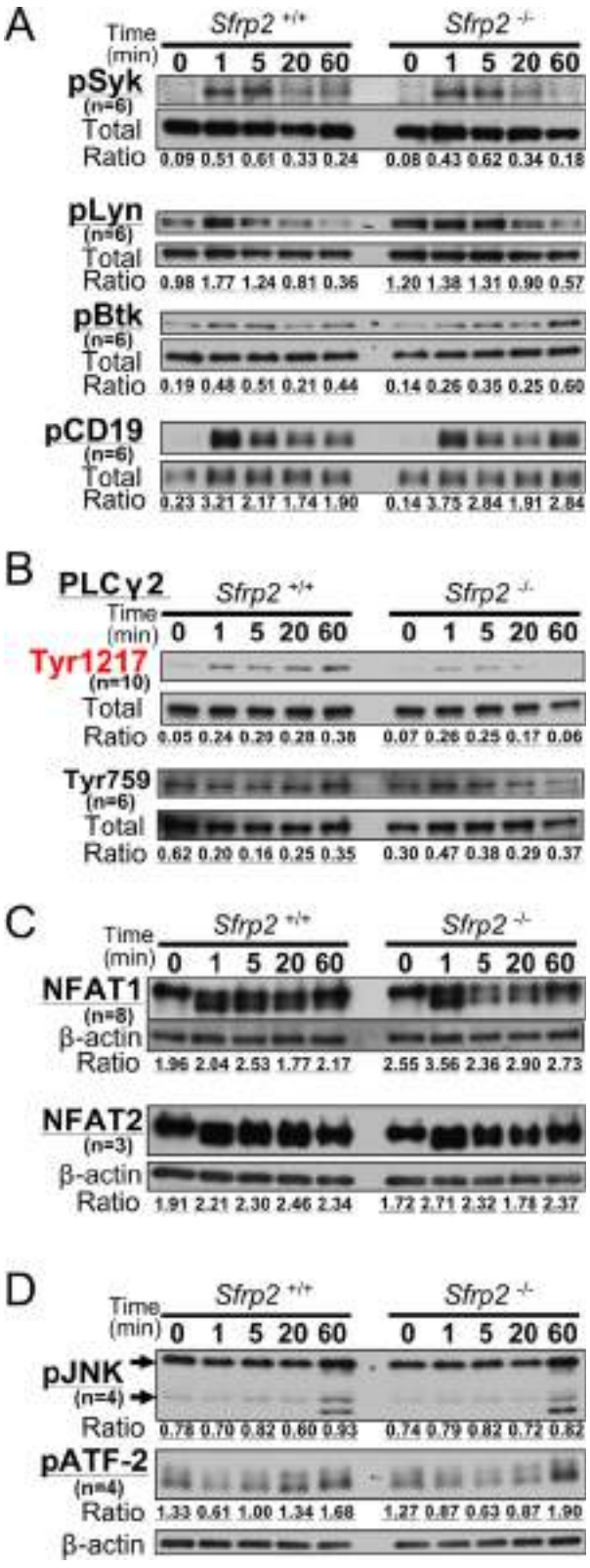

Figure 4 (See legend on next page.)

(See figure on previous page.)
Figure 4 Western blotting results of PLCγ2 splenic B cell. The representative results of western blotting were displayed. Splenic B cells were stimulated with anti-IgM. All experiments were replicated and confirmed three times at least. "n" indicates the number of total tested sample for each protein. **(A)** The phosphorylation of Syk (Tyr525/526; pSyk), Lyn (Tyr507; pLyn), Btk (Tyr223; pBtk), and CD19 (Tyr531; pCD19) sites and **(B)** Tyr1217 and Tyr759 phosphorylation of PLCγ2 were demonstrated with "Total" as the controls, which indicate the amount of each applied protein. **(C)** The expressions of NFAT1 and NFAT2 were indicated with β-actin. **(D)** The phosphorylation of SAPK/JNK (Thr183/Tyr185; pJNK) and ATF-2 (Thr71; pATF-2) were indicated with β-actin. Note that there were two bands for JNK in 54 and 46 kDa due to isoforms as noted by arrows. The ratio of expression level of each sample was calculated by using ImageJ.

The calcium signaling plays a very critical role in the immune system including B cells [23], and so the calcium influx for splenic B cells with *Sfrp2* defect was selectively examined. We showed that the calcium signal transduction by BCR activation was slightly increased in $Sfrp2^{+/+}$ as well as $Sfrp2^{-/-}$ splenic B cells under calcium free condition (open arrows in Figure 2). Moreover, no difference of ER abundance was observed between these B cells (Figure 3). Thus, we could conclude that no significant difference was observed in the intracellular calcium store in both $Sfrp2^{+/+}$and $Sfrp2^{-/-}$ splenic B cells. However, when the calcium was added in the extracellular space (dotted arrows in Figure 2), intracellular calcium levels were rapidly increased in both $Sfrp2^{+/+}$ and $Sfrp2^{-/-}$ splenic B cells due to the influx of extracellular calcium by the BCR stimulation. This was considered to be attributed to the activation of calcium release-activated calcium channel in the plasma membrane triggered by emptying of ER calcium stores under calcium free condition and the first IgM stimulation (open arrows in Figure 2) [23]. Subsequently, intracellular calcium levels gradually decreased and differed significantly between $Sfrp2^{+/+}$ and $Sfrp2^{-/-}$ splenic B cells (Figure 2A). By contrast, intracellular calcium levels were rapidly decreased to the same levels in both splenic B cells after EGTA addition (Figure 2B). Therefore, this phenomenon was observed as a result of the difference of the calcium influx from extracellular to intracellular space between $Sfrp2^{+/+}$ and $Sfrp2^{-/-}$ splenic B cells.

This calcium influx phenomenon is known to be associated with the activation of several proteins involved in the regulation of cell homeostasis. Specifically, protein tyrosine kinases such as Syk and Lyn are initially activated in response to BCR stimulation, which leads to the activation of Btk and CD19. PLCγ2 is then activated by Btk, and cleaves phosphatidylinositol-bisphosphate (PIP_2) into diacylglycerol and inositol (1, 4, 5)-trisphosphate (IP_3) by hydrolysis. Subsequently, IP_3 induced calcium release from intracellular ER calcium stores by binding to the IP_3 receptor. The catalytic hydrolysis of PIP_2 is suggested to require the phosphorylation of Tyr759 in PLCγ2 [24,25]. Moreover, the role of Tyr759 phosphorylation is considered to be different from that of Tyr1217 in PLCγ2 according to the types of cells or stimulations [26]. Our results clearly showed that the defect of *Sfrp2* does not affect the phosphorylation of Syk, Lyn, Btk, and CD19, but reduces the phosphorylation of PLCγ2 at Tyr1217, whereas Tyr759 phosphorylation remained unaffected (Figure 4B). This result may indicate that the *Sfrp2* participates in not pivotally regulating the catalytic hydrolysis of PIP_2 but modulating the calcium signal transduction.

It was unknown if the effect of these defective *Sfrp2* on PLCγ2 is correlated with other abnormal mechanisms in the canonical and/or non-canonical pathways. First, since SFRP2 is not expressed in the hematopoietic cells, especially in splenic B cells compared to BM cells in $Sfrp2^{+/+}$ mice (Additional file 1), exogenous SFRP2 provided from other tissues may contribute to the calcium signaling in the splenic B cell. Moreover, since β-catenin is rarely detectable as protein levels in these splenic B cells (Additional file 2), exogenous SFRP2 may act on the calcium signaling through non-canonical pathway. However, NFAT1, NFAT2, JNK, and ATF-2, which are considered as members of a cascade in downstream of non-canonical signaling pathway, were found not to play a significant role in the $Sfrp2^{-/-}$ splenic B cells (Figure 4C and D). Taken together, the dysregulation of calcium signaling in the $Sfrp2^{-/-}$ splenic B cells occurs under BCR stimulation and is likely to be correlated with unknown common underlying signal pathway(s) of both BCR and non-canonical signalings.

As previously reported, the expression of SFRP2 was down-regulated by methylation in cancer [14,15]. Because calcium signaling was reduced by defect of *Sfrp2*, down-regulation of SFRP2 is assumed to impair the calcium signal transduction in each tissue or cell. However the immune dysfunction was not observed in our SFRP2 deficient mice under the SPF condition, it was reported the association between the methylation of SFRP2 and cancer [14-17]. Although further examination is needed, our results might give us the new insights to understand the functions of SFRP2 under the BCR and calcium signal pathway and the mechanisms of several human diseases.

Conclusions

The defect of *Sfrp2* in mice splenic B cells causes the impairment of calcium influx and the activation of PLCγ2 in the BCR signaling pathway. This phenomenon is speculated to be indirectly related to the activations of Wnt pathways.

Additional files

Additional file 1: The RT-PCR results for SFRP2.

Additional file 2: The expression analyses for β-catenin.

Additional file 3: The results of the phosphorylation experiments with splenic B cells.

Competing interests
The authors declare that they have no competing interests.

Authors' contributions
YT performed a part of experiments, analyzed and summarized all resulting data, and drafted the manuscript; MT centrally kept examined mice and participated in all of experiments; TY participated in all of experiments, designed concrete experimental plan, and helped to draft the manuscript; KT designed general experimental plan and helped to draft the manuscript; All the authors read and approved the final manuscript.

Acknowledgements
We thank T. Ichikawa for excellent secretarial assistance and Dr. S. Imashuku for suggestion and reviewing the manuscript. This work was supported by a Grant-in-Aid for Scientific Research (C: 23590368 to TY) from the Ministry of Education, Culture, Sports, Science and Technology of Japan.

Received: 16 October 2013 Accepted: 24 October 2014
Published: 4 November 2014

References
1. Miller JR: **The Wnts.** *Genome Biol* 2002, **3:**REVIEWS3001.
2. Huelsken J, Behrens J: **The Wnt signalling pathway.** *J Cell Sci* 2002, **115:**3977–3978.
3. Reya T, Clevers H: **Wnt signalling in stem cells and cancer.** *Nature* 2005, **434:**843–850.
4. Suda T, Arai F: **Wnt signaling in the niche.** *Cell* 2008, **132:**729–730.
5. Rao TP, Kuhl M: **An updated overview on Wnt signaling pathways: a prelude for more.** *Circ Res* 2010, **106:**1798–1806.
6. Sugimura R, He XC, Venkatraman A, Arai F, Box A, Semerad C, Haug JS, Peng L, Zhong XB, Suda T, Li L: **Noncanonical Wnt signaling maintains hematopoietic stem cells in the niche.** *Cell* 2012, **150:**351–365.
7. Sugimura R, Li L: **Noncanonical Wnt signaling in vertebrate development, stem cells, and diseases.** *Birth Defects Res C Embryo Today* 2010, **90:**243–256.
8. Cruciat CM, Niehrs C: **Secreted and transmembrane wnt inhibitors and activators.** *Cold Spring Harb Perspect Biol* 2013, **5:**a015081.
9. Shirozu M, Tada H, Tashiro K, Nakamura T, Lopez ND, Nazarea M, Hamada T, Sato T, Nakano T, Honjo T: **Characterization of novel secreted and membrane proteins isolated by the signal sequence trap method.** *Genomics* 1996, **37:**273–280.
10. Satoh W, Matsuyama M, Takemura H, Aizawa S, Shimono A: **Sfrp1, Sfrp2, and Sfrp5 regulate the Wnt/beta-catenin and the planar cell polarity pathways during early trunk formation in mouse.** *Genesis* 2008, **46:**92–103.
11. Mii Y, Taira M: **Secreted Wnt "inhibitors" are not just inhibitors: regulation of extracellular Wnt by secreted Frizzled-related proteins.** *Dev Growth Differ* 2011, **53:**911–923.
12. Morello R, Bertin TK, Schlaubitz S, Shaw CA, Kakuru S, Munivez E, Hermanns P, Chen Y, Zabel B, Lee B: **Brachy-syndactyly caused by loss of Sfrp2 function.** *J Cell Physiol* 2008, **217:**127–137.
13. Ikegawa M, Han H, Okamoto A, Matsui R, Tanaka M, Omi N, Miyamae M, Toguchida J, Tashiro K: **Syndactyly and preaxial synpolydactyly in the single Sfrp2 deleted mutant mice.** *Dev Dyn* 2008, **237:**2506–2517.
14. Perry AS, O'Hurley G, Raheem OA, Brennan K, Wong S, O'Grady A, Kennedy AM, Marignol L, Murphy TM, Sullivan L, Barrett C, Loftus B, Thornhill J, Hewitt SM, Lawler M, Kay E, Lynch T, Hollywood D: **Gene expression and epigenetic discovery screen reveal methylation of SFRP2 in prostate cancer.** *Int J Cancer* 2013, **132:**1771–1780.
15. Cheng YY, Yu J, Wong YP, Man EP, To KF, Jin VX, Li J, Tao Q, Sung JJ, Chan FK, Leung WK: **Frequent epigenetic inactivation of secreted frizzled-related protein 2 (SFRP2) by promoter methylation in human gastric cancer.** *Br J Cancer* 2007, **97:**895–901.
16. Huang Z, Li L, Wang J: **Hypermethylation of SFRP2 as a potential marker for stool-based detection of colorectal cancer and precancerous lesions.** *Dig Dis Sci* 2007, **52:**2287–2291.
17. Oshima T, Abe M, Asano J, Hara T, Kitazoe K, Sekimoto E, Tanaka Y, Shibata H, Hashimoto T, Ozaki S, Kido S, Inoue D, Matsumoto T: **Myeloma cells suppress bone formation by secreting a soluble Wnt inhibitor, sFRP-2.** *Blood* 2005, **106:**3160–3165.
18. Fleming HE, Janzen V, Lo Celso C, Guo J, Leahy KM, Kronenberg HM, Scadden DT: **Wnt signaling in the niche enforces hematopoietic stem cell quiescence and is necessary to preserve self-renewal in vivo.** *Cell Stem Cell* 2008, **2:**274–283.
19. Cain CJ, Manilay JO: **Hematopoietic stem cell fate decisions are regulated by Wnt antagonists: comparisons and current controversies.** *Exp Hematol* 2013, **41:**3–16.
20. Nakajima H, Ito M, Morikawa Y, Komori T, Fukuchi Y, Shibata F, Okamoto S, Kitamura T: **Wnt modulators, SFRP-1, and SFRP-2 are expressed in osteoblasts and differentially regulate hematopoietic stem cells.** *Biochem Biophys Res Commun* 2009, **390:**65–70.
21. Novak EJ, Rabinovitch PS: **Improved sensitivity in flow cytometric intracellular ionized calcium measurement using fluo-3/Fura Red fluorescence ratios.** *Cytometry* 1994, **17:**135–141.
22. Aragon IV, Barrington RA, Jackowski S, Mori K, Brewer JW: **The specialized unfolded protein response of B lymphocytes: ATF6alpha-independent development of antibody-secreting B cells.** *Mol Immunol* 2012, **51:**347–355.
23. Baba Y, Kurosaki T: **Impact of Ca2+ signaling on B cell function.** *Trends Immunol* 2011, **32:**589–594.
24. Humphries LA, Dangelmaier C, Sommer K, Kipp K, Kato RM, Griffith N, Bakman I, Turk CW, Daniel JL, Rawlings DJ: **Tec kinases mediate sustained calcium influx via site-specific tyrosine phosphorylation of the phospholipase Cgamma Src homology 2-Src homology 3 linker.** *J Biol Chem* 2004, **279:**37651–37661.
25. Bunney TD, Katan M: **PLC regulation: emerging pictures for molecular mechanisms.** *Trends Biochem Sci* 2011, **36:**88–96.
26. Kim YJ, Sekiya F, Poulin B, Bae YS, Rhee SG: **Mechanism of B-cell receptor-induced phosphorylation and activation of phospholipase C-gamma2.** *Mol Cell Biol* 2004, **24:**9986–9999.

doi:10.1186/1756-0500-7-780
Cite this article as: Tokuda *et al.*: The defect of SFRP2 modulates an influx of extracellular calcium in B lymphocytes. *BMC Research Notes* 2014 **7**:780.

OPEN ACCESS

Clinical features and management of cytomegalovirus corneal endotheliitis: analysis of 106 cases from the Japan corneal endotheliitis study

Noriko Koizumi,[1,2] Tsutomu Inatomi,[1] Takashi Suzuki,[3] Atsushi Shiraishi,[3] Yuichi Ohashi,[3] Michiko Kandori,[4] Dai Miyazaki,[4] Yoshitsugu Inoue,[4] Takeshi Soma,[5] Kohji Nishida,[5] Hiroshi Takase,[6] Sunao Sugita,[6] Manabu Mochizuki,[6] Shigeru Kinoshita,[1] for the Japan Corneal Endotheliitis Study Group

▸ Additional material is published online only. To view please visit the journal online (http://dx.doi.org/10.1136/bjophthalmol-2013-304625).

For numbered affiliations see end of article.

Correspondence to
Professor Noriko Koizumi, Department of Ophthalmology, Kyoto Prefectural University of Medicine, 465 Kajii-cho, Hirokoji-agaru, Kawaramachi-dori, Kamigyo-ku, Kyoto 602-0841, Japan; norikoiz@koto.kpu-m.ac.jp

Received 15 November 2013
Revised 17 April 2014
Accepted 6 July 2014
Published Online First 29 July 2014

ABSTRACT

Aims The purpose of this study is to elucidate the clinical manifestations and the current treatment status of cytomegalovirus (CMV) endotheliitis via a large case series obtained from a national survey conducted in Japan.

Methods The Japan Corneal Endotheliitis Study Group proposed diagnostic criteria for CMV endotheliitis based on a viral examination by PCR of aqueous humour, in combination with clinical manifestations. A national survey was then retrospectively conducted among 1160 members of the Japan Cornea Society. The study reviewed the patient profiles, clinical manifestations, and treatment modalities of individuals who met the diagnostic criteria for CMV endotheliitis.

Results The study included 109 eyes of 106 patients. Mean patient age was 66.9±10.9 years (85 males (80.2%), 21 females (19.8%)). Patients were commonly diagnosed with anterior uveitis and ocular hypertension prior to confirmation of CMV endotheliitis. Coin-shaped lesions were observed in 70.6%, and linear keratic precipitates in 8.3% of the patients, respectively. 95% of cases were treated with anti-CMV drugs.

Conclusions CMV endotheliitis is most common in middle-aged and elderly men. CMV endotheliitis should be suspected when patients present with corneal endotheliitis involving coin-shaped lesions accompanied by anterior uveitis and ocular hypertension.

Open Access
Scan to access more free content

CrossMark

To cite: Koizumi N, Inatomi T, Suzuki T, *et al*. *Br J Ophthalmol* 2015;**99**: 54–58.

INTRODUCTION

Corneal endotheliitis is a corneal endothelium-specific inflammation first described by Khodadoust and Attarzadeh in 1982.[1] It is characterised by corneal oedema, keratic precipitates (KPs), a mild anterior chamber reaction, and the destruction of corneal endothelium. There are reportedly four clinical forms of cornea endotheliitis, of which, linear corneal endotheliitis is considered the most serious form due to the progressive loss of corneal endothelial cells.[2] Corneal endotheliitis is thought to be a viral infection,[3] especially in association with herpes simplex virus (HSV),[4 5] varicella-zoster virus (VZV)[6] and mumps virus.[7] However, cases of corneal endotheliitis are often observed to be negative for HSV and VZV, and unresponsive to acyclovir treatment. Such cases are diagnosed as 'idiopathic corneal endotheliitis',[3] and their prognosis is poor due to the progressive destruction of corneal endothelium that is resistant to antiviral medication.

In 2006, we reported the first case of cytomegalovirus (CMV)-induced corneal endotheliitis in which CMV DNA was detected from the aqueous humour of the patient via PCR, and that showed a positive response to ganciclovir treatment.[8] Clinical evidence of CMV endotheliitis has been accumulated,[8–24] and the current emphasis is on the importance of early diagnosis and treatment. However, few large series have been reported, and diagnostic criteria for the disease have yet to be established.

The purpose of this study was to elucidate the clinical manifestations, as well as the current status of clinical diagnosis and treatment of CMV endotheliitis via a large case series obtained from the national survey conducted by the Japan Corneal Endotheliitis Study Group (JCESG) in accordance with the diagnostic criteria for CMV endotheliitis instituted by the JCESG.

METHODS

Prior to this survey, the JCESG proposed diagnostic criteria for CMV endotheliitis (box 1, figure 1), which were authorised by the Japanese Ministry of Health, Labour and Welfare. Questionnaire surveys on diagnostic criteria were distributed to 1160 members of the Japan Cornea Society. Members with patients who met the diagnostic criteria for CMV endotheliitis were requested to provide relevant data for each patient diagnosed with the disease between November 2004 and November 2011, comprising: demographics, clinical aspects, diagnostic protocol and treatment. This retrospective study was approved by the University Ethical Committees of Kyoto Prefectural University of Medicine, Doshisha University, and each of the other university hospitals associated with the study group.

Statistical analysis

Statistical analysis was performed using JMP software (V.9.1, SAS Institute, Cary, North Carolina, USA). The association between the duration of disease and best-corrected visual acuity (BCVA), as well as between patient age and corneal endothelial cell density, were analysed via Spearman's test. The effect of anti-CMV medication was analysed via

Box 1 Diagnostic criteria of cytomegalovirus corneal endotheliitis (established by the Japan Corneal Endotheliitis Study Group which was authorised by the Japanese Ministry of Health, Labour and Welfare)

I. Viral examination by PCR of aqueous humour Positive for CMV DNA, but negative for HSV DNA and VZV DNA
II. Clinical manifestations
  i. Corneal endotheliitis with coin-shaped lesion or linear KPs similar to the rejection line.
  ii. Corneal endotheliitis with localised corneal oedema with KPs associated with two of the following signs:
    - recurrent/chronic anterior uveitis
    - ocular hypertension/secondary glaucoma
    - corneal endothelial cell loss.

⇩

Typical CMV endotheliitis: I and II-i
Atypical CMV endotheliitis: I and II-ii

CMV, cytomegalovirus; HSV, herpes simplex virus; KP, keratic precipitate; PCR, polymerase chain reaction; VZV, varicella-zoster virus.

Welch's test. The association between pretreatment and post-treatment BCVA was analysed via paired t test.

RESULTS

A total of 109 eyes of 106 patients were reported from 30 facilities (all hospitals are listed in the online supplementary appendix). Three patients had bilateral eye involvement; 79 were diagnosed as 'typical CMV endotheliitis' and 30 were diagnosed as 'atypical CMV endotheliitis'. The mean follow-up period postdiagnosis of CMV endotheliitis was 27.2±18.8 months.

Patient age and gender

The age and gender of patients diagnosed with CMV endotheliitis is shown in figure 2. Mean age was 66.9±10.9 years (range: 40–85 years). Eighty-five cases (80.2%) were male and 21 (19.8%) cases were female.

History of systemic and ocular disease

Seventeen patients (16.0%) had been diagnosed with diabetes, 22 (20.8%) with hypertension, and 10 (9.4%) with cancer (under treatment or treated). There were no reports of HIV infection. Almost half the patients had been previously diagnosed with anterior uveitis (48.6%), Posner–Schlossman syndrome (36.7%) or secondary glaucoma/ocular hypertension (39.4%). With regard to surgical treatment prior to the diagnosis of CMV endotheliitis, corneal transplantation was performed in 29 eyes (25.7%), glaucoma surgery in 33 eyes (30.3%) and cataract surgery in 60 eyes (55%).

History of medical treatment prior to diagnosis of CMV endotheliitis

Steroids and immunosuppressive agents

Fifteen patients (14.2%) received systemic administration of steroids, and 105 eyes of 103 patients (97.1%) received topical administration. Three patients who had multiple grafts (three repeated grafts in each case) had received systemic immunosuppressive agents to prevent graft rejection. Two of those patients received systemic cyclosporine and one patient received systemic tacrolimus (FK506).

Antiviral agents

Topical aciclovir ointment was previously used in 35 eyes (32.1%) and oral valaciclovir was used in 28 patients (26.4%). Systemic acyclovir, ganciclovir or valganciclovir were also used in 1 patient each.

Antiglaucoma agents

Seventy-one eyes (65.1%) had undergone treatment with topical antiglaucoma agents. Acetazolamide tablets were also administered to 28 patients (26.4%).

Viral examination

Qualitative and/or quantitative PCR examination using an aqueous sample obtained from each of the 109 eyes (100%) showed positive for CMV DNA, but negative for HSV and VZV DNA (all being diagnostic criteria for CMV endotheliitis). Serum CMV immunoglobulin G (IgG) and immunoglobulin M (IgM) antibodies had been tested in 30 and 20 patients, respectively. All the 30 patients (100%) tested positive for CMV IgG antibody and all the 20 patients (100%) tested negative for IgM antibody. Twenty-two patients had been serum tested for CMV pp65 antigen, and all tested negative.

Clinical investigations and ocular manifestations at the diagnosis of CMV endotheliitis

BCVA

Mean BCVA (logMAR) at the time of diagnosis was 0.448. No correlation was found between duration of disease and BCVA at the time of diagnosis (Spearman's test, p=0.402).

Intraocular pressure

Mean intraocular pressure (IOP) was 19.6±9.8 mm Hg (mean±SD). Despite the use of antiglaucoma therapy in 71 eyes and previous glaucoma surgery in 33 eyes, 42 eyes (38.5%) showed high IOP (>22 mm Hg) at the time of diagnosis of CMV endotheliitis.

Corneal endothelial density

Corneal endothelial density (CED) was measured in 62 eyes, and mean CED was 1346.2±729.2 cells/mm^2 (mean±SD). CEDs were broadly distributed among the patients, and no correlation was found between patient age and CED at the time of diagnosis (Spearman's test, p=0.513).

Clinical findings at diagnosis

Coin-shaped lesion KPs and corneal oedema were observed in 70.6% and 73.4% of the eyes, respectively. Linear KPs were noted in 8.3% of the eyes, and anterior chamber inflammation was detected in 67.9% of the eyes. Investigation of lens, angle and vitreoretinal abnormality revealed 20 eyes (18.3%) with cataract and 60 eyes (55.0%) that had undergone intraocular lens implantation. Gonioscopic examination results were reported for 33 eyes (30.2%), of which 13 showed some findings such as peripheral anterior synechia, or decreased/increased pigmentation of the trabecular meshwork.

Medical treatment for CMV endotheliitis

In Japan, ganciclovir is available for the treatment of intravenous infusion, and valganciclovir hydrochloride tablets for CMV

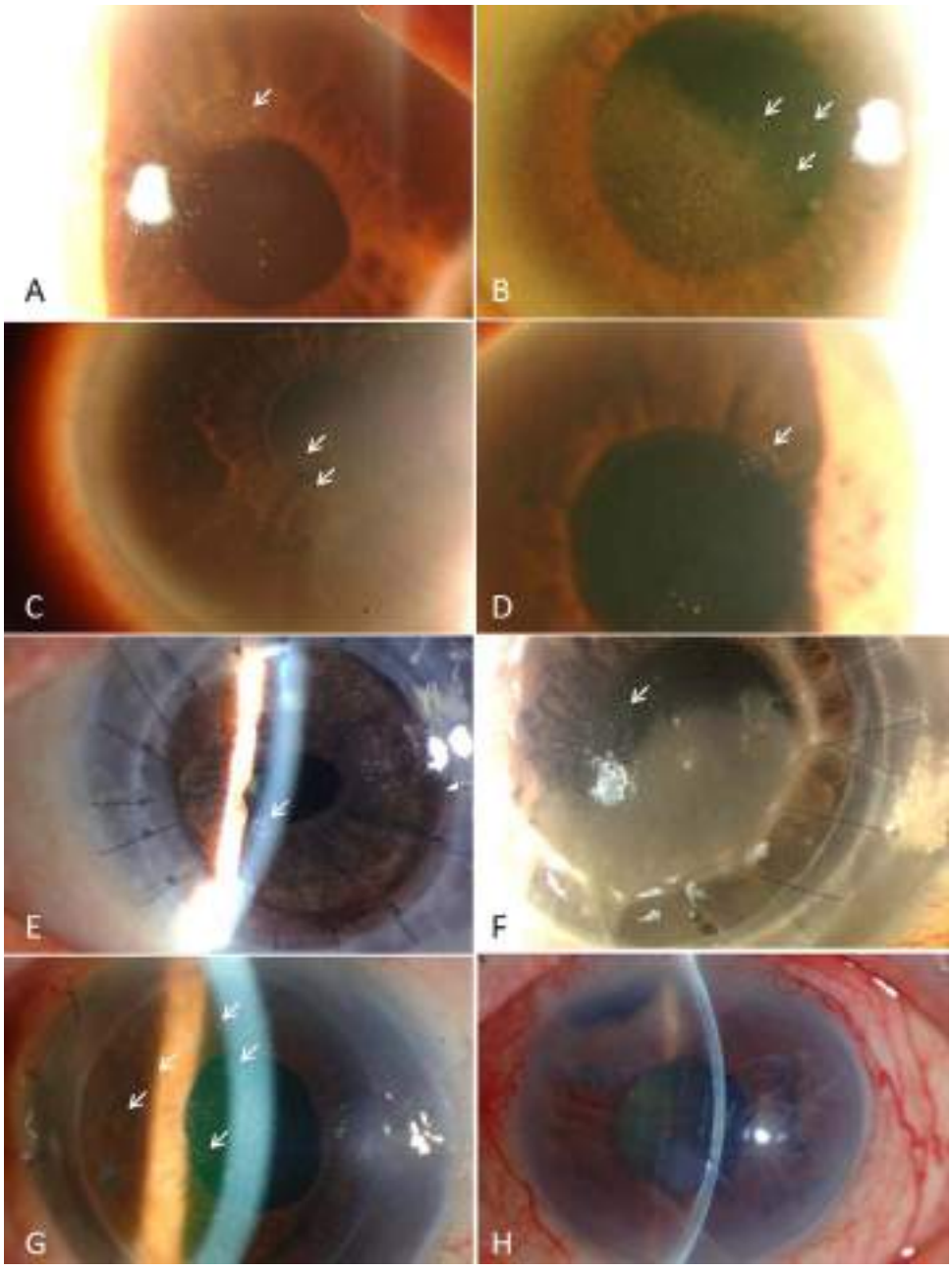

Figure 1 Representative anterior-segment photographs of cytomegalovirus (CMV) corneal endotheliitis. (A–G) Typical CMV endotheliitis: CMV endotheliitis-associated coin-shaped lesions (white arrows). (H) Atypical CMV endotheliitis: CMV endotheliitis not associated with coin-shaped lesions. This case showed corneal oedema with keratic precipitates associated with recurrent anterior uveitis and secondary glaucoma.

infection. The results of our survey showed that anti-CMV agents were used in 104 of the total 109 eyes, either systemically, topically, or both. Systemic administration of anti-CMV drugs (either ganciclovir or valganciclovir) was performed in 74 eyes (67.9%), and topical administration of ganciclovir prepared from vials for intravenous infusion[11 13] was also used in 82 eyes (75.2%). Fifty-two eyes (47.7%) received both systemic and topical anti-CMV treatment. The effect of anti-CMV treatment was clinically evaluated 1 month after initiation of anti-CMV treatment in 96 eyes, and was scored from 0 to 2— 0: ineffective (no change in corneal findings); 1: partially effective (corneal oedema and KPs improved, yet did not completely disappear); 2: greatly effective (significant improvement of corneal oedema and KPs)) (table 1). Combined anti-CMV therapy (systemic and topical) was more effective than systemic or topical anti-CMV treatment alone (Welch's test, $p=0.09$), but the difference was non-significant. During the observation period, 39 eyes (36%) showed recurrence of inflammation, and anti-CMV treatment was repeated on those eyes.

Corneal endothelial function and BCVA at final examination

At the final examination, corneal clarity was successfully retained in 66 eyes (60.6%) without additional corneal transplantation, and the mean corneal endothelial cell density among those cases was 1174.5 ± 69.3 cells/mm^2 (mean±SD). Forty-three eyes (39.4%) failed to retain corneal endothelial function during the observation period. Of those, 20 eyes (18.3%) recovered corneal clarity after undergoing corneal transplantation; the remaining 23 eyes (21.1%) with corneal endothelial dysfunction were under consideration for corneal transplantation or were

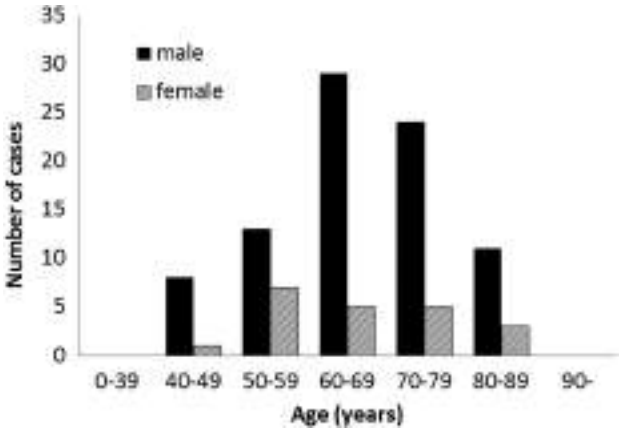

Figure 2 Age and gender of patients with cytomegalovirus (CMV) corneal endotheliitis. Mean patient age was 66.9±10.9 years (range: 40–85 years). Eighty-five cases: (80.2%) were men and 21 (19.8%) cases were women (n=106).

unsuitable for corneal transplantation due to glaucomatous optic disc atrophy. At the final examination, BCVA was evaluated in 107 eyes, and the mean BCVA at follow-up was 0.403 (logMAR). No significant difference was found between pretreatment BCVAs and those at the final examination (paired t test, p=0.376).

DISCUSSION

CMV endotheliitis are most common among middle-aged and elderly men. This finding of male dominancy is consistent with those of previous case-series reports involving non-Japanese populations.[9 20–22]

We previously reported coin-shaped lesions (or nummular KPs) and linear KPs as characteristic findings of CMV endotheliitis,[8 13] and they are often reported in other cases of CMV endotheliitis.[9–11 15 17 18 20 23] In this present study, coin-shaped lesions and linear KPs were noted in 70.6% and 8.3% of eyes, respectively. Although we were unable to compare these findings with the incidence in CMV-negative corneal endotheliitis, we consider that coin-shaped lesions and linear KPs are highly typical of CMV endotheliitis. It should be also noted that the presence of coin-shaped lesions and linear KPs can be transient. We expected to identify CMV endotheliitis cases without coin-shaped lesions or linear KPs via the diagnostic criteria for 'atypical CMV endotheliitis'. In our study, 30 eyes were reported as atypical CMV endotheliitis. Our findings confirmed the existence of overlap cases of CMV corneal endotheliitis and CMV anterior uveitis or inflammatory ocular hypertensive syndrome. The results also revealed that a large number of cases had previously undergone corneal transplantations, indicating the importance of a high index of suspicion for CMV endotheliitis as a cause of graft failure, or a primary cause of corneal endothelial dysfunction that led to the corneal transplantation. Anti-CMV agents had been widely used. When both systemic and topical anti-CMV agents were administered, most patients achieved improvement or complete remission of KPs and corneal oedema. However, 5.8% of cases treated by systemic and topical anti-CMV agents in combination failed to respond to the treatment. Those cases had severe corneal endothelial damage at the time of diagnosis. The data for those patients show that anti-CMV agents are effective for the treatment of active CMV endotheliitis; however, if corneal endothelial damage is severe, CMV endotheliitis often results in irreversible corneal endothelial dysfunction. In terms of visual acuity, no significant improvement in BCVA was found between pretreatment and final examination. We speculate that this study included non-negligible number of patients who had a long history of idiopathic corneal endotheliitis that was resistant to antiherpetic medication. This possibility highlights the need for early recognition and treatment of CMV endotheliitis in order to prevent irreversible corneal endothelial dysfunction. Since this survey was conducted retrospectively, it has limited ability to evaluate the effect of anti-CMV treatment. Further research is needed to evaluate the effect of antiviral treatment by comparing the viral load of aqueous humour before and after treatment via real-time PCR, as some members of the study group have reported previously.[15 16] In this retrospective study, we were unable to obtain any Goldmann–Witmer coefficient data for CMV because the anti-CMV IgG titre in aqueous humour was not examined in most of the cases. However, calculation of the Goldmann–Witmer coefficient might be a useful diagnostic tool in addition to the PCR analysis for the diagnosis of CMV endotheliitis, especially in atypical cases.

Table 1 Effects of anti-CMV treatment

	Effective (%)	Partially effective (%)	Not effective (%)
Systemic or topical GCV (n=44)	52.3	34.1	13.6
Systemic and topical GCV (n=52)	67.3	26.9	5.8

CMV, cytomegalovirus; GCV, ganciclovir.

The pathogenic mechanism of CMV endotheliitis has yet to be defined. Previously, Zhen *et al*[25] reported that anterior chamber-associated immune deviation may play an important role in the pathogenesis of herpetic corneal endotheliitis. One possible background factor for the reactivation of CMV within the anterior chamber is local or systemic use of intensive immunosuppressive medication. It should be noted that topical steroid eye drops were applied to 96.3% of the eyes at the time of CMV endotheliitis diagnosis. Although none of the patients were HIV-positive, we theorise that local immunosuppression might have facilitated CMV reactivation. From another perspective, 25.7% of eyes had previously received corneal transplantation. Although idiopathic corneal endotheliitis (presumably caused by CMV) was reported as the primary diagnosis in most of those cases, the possibility of CMV transmission via donor tissue cannot be excluded.[21] However, the suitability of CMV-seropositive donor tissue for corneal transplantation requires further study because serological examination of the donors for CMV was not performed in this study. To prevent recurrence of CMV endotheliitis and to preserve long-term corneal endothelial function, a maintenance therapy using topical anti-CMV agents needs to be developed.

In conclusion, this large case-series study revealed that CMV endotheliitis was common in middle-aged and elderly men. CMV endotheliitis should be suspected, and the performance of PCR of aqueous humour should be evaluated when encountering patients with corneal endotheliitis with coin-shaped lesions or linear KPs, corneal endotheliitis associated with anterior uveitis, elevated IOP, or corneal endothelial cell loss. The findings of this study suggest the effectiveness of antiviral treatment for CMV endotheliitis; however, further study is needed to establish treatment regimens for the disease in order to prevent corneal endothelial dysfunction. To the best of our knowledge, this is the largest case-series of CMV endotheliitis to report the comprehensive clinical features of this newly identified infectious corneal disease.

Author affiliations
[1]Department of Ophthalmology, Kyoto Prefectural University of Medicine, Kyoto, Japan
[2]Department of Biomedical Engineering, Faculty of Life and Medical Sciences, Doshisha University, Kyotanabe, Japan
[3]Department of Ophthalmology, Ehime University School of Medicine, Ehime, Japan
[4]Division of Ophthalmology and Visual Science, Faculty of Medicine, Tottori University, Tottori, Japan
[5]Department of Ophthalmology, Osaka University Graduate School of Medicine, Osaka, Japan
[6]Department of Ophthalmology and Vision Science, Tokyo Medical and Dental University Graduate School of Medicine, Tokyo, Japan

Acknowledgements The authors wish to thank Drs Kozaburo Hayashi (Kinki University), Chie Sotozono (Kyoto Prefectural University of Medicine), Kazuichi Maruyama (Tohoku University), Hiroko Nakagawa (Kyoto Prefectural University of Medicine), Akiko Fukumoto (Kyoto Prefectural University of Medicine), and Naoki Okumura (Doshisha University)—all of whom are members of the Japan Corneal Endotheliitis Study Group, for collecting the clinical data, and for their useful discussion; Mr John Bush for reviewing the manuscript; and Dr Katsumi Yagi (Senior Researcher, Louis Pasteur Center for Medical Research) for the statistical analysis.

Contributors Conception and design of the study (NK, TI, SK); analysis and interpretation (NK, TI, TS, AS, YO, MK, DM, YI, TS, KN, HT, SS, MM, SK); writing of the article (NK, TI, YI); critical revision of the article (YO, YI, KN, MM, SK); final approval of the article (NK, TI, ST, AS, YO, MK, DM, YI, TS, KN, HT, SS, MM, SK); data collection (NK, TI, TS, AS, YO, MK, DM, YI, TS, KN, HT, SS, MM, SK); obtaining funding (NK, TI, YO, YI, KN, MM); literature search (NK, TI, YI); administrative, technical, or logistic support (YI, MM, SK).

Funding This work was supported in part by Health and Labour Sciences Research Grants (Research on Intractable Diseases) from the Ministry of Health, Labour and Welfare of Japan.

Competing interests None.

Ethics approval The University Ethical Committees of Kyoto Prefectural University of Medicine and Doshisha University.

Provenance and peer review Not commissioned; externally peer reviewed.

REFERENCES

1 Khodadoust AA, Attarzadeh A. Presumed autoimmune corneal endotheliopathy. *Am J Ophthalmol* 1982;93:718–22.
2 Suzuki T, Ohashi Y. Corneal endotheliitis. *Semin Ophthalmol* 2008;23:235–40.
3 Ohashi Y, Kinoshita S, Mano T, *et al*. Idiopathic corneal endotheliopathy. A report of two cases. *Arch Ophthalmol* 1985;103:1666–8.
4 Robin JB, Steigner JB, Kaufman HE. Progressive herpetic corneal endotheliitis. *Am J Ophthalmol* 1985;100:336–7.
5 Ohashi Y, Yamamoto S, Nishida K, *et al*. Demonstration of herpes simplex virus DNA in idiopathic corneal endotheliopathy. *Am J Ophthalmol* 1991;112:419–23.
6 Maudgal PC, Missotten L, De Clercq E, *et al*. Varicella-zoster virus in the human corneal endothelium: a case report. *Bull Soc Belge Ophtalmol* 1980;190:71–86.
7 Singh K, Sodhi PK. Mumps-induced corneal endotheliitis. *Cornea* 2004;23:400–2.
8 Koizumi N, Yamasaki K, Kawasaki S, *et al*. Cytomegalovirus in aqueous humor from an eye with corneal endotheliitis. *Am J Ophthalmol* 2006;141:564–5.
9 Chee SP, Bacsal K, Jap A, *et al*. Corneal endotheliitis associated with evidence of cytomegalovirus infection. *Ophthalmology* 2007;114:798–803.
10 Shiraishi A, Hara Y, Takahashi M, *et al*. Demonstration of "owl's eye" morphology by confocal microscopy in a patient with presumed cytomegalovirus corneal endotheliitis. *Am J Ophthalmol* 2007;143:715–17.
11 Suzuki T, Hara Y, Uno T, *et al*. DNA of cytomegalovirus detected by PCR in aqueous of patient with corneal endotheliitis after penetrating keratoplasty. *Cornea* 2007;26:370–2.
12 Yamauchi Y, Suzuki J, Sakai J, *et al*. A case of hypertensive keratouveitis with endotheliitis associated with cytomegalovirus. *Ocul Immunol Inflamm* 2007;15:399–401.
13 Koizumi N, Suzuki T, Uno T, *et al*. Cytomegalovirus as an etiologic factor in corneal endotheliitis. *Ophthalmology* 2008;115:292–7.
14 Anshu A, Chee SP, Mehta JS, *et al*. Cytomegalovirus endotheliitis in Descemet's stripping endothelial keratoplasty. *Ophthalmology* 2009;116:624–30.
15 Kandori M, Inoue T, Takamatsu F, *et al*. Prevalence and features of keratitis with quantitative polymerase chain reaction positive for cytomegalovirus. *Ophthalmology* 2010;117:216–22.
16 Miyanaga M, Sugita S, Shimizu N, *et al*. A significant association of viral loads with corneal endothelial cell damage in cytomegalovirus anterior uveitis. *Br J Ophthalmol* 2010;94:336–40.
17 Kandori M, Miyazaki D, Yakura K, *et al*. Relationship between the number of cytomegalovirus in anterior chamber and severity of anterior segment inflammation. *Jpn J Ophthalmol* 2013;57:497–502.
18 Shimazaki J, Harashima A, Tanaka Y. Corneal endotheliitis with cytomegalovirus infection of corneal stroma. *Eye (Lond)* 2010;24:1105–7.
19 Chee SP, Jap A. Immune ring formation associated with cytomegalovirus endotheliitis. *Am J Ophthalmol* 2011;152:449–53.
20 Hwang YS, Shen CR, Chang SH, *et al*. The validity of clinical feature profiles for cytomegaloviral anterior segment infection. *Graefes Arch Clin Exp Ophthalmol* 2011;249:103–10.
21 Lusthaus JA, Kim P, Steller AK, *et al*. Successful corneal autograft after clearance of anterior chamber cytomegalovirus with oral valganciclovir in a patient with multiple failed corneal allografts. *Cornea* 2011;30:1054–7.
22 Chee SP, Jap A. Treatment outcome and risk factors for visual loss in Cytomegalovirus endotheliitis. *Graefes Arch Clin Exp Ophthalmol* 2012;250:383–9.
23 Chu HY, Sun CC, Chuang WY, *et al*. Cytomegalovirus associated corneal endotheliitis after penetrating keratoplasty in a patient with Fuchs corneal endothelial dystrophy. *Br J Ophthalmol* 2012;96:300–1.
24 Kobayashi A, Yokogawa H, Higashide T, *et al*. Clinical significance of owl eye morphologic features by in vivo laser confocal microscopy in patients with cytomegalovirus corneal endotheliitis. *Am J Ophthalmol* 2012;153:445–53.
25 Zheng X, Yamaguchi M, Goto T, *et al*. Experimental corneal endotheliitis in rabbit. *Invest Ophthalmol Vis Sci* 2000;41:377–85.

Clinical features and management of cytomegalovirus corneal endotheliitis: analysis of 106 cases from the Japan corneal endotheliitis study

Noriko Koizumi, Tsutomu Inatomi, Takashi Suzuki, Atsushi Shiraishi, Yuichi Ohashi, Michiko Kandori, Dai Miyazaki, Yoshitsugu Inoue, Takeshi Soma, Kohji Nishida, Hiroshi Takase, Sunao Sugita, Manabu Mochizuki and Shigeru Kinoshita

Br J Ophthalmol 2015 99: 54-58 originally published online July 29, 2014
doi: 10.1136/bjophthalmol-2013-304625

Notes

HHS Public Access

Author manuscript

Nat Genet. Author manuscript; available in PMC 2015 October 14.

Published in final edited form as:

Nat Genet. 2015 April ; 47(4): 387–392. doi:10.1038/ng.3226.

A common variant mapping to *CACNA1A* is associated with susceptibility to Exfoliation syndrome

A full list of authors and affiliations appears at the end of the article.

Abstract

Exfoliation syndrome (XFS) is the commonest recognizable cause of open angle glaucoma worldwide. To better understand the etiology of XFS, we conducted a genome-wide association study (GWAS) on 1,484 patients and 1,188 controls from Japan, and followed up the most significant findings on a further 6,901 patients and 20,727 controls from 17 countries across 6 continents. We discovered a significant association between a new locus (*CACNA1A* rs4926244) and increased susceptibility to XFS (Odds ratio [OR] = 1.16, $P = 3.36 \times 10^{-11}$). Although overwhelming association at the *LOXL1* locus was confirmed, the key SNP marker (*LOXL1* rs4886776) demonstrated allelic reversal depending on ethnic grouping (In Japanese: $OR_{A\text{-}allele} = 9.87$, $P = 2.13 \times 10^{-217}$; In non-Japanese: $OR_{A\text{-}allele} = 0.49$, $P = 2.35 \times 10^{-31}$). Our findings represent the first genetic locus outside of *LOXL1* which surpasses genome-wide significance for XFS, and provides insight into the biology and pathogenesis of the disease.

XFS is a generalized disorder of the extracellular matrix that manifests most conspicuously in the eye. The exfoliation material consists of cross-linked, amyloid-like fibrillar material and glycoproteins. Apart from ocular tissues, this material deposits around blood vessels

Correspondence should be addressed to T.A. aung_tin@yahoo.co.uk, or to C.C.K khorcc@gis.a-star.edu.sg.

*These authors contributed equally to this work

**These authors jointly supervised this work

[73]A full list of members and affiliations appears in the Supplementary Note

Author Contributions

T.A., M.O., & C.C.K. conceived the project. M.O., T.M., R.R.A., A.H., S.N., J.E.C., A.W.H., D.A.M., P.M., J.J.W., Y.S.A., J.C.Z., Y.N., T.Z., M.P.,L.J., Y.X.W., S.W., D.P., PG.S., Y.I., R.S.K., M.U., S.Manabe., K.H., S.Kazama., R.I., Y.M., K.Miyata., K.S., T.H., E.C., K.I., S.I., A.Y., M.Y., Y.K., M.A., T.O., T.Sakurai, T.Sugimoto, H.C., K.Y., S.Y.A., E.A.O., S.A.A-O., O.O., L.A-J, S.A.S., Y.Y., C.O., M.R.K., A.N.B., S.Y., E.L.A., E.K-J., U.L., P.C., R.M.R., A.Z., T.C., R.Ramakrishnan., K.N., R.V., P.Z., X.C., D.G-V., S.A.P., R.H., S-L.H., U-C.W-L., C.M., U.S-S., S.Moebus., N.Weisschuh., R.S., A.G., I.L., J.G.C., M.C., Q.Y., V.V., P.Founti., A.C., A.L., E.A., A.L.C., M.R.W., D.J.R., I.M-B., K.Mori, S.Heegaard., W.L.M.A., J.B.J., L.X., J.M.L., F.L., N.Wang., P.Frezzotti., S.Kinoshita, J.H.F., M.I., D.P.E., L.R.P., T.K., J.L.W., F.T., N.Y., & R.Ritch conducted patient recruitment and phenotyping. Z.L., S.U., M.K., K.P.B., M.A.B., J.J.W., Y.G., K.Y.T., L.H., W.Y.M., S.Q.P., B.Z., J.S., N.Z., Z.Y., & S.V. performed genotyping experiments. J.M.H., A.S.Y.C., M.C.L., E.N.V., G.R.H., & S.W.M.J. led and performed immunohistochemistry and immunofluorescence experiments. Z.L., K.P.B., R.A.F., P.L., K.K.A-A., L.A.S., L.H., K.S.S., J.N.F., M.N., F.M., N.G., M.M., S.U., M.K., Y.Y.T., J.H.K., A.E.A.K., S.Herms, Y.L., K.T., B.Z., J.S., N.Z., S.V., Z.Y., G.R.H., A.C.O., F.P., & A.G., performed analysis. E.N.V., T.Y.W., C.Y.C., A.M.H., M.M.N., B.C., E.S., M.S., & A.R. contributed genetic and genotyping data from control populations. The manuscript was drafted by C.C.K., with critical input from T.A., R.R.A., L.R.P., J.L.W., F.P., F.T., M.D., S.W.M.J., R.Ritch, and M.A.H. The manuscript was approved by all authors. C.C.K was responsible for obtaining financial support for this study.

URLs

Illumina, www.illumina.com; Sequenom, www.sequenom.com; Applied Biosystems, http://www.appliedbiosystems.com/; PLINK, http://pngu.mgh.harvard.edu/~purcell/plink/; R statistical program package, www.r-project.org; IMPUTE2, http://mathgen.stats.ox.ac.uk/impute/impute_v2.html

COMPETING FINANCIAL INTERESTS

The authors declare no competing financial interests.

particularly in association with elastic connective tissue, and could be found in other organs[1]. The build-up of exfoliation material deposits and pigment in the trabecular meshwork can damage this tissue and impede the drainage of aqueous humor from the eye thus resulting in elevated intraocular pressure and glaucomatous optic neuropathy. Exfoliation glaucoma is the most serious known complication of XFS[2].

The first GWAS on XFS was reported in 2007 and successfully identified *LOXL1* as a major susceptibility locus for XFS[3]. Since then, multiple studies have uniformly corroborated the association of genetic variants of *LOXL1* with XFS[4–21]. However, data from these studies showed associated alleles for *LOXL1* SNPs frequently undergo allelic reversal depending on ethnic group[22]. These findings suggest that complex genetic mechanisms are present for XFS pathogenesis, and the possibility that additional susceptibility loci for XFS remain to be identified. We assembled an international, multi-institutional collaborative effort across 6 continents comprising 17 countries to conduct a GWAS discovery and two-staged replication study of XFS (see **Methods**, Supplementary Table 1, and Supplementary Figure 1). Participating subjects provided written informed consent under the oversight of all local institutional review boards in accordance with the tenets of the Declaration of Helsinki.

For the GWAS discovery stage, we genotyped 717,991 SNP markers on 1,578 Japanese patients with XFS and 1,215 controls using the Illumina OmniExpress microarray. Control subjects were drawn from the same hospital where the XFS patients were first identified. A total of 1,484 cases and 1,188 controls passed quality control (QC) filters for call-rate, relatedness, heterozygosity and ancestry (see **Methods** for QC details) and were included for downstream association analysis. Multiple markers in strong linkage disequilibrium (LD) at the *LOXL1* locus showed strong evidence of association with XFS (Supplementary Figure 2a), with rs4886776 ($P = 7.37 \times 10^{-137}$) serving as the sentinel SNP.

A total of 66 SNPs outside of *LOXL1* showed evidence of association with XFS surpassing $P < 1 \times 10^{-4}$ at the GWAS discovery stage. We thus designed validation assays for these 66 SNP markers, together with *LOXL1* rs4886776, and genotyped them in a follow up collection of 2,628 XFS cases and 8,947 controls drawn from 9 countries (Stage 1 validation, see Supplementary Table 1). For each SNP examined, we conducted a fixed-effects meta-analysis to summarize the observations across the nine studies. One SNP marker (rs4926244), mapping within the *CACNA1A* gene that showed association in the GWAS discovery stage at $P = 5.50 \times 10^{-5}$ ($OR_{G\text{-allele}} = 1.29$) was also significant in this validation stage ($OR_{G\text{-allele}} = 1.17$, $P = 4.17 \times 10^{-5}$). Thus for rs4926244, meta-analysis of both the discovery and validation stages revealed genome-wide significant association ($OR_{G\text{-allele}} = 1.20$, $P = 2.45 \times 10^{-8}$) (Figure 1, Supplementary Table 2, and Supplementary Figure 2b). Results for all 67 SNP markers from the GWAS discovery and Stage 1 replication are appended in Supplementary Table 2. We did not observe consistent evidence of association at *CNTNAP2*, a locus previously reported to associate with XFS from a pooled GWAS study[23], as well as other previously reported candidate genes (Supplementary Table 3).

We subjected *CACNA1A* rs4926244 to further technical scrutiny in a third, independent dataset consisting of 4,273 XFS cases and 11,780 controls drawn from 8 additional countries

(Stage 2, replication; see Supplementary Table 1). The association maintained significance, consistent with findings observed in the two previous stages ($OR_{G\text{-allele}} = 1.13$, $P = 1.14 \times 10^{-4}$). Together, the combined discovery and two-stage replication patient collections consisting of 8,385 XFS cases and 21,915 controls provide evidence for association between the minor G allele at rs4926244 and XFS ($P = 3.36 \times 10^{-11}$). These data suggest risk for XFS increases approximately 1.16 fold for each copy of the minor G allele (Figure 1 and Supplementary Table 4). This association appears to be consistent with minimal heterogeneity when stratified for Asian ($OR_{G\text{-allele}} = 1.14$, $P = 7.46\times10^{-6}$), European ($OR_{G\text{-allele}}=1.19$, $P=1.90\times10^{-6}$) or South African ($OR_{G\text{-allele}} = 1.33$, $P = 0.11$)($P_{het} = 0.5$, $I^2 = 0\%$) ethnic groups (Figure 1).

SNP rs4926244 resides within an intronic region near the 3′ end of *CACNA1A*. It is flanked closely by recombination events (Figure 2) and is confined to its own linkage disequilibrium (LD) block (Supplementary Figure 3). We did not observe association with any genetic marker surpassing the nominal threshold of $P < 0.001$ outside of this critical region (Figure 2)[24]. We next performed imputation for unobserved SNPs at the *CACNA1A* locus on the basis of 1,000 Genomes cosmopolitan project data using the Phase 3 release (June 2014, see **Methods**) across the GWAS discovery collection. We were able to successfully impute 5602 SNPs across the *CACNA1A* locus. However, subsequent association analysis utilizing the imputed SNPs did not identify additional genetic associations that surpassed the statistical significance of rs4926244 (Supplementary Figure 4). Notably, the most significant SNPs emerging from the cosmopolitan imputation analysis are intronic and are all moderate-to-highly correlated with rs4926244 (Supplementary Table 5). None of these correlated SNP markers lies in strong motifs for transcription factor binding sites as identified by ENCODE. They also do not tag any common non-synonymous variants in *CACNA1A* (Supplementary Table 6). Haplotype association analysis assessing SNPs in a 2, 3, and 4 marker sliding window did not reveal evidence of association surpassing that observed for rs4926244 (lowest haplotype *P*-value = 0.00021; Supplementary Table 7), and we further note that all but one haplotype showing evidence of association exceeding $P < 0.0005$ in the GWAS dataset contained SNP rs4926244 (Supplementary Table 7). This suggests that rs4926244 is likely driving the common-variant haplotype association results, and that detailed fine-mapping of this locus using deep re-sequencing may be required. Examination of a recently available large-scale eQTL mapping database indicates the risk allele G at rs4926244 is modestly correlated with lower *CACNA1A* mRNA levels in peripheral blood cells ($Z=-3.00$, $P=0.0027$), suggesting that it may influence XFS risk through an effect on *CACNA1A* expression[25]. Further work will be needed to evaluate its effect in human ocular tissues.

Initial analysis of the *LOXL1* locus in the GWAS discovery dataset of Japanese descent demonstrated strong association at rs4886776 ($OR_{A\text{-allele}} = 8.31$, $P = 7.37 \times 10^{-137}$). The strength of this association vastly exceeded that of marker rs3825942 (responsible for a p.G153D substitution in exon 1 of *LOXL1*), which has been the most widely tested and reported SNP association prior to this analysis[22]. Performing the analysis after conditioning for the allele dosage of rs4886776 extinguished the signal of association for every other genetic marker within the *LOXL1* locus. Conversely, conditioning the analysis for allele dosage at rs3825942 still resulted in genome-wide significant association at many of the

other *LOXL1* SNPs, including rs4886776 (Supplementary Table 8). These data suggest that within the Japanese GWAS discovery set, the observed association at *LOXL1* can be attributed to rs4886776 alone. We note that rs4886776 is in high LD with rs1048661 (r^2=0.98 in 1000 genomes Asians), a SNP responsible for another non-synonymous substitution (p.R141L) in *LOXL1* but was not directly genotyped in our dataset. However, we were able to successfully impute rs1048661 in our GWAS discovery dataset and we confirmed strong association between it and XFS ($OR_{T\text{-allele}} = 8.13$, $P = 1.32 \times 10^{-126}$). SNP rs1048661 has been previously reported to show strong association with XFS in multiple populations, although the risk allele is reversed depending on which ethnic group is being studied[11,22]. This SNP is also in LD with several other *LOXL1* SNPs in potential transcription factor binding sites (Supplementary Table 6)[26,27].

Both rs4886776 and rs3825942 are in moderate pair-wise linkage disequilibrium ($r^2 = 0.23$). When we genotyped rs4886776 through the 2,628 XFS cases and 8,947 controls from Stage 1 validation (Supplementary Table 1), we noted very strong evidence of consistent association in the Japanese ($OR_{A\text{-allele}} = 21.7$, $P = 1.54 \times 10^{-135}$), leading to an overwhelmingly significant association in the Japanese cases and controls analyzed ($OR_{A\text{-allele}} = 9.87$, $P = 2.13 \times 10^{-217}$). Strikingly in non-Japanese, the direction of the association was opposite to that seen in the Japanese ($OR_{A\text{-allele}} = 0.49$, $P = 2.35 \times 10^{-31}$) (Supplementary Figure 5). Such a scenario echoes recently reported observations for the reversed effect of rs3825942 on XFS risk in South Africans, and suggests that the genetic mechanism whereby *LOXL1* exerts its effect on individual susceptibility to XFS is complex[22]. We failed to detect any evidence of statistically significant interaction between *CACNA1A* rs4926244 and the sentinel *LOXL1* polymorphisms, suggesting that both loci impact XFS risk via distinct biological pathways.

CACNA1A encodes for the alpha 1A subunit of the type P/Q voltage-dependant calcium channel. Calcium channels are responsible for the transport of calcium ions across cell membranes and play a key role in a cell's ability to generate and transmit electrical signals. Previous electron microscopy studies on human XFS eyes showed the presence of high calcium concentration in direct association with aggregating XFS fibrils[28]. In addition it is well known that fibrillin utilizes calcium to form stable aggregates[29]. Thus, it can be hypothesized that altered function of a calcium channel could lead to alterations of calcium concentrations that may facilitate the formation of XFS aggregates.

As there is a paucity of information on *CACNA1A* expression in the eye, we examined the mRNA expression profile and protein expression of *CACNA1A* from a variety of human ocular tissues and cell lines respectively (Supplementary Figure 6). *CACNA1A* mRNA expression was detected in all of the ocular tissues we studied with the exception of the optic nerve head (Supplementary Figure 6, panel A). Expression of different CACNA1A isoforms appear to be higher in human ocular tissue-derived cells than in cells of non-ocular origin (Supplementary Figure 6, panel B). Immunofluorescence and immunohistochemistry analysis was also performed on adult human eyes which showed positive immunoreactivity for CACNA1A in multiple human ocular tissues (Figure 3, Supplementary Figure 7 & 8). The distribution of CACNA1A was similar in human ocular tissues of individuals with or without XFS (Figure 3, Supplementary Figures 8 & 9). Positive staining and localization of

CACNA1A in the human eye was further corroborated by immunofluorescence microscopy analysis in mouse eyes. (Supplementary Figure 10). In the human eyes, we observed positive CACNA1A immunoreactivity in the ciliary body and iris (Figure 3). Positive staining of CACNA1A was also seen in the anterior lens epithelium but not in the acellular capsule and the cornea (Supplementary Figure 7 & 9). The optic nerve glia and vascular endothelial cells also showed positive immunoreactivity with CACNA1A (Supplementary Figure 9). In the retina, strong diffuse CACNA1A staining was seen in the photoreceptor inner segments (IS), inner nuclear layer (INL) and outer nuclear layer (ONL) and nerve fibre layer (NFL) of non XFS globes in comparison to the XFS globes where focal and patchy immunostaining of the IS, ONL, INL and NFL was observed. Light microscopy comparison of the irides in XFS eyes against non-XFS eyes showed typical XFS findings of exfoliated material on the posterior iris and atrophic iris pigment epithelium, as well as the possible atrophy of the iris dilator muscle in XFS eyes (Figure 3). Double immunofluorescence microscopy for CACNA1A and LOXL1 was also performed in human eyes with XFS and without XFS and showed co-localisation of CACNA1A and LOXL1 only in the epithelium of the ciliary processes. The exfoliated material in XFS eyes showed LOXL1 positive staining with negligible CACNA1A immunoreactivity. The ciliary body and iris smooth musculature had CACNA1A positive immunostaining but were negatively stained for LOXL1 in both XFS and non-XFS eyes (Figure 3). This observation raises the possibility that CACNA1A and LOXL1 contribute to XFS pathology through different mechanisms at different ocular sites.

In summary, we have identified a susceptibility locus mapping to *CACNA1A* using a three-staged GWAS study design. Further investigation of this locus is now warranted to uncover the mechanisms via which CACNA1A affects individual susceptibility to XFS.

Online Methods

Patient recruitment

Detailed information on all XFS sample collections can be found in Supplementary note. All patients and controls were enrolled into the study following informed consent and ethical approval from the relevant national and regional institutional review boards for each sample collection. DNA was extracted from patient blood samples using standard, well-described laboratory procedures for genetic analysis.

Genotyping

For the GWAS discovery stage, genome-wide genotyping was performed using the Illumina OmniExpress beadchips, following manufacturer's instructions (see URLs). For validation (Stage 1), genotyping was performed using the Sequenom MassArray platform (see URLs). For replication (Stage 2), genotyping was performed using Applied Biosystems Taqman probes (see URLs) for India, Germany, Italy, China, Iran, Poland, and Argentina. The Australian replication collection had GWAS genotyping on all cases and controls using Illumina genome-wide arrays, and *CACNA1A* rs4926244 was directly genotyped from the GWAS arrays. We perform cross-platform concordance checks and verify >99.9% concordance of genotypes for SNP markers of interest reported here (e.g. rs4926244).

Statistical analysis

Stringent quality control filters were used to remove poorly performing samples and SNP markers in both the GWAS discovery and validation phases. The SNPs with call rates of less than 95%, minor allele frequency of less than 1 percent, or showing significant deviation from Hardy-Weinberg Equilibrium (*P*-value for deviation $< 1 \times 10^{-6}$) were removed from further statistical analysis. Likewise, samples with an overall genotyping success rate of less than 95% were removed from further analysis. The remaining samples were then subjected to biological relationship verification by using the principle of variability in allele sharing. Identity-by-state information was derived using PLINK (see URLs). For those pairs of individuals who showed evidence of cryptic relatedness (possibly either due to duplicated or biologically related samples), we removed the sample with the lower call rate before performing principal component (PC) analysis. PC analysis was undertaken to account for spurious associations resulting from ancestral differences of individual SNPs and PC plots were performed using the R statistical program package (see URLs). For the GWAS discovery stage, all XFS cases had genetically matched controls as visualized spatially on PC analysis (Supplementary Figures 11a and 11b). A total of 581,023 autosomal SNPs passed quality filters for call rate and minor allele frequency (see **Methods**) and were included for further analysis. Genotypes were contrasted between XFS cases and controls using logistic regression, with adjustments for the top 6 principal components of genetic ancestry to further minimize confounding due to cryptic population stratification. We did not observe any evidence of genomic inflation ($\lambda gc = 1$; Supplementary Figure 12), suggesting that the association results were not confounded by external artefacts such as genetic mismatch between cases and controls. Crucially, we did not observe any deviation or dispersion of test statistics when patients with XFS without glaucoma were compared to patients with exfoliation glaucoma (Supplementary Figure 13). This suggests that our primary analysis approach in combining all XFS patients into an overall case group is valid.

For the GWAS discovery, validation, and replication stages, analysis of association with XFS disease status was carried out using allele-based score tests (1 degree of freedom), which models additive effects of the minor allele on disease risk. For the GWAS discovery stage, we incorporated the top six principal components of genetic stratification into the logistic regression model while performing the analysis for association to minimize the effect of residual population stratification. As the follow up validation (Stage 1) and replication (Stage 2) phases only tested a limited number of genetic markers, we were unable to adjust for population stratification in these follow up sample collections. However, association tests were performed by site to minimize population stratification and then subsequently combined in meta-analysis as described below. All *P*-values reported here are two-tailed.

Meta-analysis was conducted using inverse variance weights for each sample collection, which calculates an overall Z-statistic, its corresponding *P*-value, and accompanying odds ratios for each SNP analyzed. The meta-analysis is performed under the fixed effects model[30]. Analysis of linkage disequilibrium was performed using the R software package (version 2.9.0) and associated rmeta and RColorBrewer analytical packages.

Genotype Imputation

Fine-scale imputation at *CACNA1A* was performed using all 1,484 XFS cases and 1,188 controls passing the standard GWAS QC checks. The imputation and phasing of genotypes were carried out using IMPUTE2 (see URLs) with cosmopolitan population haplotypes based on data from 2535 individuals from 26 distinct populations around the world obtained from the 1000 Genomes project Phase 3 (Jun 2014) release for reference panel construction. Imputed genotypes were called with an impute probability threshold of 0.90 with all other genotypes classified as missing. Additional quality control filters were applied to remove SNPs with a call rate of < 99% should the SNP have a minor allele frequency (MAF) below 5% in either cases or controls. For common SNPS with MAF above 5%, the filtering criteria were set at less than 95% call rate.

Power calculations

All statistical power calculations were performed as previously described[31]. We present these power calculations for each of the following conditions; a) GWAS discovery stage only, b) GWAS discovery plus stage 1 validation, and c) GWAS discovery plus stage 1 validation plus stage 2 replication (Supplementary Table 9).

Expression analysis

RT-PCR in human ocular tissues: Multiple transcript variants encoding different isoforms have been found for *CACNA1A*. Here we assessed for the presence of either of the two major transcripts known for *CACNA1A*, which encode 2506 and 2261 amino acid isoforms, $Ca_V2.1$ variant-1 and 2 ($Ca_V2.1$_V2 and $Ca_V2.1$_V1, NCBI Reference Sequences: NM_001127222.1/NP_001120694.1 and NM_001127221.1/NP_001120693.1). All of the known critical regulatory elements of the $Ca_V2.1$ C-terminal tail are included in both variants, but the polyQ domain is excluded from the short-tail $Ca_V2.1$_V1 isoform[32]. We utilized 5 pairs of primers spread across and common to both transcripts to assess the presence of either transcript in eye tissues (Supplementary Table 10) *CACNA1A* transcript expression was assessed by semi quantitative reverse transcription PCR (RT-PCR) using the above mentioned *CACNA1A* specific primers on total RNA extracted from a variety of ocular tissues (anterior sclera, cornea, iris, trabecular meshwork, lens capsule, retina, choroid, optic nerve head and optic nerve) with TRIzol® Reagent (Invitrogen, Carlsbad, California) in accordance with the manufacturer's protocol. First-strand cDNA synthesis was performed with SuperScript First-Strand Synthesis System for RT-PCR (Invitrogen, Carlsbad, California). Semi quantitative RT-PCR was performed according to manufacturer's protocol, with the SYBR® Green Master Mix (Invitrogen, Carlsbad, California) using the above *CACNA1A* primers. RT-PCR products were separated on a 2% agarose gel and visualized by ethidium bromide staining. The ubiquitously expressed beta-actin *(ACTB)* gene was amplified using specific primers (Supplementary Table 10) and used as amplification and normalizing control.

Western Blotting

Cell lines obtained from American Type Culture Collection (Manassas, VA, USA) were the human retinal pigment epithelial cell line (APRE19), human cervical adenocarcinoma cell

line (Hela S), human breast adenocarcinoma cell line (MCF7), and human embryonic kidney epithelial cell line (HEK 293). Human nonpigmented ciliary epithelial cell line (NPCE) is a kind gift from Prof. Miguel Coca-Prados from Yale School of Medicine. Human Trabecular Meshwork cell line (HTM) was purchased from PromoCell GmbH (Heidelberg, Germany). Cell lysates were obtained by lysing individual cell lines with lysis buffer (50 mM Tris-HCl, pH 8, 150 mM NaCl, 1.0% Nonidet P-40, 0.5% deoxycholate, 0.1% SDS, 0.2 mM $NaVO_4$, 10 mM NaF, 0.4 mM EDTA, and 10% glycerol). SDS-PAGE resolved proteins were transferred to Hybond-C Extra nitrocellulose membranes (Amersham Life Science Inc., Arlington Heights, IL, USA). Membranes were blocked by 5% nonfat milk, 0.1% Tween 20 in Tris-buffered saline (20 mM Tris-HCl, pH 7.6, 150 mM NaCl) for 1 h before incubation with CACNA1A (1:1000) from Abcam Inc. (Cambridge, MA, USA), Actin-horseradish peroxidase (HRP) (1:50000) from Santa Cruz Biotechnology (Dallas, TX, USA). Blocking and blotting of antibodies were performed in 10% horse serum (Sigma-Aldrich Corp., St. Louis, MO, USA), 0.1% Tween 20 in phosphate-buffered saline for 1 h. The bound primary antibodies were detected by horseradish peroxidase-conjugated secondary antibodies (GE Healthcare Biosciences, Pittsburgh, PA, USA), and visualized by Luminata Forte Western HRP substrate (Millipore, Bedford, MA, USA).

Immunofluorescence Confocal Microscopy

Immunofluorescence confocal microscopy was performed on antigen retrieved 4μm paraffin sections. Blocking of tissue sections was performed with blocking buffer (10% FBS, 0.1% PBS-Tween; 1x pen/strep) for 1 hour at RT. CACNA1A (Abcam Inc., Catalog[#]: Ab81011 from Abcam) and LOXL1 (ABNOVA, Catalog [#] : H00004016-B01P from Abnova) antibodies were diluted at 1:300 ratio with blocking buffer and incubated overnight at 4°C. Secondary FITC (1:300) or Cy3 (1:300) labeled anti-mouse or anti-rabbit antibodies (Jackson Laboratories, Westgrove, PA, USA) were also diluted in blocking buffer and incubated at RT for 1 hour followed by application of Vectashield with 4′,6-diamidino-2-phenyl-indole (DAPI) (Vector Laboratories, Burlingame, CA, USA). Cover-slips were then used to overlay the sections and stored in the dark at 4°C until viewing with Olympus Fluoview 1000 confocal microscope (Olympus Optical Co. Ltd., Tokyo, Japan).

Immunohistochemistry

A total of 7 archival enucleated globes were retrieved for IHC analysis with CACNA1A (1:50) (Abcam Inc., Cambridge, MA, USA) and LOXL1 (1:50) (ABNOVA, Taipei, Taiwan) antibodies. Three human eye globes from Saudi Arabia and 1 from Denmark with a history of advanced XFS were obtained courtesy of Deepak Edward (KKESH, Riyadh Saudi Arabia) and Steffen Heegaard (University of Copenhagen, Denmark) respectively. Three additional eyes from Singapore (SGH-SNEC Ophthalmic pathology service, SGH Pathology) that were exenterated for other external pathological diagnoses that did not involve the globe were used as non-XFS controls. Immunohistochemistry (IHC) analysis was performed according to our previously published protocol[33]. In brief, paraffin sections were cut at 4μm and placed on coated slides. Immunohistochemistry was performed using the Leica Bond Polymer Refine detection kit DS9800 (Leica Microsystems GmbH, Wetzlar,

[#]Members of consortia and study groups are listed in the Supplementary Note.

Germany). Slides were heated for 20 minutes at 60°C and then loaded onto the Leica Bond III autostainer for immunohistochemical staining. Staining on the autostainer consisted of dewaxing, antigen retrieval using Leica Bond ER2 solution for 20mins at 100°C, antibody incubation for 20minutes at room temperature followed by staining using the Bond polymer refine kit. Polymeric alkaline phosphatase-AP linker antibody conjugate system (Vision Biosystems, Norwell, MA, USA) and counterstaining with haematoxylin were applied for visualization, after which the slides were dehydrated and cover-slipped.

Immunofluorescence confocal microscopy in mice

C57BL/6J and B6(Cg)-Tyrc-2J/J mice were obtained from The Jackson Laboratory production facility. Mice were housed with a 14-hour-light/10-hour-dark cycle, under the same conditions as previously described[34]. All experiments were performed in compliance with the ARVO statement for use of animals in ophthalmic and vision research and approved by The Jackson Laboratory Animal Care and Use Committee. Adult mice were deeply anesthetized and perfused with 1X phosphate buffered saline (PBS) and eyes were enucleated. Fresh tissue was frozen in optimal cutting temperature (OCT) compound frozen by liquid nitrogen cooled isopentane and stored at −80°C or eyes were fixed overnight in 4% paraformaldehyde. Fixed eyes were cyroprotected in 30% sucrose, rinsed in 1X PBS and frozen in OCT for sectioning. Eyes were cut into 12 μm sections. Primary antibodies used to stain sections included anti-CACNA1A (1:500, Millipore, Billerica, MA, USA), anti-Endomucin (EMCN; 1:500; eBioscience, San Diego, CA, USA), and anti-smooth muscle Actin (ACTA2; 1:500; Abcam, Cambridge, MA, USA). Alexafluor secondary antibodies from Invitrogen were used to label by immunofluorescence. Sections were desiccated, washed in 1X PBS with 0.5% Triton and incubated with primary antibodies overnight. Sections were subsequently washed in 1X PBS and incubated with secondary antibodies for 60 minutes. DAPI was used to stain nuclei. For each experiment, at least four sections from four eyes were assessed. Microscopy was performed on the Axio Imager (Zeiss).

Supplementary Material

Refer to Web version on PubMed Central for supplementary material.

Authors

Tin Aung[1,2,3,*], Mineo Ozaki[*,4,34], Takanori Mizoguchi[*,5], R Rand Allingham[6,*], Zheng Li[7], Aravind Haripriya[8], Satoko Nakano[9], Steffen Uebe[10], Jeffrey M. Harder[11], Anita S.Y. Chan[1,2], Mei Chin Lee[1], Kathryn P. Burdon[12,13], Yury S. Astakhov[14], Khaled K. Abu-Amero[15,16], Juan C. Zenteno[17,18], Yildirim Nilgün[19], Tomasz Zarnowski[20], Mohammad Pakravan[21], Leen Abu Safieh[22], Liyun Jia[23], Ya Xing Wang[24], Susan Williams[25], Daniela Paoli[26], Patricio G Schlottmann[27], Lulin Huang[28,29,30], Kar Seng Sim[7], Jia Nee Foo[7], Masakazu Nakano[31], Yoko Ikeda[32], Rajesh S Kumar[33], Morio Ueno[32], Shin-ichi Manabe[34], Ken Hayashi[34], Shigeyasu Kazama[35], Ryuichi Ideta[36], Yosai Mori[37], Kazunori Miyata[37,38], Kazuhisa Sugiyama[39], Tomomi Higashide[39], Etsuo Chihara[40], Kenji Inoue[41], Satoshi Ishiko[42], Akitoshi Yoshida[43], Masahide Yanagi[44], Yoshiaki Kiuchi[44], Makoto Aihara[45], Tsutomu Ohashi[46], Toshiya Sakurai[47], Takako Sugimoto[38], Hideki

Chuman[38], Fumihiko Matsuda[48], Kenji Yamashiro[49], Norimoto Gotoh[49], Masahiro Miyake[48,49], Sergei Y. Astakhov[14], Essam A. Osman[15], Saleh A. Al-Obeidan[15], Ohoud Owaidhah[21], Leyla Al-Jasim[21], Sami Al Shahwan[21], Rhys A. Fogarty[12], Paul Leo[50], Yaz Yetkin[19], Çilingir Oğuz[19], Mozhgan Rezaei Kanavi[21], Afsaneh Naderi Beni[21], Shahin Yazdani[21], Evgeny L. Akopov[14], Kai-Yee Toh[7], Gareth R Howell[11], Andrew C. Orr[51], Yufen Goh[7], Wee Yang Meah[7], Su Qin Peh[7], Ewa Kosior-Jarecka[20], Urszula Lukasik[20], Mandy Krumbiegel[10], Eranga N Vithana[1], Tien Yin Wong[1,2,3], Yutao Liu[52,53], Allison E. Ashley Koch[52], Pratap Challa[6], Robyn M Rautenbach[54], David A. Mackey[55], Alex W Hewitt[13,56], Paul Mitchell[57], Jie Jin Wang[57], Ari Ziskind[54], Trevor Carmichael[25], Rangappa Ramakrishnan[8], Kalpana Narendran[8], Rangaraj Venkatesh[8], Saravanan Vijayan[58], Peiquan Zhao[59], Xueyi Chen[60], Dalia Guadarrama-Vallejo[17,18], Ching Yu Cheng[1,3], Shamira A Perera[1,2], Rahat Husain[1,2], Su-Ling Ho[61], Ulrich-Christoph Welge-Luessen[62], Christian Mardin[62], Ursula Schloetzer-Schrehardt[62], Axel M. Hillmer[63], Stefan Herms[64,65,66,67], Susanne Moebus[68], Markus M. Nöthen[64,65], Nicole Weisschuh[69], Rohit Shetty[33], Arkasubhra Ghosh[1,70], Yik Ying Teo[7,71], Matthew A Brown[50], Ignacio Lischinsky[72], The Blue Mountains Eye Study GWAS team[73], Wellcome Trust Case Control Consortium[2,73], Jonathan G Crowston[56,74], Michael Coote[56,74], Bowen Zhao[22], Jinghong Sang[23], Nihong Zhang[23], Qisheng You[24], Vera Vysochinskaya[75], Panayiota Founti[76], Anthoula Chatzikyriakidou[77], Alexandros Lambropoulos[77], Eleftherios Anastasopoulos[76], Anne L Coleman[78], M Roy Wilson[79], Douglas J Rhee[80], Jae Hee Kang[81], Inna May-Bolchakova[82], Steffen Heegaard[83,84], Kazuhiko Mori[32], Wallace L.M. Alward[85,86], Jost B Jonas[87], Liang Xu[24], Jeffrey M Liebmann[88], Balram Chowbay[89], Elke Schaeffeler[90], Matthias Schwab[90,91,92], Fabian Lerner[93], Ningli Wang[23], Zhenglin Yang[28,29,30], Paolo Frezzotti[94], Shigeru Kinoshita[32], John H. Fingert[85,86], Masaru Inatani[95], Kei Tashiro[31], André Reis[10], Deepak P. Edward[22,96], Louis R. Pasquale[80,81], Toshiaki Kubota[9], Janey L. Wiggs[80,**], Francesca Pasutto[10,**], Fotis Topouzis[76,**], Michael Dubina[14,75,**], Jamie E. Craig[12,**], Nagahisa Yoshimura[49,**], Periasamy Sundaresan[58,**], Simon W.M. John[11,**], Robert Ritch[97,**], Michael A Hauser[6,52,**], and Chiea-Chuen Khor[3,7,**]

Affiliations

[1]Singapore Eye Research Institute, 11 Third Hospital Avenue, Singapore 168751 [2]Singapore National Eye Center, 11 Third Hospital Avenue, Singapore 168751 [3]Department of Ophthalmology, Yong Loo Lin School of Medicine, National University of Singapore [4]Ozaki Eye Hospital, 1-15, Kamezaki, Hyuga, Miyazaki 883-0066 Japan [5]Mizoguchi Eye Hospital, 6-13 Tawara-machi, Sasebo, Nagasaki, Japan 857-0016 [6]Department of Ophthalmology, Duke University Eye Center, Durham, NC [7]Division of Human Genetics, Genome Institute of Singapore [8]Intraocular Lens and Cataract Clinic, Aravind Eye Hospital, Madurai, India [9]Department of Ophthalmology, Oita University Faculty of Medicine [10]Institute of Human Genetics, Friedrich-Alexander-Universität Erlangen-Nürnberg, Germany [11]The Howard Hughes Medical Institute, the Jackson Laboratory 600 Main Street, Bar Harbor, ME 04609 [12]Department of Ophthalmology, Flinders University,

Adelaide, SA, Australia [13]Menzies Institute for Medical Research, University of Tasmania [14]Department of Ophthalmology, First Pavlov State Medical University of St. Petersburg, 6/8 L'va Tolstogo Street, 197022 St. Petersburg, Russia [15]Department of Ophthalmology, College of Medicine, King Saud University, Riyadh, Saudi Arabia [16]Department of Ophthalmology, College of Medicine, University of Florida, Jacksonville, FL, USA [17]Genetics Department, Institute of Ophthalmology "Conde de Valenciana", Mexico [18]Biochemistry Department, Faculty of Medicine, UNAM, Mexico City, Mexico [19]Department of Ophthalmology, Eskisehir Osmangazi University, Meselik, Eskisehir, Turkey [20]Department of Diagnostics and Microsurgery of Glaucoma, Medical University, Lublin, Poland, Chmielna 1, 20-079 Lublin, Poland [21]Ophthalmic Research Center, Ophthalmology department, Labbafinejad Medical Center, Shahid Beheshti University of Medical Sciences, Tehran, Iran [22]King Khaled Eye Specialist Hospital, Riyadh, Kingdom of Saudi Arabia [23]Beijing Ophthalmology & Visual Sciences Key Laboratory, Beijing Tongren Eye Centre, Beijing Tongren Hospital, Capital Medical University, Beijing, China [24]Beijing Institute of Ophthalmology, Beijing Tongren Hospital, Capital University of Medical Science, Beijing, China [25]Division of Ophthalmology, Department of Neurosciences, University of the Witwatersrand, Johannesburg, South Africa [26]Department of Ophthalmology, Monfalcone Hospital, Gorizia, Italy [27]Organización Médica de Investigación, Uruguay 725 – PB, Buenos Aires (C1015ABO) Argentina [28]Sichuan Provincial Key Laboratory for Human Disease Gene Study, Hospital of the University of Electronic Science and Technology of China and Sichuan Provincial People's Hospital, Chengdu, China [29]School of Medicine, University of Electronic Science and Technology of China, Chengdu, China [30]Sichuan Translational Medicine Hospital, Chinese Academy of Sciences, Chengdu, China [31]Department of Genomic Medical Sciences, Kyoto Prefectural University of Medicine, Kyoto, Japan [32]Department of Ophthalmology, Kyoto Prefectural University of Medicine, Kyoto, Japan [33]Glaucoma services, Narayana Nethralaya Eye Hospital, 121/C, Chord Road, Rajajinagar, 1st R Block, Bangalore 560 010, India [34]Hayashi Eye Hospital, 4-23-35, Hakataekimae, Hakata-ku, Fukuoka, Japan [35]Shinjo Eye Clinic, 889-1,Mego, Simokitakatamachi, Miyazaki-shi, Miyazaki 880-0035,Japan [36]Ideta Eye Hospital, Kumamoto, Japan [37]Miyata Eye Hospital, 6-3, Kurahara, Miyakonojo, Miyazaki 885-0051 Japan [38]Department of Ophthalmology, Faculty of Medicine, University of Miyazaki, Miyazaki, Japan [39]Department of Ophthalmology and Visual Science, Kanazawa University Graduate School of Medical Science, Kanazawa University, 13-1 Takara-machi, Kanazawa, 920-8641, Japan [40]Sensho-kai Eye Institute, Minamiyama 50-1, Iseda, Uji, Kyoto 611-0043, Japan [41]Inouye Eye Hospital, Tokyo, Japan [42]Department of Medicine and Engineering Combined Research Institute, Asahikawa Medical University, Asahikawa, Japan [43]Department of Ophthalmology, Asahikawa Medical University, Asahikawa, Japan [44]Department of Ophthalmology and Visual Science, Hiroshima University, Hiroshima, Japan [45]Yotsuya Shirato Eye Clinic, Tokyo, Japan [46]Ohashi eye center, Kita1-1 Hondori6 Shiroishi-ku Sapporo 003-0027 Japan [47]Tane Memorial Eye Hospital, Osaka [48]Center for Genomic Medicine/Inserm U.

852, Kyoto University Graduate School of Medicine, Kyoto, Japan [49]Department of Ophthalmology and Visual Sciences, Kyoto University Graduate School of Medicine, Kyoto, Japan [50]University of Queensland Diamantina Institute, Translational Research Institute, Princess Alexandra Hospital, Brisbane, Qld, Australia [51]Department of Ophthalmology and Visual Sciences, Dalhousie University, Halifax, Canada [52]Department of Medicine, Duke University Medical Center, Durham, North Carolina [53]Department of Cellular Biology and Anatomy, Georgia Regents University, Augusta, Georgia [54]Division of Ophthalmology, Faculty of Medicine and Health Sciences, University of Stellenbosch, Cape Town, South Africa [55]Centre for Ophthalmology and Visual Science, Lions Eye Institute, University of Western Australia, Perth, Australia [56]Centre for Eye Research Australia (CERA), University of Melbourne, Royal Victorian Eye and Ear Hospital, Melbourne, Victoria, Australia [57]Centre for Vision Research, Department of Ophthalmology and Westmead Millennium Institute, University of Sydney, NSW Australia [58]Department of Genetics, Aravind Medical Research Foundation, Madurai, India [59]Department of Ophthalmology, Xin Hua Hospital affiliated to Shanghai Jiao Tong University, School of Medicine, No. 1665, Kongjiang Road, Shanghai 200092, China [60]Department of Ophthalmology, the First Affiliated Hospital of Xinjiang Medical University, Urumchi 830054, Xinjiang Uygur Autonomous Region, China [61]National Healthcare Group Eye Institute, Tan Tock Seng Hospital, Singapore [62]Department of Ophthalmology, Friedrich-Alexander-Universität Erlangen-Nürnberg, Germany [63]Cancer Therapeutics and Stratified Oncology, Genome Institute of Singapore [64]Institute of Human Genetics, University of Bonn, Bonn, Germany [65]Department of Genomics, Life & Brain Center, University of Bonn, Bonn, Germany [66]Division of Medical Genetics, University Hospital, Basel, Switzerland [67]Human Genetics Research Group, Department of Biomedicine, University of Basel, Basel, Switzerland [68]Institute for Medical Informatics, Biometry and Epidemiology, University Hospital of Essen, University Duisburg-Essen, Essen, Germany [69]University Eye Hospital, Wuerzburg, Germany [70]Genes, Repair and Regeneration in Ophthalmic Workstation Research Lab, Narayana Nethralaya Foundation, Bangalore, India [71]Saw Swee Hock School of Public Health, National University of Singapore, Singapore [72]Centro Oftalmologico Lischinsky, Junin 692, Tucuman (4000) – Argentina [74]Department of Ophthalmology, University of Melbourne [75]St. Petersburg Academic University, 8/3 Klopina Street, 194021 St. Petersburg, Russia [76]Department of Ophthalmology, Faculty of Medicine, Aristotle University of Thessaloniki, AHEPA Hospital, Thessaloniki, Greece [77]Department of Biology and Genetics, Faculty of Medicine, Aristotle University of Thessaloniki, Greece [78]Center for Community Outreach and Policy, Stein Eye Institute, David Geffen School of Medicine at UCLA, Los Angeles, CA 90095 United States [79]Wayne State University, Detroit, 48202, United States [80]Department of Ophthalmology, Harvard Medical School, Massachusetts Eye and Ear Infirmary, Boston, Massachusetts, United States of America [81]Channing Division of Network Medicine, Brigham and Women's Hospital, Boston, Massachusetts, United States of America [82]Ophthalmology Department, Military Hospital Begin, Paris, France [83]Eye

Pathology Institute, Department of Neuroscience and Pharmacology, University of Copenhagen, Copenhagen, Denmark [84]Department of Ophthalmology, Glostrup University Hospital, Glostrup, Denmark [85]Stephen A. Wynn Institute for Vision Research, University of Iowa, USA [86]Department of Ophthalmology and Visual Sciences, Carver College of Medicine, University of Iowa, Iowa City [87]Department of Ophthalmology, Medical Faculty Mannheim of the Ruprecht-Karls-University Heidelberg, Germany [88]New York University School of Medicine; Manhattan Eye, Ear and Throat Hospital, New York [89]Division of Medical Sciences, Humphrey Oei Institute of Cancer Research, National Cancer Centre of Singapore [90]Dr. Margarete Fischer-Bosch-Institute of Clinical Pharmacology, Stuttgart, and University Tuebingen, Germany [91]Department of Clinical Pharmacology, University Hospital, Tuebingen, Germany [92]German Cancer Consortium (DKTK), German Cancer Research Center, Heidelberg, Germany [93]Fundacion para el Estudio del Glaucoma, Marcelo T de Alvear 2010 - 2A Buenos Aires (C1122AAF) Argentina [94]Department of Surgery, Section of Ophthalmology, University of Siena, Siena, Italy [95]Department of Ophthalmology, Faculty of Medical Science, University of Fukui, 23-3 Shimoaizuki, Matsuoka, Eiheiji, Yoshida, Fukui, 910-1193, Japan [96]Wilmer Eye Institute, Johns Hopkins University School of Medicine, Baltimore, Maryland, United States of America [97]Einhorn Clinical Research Center, New York Eye and Ear Infirmary of Mount Sinai, New York, NY, United States of America

Acknowledgments

The authors thank the staff and participants of all studies for their important contributions. We thank Khai-Koon Heng, Xiao-Yin Chen, Hui-Meng Soo, Shi-Qi Mok, Andrea Jamuth, Nicole Foxworth and Monika Elbl for technical assistance. This research was funded by the Biomedical Research Council, Agency for Science, Technology and Research, Singapore. J.L.W. acknowledges support from the National Institutes of Health/National Eye Institute grants (NIH/NEI R01 EY020928 and NIH/NEI P30 EY014104). SWMJ acknowledges support from EY11721 and is an Investigator of the Howard Hughes Medical Institute. L.R.P. acknowledges support from a Harvard Medical School Distinguished Ophthalmology Scholar Award and the Harvard Glaucoma Center of Excellence. J.H.F. acknowledges support from the National Institutes of Health/National Eye Institute grants (EY023512 and EY018825). Zhenglin Yang acknowledges support from the National Natural Science Foundation of China (81025006, and 81170883), as well as from the Department of Science and Technology of Sichuan Province, China (2012SZ0219 (Z.Y.) and 2011jtd0020 (Z.Y.). M. Schwab acknowledges support from the Robert Bosch Stiftung, Stuttgart, Germany and The German Cancer Consortium (DKTK), Germany. The Australian case cohort was funded by grants from the Ophthalmic Research Institute of Australia and the National Health and Medical Research Council (NHMRC) project #535044. The Thessaloniki Eye Study was co-funded by the European Union (European Social Fund) and Greek national funds under the Act “Aristia” of the Operational Program “Education and Lifelong Learning” (see Supplementary Note). The Blue Mountains Eye Study (BMES) GWAS and genotyping costs was supported by Australian NHMRC, Canberra Australia (NHMRC project grant IDs 512423, 475604 and 529912), and the Wellcome Trust, UK as part of Wellcome Trust Case Control Consortium 2 (A Viswanathan, P McGuffin, P Mitchell, F Topouzis, P Foster, grant IDs 085475/B/08/Z and 085475/08/Z). K.P.B. is an NHMRC Senior Research Fellow and J.E.C. is an NHMRC Practitioner Fellow. M.A.B. is a NHMRC Principal Research Fellow. A.W.H. is a NHMRC Peter Doherty Fellow.

References for main text

1. Schlotzer-Schrehardt U, Naumann GO. Ocular and systemic pseudoexfoliation syndrome. Am J Ophthalmol. 2006; 141:921–937. [PubMed: 16678509]
2. Ritch R, Schlotzer-Schrehardt U. Exfoliation syndrome. Surv Ophthalmol. 2001; 45:265–315. [PubMed: 11166342]

3. Thorleifsson G, et al. Common sequence variants in the LOXL1 gene confer susceptibility to exfoliation glaucoma. Science. 2007; 317:1397–400. [PubMed: 17690259]
4. Chen H, et al. Ethnicity-based subgroup meta-analysis of the association of LOXL1 polymorphisms with glaucoma. Mol Vis. 2010; 16:167–77. [PubMed: 20142848]
5. Fingert JH, et al. LOXL1 mutations are associated with exfoliation syndrome in patients from the midwestern United States. Am J Ophthalmol. 2007; 144:974–975. [PubMed: 18036875]
6. Hayashi H, Gotoh N, Ueda Y, Nakanishi H, Yoshimura N. Lysyl oxidase-like 1 polymorphisms and exfoliation syndrome in the Japanese population. Am J Ophthalmol. 2008; 145:582–585. [PubMed: 18201684]
7. Fan BJ, et al. DNA sequence variants in the LOXL1 gene are associated with pseudoexfoliation glaucoma in a U.S. clinic-based population with broad ethnic diversity. BMC Med Genet. 2008; 9:5. [PubMed: 18254956]
8. Yang X, et al. Genetic association of LOXL1 gene variants and exfoliation glaucoma in a Utah cohort. Cell Cycle. 2008; 7:521–4. [PubMed: 18287813]
9. Hewitt AW, et al. Ancestral LOXL1 variants are associated with pseudoexfoliation in Caucasian Australians but with markedly lower penetrance than in Nordic people. Hum Mol Genet. 2008; 17:710–6. [PubMed: 18037624]
10. Pasutto F, et al. Association of LOXL1 common sequence variants in German and Italian patients with pseudoexfoliation syndrome and pseudoexfoliation glaucoma. Invest Ophthalmol Vis Sci. 2008; 49:1459–63. [PubMed: 18385063]
11. Ozaki M, et al. Association of LOXL1 gene polymorphisms with pseudoexfoliation in the Japanese. Invest Ophthalmol Vis Sci. 2008; 49:3976–80. [PubMed: 18450598]
12. Fan BJ, et al. LOXL1 promoter haplotypes are associated with exfoliation syndrome in a U.S. Caucasian population. Invest Ophthalmol Vis Sci. 2011; 52:2372–8. [PubMed: 21212179]
13. Wolf C, et al. Lysyl oxidase-like 1 gene polymorphisms in German patients with normal tension glaucoma, pigmentary glaucoma and exfoliation glaucoma. J Glaucoma. 2010; 19:136–41. [PubMed: 19373106]
14. Lemmela S, et al. Association of LOXL1 gene with Finnish exfoliation syndrome patients. J Hum Genet. 2009; 54:289–97. [PubMed: 19343041]
15. Aragon-Martin JA, et al. Evaluation of LOXL1 gene polymorphisms in exfoliation syndrome and exfoliation glaucoma. Mol Vis. 2008; 14:533–41. [PubMed: 18385788]
16. Chen L, et al. Evaluation of LOXL1 polymorphisms in exfoliation syndrome in a Chinese population. Mol Vis. 2009; 15:2349–57. [PubMed: 19936304]
17. Mossbock G, et al. Lysyl oxidase-like protein 1 (LOXL1) gene polymorphisms and exfoliation glaucoma in a Central European population. Mol Vis. 2008; 14:857–61. [PubMed: 18483563]
18. Challa P, et al. Analysis of LOXL1 polymorphisms in a United States population with pseudoexfoliation glaucoma. Mol Vis. 2008; 14:146–9. [PubMed: 18334928]
19. Ramprasad VL, et al. Association of non-synonymous single nucleotide polymorphisms in the LOXL1 gene with pseudoexfoliation syndrome in India. Mol Vis. 2008; 14:318–22. [PubMed: 18334947]
20. Nakano M, et al. Novel common variants and susceptible haplotype for exfoliation glaucoma specific to Asian population. Sci Rep. 2014; 4:5340. [PubMed: 24938310]
21. Mori K, et al. LOXL1 genetic polymorphisms are associated with exfoliation glaucoma in the Japanese population. Mol Vis. 2008; 14:1037–40. [PubMed: 18552979]
22. Williams SE, et al. Major LOXL1 risk allele is reversed in exfoliation glaucoma in a black South African population. Mol Vis. 2010; 16:705–12. [PubMed: 20431720]
23. Krumbiegel M, et al. Genome-wide association study with DNA pooling identifies variants at CNTNAP2 associated with pseudoexfoliation syndrome. Eur J Hum Genet. 2011; 19:186–93. [PubMed: 20808326]
24. Rioux JD, et al. Genetic variation in the 5q31 cytokine gene cluster confers susceptibility to Crohn disease. Nat Genet. 2001; 29:223–8. [PubMed: 11586304]
25. Westra HJ, et al. Systematic identification of trans eQTLs as putative drivers of known disease associations. Nat Genet. 2013; 45:1238–43. [PubMed: 24013639]

26. Boyle AP, et al. Annotation of functional variation in personal genomes using RegulomeDB. Genome Res. 2012; 22:1790–7. [PubMed: 22955989]
27. Ward LD, Kellis M. HaploReg: a resource for exploring chromatin states, conservation, and regulatory motif alterations within sets of genetically linked variants. Nucleic Acids Res. 2012; 40:D930–4. [PubMed: 22064851]
28. Schlotzer-Schrehardt U, Kortje KH, Erb C. Energy-filtering transmission electron microscopy (EFTEM) in the elemental analysis of pseudoexfoliative material. Curr Eye Res. 2001; 22:154–62. [PubMed: 11402393]
29. Reinhardt DP, Ono RN, Sakai LY. Calcium stabilizes fibrillin-1 against proteolytic degradation. J Biol Chem. 1997; 272:1231–6. [PubMed: 8995426]
30. Willer CJ, Li Y, Abecasis GR. METAL: fast and efficient meta-analysis of genomewide association scans. Bioinformatics. 2010; 26:2190–1. [PubMed: 20616382]
31. Purcell S, Cherny SS, Sham PC. Genetic Power Calculator: design of linkage and association genetic mapping studies of complex traits. Bioinformatics. 2003; 19:149–50. [PubMed: 12499305]
32. Tsou WL, Soong BW, Paulson HL, Rodriguez-Lebron E. Splice isoform-specific suppression of the Cav2.1 variant underlying spinocerebellar ataxia type 6. Neurobiol Dis. 2011; 43:533–42. [PubMed: 21550405]
33. Lee MC, et al. Expression of the Primary Angle Closure Glaucoma (PACG) Susceptibility Gene PLEKHA7 in Endothelial and Epithelial Cell Junctions in the Eye. Invest Ophthalmol Vis Sci. 2014; 55:3833–41. [PubMed: 24801512]
34. Smith RS, et al. Haploinsufficiency of the transcription factors FOXC1 and FOXC2 results in aberrant ocular development. Hum Mol Genet. 2000; 9:1021–32. [PubMed: 10767326]

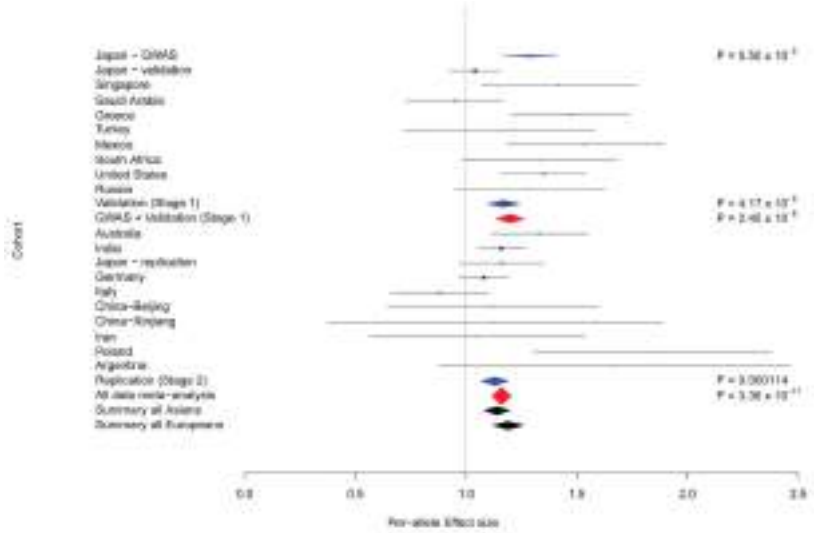

Figure 1.

Forest plot for the associations between *CACNA1A* rs4926244 and Exfoliation syndrome in discovery and follow up case-control collections. The black lines denote the 95% confidence intervals of the odds ratio for each collection. The diamonds denote summary results for the GWAS, Validation and Replication stages (blue), as well as the GWAS and Validation meta-analysis, and meta-analysis of data from all collections (red). Asian and European ethnic summaries are in black diamonds.

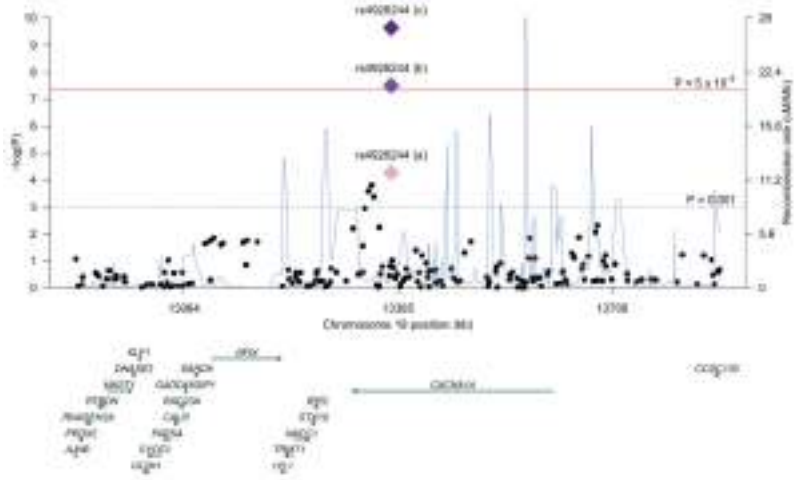

Figure 2.

Regional association and recombination rate plot for the *CACNA1A* rs4926244 locus. The left *y* axis represents –log10 *P* values for association with exfoliation syndrome and the right *y* axis represents the recombination rate. The *x* axis represents base-pair positions along the chromosome (human genome Build 37). The diamonds denote the summary of each experimental stage, a) for the GWAS discovery, b) for the meta-analysis between GWAS discovery and validation stages, and c) for the meta-analysis between GWAS discovery, validation, and replication stages.

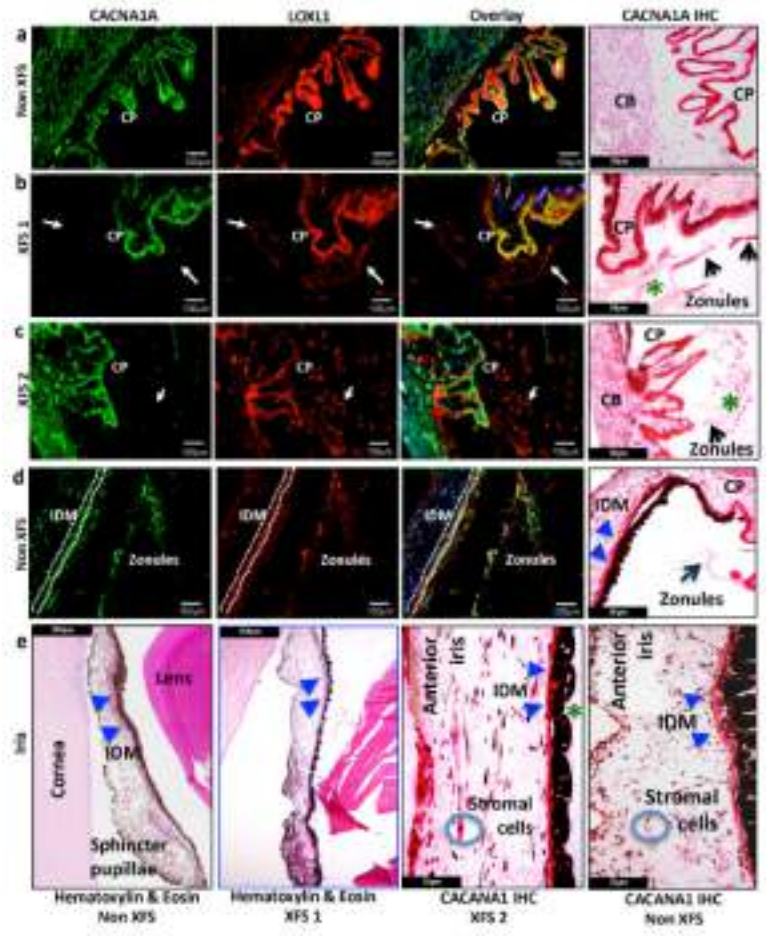

Figure 3.

CACNA1A and LOXL1 protein expression and light microscopic analysis in XFS and non-XFS control eyes. Immunolocalisation of CACNA1A in human non-XFS and XFS globes show CACNA1A positive immunoreactivity in the smooth musculature of the ciliary body (CB) and pigmented and non-pigmented ciliary process (CP) epithelium with variable staining in the zonules (Panels a to c: CACNA1A immunofluorescence (IF) panel; CACNA1A immunohistochemical (IHC) panel, 40x; zonules, white and black arrows; exfoliated material, green asterix). In contrast, LOXL1 immunoreactivity is present only in the exfoliated material and the CP epithelium, (LOXL1 IF panel; zonules, white arrows). Double immunofluorecence analysis shows colocalisation of CACNA1A and LOXL1 within the non-pigmented and pigmented epithelium of the CP but not in the CB smooth muscles or the zonules (IF overlay panel; zonules, white arrows). Light microscopy comparison of non-XFS and XFS irides show the typical XFS findings of exfoliated material (green asterix) on the posterior iris and atrophic iris pigment epithelium with possible atrophy of the iris dilator muscle (blue arrowheads) in XFS irides. The sphincter pupillae in both non-XFS and XFS shows negligible differences (H&E panels). CACNA1A positive immunoreactivity is also seen in the anterior iris border, iris stromal cells, the iris dilator (blue arrowheads, H&E and IHC panels) and sphincter muscles as well as the iris pigmented epithelium in both XFS and Non-XFS irides (Panel d & e: CACNA1A IF and CACNA1A IHC panels). Stromal cells are

highlighted by the blue circles. For CACNA1A, LOXL1, and overlay panels a) through to d), each unit on the scale bar represents 100 μm. For CACNA1A IHC panels a) to d), each unit on the scale bar represents 50 μm. For panel e) hematoxylin & eosin non-XFS as well as hematoxylin & eosin XFS1, each unit on the scale bar represents 200 μm. For panel e) CACNA1A IHC XFS2 as well as CACNA1A IHC non-XFS, each unit on the scale bar represents 25 μm.

Trinucleotide Repeat Expansion in the *TCF4* Gene in Fuchs' Endothelial Corneal Dystrophy in Japanese

Masakazu Nakano,[1] Naoki Okumura,[2,3] Hiroko Nakagawa,[3] Noriko Koizumi,[2] Yoko Ikeda,[3] Morio Ueno,[3] Kengo Yoshii,[4] Hiroko Adachi,[1] Ross A. Aleff,[5] Malinda L. Butz,[6] W. Edward Highsmith,[6] Kei Tashiro,[1] Eric D. Wieben,[5] Shigeru Kinoshita,[3] and Keith H. Baratz[7]

[1]Department of Genomic Medical Sciences, Kyoto Prefectural University of Medicine, Kyoto, Japan
[2]Department of Biomedical Engineering, Faculty of Life and Medical Sciences, Doshisha University, Kyotanabe, Japan
[3]Department of Ophthalmology, Kyoto Prefectural University of Medicine, Kyoto, Japan
[4]Department of Medical Statistics, Kyoto Prefectural University of Medicine, Kyoto, Japan
[5]Department of Biochemistry and Molecular Biology, Mayo Clinic, Rochester, Minnesota, United States
[6]Department of Laboratory Medicine and Pathology, Mayo Clinic, Rochester, Minnesota, United States
[7]Department of Ophthalmology, Mayo Clinic, Rochester, Minnesota, United States

Correspondence: Keith H. Baratz, Department of Ophthalmology, Mayo Clinic, 200 First Street, SW, Rochester, MN 55905, USA; baratz.keith@mayo.edu.

MN and NO are joint first authors.

Submitted: April 11, 2015
Accepted: May 17, 2015

Citation: Nakano M, Okumura N, Nakagawa H, et al. Trinucleotide repeat expansion in the *TCF4* gene in Fuchs' endothelial corneal dystrophy in Japanese. *Invest Ophthalmol Vis Sci*. 2015;56:4865–4869. DOI:10.1167/iovs.15-17082

Purpose. The purpose of this study was to evaluate the association between the intronic expansion of a trinucleotide repeat (TNR) in the *TCF4* gene and Fuchs' endothelial corneal dystrophy (FECD) in a Japanese population.

Methods. Forty-seven Japanese FECD patients and 96 age-matched controls were recruited. FECD patients and controls were examined by slit-lamp and noncontact specular microscopy. The repeat length was determined by direct sequencing and short tandem repeat assay of PCR-amplified DNA and Southern blotting of unamplified DNA.

Results. A TNR expansion, defined as >50 CTG repeats in the *TCF4* gene was identified in 12 of 47 FECD cases (26%) and 0 of 96 controls (0%; $P < 0.001$). Sensitivity and specificity in this study were 26% and 100%, respectively. The clinical characteristics of FECD patients with TNR expansion were not distinct from those without TNR expansion.

Conclusions. These findings show for the first time in a Japanese population the association of the TNR expansion in *TCF4* with FECD. In contrast to Caucasian cohorts in whom the TNR expansion is present in most patients with FECD, a CTG expansion is present in a minority of Japanese subjects, indicating other genetic variants as common causes of phenotypically identical disease in this population.

Keywords: corneal endothelium, Fuchs' endothelial corneal dystrophy, *TCF4*

Fuchs' endothelial corneal dystrophy (FECD) is a bilateral, inherited degenerative disease of the corneal endothelium. This nonreplicating tissue layer is essential for maintaining corneal clarity through an active ionic pump function and barrier function. Mild FECD is asymptomatic, but advanced stages result in a functional impairment of the endothelial layer with eventual corneal edema, vision loss, and pain. Corneal transplantation is the only therapeutic option for treating FECD,[1] and it is the most frequent indication for corneal transplantation, accounting for more than 60% of endothelial keratoplasty procedures performed in the United States.[2]

FECD is an autosomal dominant disease with wide variation in penetrance and expression.[3] A rare form of early onset FECD is associated with a mutation in *COL8A2*.[4,5] The common form of late-onset FECD has been linked to chromosomes 13,[6,7] 18,[8] 5,[9] and 9.[10] In addition, missense mutations in the zinc finger E-box binding homeobox 1 (*ZEB1*) gene[10,11] and the solute carrier family member 4A11 (*SLC4A11*) gene[12,13] were suggested to be causes of late-onset FECD, although those mutations were detected in a small proportion of the FECD population.

A genome-wide association study by Baratz et al.[14] identified an association between late-onset FECD and the intronic single nucleotide polymorphism rs613872 in the transcription factor 4 (*TCF4*) gene on chromosome 18, and both association and linkage analyses performed by subsequent investigators replicated this association.[15–18] Another study reported that FECD in families mapped to the FCD2 locus on chromosome 18 did not cosegregate with rs613872, suggesting that FCD2 was independent of this minor allele.[15,16] In 2012, Wieben et al.[19] revealed that the expansion of a CTG trinucleotide repeat (TNR) in a different intron of *TCF4* was commonly detected in FECD and that the sensitivity and specificity of >50 repeats identifying FECD were 79% and 96%, respectively. In addition, subsequent investigators recently replicated the TNR expansion in other FECD cohorts.[20–22]

Here we present additional evidence for the association between the intronic CTG expansion in *TCF4* with late-onset FECD in Japanese. We demonstrated that a repeat length >50 repeats was identified in 12 of 47 FECD cases (26%) and 0 of 96 controls (0%), with a sensitivity and specificity of 26% and 100%, respectively. We also showed that the clinical phenotype and severity of disease status of FECD patients with TNR expansion were not different from those without expansion, suggesting that genetic abnormalities responsible for non-

expansion-associated disease cause an indistinguishable phenotype.

Materials and Methods

Ethical Statements

This study was approved by the Institutional Review Boards of Kyoto Prefectural University of Medicine and the Mayo Clinic and was conducted in accordance with the ethical principles of the Declaration of Helsinki. Written informed consent was obtained from all FECD and normal participants.

FECD Patients and Control Subjects

Forty-seven FECD and 96 healthy Japanese subjects were recruited between September 2010 and April 2014 at the University Hospital of Kyoto Prefectural University of Medicine in order to provide peripheral blood samples. An investigator who was masked to both the blood sampling and the experiments assigned an anonymous code to each blood sample.

All participants were examined by slit-lamp biomicroscopy (Pentacam; Oculus Optikgeräte GmbH, Wetzlar, Germany) and noncontact specular microscopy (EM3000; Tomey Corporation, Nagoya, Japan; if images were obtainable). FECD cases were graded based on a scale proposed by Krachmer et al.[23] and had a minimum grade of 1, which represented 12 or more central nonconfluent guttae. Control subjects were selected based on (1) age > 60 years old, (2) absence of guttae observed by slit-lamp microscopy and noncontact specular microscopy, and (3) no other corneal disease.

Measurement of *TCF4* Triplet Repeat Length

Genomic DNA was isolated from 350 μL of peripheral blood by BioRobot EZ1 (Qiagen, Valencia, CA, USA) using the EZ1 DNA blood 350 μL mini-kit (Qiagen), according to the manufacturer's instructions. The amount and quality of each isolated DNA sample was analyzed by UV spectrophotometer (NanoDrop; NanoDrop Technologies, DE, USA) and stored at –80°C until use. In order to measure the length of the CTG repeat in the third intron of the *TCF4* gene, we first performed a short tandem repeat assay as described previously.[19] Briefly, PCR of the repeat region was performed using one fluorescent-labeled primer. Following amplification, the size of the product was determined by capillary electrophoresis (3730xl model DNA analyzer; Applied Biosystems, Grand Island, NY, USA).

For samples demonstrating a single signal from the short tandem repeat assay, we performed Southern blotting using unamplified DNA as previously described[19] to confirm whether each subject possessed either two short alleles of the same repeat length or had an additional allele with a CTG expansion too large to detect by the PCR-based short tandem repeat assay.

Statistical Analysis

In order to examine the possible confounding effects of sex and age of the subjects, we assessed the correlations between the case and control samples by means of Student's *t*-test or chi-square test (Table 1). Fisher's exact test was used for analyzing the difference in the frequency of patients and controls in the three groups divided by the length of TNR (>50, 40–50, and <40 repeats) (Table 2). We also applied the Wilcoxon rank sum test and Spearman's rank correlation coefficient to determine whether there were significant correlations between the clinical parameters and the TNR length. Results are expressed as means ± SD.

Table 1. Sample Information

Subjects	FECD Cases	Controls	*P* Value
No. of subjects	47	96	
Female-to-male ratio	1.8	1.3	>0.05*
Age, y	68.4 ± 12.7	67.2 ± 5.5	>0.05†

* *P* value of χ^2 test for case and control comparisons.
† *P* value of Student's *t* test for case and control comparisons.

Results

Clinical Manifestations of FECD in Japanese Patients

Demographics of the subjects participating in this study are shown in Table 1. No differences were observed in male-to-female ratios or subject age between the FECD and control groups. All control subjects exhibited a normal morphological corneal endothelium without guttae (Fig. 1A). In contrast, all FECD patients exhibited guttae formation associated with decreased corneal endothelial cell density. Coincident with FECD in Caucasians, guttae formation and morphological abnormalities of the endothelium were more evident in the center than in the periphery of corneas, and edema started from the center in early FECD cases (Figs. 1B, 1C).

CTG Repeat Expansion of *TCF4* in Japanese Subjects

The lengths of CTG TNRs for 47 FECD cases and 96 controls are listed in Table 2. Among FECD participants, 12 of 47 cases (26%) possessed >50 CTG repeats (Table 2); of note, one FECD patient had >100 repeats, and Southern blotting confirmed an expansion of ~2600 repeats. Similar to findings in a previous study,[19] the distribution of repeat length among affected subjects was bimodal; no subjects had between 31 and 59 repeats (Fig. 2). No control subject possessed more than 41 repeats. The sensitivity and specificity values of an expanded repeat length to determine an FECD case in our subjects were 26% and 100%, respectively; however, the threshold value of an "expanded repeat" could not be determined due to the absence of cases or controls with repeat lengths between 42 and 59.

Correlation Between Clinical Parameters and Repeat Length

We assessed the correlation between the TNR length and clinical parameters in the case subjects. As a result, there was no significant correlation between the length of TNR and visual acuity ($P = 0.989$) or central corneal thickness ($P = 0.124$). Additionally, there were no differences in these parameters between the FECD groups, based on the presence or absence of TNR expansion (Figs. 3A–D). Notably, the mean ages of the two groups were similar (TNR+ mean age = 68.3 ± 9.3 years; TNR– mean age = 68.5 ± 13.8 years.) Our subjective evaluation of corneal appearance by slit-lamp biomicroscopy and noncontact specular microscopy was unable to distinguish between cases with and without TNR expansion (Figs. 4A–F).

Table 2. TGC Repeat Length in *TCF4* Genes of FECD Patients and Normal Controls

	FECD Cases*			Controls		
No. of Repeats	**>50**	**40–50**	**<40**	**>50**	**40–50**	**<40**
No. of subjects	12	0	35	0	1	95
% of subjects	26%	0%	74%	0%	1%	99%

* $P < 0.001$ for FECD cases versus controls by Fisher's exact test.

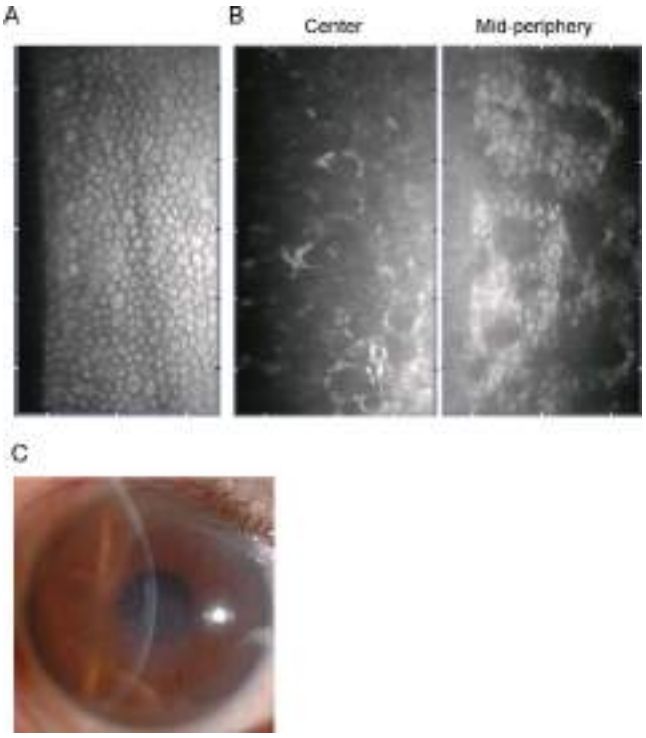

FIGURE 1. Clinical manifestations of FECD in Japanese patients. (**A**) Noncontact specular microscopy image of normal subject. (**B**) Noncontact specular microscopy images of an FECD patient with 30 CTG repeats. Images were obtained from the corneal center and mid-periphery. (**C**) Representative slit-lamp photograph from an FECD patient with 70 CTG repeats.

DISCUSSION

FECD is the most common inherited corneal dystrophy, and as many as 5% of the population over 40 years of age in the United States may exhibit guttae.[24] Accordingly, visual loss due to FECD is the most frequent indication for corneal transplantation in the United States[2] but less commonly so in Asian countries such as Japan. Data comprising the prevalence of FECD in Japan is not well elucidated, but a national survey described FECD as an indication for keratoplasty in 1.9% of cases of bullous keratopathy between 1999 and 2001.[25] Similarly, FECD accounted for only 16.6% of penetrating keratoplasty in India.[26]

Evidence is accumulating that variation in *TCF4* and particularly the intronic CTG repeat expansion[19–22,27] contributes to FECD. The apparent differences in prevalence of FECD between Caucasian and Asian populations led us to investigate whether Japanese FECD patients share the intronic TNR expansion in *TCF4*. In this study, we showed that 12 of 47 FECD patients (sensitivity = 26%) harbored a heterozygous CTG expansion of >50 repeats in comparison to no control patients (specificity = 100%). A homozygous expansion was not found in any participant. The prevalence of repeat expansion in the current study population is lower than the 79% reported in the initial report in a Caucasian population[19] and an independent U.S. cohort reported by Mootha et al.[20] confirming repeat expansion in 88 of 120 cases (73%) and in 5 of 70 control subjects (7%). The results of this current study are more comparable to the prevalence in an Indian population in which 14 of 44 subjects (34%) were found to have repeat expansion.[21] A study describing ethnic Chinese in Singapore found a prevalence of repeat expansion in 25 of 57 FECD subjects (44%), but the definition of CTG expansion was >40 repeats.[22]

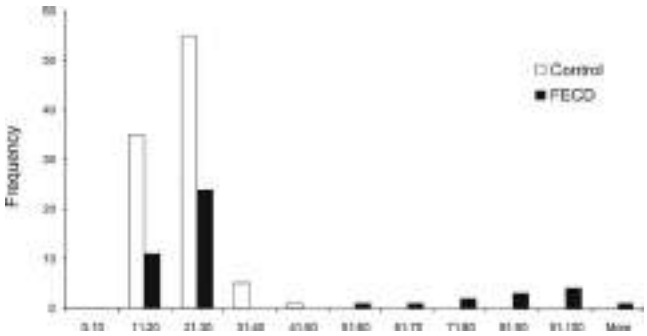

FIGURE 2. Frequency histogram of the CTG repeat length. CTG repeat length of the longest allele in all samples of both FECD cases (*black bars*) and normal control (*white bars*) samples. Note that one FECD patient had more than 100 repeats.

The lack of CTG expansion in any of our control subjects is also in contrast to these prior studies in which a small proportion of normal subjects harbored repeat expansion. The U.S. cohorts reported *TCF4* repeat expansion in 3 of 63 subjects (5%)[19] and 7 of 100 subjects (7%),[20] respectively. Repeat expansion was found in 5 of 97 normal subjects (5%) in an Indian study by Nanda et al.[21] and in 2 of 121 controls (2%) in a study of ethnic Chinese by Xing et al.[22] One consideration in comparing studies is the threshold defined for repeat expansion. Nanda et al.[21] used a threshold of 50 repeats, whereas the other studies considered CTG expansion as >40 repeats. However, in any population, CTG repeat sizes between 40 and 50 are uncommon in either control or FECD participants. In the original U.S. study, 1 control subject and 1 FECD subject had repeat lengths in this range.[19] Of course, the functional significance of these intermediate repeat lengths or the threshold size for a pathogenic expansion is currently unknown.

The *TCF4* gene (also known as *ITF2* and *SEF2*, and not to be confused with T-cell factor 4, which is now known as *TCF7L2*) encodes the E2-2 protein that is a member of the helix-loop-helix (bHLH) family of transcription factors and plays an important role in a variety of developmental processes.[28] *TCF4* was shown to be one of the first genes associated with schizophrenia in a large-scale genetic association study.[29] In addition, *TCF4* is associated with primary sclerosing cholangitis and Pitt-Hopkins syndrome, a form of severe developmental retardation.[28] Except for Pitt-Hopkins syndrome, which results from a haploinsufficiency of *TCF4*, the involvement of *TCF4* in the pathogenesis of other diseases has not been elucidated.[30]

Du et al.[31] recently reported that transcription of CTG repeats resulted in nuclear foci containing condensed poly$(CUG)_n$ RNA and muscleblind-like1 (MBNL1) protein, an mRNA-splicing factor, in corneal endothelial cells from FECD patients with repeat expansions but not in an FECD patient without repeat expansion, and these results have been replicated by Mootha et al.[32] Loss of MBNL1 activity due to sequestration in these toxic RNA foci has been shown to be a pathogenic event in myotonic dystrophy type 1, leading to a pattern of missplicing of MBNL1-regulated mRNAs that was also duplicated in FECD endothelium.[31] Previous work has also demonstrated that MBNL1 plays a role in epithelial-to-mesenchymal transition (EMT),[33,34] which has been proposed as an important event in the pathogenesis of FECD.[14,31,35] Thus, TNR expansion in *TCF4* could play a role in the development of FECD cases in a subset of the Japanese population through several possible mechanisms, including RNA toxicity. However, other genetic and/or environmental factors must be responsible for most cases in Japan. We recently reported that a Rho kinase inhibitor eye drop is effective for Japanese FECD patients.[36,37] Two FECD

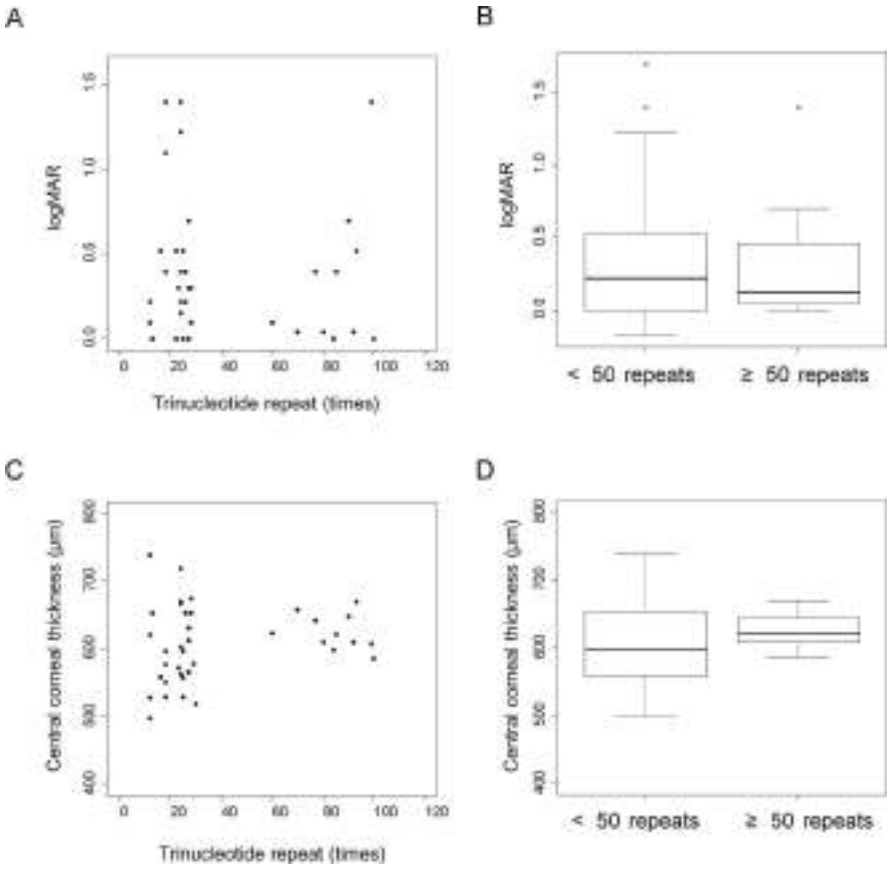

Figure 3. Correlation between the TGC repeat length and visual acuity; central corneal thickness in the case subjects. (**A**, **B**) Graph shows the correlation between TGC repeat length and visual acuity. (**C**, **D**) Graph shows the correlation between TGC repeat length and central corneal thickness.

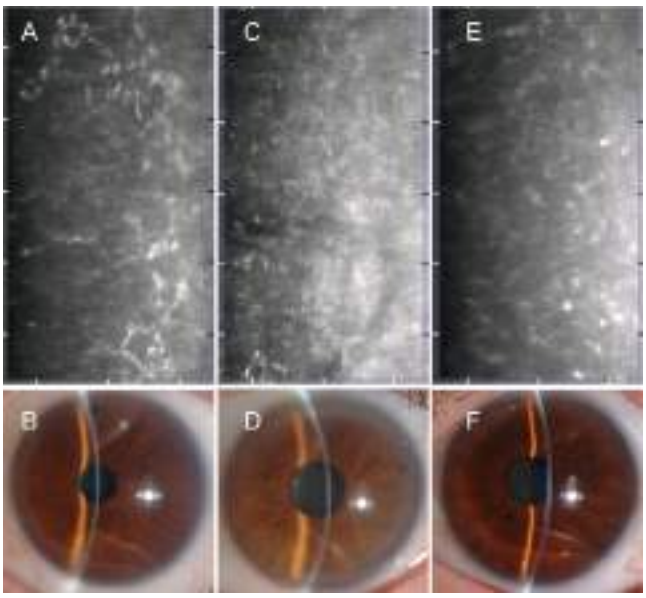

Figure 4. Noncontact specular microscopy images and slit-lamp photographs of FECD patients. (**A**, **B**) A 56-year-old woman with 25 CTG repeats. (**C**, **D**) A 55-year-old man with 100 CTG repeats. (**E**, **F**) A 68-year-old woman with ~2600 CTG repeats.

patients who were successfully treated with Rho kinase inhibitor were included in the current study; 1 patient had a TNR expansion and 1 patient had no TNR expansion. This very preliminary finding that Rho kinase inhibition may be useful regardless of the *TCF4* TNR status warrants more detailed investigation but also motivates us to expand our clinical studies of Rho kinase inhibitors to Caucasian populations.

We also showed that clinical manifestations of FECD, such as guttae, corneal thickness, and visual acuity, were indistinguishable between patients who carry a CTG repeat expansion and those who lack the expansion. Our data are consistent with the knowledge that FECD is a genetically heterogeneous disease and suggest that one or more additional undiscovered variants may be common causes of FECD in Japan.

Acknowledgments

The authors thank all the patients and volunteers who enrolled in the study.

Supported by an unrestricted grant from Research to Prevent Blindness, Inc., to the Mayo Clinic Department of Ophthalmology, by a Health Labour Sciences research grant (KS and TK), and by Research Funding for Longevity Sciences from National Center for Geriatrics and Gerontology (KS, TK, and UM).

Disclosure: **M. Nakano**, None; **N. Okumura**, None; **H. Nakagawa**, None; **N. Koizumi**, None; **Y. Ikeda**, None; **M Ueno**, None; **K. Yoshii**, None; **H. Adachi**, None; **R.A. Aleff**, None; **M.L. Butz**, None; **W.E. Highsmith**, None; **K. Tashiro**, None; **E.D. Wieben**, None; **S. Kinoshita**, None; **K.H. Baratz**, None

References

1. Tan DT, Dart JK, Holland EJ, Kinoshita S. Corneal transplantation. *Lancet*. 2012;379:1749–1761.
2. Eye Bank Association of America. *Eye Banking Statistical Report*. Washington, DC: Eye Bank Association of America; 2013.
3. Aldave AJ, Han J, Frausto RF. Genetics of the corneal endothelial dystrophies: an evidence-based review. *Clin Genet*. 2013;84:109–119.
4. Biswas S, Munier FL, Yardley J, et al. Missense mutations in COL8A2, the gene encoding the alpha2 chain of type VIII collagen, cause two forms of corneal endothelial dystrophy. *Hum Mol Genet*. 2001;10:2415–2423.
5. Gottsch JD, Sundin OH, Liu SH, et al. Inheritance of a novel COL8A2 mutation defines a distinct early-onset subtype of Fuchs' corneal dystrophy. *Invest Ophthalmol Vis Sci*. 2005;46:1934–1939.
6. Sundin OH, Jun AS, Broman KW, et al. Linkage of late-onset Fuchs' corneal dystrophy to a novel locus at 13pTel-13q12.13. *Invest Ophthalmol Vis Sci*. 2006;47:140–145.
7. Meadows DN, Eghrari AO, Riazuddin SA, Emmert DG, Katsanis N, Gottsch JD. Progression of Fuchs' corneal dystrophy in a family linked to the FCD1 locus. *Invest Ophthalmol Vis Sci*. 2009;50:5662–5666.
8. Sundin OH, Broman KW, Chang HH, Vito EC, Stark WJ, Gottsch JD. A common locus for late-onset Fuchs' corneal dystrophy maps to 18q21.2-q21.32. *Invest Ophthalmol Vis Sci*. 2006;47:3919–3926.
9. Riazuddin SA, Eghrari AO, Al-Saif A, et al. Linkage of a mild late-onset phenotype of Fuchs' corneal dystrophy to a novel locus at 5q33.1-q35.2. *Invest Ophthalmol Vis Sci*. 2009;50:5667–5671.
10. Riazuddin SA, Zaghloul NA, Al-Saif A, et al. Missense mutations in TCF8 cause late-onset Fuchs' corneal dystrophy and interact with FCD4 on chromosome 9p. *Am J Hum Genet*. 2010;86:45–53.
11. Mehta JS, Vithana EN, Tan DT, et al. Analysis of the posterior polymorphous corneal dystrophy 3 gene, TCF8, in late-onset Fuchs' endothelial corneal dystrophy. *Invest Ophthalmol Vis Sci*. 2008;49:184–188.
12. Vithana EN, Morgan PE, Ramprasad V, et al. SLC4A11 mutations in Fuchs' endothelial corneal dystrophy. *Hum Mol Genet*. 2008;17:656–666.
13. Riazuddin SA, Vithana EN, Seet LF, et al. Missense mutations in the sodium borate cotransporter SLC4A11 cause late-onset Fuchs' corneal dystrophy. *Hum Mutat*. 2010;31:1261–1268.
14. Baratz KH, Tosakulwong N, Ryu E, et al. E2-2 protein and Fuchs' corneal dystrophy. *N Engl J Med*. 2010;363:1016–1024.
15. Li YJ, Minear MA, Rimmler J, et al. Replication of TCF4 through association and linkage studies in late-onset Fuchs' endothelial corneal dystrophy. *PLoS One*. 2011;6:e18044.
16. Riazuddin SA, McGlumphy EJ, Yeo WS, Wang J, Katsanis N, Gottsch JD. Replication of the TCF4 intronic variant in late-onset Fuchs' corneal dystrophy and evidence of independence from the FCD2 locus. *Invest Ophthalmol Vis Sci*. 2011;52:2825–2829.
17. Igo RP Jr, Kopplin LJ, Joseph P, et al. Differing roles for TCF4 and COL8A2 in central corneal thickness and Fuchs' endothelial corneal dystrophy. *PLoS One*. 2012;7:e46742.
18. Kuot A, Hewitt AW, Griggs K, et al. Association of TCF4 and CLU polymorphisms with Fuchs' endothelial dystrophy and implication of CLU and TGFBI proteins in the disease process. *Eur J Hum Genet*. 2012;20:632–638.
19. Wieben ED, Aleff RA, Tosakulwong N, et al. A common trinucleotide repeat expansion within the transcription factor 4 (TCF4, E2-2) gene predicts Fuchs' corneal dystrophy. *PLoS One*. 2012;7:e49083.
20. Mootha VV, Gong X, Ku HC, Xing C. Association and familial segregation of CTG18.1 trinucleotide repeat expansion of TCF4 gene in Fuchs' endothelial corneal dystrophy. *Invest Ophthalmol Vis Sci*. 2014;55:33–42.
21. Nanda GG, Padhy B, Samal S, Das S, Alone DP. Genetic association of TCF4 intronic polymorphisms, CTG18.1 and rs17089887, with Fuchs' endothelial corneal dystrophy in an Indian population. *Invest Ophthalmol Vis Sci*. 2014;55:7674–7680.
22. Xing C, Gong X, Hussain I, et al. Transethnic replication of association of CTG18.1 repeat expansion of TCF4 gene with Fuchs' corneal dystrophy in Chinese implies common causal variant. *Invest Ophthalmol Vis Sci*. 2014;55:7073–7078.
23. Krachmer JH, Purcell JJ Jr, Young CW, Bucher KD. Corneal endothelial dystrophy. A study of 64 families. *Arch Ophthalmol*. 1978;96:2036–2039.
24. Lorenzetti DW, Uotila MH, Parikh N, Kaufman HE. Central cornea guttata. Incidence in the general population. *Am J Ophthalmol*. 1967;64:1155–1158.
25. Shimazaki J, Amano S, Uno T, Maeda N, Yokoi N. Japan Bullous Keratopathy Study G. National survey on bullous keratopathy in Japan. *Cornea*. 2007;26:274–278.
26. Pandrowala H, Bansal A, Vemuganti GK, Rao GN. Frequency, distribution, and outcome of keratoplasty for corneal dystrophies at a tertiary eye care center in south India. *Cornea*. 2004;23:541–546.
27. Wieben ED, Aleff RA, Eckloff BW, et al. Comprehensive assessment of genetic variants within TCF4 in Fuchs' endothelial corneal dystrophy. *Invest Ophthalmol Vis Sci*. 2014;55:6101–6107.
28. Forrest MP, Hill MJ, Quantock AJ, Martin-Rendon E, Blake DJ. The emerging roles of TCF4 in disease and development. *Trends Mol Med*. 2014;20:322–331.
29. Stefansson H, Ophoff RA, Steinberg S, et al. Common variants conferring risk of schizophrenia. *Nature*. 2009;460:744–747.
30. Amiel J, Rio M, de Pontual L, et al. Mutations in TCF4, encoding a class I basic helix-loop-helix transcription factor, are responsible for Pitt-Hopkins syndrome, a severe epileptic encephalopathy associated with autonomic dysfunction. *Am J Hum Genet*. 2007;80:988–993.
31. Du J, Aleff RA, Soragni E, et al. RNA toxicity and missplicing in the common eye disease fuchs endothelial corneal dystrophy. *J Biol Chem*. 2015;290:5979–5990.
32. Mootha VV, Hussain I, Cunnusamy K, et al. TCF4 triplet repeat expansion and nuclear RNA foci in Fuchs' endothelial corneal dystrophy. *Invest Ophthalmol Vis Sci*. 2015;56:2003–2011.
33. LeMasters KE, Blech-Hermoni Y, Stillwagon SJ, Vajda NA, Ladd AN. Loss of muscle blind-like 1 promotes invasive mesenchyme formation in endocardial cushions by stimulating autocrine TGFbeta3. *BMC Dev Biol*. 2012;12:22.
34. Venables JP, Brosseau JP, Gadea G, et al. RBFOX2 is an important regulator of mesenchymal tissue-specific splicing in both normal and cancer tissues. *Mol Cell Biol*. 2013;33:396–405.
35. Iliff BW, Riazuddin SA, Gottsch JD. The genetics of Fuchs' corneal dystrophy. *Expert Rev Ophthalmol*. 2012;7:363–375.
36. Koizumi N, Okumura N, Ueno M, Nakagawa H, Hamuro J, Kinoshita S. Rho-associated kinase inhibitor eye drop treatment as a possible medical treatment for Fuchs corneal dystrophy. *Cornea*. 2013;32:1167–1170.
37. Okumura N, Koizumi N, Kay EP, et al. The ROCK inhibitor eye drop accelerates corneal endothelium wound healing. *Invest Ophthalmol Vis Sci*. 2013;54:2493–2502.

Investigative Ophthalmology & Visual Science

PLOS | ONE

RESEARCH ARTICLE

Morphological Changes of Human Corneal Endothelial Cells after Rho-Associated Kinase Inhibitor Eye Drop (Ripasudil) Administration: A Prospective Open-Label Clinical Study

Hiroko Nakagawa[1☯], Noriko Koizumi[1,2☯*], Naoki Okumura[1,2], Hideki Suganami[3], Shigeru Kinoshita[1¤]

1 Department of Ophthalmology, Kyoto Prefectural University of Medicine, Kyoto, Kyoto, Japan, **2** Department of Biomedical Engineering, Faculty of Life and Medical Sciences, Doshisha University, Kyotanabe, Kyoto, Japan, **3** Kowa Company, Ltd, Nagoya, Aichi, Japan

☯ These authors contributed equally to this work.
¤ Current address: Department of Frontier Medical Science and Technology for Ophthalmology, Kyoto Prefectural University of Medicine, Kyoto, Kyoto, Japan
* nkoizumi@mail.doshisha.ac.jp

OPEN ACCESS

Citation: Nakagawa H, Koizumi N, Okumura N, Suganami H, Kinoshita S (2015) Morphological Changes of Human Corneal Endothelial Cells after Rho-Associated Kinase Inhibitor Eye Drop (Ripasudil) Administration: A Prospective Open-Label Clinical Study. PLoS ONE 10(9): e0136802. doi:10.1371/journal.pone.0136802

Editor: Vishal Jhanji, The Chinese University of Hong Kong, HONG KONG

Received: May 26, 2015

Accepted: August 5, 2015

Published: September 14, 2015

Data Availability Statement: All relevant data are within the paper and Supporting Information files.

Funding: This study was sponsored by Kowa Company, Ltd, Nagoya, Japan. The sponsor participated in design, study conduct, data collection, data management, data analysis, interpretation of the data of the study, and preparation, review, and approval of the manuscript.

Competing Interests: This study was sponsored by Kowa Company, Ltd. HS is an employee of Kowa

Abstract

Purpose

To investigate the effect and safety of a selective Rho kinase inhibitor, ripasudil 0.4% eye drops, on corneal endothelial cells of healthy subjects.

Design

Prospective, interventional case series.

Methods

In this study, 6 healthy subjects were administered ripasudil 0.4% in the right eye twice daily for 1 week. Morphological changes and corneal endothelial cell density were examined by noncontact and contact specular microscopy. Central corneal thickness and corneal volume of 5 mm-diameter area of center cornea were analyzed by Pentacam Scheimpflug topography. All the above measurements were conducted in both eyes before administration, 1.5 and 6 hours after the initial administration on day 0; and in the same manner after the final administration on day 7.

Results

By noncontact specular microscopy, indistinct cell borders with pseudo guttae were observed, but by contact specular microscopy, morphological changes of corneal endothelial cells were mild and pseudo guttae was not observed after single and repeated administration of ripasudil in all subjects. These changes resolved prior to the next administration,

Company, Ltd. NK has received consulting fees from Kowa, Senju Pharmaceutical, and M's Science Corporation, and grants from Japanese Ministry of Education, Culture, Sports, Science and Technology, and Japanese Ministry of Health, Labour and Welfare Ministry. SK has received consulting fees from Kowa, Senju Pharmaceutical, Santen Pharmaceutical, Otsuka Pharmaceutical, Alcon Japan, AMO Japan, HOYA, and has the following patents with Senju Pharmaceutical (Agent for promoting corneal endothelial cell adhesion, JP 5657252). There are no further patents, products in development or marketed products to declare. This does not alter the authors' adherence to all the PLOS ONE policies on sharing data and materials.

and corneal endothelial cell density, central corneal thickness and corneal volume were not changed throughout the study period.

Conclusion

Transient morphological changes of corneal endothelial cells such as indistinct cell borders with pseudo guttae were observed by noncontact specular microscopy in healthy subjects after ripasudil administration. Corneal edema was not observed and corneal endothelial cell density did not decrease after 1 week repetitive administration. These morphological changes were reversible and corneal endothelial cell morphology returned to normal prior to the next administration.

Trial Registration

JAPIC Clinical Trials Information 142705

Introduction

Rho-associated, coiled-coil containing protein kinase (ROCK), serine/threonine kinase is involved in diverse physiological functions, such as cytoskeletal rearrangement related to cell shape, smooth muscle contraction, and gene expression [1,2]. Recently, by focusing on these physiological functions, many researchers are investigating clinical applications for ROCK inhibitors [3–6]. Some selective ROCK inhibitors are actually used in clinical practice, for example, fasudil and ripasudil are therapeutic agents for cerebral vasospasm and glaucoma, respectively. The mechanism of intraocular pressure-lowering by ROCK inhibitors, including ripasudil, is hypothesized to be due to ROCK inhibitors increase in conventional outflow of aqueous humor by directly altering cell shape in the trabecular meshwork and increasing the permeability of the Schlemm's canal endothelial cells [4,7–9].

Currently, treatment of corneal endothelial dysfunction is mainly corneal transplantation, in addition, various alternative therapies are propounded [10,11]. Recently, attention has been focused on the effect of ROCK inhibitor on corneal endothelial cells (CECs). Okumura et al. reported that the selective ROCK inhibitor Y-27632 promotes cell adhesion and proliferation, and inhibits the apoptosis of primate CECs in culture [12]. In rabbit and monkey models of partial endothelial dysfunction, they showed that corneal endothelial wound healing was accelerated via the topical application of Y-27632 and Y-39983 to the ocular surface, resulting in regeneration of a corneal endothelial monolayer with a high endothelial cell density (ECD) [13–15]. In addition, the positive effect of Y-27632 eye drops in treating patients with central corneal edema due to Fuchs corneal endothelial dystrophy was reported [5,13,16].

Ripasudil 0.4% (K-115, Glanatec; Kowa Company, Ltd, Nagoya, Japan) is an ophthalmic solution which was approved in Japan for the treatment of glaucoma and ocular hypertension in September 2014 [17]. In a preclinical study of ripasudil in cynomolgus monkeys, some morphological changes in CECs and limited decrease in corneal thickness were observed after both single and repeated instillation of ripasudil [18]. These findings lead us to consider the possibility of the effect of ripasudil on CECs. In this prospective study, to investigate the effect and safety of ripasudil 0.4% ophthalmic solution on human CECs, we examined morphological changes and ECD in healthy subjects after single and 1 week of ripasudil administration.

Methods

A prospective, open-label clinical study was conducted at University Hospital, Kyoto Prefectural University of Medicine (KPUM) in accordance with the ethical principles of the Declaration of Helsinki. Heishinkai Medical Group Incorporated, OPHAC Hospital, which is not part of KPUM, was in charge of subject screening. The study protocol was approved prior to beginning the study by each institutional review board as follows, KPUM Institutional Review Board; OPHAC Hospital Institutional Review Board. Subjects for the clinical study received complete information regarding the protocol, and written informed consent was obtained from each participant before entry to the study. This study is registered at www.clinicaltrials.jp as study no. 142705.

Inclusion criteria were healthy Japanese subjects, aged from 20 to 64 years. Subjects with ocular disease (including corneal guttae) or who had undergone ocular surgery (including laser treatment) in either eye were excluded from the study. Subjects with central ECD of lower than 2000 cells/mm^2, with CCT of 600 μm or more, or with their best-corrected visual acuity of worse than logMAR visual acuity 0.0 (decimal visual acuity 1.0) in either eye were also excluded. Throughout the study period, subjects were prohibited from receiving medical therapy (excluding medical therapy for adverse events), ocular surgery, laser treatment, ocular treatment, and wearing contact lenses.

Subjects fulfilling the above criteria were screened in OPHAC Hospital, and then transferred to KPUM within the 4 week observation period (during which they did not receive medical therapy or ripasudil). During the administration period, subjects were administered 1 drop of ripasudil 0.4% into the right eye twice daily for 1 week.

To investigate the effect of ripasudil administration on CECs, corneal endothelial cell morphology and ECD were examined by noncontact and specially-designed contact specular microscopy. Automated image capture and corneal endothelial cell count by the software associated with the device was performed by EM3000 noncontact specular microscopy (Tomey corporation, Nagoya, Japan). Subsequently, endothelial cell examination was performed with KSSP laser scanning wide-field contact specular microscopy (Konan Medical, Inc, Nishinomiya, Japan). Oxybuprocaine 0.4% eye drops were used to anaesthetize the eyes and subjects were asked to concentrate on the fixation light in the microscope and the contact cone lens (×40 magnification) was used to record pictures. The images from the center cornea with good contrast were selected and ECD was analyzed by using the manufacturer's software by the center method. To evaluate the corneal endothelial function, CCT and corneal volume of 5 mm-diameter area of the center cornea were analyzed by Pentacam Scheimpflug topography (Oculus Optikgeräte GmbH, Wetzlar, Germany).

These ocular examinations were conducted in both eyes before administration, 1.5 and 6 hours after the initial administration on day 0; and in the same manner after the final administration on day 7. Between 4 to 8 weeks after the final administration on day 7, the ocular examinations were repeated for follow-up observation. Other ocular examinations including slit-lamp microscopy, noncontact tonometry, and best-corrected visual acuity measurements were conducted, and adverse events were collected throughout the study period.

The changes of ECD, CCT, slit-lamp examination, best-corrected visual acuity, and intraocular pressure from before the initial administration to each subsequent time point was evaluated in both eyes for each subject at day 0, day 7 and at the follow-up observation. The palpebral and bulbar conjunctiva, cornea, anterior chamber, iris, and lens were examined with slit-lamp microscopy throughout the study.

Results

The enrollment of subjects began in November 2014 and follow-up observation was completed in February 2015. In this study, 10 subjects were enrolled for screening. Four subjects were

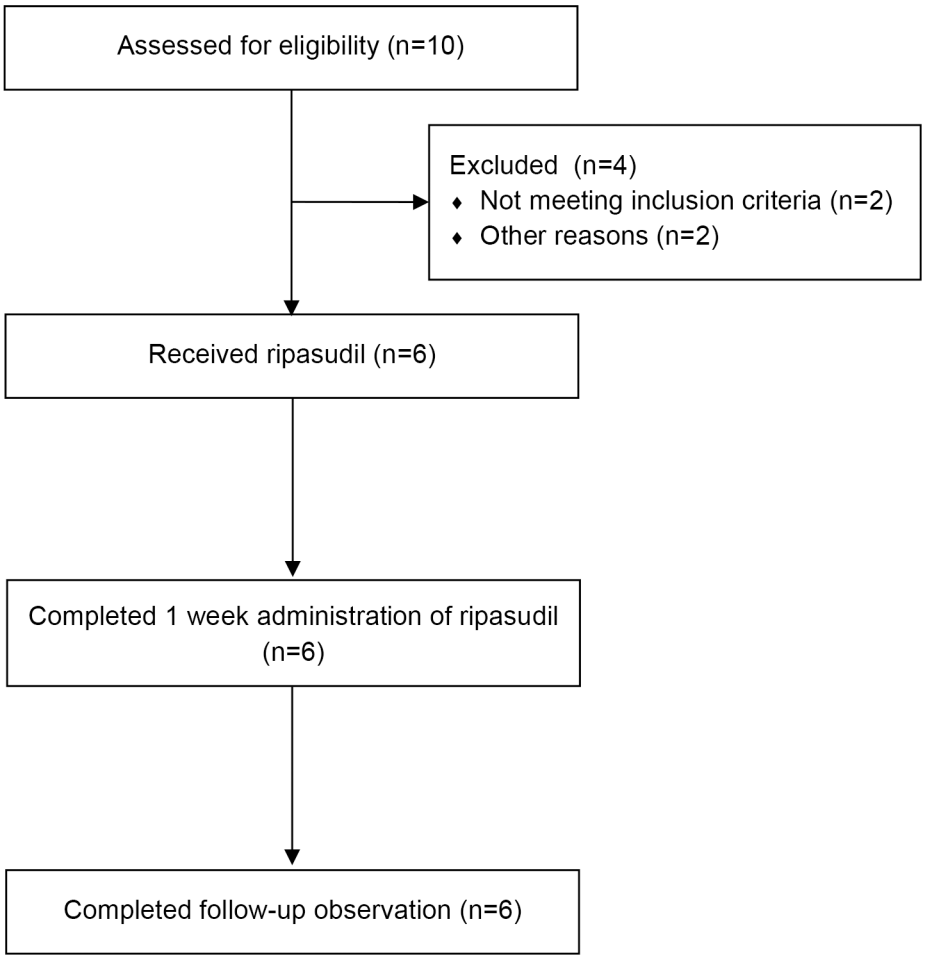

Fig 1. Flow diagram of the study.

doi:10.1371/journal.pone.0136802.g001

excluded; 2 subjects did not satisfy inclusion criteria owing to abnormal laboratory value; 1 subject could not participate for study schedule; ocular examinations were difficult for another 1 subject due to having long eyelashes. The remaining 6 healthy male without any ocular diseases were enrolled in this study and had ripasudil 0.4% administered twice daily for 1 week (Fig 1). The mean age of the subjects was 27.7 ± 5.1 (mean ± SD) (ranged from 20 to 32).

By noncontact specular microscopic examination, distinctive morphological changes of CECs were evident in all 6 subjects 1.5 hours after the initial administration of ripasudil (Fig 2). Highly irregular and blurred images by noncontact specular microscopy were obtained at 1.5 hours after ripasudil administration in all the subjects. Cell borders of CECs which are usually seen as black lines by specular microscopy were observed as white lines due to reflection of the light and as irregular forms. Guttae like dark cells with irregular and indistinct cell borders were detected in all the 6 subjects. In subject 5, the endothelial image was considerably affected and was hardly distinguished by noncontact specular microscopy (Fig 2, right, second). In contrast, using contact specular microscopy, 1.5 hours after ripasudil administration CECs showed less definitive morphological change though there were some irregular cell borders. A very few dark or swollen cells were observed only sporadically and they did not show the characteristic morphology of guttae (Fig 3, right, second). These morphological changes were detected in common in all of 6 subjects. These changes resolved and CEC morphology returned to normal

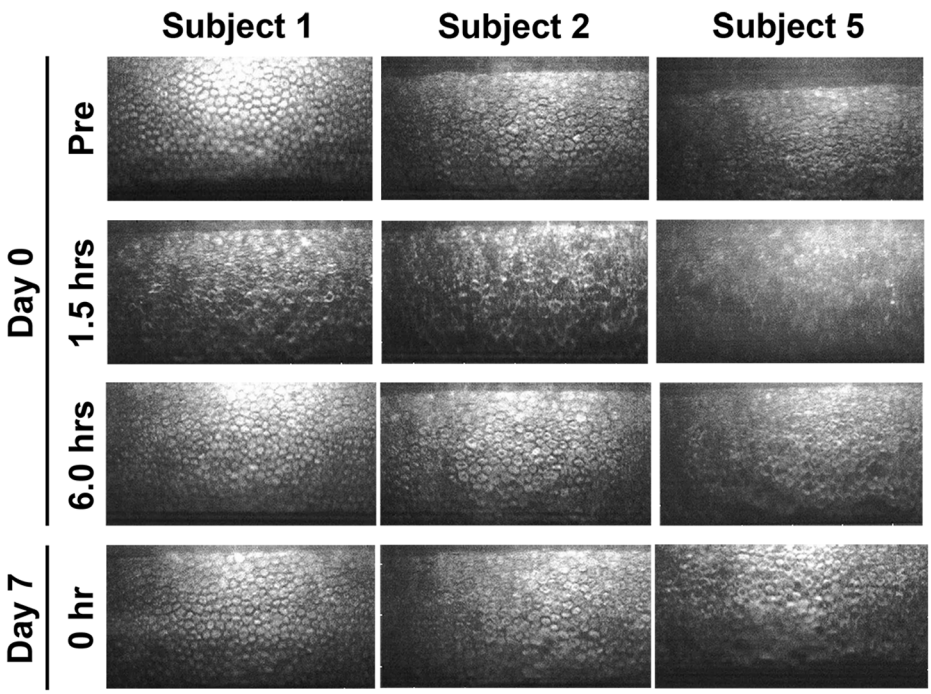

Fig 2. Noncontact specular microscopy images of corneal endothelium before and after ripasudil administration in instilled eye. In 3 of 6 typical healthy subjects, before administration (Top row), 1.5 hours after the initial administration on day 0 (Second row), 6 hours after the initial administration on day 0 (Third row), and before the final administration on day 7 (Bottom row), in subject 1 (Left column), subject 2 (Middle column), and subject 5 (Right column). Before ripasudil administration, corneal endothelial cells showed regular hexagonal monolayer with clear cell borders in all subjects (Top row). One and half hours after ripasudil administration, endothelial cell showed irregular and indistinct cell borders with guttae like dark cells in subjects 1 (Left, second) and 2 (Middle, second). In subject 5, no analyzable image was obtained by noncontact specular microscopy (Right, second). At 6 hours post-dose or later, corneal endothelial morphology returned to normal in subjects 1 and 2. Some guttae like dark cells were still observed in subject 5 at 6 hours on day 0 (Right, third) and prior to the final administration on day 7 (Right, bottom).

doi:10.1371/journal.pone.0136802.g002

by 6 hours after administration in 5 of 6 subjects by specular microscopy (Figs 2 and 3, left and middle columns). In subject 5, minor guttae like dark cells was still detectable at 6 hours after administration using noncontact specular microscopy (Fig 2, right, third) but were not evident by contact specular microscopy (Fig 3, right, third). After repeated administration of ripasudil, contact specular microscopic images of CECs in all subjects showed healthy morphology prior to the final administration on day 7 (Fig 3, bottom). At the follow-up observation, no abnormal findings of CECs were detected by contact or noncontact specular microscopy in any subjects (data not shown). Serial observations of CECs by noncontact and contact specular microscopies on day 0 and day 7 revealed the morphological changes to be reversible and no morphological abnormalities were observed in the CECs.

ECD was evaluated at 6 time points and at the follow-up observation by noncontact and contact specular microscopies (Tables 1 and 2). ECD did not change throughout observation period other than 1.5 hours after ripasudil administration. At 1.5 hours, ECD was difficult to evaluate for all 6 subjects by noncontact specular microscopy and in 3 subjects by contact specular microscopy due to the blurred images with considerable morphological changes. Reliable data was obtained from subjects 1, 3 and 4 at 1.5 hours by contact specular microscopy and decreased ECD was not observed in these subjects. Moreover none of the 6 subjects showed decreased ECD at the follow-up observation.

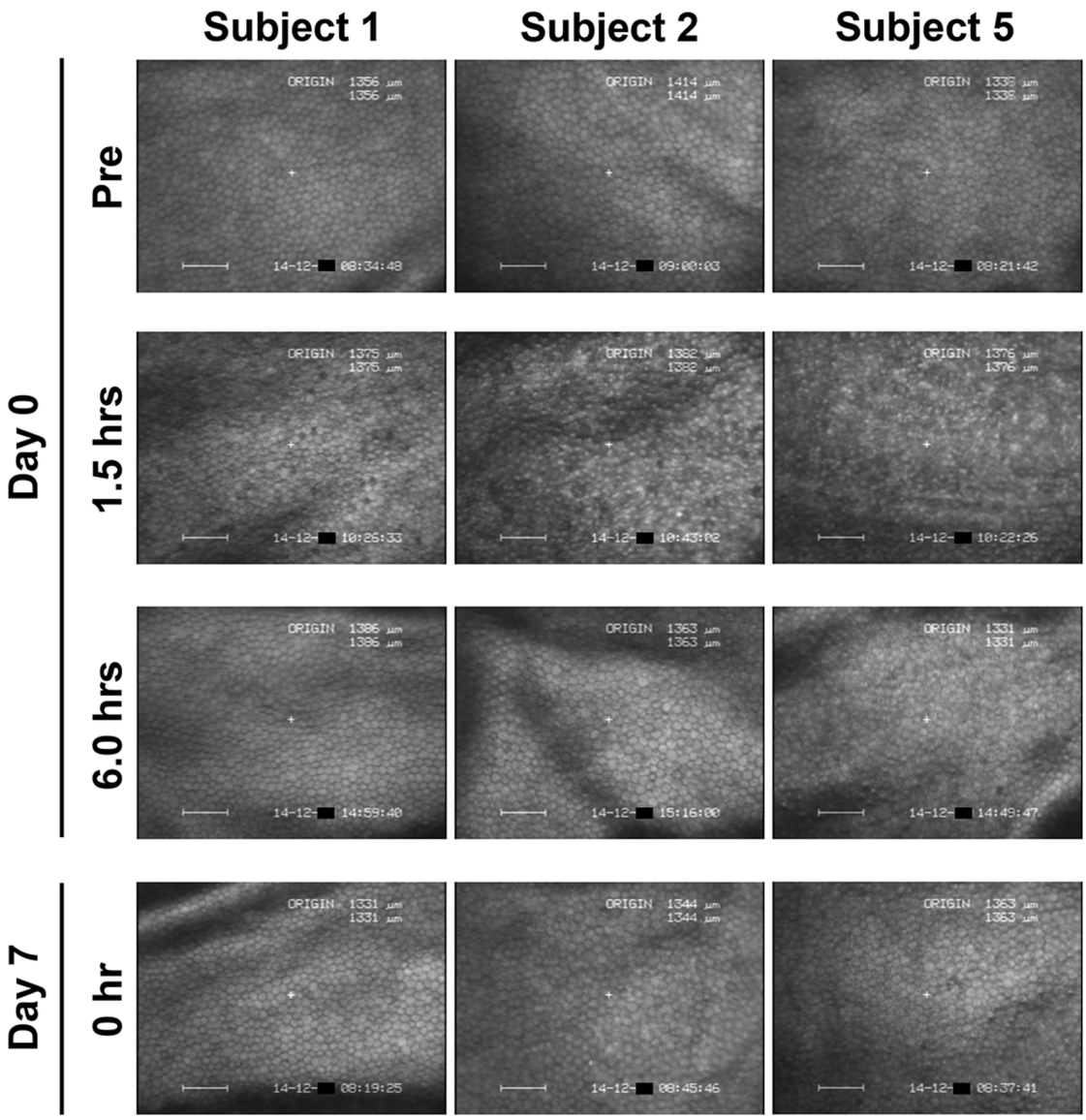

Fig 3. Contact specular microscopy images of corneal endothelium before and after ripasudil administration in instilled eye. In 3 of 6 typical healthy subjects, before administration (Top row), 1.5 hours after the initial administration on day 0 (Second row), 6 hours after the initial administration on day 0 (Third row), and before the final administration on day 7 (Bottom row), in subject 1 (Left column), subject 2 (Middle column), and subject 5 (Right column). Before ripasudil administration, wide-field contact specular microscopy revealed regular hexagonal monolayer of corneal endothelial cells in all subjects (Top row). One and half hours after ripasudil administration, corneal endothelial cells showed indistinct cell borders with a very few dark cells (Second row), but characteristic morphology of guttae was not observed. These morphological changes were detected in common in all subjects. At 6 hours post-dose or later, corneal endothelial morphology came back to normal in all subjects (Third and bottom rows).

doi:10.1371/journal.pone.0136802.g003

To examine the effect of ripasudil on corneal endothelial function of healthy subjects, we evaluated CCT (Table 3) and corneal volume of the 5 mm-diameter area at the central cornea (Table 4) at 6 time points and at the follow-up observation using Pentacam Scheimpflug topography. We did not find any changes for either CCT or corneal volume for any of the 6 subjects. Corneal pachymetry mapping data obtained by Pentacam Scheimpflug topography supported the findings obtained by CCT and corneal volume (Fig 4). Best-corrected visual acuity did not change in any of the subjects eyes. In the non-instilled eye, there were no morphological changes in CECs (Figs 5 and 6), changes of ECD (Tables 5 and 6), or change in CCT (Table 7)

Table 1. Endothelial Cell Density Examined by Noncontact Specular Microscopy Before and After the Administrations of Ripasudil in Instilled Eye. N/A = not able to be calculated or unreliable data, SD = standard deviation. Values are the number of corneal endothelial cells (/mm^2).

Subject	Day 0			Day 7			Follow-up
	Pre[a]	1.5 hrs.	6 hrs.	0 hr[b]	1.5 hrs.	6 hrs.	
1	3252	N/A	3280	3201	N/A	3210	3175
2	2692	N/A	2583	2664	N/A	2478	2590
3	3001	N/A	2874	2974	N/A	2929	2881
4	2567	N/A	2426	2628	N/A	2613	2597
5	2384	N/A	2296	2283	N/A	2427	2614
6	2824	N/A	2702	3010	N/A	2825	2982
Mean	2786.7	-	2693.5	2793.3	-	2747.0	2806.5
SD	310.9	-	351.7	331.7	-	298.8	244.9

[a] Before the administration of ripasudil.

[b] Before the final administrations of ripasudil (Twelve hours after administration).

doi:10.1371/journal.pone.0136802.t001

Table 2. Endothelial Cell Density Examined by Contact Specular Microscopy Before and After the Administrations of Ripasudil in Instilled Eye. N/A = not able to be calculated or unreliable data, SD = standard deviation. Values are the number of corneal endothelial cells (/mm^2).

Subject	Day 0			Day 7			Follow-up
	Pre[a]	1.5 hrs.	6 hrs.	0 hr[b]	1.5 hrs.	6 hrs.	
1	3175	3135	3155	3390	3378	3378	3300
2	2646	N/A	2688	2604	N/A	2611	2545
3	3125	3115	3226	3215	3145	3165	3145
4	2283	2247	2353	2525	2506	2564	2421
5	2755	N/A	2725	2849	N/A	2933	2833
6	3058	N/A	2941	2967	N/A	2994	3096
Mean	2840.3	-	2848.0	2925.0	-	2940.8	2890.0
SD	345.3	-	326.0	337.9	-	314.7	351.5

[a] Before the administration of ripasudil.

[b] Before the final administrations of ripasudil (Twelve hours after administration).

doi:10.1371/journal.pone.0136802.t002

or corneal volume (Table 8) observed in any of the subjects. The only drug related adverse events observed were mild conjunctival hyperemia, which was detected in 5 of 6 subjects (except subject 1), and resolved prior to the next administration in all cases. By slit-lamp microscopy, the cornea remained clear throughout the observation period and corneal stromal and epithelial edema was not detected in any subject. Mild guttae like endothelial reflection, corresponding to the specular microscopic image, was observed at 1.5 hours after the initial administration in 1 subject (subject 2). This finding was resolved by 6 hours.

Discussion

This study was designed and conducted to examine the effect and safety of a selective ROCK inhibitor, ripasudil 0.4% ophthalmic solution, on CECs in healthy subjects. Six healthy subjects with healthy cornea were instilled with ripasudil 0.4% twice daily for 1 week. Considerable morphological changes in CECs were observed by noncontact specular microscopy in all subjects at 1.5 hours after ripasudil administration. Since these changes were detected only in

Table 3. Central Corneal Thickness Before and After the Administrations of Ripasudil in Instilled Eye. SD = standard deviation. Values are the central corneal thickness (μm) examined by Pentacam Scheimpflug topography.

Subject	Day 0			Day 7			Follow-up
	Pre[a]	1.5 hrs.	6 hrs.	0 hr[b]	1.5 hrs.	6 hrs.	
1	559	550	556	558	555	555	555
2	559	575	569	564	561	561	564
3	587	575	575	568	566	575	580
4	560	554	556	558	559	554	567
5	558	553	559	554	556	555	562
6	561	559	555	561	562	561	559
Mean	564.0	561.0	561.7	560.5	559.8	560.2	564.5
SD	11.3	11.2	8.3	5.0	4.1	7.9	8.6

[a] Before the administration of ripasudil.

[b] Before the final administrations of ripasudil (Twelve hours after administration).

doi:10.1371/journal.pone.0136802.t003

ripasudil instilled eyes but not in non-instilled eyes, it was considered to be a phenomenon associated with ripasudil administration.

One and half hours after ripasudil administration, irregularity of cell borders with guttae like dark cells was observed in CEC images taken by noncontact specular microscope. These findings were similar to the results from previous studies in cynomolgus monkeys [18], so these corneal endothelial responses to ripasudil might be common in primates. The reason for these findings detected in the animal study was considered to be due to the reflected light of specular microscopy being scattered by CECs with morphological changes [18]. However, the actual changes in CECs were not adequately examined due to the limitation of quality of CECs observed by noncontact specular microscopy.

In this clinical study, we used specially designed, slit-scanning, wide-field contact specular microscope to analyze the effect of ripasudil on corneal endothelial morphology, and we successfully obtained clearer images than those of noncontact specular microscopy. The contact specular microscope we used in this study is a machine KSSP made by Konan Medical, Inc. This machine has a slit-scanning system and effectively reduces the light scattering by CECs. In

Table 4. Corneal Volume of 5mm Diameter Area of Central Cornea Before and After the Administrations of Ripasudil in Instilled Eye. SD = standard deviation. Values are the corneal volume of 5mm diameter area (mm^3).

Subject	Day 0			Day 7			Follow-up
	Pre[a]	1.5 hrs.	6 hrs.	0 hr[b]	1.5 hrs.	6 hrs.	
1	12.1	11.9	12.0	12.1	12.1	12.0	12.0
2	11.9	12.2	12.1	12.1	11.9	11.9	11.9
3	12.0	12.1	12.1	12.1	11.9	12.1	12.3
4	11.9	11.7	11.8	11.8	11.8	11.7	12.0
5	11.9	11.8	12.0	11.9	11.9	11.8	12.0
6	11.9	11.9	11.8	11.9	12.0	11.9	11.9
Mean	11.95	11.93	11.97	11.98	11.93	11.90	12.02
SD	0.08	0.19	0.14	0.13	0.10	0.14	0.15

[a] Before the administration of ripasudil.

[b] Before the final administrations of ripasudil (Twelve hours after administration).

doi:10.1371/journal.pone.0136802.t004

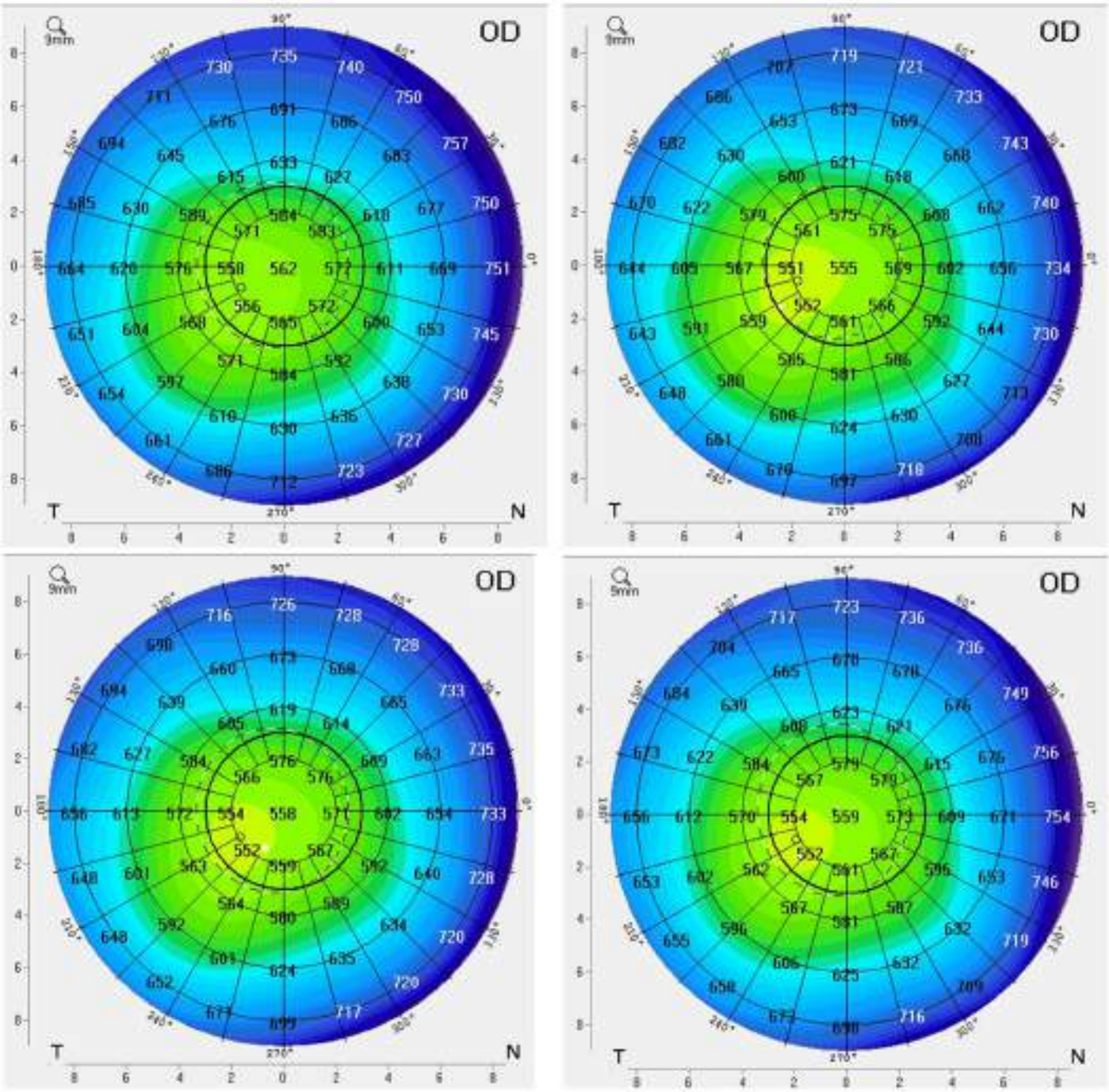

Fig 4. Corneal pachymetry mapping in instilled eye. Corneal pachymetry mapping of subject 4 on day 0 before administration (Top left), 1.5 hours (Top right) and 6 hours (Bottom left) after the initial administration and on day 7 prior to the final administration (Bottom right) of ripasudil in instilled eye. Throughout the observation period, there was no change of corneal thickness of the center and peripheral cornea.

doi:10.1371/journal.pone.0136802.g004

this study, we were able to observe the morphological changes of CECs caused by ripasudil administration in detail using contact specular microscopy. We found that CECs showed indistinct cell borders with a very few dark or swollen cells but there was no findings of loss of CECs. Considerable morphological changes with multiple guttae like cells which was observed

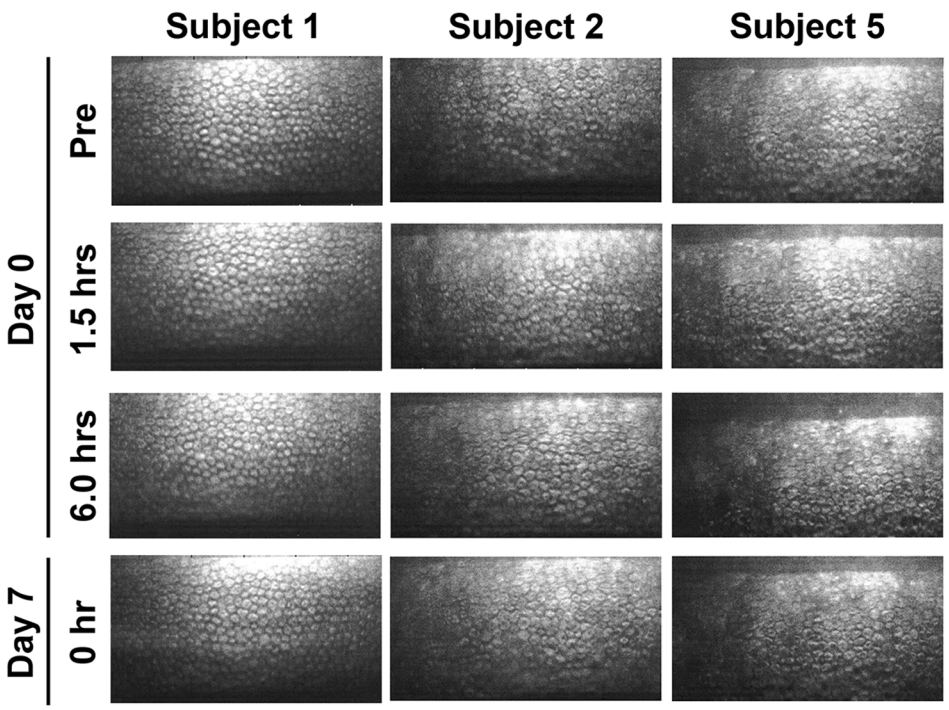

Fig 5. Noncontact specular microscopy images of corneal endothelium before and after ripasudil administration in non-instilled eye. In 3 of 6 typical healthy subjects, before administration (Top row), 1.5 hours after the initial administration on day 0 (Second row), 6 hours after the initial administration on day 0 (Third row), and before the final administration on day 7 (Bottom row) of ripasudil in non-instilled eye, in subject 1 (Left column), subject 2 (Middle column), and subject 5 (Right column). Throughout the observation period, there were no morphological changes of corneal endothelial cells in non-instilled eye.

doi:10.1371/journal.pone.0136802.g005

by noncontact specular microscopy was not actually detected using contact specular microscopy.

As pharmacological effects of ROCK inhibitor, cell morphological changes induced by disruption of actin microfilament bundles and impairment of focal adhesion formation were reported [4,19], and similar morphological changes of CECs might also be induced by ripasudil. Moreover, similar findings were reported from previous studies in cynomolgus monkeys by instillation of both ripasudil and Y-39983 [18], and therefore, morphological changes of CECs could be a common characteristic of ROCK inhibitors. The reason that images using contact specular microscopy were clearer than those by noncontact specular microscopy, was thought to be due to a decrease in the influence of scattering of reflected light owing to the device being in contact with the corneal surface.

Similar morphological change of CECs detected by specular microscopy was previously reported in cynomolgus monkey after the administration of H-7, serine-threonine kinase inhibitor [20]. In that paper, it was reported that CEC borders became indistinct by 1 hour after H-7 administration but cell morphology was mostly recovered by 3–5 hours and had completely recovered to normal by 24 hours without changes in ECD. H-7 is a serine-threonine kinase which decreases intraocular pressure by relaxing and expanding the trabecular meshwork and Schlemm's canal, which is a similar mechanism as ripasudil on intraocular pressure. It is interesting that CECs of human subjects with ripasudil administration showed a similar change with that of cynomolgus monkey administered H-7. Though the mechanism of this pseudo guttae formation is yet to be elucidated, it might have occurred due to morphological

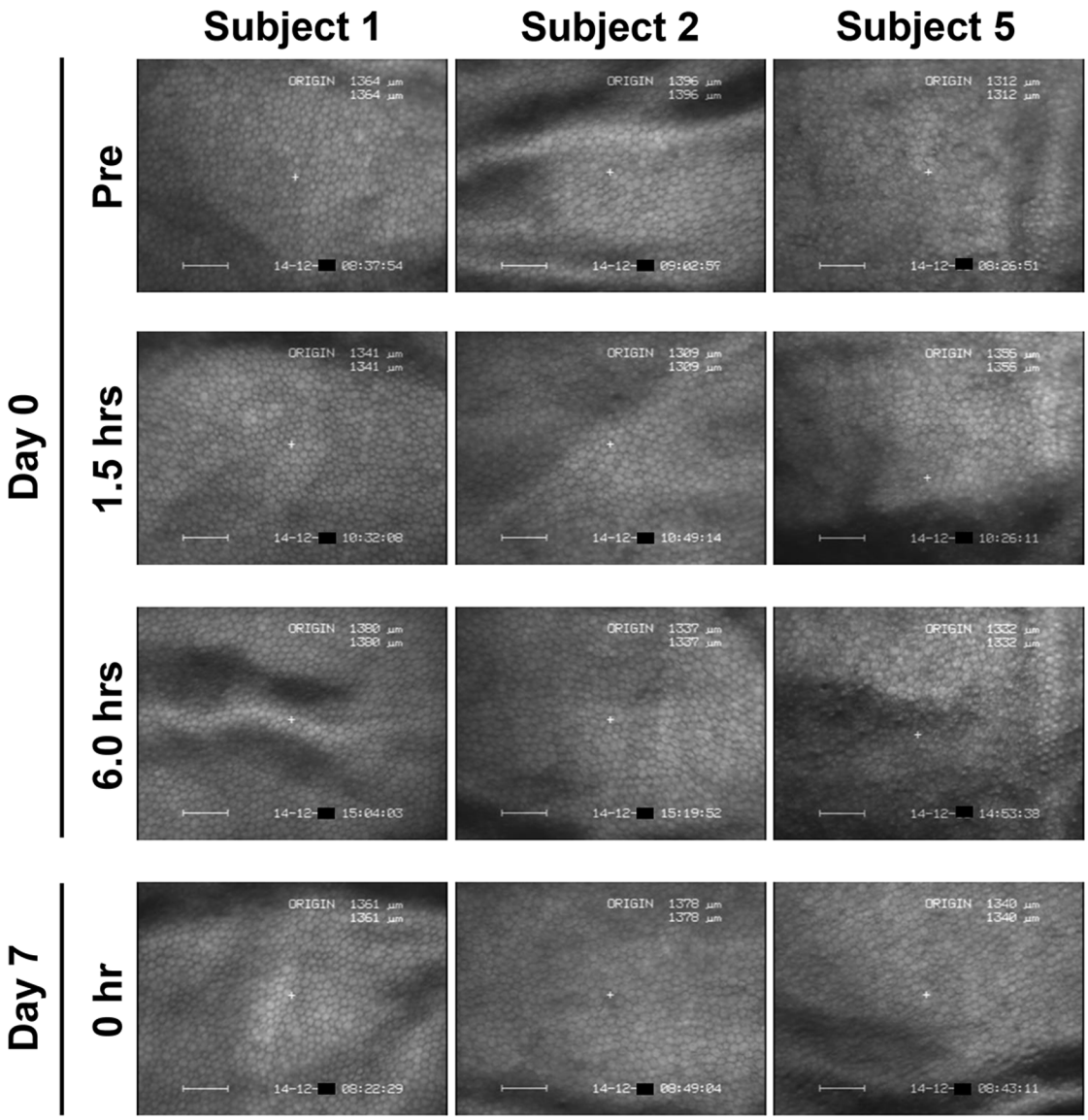

Fig 6. Contact specular microscopy images of corneal endothelium before and after ripasudil administration in non-instilled eye. In 3 of 6 typical healthy subjects, before administration (Top row), 1.5 hours after the initial administration on day 0 (Second row), 6 hours after the initial administration on day 0 (Third row), and before the final administration on day 7 (Bottom row) of ripasudil in non-instilled eye, in subject 1 (Left column), subject 2 (Middle column), and subject 5 (Right column). Throughout the observation period, there were no morphological changes of corneal endothelial cells in non-instilled eye.

doi:10.1371/journal.pone.0136802.g006

changes of CECs induced by the pharmacological effect of ripasudil on actin microfilament which might lead to strongly-scattered reflected light from the specular microscopy.

In previous studies, pseudo guttae with circumscribed black zones were observed after insertion of soft contact lenses in unadapted patients and they were referred to as "endothelial bleb" [21]. The causes of endothelial blebs from wearing soft contact lenses were ascribed to several factors, including the mechanical effects of the lens, reduced corneal oxygenation, interference with carbon dioxide (CO_2) efflux and changes in corneal pH [22]. These factors are not likely to be involved in subjects with ripasudil administration, so the mechanism of pseudo guttae formation in ripasudil instilled eyes is likely different from patients wearing soft contact lenses.

Table 5. Endothelial Cell Density Examined by Noncontact Specular Microscopy Before and After the Administrations of Ripasudil in Non-instilled Eye. SD = standard deviation. Time points indicate administrations of ripasudil in instilled eye. Values are the number of corneal endothelial cells (/mm^2).

Subject	Day 0			Day 7			Follow-up
	Pre[a]	1.5 hrs.	6 hrs.	0 hr[b]	1.5 hrs.	6 hrs.	
1	3187	3175	3201	3300	3274	3135	3221
2	2648	2578	2517	2543	2566	2544	2626
3	3006	3074	2886	3130	3042	3036	3074
4	2459	2404	2472	2465	2437	2380	2476
5	2690	2548	2657	2507	2611	2697	2618
6	2864	2744	2873	2978	2805	2819	2955
Mean	2809.0	2753.8	2767.7	2820.5	2789.2	2768.5	2828.3
SD	263.6	308.4	274.0	361.2	317.7	288.1	296.6

[a] Before the administrations of ripasudil in instilled eye.

[b] Twelve hours after the administrations of ripasudil in instilled eye.

doi:10.1371/journal.pone.0136802.t005

Table 6. Endothelial Cell Density Examined by Contact Specular Microscopy Before and After the Administrations of Ripasudil in Non-instilled Eye. SD = standard deviation. Time points indicate administrations of ripasudil in instilled eye. Values are the number of corneal endothelial cells (/mm^2).

Subject	Day 0			Day 7			Follow-up
	Pre[a]	1.5 hrs.	6 hrs.	0 hr[b]	1.5 hrs.	6 hrs.	
1	3185	3344	3236	3247	3236	3226	3195
2	2681	2695	2710	2618	2717	2625	2558
3	3040	3289	3030	3106	3155	3125	3086
4	2381	2463	2364	2353	2488	2433	2358
5	2681	2786	2710	2865	2770	2747	2762
6	2976	2915	2778	2809	2801	2809	3067
Mean	2824.0	2915.3	2804.7	2833.0	2861.2	2827.5	2837.7
SD	295.7	344.5	299.9	323.8	282.4	300.3	333.5

[a] Before the administrations of ripasudil in instilled eye.

[b] Twelve hours after the administrations of ripasudil in instilled eye.

doi:10.1371/journal.pone.0136802.t006

Table 7. Central Corneal Thickness in Non-instilled Eye. SD = standard deviation. Time points indicate administrations of ripasudil in instilled eye. Values are the central corneal thickness measured by Pentacam Scheimpflug topography (μm).

Subject	Day 0			Day 7			Follow-up
	Pre[a]	1.5 hrs.	6 hrs.	0 hr[b]	1.5 hrs.	6 hrs.	
1	552	551	549	554	557	549	551
2	556	562	563	565	562	567	555
3	565	573	575	567	571	575	572
4	559	564	557	564	559	560	562
5	551	550	553	554	551	549	553
6	552	550	554	558	551	552	556
Mean	555.8	558.3	558.5	560.3	558.5	558.7	558.2
SD	5.4	9.5	9.3	5.8	7.5	10.7	7.7

[a] Before the administrations of ripasudil in instilled eye.

[b] Twelve hours after the administrations of ripasudil in instilled eye.

doi:10.1371/journal.pone.0136802.t007

Table 8. Corneal Volume of 5mm Diameter Area of Central Cornea in Non-instilled Eye. SD = standard deviation. Time points indicate administrations of ripasudil in instilled eye. Values are the corneal volume (mm^3).

Subject	Day 0			Day 7			Follow-up
	Pre[a]	1.5 hrs.	6 hrs.	0 hr[b]	1.5 hrs.	6 hrs.	
1	11.8	11.9	11.8	11.9	12.0	11.8	11.8
2	11.8	11.9	11.9	12.0	11.9	12.0	11.7
3	12.0	12.2	12.2	12.1	12.1	12.2	12.2
4	11.9	12.0	11.8	12.0	11.8	11.9	12.0
5	11.8	11.8	11.8	11.9	11.8	11.8	11.8
6	11.6	11.6	11.7	11.8	11.6	11.6	11.7
Mean	11.82	11.90	11.87	11.95	11.87	11.88	11.87
SD	0.13	0.20	0.18	0.10	0.18	0.20	0.20

[a] Before the administrations of ripasudil in instilled eye.

[b] Twelve hours after the administrations of ripasudil in instilled eye.

doi:10.1371/journal.pone.0136802.t008

The morphological changes in CECs after ripasudil administration were confirmed to be reversible effects and CECs returned to normal prior to the next administration for all subjects. In addition, ECD, CCT, corneal volume, and best-corrected visual acuity remained stable for all subjects. We conducted post hoc Wilcoxon signed rank test for changes from before administration on Day 0 in ECD, CCT and corneal volume. No significant differences were found in the instilled eye, and significant differences were found for only 1 time point for 2 ocular examinations in the non-instilled eye; CCT before administration on Day 7 ($P = 0.03$, two-sided); and corneal volume before administration on Day 7 ($P = 0.03$, two-sided). These differences were thought to be due to random fluctuations in the non-instilled eye. Thus, no findings of cell loss in CECs might have occurred, and we assumed that the findings similar to guttae were pseudo guttae which might have occurred due to transient morphological change of CECs. Pseudo guttae formation was a transient effect of ripasudil and these changes were different from "real" guttae where accumulation of abnormal extracellular matrix is often observed in corneal endothelial diseases such as Fuchs endothelial corneal dystrophy. Additionally, 1-year clinical evaluation of ripasudil 0.4% in patients with open-angle glaucoma and ocular hypertension revealed acceptable safety profile and there were no corneal endothelial disorders reported as adverse events in the long-term study [23].

In conclusion, this study revealed that transient morphological changes identified by indistinct cell borders and appearance of pseudo guttae were observed in CECs after ripasudil administration using noncontact specular microscopy. This may induce a transient functional alteration of corneal endothelium. However, the morphological changes were mild when observed by contact specular microscopy and there were no findings of CEC loss. These morphological changes did not effect corneal thickness or ECD. The recovery of CECs was confirmed by contact specular microscopy prior to the next administration of ripasudil. These results support the safety of short-term use of ripasudil on CECs in subjects with healthy cornea. Further studies are needed in order to explore the long-term effects of ripasudil and the underlying cellular mechanism of the effect on CECs.

Supporting Information

S1 Protocol. Trial Protocol.
(PDF)

S1 TREND Checklist. TREND Checklist.
(PDF)

Acknowledgments

We thank Hiroshi Mikami, Heishinkai Medical Group Incorporated, OPHAC Hospital, Yodogawa, Osaka, contribution to data collection.

Author Contributions

Conceived and designed the experiments: HN NK NO HS SK. Performed the experiments: HN NK NO HS SK. Analyzed the data: HS. Contributed reagents/materials/analysis tools: HS SK. Wrote the paper: HN NK NO HS.

References

1. Ishizaki T, Maekawa M, Fujisawa K, Okawa K, Iwamatsu A, Fujita A, et al. The small GTP-binding protein Rho binds to and activates a 160 kDa Ser/Thr protein kinase homologous to myotonic dystrophy kinase. EMBO J 1996; 15: 1885–1893. PMID: 8617235
2. Shimokawa H, Takeshita A. Rho-kinase is an important therapeutic target in cardiovascular medicine. Arterioscler Thromb Vasc Biol 2005; 25: 1767–1775. PMID: 16002741
3. Shibuya M, Suzuki Y, Sugita K, Saito I, Sasaki T, Takakura K, et al. Effect of AT877 on cerebral vasospasm after aneurysmal subarachnoid hemorrhage. Results of a prospective placebo-controlled double-blind trial. J Neurosurg 1992; 76: 571–577. PMID: 1545249
4. Honjo M, Tanihara H, Inatani M, Kido N, Sawamura T, Yue BY, et al. Effects of rho-associated protein kinase inhibitor Y-27632 on intraocular pressure and outflow facility. Invest Ophthalmol Vis Sci 2001; 42: 137–144. PMID: 11133858
5. Koizumi N, Okumura N, Ueno M, Kinoshita S. New therapeutic modality for corneal endothelial disease using Rho-associated kinase inhibitor eye drops. Cornea 2014; 33: S25–31. PMID: 25289721
6. Arita R, Hata Y, Nakao S, Kita T, Miura M, Kawahara S, et al. Rho kinase inhibition by fasudil ameliorates diabetes-induced microvascular damage. Diabetes 2009; 58: 215–226. doi: 10.2337/db08-0762 PMID: 18840783
7. Isobe T, Mizuno K, Kaneko Y, Ohta M, Koide T, Tanabe S. Effects of K-115, a rho-kinase inhibitor, on aqueous humor dynamics in rabbits. Curr Eye Res 2014; 39: 813–822. doi: 10.3109/02713683.2013.874444 PMID: 24502505
8. Koga T, Koga T, Awai M, Tsutsui J, Yue BY, Tanihara H. Rho-associated protein kinase inhibitor, Y-27632, induces alterations in adhesion, contraction and motility in cultured human trabecular meshwork cells. Exp Eye Res 2006; 82: 362–370. PMID: 16125171
9. Kameda T, Inoue T, Inatani M, Fujimoto T, Honjo M, Kasaoka N, et al. The effect of rho-associated protein kinase inhibitor on monkey Schlemm's canal endothelial cells. Invest Ophthalmol Vis Sci 2012; 53: 3092–3103. doi: 10.1167/iovs.11-8018 PMID: 22491412
10. Jhanji V, Mehta JS, Sharma N, Sharma B, Vajpayee RB. Targeted corneal transplantation. Curr Opin Ophthalmol. 2012; 23:324–329. PMID: 22569469
11. Jhanji V, Sharma N, Agarwal T, Vajpayee RB. Alternatives to allograft corneal transplantation. Curr Opin Ophthalmol. 2010; 21:301–309. PMID: 20560170
12. Okumura N, Ueno M, Koizumi N, Sakamoto Y, Hirata K, Hamuro J, et al. Enhancement on primate corneal endothelial cell survival in vitro by a ROCK inhibitor. Invest Ophthalmol Vis Sci 2009; 50: 3680–3687. doi: 10.1167/iovs.08-2634 PMID: 19387080
13. Okumura N, Koizumi N, Kay EP, Ueno M, Sakamoto Y, Nakamura S, et al. The ROCK inhibitor eye drop accelerates corneal endothelium wound healing. Invest Ophthalmol Vis Sci 2013; 54: 2493–2502. doi: 10.1167/iovs.12-11320 PMID: 23462749
14. Okumura N, Nakano S, Kay EP, Numata R, Ota A, Sowa Y, et al. Involvement of cyclin D and p27 in cell proliferation mediated by ROCK inhibitors Y-27632 and Y-39983 during corneal endothelium wound healing. Invest Ophthalmol Vis Sci. 2014; 55: 318–329. doi: 10.1167/iovs.13-12225 PMID: 24106120
15. Okumura N, Koizumi N, Ueno M, Sakamoto Y, Takahashi H, Hirata K, et al. Enhancement of corneal endothelium wound healing by Rho-associated kinase (ROCK) inhibitor eye drops. Br J Ophthalmol 2011; 95: 1006–1009. doi: 10.1136/bjo.2010.194571 PMID: 21398412

16. Koizumi N, Okumura N, Ueno M, Nakagawa H, Hamuro J, Kinoshita S. Rho-associated kinase inhibitor eye drop treatment as a possible medical treatment for Fuchs corneal dystrophy. Cornea 2013; 32: 1167–1170. PMID: 23715376

17. Garnock-Jones KP. Ripasudil: first global approval. Drugs 2014; 74: 2211–2215. doi: 10.1007/s40265-014-0333-2 PMID: 25414122

18. Wato E, Omichi K, Yoneyama S, Tanaka M, Kagawa M, Amano Y. Safety evaluation of morphological changes in corneal endothelial cells induced by K-115 in cynomolgus monkeys. Fund Toxicol Sci 2014; 1: 39–47.

19. Nagayama K, Matsumoto T. Contribution of actin filaments and microtubules to quasi-in situ tensile properties and internal force balance of cultured smooth muscle cells on a substrate. Am J Physiol Cell Physiol 2008; 295: C1569–1578. doi: 10.1152/ajpcell.00098.2008 PMID: 18923059

20. Tian B, Sabanay I, Peterson JA, Hubbard WC, Geiger B, Kaufman PL. Acute effects of H-7 on ciliary epithelium and corneal endothelium in monkey eyes. Curr Eye Res 2001; 22: 109–120 PMID: 11402388

21. Zantos SG, Holden BA. Transient endothelial changes soon after wearing soft contact lenses. Am J Optom Physiol Opt 1977; 54: 856–858. PMID: 612228

22. Holden BA, Williams L, Zantos SG. The etiology of transient endothelial changes in the human cornea. Invest Ophthalmol Vis Sci 1985; 26: 1354–1359. PMID: 3930418

23. Tanihara H, Inoue T, Yamamoto T, Kuwayama Y, Abe H, Suganami H, et al. One-Year Clinical Evaluation of 0.4% Ripasudil (K-115) in Patients with Open-Angle Glaucoma and Ocular Hypertension. Acta Ophthalmol 2015; in press.

Laboratory Investigation (2015), 1–14

Involvement of ZEB1 and Snail1 in excessive production of extracellular matrix in Fuchs endothelial corneal dystrophy

Naoki Okumura[1,2], Ryuki Minamiyama[1], Leona TY Ho[1], EunDuck P Kay[1], Satoshi Kawasaki[2], Theofilos Tourtas[3], Ursula Schlötzer-Schrehardt[3], Friedrich E Kruse[3], Robert D Young[4], Andrew J Quantock[4], Shigeru Kinoshita[2] and Noriko Koizumi[1]

Fuchs endothelial corneal dystrophy (FECD) due to corneal endothelial cell degeneration is a major cause of corneal transplantation. It is characterized by abnormal deposition of extracellular matrix (ECM), such as corneal guttae, accompanied by a loss of endothelial cells. Although recent studies have revealed several genomic factors, the molecular pathophysiology of FECD has not yet been revealed. In this study, we establish a cellular *in vitro* model by using immortalized corneal endothelial cells obtained from late-onset FECD and control patients and examined the involvement of epithelial mesenchymal transition (EMT) on excessive ECM production. We demonstrate that the EMT-inducing genes *ZEB1* and *SNAI1* were highly expressed in corneal endothelial cells in FECD and were involved in excessive production of ECM proteins, such as type I collagen and fibronectin through the transforming growth factor (TGF)-β signaling pathway. Furthermore, we found that SB431542, a specific inhibitor of TGF-β type I ALK receptors, suppressed the expression of ZEB1 and Snail1 followed by reduced production of ECM. These findings suggest that increased expression levels of ZEB1 and Snail1 in FECD cells were responsible for an increased responsiveness to TGF-β present in the aqueous humor and excessive production of ECM. In addition, these results suggest that the regulation of EMT-related genes by blocking the TGF-β signaling pathway may be a feasible therapeutic strategy for FECD.
Laboratory Investigation advance online publication, 24 August 2015; doi:10.1038/labinvest.2015.111

Fuchs endothelial corneal dystrophy (FECD) is a degenerative disease of the corneal endothelium. The phenotypic clinical features of FECD are characterized by the presence/formation of corneal guttae, which are collagenous excrescences of the corneal endothelial basement membrane (Descemet's membrane).[1] As the disease progresses, an increasing density of guttae and an aberrant thickening of Descemet's membrane becomes evident; this is caused by the abnormal/excessive accumulation of extracellular matrix (ECM). This accumulation of ECM is accompanied by a gradual loss of corneal endothelial cells (CECs), thereby leading to a functional impairment of the endothelium to pump excess fluid out of the corneal stroma.[2] This eventually results in corneal edema and ultimately in vision loss and pain. Currently, corneal transplantation using post-mortem donor tissue is the only therapeutic choice for the treatment of FECD.[3] In the United States, FECD affects as much as 5% of the population aged over 40.[4] Visual disturbance due to FECD is the most common indication for corneal transplantation in the US.[5]

There are two forms of FECD that are defined by the age of onset, the less common early-onset FECD, and the classic late-onset FECD. Genetic linkage and association studies revealed that early-onset FECD exhibits linkage to chromosome 1q and that late-onset FECD has been linked to chromosomes 13 (FCD1), 18 (FCD2), 5 (FCD3), and 9 (FCD4). Late-onset classic FECD can either be familial or sporadic, with an onset typically occurring after the age of 40 years. Although mutations in the zinc-finger E-box binding homeobox 1 (*ZEB1*) gene[6,7] and the solute carrier family 4 member 11 (*SLC4A11*) gene[8,9] have been reported as causative of late-onset

[1]Department of Biomedical Engineering, Faculty of Life and Medical Sciences, Doshisha University, Kyotanabe, Japan; [2]Department of Ophthalmology, Kyoto Prefectural University of Medicine, Kyoto, Japan; [3]Department of Ophthalmology, University of Erlangen-Nürnberg, Erlangen, Germany and [4]Structural Biophysics Group, School of Optometry and Vision Sciences, Cardiff University, Cardiff, UK
Correspondence: Professor N Koizumi, MD, PhD, Department of Biomedical Engineering, Faculty of Life and Medical Sciences, Doshisha University, Kyotanabe 610-0321, Japan.
E-mail: nkoizumi@mail.doshisha.ac.jp

Received 5 December 2014; revised 30 May 2015; accepted 30 June 2015; published online 24 August 2015

FECD, these mutations were only rarely observed in the patient population. On the other hand, Baratz *et al*[10] reported that a genome-wide association study (GWAS) revealed a highly significant association between single nucleotide polymorphisms in transcription factor 4 genes (*TCF4*) in classic late-onset FECD. In addition, involvement of EMT in FECD was hypothesized, as the E-protein family (E2-2)—which is coded by *TCF4*—has a role in EMT. Contrary to the increased genetic evidence of FECD, little is known about the molecular pathogenesis of gradual CEC damage in association with excessive accumulation of ECM.

In this study, we investigated the molecular mechanisms of excessive ECM production as a possible cause of ER stress[11] in CECs in FECD. For this purpose, we established an FECD cellular *in vitro* model using immortalized cell lines derived from FECD and control patients. Since the involvement of EMT in FECD is hypothesized from GWAS analysis,[10] EMT-inducing genes and their effect on excessive production of ECM were investigated. In addition, we assessed the involvement of the transforming growth factor (TGF)-β signaling pathway in the expression of EMT-related genes and ECM production. Finally, we tested the inhibition of TGF-β signaling to suppress excessive ECM production and its feasibility as a possible therapeutic target for treating FECD.

MATERIALS AND METHODS

Materials

Dulbecco's modified Eagle's medium was purchased from Nacalai Tesque (Kyoto, Japan). FNC Coating Mix was purchased from Athena Environmental Sciences (Baltimore, MD). Collagenase A was purchased from Roche Applied Science (Penzberg, Germany). Epidermal growth factor, ascorbic acid, calcium chloride, collagen type I antibody, and propidium iodide were purchased from Sigma-Aldrich (St Louis, MO). DAPI was purchased from Vector Laboratories (Burlingame, CA), and fibronectin antibody was purchased from BD Biosciences (San Jose, CA, USA), Further, Na^+/K^+-ATPase antibody was purchased from Upstate Biotec (Lake Placid, NY), ZO-1 antibody was purchased from Zymed Laboratories (South San Francisco, CA), collagen type IV antibody was purchased from Abcam (Cambridge, UK), and collagen type (α2) VIII antibody was purchased from Abgent (San Diego, CA). The primary antibodies of ZEB1 and Snail1 were purchased from Cell Signaling Technology (Danvers, MA, USA). TGFβ1, TGFβ2, and TGFβ neutralizing antibodies were purchased from R&D Systems (Minneapolis, MN). SB431542 was purchased from Tocris Bioscience (Bristol, UK). Further, Smad3 inhibitor was purchased from Merck Millipore (Billerica, MA). FGF-2, Trypsin–ethylenediaminetetraacetic acid (EDTA), OptiMEM-I, Alexa Fluor 488-conjugated goat anti-mouse IgG, Alexa Fluor 488-conjugated Donkey anti-rabbit IgG, Alexa Fluor 594-conjugated donkey anti-mouse IgG, Alexa Fluor 594-conjugated Donkey anti-rabbit IgG, Snail1 Stealth RNAi ((SNAI_1; HSS143995, SNAI_2; HSS143996, SNAI_3; HSS143997), ZEB1 Stealth RNAi ((ZEB1_1; HSS110548, ZEB_2; HSS110549. ZEB1_3; HSS186235), Stealth RNAi negative control low GC ♯2, Lipofectamine RNAiMAX, lentiviral vector (pLenti6.3_V5-TOPO), and helper plasmids (pLP1, pLP2, and pLP/VSVG) were purchased from Life Technologies (Carlsbad, CA). Transfection reagent was purchased from (Fugene HD; Promega, Madison, WI). RNeasy mini kit was purchased from Qiagen (Hilden, Germany). ReverTra Ace was purchased from Toyobo (Osaka, Japan).

Ethics Statement

The human tissue used in this study was handled under the guidelines based on the ethical principles of the Declaration of Helsinki. Written informed consent was acquired from FECD patients, corneal buttons were obtained during the procedure of penetrating keratoplasty, and stripped Descemet's membranes with CECs were obtained during Descemet's membrane endothelial keratoplasty (DMEK). Normal human donor corneas were obtained from SightLife, Seattle, WA (http://www.sightlife.org/).

Immortalization of CECs

Descemet's membranes, including the CECs, were stripped from three normal human donor corneas and from corneas of three FECD patients during DMEK, and were cultured according to modified published protocols.[12,13] After culturing for 14 days, the FECD-derived CECs and the control CECs were immortalized using SV40 and hTERT to produce iFECD and iHCEC cell lines, respectively. The coding sequences of the SV40 large T antigen and hTERT genes were amplified by PCR and were TA-cloned into a commercial lentiviral vector. Thereafter, the lentiviral vectors were transfected to human embryonic kidney 293 T cells (RCB2202; Riken Bioresource Center, Ibaraki, Japan) along with three helper plasmids (pLP1, pLP2, and pLP/VSVG) using a transfection reagent. After 48 h of transfection, the supernatant of the culture medium was harvested. For lentiviral transduction, the virus-containing supernatants of both genes were added to the cultures of HCECs in the presence of 5 μg/ml of polybrene.

Cell Culture

The immortalized cells were cultured in Dulbecco's Modified Eagle's Medium (DMEM) containing 10% FBS and 1% penicillin and streptomycin. Once the immortalized cells were 80% confluent, the cells were trypsinized with 0.05% Trypsin-EDTA and passaged. For general usage, prior to seeding the cells, the culturing plates were coated with FNC-coating mix. However, for the analysis of ECM production, the culturing plates were uncoated. To test the effect of TGFβ on immortalized cells, the cells were grown to 60–70% confluence and starved in a serum-free medium for 24 h. A supplement of TGFβ1 (1, 3, and 10 ng/ml) or TGFβ2 (10 ng/ml) was added to the serum-free media for 24 h of incubation. For inhibition of the TGFβ signaling pathway, cells were supplemented with SB431542 (1, 3, and 10 μM),

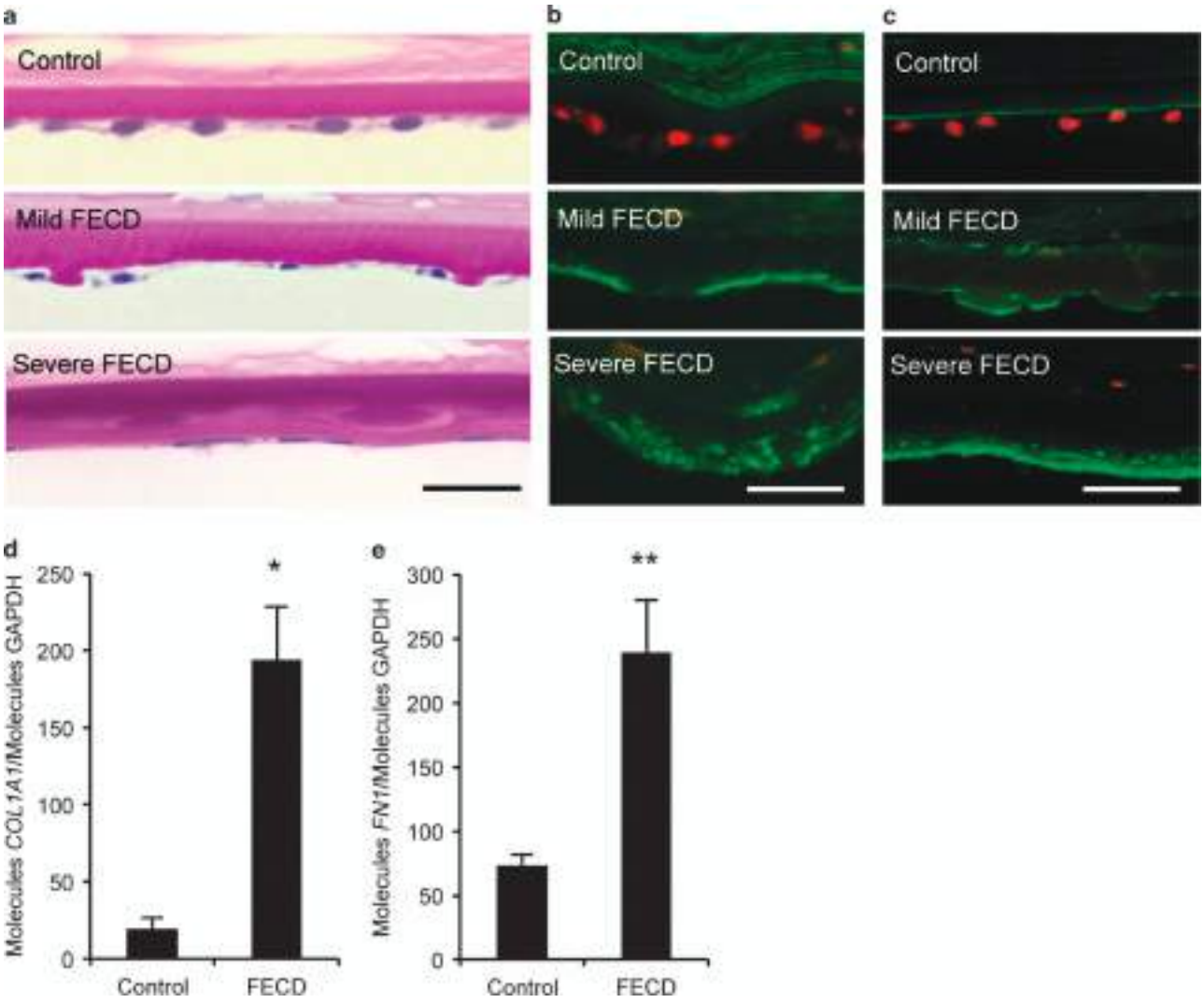

Figure 1 Expression levels of extracellular matrix (ECM) in CECs and Descemet's membrane of FECD patients. (**a**) Representative PAS staining images of healthy donor cornea and FECD patient cornea. Scale bar, 50 μm. (**b** and **c**) Expression of collagen type I (**b**) and fibronectin (**c**) in healthy donor cornea and FECD patient cornea was assessed using immunofluorescence staining. Nuclei were stained by propidium Iodide. Scale bar, 50 μm. (**d** and **e**) Quantitative determination of mRNA levels of *COL1A1* (**d**) and *FN1* (**e**) in corneal endothelial specimens from donor cornea and patients with Fuchs corneal dystrophy using real-time PCR. Data were normalized to GAPDH and are expressed as molecules of interest per molecules GAPDH. $^{*}P<0.01$, $^{**}P<0.05$. CECs, corneal endothelial cells; FECD, Fuchs endothelial corneal dystrophy; GAPDH, glyceraldehyde-3-phosphate dehydrogenase; PAS, periodic acid-Schiff.

Smad3 inhibitor (3 μM), or TGFβ1-neutralizing antibody (500 ng/ml) in serum-free medium and incubated for 24 h.

Knockdown of Genes by siRNA

The immortalized cells were seeded at a density of 2×10^4 cells/cm^2 into a 24-well plate and incubated with RNAi duplex (ZEB1: ZEB1_1, ZEB1_2, and ZEB1_3; Snail1: SNAI_1, SNAI1_2, and SNAI1_3) and Lipofectamine RNAiMAX according to the manufacturer's protocol. Random RNAi low GC was used as a control and quantitative real-time PCR was performed to assess the knockdown of the ZEB1 or Snail1 genes.

ECM Production Assay

To evaluate the ECM deposition, 1×10^5 cells were seeded onto Corning Transwell polyester membrane cell culture inserts and grown until confluence. The entire Transwell inserts were fixed with 2.5% glutaraldehyde and 2% paraformaldehyde in 0.1 M Sorensen phosphate buffer. The membranes were embedded into either OCT compound or prepared for transmission electron microscopy analysis. Cryosectioned specimens were used for hematoxylin–eosin (HE) staining and immunofluorescence staining analysis.

Periodic Acid-Schiff (PAS) Staining and Immunocytochemistry

Cryosectioned corneas were fixed with 4% paraformaldehyde and stained with PAS for inspection at the light microscope level. For immunocytochemistry, cryosectioned specimens or CECs cultured on glass slides were fixed with 4%

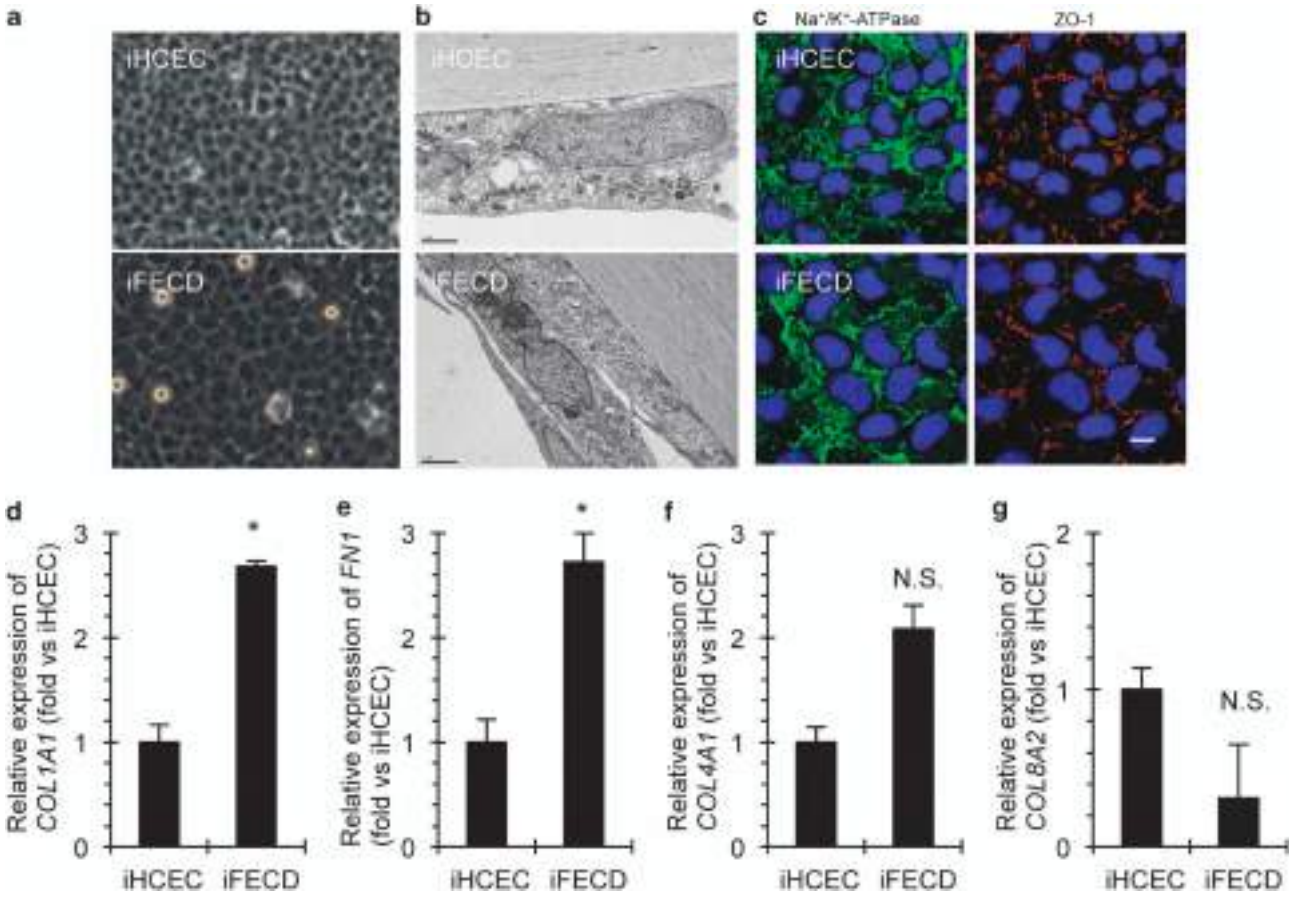

Figure 2 Excessive production of extracellular matrix (ECM) by iFECD. (**a**) Representative phase contrast images of immortalized HCEC established from three individual donor corneas (iHCEC) and immortalized HCEC established from three individual FECD patients (iFECD). Scale bar = 100 μm. (**b**) Ultra structural analysis of both iHCEC and iFECD cultured on Corning Transwell polyester membrane cell culture inserts was observed using TEM. Scale bar = 2 μm. (**c**) Function related markers of CECs (Na^+/K^+-ATPase and ZO-1) were immunostained in iHCEC and iFECD. Nuclei was stained by DAPI. Scale bar = 100 μm. (**d**–**g**) Real-time PCR was performed to analyze the expression levels of pathologic ECMs of Descemet's membrane (*COL1A1* and *FN1*) and Descemet's membrane component ECMs (*COL4A1* and *COL8A2*) both in iHCEC and iFECD. Triplicate experiments were performed in three independent iHCEC and iFECD. Representative data were shown both in iHCEC and iFECD batches. *$P < 0.01$. (**h**–**k**) iHCEC and iFECD were cultured, and the expression of collagen type I, fibronectin, and collagen types IV and VIII were assessed using immunofluorescence staining. The pictures depict three independent experiments. Scale bar = 100 μm. (**l**) ECM was morphologically analyzed by transmission electron microscopy (TEM) in iHCEC and iFECD cultured on a Corning Transwell polyester membrane cell culture insert. The representative TEM image shows that iHCEC cells maintained the normal ultra-structure morphology (i), iFECD cells exhibited indications of intracellular ECM production (ii), fibrillar ECM between cells (iii), and extracellular ECM (iv). Asterisk indicates ECM. Scale bar = **a** and **b**, 1 μm; **c**, 100 nm; and **d**, 200 nm. The pictures are representative of iHCEC and iFECD established from three independent donors and patients, respectively. (**m** and **n**) The ECM deposition was assessed by HE staining of cross-sectioned iHCEC and iFECD cultured on Corning Transwell polyester membrane cell culture inserts. The thickness of ECM was quantified by Image J software ($n = 3$). The experiment was performed in triplicate. *$P < 0.01$. Scale bar = 50 μm. CECs, corneal endothelial cells; DAPI, 4',6-diamidino-2-phenylindole; FECD, Fuchs endothelial corneal dystrophy; HE, hematoxylin and eosin; Na^+/K^+-ATPase, sodium-potassium adenosine triphosphatase; N.S., not significant; ZO-1, zonula occludens-1.

paraformaldehyde, washed with phosphate buffered saline (PBS), and blocked with 2% bovine serum albumin. Samples were incubated with antibodies against Na^+/K^+-ATPase (1:200 diluted in PBS), ZO-1 (1:300 diluted in PBS), collagen type I (1:200 diluted in PBS), collagen type IV (1:200 diluted in PBS), collagen type (α2) VIII (1:50 diluted in PBS), and fibronectin (1:200 diluted in PBS) overnight at 4 °C; washed in PBS; and incubated with a 1:1000 dilution of Alexa Fluor 488-conjugated secondary antibodies for 1 h at room temperature. Cell nuclei were stained with DAPI; then, the slides were inspected using fluorescence microscopy (TCS SP2 AOBS; Leica Microsystems, Wetzlar, Germany).

Transmission Electron Microscopy

Transwell membrane samples were washed in 0.1M Sorensen phosphate buffer, processed through 0.5% uranyl acetate *en bloc* staining, and subsequently dehydrated using an ascending ethanol series. After transferring the specimens to propylene oxide, the samples were infiltrated and embedded in Araldite CY212 resin. Ultrathin sections were collected on uncoated

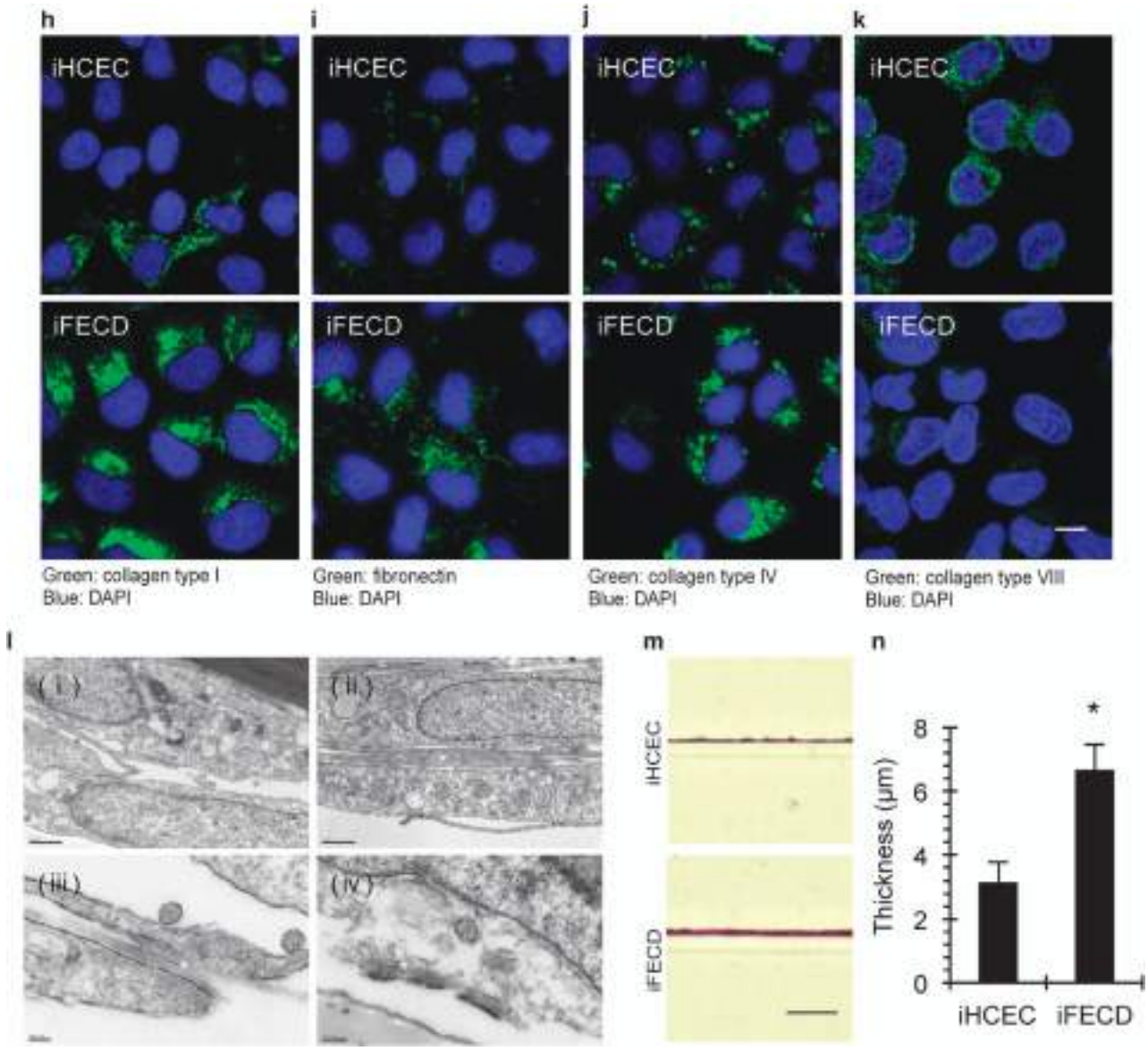

Figure 2 Continued.

G300 copper grids and stained with 1% aqueous phosphotungstic acid and uranyl acetate. Sections were examined under a transmission electron microscope (JEOL 1010; JEOL, Tokyo, Japan) equipped with a charge-coupled device camera (Orius SC1000; Gatan, Pleasanton, CA).

Quantitative Real-Time PCR

Total RNA was extracted from the corneal endothelium of the FECD patient and donor corneas, and cDNA was synthesized by utilizing 200 U Superscript II reverse transcriptase (Invitrogen, Karlsruhe, Germany) and random primers (Invitrogen). Quantitative real-time PCR was performed by MyIQ Thermal Cycler and software (Biorad, Munich, Germany). All samples were analyzed in duplicates with a program of 95 °C for 10 min and 40 cycles of 95 °C for 10 s and 60 °C for 30 s. For quantification, standard curves using serial dilutions (10^2–10^7 copies) of plasmid-cloned amplicons were run in parallel. For normalization of gene expression levels, ratios relative to glyceraldehyde-3-phosphate dehydrogenase (GAPDH) were calculated.

Gene expression levels of iHCECs and iFECDs were analyzed using TaqMan real-time PCR. Total RNA was extracted from the immortalized cells using RNeasy mini kit, and cDNA was synthesized by the use of ReverTra Ace. TaqMan primers for *COL1A1*, Hs00164004_ml; *COL4A1*, Hs00266237_ml; *COL8A2*, Hs00697025; *FN1*, Hs01549976_ml; *SNAI1*, Hs00195591_ml; *SNAI2*, Hs00950344_ml; *ZEB1*, Hs00232783_ml; and TaqMan pre-development human GAPDH (Applied Biosystems) were used. The PCR was performed using the StepOne (Applied Biosystems) real-time PCR system. GAPDH was used as an internal standard.

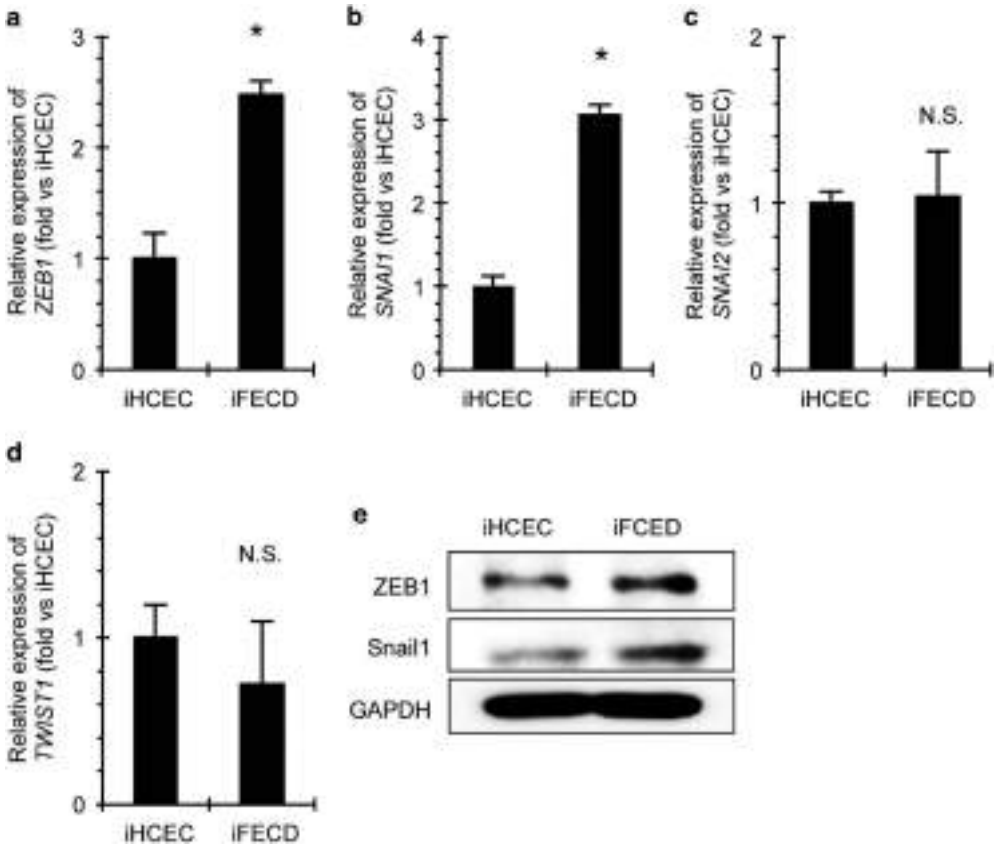

Figure 3 Expression levels of EMT-related markers in iFECD. (**a**–**d**) Expression levels of EMT-related markers (*ZEB1*, *SNAI1*, *SNAI2*, and *TWIST1*) in iHCEC and iFECD were evaluated using real-time PCR. The mean expression levels of iHCEC and iFECD established from three independent donors and patients were plotted. Triplicate experiments were performed in three independent iHCEC and iFECD. Representative data were shown both in iHCEC and iFECD batches. *$P<0.01$. (**e**) Expression levels of ZEB1 and Snail1 protein in iHCEC and iFECD were evaluated by western blotting. Experiments were performed in triplicate. EMT, epithelial mesenchymal transition; FECD, Fuchs endothelial corneal dystrophy; GAPDH, glyceraldehyde-3-phosphate dehydrogenase; N.S., not significant.

Immunoblotting

The iHCECs and iFECDs were washed with ice-cold PBS and then lysed with ice-cold RIPA buffer containing Phosphatase Inhibitor Cocktail 2 and Protease Inhibitor Cocktail. Following centrifugation at 15 000 r.p.m. for 10 min, the supernatant representing total proteins was collected. The protein concentration of the sample was assessed by use of the BCA Protein Assay Kit (Takara Bio, Otsu, Japan). The protein samples were fractionated by SDS–PAGE; proteins were transferred to PVDF membranes. The membranes were blocked with 3% non-fat dry milk for 1 h at RT and were incubated overnight at 4 °C with the following primary antibodies: ZEB1 (1:1000), Snail1 (1:1000), fibronectin (1:1000), and GAPDH (1:3000). After washing, the blots were incubated with horseradish peroxidase-conjugated secondary antibodies (1:5000). The blots were then developed with luminal for enhanced chemiluminescence using the ECL Advanced Western Blotting Detection Kit (GE Healthcare, Piscataway, NJ), documented using an LAS4000S (Fuji Film, Tokyo, Japan).

Statistical Analysis

The statistical significance (*P*-value) of differences between mean values of the two-sample comparison was determined by use of the Student's *t*-test. The comparison of multiple sample sets was analyzed using Dunnett's multiple-comparison test. The values shown in the graphs represent the mean ± s.e.m.

RESULTS

FECD Cellular Model Shows Excessive ECM Production

PAS staining showed that Descemet's membrane was thicker in FECD patients associated with excrescences 'clinically called guttae' than that in control patients (Figure 1a). Similar to previous reports,[14,15] thickened Descemet's membrane expressed type I collagen and fibronection (Figures 1b and c). Real-time PCR demonstrated that the expression of FECD-related ECM, *COL1A1* and *FN1*, were significantly higher in FECD than in control (Figures 1d and e). Next, we cultured CECs derived from three FECD patients and three normal control corneas and immortalized by introduction of SV40 and hTERT genes to establish the cellular model of FECD.

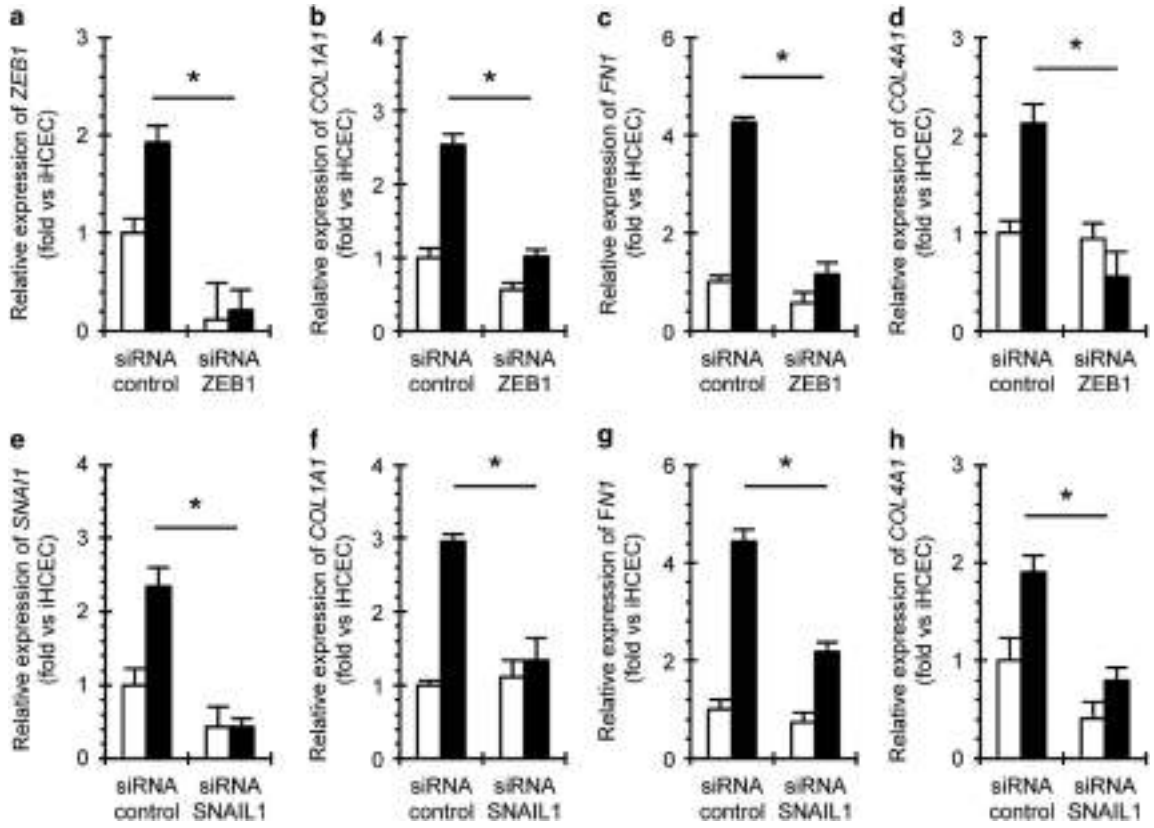

Figure 4 An upregulation of EMT-related genes was seen in iFECD cells. (**a**) Knockdown of ZEB1 gene by siRNA was confirmed by real-time PCR. *$P<0.01$. (**b**–**d**) ZEB1 gene was knocked down by siRNA, and expression levels of *COL1A1*, *FN1*, and *COL4A1* were analyzed using real-time PCR. *$P<0.01$. (**e**) Knockdown of Snail1 gene by siRNA was confirmed by real-time PCR. *$P<0.01$. (**f**–**h**) Snail1 gene was knocked down by siRNA, and expression levels of *COL1A1*, *FN1*, and *COL4A1* were analyzed using real-time PCR. *$P<0.01$. (**i**–**k**) ZEB1 and Snail1 was, respectively, knocked down by siRNA in iHCEC and iFECD, and production of collagen type I, fibronectin, and collagen types IV was evaluated using immunostaining. Scale bar = 100 μm. (**l** and **m**) iHCEC and iFECD of which ZEB1 and Snail1 gene was knocked down by siRNA were cultured on Corning Transwell polyester membrane cell culture inserts for 48 h. The thickness of ECM was stained by HE and was quantified by Image J software ($n=3$). The experiment was performed in triplicate. *$P<0.01$. Scale bar = 50 μm. DAPI, 4',6-diamidino-2-phenylindole; EMT, epithelial mesenchymal transition; FECD, Fuchs endothelial corneal dystrophy; HE, hematoxylin and eosin.

Phase contrast microscopy and transmission electron microscopy (TEM) of representative iHCEC and iFECD demonstrated that both cell lines formed a regular monolayer comprising contact-inhibited hexagonal cells resembling an endothelial monolayer *in vivo* (Figures 2a and b). The two cell lines were further examined for the expression of markers indicating endothelial cell function, thereby revealing characteristic staining patterns for Na^+/K^+-ATPase and ZO-1 at the plasma membranes (Figure 2c). An analysis of the expression of FECD-related ECM genes using real-time PCR demonstrated that expression levels of *COL1A1* and *FN1* were significant and those for *COL4A1* were increased in iFECD compared with iHCEC, whereas expression levels of *COL8A2* were reduced in iFECD compared with those in iHCEC (Figures 2d–g). Corresponding immunofluorescence analyses showed that the protein expression of type I collagen, fibronectin, and type IV collagen was more pronounced in iFECD than in iHCEC, whereas staining of type VIII collagen was negligible in iFECD cells (Figures 2h–k), thereby confirming the mRNA expression data. Furthermore, TEM analysis showed the obvious presence of fibrillar ECM in-between cells, intracellular, and between cell and substrate in iFECD; iHCEC cells maintained normal ultra-structure morphology (Figure 2l). To analyze the amount of ECM produced by iFECD and iHCEC, cells were cultured on Corning Transwell polyester membrane culture inserts until confluence. The accumulated ECM comprising types I, IV, and VIII collagen and fibronectin (Supplementary Figure S1) was visualized by HE staining and was found to be significantly broader in iFECD cultures than in iHCEC (6.65 ± 0.82 μm and 3.14 ± 0.64 μm, respectively) (Figures 2m and n). To analyze the potential molecular mechanisms of increased ECM production in iFECD, we investigated the expression of EMT-inducing genes—*ZEB1*, *SNAI1*, *SNAI2*, and *TWIST1*—in both cell lines (Figures 3a–d). The expression of *ZEB1* and *SNAI1* was significantly upregulated in iFECD as compared with iHCEC, while *SNAI2* and *TWIST1* did not show any significant differences in expression levels. Coincidentally, western blotting demonstrated that the expression of ZEB1 and Snail1 was upregulated in iFECD as compared with that in iHCEC at protein level (Figure 3e).

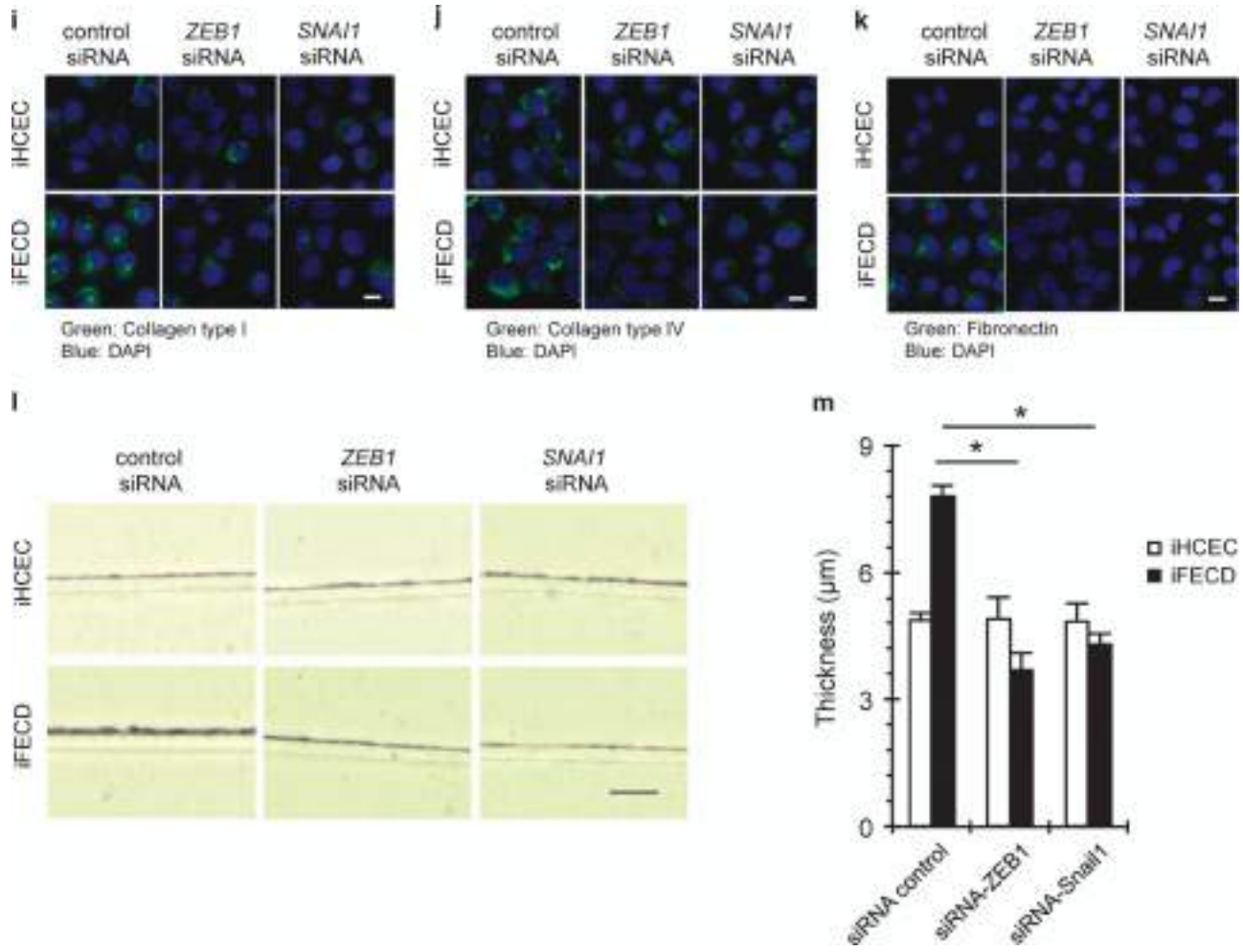

Figure 4 Continued.

ZEB1 and Snail1 Regulate the Excessive Production of ECM in FECD

To further elucidate the involvement of ZEB1 and Snail1 in the production of excessive ECM in FECD cells, we employed a gene knockdown strategy using siRNA. Real-time PCR analysis showed that expression levels of *COL1A1*, *FN1*, and *COL4A1* were significantly decreased in iFECD, but not in iHCEC after knockdown of both ZEB1 and Snail1 genes (Figures 4a–h). In accordance, immunofluorescent staining showed decreased production of type I collagen, fibronectin, and type IV collagen following downregulation of ZEB1 and Snail1 only in iFECD (Figures 4i–k). Consistently, the thickness of ECM deposited by iFECD treated with *ZEB1* siRNA or *SNAI1* siRNA was significantly lower than that treated with random siRNA ($3.70 \pm 0.4\,\mu$m, $4.31 \pm 0.3\,\mu$m, and $7.79 \pm 0.3\,\mu$m, respectively), whereas the thickness of ECM deposited by iHCEC was unaffected (Figures 4l and m). These observations suggested that both ZEB1 and Snail1 played a crucial role in regulating the ECM production in FECD cells.

TGF-β Induces ECM in FECD via Upregulation of ZEB1 and Snail1

Since TGF-β signaling is known to be involved in the activation of EMT-related genes in various tissues,[16] we assessed the effect of exogenous TGF-β on expression of ZEB1 and Snail1 in CECs. We demonstrated that TGF-β1 increased the expression of *ZEB1* in iFECD, but not in iHCEC (Figure 5a), as well as the expression of *SNAI1* both in iFECD and iHCEC in a dose-dependent manner (Figure 5b). Moreover, expression levels of *COL1A1*, *COL4A1*, *FN1*, and *COL8A2* were significantly upregulated in iFECD, but not in iHCEC by TGF-β in a dose-dependent manner (Figures 5c–f). Western blotting demonstrated that TGF-β increased the expression of ZEB1 in iFECD, but not in iHCEC. Moreover, production of fibronection was evident in iFECD by TGF-β stimulation, but less evident in iHCEC (Figure 5g). Correspondingly, the thickness of ECM increased significantly from 6.42 ± 0.2 to $8.71 \pm 0.3\,\mu$m in iFECD on TGF-β stimulation, whereas it was not altered by TGF-β in iHCEC (Figures 5h and i). These observations suggest that excessive ECM production in iFECD

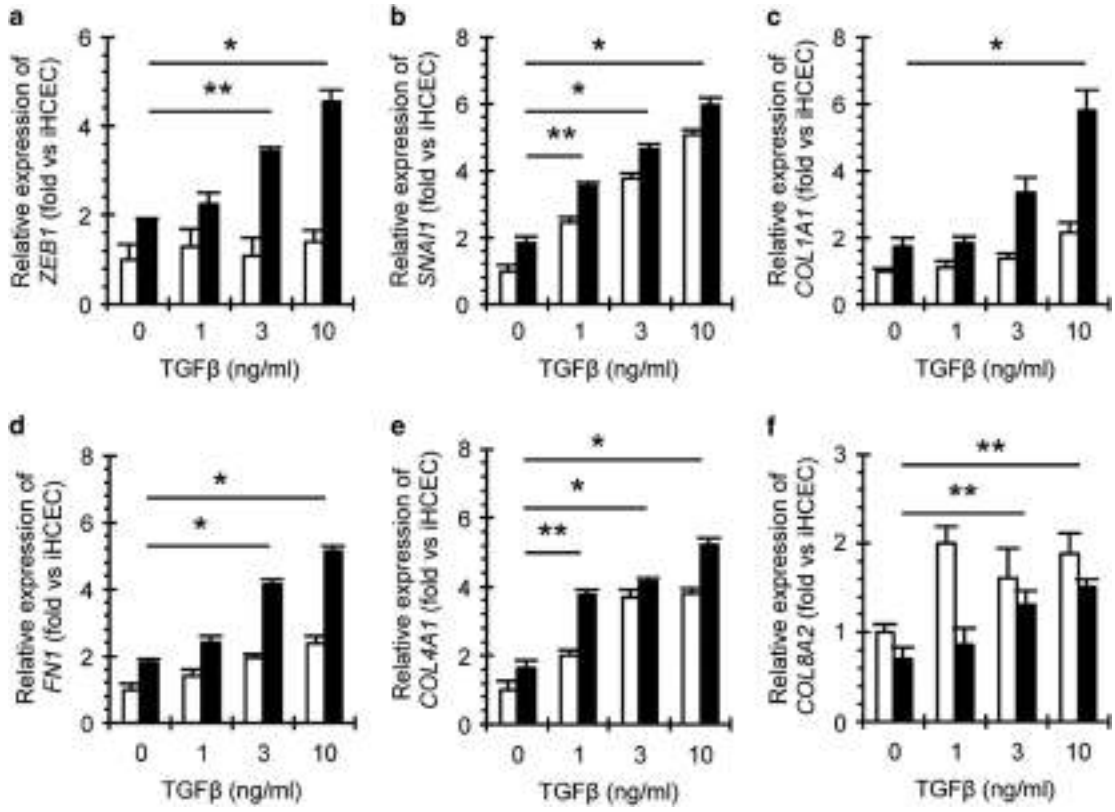

Figure 5 The effect of TGFβ on ZEB1, Snail1 expression, and on the production of ECM in iFECD. Upregulation of ZEB1 and Snail1 in iFECD cells hyper-responded against TGFβ. (**a**–**f**) iHCEC and iFECD were stimulated by TGFβ1 (0, 1, 3, and 10 ng/ml) for 24 h. Expression mRNA of *ZEB1*, *SNAI1*, *COL1A1*, *FN1*, and *COL4A1* was evaluated by real-time PCR. The experiments were performed in duplicate in three independent batches of iHCEC and iFECD. $^{*}P<0.01$. $^{**}P<0.05$. (**g**) iHCEC and iFECD were stimulated by TGFβ1 (10 ng/ml) for 24 h following 24-h serum starvation. Expression levels of ZEB1, Snail1, and fibronectin in iHCEC and iFECD were evaluated by western blotting. Experiments were performed in triplicate. (**h** and **i**) iHCEC and iFECD were cultured on Corning Transwell polyester membrane cell culture inserts and were stimulated by TGFβ1 (10 ng/ml) for 24 h. The thickness of ECM was stained by HE and was quantified by Image J software ($n=3$). The experiment was performed in triplicate. $^{*}P<0.01$. Scale bar = 50 μm. ECM, extracellular matrix; FECD, Fuchs endothelial corneal dystrophy; GAPDH, glyceraldehyde-3-phosphate dehydrogenase; HE, hematoxylin and eosin.

may be the consequence of an increased responsiveness to TGF-β stimulation as compared with iHCEC.

Inhibition of TGF-β Signaling Pathway Suppresses Excessive ECM Production via Downregulation of ZEB1 and Snail1

The observations that the downregulation of ZEB1 and Snail1 suppressed ECM production and that TGF-β increased expression of ZEB1 and Snail1 in iFECD led us to assess the effect of inhibition of TGF-β signaling on ECM production. Treatment of cells with SB431542, an inhibitor of TGF-β type I ALK receptors, significantly suppressed expression levels of *ZEB1* and *SNAI1* in iFECD (Figures 6a and b). Moreover, the mRNA levels of *COL1A1*, *FN1*, *COL4A1*, and *COL8A2* were significantly reduced by SB431542 in iFECD (Figures 6c–f). Although TGF-β-stimulated ECM production was more pronounced in iFECD than in iHCEC, SB431542 decreased the expression of ECM proteins in iFECD and iHCEC to similar levels (Figures 6g–j). The thickness of ECM produced by iFECD (5.5 ± 0.3 μm) was significantly increased by TGF-β2 (7.3 ± 0.6 μm), as well as TGF-β1 (9.4 ± 0.3 μm) (Figures 7a and b). We also demonstrated that Smad3 inhibitor (3 μM) and TGF-β1-neutralizing antibody (500 ng/ml) suppressed the production of ECM to a level similar to that achieved by SB431542 in iFECD after 48-h cultivation (Figures 7a and b), thereby suggesting that inhibition of TGF-β signaling downregulates excessive ECM production.

DISCUSSION

In the case of FECD, Descemet's membrane is thickened two to threefold.[17] The thickened Descemet's membrane and excrescences comprise several ECMs such as collagen types I, IV, and VIII; fibronection; and laminin—these were considered to be secreted by affected CECs.[14] Since small sample size obtained from FECD patients is an obstacle for researchers,[11] we established an *in vitro* cellular model of FECD by immortalization of the CECs received from late-onset FECD patients. The data presented in this study identified potential overexpressed ECM proteins, which include collagen type I and fibronectin at both mRNA and protein levels and probably contribute to the excessive ECM deposition found in Descemet's membrane in FECD.

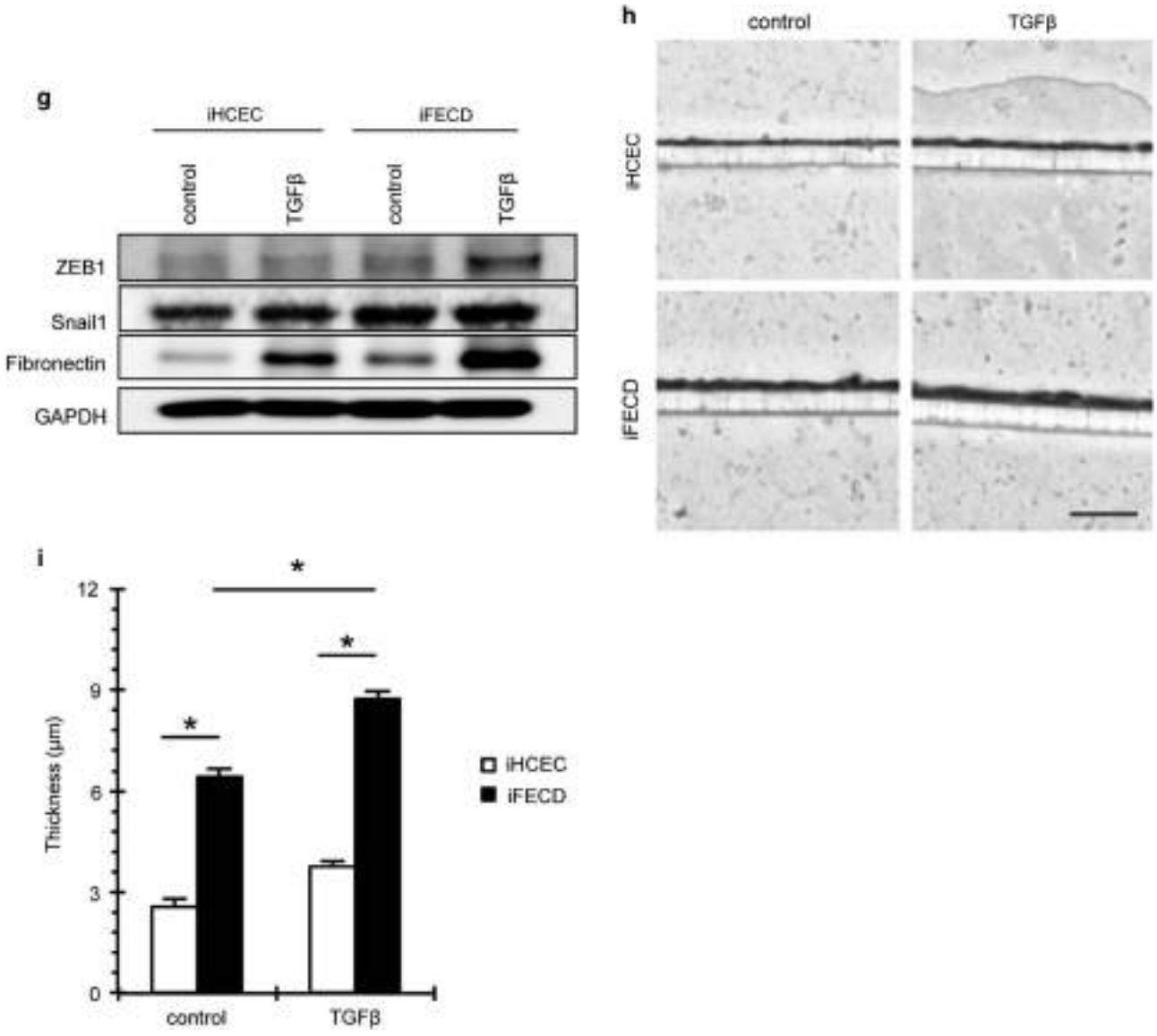

Figure 5 Continued.

However, the pathology of excessive secretion and deposition of ECM in Descemet's membrane was not clearly understood. Our current study highlights that the EMT inducer genes cause excessive ECM in FECD. EMT has an important role in appropriate embryonic development, wound healing, tissue regeneration, organ fibrosis, and cancer progression.[18,19] Although the expression of EMT inducers is silenced in the adult organism, reactivation occurs when epithelial homeostasis is disturbed, such as during the fibroblastic process that occurs during organ degeneration.[18] The corneal endothelium can undergo fibroblastic transformation in association with fibrotic ECM alterations in advanced stages of several disorders that involve progressive endothelial dysfunction, such as FECD, pseudoexfoliation syndrome, corneal endotheliitis, and corneal trauma; these fibroblastic changes are recognized as EMT.[20–23] Here, we provide evidence that the upregulation of ECM components in FECD is caused by EMT inducers such as ZEB1 and Snail1, even though cell morphology is maintained as an endothelial phenotype without fibroblastic transformation.

Wieben *et al*[24] demonstrated that the trinucleotide repeat expansion in *TCF4* is strongly associated with late-onset FECD; >50 trinucleotide repeats were found in 79% of FECD and 3% of control. Furthermore, transcription of CTG repeats resulted in nuclear foci containing condensed poly $(CUG)_n$ RNA and muscleblind-like1 (MBNL1) protein, an mRNA-splicing factor.[25,26] As MBNL1 is known to have a role in EMT in other types of cells,[27,28] the possibility that CTG repeats in *TCF4* are related to the activation of EMT inducer genes in FECD needs to be further investigated to elucidate the pathophysiology of FECD. The cellular models of FECD were established from three different patients in our current

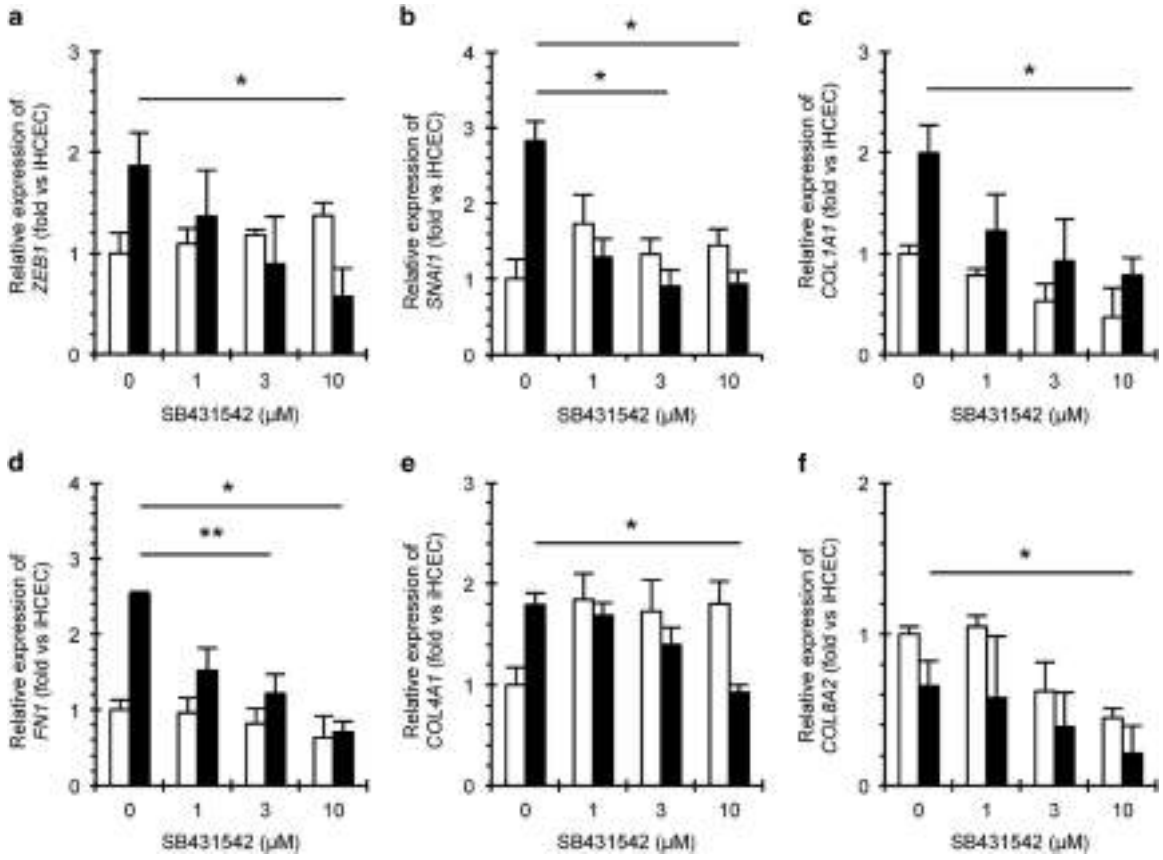

Figure 6 The effect of inhibiting TGFβ signaling pathway on suppressing ZEB1 and Snail1 gene expression, as well as on the production of ECM in iFECD. (**a**–**f**) iHCEC and iFECD were cultured with SB431542 (1, 3, and 10 μM) for 24 h. Expression mRNA of *ZEB1*, *SNAI1*, *COL1A1*, *FN1*, and *COL4A1* was evaluated using real-time PCR. The experiments were performed in duplicate in three independent batches of iHCEC and iFECD. $^{*}P<0.01$. $^{**}P<0.05$. (**g**–**j**) iHCEC and iFECD were cultured with SB431542 (10 μM) for 24 h and production of collagen type I, fibronectin, and collagen type IV was evaluated using immunofluorescence staining. The experiments were performed in three independent batches of iHCEC and iFECD. Scale bar = 100 μm. DAPI, 4',6-diamidino-2-phenylindole; ECM, extracellular matrix; FECD, Fuchs endothelial corneal dystrophy.

experiments, but whether patients possess CTG repeats in TCF4 was not investigated. Future experiments that establish cellular models derived from FECD patients associated with CTG repeats in TCF4 might provide a better understanding of how repeats cause the disease.

ZEB1, a zinc-finger transcription factor that binds to E2 box DNA sequence is involved in EMT through its regulation by TGF-β, FGF, and the miR200 family of microRNAs.[16] The *TCF4* codes for the helix-loop-helix transcription factor E2-2 that regulates cell growth and differentiation.[29] Since E2-2 regulates ZEB1 expression, it is hypothesized that altering E2-2 function by *TCF4* variants affects ZEB1 in late-onset FECD.[10] Our study provided evidence that supports the hypothesis that ZEB1 is highly expressed in FECD and induces an EMT-like phenotype with a hallmark phenotype of FECD—secretion of excessive ECM. Interestingly, *ZEB1* missense mutations were found in 7 of 384 unrelated individuals with FECD;[7] this also suggests that ZEB1 has a role in the pathogenesis of FECD.

Snail is a common downstream target of various signaling pathways that regulate EMT.[30] Although Snail1 and Snaill2 in Snail family members of zinc-finger proteins (Snail1, Snail2, and Snail3) are reported to mediate EMT in various organs,[30] we found that Snail1, not Snail2, is highly expressed in FECD. Snail regulates EMT phenotypes, such as increased expression of mesenchymal cell markers and decreased expression of epithelial markers.[30] Although Snail1 is well-recognized as an EMT inducer, an EMT-independent role is also reported.[30] In an EMT-independent role, Snail1 acts as a potent survival factor against apoptotic stimuli through the death receptor and DNA damage.[31,32] Therefore, the possibility that Snail1 is induced in FECD by an apoptotic signal and acts as a pro-apoptotic factor must be further studied.

Our study highlights that the inhibition of TGF-β signaling represses excessive ECM production by suppressing ZEB1 and Snail1 expression in FECD, thereby confirming the findings of previous studies that TGF-β induces the expression of transcription factors and transcription regulators involved in EMT in several tissues.[33] Furthermore, with regard to the

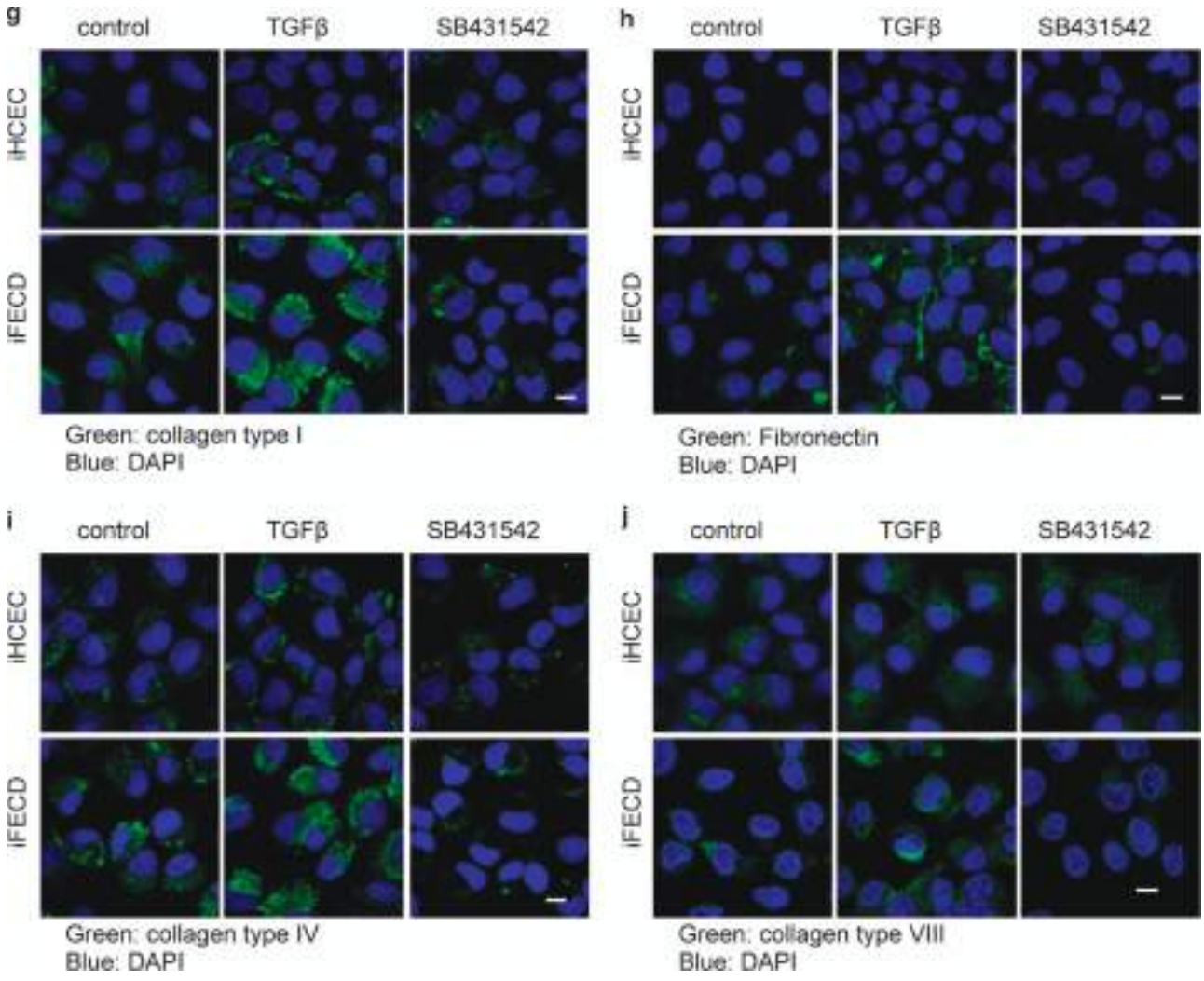

Figure 6 Continued.

corneal endothelium, we recently reported that TGF-β triggers the secretion of fibrillar ECM proteins, such as type I collagen and fibronectin, in CECs.[12] Since concentration of TGF-β is higher in the aqueous humor than in serum, and TGF-β is believed to be involved in the pathogenesis of FECD, as well as the homeostasis of the corneal endothelium.[34] In this regard, we proposed that highly expressed ZEB1 and Snail1 in FECD were responsible for the hyper-response to TGF-β in the aqueous humor and excessive production of ECM. Further, since abundant production of ECM proteins increase the amount of unfolded protein at endoplasmic reticulum (ER) stress,[11] we speculated that excessive ECM causes not only guttae and thickening of Descemet's membrane, but also apoptosis caused by ER stress. The ER is the cellular compartment that is involved in protein folding and maturation, and many different perturbations lead to the accumulation of unfolded or misfolded proteins in the ER, thereby causing ER stress.[35] Further studies that clarify whether excessive production of ECM induces ER stress and then triggers apoptosis of CECs of FECD are necessary.

To the best of our knowledge, this is the first report of EMT-related genes such as ZEB1 and Snail1 as a mechanism of inducing excessive ECM proteins in late-onset FECD. Although future research is needed to elucidate whether excessive ECM proteins induce apoptosis of the corneal endothelium caused by ER stress, in this study we proposed that regulating EMT inducer genes by the suppression of the TGF-β signaling pathway may be a feasible therapeutic tool for FECD.

Supplementary Information accompanies the paper on the Laboratory Investigation website (http://www.laboratoryinvestigation.org)

ACKNOWLEDGMENTS

We are grateful to Dr Matthias Zenkel for the valuable advice and Dr Kenta Yamasaki for providing technical assistance. This work was supported by The Funding Program for Next Generation World-Leading Researchers from the Cabinet Office in Japan (Koizumi N: LS117).

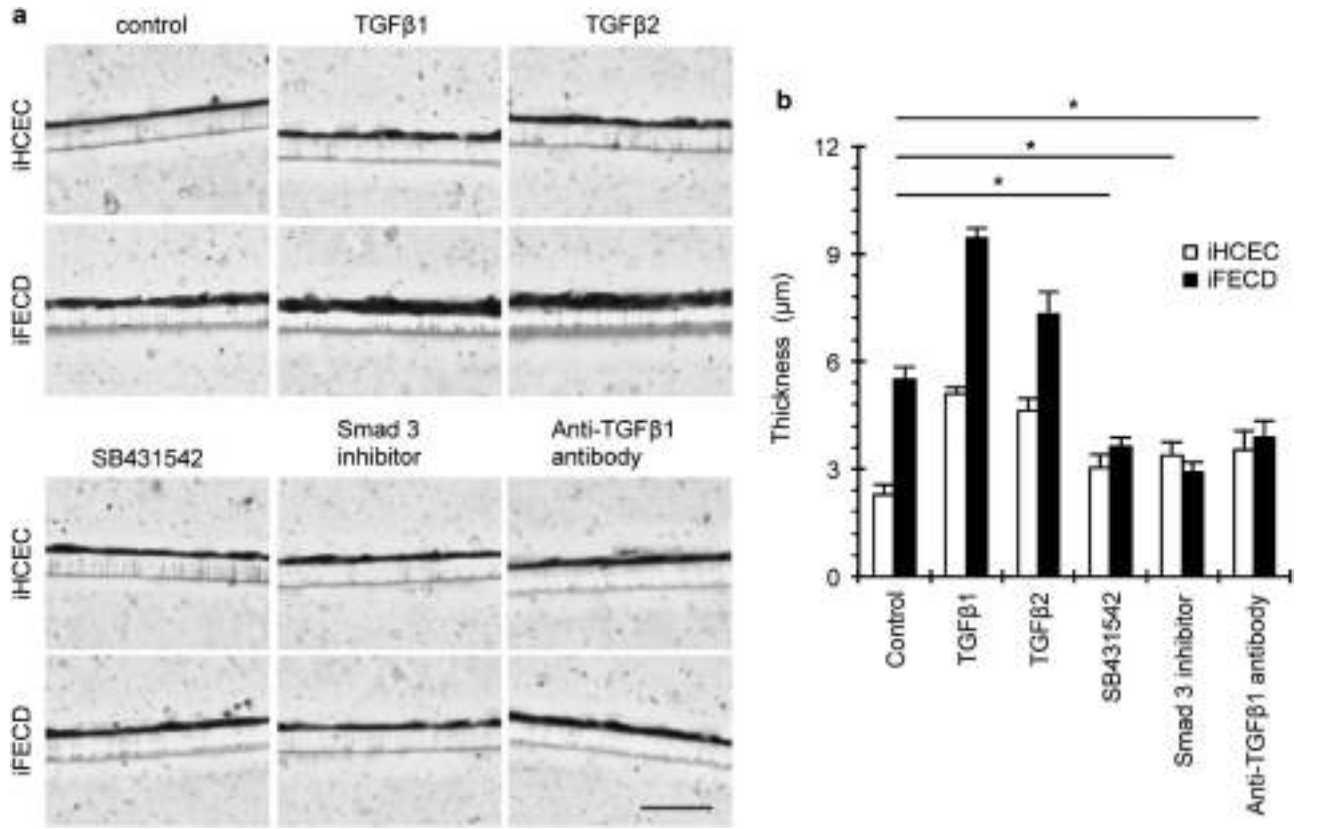

Figure 7 Effect of inhibition of the TGFβ signaling pathway on excessive production of ECM in iFECD. (**a**) iHCEC and iFECD were cultured on Corning Transwell polyester membrane cell culture inserts and were treated with TGFβ1 (10 ng/ml), TGFβ2 (10 ng/ml), SB431542 (10 μM), Smad3 inhibitor (3 μM), or anti-TGFβ1 antibody (500 ng/ml) for 24 h. Accumulated ECM was evaluated using HE staining. (**b**) The thickness of ECM was quantified by Image J software ($n = 3$). The experiment was performed in triplicate. *$P < 0.01$. Scale bar = 50 μm. ECM, extracellular matrix; FECD, Fuchs endothelial corneal dystrophy; HE, hematoxylin and eosin.

DISCLOSURE/CONFLICT OF INTEREST

NO, US-S, FEK, SK, and NK have potential financial competing interests (patents currently pending). LTYH, EPK, SK, TT, RDY and AJQ declare no conflict of interest.

1. Chi HH, Teng CC, Katzin HM. Histopathology of primary endothelial-epithelial dystrophy of the cornea. Am J Ophthalmol 1958;45:518–535.
2. Kenney MC, Labermeier U, Hinds D *et al.* Characterization of the descemet's membrane/posterior collagenous layer isolated from fuchs' endothelial dystrophy corneas. Exp Eye Res 1984;39:267–277.
3. Tan DT, Dart JK, Holland EJ *et al.* Corneal transplantation. Lancet 2012;379:1749–1761.
4. Lorenzetti DW, Uotila MH, Parikh N *et al.* Central cornea guttata. incidence in the general population. Am J Ophthalmol 1967;64: 1155–1158.
5. America Eye Bank Association of America. Eye Banking Statistical Report. Washington, DC, USA 2012.
6. Mehta JS, Vithana EN, Tan DT *et al.* Analysis of the posterior polymorphous corneal dystrophy 3 gene, Tcf8, in late-onset fuchs endothelial corneal dystrophy. Invest Ophthalmol Vis Sci 2008;49:184–188.
7. Riazuddin SA, Zaghloul NA, Al-Saif A *et al.* Missense mutations in Tcf8 cause late-onset fuchs corneal dystrophy and interact with Fcd4 on chromosome 9p. Am J Hum Genet 2010;86:45–53.
8. Vithana EN, Morgan PE, Ramprasad V *et al.* slc4a11 mutations in fuchs endothelial corneal dystrophy. Hum Mol Genet 2008;17:656–666.
9. Riazuddin SA, Vithana EN, Seet LF *et al.* Missense mutations in the sodium borate cotransporter Slc4a11 cause late-onset fuchs corneal dystrophy. Hum Mutat 2010;31:1261–1268.
10. Baratz KH, Tosakulwong N, Ryu E *et al.* E2-2 protein and fuchs's corneal dystrophy. N Engl J Med 2010;363:1016–1024.
11. Engler C, Kelliher C, Spitze AR *et al.* Unfolded protein response in fuchs endothelial corneal dystrophy: a unifying pathogenic pathway? Am J Ophthalmol 2010;149:194–202.
12. Okumura N, Kay EP, Nakahara M *et al.* Inhibition of Tgf-Beta signaling enables human corneal endothelial cell expansion *in vitro* for use in regenerative medicine. PLoS One 2013;8:e58000.
13. Okumura N, Nakano S, Kay EP *et al.* Involvement of cyclin D and P27 in cell proliferation mediated by rock inhibitors Y-27632 and Y-39983 during corneal endothelium wound healing. Invest Ophthalmol Vis Sci 2014;55:318–329.
14. Gottsch JD, Zhang C, Sundin OH *et al.* Fuchs corneal dystrophy: aberrant collagen distribution in an L450w mutant of the Col8a2 gene. Invest Ophthalmol Vis Sci 2005;46:4504–4511.
15. Weller JM, Zenkel M, Schlotzer-Schrehardt U *et al.* Extracellular matrix alterations in late-onset fuchs' corneal dystrophy. Invest Ophthalmol Vis Sci 2014;55:3700–3708.
16. Miyazono K. Transforming growth factor-beta signaling in epithelial-mesenchymal transition and progression of cancer. Proc Jpn Acad Ser B Phys Biol Sci 2009;85:314–323.
17. Goar EL. Dystrophy of the corneal endothelium (cornea guttata), with report of a histologic examination. Trans Am Ophthalmol Soc 1933;31:48–59.
18. Acloque H, Adams MS, Fishwick K *et al.* Epithelial-mesenchymal transitions: the importance of changing cell state in development and disease. J Clin Invest 2009;119:1438–1449.
19. Kalluri R. Emt: when epithelial cells decide to become mesenchymal-like cells. J Clin Invest 2009;119:1417–1419.

20. Naumann GO, Schlotzer-Schrehardt U. Keratopathy in pseudoexfoliation syndrome as a cause of corneal endothelial decompensation: a clinicopathologic study. Ophthalmology 2000;107:1111–1124.
21. Kawaguchi R, Saika S, Wakayama M *et al.* Extracellular matrix components in a case of retrocorneal membrane associated with syphilitic interstitial keratitis. Cornea 2001;20:100–103.
22. Koizumi N, Suzuki T, Uno T *et al.* Cytomegalovirus as an etiologic factor in corneal endotheliitis. Ophthalmology 2008;115:292–297.
23. Song JS, Lee JG, Kay EP. Induction of Fgf-2 synthesis by Il-1beta in aqueous humor through P13-kinase and P38 in rabbit corneal endothelium. Invest Ophthalmol Vis Sci 2010;51:822–829.
24. Wieben ED, Aleff RA, Tosakulwong N *et al.* A common trinucleotide repeat expansion within the transcription factor 4 (Tcf4, E2-2) gene predicts fuchs corneal dystrophy. PLoS One 2012;7:e49083.
25. Du J, Aleff RA, Soragni E *et al.* RNA toxicity and missplicing in the common eye disease fuchs endothelial corneal dystrophy. J Biol Chem 2015;290:5979–5990.
26. Mootha VV, Hussain I, Cunnusamy K *et al.* Tcf4 triplet repeat expansion and nuclear RNA foci in Fuchs' endothelial corneal dystrophy. Invest Ophthalmol Vis Sci 2015;56:2003–2011.
27. LeMasters KE, Blech-Hermoni Y, Stillwagon SJ *et al.* Loss of muscleblind-like 1 promotes invasive mesenchyme formation in endocardial cushions by stimulating autocrine Tgfbeta3. BMC Dev Biol 2012;12:22.
28. Venables JP, Brosseau JP, Gadea G *et al.* Rbfox2 is an important regulator of mesenchymal tissue-specific splicing in both normal and cancer tissues. Mol Cell Biol 2013;33:396–405.
29. Murre C, Bain G, van Dijk MA *et al.* Structure and function of helix-loop-helix proteins. Biochim Biophys Acta 1994;1218: 129–135.
30. Barrallo-Gimeno A, Nieto MA. The snail genes as inducers of cell movement and survival: implications in development and cancer. Development 2005;132:3151–3161.
31. Kajita M, McClinic KN, Wade PA. Aberrant expression of the transcription factors snail and slug alters the response to genotoxic stress. Mol Cell Biol 2004;24:7559–7566.
32. Martinez-Alvarez C, Blanco MJ, Perez R *et al.* Snail family members and cell survival in physiological and pathological cleft palates. Dev Biol 2004;265:207–218.
33. Argast GM, Krueger JS, Thomson S *et al.* Inducible expression of Tgfbeta, Snail and Zeb1 recapitulates Emt *in vitro* and *in vivo* in a Nsclc model. Clin Exp Metastasis 2011;28:593–614.
34. Klenkler B, Sheardown H. Growth factors in the anterior segment: role in tissue maintenance, wound healing and ocular pathology. Exp Eye Res 2004;79:677–688.
35. Hetz C, Chevet E, Harding HP. Targeting the unfolded protein response in disease. Nat Rev Drug Discov 2013;12:703–719.

OXFORD

Human Molecular Genetics, 2015, Vol. 24, No. 13 3880–3892

doi: 10.1093/hmg/ddv128
Advance Access Publication Date: 10 April 2015
Original Article

ORIGINAL ARTICLE

A common variant near *TGFBR3* is associated with primary open angle glaucoma

Zheng Li[1,3,†], R. Rand Allingham[4,†], Masakazu Nakano[5,†], Liyun Jia[8,†], Yuhong Chen[9,†], Yoko Ikeda[6], Baskaran Mani[1,11,13], Li-Jia Chen[14], Changwon Kee[15], David F. Garway-Heath[16], Sarangapani Sripriya[17], Nobuo Fuse[18], Khaled K. Abu-Amero[19,20], Chukai Huang[21], Prasanthi Namburi[22], Kathryn Burdon[23,24], Shamira A. Perera[1,13,2], Puya Gharahkhani[25], Ying Lin[26,27], Morio Ueno[6], Mineo Ozaki[28], Takanori Mizoguchi[29], Subbiah Ramasamy Krishnadas[30], Essam A. Osman[19], Mei Chin Lee[1], Anita S.Y. Chan[1,2], Liza-Sharmini A. Tajudin[31], Tan Do[32], Aurelien Goncalves[33], Pascal Reynier[34], Hong Zhang[35], Rupert Bourne[36], David Goh[2], David Broadway[37], Rahat Husain[2], Anil K. Negi[38], Daniel H Su[2], Ching-Lin Ho[2], Augusto Azuara Blanco[39], Christopher K.S. Leung[14], Tina T. Wong[1,13,2], Azhany Yakub[31], Yutao Liu[40,41], Monisha E. Nongpiur[1,11,13], Jong Chul Han[15], Do Nhu Hon[32], Balekudaru Shantha[42], Bowen Zhao[8], Jinghong Sang[8], NiHong Zhang[8], Ryuichi Sato[5], Kengo Yoshii[7], Songhomita Panda-Jonas[43], Allison E. Ashley Koch[40], Leon W. Herndon[4], Sayoko E. Moroi[44], Pratap Challa[4], Jia Nee Foo[3], Jin-Xin Bei[46,47], Yi-Xin Zeng[46,47], Cameron P. Simmons[48,49], Tran Nguyen Bich Chau[48], Philomenadin Ferdinamarie Sharmila[17], Merwyn Chew[1], Blanche Lim[1], Pansy O.S. Tam[14], Elaine Chua[1], Xiao Yu Ng[1], Victor H.K. Yong[1], Yaan Fun Chong[1], Wee Yang Meah[3], Saravanan Vijayan[22], Sohn Seongsoo[15], Wang Xu[12], Yik Ying Teo[3,12], Jessica N. Cooke Bailey[50], Jae H. Kang[51], Jonathan L. Haines[50], Ching Yu Cheng[1,11,13,2], Seang-Mei Saw[1,12], E-Shyong Tai[52], ICAARE-Glaucoma Consortium[‡], NEIGHBORHOOD Consortium[‡], Julia E. Richards[44,45], Robert Ritch[53], Douglas E. Gaasterland[54],

[†] These authors contributed equally to this work.
[‡] A list of members of each consortium appears in the Supplementary Material, Note.
[¶] These authors also contributed equally to this work.
Received: December 1, 2014. **Revised:** March 9, 2015. **Accepted:** April 8, 2015

Louis R. Pasquale[51,55], Jianjun Liu[3], Jost B. Jonas[43], Dan Milea[1,13,2], Ronnie George[42], Saleh A. Al-Obeidan[19], Kazuhiko Mori[6], Stuart Macgregor[25], Alex W. Hewitt[23,56], Christopher A. Girkin[57], Mingzhi Zhang[21], Periasamy Sundaresan[22], Lingam Vijaya[42], David A. Mackey[23,58], Tien Yin Wong[1,2,11], Jamie E. Craig[24], Xinghuai Sun[9,10,59], Shigeru Kinoshita[6], Janey L. Wiggs[57,¶], Chiea-Chuen Khor[3,11,¶,*], Zhenglin Yang[26,27,60,¶], Chi Pui Pang[14,¶], Ningli Wang[8,¶], Michael A. Hauser[4,40,¶], Kei Tashiro[5,¶], Tin Aung[1,2,11,13,¶] and Eranga N. Vithana[1,11,13,¶,*]

[1]Singapore Eye Research Institute, [2]Singapore National Eye Center, Singapore, Singapore, [3]Division of Human Genetics, Genome Institute of Singapore, Singapore, Singapore, [4]Department of Ophthalmology, Duke University Eye Center, Durham, NC, USA, [5]Department of Genomic Medical Sciences, [6]Department of Ophthalmology, [7]Department of Medical Statistics, Kyoto Prefectural University of Medicine, Kyoto, Japan, [8]Beijing Ophthalmology & Visual Sciences Key Laboratory, Beijing Tongren Eye Centre, Beijing Tongren Hospital, Capital Medical University, Beijing, China, [9]Department of Ophthalmology and Visual Science, Eye and ENT Hospital, Shanghai Medical School, [10]State Key Laboratory of Medical Neurobiology, Institutes of Brain Science, Fudan University, Shanghai, China, [11]Department of Ophthalmology, Yong Loo Lin School of Medicine, [12]Saw Swee Hock School of Public Health, National University of Singapore, Singapore, Singapore, [13]Duke-NUS Graduate Medical School, Singapore, Singapore, [14]Department of Ophthalmology and Visual Sciences, The Chinese Uuniversity of Hong Kong Eye Hospital, Hong Kong, China, [15]Department of Ophthalmology, Samsung Medical Center, Sungkyunkwan University, School of Medicine, Seoul, Seoul Korea, [16]National Institute for Health Research Biomedical Research Centre at Moorfields Eye Hospital NHS Foundation Trust and University College London Institute of Ophthalmology, London, UK, [17]SNONGC Department of Genetics and Molecular Biology, Vision Research Foundation, Sankara Nethralaya, Chennai, India, [18]Department of Integrative Genomics, Tohoku Medical Megabank Organization, Sendai, Japan, [19]Department of Ophthalmology, College of Medicine, King Saud University, Riyadh, Saudi Arabia, [20]Department of Ophthalmology, College of Medicine, University of Florida, Jacksonville, FL, USA, [21]Chinese University of Hong Kong Joint Shantou International Eye Center, Shantou University, Shantou, China, [22]Department of Genetics, Aravind Medical Research Foundation, Madurai, Tamilnadu, India, [23]Menzies Institute for Medical Research, University of Tasmania, Hobart, Australia, [24]Department of Ophthalmology, Flinders University, Adelaide, Australia, [25]Department of Genetics and Computational Biology, Statistical Genetics, QIMR Berghofer Medical Research Institute, Brisbane, QLD, Australia, [26]Sichuan Provincial Key Laboratory for Human Disease Gene Study, Hospital of the University of Electronic Science and Technology of China and Sichuan Provincial People's Hospital, Chengdu, China, [27]School of Medicine, University of Electronic Science and Technology of China, Chengdu, China, [28]Ozaki Eye Hospital, 1–15, Kamezaki, Hyuga, Miyazaki 883-0066, Japan, [29]Mizoguchi Eye Hospital, 6-13 Tawara-machi, Sasebo, Nagasaki 857-0016, Japan, [30]Glaucoma Services, Aravind Eye Hospital, Madurai, Tamilnadu, India, [31]Department of Ophthalmology, School of Medical Sciences, Universiti Sains Malaysia, Kota Bharu, Kelantan, Malaysia, [32]Vietnam National Institute of Ophthalmology, Hanoi, Vietnam, [33]Ophthalmology Department, [34]Biochemistry Department, Angers University Hospital, Angers, France, [35]Department of Ophthalmology, Tongji Hospital of Tongji Medical College, Huazhong University of Science and Technology, Wuhan, China, [36]Huntingdon Glaucoma Diagnostic & Research Centre, Hinchingbrooke Hospital, Huntingdon, UK, [37]Norfolk & Norwich University Hospital NHS Trust, Norwich, UK, [38]Heart of UK NHS Foundation Trust, Birmingham, UK, [39]School of Medicine, Dentistry and Biomedical Sciences, Centre for Experimental Medicine, Queen's University Belfast, Northern Ireland, UK, [40]Department of Medicine, Duke University Medical Center, Durham, NC, USA, [41]Department of Cellular Biology and Anatomy, Georgia Regents University, Augusta, Georgia, [42]Medical Research Foundation, Sankara Nethralaya, Chennai, India, [43]Department of Ophthalmology, Medical Faculty Mannheim of the Ruprecht-Karls-University Heidelberg, Heidelberg, Germany, [44]Department of Ophthalmology and Visual Sciences, [45]Department of Epidemiology, University of Michigan, Ann Arbor, MI, USA, [46]State Key Laboratory of Oncology in Southern China, Guangzhou, China, [47]Department of Experimental Research, Sun Yat-Sen

University Cancer Centre, Guangzhou, China, [48]Clinical Research Unit, Oxford University, 190 Ben Ham Tu, Ho Chi Minh City, Vietnam, [49]Centre for Tropical Medicine, Nuffield Department of Clinical Medicine, Oxford University, Oxford OX3 7LJ, UK, [50]Department of Epidemiology and Biostatistics, Case Western Reserve University, Cleveland, OH, USA, [51]Channing Division of Network Medicine, Brigham and Women's Hospital, Boston, MA, USA, [52]Department of Medicine, National University Health System & National University of Singapore, Singapore, [53]Einhorn Clinical Research Center, Department of Ophthalmology, New York Eye and Ear Infirmary, New York, NY, USA, [54]Eye Doctors of Washington DC, Washington, DC, USA, [55]Department of Ophthalmology, Harvard Medical School, Massachusetts Eye and Ear Infirmary, Boston, MA, USA, [56]Centre for Eye Research Australia (CERA), University of Melbourne, Royal Victorian Eye and Ear Hospital, Melbourne, VIC, Australia, [57]Department of Ophthalmology, University of Alabama at Birmingham, Birmingham, AL, USA, [58]Centre for Ophthalmology and Visual Science, Lions Eye Institute, University of Western Australia, Perth, WA, Australia, [59]Myopia Key Laboratory of the Ministry of Health of China, Shanghai, China and [60]Chinese Academy of Sciences, Sichuan Translational Medicine Hospital, Chengdu, China

*To whom correspondence should be addressed at: The Academia, 20 College Road, Discovery Tower level 6, Singapore 169856, Singapore. Tel: +65 65767216; Fax: +65 62252568. Email: eranga.n.v@sericom.sg (E. N. V.); 60 Biopolis Street, #02-01 Genome Building, Genome Institute of Singapore, Singapore 138672, Singapore. Tel: +65 68088200; Fax: +65 68088034. Email: khorcc@gis.a-star.edu.sg (C.-C. K.)

Abstract

Primary open angle glaucoma (POAG), a major cause of blindness worldwide, is a complex disease with a significant genetic contribution. We performed Exome Array (Illumina) analysis on 3504 POAG cases and 9746 controls with replication of the most significant findings in 9173 POAG cases and 26 780 controls across 18 collections of Asian, African and European descent. Apart from confirming strong evidence of association at *CDKN2B-AS1* (rs2157719 [G], odds ratio [OR] = 0.71, $P = 2.81 \times 10^{-33}$), we observed one SNP showing significant association to POAG (*CDC7–TGFBR3* rs1192415, $OR_{G\text{-allele}} = 1.13$, $P_{meta} = 1.60 \times 10^{-8}$). This particular SNP has previously been shown to be strongly associated with optic disc area and vertical cup-to-disc ratio, which are regarded as glaucoma-related quantitative traits. Our study now extends this by directly implicating it in POAG disease pathogenesis.

Introduction

Glaucoma is the leading cause of irreversible visual impairment and blindness, affecting >60 million people worldwide, and it is estimated that the number of affected individuals will reach 80 million in 2020 (1–3). Primary open angle glaucoma (POAG) is the most prevalent form of glaucoma in most populations and is characterized by progressive retinal ganglion cell (RGC) loss that causes characteristic structural changes of the optic nerve with associated with visual field loss in the face of an open drainage angle in the eye. POAG has a strong genetic component that has been well documented (4). Indeed, several susceptibility loci have been identified for POAG through the use of linkage and association studies (5). Genes known to contribute to glaucoma include myocillin (*MYOC*), optineurin (*OPTN*), TANK-binding kinase 1 (*TBK1*) and WD repeat domain 36 (*WDR36*) (6–12). However, mutations in these genes account for no >5–10% of all POAG cases in the general population (5).

It is likely that POAG, as a complex trait, results from the interactions of multiple genes and environmental factors (13–15). Genome-wide association studies (GWAS) have provided further insights into the genetic basis of POAG (16). The first GWAS on POAG was conducted on 1263 POAG cases and 34 877 controls from Iceland. Genome-wide significant association was detected at the CAV1–CAV2 locus on Chromosome 7q31 and subsequently was replicated in a multi-ethnic sample collection from Sweden, the UK, Australia, Hong Kong and China (17). This was rapidly followed by five other GWAS studies, which utilized either advanced or non-advanced POAG cases derived from populations of European or East Asian ancestries (18–22). These latter studies led to the discovery of nine additional genetic regions associated with POAG disease risk (*TMCO1*, *CDKN2B-AS1*, *SIX1-SIX6*, an intergenic region on chromosome *8q22*, *ABCA1*, *GAS7*, *AFAP1*, *GMDS* and *PMM2*). Several of these genetic loci have been replicated in ethnically diverse populations, demonstrating them to be bona fide POAG associations with global implications (23–25).

Similar in concept and laboratory chemistry to the whole-genome genotyping chip design, the exome array approach evaluates putative functional coding variants selected from the exome sequences of >12 000 individuals (26). In addition, the exome array also contains >5000 common variant SNPs from GWAS arrays with a minor allele frequency (MAF) exceeding 5% which can serve as ancestry informative markers. Exome array genotyping allows us to specifically explore the possible contribution of potentially functional coding variants in POAG disease susceptibility.

Results

Common genetic variants in *CDKN2B-AS1* and *TGFBR3-CDC7* are associated with POAG

We conducted a two-stage Exome Chip discovery and replication on POAG cases and normal controls. For the discovery stage (Stage 1), genotyping was performed using the Illumina Infinium HumanExomeBeadChip (v1.0) on a total of 3822 POAG cases and 10 426 normal controls drawn from seven countries (Table 1). In addition to the ≈247 000 SNP markers present on the standard

Table 1. Sample collections of POAG cases and controls for Stages 1 (discovery) and 2 (replication)

Collection	N cases	N controls	Ethnicity	Age of cases	Age of controls[a]	Collection comment
Singapore	850	2347	Singaporean Chinese	71.6 ± 10.1	58.88 ± 9.6	New recruitment
Japan	923	640	Japanese	65.3 ± 13.1	71.9 ± 5.8	Previously GWAS in Nakano *et al.* (25)
USA-African-Americans	590	636	African American	65.4 ± 12.3	54.8 ± 9.8	New recruitment
China-Beijing	587	461	Northern Chinese	58.5 ± 12.5	Population-based controls	New recruitment
Hong Kong	375	2962	Southern Chinese	62.3 ± 15.3	Population-based controls	Previously described for replication in Thorleifsson *et al.* (17)
South India	121	716	Indian	60.9 ± 12.0	51.0 ± 6.5	New recruitment
Vietnam	58	1984	Vietnamese	63 ± 7.1	Population-based controls	New recruitment
Total discovery	3504	9746				2206 cases are new discovery samples
Stage 2 replication						
Singapore-2	520	5473	Singaporean Chinese	71.1 ± 10	Population-based controls	New recruitment
Japan-2	935	996	Japanese	64.3 ± 14.0	57.5 ± 13.9	$N = 411$ used for replication in Nakano *et al.* (25)
USA-Afican-American 2	497	304	African-American	69.1 ± 11.0	66.7 ± 13.1	New recruitment
South India-2	453	2496	Indian	62.5 ± 9.9	58.9 ± 10.1	New recruitment
Korea	400	454	Korean	59.0 ± 11.8	40.3 ± 14.1	New recruitment
Saudi Arabia	236	655	Middle Eastern	60.8 ± 12.7	54.4 ± 11.7	New recruitment
Malaysia	132	2540	Malay	65.1 ± 8.2	58.7 ± 11.0	New recruitment
China-Beijing 2	115	251	Northern Chinese	54.2 ± 12.4	71.53 ± 7.16	New recruitment
UK	336	6090	European	71.4 ± 10.8	Population-based controls	New recruitment
China-Shantou	247	289	Southern Chinese	52.9 ± 19.4	75.7 ± 6.1	Previously described for replication in Thorleifsson *et al.* (17)
Germany	56	142	European	67.9 ± 11.4	78.4 ± 8.9	New recruitment
Vietnam-2	76	245	Vietnamese	52.4 ± 17.4	51.3 ± 17.8	New recruitment
France	80	75	European	75.6 ± 8.5	73.5 ± 8.3	New recruitment
China-Shanghai, Chengdu 2	181	286	Southern Chinese	54.7 ± 16.5	84.7 ± 11.7	Previously described in Chen *et al.* (19)
China-Shanghai, Chengdu	608	1005	Southern Chinese	49.6 ± 17.0	62.9 ± 12.1	Previously described in Chen *et al.* (19)
USA (NEIGHBOR)	2170	2347	European descendant	66.4	68	Previously described in Wiggs *et al.* (22)
USA (GLAUGEN)	976	1140	European descendant	63.6	65.5	Previously described in Wiggs *et al.* (22)
Australia (ANZRAG)	1155	1992	European descendant	60.5 ± 14.3	55.6 ± 14.4	Previously described in Gharahkhani *et al.* (20)
Total replication	9173	26 780				3425 cases are new replication samples
Total all samples	12 677	36 526				5631 cases are new in this report.

[a]Population-based controls are ascertained from large-scale studies and do not have demographic data available. Based on many well-described examples, both by others and us, the frequency of POAG in the general population is uncommon (i.e. <5%). In this regard, the false-negative rate for POAG status in the population-based controls is likely to be low and thus the effect of loss of statistical power is negligible.

Illumina Exome array (26), we also included an extra 25 000 coding frame SNP markers obtained from exome sequencing of 2000 individuals of East Asian descent. Stringent quality control (QC) filters were applied to both SNPs and samples: per SNP call rate ≥99%, per-sample call rate ≥95%, non-monomorphic SNPs and non-significant deviation from Hardy–Weinberg equilibrium (HWE) $P \geq 10^{-6}$. Samples under suspicion of cross-contamination and biologically related samples were removed by verification of extreme heterozygosity and identical by descent/identical by state information, if applicable. We further performed principal component analysis (PCA) to verify that cases and controls were well-matched ancestrally (Supplementary Material, Fig. S1) (27–32). As a result, a total of 3504 POAG cases and 9746 controls passing QC filters were included for association analysis using unconditional logistic regression, with adjustments for the principal components (PCs). From these datasets, a total of 2206 POAG cases represent entirely new patient collections, which have not been previously reported (Supplementary Material, Table S1). Each study-specific point estimate was then summarized using fixed-effects meta-analysis ($N_{\text{meta-analysis}} = 7$ collections). A quantile–quantile plot derived from the meta-analysis *P*-values showed no significant dispersion of test statistics from the expected distribution ($\lambda_{GC} = 1.042$; Supplementary Material, Fig. S2) suggesting that the association results were not confounded by cryptic population stratification. Using additive effect models, we observed experiment-wide significant

($P = 0.05/272\,000$ SNPs $= 1.84 \times 10^{-7}$) evidence of association at *CDKN2B-AS1* (rs2157719 [G], per-allele OR = 0.73, $P = 1.10 \times 10^{-7}$) (Supplementary Material, Fig. S3).

All SNP markers showing $P < 0.0005$ in the discovery stage were followed up in a validation stage (Stage 2) comprised of up to 9173 POAG cases and 26 780 controls. A total of 21 SNPs at 20 independent loci were brought forward for validation genotyping using Sequenom MassARRAY iPLEX or *in silico* look-ups if genome-wide genotyping data were available (see Supplementary Material, Table S2).

CDKN2B-AS1 rs2157719 once again showed significant evidence of association in the meta-analysis of all replication collections (OR = 0.70, $P = 2.48 \times 10^{-27}$) as well as meta-analysis of all samples tested (rs2157719 [G], OR = 0.71, $P_{meta} = 2.81 \times 10^{-33}$) (Supplementary Material, Table S2 and Fig. S4). No heterogeneity of effect between Asians (OR = 0.72, $P = 1.15 \times 10^{-15}$) and Europeans (OR = 0.69, $P = 5.54 \times 10^{-19}$) were detected for this marker (Fig. 1A), consistent with the multiple previous reports describing association at this locus (18,22,25). Apart from *CDKN2B-AS1* rs2157719, a second SNP marker (*CDC7-TGFBR3* rs1192415) showed clear evidence of replication in Stage 2 (OR = 1.12, $P = 1.04 \times 10^{-5}$, Fig. 1B and Supplementary Material, Table S2). On meta-analysis with the exome-chip discovery findings, genome-wide significant evidence of association was observed for rs1192415 (OR = 1.13, $P_{meta} = 1.6 \times 10^{-8}$) (Fig. 1B; Supplementary Material, Table S2). Although the risk allele ranged from between 11 and 34% across all ethnic groups studied for this marker, the association observed appeared to be uniform and consistent across most groups with little overall heterogeneity (I^2 index < 20%, Supplementary Material, Table S3). For rs1192514, the association appeared stronger in Asians (OR = 1.17, $P = 1.48 \times 10^{-7}$) compared with Europeans (OR = 1.10, $P = 0.01$) (Fig. 1B), although the difference was not statistically significant ($P_{het} = 0.17$). One other marker (*FNDC3B* rs4894796) was nominally significant in the replication stage (OR = 0.95, $P = 0.02$) and remained suggestively associated with POAG in the overall meta-analysis (OR = 0.93, $P = 1.40 \times 10^{-5}$) (Fig. 1C; Supplementary Material, Table S2). However, the association appeared to be nearly entirely driven by the Asian POAG collections (OR = 0.89) compared with the Europeans (OR = 0.99, P_{het} between Asians and Europeans = 0.0042) (Fig. 1C). A recently reported GWAS on POAG showed strong association with common SNP markers mapping to *AFAP1* (rs4478172) (20). Looking up on our exome dataset, we successfully genotyped rs7437940 ($r^2 = 0.18$, $D' = 0.97$ with rs4478172) which also mapped within *AFAP1*. We note significant association at this *AFAP1* marker (rs7437940: Stage 1 $P = 1.94 \times 10^{-5}$, Stage 2 $P = 0.08$, *P*-value for meta-analysis $= 4.25 \times 10^{-6}$) (Supplementary Material, Table S2), which supports the previous report (20).

Expression of POAG-associated genes in ocular tissues

We examined the mRNA expression of *CDC7*, *TGFBR3* and *FNDC3B* in multiple eye tissues. Expression of all three genes was observed in tissues relevant to POAG such as the trabecular meshwork, optic disc and nerve. In contrast to *TGFBR3* and *FNDC3B*, which were expressed in all tested ocular tissues, *CDC7* expression was absent in the iris, ciliary body and choroid (Fig. 2).

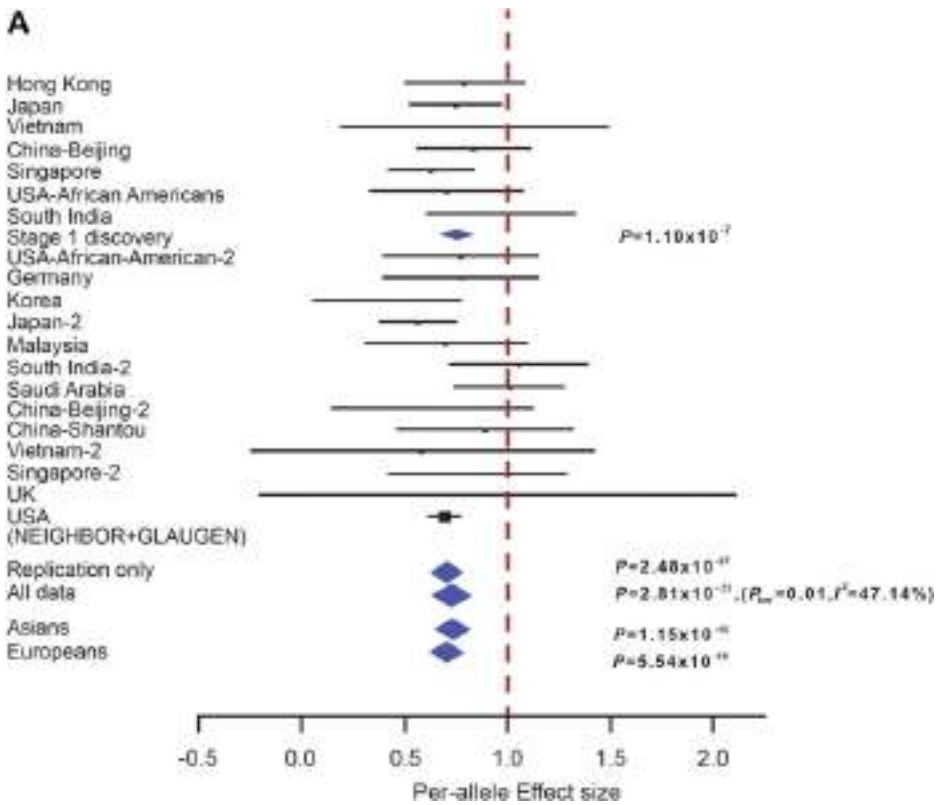

Figure 1. Forest plots showing evidence of association between SNPs: (**A**) *CDKN2B-AS1* rs2157719, (**B**) *CDC7/TGFBR3* rs1192415 and (**C**) *FNDC3B* rs4894796. The vertical line represents a per-allele odds ratio of 1.00. The oblongs represent point estimates (referring to the per-allele odds ratio), with the height of the oblongs inversely proportional to the standard error of the point estimates. Horizontal lines indicate the 95% confidence interval for each point estimate. Meta-analysis of Stages 1 and 2, OR, P_{meta} and I^2 was labeled on the right-hand side for corresponding analysis. For rs4894796 genotyping, see Supplementary Material, Information for sample collections.

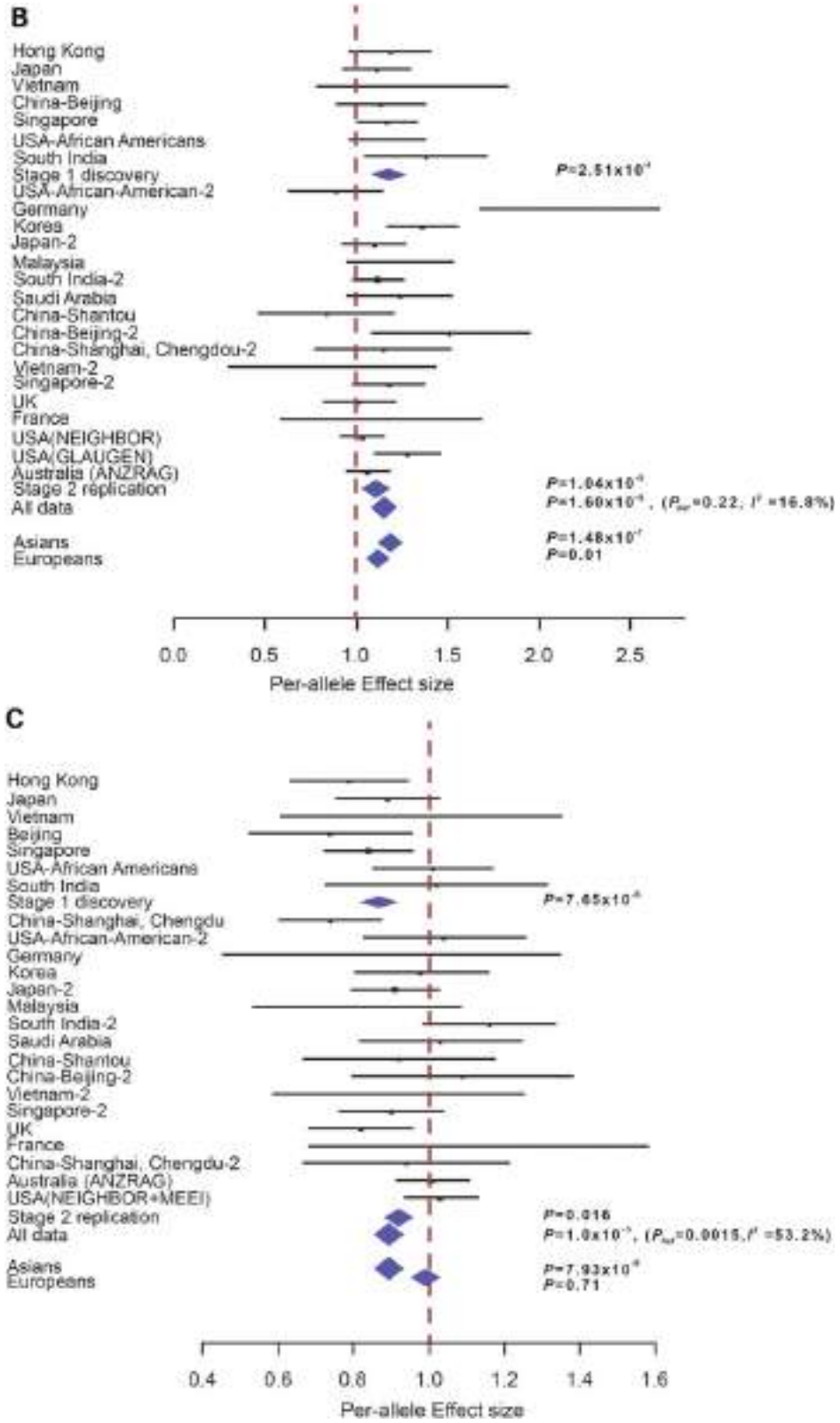

Figure 1 Continued

We also investigated the localization of FNDC3B protein in normal ocular tissues, focusing our attention on cornea and the tissues of the outflow pathway. FNDC3B could be immunolocalized to cells in the trabecular meshwork and all three layers of the cornea (Fig. 2). Immunolocalization of TGFBR3 and CDC7 could not be similarly investigated due to lack of availability of specific antibodies.

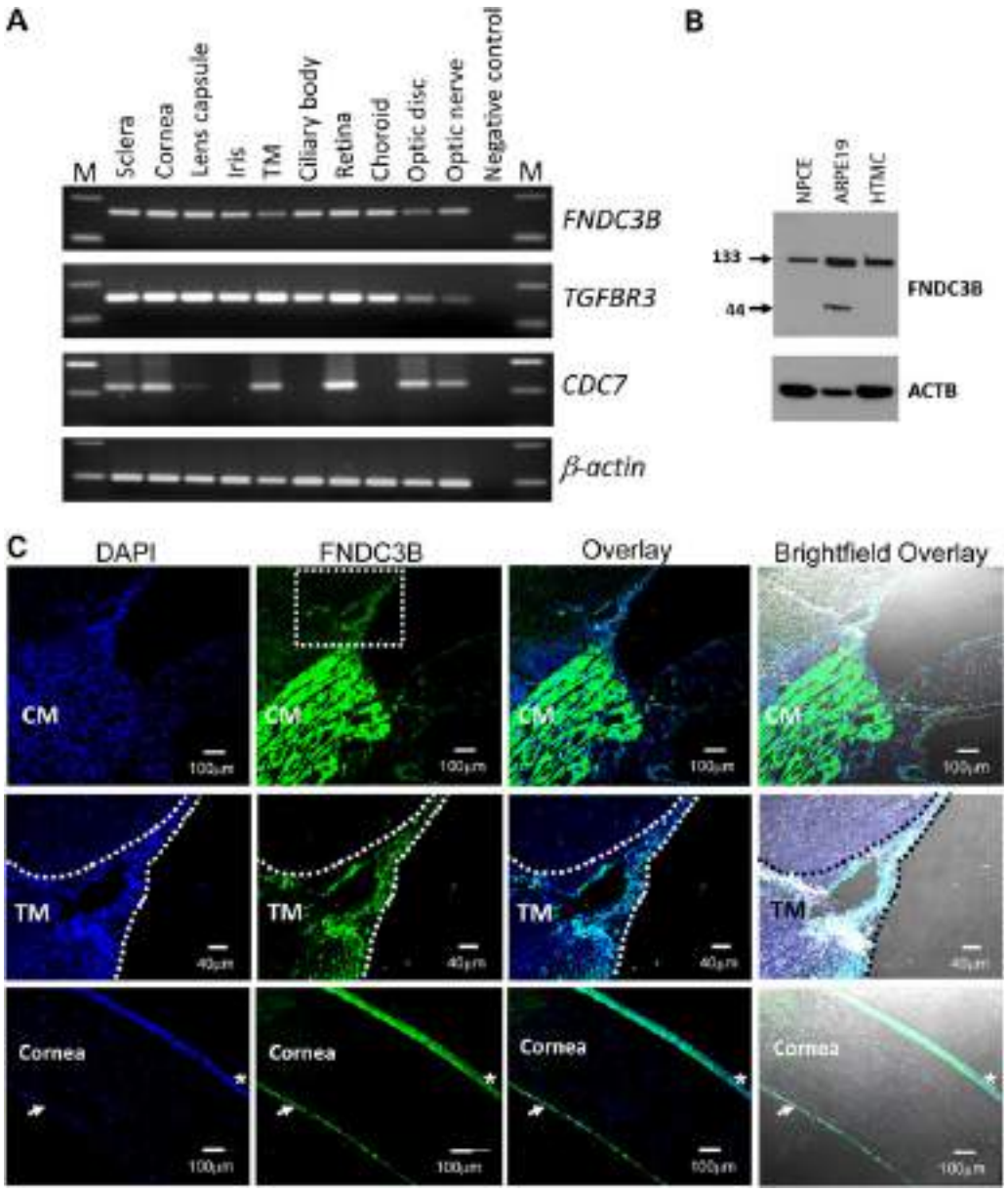

Figure 2. Analysis of *FNDC3B*, *TGFBR3* and *CDC7* expression in ocular tissues. (**A**) The *FNDC3B*-specific 162 bp and *TGFBR3*-specific 152 bp amplification product was observed in all analyzed ocular tissues. *CDC7*-specific 242 bp product was observed in sclera, cornea, trabecular meshwork, retina, optic disc and optic nerve. The ubiquitously expressed gene, *ACTB* was used as the normalizing control. A no template sample acted as the negative control (NC) to ensure non-contamination of the RT–PCR reaction mix. The variable *M* denotes molecular-weight marker. (**B**) Immunoblot of whole cell lysates from NPCE, retinal pigment epithelial (ARPE19) and HTM cells, probed for FNDC3B and β-actin, as a loading control. Positions of the ~133 and ~44 kDa forms of FNDC3B are indicated. All ocular cells analyzed expressed the ~133 kDa protein, while ARPE19 cells expressed a smaller ~44 kDa isoform of FNDC3B. (**C**) Immunolocalization of FNDC3B in human eye tissues. Strong immunofluorescence labeling of FNDC3B (green) was seen in the ciliary muscle (CM) (top row). Scale bar: 100 μm. In the trabecular meshwork (TM, middle row), FNDC3B (green) labeling was relatively weaker. Scale bar: 40 μm. FNDC3B positive immunoreactivity was also observed in cornea epithelial (*) and cornea endothelial cells (white arrows) (bottom row). Nuclei were stained with DAPI (blue). Scale bar: 100 μm.

Analysis of rare variants from the exome-chip discovery collection

We next proceeded to conduct gene-based tests on mutational load to further investigate the role of low-frequency variants in POAG for all patient collections in the discovery stage. Gene-based tests are an alternative to single-marker tests for association, which are often underpowered to detect association with rare variants. To more directly address the impact of low frequency, non-synonymous genetic variants, we considered only the variants with MAF of <5% (33). As a result, we were able to assess a total of 7822 genes having at least two such variants using the sequence kernel association optimal test (34). We note two genes (*MYO18A* and *SULF2*) which showed nominal evidence of association on burden test ($P = 6.26 \times 10^{-7}$ and $P = 5.78 \times 10^{-5}$, respectively), but these findings are primarily driven by the small Vietnamese collection ($N = 58$ cases and $N = 1984$ controls). Removal of this dataset resulted in a marked reduction of the burden test association results (Supplementary Material, Table S4).

Discussion

The present study supports the association of POAG a locus that has been previously implicated with vertical cup-disc ratio, a glaucoma-associated endophenotype. This locus is defined by rs1192415, a common SNP marker mapping to the intergenic region between *CDC7* and *TGFBR3* (allele [G], OR = 1.13, $P_{meta} = 1.6 \times 10^{-8}$). We were also able to strongly corroborate the established association of POAG with *CDKN2B-AS1.CDC7-TGFBR3* rs1192415 has previously been reported to be strongly associated with overall optic disc area, which together with VCDR is a glaucoma-related quantitative trait (35,36). Examination of this locus in >4700 POAG cases and >90 000 controls of European descent in a recent study showed direction of effect consistent with our data (OR = 1.06, $P = 0.12$) (37). Indeed, in the European section of our study ($N = 4773$ cases and 11786 controls), we note a similar effect size (OR = 1.10, $P = 0.01$) in keeping with that shown by Springelkamp and others. The effect of this locus appeared to be much stronger in Asians (OR = 1.17, $P = 1.48 \times 10^{-7}$), leading to a genome-wide significant association upon meta-analysis of all collections. Each copy of the rs1192415 minor allele is associated with a relatively modest increase in POAG risk of 1.13 at exome-wide significance. The consistency of the effect across 21 of 24 POAG collections ($P_{het} = 0.22$, I^2 index for heterogeneity = 16.9%), lend further credence to the observed association.

It is of note that the G allele of the rs1192415 is associated with increase in disc area and therefore a larger VCDR. This may indicate a lower threshold for diagnosing glaucoma in those individuals harboring the risk allele (38). However, as the diagnosis of POAG in this study was not based solely upon the presence of an increased cup–disc ratio but also compatible visual field loss, it is unlikely that selection bias has influenced the result obtained with rs1192415. We note that *FNDC3B* was one of 16 loci associated with central corneal thickness (sentinel SNP being rs4894535) in a meta-analysis conducted on >20 000 individuals of European and Asian descent (39). That study also showed marker rs4894535 to be associated with POAG in 2979 cases and 7399 controls of European descent (OR = 0.83, $P = 5.6 \times 10^{-4}$). We were able to confirm association of rs4894535 with POAG in 5810 cases and 13 175 controls with readily available DNA for genotyping across 13 collections in this study (OR = 0.91, $P = 0.0018$; Supplementary Material, Table S5), thus lending further support for this association.

It is noteworthy that the *FNDC3B* SNP we report here (rs4894796) was nominally associated with POAG in the overall meta-analyses (OR = 0.93, $P = 1.4 \times 10^{-5}$). In particular, the association at rs4894796 was observed to be particularly strong in Asians (OR = 0.89, $P = 7.93 \times 10^{-8}$) compared with Europeans (OR = 0.99, $P = 0.71$). Unsurprisingly, rs4894796 was found within a different linkage disequilibrium (LD) block than the SNP associated with central corneal thickness and POAG (rs4894535). The low LD between rs4894796 and rs4894535 suggests that the association signal at the latter SNP is not likely to be driven by rs4894796. An in-depth inspection of the LD patterns of this genetic region between European and East Asian populations, which currently appear visually identical according to available heat maps (http://www.hapmap.org), may be useful to better understand the degree of LD dissimilarity between populations and its bearing on the results obtained for *FNDC3B*. Of note, a further SNP (rs6445055) at *FNDC3B* showed genome-wide significant association for intraocular pressure (IOP) ($P = 4.9 \times 10^{-8}$), but only marginal association was seen for POAG per se ($P = 0.03$, OR = 0.92) in 4284 POAG cases and 95 560 controls of European descent (21). As the *FNDC3B* SNP associations with POAG are still suggestive rather than affirmative it is presumptive at this stage to speculate that it could be one of the links for IOP-dependent mechanisms of POAG.

This is one of the largest studies on the genetics of POAG, yet the power to detect genes with small effects was limited. One crucial reason for this apparent loss of power could be the scope of the genetic content which was used for interrogation (as exomic content only comprises <2% of the entire human genome, much useful data could be missed if the bulk of the true positive genetic associations for POAG lie in the non-coding regions of the genome). The fact that our discovery cohort was not mono-ethnic may also have reduced the power to detect ethnic specific variants of small effect sizes due to significant differences in allele frequencies between ethnic groups. The phenotypic heterogeneity and the lack of standardized clinical criteria across the cohorts may also have contributed to a loss in power. The level of IOP is commonly used to subdivide POAG into two subtypes: POAG with high IOP (>21 mmHg; named high-tension glaucoma, HTG) and NTG with normal IOP (<21 mmHg). In our cohorts, we had differing number of these subtypes with some cohorts having more NTG or HTG than others. In this study, we also did not subdivide POAG subjects into HTG and NTG to discover subtype-specific variants, focusing instead on identifying genetic variants for the overarching phenotype of POAG. However, when *CDC7-TGFBR3* rs1192415 and *FNDC3B* rs4894796 were analyzed within NTG and HTG subgroups, they did not show differences in strength of association by subtype (data not shown).

All three loci we report in this study (*CDKN2B-AS1*, *TGFBR3-CDC7* and *FNDC3B*) contain genes which may contribute to the regulation of transforming growth factor-β (TGF-β) signaling. TGF-β has been implicated previously in glaucomatous optic nerve damage and RGC death (40–42). The TGF-β family includes TGFβ1, TGFβ2 and TGFβ3, all of which bind to TGF-β receptor type-2 (TGFBR2). All TGF-β family members are dimeric polypeptide growth factors that inhibit the progression of cell cycle, which in turn may lead to terminal differentiation or apoptosis (40,43,44). TGF-β also modulates developmental and repair processes in several tissues. TGF-β signaling has been implicated in a wide variety of diseases including inflammation, autoimmune disorders, fibrosis, cancer, cataracts as well as glaucoma (40,43,44). The most strongly POAG-associated locus, CDKN2B-AS1, has been shown to regulate the transcription of cyclin-dependent kinase inhibitor 2A and 2B (CDKN2A and CDKN2B) (45), which inhibit cell proliferation via the TGF-β pathway by inducing G1-phase cell cycle arrest (44). Burdon *et al.* reported the up-regulation of *CDKN2A* and *CDKN2B* in response to elevated IOP (18). Collectively, these data suggest a link between the most well-recognized physiological risk factor of POAG and a downstream molecular response that may lead to RGC death. In this context, both CDC7 and TGFBR3 are also of interest and could have relevance to glaucomatous optic nerve damage and RGC death.

CDC7 encodes a cell division cycle protein with kinase activity that also interacts with CDKN2A. TGFBR3 is a TGF-β super family co-receptor, and is the most abundant of all TGF-β receptors (46). Through protein crystallography, murine TGFR-3 ZP domain (ZP-C) has been recently identified as a novel major TGF-β-binding site (47). It has been suggested that TGFBR3 may serve to enhance the binding of TGF-β ligands to TGF-β type II receptors by binding TGF-β and presenting it to TGFBR2, the receptor for all three TGF-β ligands. A linkage between FNDC3B, an oncogene and TGF-β signaling was also reported recently by Cai *et al.* Overexpression of FNDC3B was shown to induce epithelial-to-mesenchymal transition and activate several cancer pathways, including PI3-kinase/

Akt, Rb1 and TGF-β signaling (48). FNDC3B also induced expression of all three TGF-β ligands and promoted TGFBR1 cell-surface localization (48). This connection of POAG-associated genes/loci with the TGF-β signaling pathway therefore lends further credence to the hypothesis of TGFB pathway involvement in glaucoma.

However, despite these attractive speculations on the genes vicinal to the associated SNPs, it is possible that these variants may also affect distant as yet unidentified target genes. Definitive evidence for the involvement of these genes in the pathogenesis of POAG awaits confirmation in other datasets, as well as the identification and characterization of functional variants.

Materials and Methods

Sample collections

Ethics statement

Ethics approval was obtained from the Centralized Institutional Review Board for the Singaporean patient sample and data collection and for the conduct of this study. All study protocols for patient and control sample collection were approved by the respective relevant Medical Ethics Committees of each participating site. All studies were conducted under the tenets of the Declaration of Helsinki with written informed consent obtained from all participants.

POAG and health controls subjects inclusion criteria

POAG cases in this study were defined by the following criteria: the presence of glaucomatous optic neuropathy (defined as loss of neuroretinal rim with a vertical cup : disc ratio of >0.7 or an inter-eye asymmetry of >0.2 and/or notching attributable to glaucoma) with compatible visual field loss, open angles on gonioscopy, and absence of secondary causes of glaucomatous optic neuropathy. POAG patients with a mean IOP without treatment that is consistently <21 mmHg on diurnal testing are classified as having NTG, whereas those with a mean IOP without treatment that is consistently >21 mmHg are classified as having HTG. Patients who were unable to give informed consent, or with secondary glaucoma due to trauma, uveitis, neovascularization, pseudoexfoliation, pigment dispersion, etc., were excluded from this study.

Controls in this study were recruited in a hospital-based or population-based manner. Hospital-based controls were all generally over the age of 40 years and confirmed to have no sign of glaucoma or other major eye diseases except for mild cataract and mild refractive errors (defined as |SE| < 3D) by an ophthalmic examination. These subjects at time of recruitment had IOP of <21 mmHg with open angles, healthy optic nerves, normal visual fields, and no family history of glaucoma. Population-based controls were ethnically matched healthy individuals over the age of 40 years, unless indicated otherwise (see Table 1; Supplementary Material for more details of the samples used in this study).

Genotyping and data QC

Study participants in the discovery stage were genotyped using the Illumina's Infinium HumanExomeBeadChip (Version 1.0) + Semi-Custom BeadChip (Illumina Inc.) that contains ~250 000 SNPs of base content and an additional 25 000 East Asian-specific polymorphisms located on the coding frame. Stringent QC filters were applied after the laboratory work in genotyping completed. SNP markers that had missingness exceeding 5%, gross departure from HWE (*P*-value <1e−6) or were monomorphic were excluded from subsequent analysis. Likewise, individual samples with an overall call rate <95% were excluded. Samples were subjected to biological relationship verification by using the principle of variability in allele sharing according to the degree of relationship. Identity-by-state information was derived by PLINK. Those individuals who showed evidence of cryptic relatedness were removed before PC analysis was conducted. In addition, samples showing gender discrepancies between the clinical gender and genetically inferred gender were removed. A total of 1008 samples were excluded after rigorous application of QC filters (568 sample exclusions were due to PCA ancestral outliers, 246 were excluded due to per-sample call rate <95%, 168 were excluded due to first-degree familial relationships detected from the discovery stage exome-chip genotyping, and 26 were excluded due to suspicions of sample contamination). PC analysis was undertaken using EIGENSTRAT to account for spurious associations resulting from ancestral differences of individual SNPs (49). PCs showing significant effect on univariate analysis were used to correct for any underlying population substructure. We adjusted for the top three PCs (PC1–PC3) for Singapore, Hong Kong, Japan, USA-African Americans, China-Beijing and Vietnam. The Indian POAG collection was adjusted for the top 10 PCs (PC1–PC10), as there was more population substructure in this collection. After adjustment, we observed minimal evidence of genomic inflation ($\lambda_{GC} = 1.042$), thereby suggesting that this well-described method of controlling for population stratification was adequate in our study. Genotyping clouds for the key SNPs *CDKN2B-AS1* rs2157719, *CDC7-TGFBR3*rs1192415 and *FNDC3B*rs4894796 were directly visualized (Supplementary Material, Fig. S5) to ensure good quality.

For Stage 2 (replication stage), genotyping was performed using the Sequenom MassArray platform (www.sequenom.com). Samples recruited at the latter stage of replication were genotyped for the key SNPs *CDC7-TGFBR3*rs1192415, and *FNDC3B*rs4894796 using pre-developed Taqman Assays (Applied Biosystems, Foster City, CA, USA; www.appliedbiosystems.com)

Statistical analysis

We contrasted the genotypes between POAG cases and healthy controls via single-SNP analysis using unconditional logistic regression fitted for genotype trend effects (1-degree-of-freedom score test). To do this, the PLINK software [version 1.07] (50) was used for modeling within a logistic regression framework, adjusting for age, gender and genetic ancestry (reflected by PCs). Manhattan and LD plots were created using Haploview [version 3.2] (51). Q–Q and regional association plots were created using the software R [www.r-project.org] (52). Meta-analysis summarizing the results across all cohorts was performed using both fixed and random-effects modeling weighted in an inverse-variance manner (53). This method weighs each study according to effective sample size and cohort-specific MAF of the associated variants. To avoid an otherwise unacceptable number of false positive signals as an artifact of multiple testing, the threshold for exome-wide significance, $P < 2 \times 10^{-7}$, was considered to be statistically significant. Heterogeneity of the meta-analyses was calculated by measuring I^2.

Expression analysis of genes

Expression of *CDC7*, *TGFBR3* and *FNDC3B* was assessed by semi-quantitative reverse transcription–PCR (RT–PCR) using gene-specific primers (*CDC7*-forward 5′-TTTTCTCCCCAGCGTGACC-3′, *CDC7*-reverse 5′-GCAATTTTCTCTTCAGGTCCTAC-3′; *TGFBR3*-forward 5′-TCTCCTCAGTCCACATCCAC-3′, *TGFBR3*-reverse 5′-TGC

TGATGAAAACTGGACCAC-3′; *FNDC3B*-forward 5′-AGCATCATCT TCCCCACACA-3′, *FNDC3B*-reverse 5′-AAGAAGGAGGGCTGTTG AGG-3′) on total RNA extracted from a variety of ocular tissues (cornea, sclera, retina and retinal pigment epithelium, iris, lens capsule and optic nerve) as described earlier (54). We used the ubiquitously expressed *ACTB* gene (forward 5′-CCAACCGCGA GAAGATGA-3′and reverse 5′-CCAGAGGCGTACAGGGATAG-3′) as amplification and normalizing control.

Western blotting

Cell lines obtained from American Type Culture Collection (Manassas, VA, USA) were the human retinal pigment epithelial cell line (APRE19), human Trabecular Meshwork cell line (HTM) was purchased from ScienCellResearch Laboratories (Carlsbad, CA, USA) and the human non-pigmented ciliary epithelial cell line (NPCE) is a kind gift from Prof. Miguel Coca-Prados from Yale School of Medicine. Cell lysates were obtained by lysing individual cell lines with lysis buffer (50 mM Tris–HCl, pH 8, 150 mM NaCl, 1.0% Nonidet P-40, 0.5% deoxycholate, 0.1% SDS, 0.2 mM $NaVO_4$, 10 mM NaF, 0.4 mM EDTA and 10% glycerol). SDS–PAGE resolved proteins were transferred to Hybond-C Extra nitrocellulose membranes (Amersham Life Science Inc., Arlington Heights, IL, USA). Membranes were blocked and blotted by 5% nonfat milk, 0.1% Tween 20 in Tris-buffered saline (20 mM Tris–HCl, pH 7.6, 150 mM NaCl) for 1 h before incubation with FNDC3Bfor 1 h (1 : 250) (Sigma-Aldrich Corp., St. Louis, MO, USA). Actin-horseradish peroxidase (HRP) (1 : 50 000) from Santa Cruz Biotechnology (Dallas, TX, USA). The bound primary antibodies were detected by horseradish peroxidase-conjugated secondary antibodies (GE Healthcare Biosciences, Pittsburgh, PA, USA), and visualized by Luminata Forte Western HRP substrate (Millipore, Bedford, MA, USA).

Immunofluorescence confocal microscopy

Immunofluorescence confocal microscopy was performed on antigen retrieved 4 µm paraffin sections. Blocking of tissue sections was performed with blocking buffer (5% nonfat milk, 5% FBS, 0.1% PBS-Tween; 1× pen/strep) for 1 h at RT. FNDC3B antibody (Sigma-Aldrich Corp.) was diluted (1 : 50) into blocking buffer and incubated overnight at 4°C. Secondary FITC (1 : 300)-labelled anti-rabbit antibody (Jackson Laboratories, Westgrove, PA, USA) was also diluted in blocking buffer and incubated at RT for 1 h followed by application of Vectashield with 4′,6-diamidino-2-phenyl-indole (DAPI) (Vector Laboratories, Burlingame, CA, USA). Coverslips were then used to overlay the sections and stored in the dark at 4°C until viewing with Olympus Fluoview 1000 confocal microscope (Olympus Optical Co. Ltd., Tokyo, Japan).

Supplementary Material

Supplementary Material is available at *HMG* online.

Acknowledgements

We thank all the study participants, the staff from all involved studies and sites who contributed to this study. The authors J.E.C., K.P.B., D.A.M., and others acknowledge the support of Ms Bronwyn Usher-Ridge in patient recruitment and data collection, and Dr Patrick Danoy and Dr Johanna Hadler for genotyping of the ANZRAG cohort. They also acknowledge David C. Whiteman and Graham Radford-Smith for providing access to the control samples used with the ANZRAG glaucoma cases. The authors D.M. thank Dr Philippe Gohier and Dr Ghislaine Jallet for patient recruitment and data collection and acknowledge the technical assistance provided by the Centre de Recherche Biologique (Dr Odile Blanchet) and Centre de Recherche Clinique (Pr Marc-Antoine Custeau), University Hospital, Angers, France. The Singapore study of E.N.V., T.A. and C.C.K was supported by a Biomedical Research Council (BMRC) grant in Singapore, Ref: BMRC 10/1/35/19/675. This research was also partly supported by a grant (NMRC/TCR/008-SERI/2013) from the Singapore National Research Foundation under its Translational and Clinical Research Flagship Programme and administered by the Singapore Ministry of Health's National Medical Research Council. We also acknowledge the following source of funding support for recruitment and genotyping of population-based cohorts SIMES and SCES: National Medical Research Council, Singapore (NMRC/TCR/002-SERI/2008, (R626/47/2008TCR), CSA R613/34/2008, NMRC 0796/2003, STaR/0003/2008), the National Research Foundation of Singapore, the Biomedical Research Council, Singapore (BMRC 09/1/35/ 19/616 and 08/1/35/19/550) and Genome Institute of Singapore (GIS/12-AR2105). The Singapore Tissue Network and the Genome Institute of Singapore, Agency for Science, Technology and Research, Singapore provided services. The research of M.A.H. was supported by NIH R01 EY023646, EY13315 (MAH) and by P30-EY005722. The Japanese sample collection from Kyoto was supported by the grants from the Collaborative Development of Innovative Seeds of Japan Science and Technology Agency (JST) to M.K. and K.T., from the Ministry of Health, Labor and Welfare of Japan to M.N., K.M., K.T. and S.K., and from Santen Pharmaceutical Co. Ltd. to S.K. and K.T. The collection of Japanese POAG cases by N.F. was supported by a grant provided by the Ministry of Health, Labor and Welfare of Japan. The glaucoma research of WNL is supported by National Natural Science Foundation of China project (81030016). The research of Y. Chen was supported by National Natural Science Foundation of China (81200723) and glaucoma research of Xinghuai Sun was supported by Special Scientific Research Project of Health Professions (201302015). This research project was supported by the National Natural Science Foundation of China (81170883 (Z.Y.) and 81430008 (Z.Y.)). The glaucoma research of C.P.P. is supported by the Health and Medical Research Fund (HMRF, Ref: 01122236 and 11120801), Hong Kong and the General Research Fund from the Research Grants Council (grant number 468810), Hong Kong. Support for recruitment of Australian & New Zealand Registry of Advanced Glaucoma (ANZRAG) was provided by the Royal Australian and New Zealand College of Ophthalmology (RANZCO) Eye Foundation. Genotyping was funded by the National Health and Medical Research Council of Australia (#535074 and #1023911). This work was also supported by funding from NHMRC #1031362 awarded to Jamie E. Craig, NHMRC #1037838 awarded to Alex W. Hewitt, NHMRC #1048037 awarded to Stuart L. Graham, NHMRC #1009844 awarded to Robert J. Casson and Ivan Goldberg, NHMRC #1031920 and an Alcon Research Institute grant awarded to David A. Mackey, an Allergan Unrestricted grant awarded to Andrew J. White, the BrightFocus Foundation and a Ramaciotti Establishment Grant. S.M. is supported by Australian Research Council (ARC) and Australian National Health & Medical Research Council (NHMRC) Fellowships. Controls for the ANZRAG discovery cohort were drawn from the Australian Cancer Study, the Study of Digestive Health, and from a study of inflammatory bowel diseases. The Australian Cancer Study was supported by the Queensland Cancer Fund and the National Health and Medical Research Council (NHMRC) of Australia (Program no. 199600, awarded to David C. Whiteman, Adele C. Green, Nicholas K. Hayward, Peter

G. Parsons, David M. Purdie and Penelope M. Webb, and program number 552429, awarded to David C. Whiteman). The Study of Digestive Health was supported by grant number 5 RO1 CA 001833 from the National Cancer Institute (awarded to David C. Whiteman). The Barrett's and Esophageal Adenocarcinoma Genetic Susceptibility Study (BEAGESS) sponsored the genotyping of oesophageal cancer and Barrett's oesophagus cases, which were used as unscreened controls in the ANZRAG discovery cohort. BEAGESS was funded by grant R01 CA136725 from the National Cancer Institute Collection of Saudi POAG cases and controls was supported by the Glaucoma Research Chair at College of Medicine, King Saud University, Riyadh, Saudi Arabia. NEI Glaucoma Human Genetics Collaboration (NEIGHBOR): genotyping services for the NEIGHBOR study were provided by the CIDR and were supported by the NEI through grant HG005259-01 (J.L.W.). Additionally, CIDR is funded through a federal contract from the NIH to The Johns Hopkins University, contract number HHSN268200782096C. Collecting and processing samples for the NEIGHBOR data set was supported by the NEI through American Recovery and Reinvestment Act (ARRA) grants 3R01EY015872-05S1 (J.L.W.) and 3R01EY019126-02S1 (M.A.H.). Genotype imputation and meta-analysis were supported by EY022305 (J.L.W.). Funding for the collection of cases and controls was provided by the following NIH grants: EY015543 (R.R. Allingham); EY006827 (D. Gaasterland); HL73042, HL073389, EY13315, EY023646 (M.A.H.); CA87969, CA49449, UM1 CA167552 (J.H. Kang); EY009149 (P.R. Lichter); HG004608 (C. McCarty); EY008208 (F.A. Medeiros); EY015473 (L.R.P.); EY012118 (M. Pericak-Vance); EY015682 (A. Realini); EY011671, EY09580 (J.E. Richards); EY013178 (J.S. Schuman); RR015574, EY015872, EY010886, EY009847, EY014104 (J.L.W.); EY011008, EY144428, EY144448 and EY18660 (K. Zhang). J.L.W. and L.R.P. are also supported by the Harvard Glaucoma Center for Excellence and Research to Prevent Blindness. J.N.C.B. is supported by NIH T32 EY007157 (CWRU) and T32 EY21453-2 (VUMC). MEEI case-control sample: genotyping for the Massachusetts Eye and Ear Infirmary (MEEI) case-control sample was performed at the Broad Institute of MIT and Harvard with funding support from the NIH GEI (Gene Environment Initiative) (U01HG04424 and U01HG004728). The GENEVA Coordinating Center (U01HG004446) assisted with genotype cleaning. Imputation was supported by NIH EY022305 (JLW). Collection of cases and controls was supported by NIH EY015872 (JLW) and NIH P30 014104 (JLW). Funding to pay the Open Access publication charges for this article was provided by Singapore Eye Research Institute.

Conflict of Interest statement. None declared.

References

1. Quigley, H.A. (1996) Number of people with glaucoma worldwide. *Br. J. Ophthalmol.*, **80**, 389–393.
2. Quigley, H.A. and Broman, A.T. (2006) The number of people with glaucoma worldwide in 2010 and 2020. *Br. J. Ophthalmol.*, **90**, 262–267.
3. Tham, Y.C., Li, X., Wong, T.Y., Quigley, H.A., Aung, T. and Cheng, C.Y. (2014) Global prevalence of glaucoma and projections of glaucoma burden through 2040: a systematic review and meta-analysis. *Ophthalmology*, **121**, 2081–2090.
4. Allingham, R.R., Liu, Y. and Rhee, D.J. (2009) The genetics of primary open-angle glaucoma: a review. *Exp. Eye Res.*, **88**, 837–844.
5. Fan, B.J., Wang, D.Y., Lam, D.S. and Pang, C.P. (2006) Gene mapping for primary open angle glaucoma. *Clin. Biochem.*, **39**, 249–258.
6. Sheffield, V.C., Stone, E.M., Alward, W.L., Drack, A.V., Johnson, A.T., Streb, L.M. and Nichols, B.E. (1993) Genetic linkage of familial open angle glaucoma to chromosome 1q21-q31. *Nat. Genet.*, **4**, 47–50.
7. Stone, E.M., Fingert, J.H., Alward, W.L., Nguyen, T.D., Polansky, J.R., Sunden, S.L., Nishimura, D., Clark, A.F., Nystuen, A., Nichols, B.E. *et al.* (1997) Identification of a gene that causes primary open angle glaucoma. *Science (New York, NY)*, **275**, 668–670.
8. Rezaie, T., Child, A., Hitchings, R., Brice, G., Miller, L., Coca-Prados, M., Heon, E., Krupin, T., Ritch, R., Kreutzer, D. *et al.* (2002) Adult-onset primary open-angle glaucoma caused by mutations in optineurin. *Science (New York, NY)*, **295**, 1077–1079.
9. Sarfarazi, M., Child, A., Stoilova, D., Brice, G., Desai, T., Trifan, O.C., Poinoosawmy, D. and Crick, R.P. (1998) Localization of the fourth locus (GLC1E) for adult-onset primary open-angle glaucoma to the 10p15-p14 region. *Am. J. Hum. Genet.*, **62**, 641–652.
10. Monemi, S., Spaeth, G., DaSilva, A., Popinchalk, S., Ilitchev, E., Liebmann, J., Ritch, R., Heon, E., Crick, R.P., Child, A. *et al.* (2005) Identification of a novel adult-onset primary open-angle glaucoma (POAG) gene on 5q22.1. *Hum. Mol. Genet.*, **14**, 725–733.
11. Fingert, J.H. (2011) Primary open-angle glaucoma genes. *Eye (London, UK)*, **25**, 587–595.
12. Fingert, J.H., Robin, A.L., Stone, J.L., Roos, B.R., Davis, L.K., Scheetz, T.E., Bennett, S.R., Wassink, T.H., Kwon, Y.H., Alward, W.L. *et al.* (2011) Copy number variations on chromosome 12q14 in patients with normal tension glaucoma. *Hum. Mol. Genet.*, **20**, 2482–2494.
13. Fan, B.J., Leung, Y.F., Wang, N., Lam, S.C., Liu, Y., Tam, O.S. and Pang, C.P. (2004) Genetic and environmental risk factors for primary open-angle glaucoma. *Chin. Med. J.*, **117**, 706–710.
14. Wiggs, J.L., Damji, K.F., Haines, J.L., Pericak-Vance, M.A. and Allingham, R.R. (1996) The distinction between juvenile and adult-onset primary open-angle glaucoma. *Am. J. Hum. Genet.*, **58**, 243–244.
15. Kang, J.H., Wiggs, J.L., Rosner, B.A., Hankinson, S.E., Abdrabou, W., Fan, B.J., Haines, J. and Pasquale, L.R. (2010) Endothelial nitric oxide synthase gene variants and primary open-angle glaucoma: interactions with sex and postmenopausal hormone use. *Invest. Ophthalmol. Visual Sci.*, **51**, 971–979.
16. Hirschhorn, J.N. and Daly, M.J. (2005) Genome-wide association studies for common diseases and complex traits. *Nat. Rev.*, **6**, 95–108.
17. Thorleifsson, G., Walters, G.B., Hewitt, A.W., Masson, G., Helgason, A., DeWan, A., Sigurdsson, A., Jonasdottir, A., Gudjonsson, S.A., Magnusson, K.P. *et al.* (2010) Common variants near CAV1 and CAV2 are associated with primary open-angle glaucoma. *Nat. Genet.*, **42**, 906–909.
18. Burdon, K.P., Macgregor, S., Hewitt, A.W., Sharma, S., Chidlow, G., Mills, R.A., Danoy, P., Casson, R., Viswanathan, A. C., Liu, J.Z. *et al.* (2011) Genome-wide association study identifies susceptibility loci for open angle glaucoma at TMCO1 and CDKN2B-AS1. *Nat. Genet.*, **43**, 574–578.
19. Chen, Y., Lin, Y., Vithana, E.N., Jia, L., Zuo, X., Wong, T.Y., Chen, L.J., Zhu, X., Tam, P.O., Gong, B. *et al.* (2014) Common variants near ABCA1 and in PMM2 are associated with primary open-angle glaucoma. *Nat. Genet.*, **46**, 1115–1119.
20. Gharahkhani, P., Burdon, K.P., Fogarty, R., Sharma, S., Hewitt, A.W., Martin, S., Law, M.H., Cremin, K., Bailey, J.N., Loomis, S.J. *et al.* (2014) Common variants near ABCA1, AFAP1 and GMDS

confer risk of primary open-angle glaucoma. *Nat. Genet.*, **46**, 1120–1125.
21. Hysi, P.G., Cheng, C.Y., Springelkamp, H., Macgregor, S., Bailey, J.N., Wojciechowski, R., Vitart, V., Nag, A., Hewitt, A.W., Hohn, R. *et al.* (2014) Genome-wide analysis of multi-ancestry cohorts identifies new loci influencing intraocular pressure and susceptibility to glaucoma. *Nat. Genet.*, **46**, 1126–1130.
22. Wiggs, J.L., Yaspan, B.L., Hauser, M.A., Kang, J.H., Allingham, R.R., Olson, L.M., Abdrabou, W., Fan, B.J., Wang, D.Y., Brodeur, W. *et al.* (2012) Common variants at 9p21 and 8q22 are associated with increased susceptibility to optic nerve degeneration in glaucoma. *PLoS Genet.*, **8**, e1002654.
23. Fan, B.J., Wang, D.Y., Pasquale, L.R., Haines, J.L. and Wiggs, J.L. (2011) Genetic variants associated with optic nerve vertical cup-to-disc ratio are risk factors for primary open angle glaucoma in a US Caucasian population. *Invest. Ophthalmol. Visual Sci.*, **52**, 1788–1792.
24. Cao, D., Jiao, X., Liu, X., Hennis, A., Leske, M.C., Nemesure, B. and Hejtmancik, J.F. (2012) CDKN2B polymorphism is associated with primary open-angle glaucoma (POAG) in the Afro-Caribbean population of Barbados, West Indies. *PLoS ONE*, **7**, e39278.
25. Nakano, M., Ikeda, Y., Tokuda, Y., Fuwa, M., Omi, N., Ueno, M., Imai, K., Adachi, H., Kageyama, M., Mori, K. *et al.* (2012) Common variants in CDKN2B-AS1 associated with optic-nerve vulnerability of glaucoma identified by genome-wide association studies in Japanese. *PLoS ONE*, **7**, e33389.
26. Huyghe, J.R., Jackson, A.U., Fogarty, M.P., Buchkovich, M.L., Stancakova, A., Stringham, H.M., Sim, X., Yang, L., Fuchsberger, C., Cederberg, H. *et al.* (2013) Exome array analysis identifies new loci and low-frequency variants influencing insulin processing and secretion. *Nat. Genet.*, **45**, 197–201.
27. (ANZgene), Australia and New Zealand Multiple Sclerosis Genetics Consortium. (2009) Genome-wide association study identifies new multiple sclerosis susceptibility loci on chromosomes 12 and 20. *Nat. Genet.*, **41**, 824–828.
28. Kooner, J.S., Saleheen, D., Sim, X., Sehmi, J., Zhang, W., Frossard, P., Been, L.F., Chia, K.S., Dimas, A.S., Hassanali, N. *et al.* (2011) Genome-wide association study in individuals of South Asian ancestry identifies six new type 2 diabetes susceptibility loci. *Nat. Genet.*, **43**, 984–989.
29. Reveille, J.D., Sims, A.M., Danoy, P., Evans, D.M., Leo, P., Pointon, J.J., Jin, R., Zhou, X., Bradbury, L.A., Appleton, L.H. *et al.* (2010) Genome-wide association study of ankylosing spondylitis identifies non-MHC susceptibility loci. *Nat. Genet.*, **42**, 123–127.
30. Hoglinger, G.U., Melhem, N.M., Dickson, D.W., Sleiman, P.M., Wang, L.S., Klei, L., Rademakers, R., de Silva, R., Litvan, I., Riley, D.E. *et al.* (2011) Identification of common variants influencing risk of the tauopathy progressive supranuclear palsy. *Nat. Genet.*, **43**, 699–705.
31. Khor, C.C., Davila, S., Breunis, W.B., Lee, Y.C., Shimizu, C., Wright, V.J., Yeung, R.S., Tan, D.E., Sim, K.S., Wang, J.J. *et al.* (2011) Genome-wide association study identifies FCGR2A as a susceptibility locus for Kawasaki disease. *Nat. Genet.*, **43**, 1241–1246.
32. Sawcer, S., Hellenthal, G., Pirinen, M., Spencer, C.C., Patsopoulos, N.A., Moutsianas, L., Dilthey, A., Su, Z., Freeman, C., Hunt, S.E. *et al.* (2011) Genetic risk and a primary role for cell-mediated immune mechanisms in multiple sclerosis. *Nature*, **476**, 214–219.
33. Bonnefond, A., Skrobek, B., Lobbens, S., Eury, E., Thuillier, D., Cauchi, S., Lantieri, O., Balkau, B., Riboli, E., Marre, M. *et al.* (2013) Association between large detectable clonal mosaicism and type 2 diabetes with vascular complications. *Nat. Genet.*, **45**, 1040–1043.
34. Lee, S., Wu, M.C. and Lin, X. (2012) Optimal tests for rare variant effects in sequencing association studies. *Biostatistics*, **13**, 762–775.
35. Ramdas, W.D., van Koolwijk, L.M., Ikram, M.K., Jansonius, N. M., de Jong, P.T., Bergen, A.A., Isaacs, A., Amin, N., Aulchenko, Y.S., Wolfs, R.C. *et al.* (2010) A genome-wide association study of optic disc parameters. *PLoS Genet.*, **6**, e1000978.
36. Khor, C.C., Ramdas, W.D., Vithana, E.N., Cornes, B.K., Sim, X., Tay, W.T., Saw, S.M., Zheng, Y., Lavanya, R., Wu, R. *et al.* (2011) Genome-wide association studies in Asians confirm the involvement of ATOH7 and TGFBR3, and further identify CARD10 as a novel locus influencing optic disc area. *Hum. Mol. Genet.*, **20**, 1864–1872.
37. Springelkamp, H., Höhn, R., Mishra, A., Hysi, P.G., Khor, C.C., Loomis, S.J., Bailey, J.N., Gibson, J., Thorleifsson, G., Janssen, S.F. *et al.* (2015) Meta-analysis of genome-wide association studies identifies novel loci that influence cupping and the glaucomatous process. *Nat. Commun.*, **5**, 4883.
38. Garway-Heath, D.F., Ruben, S.T., Viswanathan, A. and Hitchings, R.A. (1998) Vertical cup/disc ratio in relation to optic disc size: its value in the assessment of the glaucoma suspect. *Br. J. Ophthalmol.*, **82**, 1118–1124.
39. Lu, Y., Vitart, V., Burdon, K.P., Khor, C.C., Bykhovskaya, Y., Mirshahi, A., Hewitt, A.W., Koehn, D., Hysi, P.G., Ramdas, W. D. *et al.* (2013) Genome-wide association analyses identify multiple loci associated with central corneal thickness and keratoconus. *Nat. Genet.*, **45**, 155–163.
40. Fuchshofer, R. (2011) The pathogenic role of transforming growth factor-beta2 in glaucomatous damage to the optic nerve head. *Exp. Eye Res.*, **93**, 165–169.
41. Pasquale, L.R., Dorman-Pease, M.E., Lutty, G.A., Quigley, H.A. and Jampel, H.D. (1993) Immunolocalization of TGF-beta 1, TGF-beta 2, and TGF-beta 3 in the anterior segment of the human eye. *Invest. Ophthalmol. Visual Sci.*, **34**, 23–30.
42. Pena, J.D., Taylor, A.W., Ricard, C.S., Vidal, I. and Hernandez, M.R. (1999) Transforming growth factor beta isoforms in human optic nerve heads. *Br. J. Ophthalmol.*, **83**, 209–218.
43. Massague, J., Blain, S.W. and Lo, R.S. (2000) TGFbeta signaling in growth control, cancer, and heritable disorders. *Cell*, **103**, 295–309.
44. Hannon, G.J. and Beach, D. (1994) p15INK4B is a potential effector of TGF-beta-induced cell cycle arrest. *Nature*, **371**, 257–261.
45. Pasmant, E., Sabbagh, A., Vidaud, M. and Bieche, I. (2011) ANRIL, a long, noncoding RNA, is an unexpected major hotspot in GWAS. *FASEB J.*, **25**, 444–448.
46. Blobe, G.C., Liu, X., Fang, S.J., How, T. and Lodish, H.F. (2001) A novel mechanism for regulating transforming growth factor beta (TGF-beta) signaling. Functional modulation of type III TGF-beta receptor expression through interaction with the PDZ domain protein, GIPC. *J. Biol. Chem.*, **276**, 39608–39617.
47. Diestel, U., Resch, M., Meinhardt, K., Weiler, S., Hellmann, T. V., Mueller, T.D., Nickel, J., Eichler, J. and Muller, Y.A. (2013) Identification of a novel TGF-beta-binding site in the Zona Pellucida C-terminal (ZP-C) domain of TGF-beta-receptor-3 (TGFR-3). *PLoS ONE*, **8**, e67214.
48. Cai, C., Rajaram, M., Zhou, X., Liu, Q., Marchica, J., Li, J. and Powers, R.S. (2012) Activation of multiple cancer pathways and tumor maintenance function of the 3q amplified oncogene FNDC3B. *Cell Cycle (Georgetown, Tex)*, **11**, 1773–1781.
49. Price, A.L., Patterson, N.J., Plenge, R.M., Weinblatt, M.E., Shadick, N.A. and Reich, D. (2006) Principal components analysis

corrects for stratification in genome-wide association studies. *Nat. Genet.*, **38**, 904–909.
50. Purcell, S., Neale, B., Todd-Brown, K., Thomas, L., Ferreira, M.A., Bender, D., Maller, J., Sklar, P., de Bakker, P.I., Daly, M.J. *et al.* (2007) PLINK: a tool set for whole-genome association and population-based linkage analyses. *Am. J. Hum. Genet.*, **81**, 559–575.
51. Barrett, J.C., Fry, B., Maller, J. and Daly, M.J. (2005) Haploview: analysis and visualization of LD and haplotype maps. *Bioinformatics (Oxford, England)*, **21**, 263–265.
52. Ihaka, R. and Gentleman, R. (1996) R: a language for data analysis and graphics. *J. Comput. Graph. Stat.*, **5**, 299–314.
53. Nalls, M.A., Plagnol, V., Hernandez, D.G., Sharma, M., Sheerin, U.M., Saad, M., Simon-Sanchez, J., Schulte, C., Lesage, S., Sveinbjornsdottir, S. *et al.* (2011) Imputation of sequence variants for identification of genetic risks for Parkinson's disease: a meta-analysis of genome-wide association studies. *Lancet*, **377**, 641–649.
54. Vithana, E.N., Aung, T., Khor, C.C., Cornes, B.K., Tay, W.T., Sim, X., Lavanya, R., Wu, R., Zheng, Y., Hibberd, M.L. *et al.* (2011) Collagen-related genes influence the glaucoma risk factor, central corneal thickness. *Hum. Mol. Genet.*, **20**, 649–658.

Genes to Cells

Stage-specific reference genes significant for quantitative PCR during mouse retinal development

Hiroko Adachi[1], Hiroyuki Tominaga[1], Yuko Maruyama[2], Kazuhito Yoneda[2], Kazuichi Maruyama[2†], Kengo Yoshii[3], Shigeru Kinoshita[2], Masakazu Nakano[1]* and Kei Tashiro[1]

[1]*Department of Genomic Medical Sciences, Kyoto Prefectural University of Medicine, Kyoto 602-8566, Japan*
[2]*Department of Ophthalmology, Kyoto Prefectural University of Medicine, Kyoto 602-8566, Japan*
[3]*Department of Medical Statistics, Kyoto Prefectural University of Medicine, Kyoto 602-8566, Japan*

Developing mouse retina has been serving as an ideal model for investigating the molecular mechanism of neural development and angiogenesis, because several significant events associated with these physiological phenomena are drastically occurring in conjunction with retinal development. However, as many genes are influencing on each other to establish mature retina within 21 days from E10 to P12, we must carefully design the experiments, such as in the case of quantitating the amount of altered gene expression toward the establishment of retina by quantitative PCR. As we have seen considerable variations of quantitative results in different developmental stages of retina depending on the reference genes used for compensation, we here attempted to determine a reliable reference gene to accurately quantitate the target genes in each stage. According to the results of *in silico* prediction and comparison with a database of SAGE, we found that the most stable gene from early to late stages was *Sdha*, whereas one of the most popular housekeeping genes, *Actb*, was the one that could mislead the quantitative results even in the adult stage. Consequently, we pointed out the importance of selecting an appropriate reference gene, especially to quantitate the amount of gene expression in the developmental stages of a certain tissue.

Introduction

As a number of critical biological events related to neural development and angiogenesis are drastically occurring in conjunction with retinal development, mouse retina obtained during pre- and postnatal period has been considered as one of the best experimental materials for investigating these physiological phenomena. Moreover, mouse retina can readily peel off from a weakly attached retinal pigment epithelium with few contaminations, if any, of other tissues, and thus, it is practically easy to obtain the materials of different developmental stages just by dissecting the eyes at each time point. Indeed, several genes encoding key molecules have been identified using mouse retina, such as a photoreceptor-specific transcription cofactor, cone-rod homeobox gene (*Crx*), which plays a significant role in the differentiation of retinal progenitor cells into photoreceptor cells (Furukawa *et al.* 1997), and vascular endothelial growth factor (VEGF) family genes (e.g., *Vegfa*), which encode angiogenesis factors critical for expanding angioblasts to form the initial vessels and for subsequent endothelial cell migration to form vessel networks (Risau 1997; Cleaver & Krieg 1998; Coultas *et al.* 2005).

However, as the mature retina consists of ten distinct layers with five retinal neural cells and is difficult to separate into each functional component (Hoon *et al.* 2014), it is quite important to carefully design the experiments when using whole retina to correctly capture the underlying biological mechanism occurring within this complex tissue. Moreover, developing retina is more complicated because many

Communicated by: Tadashi Uemura
**Correspondence:* manakano@koto.kpu-m.ac.jp
†Present address: Department of Ophthalmology, Tohoku University Graduate School of Medicine, Sendai, Miyagi 980-8574, Japan.

DOI: 10.1111/gtc.12254

gene networks are coordinately regulating the developmental fate of retinal progenitor cells to establish structurally, as well as functionally complete ten layers within 21 days from E10 to P12 (Marquardt & Gruss 2002). Therefore, to probe the molecular mechanism of, for example, neural development and/or angiogenesis by quantitating the amount of altered gene expression reflecting the changes toward the retinal establishment, we must pay a strict attention not only to obtain the precise data but also to comprehend the data correctly to show the relationship between the genes and their contributions to each biological function.

Quantitative PCR (qPCR) is one of the most frequently used and highly sensitive methods for gene expression analysis, enabling us to quantitate the expression level of target genes precisely. To compare the relative amount of a particular gene expression within different sources, the expression level of 'housekeeping genes', such as beta-actin (*Actb*) or glyceraldehyde-3-phosphate dehydrogenase (*Gapdh*) genes, is often measured simultaneously as a reference gene for compensating the raw data of a target gene with that of the reference gene. However, we are aware that the expression levels of housekeeping genes are not always constant, depending on the target tissues or cells, especially in developing tissues, where the gene expression of cellular components is significantly changing. Therefore, it is extremely important to select an appropriate reference gene for an accurate compensation of the target gene expression, although we are prone to choose a popular housekeeping gene that is just known to be expressing ubiquitously without performing any preliminary experiments.

In this study, we found considerable variations of quantitative results during the developmental period of mouse retina depending on which reference genes were used for compensation. We therefore evaluated several reference genes by using an *in silico* prediction program, *RefFinder* (Xie *et al.* 2012), as well as by comparing the quantitative results of target genes with a mouse retinal transcriptome database derived from serial analysis of gene expression (SAGE) tags (Blackshaw *et al.* 2001, 2004). As a result, we found that, as far as we investigated, the most reliable gene from early to late stages of developmental mouse retina was succinate dehydrogenase complex, subunit A, flavoprotein (Fp) (*Sdha*), whereas, *Actb* was the one that could mislead the quantitative results even in the adult stage. Consequently, we here pointed out the importance of performing preliminary experiments to select an appropriate reference gene, especially when attempting to quantitate the amount of gene expression in developmental stages of a certain tissue.

Results

Expression stability of reference genes predicted by *RefFinder*

We first determined the variation of quantification results of *Actb* and *Sdha* derived from individual mice at the same time point (Table S1 in Supporting Information). As a result, even though the standard deviation (SD) of cycle threshold (C_t) value (defined as the number of PCR cycles required for detecting the fluorescent signal crossing the threshold as a positive signal) derived from each retina of P0 littermate mouse ($n = 3$) was larger than that from the pooled retinal RNA of those mice, the difference in C_t value seemed to be not significant between the two ways of generating replication data. We therefore decided to pool the RNA from different mice in order to minimize the possible errors created by individual variation.

To select a reliable reference gene for compensating raw quantitative data of target genes in mouse retina, we first analyzed the eight candidate genes in three developmental stages (Table S4 in Supporting Information) by an *in silico* prediction program, *RefFinder* (Xie *et al.* 2012), and evaluated the results of 'expression stability' (i.e., how constant the reference gene is expressing in the different time points) expressed as the geometric mean of ranking (Fig. 1). As a result, among the genes we investigated, *Sdha* was the most stable gene in both early (E18 through P4) and late (P8, P10 and P14) stages (Fig. 1A,B). In the case of adult stage (4w, 8w and 12w), *Tbp* was predicted as the most stable gene, whereas *Sdha* dropped into the 6th (Fig. 1C), suggesting that the expression of housekeeping genes varies during retinal development. In contrast, the *Actb*, which is one of the most popular genes for qPCR compensation, was found to be unstable throughout the stages (Fig. 1A–C).

Quantification of target genes compensated by representative reference genes

We then attempted to quantitate the expression level of two sets of target genes, '*Crx* and *Nrl*' and '*Vegfa* and its receptor *Kdr*', which are known to be expressed in mouse retina through the stages in conjunction with neural development and

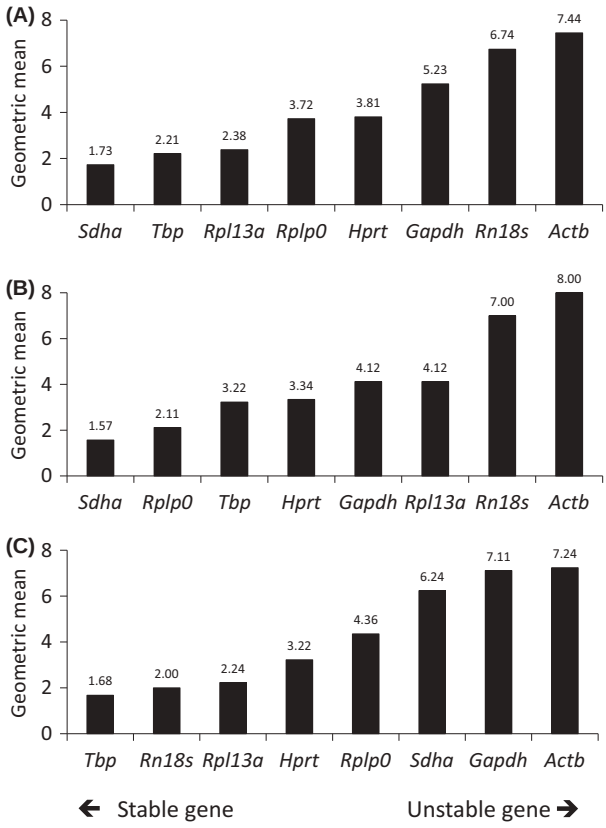

Figure 1 Expression stability of reference genes in different stages of mouse retina predicted by *RefFinder*. The results of *RefFinder* were expressed as the geometric mean of ranking determined by four major programs, *geNorm*, *NormFinder*, *BestKeeper* and *comparative* $\Delta\Delta C_t$ *method*, to evaluate how constant the reference gene is expressing in the different time points (expression stability) in (A) early (E18 through P4), (B) late (P8, P10 and P14) and (C) adult (4w, 8w and 12w) stages. Note that the smaller value of geometric mean represents the higher ranking of the expression stability.

angiogenesis, respectively (Figs S1, S2 in Supporting Information and 2), in order to compare the quantitative data compensated by different reference genes predicted by *RefFinder*. The expression level of each target gene compensated by different reference genes is shown in Figure S1 (Supporting Information). As one of our aims was to identify reliable reference gene by comparing the variations of target gene/reference gene ratio among different developmental stages, we then normalized the data of expression level to be relative to P0 (Fig. S2 in Supporting Information). To show a representative result, we selected the expression level of target genes compensated by the best two genes (*Sdha* and *Tbp*) and worst two genes (*Actb* and *Rn18s*) predicted by *RefFinder* (Fig. 2). In the case of neural development genes, the expression patterns of *Crx* (Fig. 2A) and *Nrl* (Fig. 2B), which were compensated by either *Sdha* (open circle) or *Tbp* (open triangle), appeared to be quite similar to each other throughout the stages, although the pattern of both genes compensated by *Actb* (closed triangle) looked different—a remarkable increase in expression was observed after P8 in the late stage and became consistent (Fig. 2A) or kept increasing (Fig. 2B) toward the adult stage. In the case of angiogenesis genes, the expression patterns of *Vegfa* compensated by four references genes (Fig. 2C) seemed to be similar until P14, even though the different extent of expression rate in increase/decrease during the late stage, but showed higher expression level compensated by *Rn18s* (closed circle) or *Actb* (closed triangle) than by the other genes in the adult stage (Fig. 2C). In contrast, the expression patterns of *Kdr* (Fig. 2D) compensated by either *Sdha* (open circle) or *Tbp* (open triangle) showed a peak expression at P2, followed by a gradual decrease toward the adult stage, whereas in the case of *Actb* (closed triangle), the pattern seemed to be rather opposite—a gradual increase, in general, through the development process (Fig. 2D).

Comparison with quantitative data derived from Mouse Retina SAGE Library

As we obtained some distinct expression results of target genes when compensated by different reference genes (Fig. 2), we referred an expression database of retinal SAGE tags (Mouse Retina SAGE Library) (Blackshaw *et al.* 2001, 2004), in an attempt to determine the reliable reference genes to be used for compensation in each stage. As shown in Figure S3 (Supporting Information), the tag counts of *Sdha*, *Tbp* and *Hprt* were found to be constant, whereas those of *Actb*, *Gapdh* and *Rpl13a* seemed to be considerably changing especially within the early stage. However, as the SAGE data in between P6 and P28 have not been available, we made a regression curve from the SAGE data (Fig. 3; solid line) and evaluated the consistency with the qPCR results by means of AIC (Akaike 1969) to be able to quantitatively compare the qPCR with SAGE data throughout the period (Fig. 3 and Table 2). As for the neural development genes, the plots of *Crx* with *Sdha* compensation (Fig. 3A; open circle) seemed to be well fitted to the regression curve, although when compensated by *Actb* (Fig. 3A; open triangle), the plots deviated from the

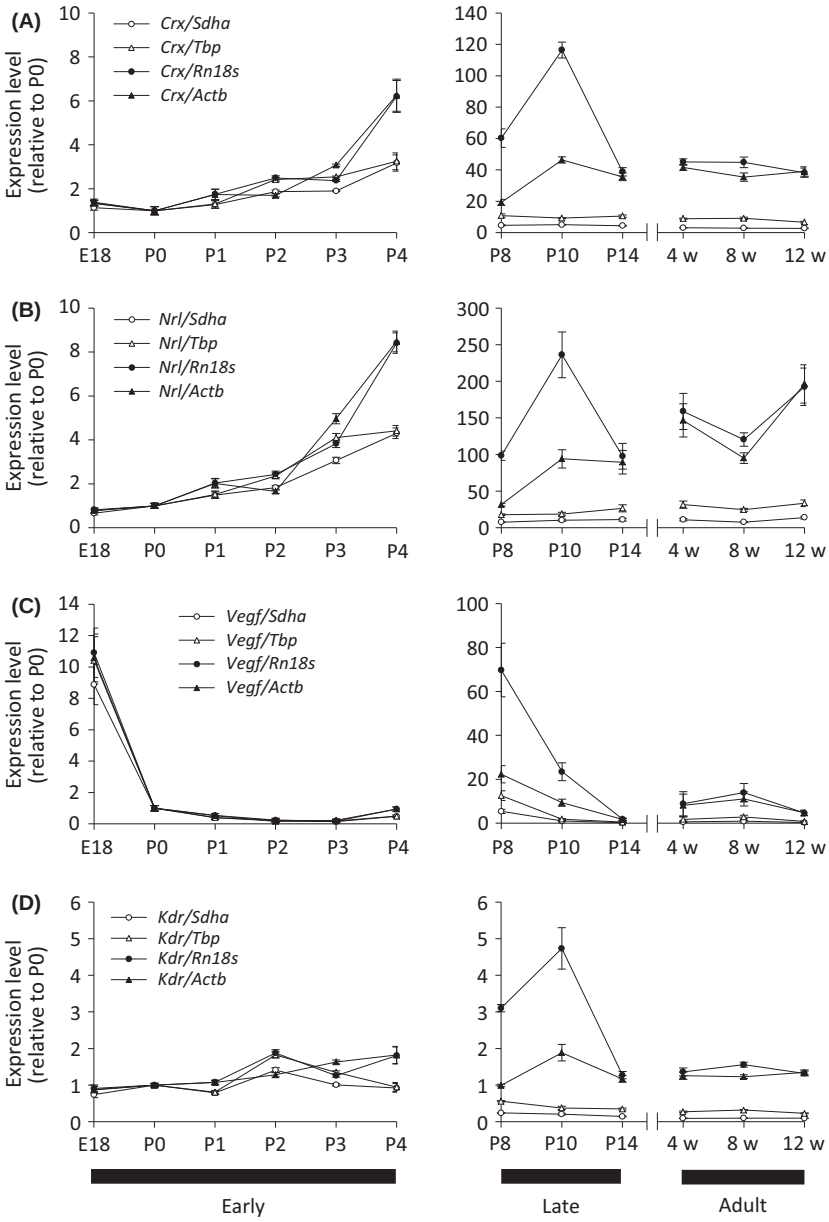

Figure 2 Expression level of target genes in mouse retina compensated by different reference genes. Expression levels of the genes related to neural development, (A) *Crx* and (B) *Nrl*, and angiogenesis, (C) *Vegfa* and (D) *Kdr*, were quantified. To calculate the expression level of each target gene, we first obtained the quantitative data of reference genes or target genes in mouse retinal cDNA by applying the C_t values to each corresponding standard curve. We then compensated the quantitative data of target genes by those of *Sdha* (predicted as the most stable gene in early and late stages), *Tbp* (so as in the adult stage), *Rn18s* (predicted as the unstable gene in early and late stages) or *Actb* (predicted as the unstable gene throughout the stages). All the results are expressed as the relative amount to the results obtained at P0. The error bars represent the standard deviation of expression level obtained by qPCR carried out in triplicate.

curve after the late stage. In contrast, the plots of *Nrl* with both *Sdha* (Fig. 3B; open circle) and *Actb* (Fig. 3B; open triangle) compensation seemed to be generally inconsistent with the regression curve. According to the ranking of proximity between the qPCR and SAGE data determined by AIC (Table 2), the qPCR results of *Crx* or *Nrl* compensated by *Actb* ranked to the 7th out of the eight genes analyzed,

whereas the ranking of the genes compensated by *Sdha* splits into the 1st (*Crx*) or the 5th (*Nrl*). The low ranking of *Nrl* might be due to the instability of *Sdha* in the adult stage (Fig. 1C) and resulted in an inaccurate expression data at P28 (Fig. 2B; open circle).

As for the angiogenesis genes, the plots of *Vegfa* with *Sdha* (Fig. 3C; open circle) or *Actb* (Fig. 3C; open triangle) compensation showed almost the same trend as in the case of *Crx* (Fig. 3A; Table 2). In contrast, the plots of *Kdr* with *Sdha* compensation (Fig. 3D; open circle) seemed to be rather close than those with *Actb* compensation (open triangle, Fig 3D) to the regression curve, showing the decreasing trend of the slope, which was supported by the ranking of AIC to be the 2nd for *Sdha* and 5th for *Actb* (Table 2).

Consequently, we here showed that the expression level of each target gene was likely to be correct when compensated by not *Actb* but *Sdha*, especially during early to late stages of retinal development, which was well correlated with the prediction results of these genes given by *RefFinder* (Fig. 1).

Discussion

In this study, we showed that the apparent expression levels of target genes in different stages of mouse retina may vary significantly when compensated by inappropriate reference genes. We therefore attempted to discover reliable genes for qPCR compensation in each stage from eight widely accepted reference genes and pointed out the significance of selecting the appropriate genes in advance of quantitating the target gene expression by using an *in silico* prediction program, as well as by comparing with the precise expression database, such as the SAGE data of mouse retina referred in this study.

For selecting an appropriate reference gene to obtain accurate quantification results of target genes, there are several useful *in silico* programs, which are freely available. These programs share a common feature for prioritizing the candidate genes based on predicting 'expression stability' of each reference gene by not only assessing the measurements of a single gene expression obtained from multiple samples, but also taking into account the expression results of different genes in the same sample. For example, *geNorm* (Vandesompele *et al.* 2002) calculates arithmetic mean of all pairwise variations from the raw expression data as 'gene-stability measure M', whereas *NormFinder* (Andersen *et al.* 2004) provides 'stability values' calculated by using Bayesian argument to estimate intra- and intergroup variations. However, as each program uses slightly, but significantly different algorithms to assess the expression stability, the ranking results of the analyzed genes tend to vary among programs, sometimes make us difficult to choose which one to use. Thus far, one of the programs, named *RefFinder* (Xie *et al.* 2012), should be the most helpful tool, because it integrates four well-known programs, *geNorm*, *NormFinder*, *BestKeeper* and *comparative* $\Delta\Delta C_t$ *method* (Vandesompele *et al.* 2002; Andersen *et al.* 2004; Pfaffl *et al.* 2004; Silver *et al.* 2006), and gives us the final answer after considering all the results brought by four different algorisms. Therefore, in this study, we decided to apply *RefFinder* for assessing the reference genes suitable for accurate quantification of the target gene expression in developing mouse retina (Fig. 1).

In addition to the *in silico* prediction for evaluating the stability of reference genes, we evaluated the accuracy of quantitative results compensated by two representative reference genes by referring a database. As there were no expression data of mouse retina in one of the most reliable expression databases, Functional Annotation of the Mammalian Genome (FANTOM), based on CAGE data (http://fantom.gsc.riken.jp), we decided to refer Mouse Retina SAGE Library (http://cepko.med.harvard.edu) (Blackshaw *et al.* 2001, 2004), composed of transcriptome data of retina through pre-, postnatal and adult stages. Although the SAGE method is practically labor-intensive to perform routinely, once the data have been acquired, it serves as an excellent standard for obtaining quantitative information of actual expression level of each gene, because it directly counts the number of unique digital sequences of cDNA tags derived from whole transcripts. We therefore compared our qPCR results compensated by different reference genes with the SAGE data by generating a regression curve from several time points (Fig. 3). Overall, we found that the expression levels of target genes were mostly close to the SAGE data when compensated by *Sdha* rather than by *Actb* determined by AIC (Akaike 1969) (Table 2). However, it should have been more accurate if we could compare the results divided into each stage, as we carried out in the experiments shown in Figures 1 and 2, and generate more precise regression curves, although we had to generate a curve reflecting the entire stages, due to the limited data of time points in the later stages (i.e., no data between P6 to P28) available from the database.

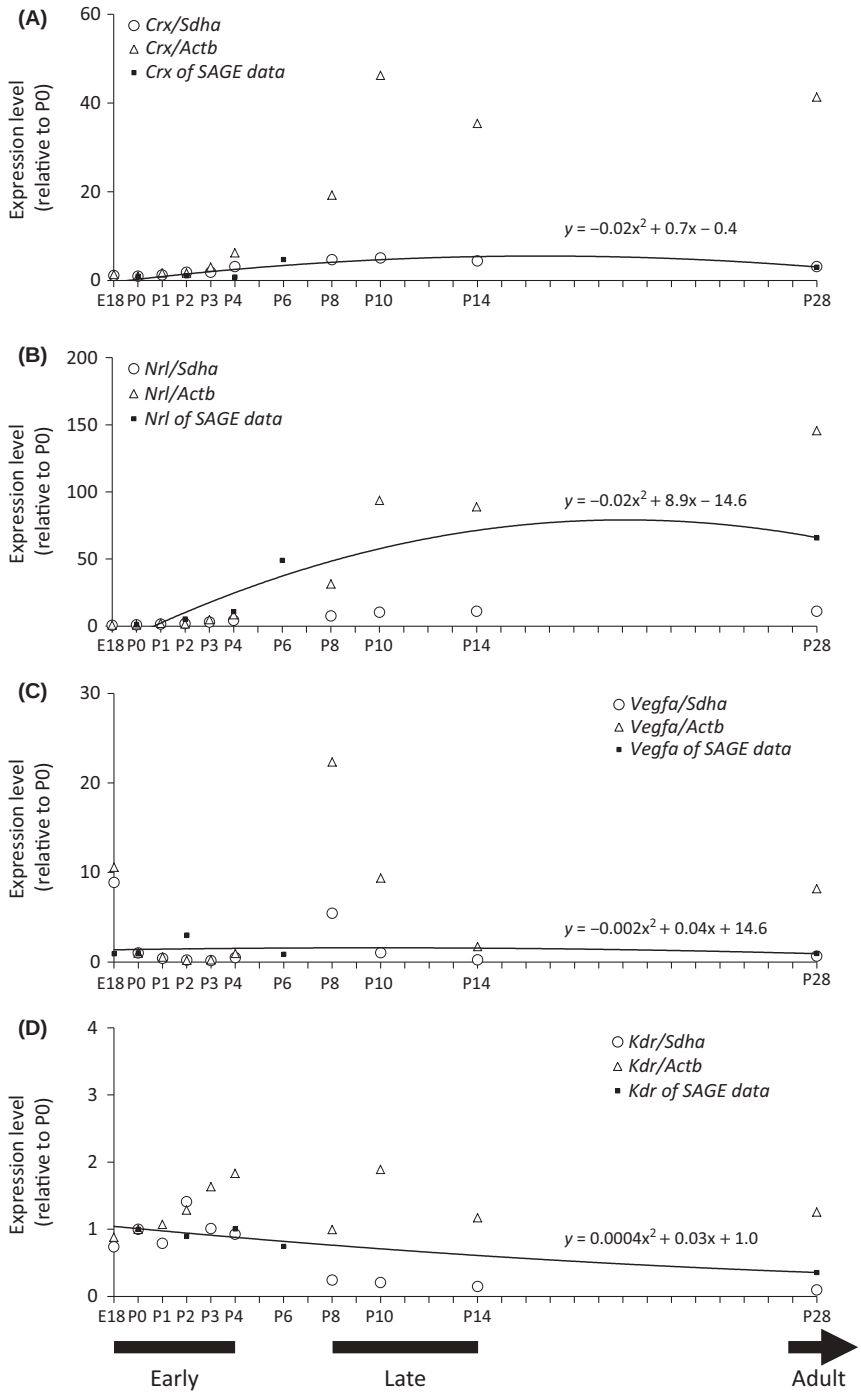

Figure 3 Comparison of expression level of target genes quantified by qPCR or SAGE. Expression levels of (A) *Crx*, (B) *Nrl*, (C) *Vegfa* and (D) *Kdr* obtained by qPCR compensated by *Sdha* (open circle) or *Actb* (open triangle) were compared with the SAGE data. Note that all the expression levels of target genes at each time point were shown as the relative amount to the results obtained at P0. The quadratic regression equation was calculated on the basis of SAGE data for each time point (closed square), and a regression curve was generated (solid line). The residual sum of expression level at each time point obtained by qPCR against the regression curve was calculated and applied to the equation of AIC to evaluate the proximity of qPCR data to SAGE data (Table 2).

According to our multiple evaluations, one of the most popular housekeeping genes, *Actb*, was found to be inappropriate for compensating the target genes irrespective of the stages. As actin is one of the three major proteins of cytoskeleton, one could readily speculate that it should be playing a pivotal role to establish complete tissue structure within a few days in the early stage of development. In fact, the apparent expression levels of all of the target genes compensated by *Actb* (Fig. 2A–D; closed triangle) seemed to be relatively high in the later stages than in the early stage when compared with the results compensated by *Sdha* (open circle) or *Tbp* (open triangle), which means that actin is highly expressing to develop retina during the early stage, and the expression level decreases in the later stages after the establishment of mature retina. Indeed, according to the results of SAGE tag counts (Figure S3 in Supporting Information), we were able to confirm the high expression level of *Actb* during the early stage, although we could not judge whether the expression level decreases or not due to the limited data points from P6 to P28. However, even in the retinal samples derived from the adult stage (4w, 8w and 12w), not only the predicted stability of *Actb* was found to be poor (Fig. 1C), but also the expression levels of target genes were disturbed by *Actb* compensation (Figs 2 and 3, Table 2). These results suggested that the expression level of *Actb* still varies widely in mature retina.

In contrast, our results suggested that *Sdha* was one of the reliable reference genes out of 8 reference genes we examined, especially in the earlier stages of retinal development, determined by both *in silico* prediction (Fig. 1) and the proximity to the SAGE data of target gene expression (Table 2). *Sdha* encodes the succinate dehydrogenase protein complex located in mitochondria and catalyzes the oxidation of succinate involved in citric acid cycle. According to Figure S3 (Supporting Information), the expression level of *Sdha* appeared to be stable probably due to its low expression level in developing retina. Therefore, we concern that the quantified results of *Sdha* could be easily influenced by experimental skills, such as the quality of RNA preparation and qPCR. Consequently, we recommend checking the quality of RNA (Table S2 in Supporting Information) and amplification efficiency of PCR (Table S3 in Supporting Information), to ensure the usefulness of *Sdha* as a reference gene in the early stage of retinal development.

In addition to *Sdha*, the genes related to metabolic pathway, such as *Gapdh*, *Hprt* or *Sdha* analyzed in this study (Table 1), could be expressing constantly through the retinal development to maintain the homeostasis of retinal cells. However, only *Sdha* ranked in the high position from early to late stages in terms of expression stability (Fig. 1A,B), whereas the expression levels of target genes compensated by these three genes, except for *Nrl* compensation, were ranked in reasonably high position in terms of the proximity to the SAGE data (Table 2). From this point of view, we categorized the eight reference genes into some functional groups as cytoskeleton (*Actb*), metabolic enzymes (*Gapdh*, *Hprt* and *Sdha*), ribosomes (*Rn18s*, *Rpl13a* and *Rplp0*) and transcription factor (*Tbp*) (Table 1) and attempted to find a rule that is determining the ranking of these genes. However, we realized that it was difficult to predict the reliability of the reference genes in each stage based on considering the relationships between retinal development and functional aspects of these genes. A large-scale identification of reference genes, such as an effort done by Frericks & Esser (2008), should be a refined way to determine and categorize reference genes by considering the functional relationships in a certain phase of developmental tissues.

Taken all together, when performing qPCR experiments to quantitate the expression level of target genes in developmental tissues, we strongly suggest selecting reliable reference genes beforehand to avoid any misinterpretations of the quantitative results. As many important genes that could explain the mechanism of tissue development are yet to be discovered, the qPCR method will still serve as a sensitive, convenient and cost-effective experimental tool to discover those genes, as long as the accurate quantitative results were obtained using an appropriate reference gene for compensation.

Experimental procedures

Animal procedures and retinal dissection

Animal experiments in this study were approved by the Institutional Animal Experiment Committee of Kyoto Prefectural University of Medicine and carried out by following the Fundamental Guidelines for Proper Conduct of Animal Experiment and Related Activities in Academic Research Institutions. Pregnant mice (C57BL/6J) carrying embryos as well as 4-week (4w), 8w and 12w-old adult mice were purchased from Japan SLC (Hamamatsu, Shizuoka, Japan). In this study, we prepared the retina samples from mice eyes at the following time points: embryonic day 18 (E18), postnatal day 0 (P0) through P4, P8, P10, P14, 4w, 8w and 12w. As all mice were born at E19, we resected the embryos from

Table 1 Primer sequences for qPCR

Gene symbol	Description	Sequence	
Candidate reference gene			
Actb	Actin, beta	Forward	GATTACTGCTCTGGCTCCTAGC
		Reverse	GACTCATCGTACTCCTGCTTGC
Gapdh	Glyceraldehyde-3-phosphate dehydrogenase	Forward	TGACGTGCCGCCTGGAGAAA
		Reverse	AGTGTAGCCCAAGATGCCCTTCAG
Hprt	Hypoxanthine phosphoribosyl transferase	Forward	CAAACTTTGCTTTCCCTGGT
		Reverse	CAAGGGCATATCCAACAACA
Rn18s	18S ribosomal RNA	Forward	CGGCTACCACATCCAAGGAA
		Reverse	GCTGGAATTACCGCGGCT
Rpl13a	Ribosomal protein L13A	Forward	TCTCAAGGTTGTTCGGCTGAA
		Reverse	GCCAGACGCCCCAGGTA
Rplp0	Ribosomal protein, large, P0	Forward	CGACCTGGAAGTCCAACTAC
		Reverse	ATCTGCTGCATCTGCTTG
Sdha	Succinate dehydrogenase complex, subunit A, flavoprotein (Fp)	Forward	GCTCCTGCCTCTGTGGTTGA
		Reverse	AGCAACACCGATGAGCCTG
Tbp	TATA box binding protein	Forward	GAAGAACAATCCAGACTAGCAGCA
		Reverse	CCTTATAGGGAACTTCACATCACAG
Target gene			
Crx	Cone-rod homeobox	Forward	CACGTGAGGAGGTTGCTCTT
		Reverse	TGGACTCCAAATGGACACGG
Nrl	Neural retina leucine zipper gene	Forward	GCTGTGCCTTTCTGGTTCTGA
		Reverse	GCTCCCGCTTTATTTCGAACT
Vegfa	Vascular endothelial growth factor A	Forward	AGCACAGCAGATGTGAATGC
		Reverse	TTTCTCCGCTCTGAACAAGG
Kdr	Kinase insert domain protein receptor	Forward	CCTGCCTACCTCACCTGTTT
		Reverse	CGGCTCTTTCGCTTACTGTT

Table 2 Ranking of proximity of the qPCR data to the SAGE data determined by AIC[†]

	Crx		*Nrl*		*Vegfa*		*Kdr*	
Ranking	Reference gene	AIC	Reference gene	AIC	Reference gene	AIC	Reference gene	AIC
1	*Sdha*	20.9	*Rplp0*	81.5	*Sdha*	56.9	*Hprt*	10.2
2	*Hprt*	34.5	*Tbp*	84.4	*Hprt*	58.5	*Sdha*	12.6
3	*Gapdh*	41.4	*Rpl13a*	86.2	*Gapdh*	62.1	*Rpl13a*	14.5
4	*Rpl13a*	48.6	*Gapdh*	89.5	*Tbp*	65.7	*Rplp0*	15.4
5	*Tbp*	50.2	*Sdha*	90.2	*Rpl13a*	66.1	*Gapdh*	15.5
6	*Rplp0*	69.4	*Hprt*	91.1	*Rplp0*	71.1	*Tbp*	15.7
7	*Actb*	83.9	*Actb*	94.6	*Actb*	74.8	*Actb*	16.6
8	*Rn18s*	97.9	*Rn18s*	107.3	*Rn18s*	96.8	*Rn18s*	36.9

[†]As AIC represents the distance between the results of qPCR and the regression curve of SAGE data, the smaller value of AIC becomes higher in the ranking.

pregnant mice the day before delivery as for the E18 samples. We defined the newborn mice within 12 h postdelivery as P0 and continued breeding the mice from then up to P14 to obtain the samples at each time point. As for the 4w, 8w and 12w retina samples, we directly dissected the eyes from purchased adult mice. We also categorized the collected samples into three groups based on those characteristics during the developmental stages as: early (E18 through P4), late (P8, P10 and P14) and adult (4w, 8w and 12w). After injecting pentobarbital into vein for euthanasia, two eyes per mouse were

removed and rinsed with phosphate-buffered saline without Mg^{++} and Ca^{++} (PBS(−)). Then, the retina was surgically dissected from each eye with particular attention to avoid the contamination of other tissues, such as a retinal pigment epithelium. Two retinas per mouse were pooled as one sample and dissolved into RNA extraction reagent, RNA STAT-60 (TEL-TEST, Friendswood, TX, USA). We collected the retina samples from three individual mice for each time point.

Total RNA extraction

Collected retina samples were homogenized in RNA STAT-60 and mixed for 15 s after adding 200 μL of chloroform (Nacalai Tesque, Kyoto, Japan). The samples were then kept at room temperature for 2 min and centrifuged at 12 000 ***g*** for 15 min at 4 °C. After removing the supernatant, we added 500 μL of isopropanol (Nacalai Tesque), mixed thoroughly and kept at room temperature for 2 min. Then, the samples were centrifuged at 12 000 ***g*** for 10 min at 4 °C, and after removing the supernatant, we added 1 mL of 75% ethanol (Nacalai Tesque) to wash the pellet of extracted total RNA. After centrifuging at 12 000 ***g*** for 5 min at 4 °C, the supernatant was carefully removed, and the pellet was air-dried for 5 min. Finally, we added 25 μL of Ambion nuclease-free water (not diethylpyrocarbonate treated) from Life Technologies (Thermo Fisher Scientific, Waltham, MA, USA) and incubated at 55 °C for 10 min to dissolve the pellet completely. The quantity and quality of total RNA were analyzed by means of NanoDrop ND-1000 (Thermo Fisher Scientific). The total RNA samples were snap-frozen in liquid nitrogen and stored at −80 °C until use.

cDNA synthesis

We pooled total RNA from three samples (500 ng each) originated from retinas of three individual mice eyes, to minimize the potential errors created by the individual variation. Then, we checked the quality of RNA by measuring RNA integrity number (RIN) using Agilent 2100 Bioanalyzer (Agilent Technologies, Santa Clara, CA, USA) (Table S2 in Supporting Information). Retinal cDNA was synthesized with SuperScript III First-Strand Synthesis System from Life Technologies (Thermo Fisher Scientific). First, the reaction mixture, consists of total RNA, primers (oligo(dT) and Random Hexamer) and dNTP, was incubated at 65 °C for 5 min. Next, after adding 10 × RT Buffer, 25 mM $MgCl_2$, 0.1 M DTT, RNaseOUT and SuperScript III Reverse Transcriptase to the reaction, the mixture was incubated at 50 °C for 50 min. The reaction was finally terminated by incubating at 85 °C for 5 min. To remove the RNA template, we added RNase H from Life Technologies (Thermo Fisher Scientific) and incubated at 37 °C for 20 min. As a source for generating standard curves, we also synthesized a cDNA derived from 1 μg of Stratagene QPCR Mouse Reference Total RNA (Agilent Technologies) in the similar way as described above.

Quantitative PCR

We carried out quantitative PCR experiments in accordance with the Minimum Information for Publication of Quantitative Real-Time PCR Experiments (MIQE) Guidelines (Bustin *et al.* 2009). In this study, we used either the published primers (Simpson *et al.* 2000; Mears *et al.* 2001; Jabs *et al.* 2004; Huang *et al.* 2005; Mamo *et al.* 2007; Feng *et al.* 2010; Omori *et al.* 2011; Veazey & Golding 2011; Al-Shabrawey *et al.* 2012) or the primers originally designed by the use of Primer Blast (http://www.ncbi.nlm.nih.gov/tools/primer-blast) and synthesized by Sigma-Aldrich (Table 1). To generate the standard curves, we first prepared PCR products amplified from 1 μL of reference cDNA by either reference gene- or target gene-specific primers. The efficiency of PCR using each gene-specific primer provided by the program of qPCR equipment called 'amplification efficiency' is shown in Table S3 (Supporting Information). Each PCR product was then diluted to 1/10 000, followed by a 10-fold serial dilution to serve as a standard curve composed of seven data points. The qPCR mixture, consists of 2.5 ng mouse retinal cDNA or 1 μL of the serially diluted standards, 6 pmol each of forward/reverse primer, THUNDERBIRD SYBR qPCR Mix (TOYOBO, Osaka, Japan) and 50 × ROX Reference dye, was prepared in a reaction volume of 20 μL, and the reaction was carried out in triplicate. We used Mx3005P Real-Time PCR System (Agilent Technologies) for qPCR under the following condition: 95 °C for 1 min as an initial degeneration step and 40 cycles of 95 °C for 15 s and 60 °C for 30 s for the PCR. Finally, the C_t values were obtained by MxPro-Mx3005P v4.10 (Agilent Technologies) on the basis of PCR amplification curve.

In silico prediction of reference gene stability

To evaluate the expression stability of reference genes in mouse retina, C_t values, which is defined as the number of PCR cycles required for detecting the fluorescent signal crossing the threshold as a positive signal, of candidate genes obtained by qPCR (Table S4 in Supporting Information) were analyzed by *RefFinder* (www.leonxie.com/referencegene.php). *RefFinder* (Xie *et al.* 2012) integrates four well-known programs with different algorithms, *geNorm* (Vandesompele *et al.* 2002), *NormFinder* (Andersen *et al.* 2004), *BestKeeper* (Pfaffl *et al.* 2004) and *comparative* $\Delta\Delta C_t$ *method* (Silver *et al.* 2006), and calculates a geometric mean of the ranking value determined by four programs. We first pooled the C_t values of the reference genes obtained in triplicate from three developmental stages separately as: early (E18 through P4), late (P8, P10 and P14) and adult (4w, 8w and 12w). We then subjected the pooled data to *RefFinder* and evaluated the geometric mean of the ranking for eight candidate genes in three different stages.

Quantification of target gene expression

We quantified the expression level of two sets of target genes, '*Crx* and *Nrl*' and '*Vegfa* and its receptor *Kdr*', which

are closely related to retinal neural development and angiogenesis, respectively (Pierce *et al.* 1995; Yang & Cepko 1996; Suzuma *et al.* 1998). We first obtained the quantitative data of reference genes or target genes in mouse retinal cDNA by applying the C_t values to each corresponding standard curve. To obtain the expression levels of target genes, the quantitative data were compensated by those of the representative reference genes in each stage based on the results of *RefFinder*: *Sdha* in early and late stages and *Tbp* in the adult stage as for the most stable genes and *Actb* throughout the stages and *Rn18s* in early and late stages as for the unstable gene. We examined the expression levels of target genes at each time point as the relative amount to the results obtained at P0 to be able to compare the results of target gene expression compensated by different reference genes.

Comparison of expression levels between qPCR and mouse retinal SAGE data

To evaluate the results of target gene expression compensated by different reference genes based on the qPCR results, we referred a database of mouse retinal transcriptome data obtained from SAGE tags (Mouse Retina SAGE Library, http://cepko.med.harvard.edu) (Blackshaw *et al.* 2001, 2004) (hereafter referred to as 'SAGE data'). To this end, we applied Akaike information criterion (AIC) (Akaike 1969) and investigated the concordance between the two data. The SAGE data were available at the time points of P0, P2, P4, P6 and P28 (regarded as equivalent to 4w) for *Crx*, *Nrl* and *Kdr*, and E18, P0, P2, P6 and P28 (the same as above) for *Vegfa*. We first normalized the expression level of target genes derived from both SAGE data and qPCR to be the relative amount of P0, of which the expression data for all of the target genes were available from both the data sets. In order to determine a quadratic regression equation from the SAGE data, we then converted each time point into the numerical number as from E18 to be $x = 0$, P0 to be $x = 1$, until P28 to be $x = 29$. Subsequently, we calculated the residual sum of the expression level at each time point obtained by qPCR against the regression curve of SAGE data and applied them to the following equation:

$$\mathrm{AIC} = n\left\{\log\left(\frac{2\pi \mathrm{Se}}{n}\right) + 1\right\} + 2(p+2)$$

n, number of time points; Se, residual sum of squares; p, explanatory variable (we assigned 2 in this study, because we applied quadratic function as a regression equation).

Acknowledgements

HA was supported by a scholarship from Japanese Association of University Women. This work was supported by JSPS KAKENHI Grant Number 26460395 to MN.

References

Akaike, H. (1969) Fitting autoregressive models for prediction. *Ann. Inst. Stat. Math*, **21**, 243–247.

Al-Shabrawey, M., Ahmad, S., Megyerdi, S., Othman, A., Baban, B., Palenski, T.L., Shin, E.S., Gurel, Z., Hsu, S. & Sheibani, N. (2012) Caspase-14: a novel caspase in the retina with a potential role in diabetic retinopathy. *Mol. Vis.* **18**, 1895–1906.

Andersen, C.L., Jensen, J.L. & Orntoft, T.F. (2004) Normalization of real-time quantitative reverse transcription-PCR data: a model-based variance estimation approach to identify genes suited for normalization, applied to bladder and colon cancer data sets. *Cancer Res.* **64**, 5245–5250.

Blackshaw, S., Fraioli, R.E., Furukawa, T. & Cepko, C.L. (2001) Comprehensive analysis of photoreceptor gene expression and the identification of candidate retinal disease genes. *Cell* **107**, 579–589.

Blackshaw, S., Harpavat, S., Trimarchi, J., Cai, L., Huang, H., Kuo, W.P., Weber, G., Lee, K., Fraioli, R.E., Cho, S.H., Yung, R., Asch, E., Ohno-Machado, L., Wong, W.H. & Cepko, C.L. (2004) Genomic analysis of mouse retinal development. *PLoS Biol.* **2**, E247.

Bustin, S.A., Benes, V., Garson, J.A., Hellemans, J., Huggett, J., Kubista, M., Mueller, R., Nolan, T., Pfaffl, M.W., Shipley, G.L., Vandesompele, J. & Wittwer, C.T. (2009) The MIQE guidelines: minimum information for publication of quantitative real-time PCR experiments. *Clin. Chem.* **55**, 611–622.

Cleaver, O. & Krieg, P.A. (1998) VEGF mediates angioblast migration during development of the dorsal aorta in *Xenopus*. *Development* **125**, 3905–3914.

Coultas, L., Chawengsaksophak, K. & Rossant, J. (2005) Endothelial cells and VEGF in vascular development. *Nature* **438**, 937–945.

Feng, J., Damrauer, S.M., Lee, M., Sellke, F.W., Ferran, C. & Abid, M.R. (2010) Endothelium-dependent coronary vasodilatation requires NADPH oxidase-derived reactive oxygen species. *Arterioscler. Thromb. Vasc. Biol.* **30**, 1703–1710.

Frericks, M. & Esser, C. (2008) A toolbox of novel murine house-keeping genes identified by meta-analysis of large scale gene expression profiles. *Biochim. Biophys. Acta* **1779**, 830–837.

Furukawa, T., Morrow, E.M. & Cepko, C.L. (1997) Crx, a novel otx-like homeobox gene, shows photoreceptor-specific expression and regulates photoreceptor differentiation. *Cell* **91**, 531–541.

Hoon, M., Okawa, H., Della Santina, L. & Wong, R.O. (2014) Functional architecture of the retina: development and disease. *Prog. Retin. Eye Res.* **42**, 44–84.

Huang, X., Barrett, R.P., McClellan, S.A. & Hazlett, L.D. (2005) Silencing Toll-like receptor-9 in *Pseudomonas aeruginosa* keratitis. *Invest. Ophthalmol. Vis. Sci.* **46**, 4209–4216.

Jabs, D.A., Gerard, H.C., Wei, Y., Campbell, A.L., Hudson, A.P., Akpek, E.K., Lee, B., Prendergast, R.A. & Whittum-Hudson, J.A. (2004) Inflammatory mediators in autoimmune lacrimal

gland disease in MRL/Mpj mice. *Invest. Ophthalmol. Vis. Sci.* **45**, 2293–2298.

Mamo, S., Gal, A.B., Bodo, S. & Dinnyes, A. (2007) Quantitative evaluation and selection of reference genes in mouse oocytes and embryos cultured in vivo and in vitro. *BMC Dev. Biol.* **7**, 14.

Marquardt, T. & Gruss, P. (2002) Generating neuronal diversity in the retina: one for nearly all. *Trends Neurosci.* **25**, 32–38.

Mears, A.J., Kondo, M., Swain, P.K., Takada, Y., Bush, R.A., Saunders, T.L., Sieving, P.A. & Swaroop, A. (2001) Nrl is required for rod photoreceptor development. *Nat. Genet.* **29**, 447–452.

Omori, Y., Katoh, K., Sato, S., Muranishi, Y., Chaya, T., Onishi, A., Minami, T., Fujikado, T. & Furukawa, T. (2011) Analysis of transcriptional regulatory pathways of photoreceptor genes by expression profiling of the Otx2-deficient retina. *PLoS One* **6**, e19685.

Pfaffl, M.W., Tichopad, A., Prgomet, C. & Neuvians, T.P. (2004) Determination of stable housekeeping genes, differentially regulated target genes and sample integrity: BestKeeper–Excel-based tool using pair-wise correlations. *Biotechnol. Lett.* **26**, 509–515.

Pierce, E.A., Avery, R.L., Foley, E.D., Aiello, L.P. & Smith, L.E. (1995) Vascular endothelial growth factor/vascular permeability factor expression in a mouse model of retinal neovascularization. *Proc. Natl Acad. Sci. USA* **92**, 905–909.

Risau, W. (1997) Mechanisms of angiogenesis. *Nature* **386**, 671–674.

Silver, N., Best, S., Jiang, J. & Thein, S.L. (2006) Selection of housekeeping genes for gene expression studies in human reticulocytes using real-time PCR. *BMC Mol. Biol.* **7**, 33.

Simpson, D.A., Feeney, S., Boyle, C. & Stitt, A.W. (2000) Retinal VEGF mRNA measured by SYBR green I fluorescence: a versatile approach to quantitative PCR. *Mol. Vis.* **6**, 178–183.

Suzuma, K., Takagi, H., Otani, A., Suzuma, I. & Honda, Y. (1998) Increased expression of KDR/Flk-1 (VEGFR-2) in murine model of ischemia-induced retinal neovascularization. *Microvasc. Res.* **56**, 183–191.

Vandesompele, J., De Preter, K., Pattyn, F., Poppe, B., Van Roy, N., De Paepe, A. & Speleman, F. (2002) Accurate normalization of real-time quantitative RT-PCR data by geometric averaging of multiple internal control genes. *Genome Biol.* **3**, RESEARCH0034.

Veazey, K.J. & Golding, M.C. (2011) Selection of stable reference genes for quantitative rt-PCR comparisons of mouse embryonic and extra-embryonic stem cells. *PLoS One* **6**, e27592.

Xie, F., Xiao, P., Chen, D., Xu, L. & Zhang, B. (2012) miRDeepFinder: a miRNA analysis tool for deep sequencing of plant small RNAs. *Plant Mol. Biol.* **80**, 75–84.

Yang, X. & Cepko, C.L. (1996) Flk-1, a receptor for vascular endothelial growth factor (VEGF), is expressed by retinal progenitor cells. *J. Neurosci.* **16**, 6089–6099.

Received: 18 March 2015
Accepted: 27 April 2015

Supporting Information

Additional Supporting Information may be found in the online version of this article at the publisher's web site:

Figure S1 Expression level of target genes in mouse retina compensated by different reference genes. Expression levels of the genes related to neural development, (A) *Crx* and (B) *Nrl*, and angiogenesis, (C) *Vegfa* and (D) *Kdr*, were quantified.

Figure S2 Expression level of target genes in mouse retina compensated by different reference genes. All the results are expressed as the relative amount to the results obtained at P0.

Figure S3 SAGE tag counts of reference genes obtained from Mouse Retina SAGE Library (http://cepko.med.harvard.edu/).

Table S1 Effect on C_t values of target genes derived from retinal RNA of each individual mouse or pooled RNA of those mice

Table S2 RIN* of pooled total RNA

Table S3 Amplification efficiency* of PCR in each primer

Table S4 C_t value input for *RefFinder*

SCIENTIFIC REPORTS

OPEN

JBP485 promotes tear and mucin secretion in ocular surface epithelia

Received: 02 December 2014
Accepted: 07 April 2015
Published: 21 May 2015

Takahiro Nakamura[1,2], Yuiko Hata[1], Maho Nagata[1], Norihiko Yokoi[1], Shumpei Yamaguchi[3], Taiichi Kaku[3] & Shigeru Kinoshita[1]

Dry eye syndrome (DES), a multifactorial disease of the tears and ocular surface, is one of the most common ocular disorders. Tear film contains ocular mucins and is essential for maintaining the homeostasis of the wet ocular surface. Since there are a limited number of clinical options for the treatment of DES, additional novel treatments are needed to improve the clinical results. In this study, we found that placental extract-derived dipeptide (JBP485) clearly promoted the expression and secretion of gel-forming mucin 5ac (Muc5ac) in rabbit conjunctival epithelium. JBP485 also elevated the expression level of cell surface-associated mucins (Muc1/4/16) in rabbit corneal epithelium. The Schirmer tear test results indicated that JBP485 induced tear secretion in the rabbit model. Moreover, JBP485 clinically improved corneal epithelial damage in a mouse dry eye model. Thus, our data indicate that JBP485 efficiently promoted mucin and aqueous tear secretion in rabbit ocular surface epithelium and has the potential to be used as a novel treatment for DES.

Dry eye syndrome (DES) is one of the most frequently encountered ocular diseases. Epidemiological investigations have reported that it is prevalent in up to one-third of the population in some countries, making it a subject of growing importance related to public health[1–3]. The International Dry Eye Workshop defined DES as a multifactorial disease of the tears and ocular surface that results in symptoms of discomfort, visual disturbance, and tear film instability, thus having the potential to damage the ocular surface[4]. In the clinical setting, DES is accompanied by increased tear-film osmolarity and ocular surface inflammation. Thus, a clear understanding of tear film dynamics and the pathogenesis of ocular inflammation is essential in order to successfully treat this type of disease.

The pre-ocular tear film is vital for the maintenance of a healthy, wet ocular surface. The film consists of an aqueous layer containing a high concentration of soluble mucin and an outermost lipid layer[5]. Recently, particular attention has been focused on the function of ocular mucins in dry eye disease. There are two types of ocular mucins that contribute, in different ways, to ocular surface homeostasis[6,7]: 1) cell surface-associated mucins (Muc1/4/16), which are expressed on ocular-surface epithelium, and 2) gel-forming mucin (Muc5ac), which is secreted by conjunctival goblet cells. Several lines of experimental and clinical evidence suggest that alterations in both cell surface-associated and gel-forming mucins occur in dry-eye-related ocular surface diseases[8–10].

Currently, the first choice of treatment in cases of DES involves the use of tear supplementation with artificial tears. However, this therapeutic pathway provides only a partial replacement of the wet ocular surface components, and repeated instillation is often required. Sodium hyaluronate and autologous serum have also shown some clinical effectiveness in DES patients[11–13]. More recently, diquafosol sodium and rebamipide, which promote tear and mucin secretion, have been reported to be effective in improving the clinical symptoms of various dry eye diseases[14,15]. Although these types of eye-drop treatments give patients more therapeutic options, new treatments with enhanced clinical effectiveness are needed to improve the symptoms in these patients.

[1]Department of Ophthalmology, Kyoto Prefectural University of Medicine, Kyoto, Japan. [2]Research Center for Inflammation and Regenerative Medicine, Doshisha University, Kyoto, Japan. [3]Japan Bio Products Co., Ltd, Tokyo, Japan. Correspondence and requests for materials should be addressed to T. N. (email: tnakamur@koto.kpu-m.ac.jp)

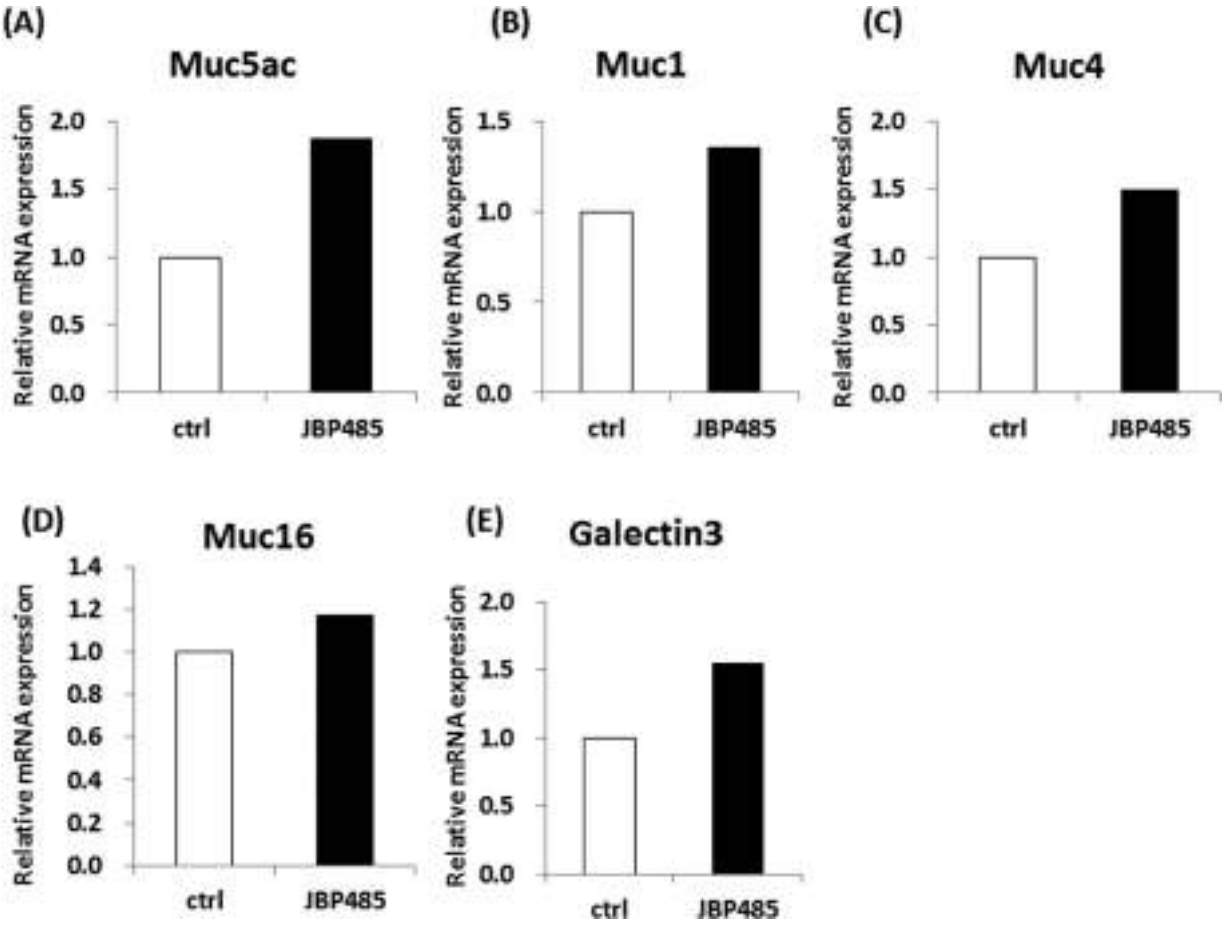

Figure 1. JBP485 promotes the expression level of mucin-related molecules in conjunctival epithelium. Relative expression of mucin-related molecules [mucin 5ac (Muc5ac), Muc1/4/16, and Galectin-3] in the control- and JBP485-treated conjunctival epithelial cells (A–E, 4 cell membrane filters, mixed). ctrl: control.

JBP485 (cyclo-trans-4-L-hydroxyprolyl-L-serine) is a dipeptide that was first isolated from placental extract (PE) as a mitogen for a kidney cell line, and it has subsequently been synthesized by chemical means[16,17]. Previous studies have demonstrated that JBP485 has anti-inflammatory and anti-apoptotic effects and that it exhibits protective properties for liver and gastrointestinal cells[17–21]. Recently, we discovered that JBP485 promotes the cell proliferation of corneal epithelium during wound healing (unpublished data). In that study, the findings of the corneal wound experiments unexpectedly revealed that rabbit eyes showed an increased level of tear secretion with JBP485. This led us to the interesting hypothesis that JBP485 might promote tear and mucin secretion in ocular surface epithelium and be a potential new treatment for DES.

The purpose of this present study was to investigate the effect of JBP485 on tear and mucin secretion in ocular surface epithelium. The findings of this study reveal for the first time that JBP485 dramatically promotes the secretion of not only ocular mucin, but also aqueous tears. In addition, we found that JBP485 repairs corneal epithelial damage in a mouse dry eye model. Thus, our data provides new insights into the function of JBP485 on the homeostasis of the ocular surface.

Results

JBP485 promotes the expression level of Muc5ac in conjunctival epithelium. To investigate the effect of JBP485 on conjunctival epithelial cells, we first examined the expression level of secretory-mucin Muc5AC in rabbit conjunctival epithelial cells (CjECs) (*ex vivo* model). For this experiment, whole rabbit eyes were first incubated in the control solution [Hank's balanced salt solution (HBSS)] and in JBP485 (100 μM) for 6 hours, and the CjECs were then collected using cell membrane filters from 4 different areas of the conjunctiva (the upper, lower, nasal, and temporal areas). The resultant 4-cell membrane filters were then mixed together and used for experiment. Interestingly, real-time polymerase chain reaction (PCR) tended to show an elevated level of Muc5ac expression in the JBP485-treated CjECs (Fig. 1A). In addition, we examined the expression of cell surface-associated mucin-related molecules (Muc1/4/16 and Galectin-3) and found that the expression levels of CjECs treated with JBP485 tended to be slightly

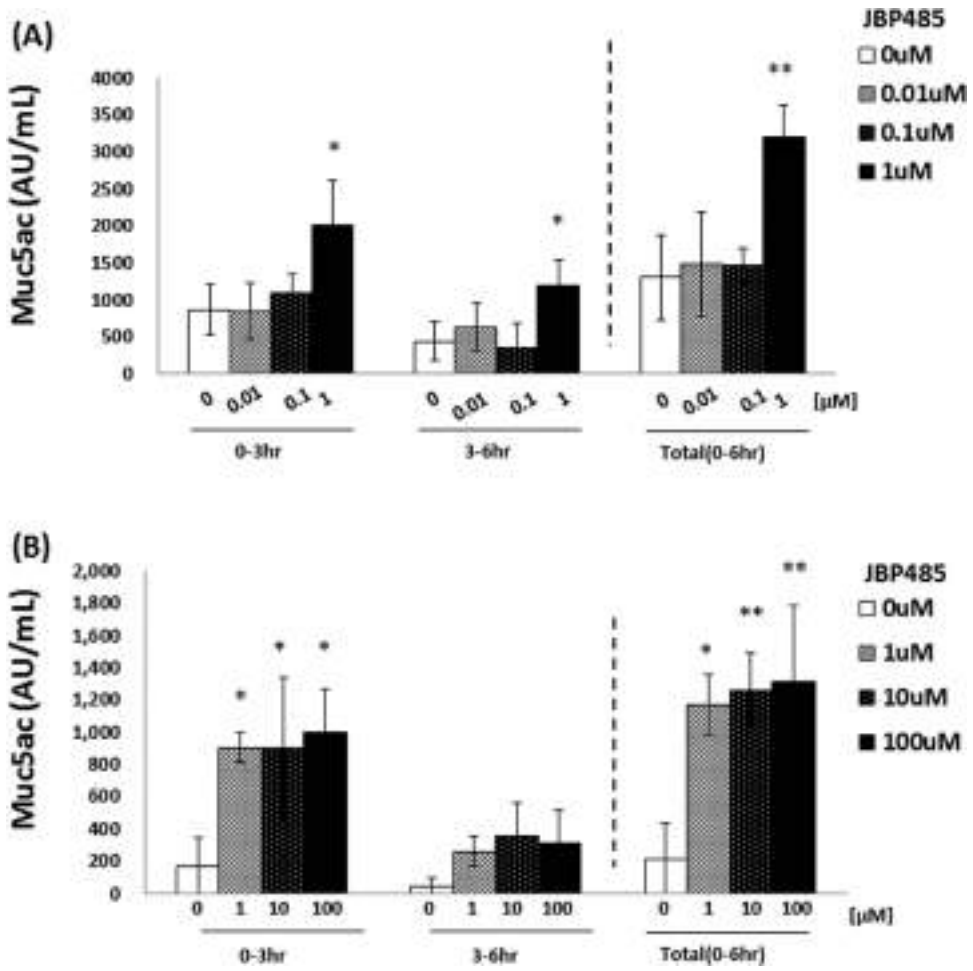

Figure 2. #JBP485 accelerates the secretion of Muc5ac in conjunctival epithelium (*ex vivo*). Protein levels of Muc5ac in conjunctival epithelium treated with JBP485 (for up to 6 hours) were examined by enzyme-linked immunosorbent assay. The concentration of JBP485 was less than 1 μM (A, n = 3) and more than 1 μM (B, n = 4). * $p < 0.05$, ** $p < 0.01$.

increased compared to the controls (Fig. 1B–E). These findings suggest that JBP485 plays some critical role in inducing the expression of ocular surface mucins.

JBP485 accelerates the secretion of Muc5ac in conjunctival epithelium. Muc5ac is a mucin that is secreted from conjunctival goblet cells. To elucidate whether JBP485 induces the secretion of Muc5ac in CjECs, quantification of Muc5ac was performed using enzyme-linked immunosorbent assay (ELISA). For this experiment, rabbit conjunctiva was obtained by use of surgical trephine (3 mm diameter) and then incubated in HBSS with or without JBP485 for up to 6 hours. At each time point (at 3 and 6 hours), supernatant was used for ELISA. After the first 3 hours of incubation, the expression level of Muc5ac in the samples treated with JBP485 (1 μM) was higher than that in the other samples (less than 1 μM) (Fig. 2A). The HBSS was then replaced with new HBBS, with or without JBP485 as above. After a further 3–6 hours of incubation, the expression level of Muc5ac in the JBP485-treated samples (1 μM) was higher than in the other samples, although the quantity of Muc5ac was less than that of at after 3 ours of incubation (Fig. 2A). We also examined the expression level of Muc5ac in samples treated with more than 1 μM of JBP485 and found that the expression patterns were similar to those in samples treated with 1 μM of JBP485 (Fig. 2B).

To directly examine the secretion of Muc5ac from the CjECs, we performed Periodic Acid Schiff (PAS) staining (that can be used to detect secretory mucin) by use of impression cytology. Briefly, 30 minutes after the topical application of JBP485 or saline solution (control), the CjECs were obtained by use of impression cytology and the PAS staining was performed. We observed that PAS stained (+) cells were distributed in almost all areas of the eyes treated with saline solution, whereas the number of those cells (not goblet cells) decreased in the JBP485-treated eyes, indicating that JBP485 promotes mucin secretion (Fig. 3A, B).

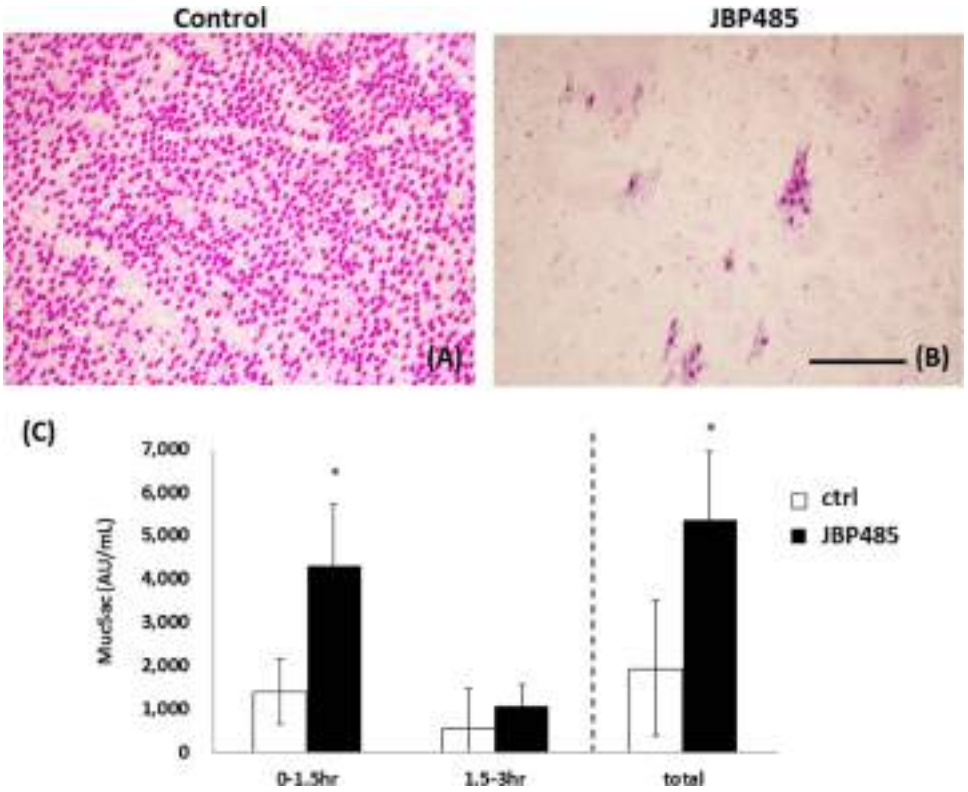

Figure 3. JBP485 accelerates the secretion of Muc5ac in conjunctival epithelium (*in vivo*). Representative Periodic Acid Schiff staining of conjunctival epithelium 30 minutes after a topical application of saline solution (**A**) and JBP485 (**B**). Protein levels of Muc5ac in the JBP485-treated (100 μM) conjunctival epithelium were examined by enzyme-linked immunosorbent assay (**C**). * $p < 0.05$ (n = 6). Scale bar, 100 μm.

Finally, we investigated whether or not a topical application of JBP485 on the eye would induce mucin secretion. Briefly, we first applied JBP485 or saline solution on the eyes 4-times daily for 3 days. Conjunctiva was then obtained from those eyes and incubated in HBSS for ELISA assay for up to 3 hours. As expected, the expression level of Muc5AC in the JBP485-treated samples (100 μM) was higher than that in the control samples (Fig. 3C). These findings clearly indicate that JBP485 accelerates the secretion of Muc5ac in CjECs.

JBP485 elevates the expression level of cell surface-associated mucin in corneal epithelium in an *in vitro* model. To investigate the effect of JBP485 on corneal epithelial cells (CECs), we first examined the expression level of cell surface-associated mucin related molecules (Muc1/4/16 and Galectin-3) in rabbit primary cultured CECs. At 2 hours before sampling, we replaced the culture medium with DMEM/F12 and incubated the cells with or without JBP485 for each time point (3, 6, 12, and 24 hours). The cells were incubated with DMEM/F12 for 24 hours as a control. For the next assay, all samples were obtained simultaneously. Real-time PCR showed that after incubation with JBP485 for 3–6 hours, relative mRNA expression of Muc1/4/16 and Galectin-3 in the cultured CECs was higher than that in the controls (Fig. 4A–D). Moreover, we noticed that at 24 hours after incubation with JBP485, the relative expression levels were similar to those in the controls (Fig. 4A–D).

***Ex vivo* model.** To further investigate the effect of JBP485 on CECs, we examined the expression level of cell surface-associated mucin related molecules (Muc1/4/16 and Galectin-3) in *ex vivo* CECs. Briefly, whole rabbit eyes were incubated in JBP485 (100 uM), and CECs were then collected by mechanical scraping at 4 time points (after 3, 6, 12, and 24 hours of incubation). Real-time PCR showed that after incubation with JBP485 for 3–6 ours, the relative mRNA expression of Muc1/4/16 in *ex vivo* CECs tended to be higher than that in the control samples (Fig. 5A–D).

***In vivo* model.** Finally, the effect of JBP485 on corneal CECs was investigated by examining the expression level of cell surface-associated mucin related molecules (Muc1/4/16 and Galectin-3) in *in vivo* CECs. Briefly, JBP485 (100 μM) or saline solution was topically applied 4-times daily for 12 days, and then the CECs were obtained by mechanical scraping. As expected, the expression levels of Muc1/4/16 and Galectin-3 in the JBP485-treated CECs tended to be higher than in the controls (Fig. 6A–D). These

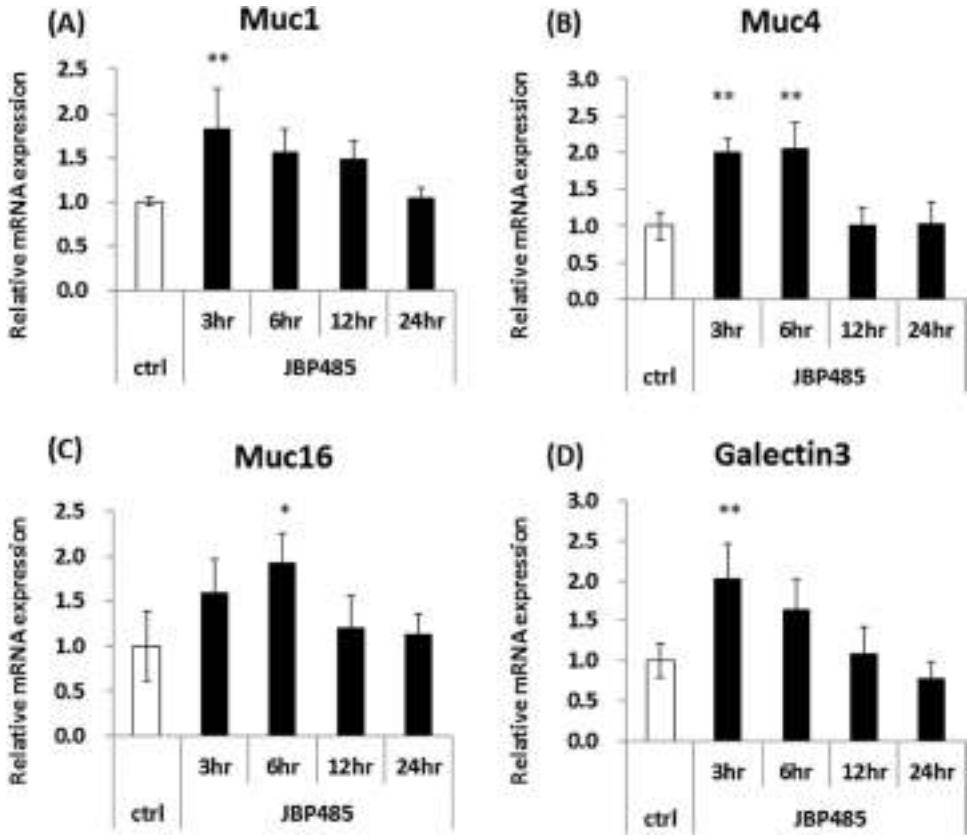

Figure 4. JBP485 elevates the expression level of cell surface-associated mucin in cultured corneal epithelium. Relative expression of mucin-related molecules (*Muc1/4/16* and *Galectin-3*) in the control- and JBP485-treated cultivated corneal epithelial cells (A–D). ctrl: control. * $p < 0.05$, ** $p < 0.01$ (n = 3).

findings clearly indicate that JBP485 promotes the expression level of cell surface-associated mucins in CECs.

JBP485 induces tear secretion in a rabbit model. To investigate the effect of JBP485 on aqueous tear-fluid secretion, we performed the Schirmer test using a rabbit model. Topical application of JBP485 (100 μM) significantly increased aqueous tear volume from 5 minutes post application, and that effect gradually decreased between 5 and 30 minutes post application (Fig. 7A). Next, we examined the effect of different concentrations of JBP485 and found that JBP485 clearly increased aqueous tear volume in a concentration-dependent manner (up to 10 mM) in rabbit eyes (Fig. 7B). These results confirm that JBP485 accelerates tear secretion in a rabbit model.

JBP485 repairs corneal epithelial damage in a mouse dry eye model. Following our findings demonstrating that JBP485 accelerates not only mucin secretion but also aqueous tear production, we investigated whether or not a topical application of JBP485 might be useful for the treatment of dry eye disease. Due to the fact that a rabbit dry eye model is difficult to establish and is too invasive and unstable to be used for evaluation, we used a simple mouse model of experimentally induced dry eye disease. Before the experiment, we confirmed that all mice showed reduced tear volume and resultant superficial punctate keratitis (SPK) on the cornea (Fig. 8A). Six days after the topical application of JBP485 (100 μM), SPK on the mice corneas were reduced in comparison to the controls (Fig. 8A). Fifteen days after the topical application of JBP485, SPK on the mice corneas was further reduced and corneal damage had clearly improved (Fig. 8A). In fact, we found that his effect was statistically significant (Fig. 8B). These findings suggest that JBP485 is useful in treating experimental dry eye conditions.

Discussion

In the current information-based society, most external information is gained through eyesight, thus leading us to we overwork our eyes. Consequently, dry eye has become one of the most common ocular diseases, and particular attention has recently been focused on the treatment of DES. Cyclosporine ophthalmic emulsion, which has an anti-inflammatory effect, is the major drug used for the treatment of dry eye in the United States[22]. Diquafosol sodium and rebamipide promote the secretion of mucin and

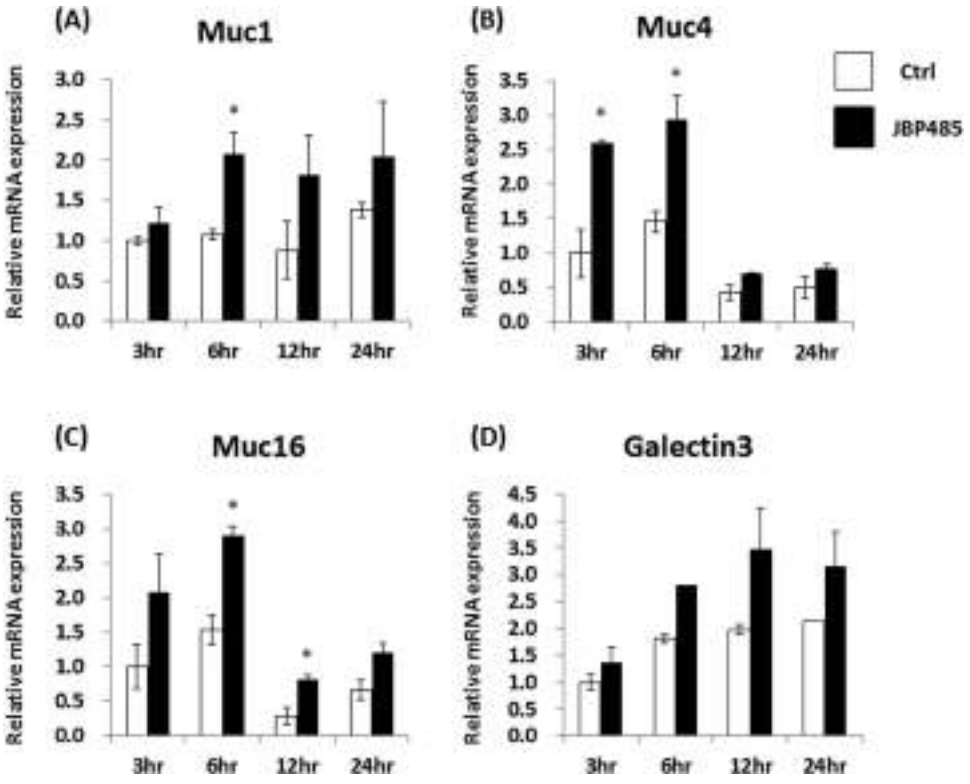

Figure 5. JBP485 elevates the expression level of cell surface-associated mucin in *ex vivo* corneal epithelium. Relative expression of mucin-related molecules (*Muc1/4/16* and *Galectin-3*) in the control- and JBP485-treated *ex vivo* corneal epithelium (A–D). ctrl: control. * $p < 0.05$ (n = 2).

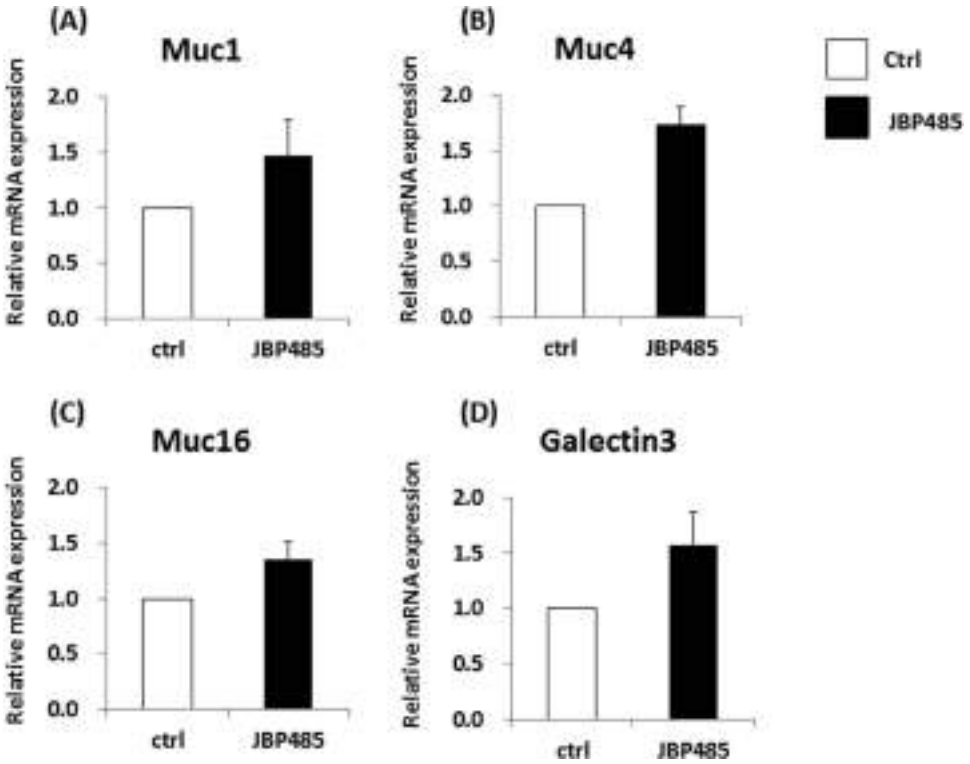

Figure 6. JBP485 elevates the expression level of cell surface-associated mucin in *in vivo* corneal epithelium. Relative expression of mucin-related molecules (*Muc1/4/16* and *Galectin-3*) in the control- and JBP485-treated *in vivo* corneal epithelium (A–D). ctrl: control (n = 3).

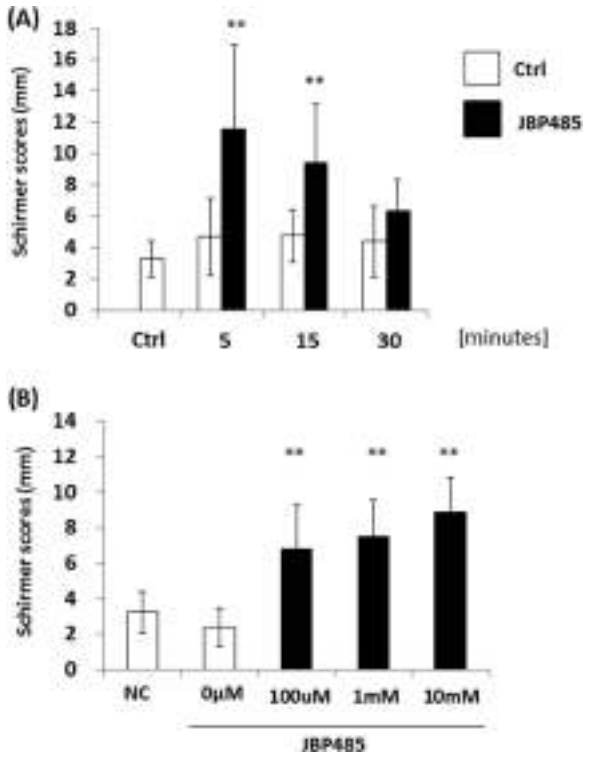

Figure 7. JBP485 induces tear secretion in a rabbit model. Schirmer test scores at different time points (up to 30 minutes) after the topical application of JBP485 solution (A, n = 8–9). Schirmer test scores for different concentrations of JBP485 after the topical application of JBP485 solution (B, n = 8-10). ** $p < 0.01$.

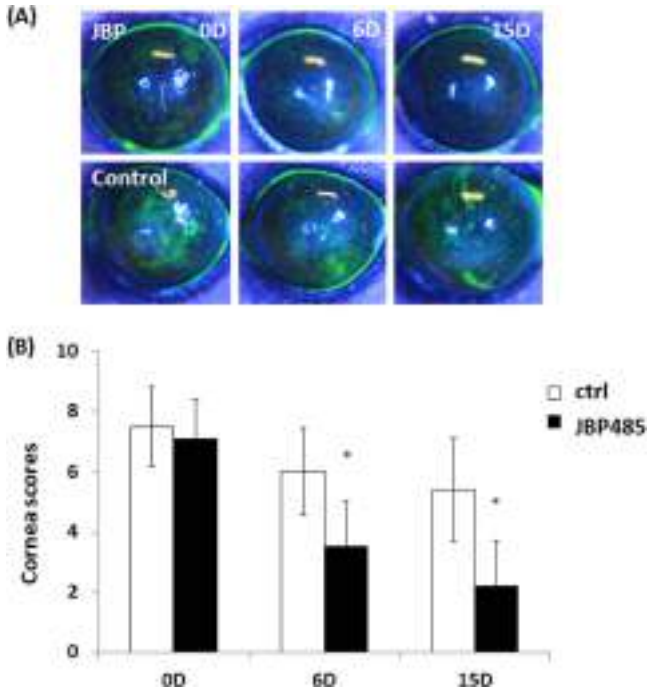

Figure 8. JBP485 repairs corneal epithelial damage in a mouse dry eye model. Fluorescent slit-lamp photographs of mouse eyes with or without JBP485 treatment for up to 15 days (**A**). Corneal fluorescein grading score at each time point after the topical application of JBP485 (**B**). * $p < 0.05$ (n = 10).

tears, and they are quickly becoming the primary eye drops used for the treatment of DES in Japan[14,15]. Although these treatments are clinically effective for many patients, alternative treatment options are

still needed. The results of this study demonstrate for the first time that JBP485 derived from PE clearly promotes the expression and secretion of mucin and tears and that it has the potential to be used as a novel treatment for dry eye.

Ocular mucins are present on the most apical surface of all mucosal epithelium in either gel-forming or cell surface-associated forms. Gel-forming secreted mucin (Muc5ac) has no transmembrane spanning domains and is specialized in various kinds of epithelial glands[10]. Our results demonstrate that JBP485 dramatically accelerates the secretion of Muc5ac from conjunctival goblet cells. In the clinical setting, the reaction time of a drug is critical for evaluating its usefulness. From our PAS staining and ELISA experiments, we found that the effect of JBP485 on conjunctival goblet cells was very fast (within 30 minutes), and these results are similar to the findings in a previous report that the topical application of INS365 (P2Y2 receptor agonist, Diquafosol sodium) dose-dependently decreased the PAS staining area up to 15 minutes[23]. Therefore, JBP485 might be a good candidate for topical application on the ocular surface. We posit that the topical administration of JBP485 must be correlated with *in vivo* analyses of Muc5ac mRNA in the conjunctiva and Muc5ac protein in tears. Unfortunately, based on our current findings, we were unable to fully demonstrate these mechanisms, and further investigation is needed to clarify these points.

Cell surface-associated mucins have a single transmembrane domain including a short cytoplasmic tail and a large glycosylated extracellular domain; they are observed in the glycocalyx of apical cell membranes of the epithelium[10]. Currently, 10 cell surface-associated mucins have been reported, and each may have a different biological function. Among them, Muc1, Muc4, and Muc16 are reportedly expressed in the ocular surface epithelium[24–27]. It has been proposed that these molecules have multiple functions, including protection, barrier function and lubrication of the ocular surface epithelium, cell signaling (EGF and Wnt), and hypothetically, osmosensors[28,29]. DES is reportedly associated with alterations in mucin expression, and expression of Muc1 and Muc16 are known to be decreased in patients with Sjogren and non-Sjogren syndrome, respectively[8,9]. Our *in vitro, ex vivo,* and *in vivo* experiments clearly showed that JBP485 elevates the expression level of these cell surface-associated mucins, suggesting that JBP485 might have the ability to normalize the apical surface of corneal and conjunctival epithelium.

Aqueous tears are vital for maintaining ocular-surface homeostasis. To the best of our knowledge, diquafosol sodium is the only eye drop that can be used to increase tear secretion[14]. Thus, additional clinical options need to be developed for the treatment of dry eye. Our results demonstrate that JBP485 accelerates tear secretion in a rabbit model in a dose-dependent manner. Interestingly, 5 minutes after the topical application of JBP485, the rabbit eyes clearly showed an increased tear volume level, and throughout the *in vivo* experiments we never observed any adverse effects such as injection, neovascularization, or inflammation. This indicates that the effect of JBP485 on the ocular surface is both safe and prompt. We theorize that the mechanism by which the level of tears is improved is an important aspect when evaluating the clinical efficacy of JBP 485. For instance, we investigated the expression of the P2Y2 receptor with or without JBP485 treatment, and found that there were no significant differences between them (data not shown). Unfortunately, we do not precisely know its mechanism, and extensive further experiments are needed to clarify these points.

JBP485 was first found as a defined hydrolysate from human placenta. Extensive and accumulating investigations demonstrate that human placenta has multiple biological functions, including anti-inflammatory effects, anti-platelet aggregation, protection and regeneration of hepatocytes, regulation of hormonal balance, modulation of immune reaction, and promotion of wound healing[30–34]. JBP485 has also consistently shown the same kinds of biological effects. However, no reports exist regarding the biological effects of JBP485 on the secretion of mucin and aqueous tear in the ocular surface epithelium. Goblet cells and glandular tissues exist in great numbers throughout the body. Therefore, our findings might provide new insight into the therapeutic effects of JBP485 not only on ocular surface epithelium but also on other related tissues and organs.

Our investigation demonstrates that JBP485 promotes the expression and secretion of mucin and aqueous tear, but using a proper animal model that simulates dry eye conditions is an important next step for the evaluation of future therapeutic treatments of dry eye diseases. Numerous mouse dry eye models have been developed to reflect the pathogenesis involved in dry eye syndrome. We decided to use a model employing the excision of the exorbital lacrimal gland simply because it is quick and easy to do. Importantly, JBP485 successfully treated the damaged corneal surface in the mouse dry eye model, providing direct evidence of the clinical efficacy of JBP485 in *in vivo* situations. However, we have not fully demonstrated that JBP485 also promotes the tear and mucin secretion in mouse ocular surface epithelia and further investigations using mouse cornea and conjunctival epithelia are needed to clarify these points.

Regarding the pathogenesis of dry eye disease, tear hyperosmolarity, tear film instability, and inflammation have been identified as core mechanisms associated with the development of the disease. Ocular inflammation may initially be accompanied by an increase in blinking and the tear reflex. This may result in a reduction in corneal sensation, leading to increased evaporation and tear-film instability. Thus, it is important to control ocular inflammation in patients with DES. Previous studies have demonstrated that JBP485 exhibits anti-inflammatory effects in the liver and intestine[17–21], and our recent findings show that JBP485 reduces inflammation in an experimental model of cultured CECs (data not shown), thus

providing additional evidence that JBP485 might have advantages over the current available treatments for dry eye disease.

In conclusion, the findings of our investigation show that PE-derived JBP485 efficiently accelerates mucin and aqueous tear secretion in ocular surface epithelium. Moreover, JBP485 was found to be effective for the treatment of corneal damage in a mouse dry eye model. Although further investigation is needed to elucidate the molecular mechanisms of its biological function, our data provides new insights into the therapeutic potential of JBP485 in the most common type of dry eye disease.

Materials and Methods

Reagent. The JBP485 used in this study was provided by Japan Bioproducts Industry Co., Ltd. (Tokyo, Japan)[16–21]. JBP485 powder was dissolved by the use of warmed saline (Otsuka Pharmaceutical Co., Ltd., Tokyo, Japan) into a 50 mM stock solution at the temperature of 50–60 °C. The solution was treated with filtration sterilization (0.22 μm), and then diluted and adjusted to the required concentration with saline for instillation or for use as a culture medium.

Animals. All animals used in this study were treated in accordance with the ARVO Statement on the Use of Animals in Ophthalmic and Vision Research. All experimental procedures were approved by the Committee for Animal Research at Kyoto Prefectural University of Medicine. Samples were taken from adult albino rabbits (2–2.5 kg in weight) under general anesthesia induced by an intramuscular injection of xylazine hydrochloride (5 mg/ml) and ketamine hydrochloride (50 mg/ml).

Cell culture. Japanese white rabbit eyes were purchased from Funakoshi Corporation (Tokyo, Japan). Rabbit corneal epithelial cells were prepared and cultured according to a previously reported method[35]. Briefly, the corneas were removed from the eyes, and the half-layers of the endothelial side were then mechanically removed by use of surgical scissors. The remaining corneal tissues were transferred to a minimum essential keratinocyte serum-free medium (Life Technologies, Carlsbad, CA) containing dispase I (Wako Pure Chemical Industries, Osaka, Japan). The tissues were then incubated at 4 °C for 24 hours and at 37 °C for 1 hour. The resultant corneal epithelium was then peeled and further incubated with TrypLE™ Select (Life Technologies) trypsin replacement enzyme at 4 °C for 30 minutes and at 37 °C for 5 minutes to dissociate the cells. The prepared rabbit CECs were suspended in CnT-20 medium (CELLnTEC, Santa Cruz, CA) and plated in collagen-coated tissue culture plates (AGC Techno Glass Co., Ltd., Shizuoka, Japan).

Real-time PCR. Real-time PCR was performed following our previously described method[36]. All samples were homogenized in lysis buffer (Buffer RLT; QIAGEN, Inc., Valencia, CA), and total RNA was eluted by use of the RNeasy® Mini Kit (QIAGEN) according to the manufacturer's instructions. The relative abundance of transcripts was detected by use of SYBR® Green PCR Master Mix (Applied Biosystems, Inc., Foster City, CA) according to the manufacturer's instructions. The primers that were used are shown in Supplemental Table 1. Sequence homology data for mucins and galectin in humans and rabbits are shown in Supplemental Information 1–5. We confirmed that our designed primers properly amplified the objective sequences using PCR and sequencing (Supplemental Fig. 1).

ELISA. Quantification of the mucin 5ac (Muc5ac) expression level was performed using ELISA by our previously reported method[37]. Each sample was incubated with HBSS (1ml/well, 24-well plates) at 37 °C. The resultant supernatant solution was incubated overnight at 40 °C. The wells were washed 3 times with 0.05% tris-buffered saline with tween20 (TBST) and incubated with 1% BSA for 1 hour at room temperature (RT). Next, the wells were incubated with anti-Muc5ac antibody (X100, Thermo Fisher Scientific, Inc., Waltham, MA) (Supplemental Fig. 2) for 1 hour at RT. The wells were then washed 3 times with TBST and incubated with secondary antibody (sheep anti-mouse IgG-HRP; GE Healthcare, Little Chalfont, UK) for 1 hour at RT. Finally, the wells were incubated with Tetramethylbenzidine (Sigma-Aldrich, St. Louis, MO) for 30 minutes at RT. The reaction was stopped by adding 0.5 M sulfuric acid solution (Nacalai Tesque Co., Kyoto, Japan). The absorbances were read at 450 nm using a microplate reader. For the experiment, the samples were run in triplicate. We set up the standard curve using an optional control well. The value shown in "Muc5ac (AU/mL)" was then calculated by the established standard curve [$y = 0.0071x + 0.2727$ ($R^2 = 0.9937$) (Fig. 2A), $y = 0.026x + 0.326$ ($R^2 = 0.9969$) (Fig. 2B)].

Impression cytology and PAS staining. After administration of the JBP485 and saline solution, membrane filters (Millipore GSWP, Billerica, MA) were placed directly on the rabbit conjunctiva for 30 seconds. The resultant membranes were then fixed in 10% formalin and oxidized in 0.5% periodic acid solution for 10 minutes. After washing with distilled water, the membranes were placed in Schiff reagent for 15 minutes. After counterstaining in hematoxylin for 1 minute, the samples were dehydrated and mounted under a coverslip using a mounting medium.

Tear fluid secretion. To measure tear secretion, we performed the Schirmer tear test (Sterilized Tear Production Measuring Strip; Showa, Tokyo, Japan) using rabbit eyes (Japanese albino rabbits, 2.5–3 kg in weight, $n = 8\sim10$)[38]. First, topical anesthesia with 0.4% oxybuprocaine hydrochloride was applied onto

the rabbit eyes. Next, at 5 minutes after the administration of 50 μL JBP485 (100 μM) or saline solution, paper strips for the Schirmer tear test were inserted into the temporal conjunctival sac of the lower eyelid for 1 minute to measure tear production. The test paper was then removed from the lower palpebral conjunctiva and the amount of moisture was measured. All tests were performed after the rabbits were attached to a fixation device and had grown quiet.

Mouse dry eye model. Excision of the exorbital lacrimal gland was performed on C57BL/6 mice at 6 weeks before examination (n = 20 eyes)[39]. Before starting the experiment, we confirmed that tear production in the mice was significantly decreased after gland excision and that SPK was clearly observed. JBP485 solution (100 μM, n = 10 eyes) and saline solution (n = 10 eyes) was topically applied on the mice eyes 4 times daily. To evaluate dry eye symptoms, fluorescein staining of the mice corneas was performed at 0, 6 and 15 days after treatment. A corneal fluorescein grading score (0: none, 1: mild, 2: moderate and 3: severe) was assigned at 3 different corneal areas (the upper, middle, and lower areas). A score of 9 points indicated severe SPK.

Statistical analysis. The statistical significance (*P*-value) in mean values of the two-sample comparison was determined by use of the Student's *t*-test. The statistical significance in the comparison of multiple sample sets was analyzed by use of the Dunnett's multiple-comparisons test. Values shown on the graphs represent the mean ± SEM.

References

1. Peral, A., Dominguez-Godinez, C. O., Carracedo, G. & Pintor, J. Therapeutic targets in dry eye syndrome. *Drug News Perspect* **21,** 166–76 (2008).
2. Gayton, J. L. Etiology, prevalence, and treatment of dry eye disease. *Clin. Ophthalmol.* **3,** 405–12 (2009).
3. Tavares, F. de P., Fernandes, R. S., Bernardes, T. F., Bonfioli, A. A. & Soares, E. J. Dry eye disease. *Semin. Ophthalmol.* **25,** 84–93 (2010).
4. The definition and classification of dry eye disease: report of the Definition and Classification Subcommittee of the International Dry Eye WorkShop (2007). *Ocul. Surf.* **5,** 75–92 (2007.).
5. Lemp, M.A. Advances in understanding and managing dry eye disease. *Am. J. Ophthalmol.* **146,** 350–356 (2008).
6. Gipson, I. K. The ocular surface: the challenge to enable and protect vision: the Friedenwald lecture. *Invest Ophthalmol. Vis. Sci.* **48,** (4390) ; 4391–8 (2007).
7. Corfield, A., Carrington, S., Hicks, S., Berry, M. & Ellingham, R. Ocular mucins: purification metabolism and function. *Progress in Retinal and Eye Research* **16,** 627 - 56 (1997).
8. Danjo, Y. *et al.* Alteration of mucin in human conjunctival epithelia in dry eye. *Invest Ophthalmol. Vis. Sci.* **39,** 2602–9 (1998).
9. Argueso, P. *et al.* Decreased levels of the goblet cell mucin MUC5AC in tears of patients with Sjogren syndrome. *Invest Ophthalmol. Vis. Sci.* **43,** 1004–11 (2002).
10. Gipson, I. K., Hori, Y. & Argueso, P. Character of ocular surface mucins and their alteration in dry eye disease. *Ocul. Surf.* **2,** 131–48 (2004).
11. Shimmura, S. *et al.* Sodium hyaluronate eyedrops in the treatment of dry eyes. *Br. J. Ophthalmol.* **79,** 1007–11 (1995).
12. Tsubota, K. *et al.* Treatment of dry eye by autologous serum application in Sjogren's syndrome. *Br. J. Ophthalmol.* **83,** 390–5 (1999).
13. Condon, P. I. *et al.* Double blind, randomised, placebo controlled, crossover, multicentre study to determine the efficacy of a 0.1% (w/v) sodium hyaluronate solution (Fermavisc) in the treatment of dry eye syndrome. *Br. J. Ophthalmol.* **83,** 1121–4 (1999).
14. Takamura, E., Tsubota, K., Watanabe, H. & Ohashi, Y. A randomised, double-masked comparison study of diquafosol versus sodium hyaluronate ophthalmic solutions in dry eye patients. *Br. J. Ophthalmol.* **96,** 1310–5 (2012).
15. Kinoshita, S. *et al.* Rebamipide (OPC-12759) in the treatment of dry eye: a randomized, double-masked, multicenter, placebo-controlled phase II study. *Ophthalmology* **119,** 2471–8 (2012).
16. Yagi, A., Nagao, M., Okamura, N., Ishizu, T. & Itoh, H. Effect of cyclo (trans-4-L-hydroxyprolyl-L-serine) from hydrolysate of human placenta on baby hamster kidney -21/C-13 cells. *Natural medicines* **52,** 156–9 (1998).
17. Liu, K. X. *et al.* Hydroxyprolylserine derivatives JBP923 and JBP485 exhibit the antihepatitis activities after gastrointestinal absorption in rats. *J. Pharmacol. Exp. Ther.* **294,** 510–5 (2000).
18. Wu, J. *et al.* Protective effect of JBP485 on concanavalin A-induced hepatocyte toxicity in primary cultured rat hepatocytes. *Eur. J. Pharmacol.* **589,** 299–305 (2008).
19. Yang, T. *et al.* Protective effect of JBP485 on concanavalin A-induced liver injury in mice. *J. Pharm. Pharmacol.* **61,** 767–74 (2009).
20. Cang, J. *et al.* Pharmacokinetics and mechanism of intestinal absorption of JBP485 in rats. *Drug. Metab. Pharmacokinet* **25,** 500–7 (2010).
21. Wang, W. *et al.* Effects of JBP485 on the expression and function of PEPT1 in indomethacin-induced intestinal injury in rats and damage in Caco-2 cells. *Peptides* **32,** 946–55 (2011).
22. Laibovitz, R. A., Solch, S., Andriano, K., O'Connell, M. & Silverman, M. H. Pilot trial of cyclosporine 1% ophthalmic ointment in the treatment of keratoconjunctivitis sicca. *Cornea* **12,** 315–23 (1993).
23. Fujihara, T., Murakami, T., Nagano, T., Nakamura, M. & Nakata, K. INS365 suppresses loss of corneal epithelial integrity by secretion of mucin-like glycoprotein in a rabbit short-term dry eye model. *J. Ocul. Pharmacol. Ther.* **18,** 363–70 (2002).
24. Inatomi, T., Spurr-Michaud, S., Tisdale, A. S. & Gipson, I. K. Human corneal and conjunctival epithelia express MUC1 mucin. *Invest Ophthalmol. Vis. Sci.* **36,** 1818–27 (1995).
25. Inatomi, T. *et al.* Expression of secretory mucin genes by human conjunctival epithelia. *Invest Ophthalmol. Vis. Sci.* **37,** 1684–92 (1996).
26. Argueso, P., Spurr-Michaud, S., Russo, C. L., Tisdale, A. & Gipson, I. K. MUC16 mucin is expressed by the human ocular surface epithelia and carries the H185 carbohydrate epitope. *Invest Ophthalmol. Vis. Sci.* **44,** 2487–95 (2003).
27. Pflugfelder, S. C. *et al.* Detection of sialomucin complex (MUC4) in human ocular surface epithelium and tear fluid. *Invest Ophthalmol. Vis. Sci.* **41,** 1316–26 (2000).
28. Hollingsworth, M. A. & Swanson, B. J. Mucins in cancer: protection and control of the cell surface. *Nat. Rev. Cancer* **4,** 45–60 (2004).
29. Govindarajan, B. & Gipson, I. K. Membrane-tethered mucins have multiple functions on the ocular surface. *Exp. Eye. Res.* **90,** 655–63 (2010).

30. Sur, T. K., Biswas, T. K., Ali, L. & Mukherjee, B. Anti-inflammatory and anti-platelet aggregation activity of human placental extract. *Acta. Pharmacol. Sin.* **24,** 187–92 (2003).
31. Liu, K. X., Kato, Y., Kaku, T. & Sugiyama, Y. Human placental extract stimulates liver regeneration in rats. *Biol. Pharm. Bull.* **21,** 44–9 (1998).
32. Kong, M. H. *et al.* Effect of human placental extract on menopausal symptoms, fatigue, and risk factors for cardiovascular disease in middle-aged Korean women. *Menopause.* **15,** 296–303 (2008).
33. Banerjee, K. K., Bishayee, A. & Chatterjee, M. Effects of human placental extract on brain monoamines and monoamine oxidase activity in rats. *Tohoku. J. Exp. Med.* **176,** 17–24 (1995).
34. Tiwary, S. K. *et al.* Effect of placental-extract gel and cream on non-healing wounds. *J. Wound Care* **15,** 325–8 (2006).
35. Nakamura, T. *et al.* Long-term phenotypic study after allogeneic cultivated corneal limbal epithelial transplantation for severe ocular surface diseases. *Ophthalmology* **117,** 2247–2254 (2010).
36. Nakamura, T. *et al.* LRIG1 inhibits STAT3-dependent inflammation to maintain corneal homeostasis. *J. Clin. Invest* **124,** 385–97 (2014).
37. Kobayashi, M. *et al.* Ocular surface reconstruction with a tissue-engineered nasal mucosal epithelial cell sheet for the treatment of severe ocular surface diseases. *Stem Cells Transl. Med. Nov. 19*. Epub ahead of print (2014).
38. Abrams, K. L., Brooks, D. E., Funk, R. S. & Theran, P. Evaluation of the Schirmer tear test in clinically normal rabbits. *Am. J. Vet. Res.* **51,** 1912–3 (1990).
39. Shinomiya, K. *et al.* Usefulness of a Dry-eye Mouse Model Produced by Exorbital Lacrimal Gland Excision and Analysis of the Increase of Caspase-1 Independent IL-1 β in the Tear Fluid of Those Mice. *Invest Ophthalmol. Vis. Sci.* **53,** *e-abstract* 2335. (2012).

Acknowledgements

The authors wish to thank T. Horikiri, S. Mano, S. Okura, M. Iwamoto, and H. Kato for assisting with the experimental procedures. This study was supported in part by Grants-in-Aid for scientific research from the research grant from Kyoto Foundation for the Promotion of Medical Science.

Author Contributions

T.N.: conception and design; T.N., Y.H. and M.N.: collection and/or assembly of data; T.N., S.Y., T.K., N.Y. and S.K.: data analysis and interpretation; T.N.: writing manuscript.

Additional Information

Supplementary information accompanies this paper at http://www.nature.com/srep

Competing financial interests: The authors declare no competing financial interests.

How to cite this article: Nakamura, T. *et al.* JBP485 promotes tear and mucin secretion in ocular surface epithelia. *Sci. Rep.* **5**, 10248; doi: 10.1038/srep10248 (2015).

SCIENTIFIC REPORTS

OPEN

JBP485 promotes corneal epithelial wound healing

Maho Nagata[1], Takahiro Nakamura[1,2], Yuiko Hata[1], Shumpei Yamaguchi[3], Taiichi Kaku[3] & Shigeru Kinoshita[1]

Received: 16 May 2015
Accepted: 08 September 2015
Published: 01 October 2015

Proper wound healing is vital for maintenance of corneal integrity and transparency. Corneal epithelial damage is one of the most frequently observed ocular disorders. Because clinical options are limited, further novel treatments are needed to improve clinical outcomes for this type of disease. In the present study, it was found that placental extract-derived dipeptide (JBP485) significantly increased the proliferation and migration of corneal epithelial cells (CECs). Moreover, JBP485 accelerated corneal epithelial wound healing *in vivo* without inflammation and neovascularization and was found to be effective for the treatment of corneal damage. These data indicate that JBP485 efficiently activates the viability of CECs and has potential as a novel treatment for various kinds of corneal epithelial disease.

The cornea is an avascular and transparent external organ of the visual system composed of three layers: epithelium, stroma and endothelium. The corneal epithelium covers the surface of the cornea as a physical barrier, protecting it by preventing infectious agents from entering the eye. It is constantly regenerated by a reservoir of stem and progenitor cells located in the limbal region[1], and responds rapidly to heal wounds, using a programmed repair mechanism to immediately close the defect and reestablish its barrier function[2]. The three major cellular events in the re-formation of the corneal epithelium are the proliferation of these cells, the migration of cells from the surrounding basal epithelium to the wounded area and differentiation of the cells into stratified layers. These wound healing processes depend on complex, orchestrated interactions of several growth factors, cytokines and extracellular matrix proteins[3,4].

Hyaluronic acid eye drops or autologous serum (AS) are commonly used to promote wound healing for treatment of corneal epithelial wounds such as superficial punctate keratitis, corneal erosion and persistent epithelial defect[5]. While these eye drops have proved successful in treating intractable corneal wounds, they lack clinical efficiency, and the problems associated with biological characteristics remain[6]. For that reason, further novel treatments with enhanced clinical usefulness are needed to improve the symptoms of these patients.

To develop a novel treatment for corneal epithelial disease, the present work focused on placental extract (PE), which has traditionally been used as a cutaneous wound healer. PE was extensively used in Chinese folk medicine because it was believed to be a rich source of therapeutic components. Nowadays, as the benefits of PE during wound healing have been reported to include anti-inflammatory, anti-fibrotic and anti-oxidative properties[7,8], aqueous PE is available and licensed in many countries for post-surgical dressings, burn injuries and chronic wounds[9–11], although it can be a potential source of infection because of its human or animal origin.

JBP485 (cyclo-trans-4-L-hydroxyprolyl-L-serine) is a dipeptide that was first isolated from Laennec (a purified hydrolysate from human placenta) as mitogens for a baby hamster kidney cell line[12]. It is noteworthy that JBP485 is completely free from any pathogens, as it can be synthesized by chemical means. Since Laennec has anti-hepatotoxic, anti-inflammatory and anti-apoptotic effects[13–15], JBP485 has been investigated for these same effects[16,17]. However, no study to date has examined JBP485's wound healing properties.

[1]Department of Ophthalmology, Kyoto Prefectural University of Medicine, Kyoto, Japan. [2]Research Center for Inflammation and Regenerative Medicine, Doshisha University, Kyoto, Japan. [3]Japan Bio Products Co., Ltd., 1-44-4, Tomigaya, Shibuya-ku, Tokyo, 151-0063, Japan. Correspondence and requests for materials should be addressed to T.N. (email: tnakamur@koto.kpu-m.ac.jp)

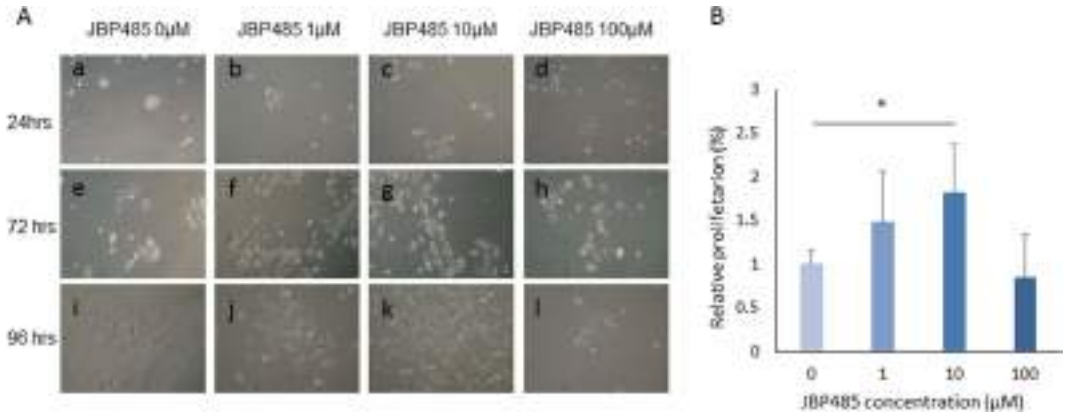

Figure 1. JBP485 accelerates proliferation of cultivated corneal epithelial cells (CECs). (**A**) Representative phase-contrast images of CECs 24 (**a–d**), 72 (**e–h**), and 96 (**i–l**) hours after the addition of JBP485 (**a,e,i**: 0 μM; **b,f,j:** 1 μM; **c,g,k:** 10 μM; **d,h,l:** 100 μM). At 72 hours after the addition of JBP485, higher cell density was observed in plates supplemented with 1 μM (**f**) and 10 μM (**g**) of JBP485 relative to control (**e**). After 96 hours, cell density was noticeably high when CECs were supplemented with 10 μM of JBP485 (**k**) as compared to the others (**I,j,l**). (**B**) BrdU assay at 72 hours after the addition of 0, 1, 10 and 100 μM JBP485, when cells reached subconfluence. Relative proliferation increased with JBP485 in a dose-dependent manner up to 10 μM, with a significant increase observed when CECs were supplemented with 10 μM of JBP485 ($p < 0.05$). CECs treated with 100 μM JBP485 showed no significant increase. Data are expressed as mean ± SD. *$p < 0.05$, ANOVA followed by a Dunnett test, $n = 5$.

The purpose of this present study was to investigate the effect of JBP485 on the proliferation, migration and wound healing of corneal epithelial cells. The findings demonstrate for the first time that JBP485 dramatically promotes the proliferation and migration of corneal epithelial cells (CECs); in addition, corneal wound healing was found to be significantly accelerated by JBP485. These data provide new insights into the function of JBP485 in the maintenance of the corneal epithelium.

Results

JBP485 accelerates proliferation of CECs *in vitro*. To determine the effect of JBP485 on the proliferative activity of CECs, cells were cultured in medium supplemented with various concentrations of JBP485 (Fig. 1A). At 72 hours after the addition of JBP485, a comparatively higher cell density was observed by microscope in those plates supplemented with 1 μM and 10 μM of JBP485 relative to control. After 96 hours, cell density was noticeably higher when CECs were supplemented with 10 μM of JBP485. At the time when cells reached subconfluence, the proliferative activity of each condition was evaluated by 5-bromo-2′-deoxyuridine (BrdU) ELISA assay (Fig. 1B) to support the microscopic findings that showed higher cell densities in the JBP485-treated group than in the control. When CECs were cultivated for 72 hours with JBP485, relative proliferation was found to be increased in a dose-dependent manner up to 10 μM, and a significant increase was observed when CECs were supplemented with 10 μM of JBP485 ($p < 0.05$, ANOVA followed by a Dunnett test). CECs treated with 100 μM JBP485 showed no significant increase. Relative proliferation value of CECs supplemented with 1 μM and 10 μM of JBP485 was 1.48 and 1.82 respectively (Fig. 1B).

JBP485 promotes migration of CECs *in vitro*. Given the importance of cell migration activity for re-epithelialization, *in vitro* scratch assay of rabbit CECs was then conducted to assess the effects of JBP485 on cell migration. Scratch assay confirmed that JBP485 accelerates closure of the gap in a dose-dependent manner up to a concentration of 100 μM at 9 hours after the scratch (Fig. 2A). A significant difference was observed relative to the control at a concentration of 100 μM ($p < 0.01$, ANOVA followed by a Dunnett test) at 9 hours after the scratch (Fig. 2B), indicating that JBP485 promotes the migration of CECs *in vitro*.

Topical administration of JBP485 promotes corneal epithelial wound healing *in vivo*. Based on the *in vitro* findings, the effect of JBP485 was then examined in an *in vivo* model of corneal epithelial wound healing. An 8-mm corneal epithelial debridement wound was mechanically created in rabbits, followed by topical administration of 100 μM JBP485 or saline to the cornea 4 times a day until the wound was closed. Representative images of healing corneas are shown in Fig. 3A. All the corneal wounds treated with JBP485 closed within 4 days without inflammation and neovascularization while all the wounds to control eyes required 5 days for wound closure. The wound area treated with JBP485 was found to be significantly smaller at 1 ($p < 0.001$), 2 ($p < 0.02$), 3 ($p < 0.02$), and 4 ($p < 0.001$) days after wounding as compared to control eyes (Fig. 3B).

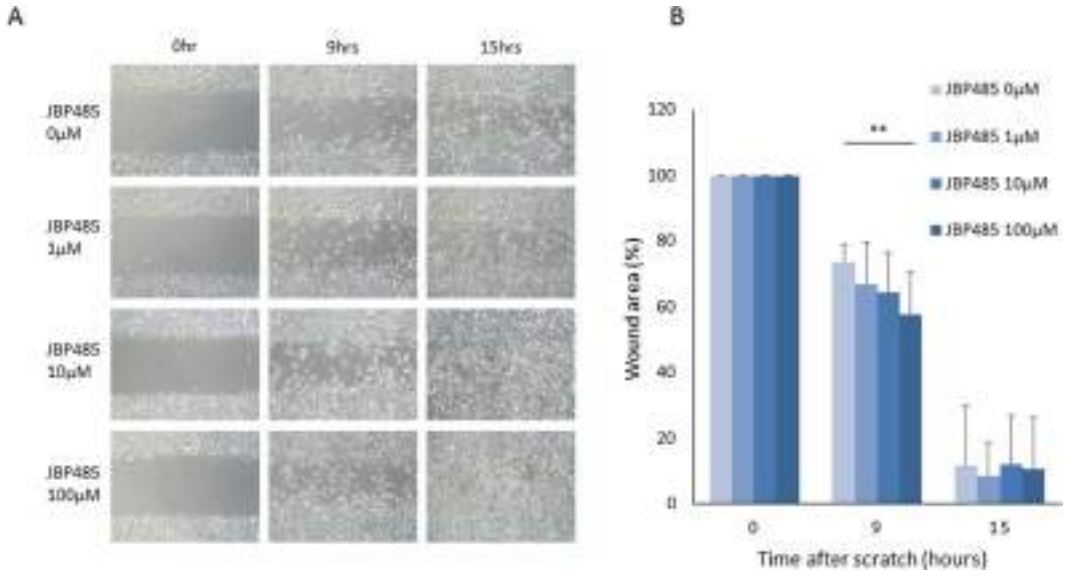

Figure 2. Enhanced migration of CECs by JBP485. (**A**) Cell migration was determined by a scratch assay. Cultivated CECs were scratched linearly. After the scratch, CECs were supplemented with 0, 1, 10 and 100 μM JBP485 and then photographed using phase-contrast microscopy, immediately and at 9 and 15 hours after scratch. (**B**) Chart of averaged wound size change against time. Wound size was significantly smaller than control (no addition of JBP485) when supplemented with 100 μM JBP485 ($p < 0.01$) at 9 hours after scratch. Data are expressed as mean ± SD. **$p < 0.01$, ANOVA followed by a Dunnett test, $n = 12$.

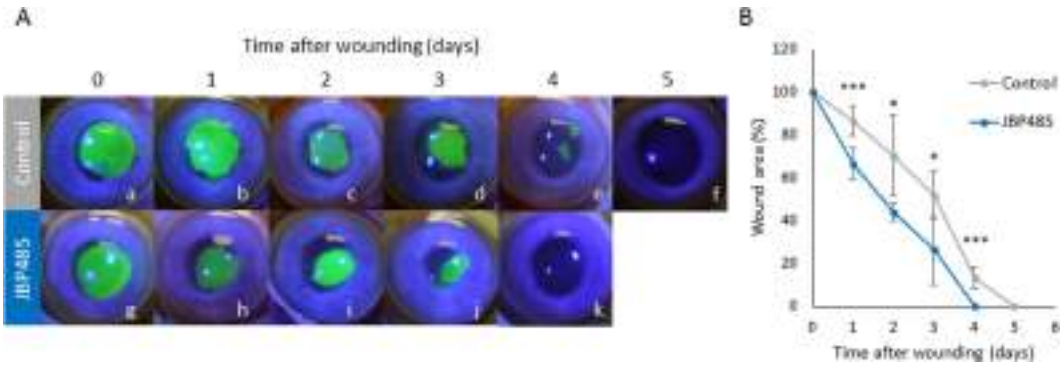

Figure 3. Acceleration of corneal epithelial wound healing by JBP485. (**A**) Representative photographs of the fluorescein-stained corneas of control and JBP485-treated eyes, immediately and 1, 2, 3, 4 and 5 days after wounding. Green-colored areas represent fluorescein-stained regions of the corneal epithelial wounds. In control eyes, corneal wounds needed 5 days to heal completely as compared to 4 days in JBP485-treated eyes. (**B**) Time course of epithelial wound healing in JBP485-treated eyes and controls. Both eyes from 5 mice were used to measure the size of epithelial defects. The wound area was significantly smaller in the JBP485-treated eyes than in control eyes at 1 ($p < 0.001$), 2 ($p < 0.02$), 3 ($p < 0.02$) and 4 ($p < 0.001$) days. At 5 days, all the wounds were closed in JBP485-treated eyes while wounds still remained in all the control eyes. Data are expressed as mean ± SD. ***$p < 0.001$, *$p < 0.05$, Student t-test, $n = 5$.

JBP485 activates viability of corneal epithelial cells. To evaluate the proliferative activity of CECs during wound healing, Ki67 expression was examined for the leading edge, peripheral, and limbal regions of rabbit corneas in each section. Sections were obtained from 12 different parts of each cornea at 1 day and 2 days after wounding. Representative images of Ki67 expression at 1 day (Fig. 4A) and 2 days (Fig. 4C) after wounding revealed a comparatively high density of Ki67 positive cells in the leading edge and limbal areas for both groups (Fig. 4A–C-a,c,d,f). To more precisely compare Ki67 expression between the groups, Ki67 labelling index was calculated. At 1 day after wounding, a significantly higher Ki67 index was observed only in the limbus ($p < 0.02$) on the JBP485-treated corneas as compared to the control corneas (Fig. 4B). On day 2, each part of those corneas generally showed increased Ki67 indexes as compared to day 1 (Fig. 4D). On day 2, leading edge part of the corneas in both groups demonstrated

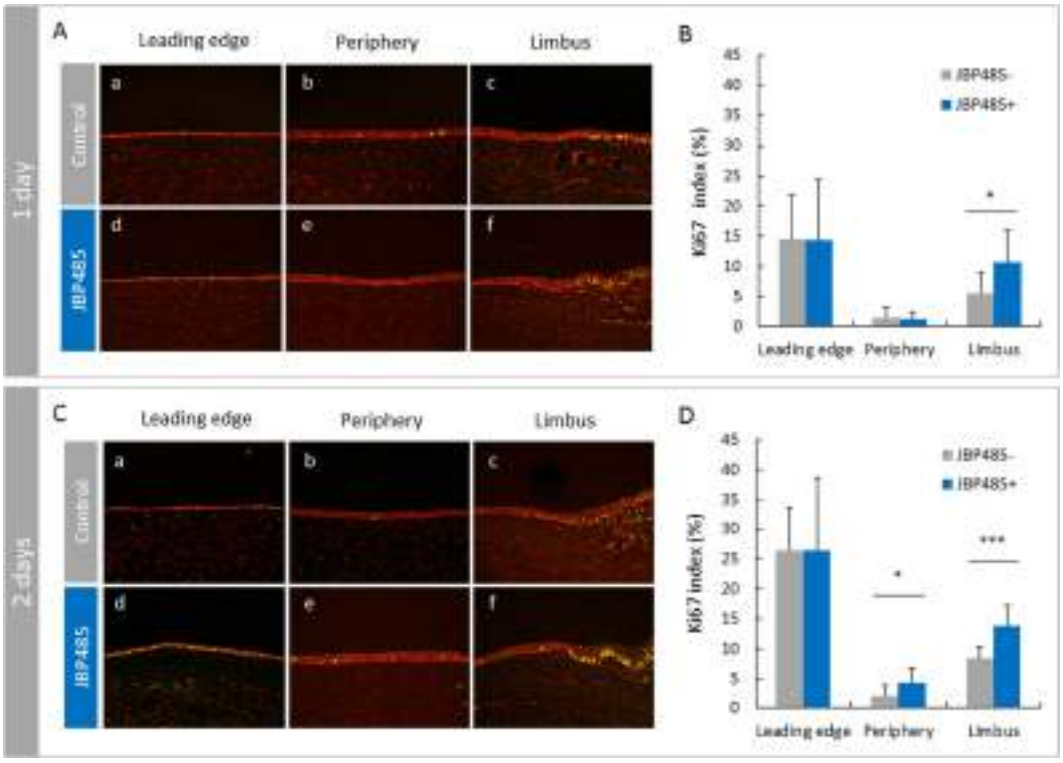

Figure 4. Enhanced proliferation by JBP485 after corneal wounding. (**A**,**C**) Representative images of immunolocalization of Ki67 in the leading edge of migrating epithelium (**a,d**), the peripheral area (**b,e**), and the limbal area (**c,f**) in control (**a–c**) and JBP485-treated corneas (**d–f**) at 1 day (**A**) and 2 days (**C**) after wounding. (**B,D**) Graphs of Ki67 index on control and JBP485-treated eyes at 1 day (**B**) and 2 days (**D**) after wounding. (**B**) At day 1, the Ki67 index of the limbal area was significantly higher in JBP485-treated eyes than in control eyes ($p < 0.02$). Ki67 indexes of the leading edge and peripheral areas showed no significant differences between groups. (**D**) At day 2, Ki67 indexes of the leading edge area showed high levels in both groups, although no significant difference was found between the groups. Ki67 indexes in the limbal ($p < 0.001$) and peripheral areas ($p < 0.02$) were significantly higher in JBP485-treated eyes than in control eyes. Data are expressed as mean ± SD, ***$p < 0.001$, *$p < 0.05$, Student t-test, $n = 12$.

high Ki67 indexes as compared to other parts, indicating that the leading edge CECs actively proliferated to cover epithelial defects in both groups. On day 2, significant differences between the groups were observed in the limbal ($p < 0.001$) and peripheral parts ($p < 0.02$) of the corneas (Fig. 4D). These findings imply that JBP485 efficiently activated the viability of CECs during wound healing even in those areas where proliferative activity of CECs was comparatively low in untreated corneas.

Discussion

The present study demonstrated for the first time that JBP485, a purified dipeptide from placenta, accelerates corneal wound healing of CECs. When corneal epithelium is wounded, CEC response includes two important steps to cover the corneal surface: cell proliferation from the surrounding area and cell migration to cover the damaged area[3]. In the present study, the effects of JBP485 on cell proliferation and on migration activity were separately evaluated to establish more precisely the mechanism of JBP485. Proliferative activity in cultivated CECs treated with JBP485 at an appropriate concentration was significantly higher than control, which aligns with a previous study in which JBP485 was isolated as mitogens for a baby hamster kidney cell line[12]. In agreement with this study, our results showed that JBP485 has an optimal concentration for cell proliferation. Scratch assay revealed that JBP485 significantly promotes migration in a dose-dependent manner up to 100 μM. These *in vitro* data demonstrate that JBP485 accelerates both proliferation and migration, as evidenced by *in vivo* corneal epithelial wound healing assay, which showed significant acceleration of re-epithelialization when JBP485 was topically administered. In this wound model, the Ki67 index level of the JBP485-treated group was high even in the limbal and peripheral areas that showed a comparatively low Ki67 index level in control corneas. In addition, statistically high significance during early stages of wound healing implied enhanced migration by JBP485, as the healing of the corneal epithelium begins via cell migration to resurface a defect, followed by the proliferation of cells[2]. These results suggest that JBP485 raises the proliferation activity level and the migration level of CECs during wound healing. We posit that, as dose-dependent experiments are ideal

for *in vivo* corneal wound experiments (8 mm in size), it is in fact quite difficult to set up their conditions. Therefore, future studies are needed to clarify this point.

Since JBP485 clearly exhibits a liver-protective property[13], the main purpose of previous studies on JBP485 has been to investigate its anti-hepatitis and liver-protective effects. The present study reports for the first time on its role in wound healing. Those previous studies speculated that the anti-hepatitis and liver-protective mechanism of JBP485 was associated with anti-oxidation and anti-apoptosis[14]. Since these mechanisms are also important for cell proliferation and wound healing[4], our findings of increased proliferative activity and migration *in vitro* and accelerated wound healing *in vivo* are compatible with previous studies of JBP485.

For treatment of delayed healing of corneal epithelial injuries, many biological substances have been applied in both animal models and human patients. Amniotic membrane has successfully been applied as a temporary biological patch to cover corneal wounds caused by ocular surface diseases such as persistent epithelial defects or infectious keratitis, or as a permanent surgical graft in ocular surface reconstruction, principally after removal of tumors or pterygium[18]. For topical instillation, AS has been applied for treatment of corneal wounds such as severe dry eye, persistent corneal epithelial defects and neurotrophic keratopathy, or for adjuvant use after limbal transplantation or ocular surface reconstruction[6]. These biological substances have successfully improved corneal wounds, but concerns about their human origin still remain. On the other hand, JBP485 also promotes wound healing and without safety concerns as it is chemically defined.

In many studies exploring wound healing in the treatment of persistent epithelial defects, several wound healing factors, including epidermal growth factor (EGF), fibronectin and combination of Substance P (SP) and insulin-like growth factor-1 (IGF-1), have been found to promote wound healing in both animal models and human patients[19–21]. Topical use of EGF has proved successful in accelerating corneal wound closure in animal models and patients by promoting cell proliferation and migration[3,19,22]. Since biosynthetic human EGF produced by yeast recombinant DNA techniques became available, topical use of EGF has been widely used, mainly in cosmetic applications. However, in the treatment of corneal wounds, corneal angiogenesis is a common complication because the cell proliferative property is related to angiogenesis[23].

Fibronectin eye drops are also effective for the treatment of corneal epithelial defects because of their ability to accelerate migration of CECs[20]. Additionally, to overcome the potential infection problems associated with the clinical use of blood products, PHSRN—a peptide corresponding to the second cell-binding domain of fibronectin—was developed as an alternative to blood-derived fibronectin eye drops[24]. Its reported beneficial effect was to stimulate migration of CECs in animal models and in clinical studies it was found useful for the treatment of persistent corneal epithelial defects[25,26]. The combination of SP and IGF-1 has also been shown to synergistically enhance corneal epithelial wound closure, especially in a rat model of neurotrophic keratopathy[27]. As a developed study of SP plus IGF-1 treatment, when applied to corneal wounds, the tetrapeptide FGLN derived from SP and the tetrapeptide SSSR derived from IGF-1 had successfully promoted corneal epithelial wound healing in both animal models and clinical studies[28]. These fibronectin eye drops, and eye drops containing SP and IGF-1 or their derivatives, aim to exploit its migratory effect. In contrast, topical application of JBP485 was found to promote both proliferation and migration.

For topical application of a wound healer with proliferative effects, sufficient wound healing must be achieved without simultaneous unintended angiogenesis, inflammation or fibrosis. If there is evidence of any adverse effect of the drug, such as angiogenesis caused by EGF eye drops, the drug is less acceptable for clinical use, even where it has sufficient wound healing capacity. In the present study, no signs of adverse effects such as angiogenesis or unintended inflammatory or fibrotic change were microscopically detected in topical application of JBP485 in the animal model. Moreover, the data showed no angiogenesis or inflammatory effect of JBP485 in mouse models or in cultivated CECs (data not shown). In systemic administration, JBP485 has already been shown to have no adverse effects in rats and mice[13–15]. Since JBP485 is thought to be excreted by organic anion transporters in the kidney, concerns might be raised about renal toxicity, but JBP485 is not toxic for the kidney and in fact protects against renal toxicity[29].

Our recent study showed that JBP485 promotes tear and mucin secretion in corneal and conjunctival cells[30]. Clinically, decreased secretion of tears sometimes makes corneal wound healing slow or intractable. Maintaining the ocular surface in a constantly wet state is thought to be important for proper healing of corneal wounds; when treating corneal wounds from dry eye, JBP485 treatment is therefore of great advantage.

In conclusion, the findings of our investigation show that PE-derived JBP485 efficiently promotes proliferation and migration of CECs. Moreover, JBP485 was found to be effective for the treatment of corneal damage. Although further investigation is needed to elucidate the molecular mechanisms of its biological function, our data provide new insights into the therapeutic potential of JBP485 across a range of corneal epithelial diseases.

Materials and Methods

JBP485 preparation. Chemically synthesized JBP485 was provided by Japan Bio Products Co., Ltd. (Tokyo, Japan). JBP485 powder was dissolved in warmed saline (Otsuka, Pharmaceutical Co., Ltd., Tokyo,

Japan) into 50 mM solution at a temperature of 50 °C and then diluted to the required concentration, with saline for instillation or with medium for culture.

Cell culture. Eyes of Japanese white rabbits were purchased from Funakoshi Corporation (Tokyo, Japan). Rabbit corneal epithelial cells were prepared and cultured according to a modified version of the previously reported method[31]. In brief, limbal tissues were removed from the eyes, and the half-layers of endothelial side were then mechanically removed by surgical scissors. The remaining corneal tissues were transferred to minimum essential keratinocyte serum-free medium (KSFM; Life Technologies, California, USA) ($[Ca^{2+}] = 0.4$ mM) containing dispase I (Wako Pure Chemical Industries, Osaka, Japan) at 250 PU/mL and then incubated at 4 °C for 24 hours and 37 °C for 1 hour. The corneal epithelial cells were then peeled and further incubated with TrypLE™ select (Life Technologies, California, USA) at 4 °C for 30 minutes and 37 °C for 5 minutes to dissociate adhesion between the cells. The prepared rabbit CECs were suspended in serum-free CnT-20 medium (CELLnTEC, Santa Cruz, CA, USA) containing 1% Antibiotic-Antimyotic (Life Technologies Corporation, Carlsbad, CA USA) to isolate and grow CECs and then plated in collagen-coated tissue culture plates (AGC Techno Grass Co., Ltd., Shizuoka, Japan). The rabbit CECs were then cultured at 37 °C with 5% CO_2, and the medium was replaced with fresh medium every 48 hours until the cells reached subconfluence.

Cell proliferation assay. A colorimetric BrdU cell proliferation ELISA (Amersham Cell Proliferation Biotrak ELISA, GE Healthcare Milan, Italy) was used to assess cell proliferation ability according to manufacturer specifications. Primary rabbit CECs were cultured in serum-free CnT-20 medium containing 1% antibiotic-antimyotic for 3 days until the cells adhered to the culture dish, and then the medium was shifted to the medium containing an appropriate concentration of JPB485 (0, 1, 10, 100 μM) until the cells reached subconfluence. On the day of assay, BrdU (final, 10 μM) was added to each well of a 24-well plate, except for negative controls that received no BrdU. CECs were incubated for 18 hours at 37 °C in a CO_2 incubator. Plates were drained and blocked with 200 μL/well of ELISA fixative for 30 minutes at room temperature (RT). After decanting, 200 μL of peroxidase-conjugated anti-BrdU solution was added to each well, and dishes were incubated for 90 minutes at RT. Finally, 200 μL of 3,3′,5,5′ -tetramethylbenzidine (TMB) solution was added to each well and incubated for 15 minutes on a shaker, and absorbance was immediately measured at 450 nm in an absorption spectrometer (Multiskan MS, Lab systems, Helsinki, Finland).

***In vitro* scratch assay.** *In vitro* wound modelling was performed using a scratch assay. Confluent monolayers of rabbit CECs, cultured as described above in serum-free Cnt-20 medium containing 1% antibiotic-antimyotic in 6-well plates, were linearly scratched with a 1000 μL plastic pipette tip to create a cell-free area. Cultures were gently washed 3 times with warmed phosphate-buffered saline (PBS) to remove loose cells. The CnT-20 medium was then added containing 0, 1, 10 or 100 μM of JBP485, and cells were incubated in a CO_2 incubator. Twelve fields of each scratch area were photographed at various time points until the cells completely covered the cell-free area. Each wound area was measured using image analyzing software (Image J; developed by Wayne Rasband, National Institutes of Health, Bethesda, MD; provided in the public domain at http://rsb,info.nih.gov/ij). The wound area was calculated as a percentage of the initial wound area.

Corneal wounding. All experiments were performed in strict accordance with the Association for Research in Vision and Ophthalmology Statement for the Use of Animals in Ophthalmic and Vision Research. All animals used in this study were maintained and handled according to the protocols approved by the Kyoto Prefectural University of Medicine. Albino Japanese rabbits were obtained from Kitayama Laboratories (Kyoto, Japan) and were maintained under pathogen-free conditions in the barrier facility. *In vivo* rabbit models of corneal wound closure were created as previously described[30]. Rabbits were anaesthetised with an intramuscular injection of ketamine hydrochloride (60 mg/kg of body mass; Daiichi Sankyo Propharma, Tokyo, Japan) and xylazine (5 mg/kg; Bayer Medical, Tokyo Japan) as well as with oxybuprocaine eye drop (Santen pharmaceutical company, Osaka, Japan). The central regions of rabbit corneas were demarcated with an 8-mm circular trephine, and epithelia within the circle were mechanically scraped with a rust ring remover (Handy Micro Motor; Inami, Tokyo, Japan). Right eyes were elected to receive treatment while left eyes were assigned to receive the placebo. The right eyes of rabbits received a topical application of 100 μM JBP485, starting immediately after surgery. Control eyes received isotonic saline (Otsuka, Pharmaceutical Co., Ltd., Tokyo, Japan). All eyes were treated 4 times per day for 5 days.

Corneal Wound Healing Evaluation. The epithelial wounds were visualized using fluorescein and photographed at 0, 1, 2, 3, 4 and 5 days after wounding, under a slit lamp microscope equipped with a digital camera (EOS 30D digital; Canon, Tokyo, Japan) with a cobalt blue filter. The area of each epithelial defect was measured using Image J image analyzing software as above. The wound area was calculated as a percentage of the initial wound area.

Immunofluorescence. Immunofluorescence analysis was performed by means of the indirect immunofluorescent technique as previously described[32]. Briefly, sectioned samples were immediately washed with PBS and embedded in optimal cutting temperature (OCT) compound. Frozen sections were sliced to a thickness of 8 μm, placed on gelatin-coated slides, air dried and fixed in 100% acetone or 4% paraformaldehyde at 4 °C. After several washings with PBS, the sections were incubated with 1% bovine serum albumin at RT for 30 minutes to block nonspecific binding. They were then incubated with primary antibody (mouse monoclonal anti-Ki67 antibody; BD Biosciences, California) for 1 hour at RT and washed 3 times in PBS containing 0.15% TRITON™ X-100 (The Dow Chemical Company, Midland, MI) for 15 minutes per wash. For negative control experiments, the equivalent serum was used. After staining with the primary antibodies, the sections were incubated at RT for 1 hour with appropriate fluorescein-conjugated secondary antibody. After several washes with PBS, they were coverslipped with mounting medium containing propidium iodide (PI; Vector Laboratories, Inc., Burlingame, CA). The slides were then examined with a confocal microscope (FluoView®; Olympus Corporation, Tokyo, Japan).

Ki67 labelling index. The sections were stained with Ki67 using the indirect immunofluorescence technique. The Ki67 protein is present during G1, S, G2 and M phases of the cell cycle and is strictly associated with cell proliferation. The epithelial cells positive for Ki67 and PI in a confocal microscopic field were manually counted, and the number of Ki67 positive cells was recorded as a percentage of the total cell count.

Statistics. Differences were evaluated by analysis of variance (ANOVA) followed by either a Dunnett multiple comparison test or a student's unpaired t-test. Values of $p < 0.05$ were considered significant.

References

1. Pellegrini, G. *et al.* Location and clonal analysis of stem cells and their differentiated progeny in the human ocular surface. *J Cell Biol* **145,** 769–782 (1999).
2. Lu, L., Reinach, P. S. & Kao, W. W. Corneal epithelial wound healing. *Exp Biol Med (Maywood)* **226,** 653–664 (2001).
3. Imanishi, J. *et al.* Growth factors: importance in wound healing and maintenance of transparency of the cornea. *Prog Retin Eye Res* **19,** 113–129 (2000).
4. Wilson, S. E. *et al.* The corneal wound healing response: cytokine-mediated interaction of the epithelium, stroma, and inflammatory cells. *Prog Retin Eye Res* **20,** 625–637 (2001).
5. Fox, R. I., Chan, R., Michelson, J. B., Belmont, J. B. & Michelson, P. E. Beneficial effect of artificial tears made with autologous serum in patients with keratoconjunctivitis sicca. *Arthritis Rheum* **27,** 459–461 (1984).
6. Quinto, G. G., Campos, M. & Behrens, A. Autologous serum for ocular surface diseases. *Arq Bras Oftalmol* **71,** 47–54 (2008).
7. Sur, T. K., Biswas, T. K., Ali, L. & Mukherjee, B. Anti-inflammatory and anti-platelet aggregation activity of human placental extract. *Acta Pharmacol Sin* **24,** 187–192 (2003).
8. Jung, J. *et al.* Placenta extract promote liver regeneration in CCl4-injured liver rat model. *Int Immunopharmacol* **11,** 976–984 (2011).
9. Biswas, T. K., Auddy, B., Bhattacharya, N. P., Bhattacharya, S. & Mukherjee, B. Wound healing activity of human placental extracts in rats. *Acta Pharmacol Sin* **22,** 1113–1116 (2001).
10. Wu, C. H., Chang, G. Y., Chang, W. C., Hsu, C. T. & Chen, R. S. Wound healing effects of porcine placental extracts on rats with thermal injury. *Br J Dermatol* **148,** 236–245 (2003).
11. Shukla, V. K., Rasheed, M. A., Kumar, M., Gupta, S. K. & Pandey, S. S. A trial to determine the role of placental extract in the treatment of chronic non-healing wounds. *J Wound Care* **13,** 177–179 (2004).
12. Yagi, A. *et al.* Effect of cyclo (trans-4-L-hydroxyprolyl-L-serine) from hydrolysate of human placenta on baby hamster kidney -21/C-13 cells. *Natural Medicine* **52,** 156–159 (1998).
13. Liu, K. X. *et al.* Hydroxyprolylserine derivatives JBP923 and JBP485 exhibit the antihepatitis activities after gastrointestinal absorption in rats. *J Pharmacol Exp Ther* **294,** 510–515 (2000).
14. Yang, T. *et al.* Protective effect of JBP485 on concanavalin A-induced liver injury in mice. *J Pharm Pharmacol* **61,** 767–774 (2009).
15. Cang, J. *et al.* Pharmacokinetics and mechanism of intestinal absorption of JBP485 in rats. *Drug Metab Pharmacokinet* **25,** 500–507 (2010).
16. Sakamoto, K., Tonooka, M., Abe, K., Usami, K. & Kasahara, T. Comparative studies on rat primary cultured and isolated hepatocytes in the evaluation of a therapeutic agents for liver disease. *Jpn J Pharmacol* **41,** 424–426 (1986).
17. Wu, J. *et al.* Laennec protects murine from concanavalin A-induced liver injury through inhibition of inflammatory reactions and hepatocyte apoptosis. *Biol Pharm Bull* **31,** 2040–2044 (2008).
18. Fernandes, M., Sridhar, M. S., Sangwan, V. S. & Rao, G. N. Amniotic membrane transplantation for ocular surface reconstruction. *Cornea* **24,** 643–653 (2005).
19. Kitazawa, T. *et al.* The mechanism of accelerated corneal epithelial healing by human epidermal growth factor. *Invest Ophthalmol Vis Sci* **31,** 1773–1778 (1990).
20. Watanabe, K., Nakagawa, S. & Nishida, T. Chemotactic and haptotactic activities of fibronectin for cultured rabbit corneal epithelial cells. *Invest Ophthalmol Vis Sci* **29,** 572–577 (1988).
21. Nishida, T. *et al.* Synergistic effects of substance P with insulin-like growth factor-1 on epithelial migration of the cornea. *J Cell Physiol* **169,** 159–166 (1996).
22. Nakamura, Y., Sotozono, C. & Kinoshita, S. The epidermal growth factor receptor (EGFR): role in corneal wound healing and homeostasis. *Exp Eye Res* **72,** 511–517 (2001).
23. Nezu, E., Ohashi, Y., Kinoshita, S. & Manabe, R. Recombinant human epidermal growth factor and corneal neovascularization. *Jpn J Ophthalmol* **36,** 401–406 (1992).
24. Aota, S., Nomizu, M. & Yamada, K. M. The short amino acid sequence Pro-His-Ser-Arg-Asn in human fibronectin enhances cell-adhesive function. *J Biol Chem* **269,** 24756–24761 (1994).
25. Kimura, K. *et al.* Stimulation of corneal epithelial migration by a synthetic peptide (PHSRN) corresponding to the second cell-binding site of fibronectin. *Invest Ophthalmol Vis Sci* **48,** 1110–1118 (2007).
26. Yamada, N. *et al.* Open clinical study of eye drops containing the fibronectin-derived peptide PHSRN for treatment of persistent corneal epithelial defects. *Cornea* **31,** 1408–1413 (2012).

27. Nagano, T. *et al.* Effects of substance P and IGF-1 in corneal epithelial barrier function and wound healing in a rat model of neurotrophic keratopathy. *Invest Ophthalmol Vis Sci* **44,** 3810–3815 (2003).
28. Yamada, N. *et al.* Open clinical study of eye-drops containing tetrapeptides derived from substance P and insulin-like growth factor-1 for treatment of persistent corneal epithelial defects associated with neurotrophic keratopathy. *Br J Ophthalmol* **92,** 896–900 (2008).
29. Liu, T. *et al.* Changes in expression of renal Oat1, Oat3 and Mrp2 in cisplatin-induced acute renal failure after treatment of JBP485 in rats. *Toxicol Appl Pharmacol* **264,** 423–430 (2012).
30. Nakamura, T. *et al.* JBP485 promotes tear and mucin secretion in ocular surface epithelia. *Scientific reports* **5,** 10248 (2015).
31. Nakamura, T. *et al.* Sterilized, freeze-dried amniotic membrane: a useful substrate for ocular surface reconstruction. *Invest Ophthalmol Vis Sci* **45,** 93–99 (2004).
32. Nagata, M. *et al.* LRIG1 as a potential novel marker for neoplastic transformation in ocular surface squamous neoplasia. *PLoS One* **9,** e93164 (2014).

Acknowledgements

The authors wish to thank T. Horikiri, S. Mano, S. Okura, M. Iwamoto, and H. Kato for assisting with the experimental procedures. This study was supported in part by Grants-in-Aid for scientific research from the research grant from Kyoto Foundation for the Promotion of Medical Science.

Author Contributions

T.N. conception and design; M.N., T.N. and Y.H. collection and/or assembly of data; T.N., S.Y., T.K. and S.K. data analysis and interpretation; M.N. and T.N. writing manuscript.

Additional Information

Competing financial interests: Yes there is potential Competing Financial Interest. T.N. and S.K. received research funding from Japan Bio Products Co., Ltd.

How to cite this article: Nagata, M. *et al.* JBP485 promotes corneal epithelial wound healing. *Sci. Rep.* **5**, 14776; doi: 10.1038/srep14776 (2015).

PLOS | ONE

RESEARCH ARTICLE

Clusterin Seals the Ocular Surface Barrier in Mouse Dry Eye

Aditi Bauskar[1], Wendy J. Mack[2], Jerome Mauris[3], Pablo Argüeso[3], Martin Heur[4], Barbara A. Nagel[5], Grant R. Kolar[6], Martin E. Gleave[7], Takahiro Nakamura[8], Shigeru Kinoshita[8], Janet Moradian-Oldak[9], Noorjahan Panjwani[10], Stephen C. Pflugfelder[11], Mark R. Wilson[12], M. Elizabeth Fini[13], Shinwu Jeong[14]*

1 USC Institute for Genetic Medicine and Graduate Program in Medical Biology, Keck School of Medicine of USC, University of Southern California, Los Angeles, California, United States of America, **2** Southern California Clinical & Translational Science Institute and Department of Preventive Medicine, Keck School of Medicine of USC, University of Southern California, Los Angeles, California, United States of America, **3** The Schepens Eye Research Institute, Massachusetts Eye & Ear and Department of Ophthalmology, Harvard Medical School, Boston, Massachusetts, United States of America, **4** USC Eye Institute, Keck School of Medicine of USC, University of Southern California, Los Angeles, California, United States of America, **5** Research Microscopy and Histology Core, Department of Pathology, Saint Louis University School of Medicine, St Louis, Missouri, United States of America, **6** Department of Pathology and Department of Ophthalmology, Saint Louis University School of Medicine, St. Louis, Missouri, United States of America, **7** The Vancouver Prostate Centre and Department of Urologic Sciences, University of British Columbia, Vancouver, British Columbia, Canada, **8** Department of Frontier Medical Science and Technology for Ophthalmology, Kyoto Prefectural University of Medicine, Kyoto, Japan, **9** Center for Craniofacial Molecular Biology, Division of Biomedical Sciences, University of Southern California, Herman Ostrow School of Dentistry of USC, Los Angeles, California, United States of America, **10** New England Eye Center/ Department of Ophthalmology and Department of Developmental, Molecular & Chemical Biology, Tufts University School of Medicine, Boston, Massachusetts, United States of America, **11** Ocular Surface Center, Department of Ophthalmology, Cullen Eye Institute, Baylor College of Medicine, Houston, Texas, United States of America, **12** Illawarra Health and Medical Research Institute, School of Biological Sciences, University of Wollongong, Wollongong, New South Wales, Australia, **13** USC Institute for Genetic Medicine and Departments of Cell & Neurobiology and Ophthalmology, Keck School of Medicine of USC, University of Southern California, Los Angeles, California, United States of America, **14** USC Institute for Genetic Medicine and Department of Ophthalmology, Keck School of Medicine of USC, University of Southern California, Los Angeles, California, United States of America

* shinwuje@usc.edu

Citation: Bauskar A, Mack WJ, Mauris J, Argüeso P, Heur M, Nagel BA, et al. (2015) Clusterin Seals the Ocular Surface Barrier in Mouse Dry Eye. PLoS ONE 10(9): e0138958. doi:10.1371/journal.pone.0138958

Editor: Alexander V. Ljubimov, Cedars-Sinai Medical Center; UCLA School of Medicine, UNITED STATES

Received: June 11, 2015

Accepted: September 4, 2015

Published: September 24, 2015

Data Availability Statement: All relevant data are within the paper.

Funding: This work was funded by an award from the James H. Zumberge Faculty Research & Innovation Fund (to SJ) (http://research.usc.edu/zumberge); National Institutes of Health grants R01-EY009828 (to MEF)(https://nei.nih.gov), R01-EY024031 (to PA) (https://nei.nih.gov), R01-DE013414 (to JM-O) (http://www.nidcr.nih.gov) and UL1-TR000130 (formerly UL1-RR031986; sub-award to WJM) (http://www.nih.gov/about/almanac/organization/NCRR.htm); an unrestricted grant from Research to Prevent Blindness, New York, NY (https://www.rpbusa.org/rpb/grants/grants) to the

Abstract

Dry eye is a common disorder caused by inadequate hydration of the ocular surface that results in disruption of barrier function. The homeostatic protein clusterin (CLU) is prominent at fluid-tissue interfaces throughout the body. CLU levels are reduced at the ocular surface in human inflammatory disorders that manifest as severe dry eye, as well as in a preclinical mouse model for desiccating stress that mimics dry eye. Using this mouse model, we show here that CLU prevents and ameliorates ocular surface barrier disruption by a remarkable sealing mechanism dependent on attainment of a critical all-or-none concentration. When the CLU level drops below the critical all-or-none threshold, the barrier becomes vulnerable to desiccating stress. CLU binds selectively to the ocular surface subjected to desiccating stress *in vivo*, and *in vitro* to the galectin LGALS3, a key barrier component. Positioned in this way, CLU not only physically seals the ocular surface barrier, but it also protects the barrier cells and prevents further damage to barrier structure. These findings define a

University of Southern California; and start-up funding from the Keck School of Medicine of USC. The funders had no role in study design, data collection and analysis, decision to publish, or preparation of the manuscript.

Competing Interests: A U.S. patent application entitled "Structure/Function of Clusterin Pharmaceuticals" (inventors: MEF and SJ) and a U. S. provision patent application entitled "Diagnostic Test to Improve Efficacy of Biotherapeutics for Dry Eye Based on Clusterin" (inventors: MEF, SJ and AB) have been filed by the University of Southern California in connection with this work. The other authors declare that they have no competing interests. This does not alter the authors' adherence to all the PLOS ONE policies on sharing data and materials.

fundamentally new mechanism for ocular surface protection and suggest CLU as a biotherapeutic for dry eye.

Introduction

The ocular surface is directly exposed to the outside environment, where it is subject to desiccation and interaction with noxious agents, thus it must function as a barrier to protect the underlying tissue [1]. Membrane-associated mucins project from the apical cell layer of the corneal and conjunctival epithelia into the tear film, where they bind multiple oligomers of the lectin LGALS3 to form a highly organized glycocalyx, creating the transcellular barrier [2, 3]. In addition, tight junctions seal the space between adjacent cells to create the paracellular barrier [4]. The barriers appear to be functionally linked via the cytoskeleton [5].

Ocular surface barrier disruption is a sign of dry eye, a disorder caused by inadequate hydration by the tears, which results in discomfort, affects quality of vision, and can cause blindness [6]. Dry eye affects ~5 million people over the age of 50 in the USA (especially women) and almost 15% of the population at all ages, comprising upwards of 30–40 million people [7]. In all forms of dry eye, reduced tear flow and/or increased evaporation leads to tear hyperosmolarity, initiating the vicious circle of dry eye pathology. Hyperosmolarity induces inflammatory cascade activation [8–10], promotes apoptosis [11–13], and stimulates expression and activity of matrix metalloproteinases (MMPs) [14, 15], leading to ocular surface barrier disruption [16]. Disruption of the ocular surface barrier is assessed clinically by measuring uptake of water-soluble dyes such as rose-bengal, lissamine green or fluorescein, which occurs in a distinctive punctate pattern in dry eye [17, 18]. The normal ocular surface exhibits variable levels of dye uptake, possibly reflecting the natural processes of cellular desquamation and shedding of mucin ectodomains [1, 18, 19]. Higher levels of dye uptake are diagnostic of dry eye, however mechanisms are not fully defined [18, 20, 21].

MMP9 is recognized as a causal mediator of ocular surface barrier disruption due to desiccating stress in both mice [14, 15], and humans [22]. To help generate hypotheses about mechanisms of dry eye, we performed a yeast two-hybrid screen for corneal proteins that interact with MMP9 [23]. A single candidate was validated: clusterin (CLU). Functional studies revealed that CLU is a potent inhibitor of MMP9 enzymatic activity, as well as activity of other MMPs. When CLU was added to confluent epithelial cell cultures treated with MMP9, tight junctions were protected against MMP9 proteolysis [23].

Human CLU is secreted as a 62-kDa glycoprotein (with an apparent mass of 70–80 kDa as evaluated by denaturing SDS-PAGE) composed of two disulfide-bonded polypeptide chains derived from proteolytic cleavage of an intracellular precursor [24]. With three sites for N-linked glycosylation on each chain, secreted CLU is 17–27% N-linked carbohydrate by weight [25]. Three long natively disordered regions linked to amphipathic helices form a dynamic, molten globule-like binding site, providing the ability to interact with a variety of molecules [26]. Also known as apolipoprotein J or ApoJ, CLU associates with discrete subclasses of high-density lipoproteins [27]. CLU is cytoprotective [28, 29] and anti-inflammatory [30], and it also functions as an extracellular molecular chaperone, acting to maintain proteostasis by inhibiting the aggregation of stress-induced misfolded proteins and facilitating their clearance from extracellular fluids [31, 32]. Consistent with this, the only known phenotype of CLU knockout mice maintained under unstressed conditions is the gradual accumulation of insoluble protein deposits in the kidney [33]. On the other hand, CLU knockout mice exhibit distinct phenotypes when conditions are created to model inflammatory diseases [30, 34].

CLU is found in bodily fluids and is expressed prominently by epithelia at fluid-tissue interfaces [35, 36]. In the context of its known properties, this expression pattern suggests that CLU protects barrier cells from the environment. With regard to the ocular surface-tear interface, CLU was identified as the most abundant transcript in the human corneal epithelium [37]. CLU is expressed in the apical corneal epithelial cell layers in both human [38] and mouse [23], and has also been identified in human tears [39–41]. Expression of CLU in the ocular surface epithelia is dramatically reduced in human inflammatory disorders that manifest as severe dry eye [38]. Similarly, we showed recently that both CLU protein and mRNA levels in the ocular surface epithelia are reduced by ~30% when desiccating stress is induced in a preclinical mouse model for dry eye [23]. In addition, a striking reduction of CLU expression was observed in cultured human corneal epithelial cells treated with inflammatory mediators [23]. Collectively, these results suggest that down-regulation of CLU expression at the ocular surface subjected to desiccating stress in dry eye is due to activation of the inflammatory cascade.

In this study we investigated the hypothesis that reduced levels of CLU result in vulnerability to barrier disruption using the preclinical mouse model.

Materials and Methods

Proteins and antibodies

HUGO nomenclature is used for genes and their products, unless otherwise indicated. The secreted form of recombinant human CLU (rhCLU) and recombinant mouse CLU (rmCLU), both of which contain a polyhistidine-tag (His6 tag) at the C-terminus, were purchased from R&D Systems (Minneapolis, MN). These proteins are expressed in mammalian cells and are fully glycosylated and processed, closely modeling secreted CLU expressed *in vivo*. Natural secreted plasma CLU (pCLU) purified from human serum was purchased from ProsPec (Ness-Ziona, Israel). Bovine serum albumin (BSA) was purchased from R&D Systems. The cytokine TNFA was purchased from Sigma (St. Louis, MO). Anti-CLU (sc-6419) and anti-LGALS3 antibodies (sc-23983) were purchased from Santa Cruz Biotech (Santa Cruz, CA). Anti-OCLN (ab168986), anti-ACTB (ab6276), and anti-His6 tag (ab18184) antibodies were purchased from Abcam (Cambridge, MA).

Preclinical mouse model

The University of Southern California's Institutional Animal Care and Use Committee approved the research protocol for use of mice in this study. Research was conducted in adherence with the Association for Research in Vision and Ophthalmology (ARVO) Statement for the Use of Animals in Ophthalmic and Visual Research.

Wild type C57Bl/6J female mice purchased from Jackson Labs (Bar Harbor, ME) were used for all experiments unless otherwise stated. Mice were housed in a pathogen-free barrier facility at USC and kept at 25±1°C, relative humidity 60%±10%, with alternating 12 h light/dark cycles. Euthanasia was performed using compressed CO_2 gas, according to the American Veterinary Medical Association Guidelines for the Euthanasia of Animals: 2013 Edition.

Desiccating stress was induced in 6–8 week old mice by the air-draft-plus-scopolamine protocol, as previously described [14]. Briefly, scopolamine hydrobromide (Sigma-Aldrich, St. Louis, MO) (0.5 mg/0.2 ml in PBS) was injected subcutaneously in alternating hindquarters, 4 times/day (7 AM, 10 AM, 1 PM, and 4 PM), to inhibit tear secretion. At the same time, mice were exposed to an air draft for 18 hours/day in a room with 80±1°F and <40% humidity at all times. Standard desiccating stress induction was done for 5 days, otherwise, for the period as indicated.

Delivery of CLU was performed as previously described [8, 14]. Eye drops of CLU or BSA were formulated in PBS vehicle and drops were delivered topically to the unanesthetized mouse eye. The standard treatment protocol was 1 uL/eye, 4 times/day, delivered at the time of scopolamine injection. In some experiments drops were delivered a single time. PBS alone was used as the vehicle control.

Corneal epithelial uptake of clinical fluorescein dye Fluoresoft® -0.35% (Holles Laboratory, Cohasset, MA) was assessed quantitatively using fluorometry, as previously described [14]. In some experiments as noted, Alexa-Fluor-dextran (Molecular Probes, Eugene, OR) was substituted.

Imaging of fluorescein uptake at the ocular surface

Laser scanning confocal microscopy was used to image the punctate pattern of fluorescein uptake, as described [42]. Mice were euthanized following treatment and whole eyes were extracted. The eyes were immersed in PBS while the optic nerve was detached, following which they were placed anterior side up, on a 0.8% agarose plate (NuSieve® GTG® Agarose, Lonza, Rockland, ME). Whole mount digital images (512 x 512 pixels) were captured with a laser-scanning confocal microscope (LSM 5 Pascal, Zeiss, Thornwood, NY) using a 10X objective. Fluorescent images in the central cornea of the samples were captured in Z-section at 1um intervals by using identical photomultiplier tube gain settings and processed using Zen 2012 software (Zeiss) and ImageJ64 software (http://imagej.nih.gov/ij/). The individual layers of the corneal epithelium were captured utilizing the Z-stack option. This technique allows for the specimen to be scanned from the surface to the basal layer of the epithelium. The Z-stack can then be projected into a flat image representing fluorescein uptake through all layers of the epithelium. The software can also combine the Z-stack images into a three-dimensional (3-D) configuration, generating a cross section that is perpendicular to the apical plane. In this way, penetration of fluorescein into the apical, sub-apical, and basal layers of the epithelium can be evaluated.

Imaging of CLU binding to the ocular surface and LGALS3 affinity chromatography

CLU binding to the ocular surface was visualized using an indirect immunofluorescent labeling technique and imaged by laser scanning confocal microscopy as described above. Antibody (50 ug) to the His6 tag on rhCLU was labeled with CF™-594 (excitation/emission = 593 nm/614 nm) using a CF dye SE protein labeling kit (Biotium, Hayward, CA). The final labeled antibody was prepared in PBS at 1.7 mg/ml after removal of unincorporated dye molecules. CLU-CF-594-Ab complex (CLU at ~110 ug/mL, which is > threshold concentration) was made before instillation to the ocular surface by incubating CLU (2 uL of 200 μg/ml) and labeled antibody (1.5 uL of 1.7 mg/ml) in the dark for 3 h at room temperature (RT). To each eye, 2 uL of CF-594-Ab alone or complex solution was applied for 15 min before extracting eyes for imaging. As a reference point for CLU binding on the ocular surface, eyes in some experiments were co-treated for 5 min before extraction with a fluorescent lipophilic membrane tracer DiO (1 uL) (3,3'-Dioctadecyloxacarbocyanine Perchlorate, Life Technologies; excitation/emission = 484/501 nm), which was dissolved at 1 ug/ml DMSO.

LGALS3 affinity chromatography was performed as previously described [3]. The CLU present in the various collected fractions was quantified by Western blotting.

Apoptosis assay and epithelial protein analysis

After 7-day DS with PBS or CLU (1μg/ml) treatments, eyes were frozen in OCT solution and cross-sectioned at 10 um thickness. To detect apoptosis, tissue slides were stained for the

terminal deoxynucleotidyl transferase dUTP nick end labeling (TUNEL) using the In Situ Cell Death Detection Kit Fluorescein (Sigma-Aldrich) according to the protocol provided by the company with permeabilisation for 12 min at 37°C, and the fluorescent images were obtained by confocal microscopy.

Protein preparation from epithelial tissue lysates was described previously [23]. Protein extracts from individual eyes in the same treatment group (7 mice/treatment) were pooled. 20 ug of protein/sample was resolved by denaturing SDS-PAGE (12% gel) for Western blotting.

Cell culture model

Cells of the telomerase-immortalized human corneal limbal epithelial cell (HCLE) line [43] were plated in a 96-well plate and left for 7 days to stratify and differentiate, as previously described [23]. To measure secreted MMP9 produced in response to treatments, cell conditioned media samples were subjected to gelatin zymography and Image J analysis [23].

Tear CLU quantification

Mouse basal tears were collected in mice by instillation of 2 ul of PBS containing 0.1% BSA into the conjunctival sac of each eye, which was then collected with a glass capillary tube from the tear meniscus in the lateral canthus as described [44]. Samples were pooled from 2 eyes. Tear volume was measured using phenol red–impregnated cotton threads (Zone-Quick; Oasis, Glendora, CA) [45]; results were similar to tear volumes reported previously [46]. CLU was quantified using the Mouse Clusterin Quantikine ELISA kit (R&D Systems), according to the protocol provided by the company, which utilized a standard curve.

CLU knockout mice

In some experiments, Clu knockout mice on the C57Bl/6J background were used. Heterozygous breeders were purchased from Jackson Labs and bred with C57Bl/6J wild type mice to obtain both heterozygotes and homozygotes on the same background. Genotypes of offspring were confirmed by PCR from genomic DNA isolated from tail tips. The PCR primers were previously described [34].

A morphological evaluation was performed on the unstressed ocular surface of CLU knockout mice of both the heterozygous $CLU^{+/-}$ and homozygous $CLU^{-/-}$ genotypes, comparing to wild type C57Bl/6J mice. First, a hand-held 20-diopter indirect lens was used to examine the ocular surface. The ocular surface of eyes from two different mice of the heterozygous $CLU^{+/-}$ genotype was compared to eyes from two different mice of the wild type genotype. Mice were not anesthetized, nor was any topical anesthetic applied to the ocular surface prior to examination. An ophthalmologist and cornea sub-specialist (MH) performed the evaluation. Similarly, the ocular surface of eyes from three different mice of the homozygous $CLU^{-/-}$ knockout genotype was evaluated.

Next, the ocular surface was evaluated by histologic techniques. Briefly, eyes were fixed in 4% formaldehyde and embedded in paraffin. Sections of 6 um were stained with hematoxylin and eosin or periodic acid-Schiff reagent and photographed with a Nikon Eclipse E400 (Garden City, NY) microscope equipped with a Nikon DXM 1200 digital camera. One eye from each of three different mice was examined from the WT, heterozygous $CLU^{+/-}$ or homozygous $CLU^{-/-}$ genotypes (nine eyes total).

Ocular surface ultrastructure was evaluated by transmission electron microscopy. Briefly, a slit was made at the corneal-scleral margin of the eye, which was then immersed in 2% glutaraldehyde, 2% paraformaldehyde in sodium cacodylate buffer, pH7.4, containing 0.025% (w/v) CaCl2, for 60 min at RT. Anterior segments were separated from the lens and posterior

segments and held in fixative overnight before being post-fixed in 1% osmium tetroxide and embedded in EmBed (EMS) resin. Thin sections (70 nm) were post-stained with uranyl acetate and lead citrate, viewed in a JEOL 1200 electron microscope, and photographed with an AMT XR-41 TEM digital camera. One eye from each of three different mice was examined from the WT or homozygous $CLU^{-/-}$ genotypes (six eyes total). An ocular pathologist (GRK) evaluated the images.

Statistical analyses

Treatment groups (DS+PBS versus DS+CLU or DS+BSA) were compared to controls (non-stressed (NS) versus DS) on the continuous study variables with generalized linear regression models, using an identity link function. In the regression model, a generalized estimating equation approach was used to explicitly incorporate the correlated outcomes between eyes within one animal [47, 48]; an exchangeable correlation structure was used. The independent sample t-test was used to compare cell culture results between groups. Two-sided $P \leq 0.05$ was considered statistically significant. Analyses were performed using the Statistical Analysis Software (SAS, Version 9.4).

Results

Topical CLU protects the ocular surface subjected to desiccating stress

To determine whether supplementation with topical CLU could protect against disruption of the ocular surface barrier subjected to desiccating stress, we applied the 5-day desiccating stress protocol to mice, and also treated topically with recombinant human CLU (rhCLU) formulated in PBS, applied 4 times/day at the same time as scopolamine was administered. After 5 days, barrier integrity was quantified by measuring uptake of fluorescein dye. Results were compared to controls treated with PBS vehicle alone. The stressed but untreated (UT) ocular surface served as the control for PBS treatment and non-stressed (NS) eyes served as the baseline control. Since CLU concentration in human serum was known to be in the range of 100±50 ug/mL [49], we used 10 or 100 ug/mL of rhCLU for our first experiments (Fig 1A). Dye uptake in stressed eyes treated with PBS alone was ~8-fold greater than NS counterparts. In contrast, dye uptake in eyes that were stressed, while also being treated with CLU at 10 or 100 ug/mL, was similar to that of NS counterparts, indicating complete protection against barrier disruption. We performed a second set of experiments using a 7-day desiccating stress protocol and rhCLU concentrations of 1 and 10 ug/mL. Again we observed nearly complete protection against barrier disruption as measured by dye uptake at both concentrations (Fig 1B). We performed a similar experiment using a 5-day desiccating stress protocol, but using human plasma CLU (pCLU) (Fig 1C) or recombinant mouse CLU (rmCLU) (Fig 1D) to rule out the possibility that the results might be unique to rhCLU. Treatment with 2 ug/mL of pCLU or rmCLU consistently protected against barrier disruption as measured by fluorescein uptake, to the same extent as rhCLU at 2 ug/mL, and was comparable to NS controls.

Topical CLU protects the ocular surface in an all-or-none response

To determine a dose-response for barrier protection by CLU, we next applied the 5-day desiccating stress protocol while simultaneously treating the ocular surface with serial 10-fold dilutions of rhCLU. Similar to results of the experiment shown above (Fig 1), treatment with 1 ug/mL or 10 ug/mL almost completely protected against fluorescein uptake. In contrast, lower concentrations had essentially no effect, with values similar to UT and PBS-treated groups (Fig 2A Left). To determine any gradation in activity between 0.1 and 1 ug/mL CLU, we tested CLU

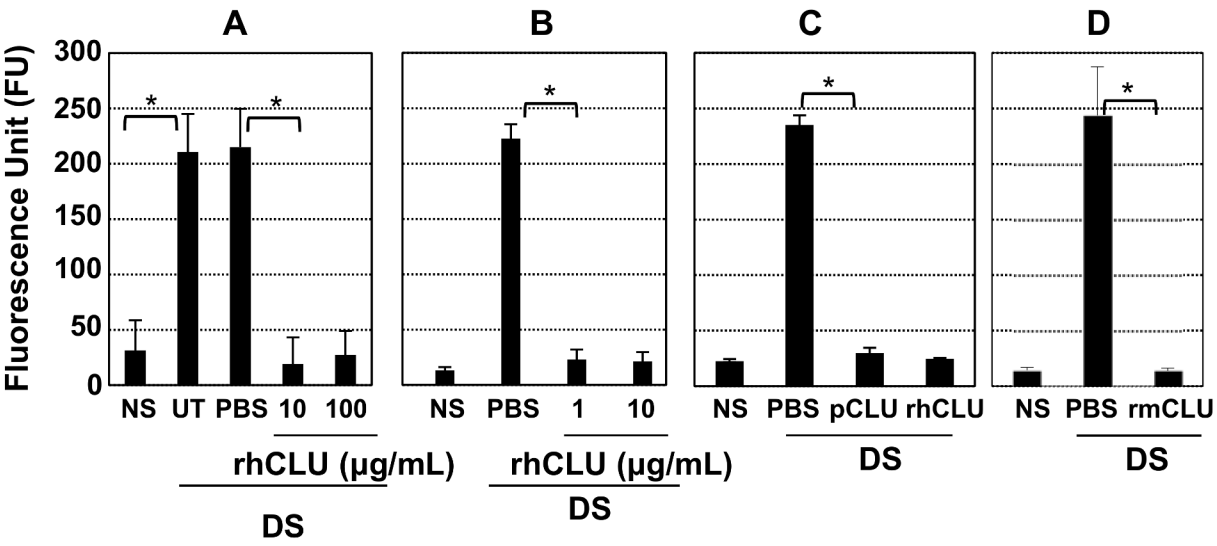

Fig 1. Topical CLU protects the ocular surface barrier against functional disruption by desiccating stress. The standard desiccating stress (DS) protocol was applied, while eyes were left untreated (UT) or treated topically 4 times/day with 1 uL of CLU formulated in PBS, or with PBS control. Non-stressed (NS) mice housed under normal ambient conditions served as a baseline control. After the indicated time period, barrier integrity was assayed by measuring corneal epithelial uptake of fluorescein (FU = Fluorescence Units at 521 nm). Values are expressed as the mean ± SD. **(A)** The desiccating stress (DS) protocol was applied for 5 days while also treating with rhCLU at 10 or 100 ug/mL. *P<0.0001 (n = 9). **(B)** The desiccating stress (DS) protocol was applied for 7 days while also treating with rhCLU at 1 or 10 ug/mL. *P<0.0001 (n = 4). **(C)** The desiccating stress (DS) protocol was applied for 5 days while also treating with human plasma CLU (pCLU) at 2 ug/mL *P<0.0001 (n = 4). (D) The desiccating stress (DS) protocol was applied for 5 days while also treating with recombinant mouse CLU (rmCLU) at 2 ug/mL. *P<0.0001 (n = 4)

doi:10.1371/journal.pone.0138958.g001

concentrations at tight intervals in between these doses (Fig 2A Middle). We observed a transition in effectiveness between 0.6 ug/mL and 1 ug/mL, essentially an all-or-none response. We also tested rmCLU; the dose transition was at exactly the same place, between 0.6 and 1 ug/mL (Fig 2A Right). Next, we tested whether BSA, as an *in vitro* protein stabilizer and as a non-CLU protein also found in serum, could enhance the protective activity of CLU at the low concentration. BSA did not show any significant protective or enhancing effect, alone or with CLU at 0.6 ug/mL, compared with 1 ug/mL of CLU alone (Fig 2B). Use of Alexa-Fluor-dextran in the fluorescein uptake assay, which is more discriminating because of its much larger molecular size [14], gave identical results (data not shown).

To determine whether a dose response effect could be observed at CLU concentrations below the threshold level exhibited by the sharp transition, we changed our experimental conditions. As before, we applied the 5-day desiccating stress protocol while simultaneously treating the ocular surface with rhCLU, but then on day 6 we stopped CLU treatment and discontinued scopolamine injections, but maintained a mild stress by continuing the air draft, elevated temperature and reduced humidity. We then waited an additional two days, following which time we assayed barrier integrity by fluorescein dye uptake (Fig 2C). Disruption of the ocular surface barrier after the 2-day moderate desiccating stress was considerably less than observed when the dye uptake assay was done directly following the 5-day desiccating stress protocol. Interestingly, in this setting, we found that the prior delivery of 0.1 ug/mL CLU, 4 times/day was as effective as 1 ug/mL. Again the result was primarily all-or-none, although we observed a small graded effect between 0.01–0.1 ug/mL, which may reflect the transition between desiccating stress conditions.

These results indicate that topical CLU protects the ocular surface barrier against disruption by desiccating stress in an all-or-none manner at a very precise threshold dose range that is highly reproducible.

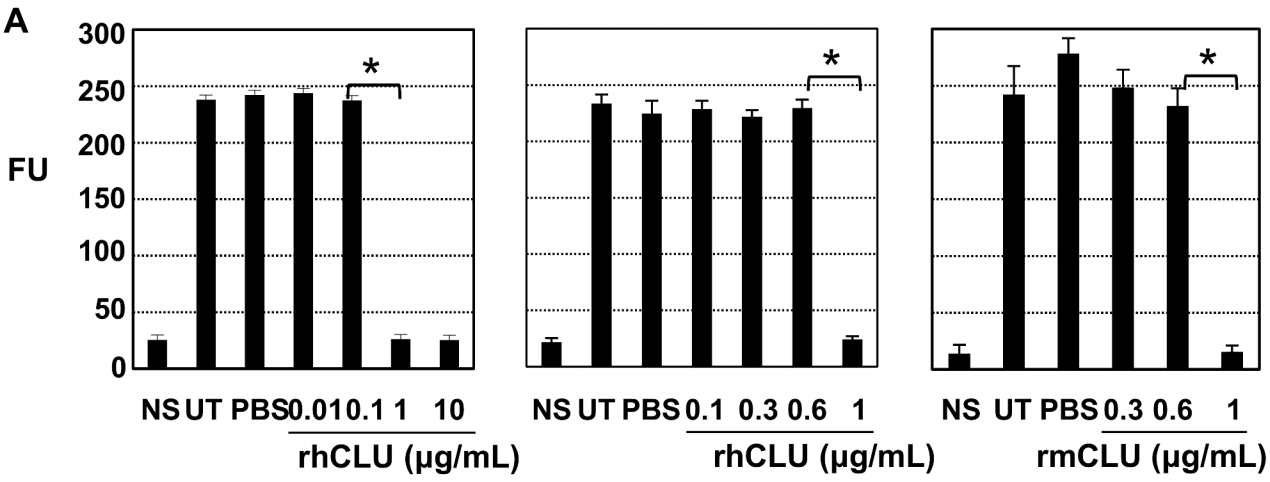

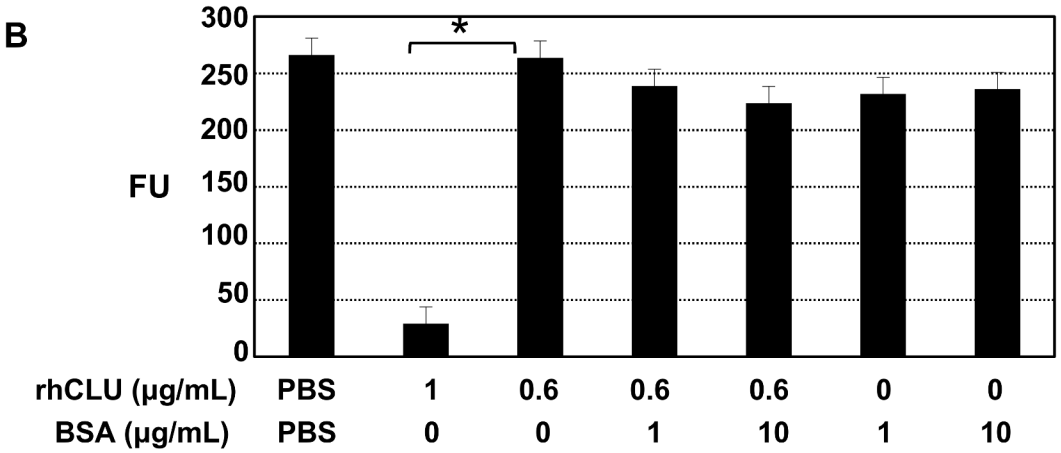

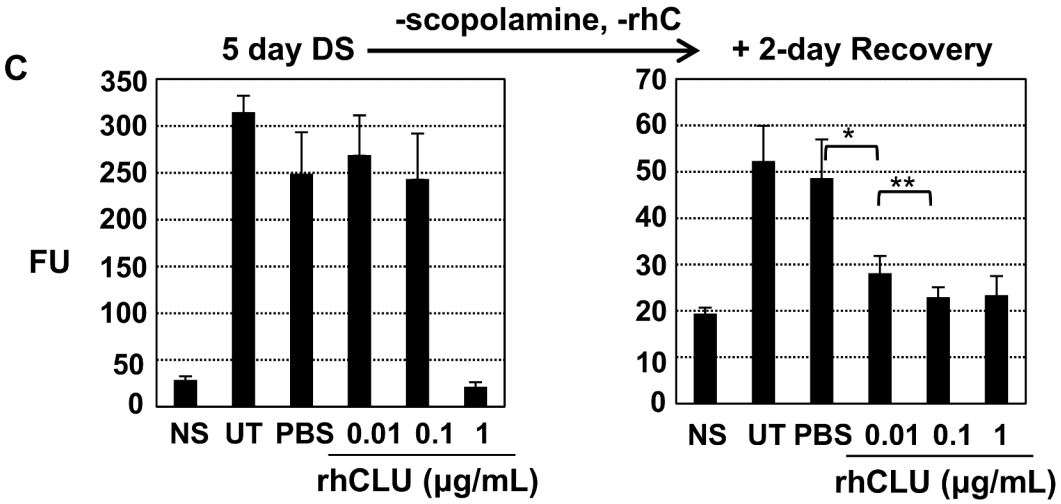

Fig 2. Topical CLU protects the ocular surface barrier via an all-or-none mechanism. The standard desiccating stress (DS) protocol was applied, while eyes were left untreated (UT) or treated topically 4 times/day with 1 uL of CLU formulated in PBS, or with PBS control. Non-stressed (NS) mice housed under

normal ambient conditions served as a baseline control. After the indicated time period, barrier integrity was assayed by measuring corneal epithelial uptake of fluorescein (FU = Fluorescence Units at 521 nm). Values are expressed as the mean ± SD. **(A) Dose response experiment.** The desiccating stress (DS) protocol was applied for 5 days while also treating with **(Left)** recombinant human CLU (rhCLU) at the indicated 10-fold dilutions (n = 6), **(Middle)** recombinant human CLU (rhCLU) at 0.1, 0.3, 0.6, or 1 ug/mL (n = 6), or **(Right)** recombinant mouse CLU (rmCLU) at 0.3, 0.6, and 1 ug/mL (n = 4). *P<0.0001. **(B) Experiment comparing CLU with BSA.** The desiccating stress (DS) protocol was applied for 5 days while also treating with recombinant human CLU (rhCLU) and BSA, individually or in combination, as indicated. *P<0.0001 (n = 4)**. (C) Stress reduction experiment.** The standard desiccating stress (DS) protocol was applied for 5 days while eyes were also treated with recombinant human CLU (rhCLU) at 0.01, 0.1, and 1 ug/mL. Using a subset (n = 4) of each treatment group the effect of each rhCLU dose on integrity of the ocular surface barrier was confirmed by the fluorescein uptake test at day 5. Then the rest of the mice in each treatment group were subjected for two more days to a more moderate desiccating stress by continuing with the air draft and heat, but omitting scopolamine and CLU treatments. The fluorescein uptake test was then performed on these remaining mice. *P = 0.004 (n = 4); **P = 0.05 (n = 4)

doi:10.1371/journal.pone.0138958.g002

Topical CLU ameliorates pre-existing ocular surface barrier disruption due to desiccating stress

Having clearly demonstrated the preventive effect of CLU in protecting the ocular surface against desiccating stress, we next assessed the potential of CLU to ameliorate pre-existing ocular surface disruption. Representative results are shown in Fig 3. In this experiment, we applied the 5-day desiccating stress protocol, and then treated topically with rhCLU at 2 ug/mL (4 times/day) for another 5 days while maintaining the same desiccating stress protocol. Following this, barrier integrity was assayed. The PBS control showed a high level of dye uptake, ~12X greater than NS controls, but the barrier was essentially intact in CLU treated mice, similar to NS controls.

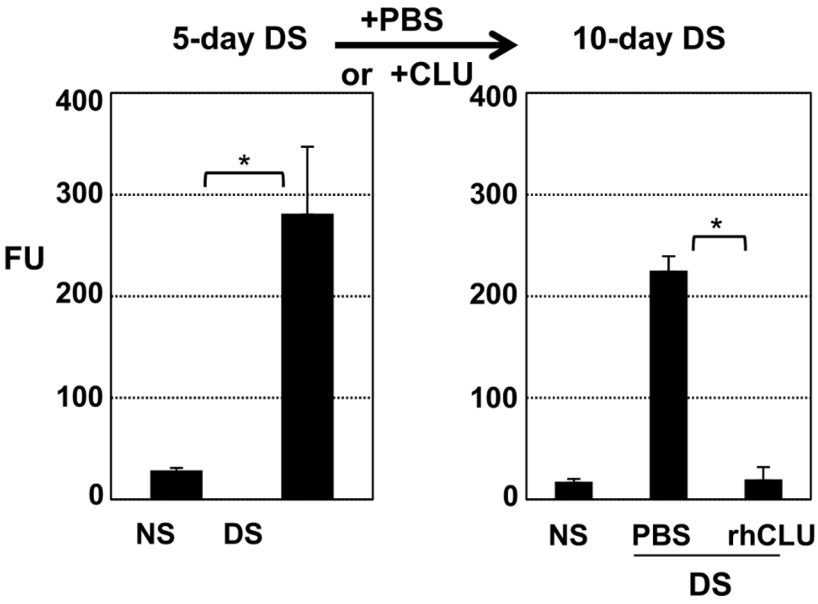

Fig 3. Topical CLU ameliorates pre-existing ocular surface barrier disruption caused by desiccating stress. (Left). The standard desiccating stress (DS) protocol was applied for 5-days to create ocular surface disruption. Non-stressed (NS) mice housed under normal ambient conditions served as a baseline control. **(Left)** After the indicated time period, barrier disruption was confirmed by measuring corneal epithelial uptake of fluorescein (FU = Fluorescence Units at 521 nm) in a subset of mice. Values are expressed as the mean ± SD. *p<0.0001 (n = 4). **(Right)** The same desiccating stress (DS) protocol was continued for another 5 days while eyes with desiccating stress were treated topically with 1 uL of recombinant human CLU (rhCLU) formulated in PBS at 2 ug/mL, or with PBS control, 4 times/day. The fluorescein uptake test was then performed on these remaining mice. Values are expressed as the mean ± SD. *p<0.0001(n = 4).

doi:10.1371/journal.pone.0138958.g003

Topical CLU directly seals the ocular surface barrier against disruption due to desiccating stress

The amelioration results outlined above (Fig 3) suggested that one of the mechanisms of CLU action might be simply to seal areas of barrier damage so that dye can no longer penetrate. To test this idea, we applied the 5-day desiccating stress protocol, and then treated with CLU, but this time assayed for dye uptake within 15 minutes of treatment, giving the ocular surface no time to recover from the more severe stress (Fig 4A). An all-or-none response was observed once again, but the transition point was higher than when CLU was applied 4 times/day. Thus CLU at 6 ug/mL, applied one time, was completely effective in preventing dye uptake, while 3 ug/mL was completely ineffective. Laser scanning confocal microscopy was used to visualize punctate staining and its amelioration (Fig 4B). Eyes of mice subjected to desiccating stress and

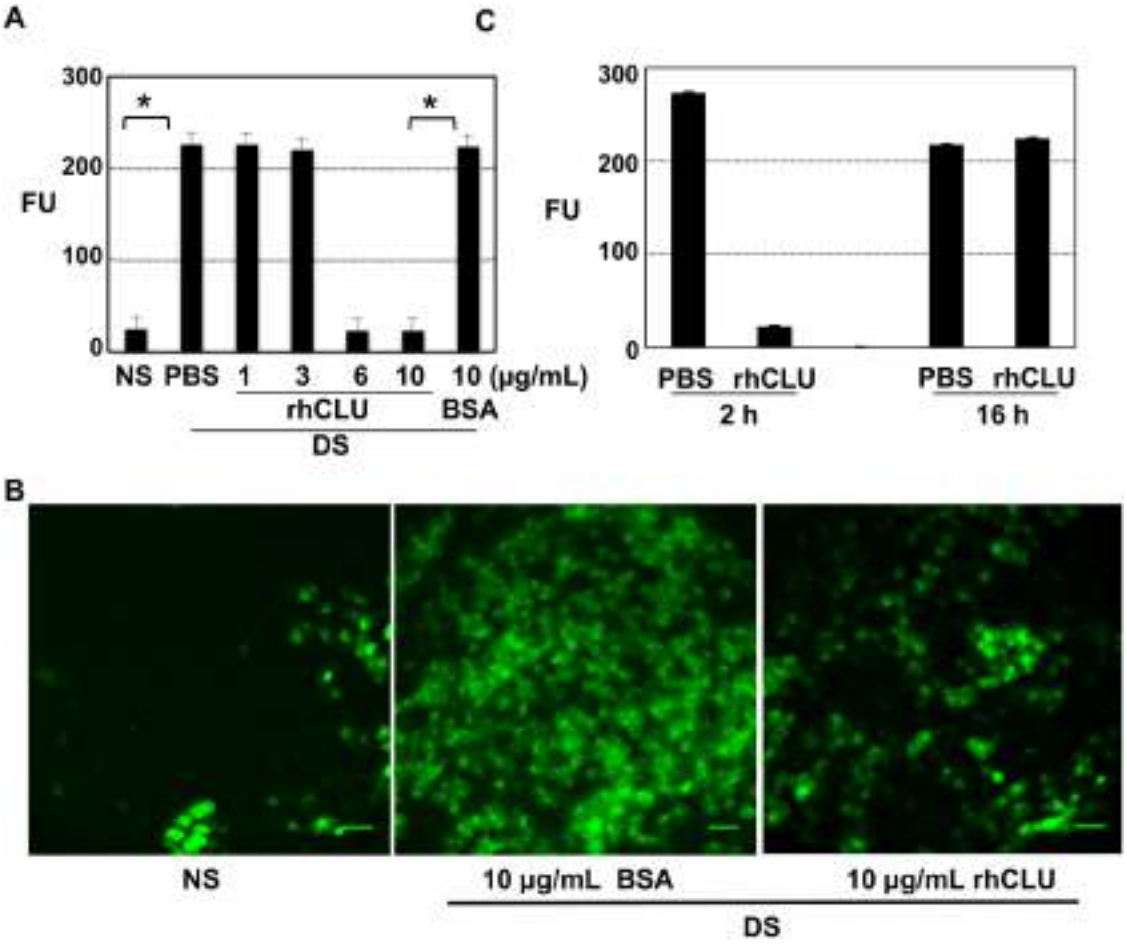

Fig 4. Topical CLU directly seals the ocular surface barrier disrupted by desiccating stress. The standard desiccating stress (DS) protocol was applied for 5-days to create ocular surface disruption. Non-stressed (NS) mice housed under normal ambient conditions served as a baseline control. Eyes with desiccating stress were then treated topically, a single time, with 1 uL of CLU formulated in PBS, 1 uL of BSA formulated in PBS for comparison, or 1 uL of PBS control. Barrier disruption was assayed by measuring corneal epithelial uptake of fluorescein (FU = Fluorescence Units at 521 nm). Values are expressed as the mean ± SD. **(A)** Eyes were treated a single time with recombinant human CLU (rhCLU) at 1, 3, 6 or 10 ug/mL, BSA at 10 ug/mL, or PBS. Fifteen minutes later, the fluorescein uptake test was performed, before there was time for barrier repair to occur. *P<0.0001 (n = 4). **(B)** Images of central cornea from the experiment shown in (A), obtained using laser scanning confocal microscopy at 10X magnification. One representative image out of two independent experiments is shown. Scale bar = 100 um. **(C)** Eyes were treated a single time with recombinant human CLU (rhCLU) at 10 ug/mL (right eyes) or PBS (left eyes). Then the mice were kept further for 2 h or 16 h while continuing with the same desiccating stress protocol. The fluorescein uptake test was performed following the indicated time period to assess the time length of CLU treatment effect. *p<0.0001 (n = 4)

doi:10.1371/journal.pone.0138958.g004

treated with BSA control showed many punctate spots of the size and shape of cells, similar to UT eyes, while desiccating stress eyes treated with CLU at 10 ug/mL showed far fewer spots, similar to the non-stressed control. In a second set of experiments we sought to determine how long the sealing effect would last. In a time course experiment, the sealing effect was maintained for 2 hours, but was lost by 16 hours (Fig 4C).

Topical CLU binds selectively to the ocular surface subjected to desiccating stress, and to LGALS3 *in vitro*

To visualize CLU binding to the ocular surface, we used the technique of direct immunostaining with an antibody conjugated to CF-594 dye. To differentiate topically applied rhCLU from endogenous CLU, we took advantage of the C-terminal His tag incorporated into the rhCLU molecule. Representative results are shown in Fig 5A. Eyes subjected to desiccating stress, then treated with CF-594 dye conjugated anti-His antibody alone, showed some diffuse fluorescence over the ocular surface subjected to desiccating stress. However, when the ocular surface of these mice was treated with rhCLU, substantial punctate binding of dye-conjugated antibody to the ocular surface subjected to desiccating stress was observed, indicating the location of direct CLU binding. In contrast, the NS eye showed far less binding. In a second set of experiments, the fluorescent lipophilic membrane tracer DiO was used to delineate individual cells. Representative results are shown in Fig 5B. This showed that the CLU "spots" were approximately the size of cells. In some cases, the CLU spots (red) filled the entire area of individual cells marked by the dyed membrane (green), overlapping completely (yellow color). In other cases, CLU spots were clearly separate.

Next we considered what kinds of ocular surface molecules might bind CLU. LGALS3, a key component of the ocular surface barrier, is a member of the galectin class of beta-galactoside-binding proteins. What is known about the glycosyl moiety of CLU is consistent with LGALS3 binding [25, 27]. CLU applied to an LGALS3-sepharose affinity column bound to the beads and was not eluted 0.1 M sucrose, a disaccharide that does not compete with LGALS3 sugar binding, but was mostly eluted with a competitive inhibitor of LGALS3 sugar binding, 0.1 M beta-lactose (Fig 5C). This suggests that CLU binding to LGALS3 is specific for the beta-galactoside-binding function.

Topical CLU is cytoprotective and proteostatic

Having demonstrated the capacity of CLU to protect the ocular surface barrier against functional disruption due to desiccating stress, we next tested its capacity to protect the cells and proteins of the barrier against physical damage. First we investigated the cytoprotective activity of topical CLU. Representative results are shown in Fig 6A. Only a few cells at the ocular surface of non-stressed (NS) eyes were positively stained in the TUNEL assay, a measure of DNA damage characteristic of apoptotic cells. In the PBS-treated DS eye, staining of epithelial cells and stroma cells was strikingly increased, consistent with previous observations [11–13, 50]. However, when the ocular surface was treated topically with CLU at the same time as it was subjected to desiccating stress, the level of TUNEL staining remained the same as in non-stressed eyes.

We next investigated protection of ocular surface barrier proteins against desiccating stress. Representative results are shown in Fig 6B. Corneal epithelial lysates were isolated from the eyes of mice maintained under ambient conditions (NS), mice subjected to desiccating stress but otherwise untreated (UT), and mice subjected to desiccating stress while also being treated with rhCLU or the PBS control. We found an increase in a truncated form of LGALS3 after desiccating stress, which suggested proteolysis. Importantly, LGALS3 was protected from

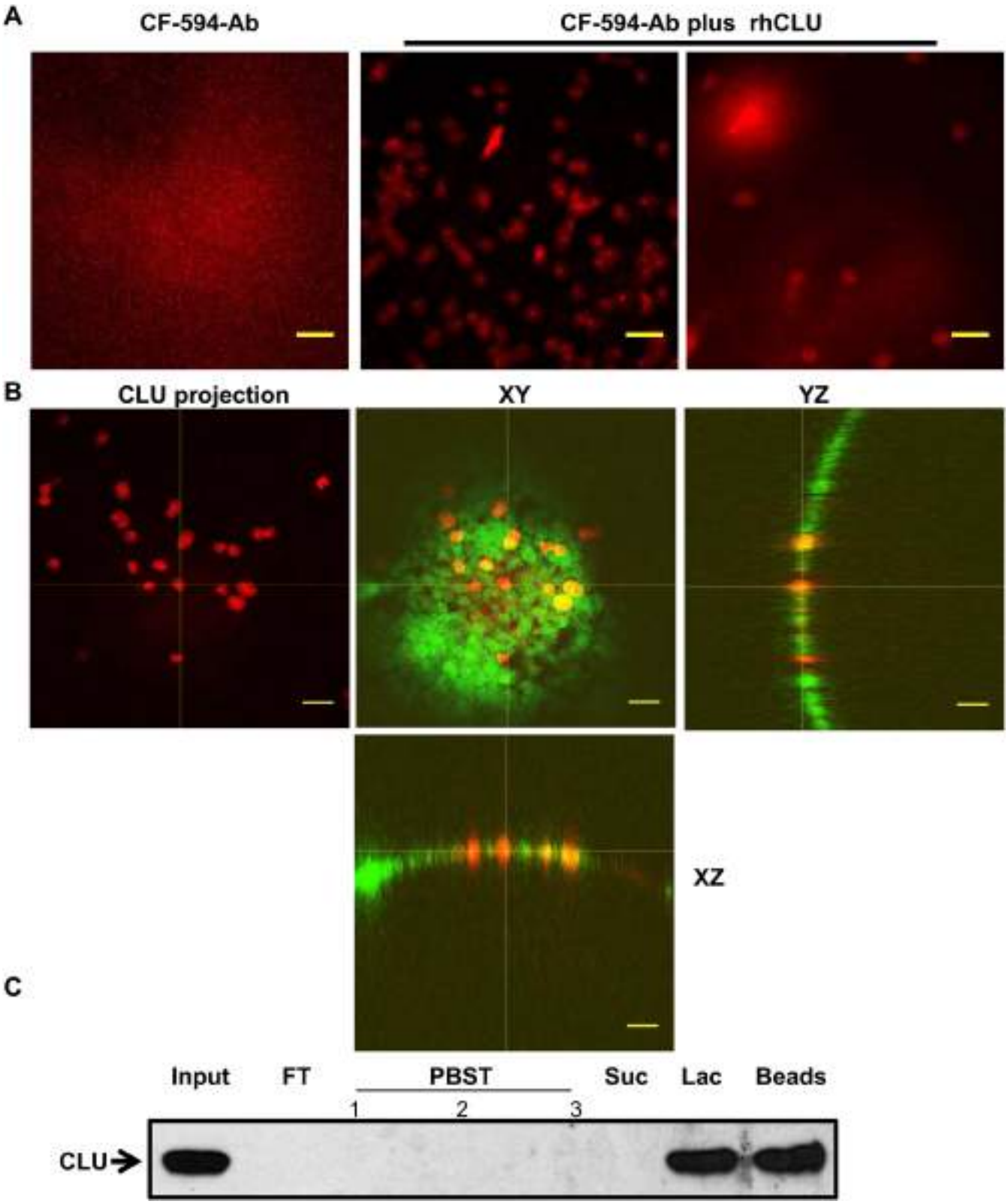

Fig 5. Topical CLU binds selectively to the ocular surface subjected to desiccating stress, and to LGALS3 *in vitro*. (A) The standard desiccating stress (DS) protocol was applied for 5-days to create ocular surface disruption. Non-stressed (NS) mice housed under normal ambient conditions were included for comparison. Eyes were treated with CF-594-anti-His antibody that binds to the His tag of recombinant human CLU (rhCLU), or with a complex of

the antibody-rhCLU for 15 min, followed by confocal imaging of central cornea. Images were taken at 10X magnification. Scale bar = 100 um. **(B)** A DS eye was treated with a complex of the antibody-rhCLU (red) as in (A), as well as a fluorescent membrane tracer DiO (green). Images were taken at 20X magnification. In the left panel only CLU was projected. The right three panels show one Z-section plane with cross-sections oriented to the XY, YZ, and XZ axes, generated using Image J software. Yellow indicates regions of co-localization of the red and green signal. Scale bar = 100 um. **(C)** LGALS3-Sepharose affinity column chromatography. 1.5 ug rhCLU was applied to a 300 uL LGALS3 affinity column equilibrated in PBS containing 0.1% Triton X-100 (PBST) and the column was washed with PBST. To test sugar-binding specificity, the column was then treated sequentially with a non-competing disaccharide, sucrose (0.1 M), and then a competing disaccharide, 0.1 M lactose, dissolved in PBST. Western blotting was used to quantify CLU in the resulting fractions. Loading of the "Lac" lane represents a 1:10 dilution of the input and the "Beads" lane is a 1:4 dilution of the input, thus ~2.5X more CLU was Lac-eluted than retained on the beads. FT = flow-through; Suc = sucrose; Lac = lactose

doi:10.1371/journal.pone.0138958.g005

truncation in the corneal epithelium of mice treated with topical CLU in PBS, but not in mice treated with PBS alone. Similarly, the amount of the tight junction protein OCLN was reduced in the corneal epithelium of eyes subjected to desiccating stress, but was restored in mice treated with topical CLU in PBS, but not when treated with PBS alone. It should be noted that the area of ocular surface barrier damage is expected to be only a small percentage of the total based on the pattern of punctate fluorescein staining. These findings provide evidence that CLU protects the protein structure of both the transcellular and paracellular barriers at the mouse ocular surface subjected to desiccating stress.

We also examined the effect of CLU on MMP9 expression using a corneal cell culture model, as shown in Fig 6C. Treatment of cells with rhCLU significantly reduced (by ~50%) the stimulatory effects of TNFA on MMP9 expression, but BSA had no effect. These results provide a second possible mechanism for ocular surface barrier protection against proteolysis.

Causal association between CLU concentration in tears and ocular surface barrier vulnerability

The concentration of endogenous CLU in mouse tears was measured using an ELISA. Representative results are shown in Fig 7A. In this experiment, the mean CLU concentration in tears from mice kept at ambient conditions was 5.2±0.4 ug/mL. This was reduced to 3.7±0.3 ug/mL in tears from mice subjected to the 5-day desiccating stress protocol, an ~30% reduction, similar to what was previously observed in the ocular surface epithelium using this mouse model [23].

CLU knockout mice could be useful for examining the causal relationship between endogenous CLU concentration in tears and ocular surface barrier vulnerability to desiccating stress if the ocular surface is normal under ambient conditions. On gross inspection, eyes of both heterozygous $CLU^{+/-}$ and homozygous $CLU^{-/-}$ knockout mice on the C57BL/6J background appeared anatomically normal. We examined the ocular surface of both of these knockout genotypes more closely using a hand-held 20-diopter indirect lens, and compared to wild type C57BL6/J mice. In all three genotypes, the tear film appeared of similar thickness and the ocular surface appeared smooth and unaffected, with no inflammatory infiltrates apparent. Histological analysis of cross-sections, revealed no differences among genotypes, and periodic acid-Schiff histochemistry revealed similar goblet cell numbers in all genotypes (data not shown).

Ocular surface epithelia examined by transmission electron microscopy revealed no differences between wild type C57Bl/6J and homozygous $CLU^{-/-}$ knockout mice. Representative images are shown in Fig 7B. There was no evidence of squamous metaplasia in the corneal or conjunctival epithelia. Microplicae at the apical cell surface appeared similar in contour and density. Junctional complexes between cells were of similar appearance and numbers. Thus the ocular surface of homozygous $CLU^{-/-}$ knockout mice maintained under ambient conditions appears to be entirely normal, i.e., the same as wild type counterparts.

Next we compared tear CLU concentration in WT and heterozygous $CLU^{+/-}$ mice maintained at ambient conditions. Representative results are shown in Fig 7C. The mean tear CLU

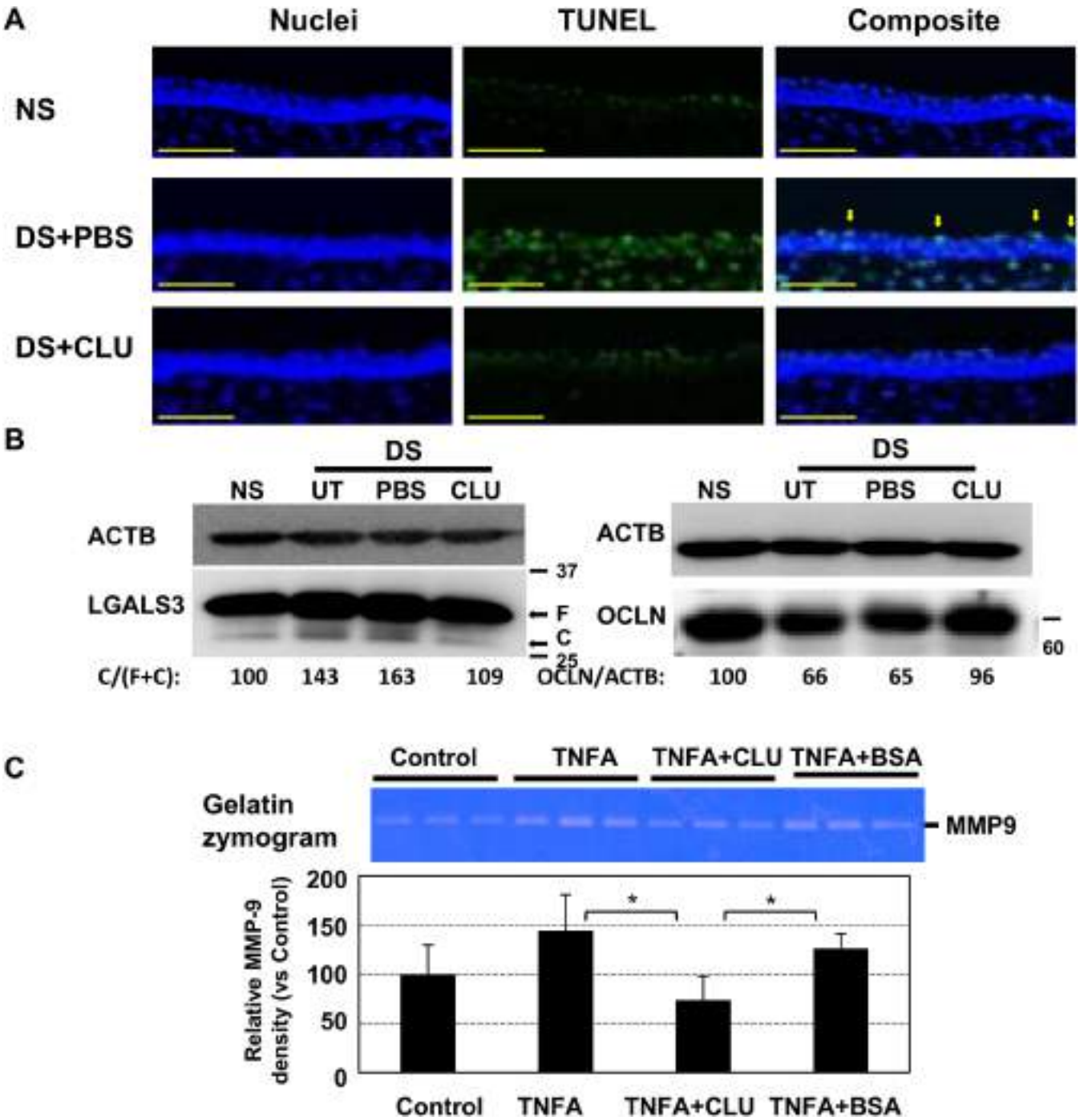

Fig 6. Topical CLU protects the ocular surface barrier against proteolytic damage due to desiccating stress. (A) The standard desiccating stress (DS) protocol was applied, while eyes were left untreated (UT) or treated topically, 4 times/day, with 1 uL of recombinant human CLU (rhCLU) formulated in PBS, or with 1 uL of PBS control. Non-stressed (NS) mice housed under normal ambient conditions were included as a control for PBS treatment. At the end of the experiment, eyes were removed and embedded for frozen sectioning at 10-um thickness. TUNEL staining was performed and nuclei were counterstained with DAPI. Images were taken at 20X magnification. Arrows indicate apoptotic cells in the apical ocular surface epithelium of DS+PBS eyes. **(B)** The standard desiccating stress (DS) protocol was applied, while eyes were left untreated (UT) or treated topically, 4 times/day, with 1 uL of recombinant human CLU (rhCLU) formulated in PBS, or with 1 uL of PBS control. Non-stressed (NS) mice housed under normal ambient conditions were included as a control for PBS treatment. Desiccating stress was applied to 7 mice per treatment group for 5 days (OCLN) or 9 days (LGALS3) while treated with PBS or CLU at 1 ug/mL. Then total proteins were extracted from the ocular surface epithelia using TRIzol, pooled among the same treatment groups, and subjected to Western blotting with anti-LGALS3 and anti-OCLN antibodies. The protein band image was obtained by Fuji Doc digital camera. "F" indicates full length LGALS3 protein, and "C" is the cleaved product of LGALS3. A digital image analyzer built into the camera was used to quantify the density of individual

protein bands. The relative cleavage of LGALS3 was calculated by ratio of the C over the total (F+C) LGALS3 protein. The relative amount of OCLN was normalized to the loading control (ACTB) in each gel lane. **(C)** Stratified HCLE cells were treated with TNFA (5 ng/mL), alone or with recombinant human CLU (rhCLU) (4 ug/mL) or BSA (40 ug/mL) for 24 h. the conditioned media were subject to gelatin zymography and the developed MMP9 image were analyzed by Image J software. *P<0.05 (n = 3, student's t-test)

doi:10.1371/journal.pone.0138958.g006

concentration in this group of WT mice was 5.5±1.2 ug/mL, while the mean concentration in heterozygous $CLU^{+/-}$ mice was 2.2±0.6 ug/mL. This is an ~50% difference and indicates that the CLU concentration in tears is roughly proportional to the number of gene copies. Significantly, the reduced level of CLU in tears of heterozygous $CLU^{+/-}$ KO mice was less than the level of CLU in tears of WT eyes subjected to desiccating stress. Thus the heterozygous $CLU^{+/-}$ KO genotype can be used to determine whether reduced CLU levels in tears alone results in vulnerability to desiccating stress.

Finally, barrier sensitivity was evaluated in WT and heterozygous $CLU^{+/-}$ KO mice. To facilitate the detection of differences, the mild desiccating stress protocol was used. Thus mice were exposed to air draft at elevated temperature and reduced humidity, but scopolamine injections were omitted (as in Fig 2C). This protocol was continued for 4-weeks, after which time, ocular surface barrier integrity was assayed. Representative results are shown in Fig 7D. Fluorescein uptake in WT eyes was only about 3X higher than NS controls. In contrast, fluorescein uptake in heterozygous $CLU^{+/-}$ KO mice was approximately 10X higher than NS controls. These results demonstrate that reduced CLU in the tears correlates with increased vulnerability of the ocular surface barrier to desiccating stress.

Discussion

CLU is a homeostatic protein, prominently expressed at fluid-tissue interfaces throughout the body including the ocular surface. Here we report that CLU prevents and ameliorates ocular surface barrier disruption due to desiccating stress by a remarkable sealing mechanism dependent on attainment of a critical concentration in the tears. When tear CLU drops below the critical threshold, the ocular surface barrier becomes vulnerable to disruption. Sealing by CLU involves selective binding to the stressed ocular surface. Positioned in this way, CLU not only physically seals the ocular surface barrier, but it also protects the barrier cells and prevents further damage to barrier structure. These findings provide an answer to the long mystery of CLU's physiological role at the ocular surface and also identify a fundamentally new mechanism for ocular surface protection.

Ocular surface sealing

Since the ocular surface barrier of the homozygous $CLU^{-/-}$ KO mouse is intact under ambient conditions, it seems unlikely that CLU is a structural component of the normal barrier, but rather that it serves a protective and surveillance role. This fits with previous reports that CLU knockout mice display a phenotype only when systems are perturbed by application of inflammatory disease models [30, 33, 34]. The selectivity of topical CLU binding for the ocular surface subjected to desiccating stress suggests that CLU seals by binding to areas of barrier disruption. This remains conjectural at this point, as we have not directly demonstrated co-localization with spots of fluorescein uptake, however the punctate character observed for binding of topical CLU at both the normal ocular surface and the ocular surface subjected to desiccating stress is consistent with this idea. Thus we propose that CLU might also act as a "spot weld" at the ocular surface, sealing damage to the barriers where needed.

A previous study suggested that CLU interacts with a lectin-type receptor on liver cells [51] and here we demonstrate CLU interaction with the galectin LGALS3. Galectins are a family of

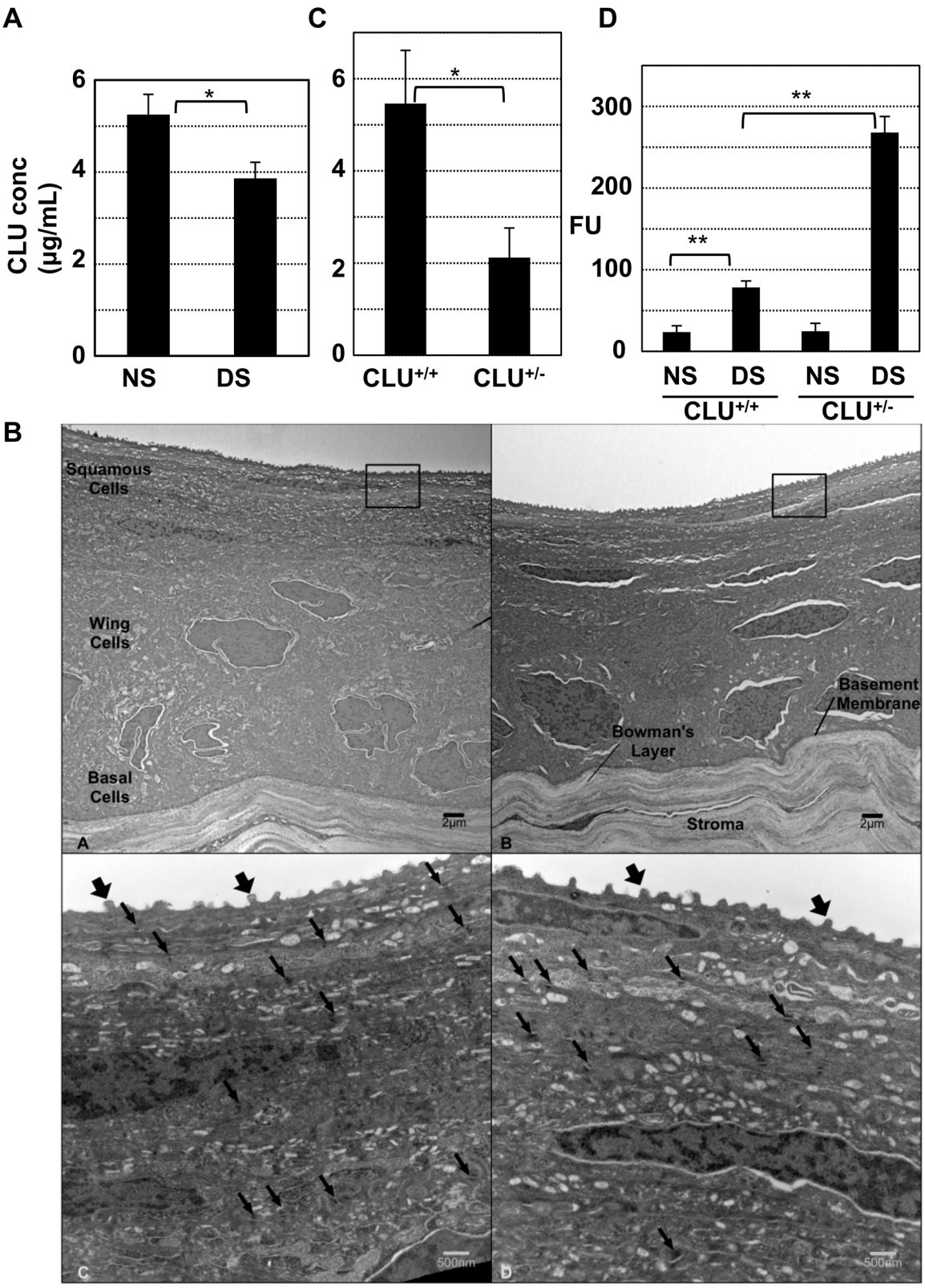

Fig 7. Causal association between endogenous CLU concentration in tears and ocular surface barrier vulnerability. (A) Tears were collected from mice housed under normal ambient conditions or after application of the standard desiccating stress (DS) protocol for 5-days, and ELISA was used to measure CLU concentration (*P = $5x10^{-8}$ n = 6, student's t-test). **(B)** Representative transmission electron microscopy comparing images of anterior cornea

from wild type C57BL6/J mice (A and C) and mice with homozygous $CLU^{-/-}$ knockout on the C57BL6/J background (B and D). In low power (4000x) magnifications (A and B), five layers of epithelial cells divided into squamous, wing, and basal cell regions are visualized along with an intact basement membrane and Bowman's layer in both types of animals. Higher power images (C and D, 20,000x) of similar regions to those boxed in panels A and B show numerous surface microplicae (fat arrows) in both genotypes. Desmosomes (thin arrows) are similar in both frequency and structure. Higher power images (not shown) demonstrate intact adherens junctions in both genotypes. **(C)** Tears from wild type or heterozygous $CLU^{+/-}$ knockout mice kept at ambient conditions were collected and ELISA was used to measure CLU concentration ($p = 2.1x10^{-5}$; n = 7, student's t-test). **(D)** Wild type mice or heterozygous $CLU^{+/-}$ knockout mice were subjected to the standard desiccating stress protocol, but without scopolamine injection for four weeks and then ocular surface barrier integrity was measured by fluorescein uptake (**p<0.0001, n = 4).

doi:10.1371/journal.pone.0138958.g007

lectin proteins defined by binding specificity for beta-galactoside containing glycans. The main family member at the human ocular surface is LGALS3 (galectin-3) [3, 52, 53]. All galectins have a C-terminal carbohydrate recognition domain, but LGALS3 is unique in also possessing an N-terminal extension with a repeating motif which enables multimer formation [54]. This gives it the capacity to form networks that bridge membrane-associated mucin ectodomains, to organize the ocular surface barrier. MMPs (and likely other proteinases) specifically cleave the multimerization domain from the body of LGALS3, reducing self-association [55–57]. LGALS3 cleavage products are found at the ocular surface and in tears of dry eye patients [58], and we provide evidence here that LGALS3 is cleaved at the mouse ocular surface subjected to desiccating stress. This suggests the possibility that LGALS3 cleavage frees it for interaction with CLU.

CLU sealing may also occur via direct interaction with the plasma membrane of damaged cells. CLU and related apolipoproteins can insert directly into the plasma membrane of cells in the wall of blood vessels [59–61]. This function appears to be due to the special structural features of CLU, in particular the helical amphipathic domains, which confer the properties of a proteinaceous detergent [26]. N-glycosylation sites are located around the disulfide bonds of CLU and may form a scaffold region in clusterin with negatively charged carbohydrates localized to this scaffold. The arms containing the amphipathic helices may extend outward from the scaffold. In this model, CLU resembles a lipid, with the charged head-group being the carbohydrate-covered scaffold of CLU and the hydrophobic tail being the arms. Sealing by CLU may thus be related to the phenomenon of lipid surfactant-mediated "sealing" of plasma membranes damaged by electroporation or other insults, which prevents leakage of fluorescein from preloaded cells [62, 63]. Importantly, insertion of CLU into the vascular wall [59–61] and surfactant-mediated sealing [62, 63] are both cytoprotective. Recently, CLU association with intracellular membranes was also shown to be cytoprotective [64, 65]. The mechanisms of sealing against fluorescein uptake will be very important to define.

Critical all-or-none threshold

The observation of a critical threshold for all-or-none sealing by topical and endogenous CLU is also quite novel and intriguing. Previous mass spectrometric analyses have indicated that CLU protein is present in human tears [39–41], however the concentration has never been measured in humans or any other species. Here we determine that the concentration of CLU in the tears of mice maintained under ambient conditions is between 5–6 ug/mL. CLU concentration was reduced by ~ 30% (from 5.2 ug/mL to 3.6 ug/mL) in the tears of mice subjected to the 5-day desiccating stress protocol, similar to the percent reduction previously reported in the ocular surface epithelia in this mouse model [23]. Heterozygous $CLU^{+/-}$ KO mice were found to have about half the tear CLU concentration of wild type mice, as would be predicted by the genetic deficiency. This reduction in concentration (to 2.5 ug/mL) results in increased vulnerability to desiccating stress. Adding CLU by topical application corrects this, resealing the barrier.

Our results suggest that the normal concentration of endogenous CLU in tears is above the critical threshold, thus ensuring that the ocular surface barrier remains sealed when subjected to stress. Desiccating stress reduces tear CLU below the threshold, thus making the ocular surface barrier vulnerable to disruption. This means the critical threshold must be somewhere between 5–6 ug/mL and 3.6 ug/mL. Perhaps significantly, this fits within the range of the all-or-none threshold for sealing by a single topical application of CLU (3–6 ug/mL). We envision that topical CLU applied as a 1 uL drop, which is ~30-fold larger than the tear volume [46], would dilute the CLU already present in the tears. Thus, tear CLU contribution to total CLU would seem to be negligible, and the topical threshold for sealing constant, regardless of tear concentration. Enigmatically, a much lower critical threshold is observed when CLU is applied multiple times a day. Perhaps this means we are, in fact, supplementing tear CLU with topical CLU. On the other hand, the mechanism could be much more complex. For example, as noted in the Introduction, CLU has anti-inflammatory properties and thus topical CLU treatment might stimulate a recovery of CLU tear levels over time.

All-or-none responses are seen in many biological processes [66–68] and often involve the assembly of multimeric complexes at a critical concentration [69]. CLU can exist in monomeric or multimeric forms [70, 71] and is found in large complexes in numerous diseases [72–74]. Thus one possible mechanism for the critical threshold effect is that CLU must co-assemble with LGALS3 (and possibly other molecules) into a multimeric complex before it can seal the barrier. Cleavage of LGALS3 alters the carbohydrate binding domain of LGALS3 so that it binds more tightly to glycoconjugates [57], and we show here that LGALS3 binds in a lactose dependent manner to CLU. Significantly, surfactant-mediated sealing of cells occurs only when the surfactant molecules reach a critical concentration in solution, enabling micelle formation. Further studies will be needed to define these important mechanisms.

Cytoprotection and proteostasis

This is the first time CLU has been demonstrated to be anti-apoptotic at the ocular surface subjected to desiccating stress, however this CLU activity has been well studied in connection with resistance to chemotherapeutics in cancer [28, 29]. Endogenously secreted CLU is re-internalized within the cell by binding to cell surface receptors of the low-density lipoprotein family such as LRP2 (megalin) [75], LPR8, or VLDLR [76], followed by endocytosis. Binding of CLU to LRP2 induces activation of AKT, which phosphorylates Bad [76]. In addition, internalized CLU binds Ku70/Bax complexes, preventing Bax activation [77], and also stabilizes NF-kappaB and IkappaBalpha [78]. Through each of these pathways, internalized CLU increases cell survival and in this way, topical CLU could prevent cells at the ocular surface from entering the apoptotic pathway when subjected to desiccating stress. We must also consider the possibility that CLU's cytoprotective effect is indirect, a result of its well-known anti-inflammatory activity [30].

An additional and novel means for protecting against apoptosis is suggested by our findings on ocular surface sealing by CLU. As mentioned in the Introduction, mechanisms whereby cells at the ocular surface take up water-soluble dyes are poorly understood. A recent study showed that fluorescein uptake occurs selectively in cultured corneal epithelial cells undergoing apoptosis in response to stress (as opposed to dead cells), suggesting an active transport process [79]. A caveat is that the cultures used in this study were non-confluent, meaning that the tight junction-regulated paracellular barrier would not be fully formed. In addition, the cultures were not stratified, meaning that they would not have expressed cell-associated mucins needed to form the transcellular barrier [23]. Nevertheless, the results suggest the intriguing idea that the immediate sealing of the ocular surface upon topical application of CLU, and the capacity

of topical CLU to protect cells from undergoing apoptosis, could be causally linked. Additional studies will be needed to investigate this potentially very important relationship.

Bound at the ocular surface via LGALS3 or other molecules, CLU would be aptly positioned, not only to seal the ocular surface barrier, but also to prevent its further structural damage. The proteostatic effects of CLU as an extracellular molecule chaperone have been well documented [31, 32]. More recently, we showed that CLU is also a potent inhibitor of MMP9 and other MMPs and protects the paracellular barrier against proteolysis by MMP9 *in vitro*. In this study, we provide the first evidence that CLU maintains proteostasis at both the transcellular and the paracellular barriers at the ocular surface subjected to desiccating stress *in vivo*. In addition, using a corneal epithelial cell culture model, we show that CLU reduces MMP9 expression stimulated by the inflammatory cytokine TNFA, providing a second way that CLU might be proteostatic. It should be noted that there are two previously published articles presenting data that CLU stimulates MMP9 expression in cell culture models: leukocytes [80] and tumor cells [81]. We do not consider these results to be conflicting with our own, as CLU activities are often seen to be enigmatic, and may be context-dependent [24]. It is well known that MMP expression can be induced by providing aggregated molecules to stimulate phagocytosis [82], thus the aggregation or multimerization status of CLU may make a difference in its effects on MMP expression.

Potential of CLU as a novel biotherapeutic for dry eye

Our results demonstrate that topical CLU is remarkably protective of the ocular surface in mice, and can completely reverse the primary sign of dry eye, fluorescein staining. The bioavailability of drugs topically applied to the ocular surface is on the order of 5% or less, due to tear washout effects and the permeability barrier [83, 84], however we show that CLU binds to the ocular surface and remains effective for many hours. These findings, combined with the observed cytoprotective and proteostatic effects of CLU, and considered in context of CLU's well-characterized anti-inflammatory properties, present a compelling case for developing CLU as a biological therapeutic for dry eye. As a natural homeostatic protein, CLU would be safe and well tolerated, making it an ideal drug. While non-eukaryotic expression systems have been problematic, hrCLU expressed in mammalian cells is full glycosylated, proteolytically processed, and fully functional as a molecular chaperone [85]. Here we show the hrCLU expressed in mammalian cells is functionally indistinguishable from CLU purified from human plasma in protection and sealing of the ocular surface against desiccating stress.

Cyclosporine A (Restasis®, Allergan) is currently the only FDA approved medication for dry eye [86]. The current standard for FDA approval is two studies showing a statistically significant superiority of the drug to its vehicle in relieving both a sign, e.g. fluorescein uptake, and a symptom, e.g., irritation, dryness, gritty feeling and burning [87, 88]. Consistent amelioration of fluorescein uptake has been a difficult criterion for investigational drugs to meet [86–88]. If the all-or-none effect of CLU treatment in mice holds in humans, the "all" part would be an important advantage. Studies in humans are needed to learn whether CLU will also improve symptoms.

Acknowledgments

The authors thank Ilene Gipson, Ph.D. (Harvard Medical School), Winston Kao, Ph.D. (University of Cincinnati College of Medicine), and Joseph Barr, O.D. (Ohio State University College of Optometry) for helpful discussions, and Drs. Tatsuo Itakura and Nitin Patel (University of Southern California) for helpful discussions and critical reading of the manuscript. Dr. Gipson is also gratefully acknowledged for providing the HCLE cell line. The authors thank

Howard Tearle (Vancouver Prostate Centre) for advice on breeding and evaluation of the knockout mice.

Author Contributions

Conceived and designed the experiments: AB MEF SJ. Performed the experiments: AB JM PA MH BAN GRK SJ. Analyzed the data: AB WJM JM PA MH BAN GRK MEF SJ. Contributed reagents/materials/analysis tools: MEG JM-O. Wrote the paper: AB WJM JM PA MH BAN GRK MEG TN SK JM-O NP SCP MRW MEF SJ. Provided consultation in specific areas of their expertise: MEG TN SK JM-O PA NP SCP MRW.

References

1. Gipson IK. The ocular surface: the challenge to enable and protect vision: the Friedenwald lecture. Investigative ophthalmology & visual science. 2007; 48(10):4390; 1–8. Epub 2007/09/28. doi: 10.1167/iovs.07-0770 PMID: 17898256; PubMed Central PMCID: PMC2886589.
2. Blalock TD, Spurr-Michaud SJ, Tisdale AS, Heimer SR, Gilmore MS, Ramesh V, et al. Functions of MUC16 in corneal epithelial cells. Investigative ophthalmology & visual science. 2007; 48(10):4509–18. Epub 2007/09/28. doi: 10.1167/iovs.07-0430 PMID: 17898272.
3. Argueso P, Guzman-Aranguez A, Mantelli F, Cao Z, Ricciuto J, Panjwani N. Association of cell surface mucins with galectin-3 contributes to the ocular surface epithelial barrier. The Journal of biological chemistry. 2009; 284(34):23037–45. Epub 2009/06/27. doi: 10.1074/jbc.M109.033332 PMID: 19556244; PubMed Central PMCID: PMC2755710.
4. Mantelli F, Massaro-Giordano M, Macchi I, Lambiase A, Bonini S. The cellular mechanisms of dry eye: from pathogenesis to treatment. Journal of cellular physiology. 2013; 228(12):2253–6. Epub 2013/05/23. doi: 10.1002/jcp.24398 PMID: 23696296.
5. Gipson IK, Spurr-Michaud S, Tisdale A, Menon BB. Comparison of the Transmembrane Mucins MUC1 and MUC16 in Epithelial Barrier Function. PloS one. 2014; 9(6):e100393. Epub 2014/06/27. doi: 10.1371/journal.pone.0100393 PMID: 24968021; PubMed Central PMCID: PMC4072602.
6. TFOS. Report of the International Dry Eye Workshop (DEWS). The ocular surface. 2007; 5:65–204.
7. Schaumberg DA, Sullivan DA, Dana MR. Epidemiology of dry eye syndrome. Adv Exp Med Biol. 2002; 506(Pt B):989–98. PMID: 12614022.
8. De Paiva CS, Corrales RM, Villarreal AL, Farley WJ, Li DQ, Stern ME, et al. Corticosteroid and doxycycline suppress MMP-9 and inflammatory cytokine expression, MAPK activation in the corneal epithelium in experimental dry eye. Experimental eye research. 2006; 83(3):526–35. Epub 2006/04/29. doi: 10.1016/j.exer.2006.02.004 PMID: 16643899.
9. Li DQ, Luo L, Chen Z, Kim HS, Song XJ, Pflugfelder SC. JNK and ERK MAP kinases mediate induction of IL-1beta, TNF-alpha and IL-8 following hyperosmolar stress in human limbal epithelial cells. Experimental eye research. 2006; 82(4):588–96. Epub 2005/10/06. doi: 10.1016/j.exer.2005.08.019 PMID: 16202406; PubMed Central PMCID: PMC2198933.
10. Pflugfelder SC, Jones D, Ji Z, Afonso A, Monroy D. Altered cytokine balance in the tear fluid and conjunctiva of patients with Sjogren's syndrome keratoconjunctivitis sicca. Current eye research. 1999; 19 (3):201–11. Epub 1999/09/17. PMID: 10487957.
11. Luo L, Li DQ, Pflugfelder SC. Hyperosmolarity-induced apoptosis in human corneal epithelial cells is mediated by cytochrome c and MAPK pathways. Cornea. 2007; 26(4):452–60. Epub 2007/04/26. doi: 10.1097/ICO.0b013e318030d259 PMID: 17457195.
12. Chen W, Zhang X, Liu M, Zhang J, Ye Y, Lin Y, et al. Trehalose protects against ocular surface disorders in experimental murine dry eye through suppression of apoptosis. Experimental eye research. 2009; 89(3):311–8. Epub 2009/04/07. doi: 10.1016/j.exer.2009.03.015 PMID: 19345212.
13. Clouzeau C, Godefroy D, Riancho L, Rostene W, Baudouin C, Brignole-Baudouin F. Hyperosmolarity potentiates toxic effects of benzalkonium chloride on conjunctival epithelial cells in vitro. Molecular vision. 2012; 18:851–63. Epub 2012/04/25. PMID: 22529703; PubMed Central PMCID: PMC3332130.
14. Pflugfelder SC, Farley W, Luo L, Chen LZ, de Paiva CS, Olmos LC, et al. Matrix metalloproteinase-9 knockout confers resistance to corneal epithelial barrier disruption in experimental dry eye. The American journal of pathology. 2005; 166(1):61–71. Epub 2005/01/06. doi: 10.1016/S0002-9440(10)62232-8 PMID: 15632000; PubMed Central PMCID: PMC1602302.
15. Li DQ, Pflugfelder SC. Matrix metalloproteinases in corneal inflammation. The ocular surface. 2005; 3(4 Suppl):S198–202. Epub 2007/01/12. PMID: 17216119.

16. Foulks GN, Pflugfelder SC. New testing options for diagnosing and grading dry eye disease. American journal of ophthalmology. 2014; 157(6):1122–9. Epub 2014/03/19. doi: 10.1016/j.ajo.2014.03.002 PMID: 24631478; PubMed Central PMCID: PMC4062650.

17. Abelson MB, Ingerman A. The Dye-namics of Dry-Eye Diagnosis. Review of Ophthalmology on-line. 2005. Epub 15 Nov 2005.

18. Bron AJ, Argueso P, Irkec M, Bright FV. Clinical staining of the ocular surface: mechanisms and interpretations. Progress in retinal and eye research. 2015; 44:36–61. doi: 10.1016/j.preteyeres.2014.10.001 PMID: 25461622.

19. Wiechmann AF, Ceresa BP, Howard EW. Diurnal variation of tight junction integrity associates inversely with matrix metalloproteinase expression in Xenopus laevis corneal epithelium: implications for circadian regulation of homeostatic surface cell desquamation. PloS one. 2014; 9(11):e113810. doi: 10.1371/journal.pone.0113810 PMID: 25412440; PubMed Central PMCID: PMC4239109.

20. Luo L, Li DQ, Doshi A, Farley W, Corrales RM, Pflugfelder SC. Experimental dry eye stimulates production of inflammatory cytokines and MMP-9 and activates MAPK signaling pathways on the ocular surface. Investigative ophthalmology & visual science. 2004; 45(12):4293–301. Epub 2004/11/24. doi: 10.1167/iovs.03-1145 PMID: 15557435.

21. Mokhtarzadeh M, Casey R, Glasgow BJ. Fluorescein punctate staining traced to superficial corneal epithelial cells by impression cytology and confocal microscopy. Investigative ophthalmology & visual science. 2011; 52(5):2127–35. Epub 2011/01/08. doi: 10.1167/iovs.10-6489 PMID: 21212176; PubMed Central PMCID: PMC3080172.

22. Chotikavanich S, de Paiva CS, Li de Q, Chen JJ, Bian F, Farley WJ, et al. Production and activity of matrix metalloproteinase-9 on the ocular surface increase in dysfunctional tear syndrome. Investigative ophthalmology & visual science. 2009; 50(7):3203–9. Epub 2009/03/04. doi: 10.1167/iovs.08-2476 PMID: 19255163; PubMed Central PMCID: PMC3594995.

23. Jeong S, Ledee DR, Gordon GM, Itakura T, Patel N, Martin A, et al. Interaction of clusterin and matrix metalloproteinase-9 and its implication for epithelial homeostasis and inflammation. The American journal of pathology. 2012; 180(5):2028–39. Epub 2012/03/24. doi: 10.1016/j.ajpath.2012.01.025 PMID: 22440257; PubMed Central PMCID: PMC3349834.

24. Jones SE, Jomary C. Clusterin. The international journal of biochemistry & cell biology. 2002; 34 (5):427–31. Epub 2002/03/22. PMID: 11906815.

25. Kapron JT, Hilliard GM, Lakins JN, Tenniswood MP, West KA, Carr SA, et al. Identification and characterization of glycosylation sites in human serum clusterin. Protein science: a publication of the Protein Society. 1997; 6(10):2120–33. Epub 1997/10/23. doi: 10.1002/pro.5560061007 PMID: 9336835; PubMed Central PMCID: PMC2143570.

26. Bailey RW, Dunker AK, Brown CJ, Garner EC, Griswold MD. Clusterin, a binding protein with a molten globule-like region. Biochemistry. 2001; 40(39):11828–40. Epub 2001/09/26. PMID: 11570883.

27. de Silva HV, Stuart WD, Park YB, Mao SJ, Gil CM, Wetterau JR, et al. Purification and characterization of apolipoprotein J. The Journal of biological chemistry. 1990; 265(24):14292–7. Epub 1990/08/25. PMID: 2387851.

28. Toren PJ, Gleave ME. Evolving landscape and novel treatments in metastatic castrate-resistant prostate cancer. Asian journal of andrology. 2013; 15(3):342–9. Epub 2013/04/16. doi: 10.1038/aja.2013.38 PMID: 23584378; PubMed Central PMCID: PMC3739642.

29. Matsumoto H, Yamamoto Y, Shiota M, Kuruma H, Beraldi E, Matsuyama H, et al. Cotargeting Androgen Receptor and Clusterin Delays Castrate-Resistant Prostate Cancer Progression by Inhibiting Adaptive Stress Response and AR Stability. Cancer Res. 2013; 73(16):5206–17. doi: 10.1158/0008-5472.CAN-13-0359 PMID: 23786771.

30. Savkovic V, Gantzer H, Reiser U, Selig L, Gaiser S, Sack U, et al. Clusterin is protective in pancreatitis through anti-apoptotic and anti-inflammatory properties. Biochemical and biophysical research communications. 2007; 356(2):431–7. Epub 2007/03/16. doi: 10.1016/j.bbrc.2007.02.148 PMID: 17359935.

31. Humphreys DT, Carver JA, Easterbrook-Smith SB, Wilson MR. Clusterin has chaperone-like activity similar to that of small heat shock proteins. The Journal of biological chemistry. 1999; 274(11):6875–81. Epub 1999/03/06. PMID: 10066740.

32. Wilson MR, Easterbrook-Smith SB. Clusterin is a secreted mammalian chaperone. Trends in biochemical sciences. 2000; 25(3):95–8. Epub 2000/03/01. PMID: 10694874.

33. Rosenberg ME, Girton R, Finkel D, Chmielewski D, Barrie A 3rd, Witte DP, et al. Apolipoprotein J/clusterin prevents a progressive glomerulopathy of aging. Molecular and cellular biology. 2002; 22 (6):1893–902. Epub 2002/02/28. PMID: 11865066; PubMed Central PMCID: PMC135592.

34. McLaughlin L, Zhu G, Mistry M, Ley-Ebert C, Stuart WD, Florio CJ, et al. Apolipoprotein J/clusterin limits the severity of murine autoimmune myocarditis. The Journal of clinical investigation. 2000; 106

(9):1105–13. Epub 2000/11/09. doi: 10.1172/JCI9037 PMID: 11067863; PubMed Central PMCID: PMC301413.

35. Aronow BJ, Lund SD, Brown TL, Harmony JA, Witte DP. Apolipoprotein J expression at fluid-tissue interfaces: potential role in barrier cytoprotection. Proceedings of the National Academy of Sciences of the United States of America. 1993; 90(2):725–9. Epub 1993/01/15. PMID: 8421712; PubMed Central PMCID: PMC45738.

36. Trougakos IP, Gonos ES. Clusterin/apolipoprotein J in human aging and cancer. The international journal of biochemistry & cell biology. 2002; 34(11):1430–48. Epub 2002/08/30. PMID: 12200037.

37. Nishida K, Adachi W, Shimizu-Matsumoto A, Kinoshita S, Mizuno K, Matsubara K, et al. A gene expression profile of human corneal epithelium and the isolation of human keratin 12 cDNA. Investigative ophthalmology & visual science. 1996; 37(9):1800–9. Epub 1996/08/01. PMID: 8759347.

38. Nakamura T, Nishida K, Dota A, Kinoshita S. Changes in conjunctival clusterin expression in severe ocular surface disease. Investigative ophthalmology & visual science. 2002; 43(6):1702–7. Epub 2002/05/31. PMID: 12036968.

39. Li N, Wang N, Zheng J, Liu XM, Lever OW, Erickson PM, et al. Characterization of human tear proteome using multiple proteomic analysis techniques. Journal of proteome research. 2005; 4(6):2052–61. Epub 2005/12/13. doi: 10.1021/pr0501970 PMID: 16335950.

40. Karnati R, Laurie DE, Laurie GW. Lacritin and the tear proteome as natural replacement therapy for dry eye. Experimental eye research. 2013; 117:39–52. Epub 2013/06/19. doi: 10.1016/j.exer.2013.05.020 PMID: 23769845; PubMed Central PMCID: PMC3844047.

41. Zhou L, Zhao SZ, Koh SK, Chen L, Vaz C, Tanavde V, et al. In-depth analysis of the human tear proteome. Journal of proteomics. 2012; 75(13):3877–85. Epub 2012/05/29. doi: 10.1016/j.jprot.2012.04.053 PMID: 22634083.

42. De Paiva CS, Corrales RM, Villarreal AL, Farley W, Li DQ, Stern ME, et al. Apical corneal barrier disruption in experimental murine dry eye is abrogated by methylprednisolone and doxycycline. Investigative ophthalmology & visual science. 2006; 47(7):2847–56. Epub 2006/06/27. doi: 10.1167/iovs.05-1281 PMID: 16799024.

43. Gipson IK, Spurr-Michaud S, Argueso P, Tisdale A, Ng TF, Russo CL. Mucin gene expression in immortalized human corneal-limbal and conjunctival epithelial cell lines. Investigative ophthalmology & visual science. 2003; 44(6):2496–506. Epub 2003/05/27. PMID: 12766048.

44. Dursun D, Wang M, Monroy D, Li DQ, Lokeshwar BL, Stern ME, et al. A mouse model of keratoconjunctivitis sicca. Investigative ophthalmology & visual science. 2002; 43(3):632–8. Epub 2002/02/28. PMID: 11867577.

45. Villareal AL, Farley W, Pflugfelder SC. Effect of topical ophthalmic epinastine and olopatadine on tear volume in mice. Eye Contact Lens. 2006; 32(6):272–6. doi: 10.1097/01.icl.0000224360.10319.b1 PMID: 17099387.

46. Li Z, Woo JM, Chung SW, Kwon MY, Choi JS, Oh HJ, et al. Therapeutic effect of topical adiponectin in a mouse model of desiccating stress-induced dry eye. Investigative ophthalmology & visual science. 2013; 54(1):155–62. Epub 2012/12/06. doi: 10.1167/iovs.12-10648 PMID: 23211823.

47. Zeger SL, Liang KY. Longitudinal data analysis for discrete and continuous outcomes. Biometrics. 1986; 42(1):121–30. PMID: 3719049.

48. Zeger SL, Liang KY, Albert PS. Models for longitudinal data: a generalized estimating equation approach. Biometrics. 1988; 44(4):1049–60. PMID: 3233245.

49. Thomas-Tikhonenko A, Viard-Leveugle I, Dews M, Wehrli P, Sevignani C, Yu D, et al. Myc-transformed epithelial cells down-regulate clusterin, which inhibits their growth in vitro and carcinogenesis in vivo. Cancer research. 2004; 64(9):3126–36. Epub 2004/05/06. PMID: 15126350.

50. Xiao B, Wang Y, Reinach PS, Ren Y, Li J, Hua S, et al. Dynamic ocular surface and lacrimal gland changes induced in experimental murine dry eye. PloS one. 2015; 10(1):e0115333. doi: 10.1371/journal.pone.0115333 PMID: 25590134; PubMed Central PMCID: PMC4295848.

51. Stewart EM, Aquilina JA, Easterbrook-Smith SB, Murphy-Durland D, Jacobsen C, Moestrup S, et al. Effects of glycosylation on the structure and function of the extracellular chaperone clusterin. Biochemistry. 2007; 46(5):1412–22. Epub 2007/01/31. doi: 10.1021/bi062082v PMID: 17260971.

52. Argueso P, Panjwani N. Focus on molecules: galectin-3. Experimental eye research. 2011; 92(1):2–3. Epub 2010/11/30. doi: 10.1016/j.exer.2010.11.009 PMID: 21111733; PubMed Central PMCID: PMC3034303.

53. Mauris J, Mantelli F, Woodward AM, Cao Z, Bertozzi CR, Panjwani N, et al. Modulation of ocular surface glycocalyx barrier function by a galectin-3 N-terminal deletion mutant and membrane-anchored synthetic glycopolymers. PloS one. 2013; 8(8):e72304. Epub 2013/08/27. doi: 10.1371/journal.pone.0072304 PMID: 23977277; PubMed Central PMCID: PMC3747151.

54. Matani P, Sharrow M, Tiemeyer M. Ligand, modulatory, and co-receptor functions of neural glycans. Frontiers in bioscience: a journal and virtual library. 2007; 12:3852–79. Epub 2007/05/09. PMID: 17485343.

55. Ochieng J, Fridman R, Nangia-Makker P, Kleiner DE, Liotta LA, Stetler-Stevenson WG, et al. Galectin-3 is a novel substrate for human matrix metalloproteinases-2 and -9. Biochemistry. 1994; 33 (47):14109–14. Epub 1994/11/29. PMID: 7947821.

56. Ulmer TA, Keeler V, Andre S, Gabius HJ, Loh L, Laferte S. The tumor-associated antigen 90K/Mac-2-binding protein secreted by human colon carcinoma cells enhances extracellular levels of promatrilysin and is a novel substrate of matrix metalloproteinases-2, -7 (matrilysin) and -9: Implications of proteolytic cleavage. Biochimica et biophysica acta. 2010; 1800(3):336–43. Epub 2009/08/12. doi: 10.1016/j.bbagen.2009.07.030 PMID: 19665518.

57. Ochieng J, Green B, Evans S, James O, Warfield P. Modulation of the biological functions of galectin-3 by matrix metalloproteinases. Biochimica et biophysica acta. 1998; 1379(1):97–106. Epub 1998/02/19. PMID: 9468337.

58. Uchino Y, Mauris J, Woodward AM, Dieckow J, Amparo F, Dana R, et al. Alteration of galectin-3 in tears of patients with dry eye disease. Am J Ophthalmol. 2015; 159(6):1027–35 e3. doi: 10.1016/j.ajo.2015.02.008 PMID: 25703476; PubMed Central PMCID: PMC4426220.

59. Navab M, Anantharamaiah GM, Reddy ST, Van Lenten BJ, Buga GM, Fogelman AM. Peptide Mimetics of Apolipoproteins Improve HDL Function. J Clin Lipidol. 2007; 1(2):142–7. doi: 10.1016/j.jacl.2007.03.002 PMID: 18449337; PubMed Central PMCID: PMC2130772.

60. Handattu SP, Garber DW, Horn DC, Hughes DW, Berno B, Bain AD, et al. ApoA-I mimetic peptides with differing ability to inhibit atherosclerosis also exhibit differences in their interactions with membrane bilayers. J Biol Chem. 2007; 282(3):1980–8. doi: 10.1074/jbc.M606231200 PMID: 17114186.

61. Chieze L, Bolanos-Garcia VM, Pinot M, Desbat B, Renault A, Beaufils S, et al. Fluid and condensed ApoA-I/phospholipid monolayers provide insights into ApoA-I membrane insertion. Journal of molecular biology. 2011; 410(1):60–76. doi: 10.1016/j.jmb.2011.04.006 PMID: 21510960.

62. Lee RC, River LP, Pan FS, Ji L, Wollmann RL. Surfactant-induced sealing of electropermeabilized skeletal muscle membranes in vivo. Proc Natl Acad Sci U S A. 1992; 89(10):4524–8. PMID: 1584787; PubMed Central PMCID: PMC49115.

63. Maskarinec SA, Hannig J, Lee RC, Lee KY. Direct observation of poloxamer 188 insertion into lipid monolayers. Biophys J. 2002; 82(3):1453–9. doi: 10.1016/S0006-3495(02)75499-4 PMID: 11867460; PubMed Central PMCID: PMC1301946.

64. Adisetiyo H, Liang M, Liao CP, Aycock-Williams A, Cohen MB, Xu S, et al. Loss of survivin in the prostate epithelium impedes carcinogenesis in a mouse model of prostate adenocarcinoma. PloS one. 2013; 8(7):e69484. Epub 2013/08/13. doi: 10.1371/journal.pone.0069484 PMID: 23936028; PubMed Central PMCID: PMC3729965.

65. Liang J, Tong P, Zhao W, Li Y, Zhang L, Xia Y, et al. The REST gene signature predicts drug sensitivity in neuroblastoma cell lines and is significantly associated with neuroblastoma tumor stage. International journal of molecular sciences. 2014; 15(7):11220–33. doi: 10.3390/ijms150711220 PMID: 24968265; PubMed Central PMCID: PMC4139778.

66. Matveev V, Wang XJ. Implications of all-or-none synaptic transmission and short-term depression beyond vesicle depletion: a computational study. The Journal of neuroscience: the official journal of the Society for Neuroscience. 2000; 20(4):1575–88. Epub 2000/02/09. PMID: 10662847.

67. Kierzek AM, Zhou L, Wanner BL. Stochastic kinetic model of two component system signalling reveals all-or-none, graded and mixed mode stochastic switching responses. Molecular bioSystems. 2010; 6 (3):531–42. Epub 2010/02/23. doi: 10.1039/b906951h PMID: 20174681.

68. Liu T, Yamaguchi Y, Shirasaki Y, Shikada K, Yamagishi M, Hoshino K, et al. Single-Cell Imaging of Caspase-1 Dynamics Reveals an All-or-None Inflammasome Signaling Response. Cell reports. 2014. Epub 2014/08/16. doi: 10.1016/j.celrep.2014.07.012 PMID: 25127135.

69. Tsianou M, Fajalia AI. Cyclodextrins and Surfactants in Aqueous Solution above CMC: Where are the Cyclodextrins Located? Langmuir: the ACS journal of surfaces and colloids. 2014. Epub 2014/08/16. doi: 10.1021/la5013999 PMID: 25126838.

70. Collard MW, Griswold MD. Biosynthesis and molecular cloning of sulfated glycoprotein 2 secreted by rat Sertoli cells. Biochemistry. 1987; 26(12):3297–303. Epub 1987/06/16. PMID: 3651384.

71. Hochgrebe T, Pankhurst GJ, Wilce J, Easterbrook-Smith SB. pH-dependent changes in the in vitro ligand-binding properties and structure of human clusterin. Biochemistry. 2000; 39(6):1411–9. Epub 2000/02/24. PMID: 10684622.

72. Crabb JW, Miyagi M, Gu X, Shadrach K, West KA, Sakaguchi H, et al. Drusen proteome analysis: an approach to the etiology of age-related macular degeneration. Proceedings of the National Academy of

Sciences of the United States of America. 2002; 99(23):14682–7. Epub 2002/10/23. doi: 10.1073/pnas.222551899 PMID: 12391305; PubMed Central PMCID: PMC137479.

73. Nishida K, Quantock AJ, Dota A, Choi-Miura NH, Kinoshita S. Apolipoproteins J and E co-localise with amyloid in gelatinous drop-like and lattice type I corneal dystrophies. The British journal of ophthalmology. 1999; 83(10):1178–82. Epub 1999/09/30. PMID: 10502582; PubMed Central PMCID: PMC1722813.

74. Calero M, Rostagno A, Matsubara E, Zlokovic B, Frangione B, Ghiso J. Apolipoprotein J (clusterin) and Alzheimer's disease. Microscopy research and technique. 2000; 50(4):305–15. Epub 2000/08/11. doi: 10.1002/1097-0029(20000815)50:4<305::AID-JEMT10>3.0.CO;2-L PMID: 10936885.

75. Kounnas MZ, Loukinova EB, Stefansson S, Harmony JA, Brewer BH, Strickland DK, et al. Identification of glycoprotein 330 as an endocytic receptor for apolipoprotein J/clusterin. The Journal of biological chemistry. 1995; 270(22):13070–5. Epub 1995/06/02. PMID: 7768901.

76. Leeb C, Eresheim C, Nimpf J. Clusterin is a ligand for apolipoprotein E receptor 2 (ApoER2) and very low density lipoprotein receptor (VLDLR) and signals via the Reelin-signaling pathway. The Journal of biological chemistry. 2014; 289(7):4161–72. Epub 2014/01/02. doi: 10.1074/jbc.M113.529271 PMID: 24381170; PubMed Central PMCID: PMC3924281.

77. Zhang H, Kim JK, Edwards CA, Xu Z, Taichman R, Wang CY. Clusterin inhibits apoptosis by interacting with activated Bax. Nature cell biology. 2005; 7(9):909–15. doi: 10.1038/ncb1291 PMID: 16113678.

78. Santilli G, Aronow BJ, Sala A. Essential requirement of apolipoprotein J (clusterin) signaling for IkappaB expression and regulation of NF-kappaB activity. The Journal of biological chemistry. 2003; 278 (40):38214–9. doi: 10.1074/jbc.C300252200 PMID: 12882985.

79. Bandamwar KL, Papas EB, Garrett Q. Fluorescein staining and physiological state of corneal epithelial cells. Contact lens & anterior eye: the journal of the British Contact Lens Association. 2014; 37(3):213–23. doi: 10.1016/j.clae.2013.11.003 PMID: 24332360.

80. Shim YJ, Kang BH, Jeon HS, Park IS, Lee KU, Lee IK, et al. Clusterin induces matrix metalloproteinase-9 expression via ERK1/2 and PI3K/Akt/NF-kappaB pathways in monocytes/macrophages. Journal of leukocyte biology. 2011; 90(4):761–9. Epub 2011/07/12. doi: 10.1189/jlb.0311110 PMID: 21742938.

81. Radziwon-Balicka A, Santos-Martinez MJ, Corbalan JJ, O'Sullivan S, Treumann A, Gilmer JF, et al. Mechanisms of platelet-stimulated colon cancer invasion: role of clusterin and thrombospondin 1 in regulation of the P38MAPK-MMP-9 pathway. Carcinogenesis. 2014; 35(2):324–32. Epub 2013/10/03. doi: 10.1093/carcin/bgt332 PMID: 24085798.

82. Fini ME, Cook JR, Mohan R, Brinckerhoff CE. Regulation of matrix metalloproteinase gene expression. In: W. P, Mecham R, editors. Matrix Metalloproteinases: Academic Press; 1998.

83. Kompella UB, Kadam RS, Lee VH. Recent advances in ophthalmic drug delivery. Therapeutic delivery. 2010; 1(3):435–56. Epub 2011/03/15. doi: 10.4155/TDE.10.40 PMID: 21399724; PubMed Central PMCID: PMC3051398.

84. Urtti A. Challenges and obstacles of ocular pharmacokinetics and drug delivery. Advanced drug delivery reviews. 2006; 58(11):1131–5. Epub 2006/11/14. doi: 10.1016/j.addr.2006.07.027 PMID: 17097758.

85. Dabbs RA, Wilson MR. Expression and purification of chaperone-active recombinant clusterin. PloS one. 2014; 9(1):e86989. Epub 2014/01/28. doi: 10.1371/journal.pone.0086989 PMID: 24466307; PubMed Central PMCID: PMC3900688.

86. Williamson JF, Huynh K, Weaver MA, Davis RM. Perceptions of dry eye disease management in current clinical practice. Eye & contact lens. 2014; 40(2):111–5. Epub 2014/02/11. doi: 10.1097/ICL.0000000000000020 PMID: 24508770.

87. Novack GD. Why aren't there more pharmacotherapies for dry eye? Ocul Surf. 2014; 12(3):227–30. doi: 10.1016/j.jtos.2014.05.001 PMID: 24999105.

88. Sullivan DA, Hammitt KM, Schaumberg DA, Sullivan BD, Begley CG, Gjorstrup P, et al. Report of the TFOS/ARVO Symposium on global treatments for dry eye disease: an unmet need. The ocular surface. 2012; 10(2):108–16. Epub 2012/04/10. doi: 10.1016/j.jtos.2012.02.001 PMID: 22482471.

Genome-wide association study identifies five new susceptibility loci for primary angle closure glaucoma

Primary angle closure glaucoma (PACG) is a major cause of blindness worldwide. We conducted a genome-wide association study (GWAS) followed by replication in a combined total of 10,503 PACG cases and 29,567 controls drawn from 24 countries across Asia, Australia, Europe, North America, and South America. We observed significant evidence of disease association at five new genetic loci upon meta-analysis of all patient collections. These loci are at *EPDR1* rs3816415 (odds ratio (OR) = 1.24, $P = 5.94 \times 10^{-15}$), *CHAT* rs1258267 (OR = 1.22, $P = 2.85 \times 10^{-16}$), *GLIS3* rs736893 (OR = 1.18, $P = 1.43 \times 10^{-14}$), *FERMT2* rs7494379 (OR = 1.14, $P = 3.43 \times 10^{-11}$), and *DPM2–FAM102A* rs3739821 (OR = 1.15, $P = 8.32 \times 10^{-12}$). We also confirmed significant association at three previously described loci ($P < 5 \times 10^{-8}$ for each sentinel SNP at *PLEKHA7*, *COL11A1*, and *PCMTD1–ST18*)[1], providing new insights into the biology of PACG.

Glaucoma is the most common cause of irreversible blindness worldwide[2]. The main forms of glaucoma are primary open angle glaucoma (POAG), PACG, and exfoliation glaucoma. All three forms of glaucoma show familial clustering, suggesting a substantial genetic component in pathogenesis. Recent genetic studies have implicated several distinct loci associated with each of these types of glaucoma[1,3–6]. For PACG, the epidemiological risk factors include advancing age, female sex, and East Asian ancestry[7,8]. Up to 80% of the estimated 15 million people afflicted with PACG live in Asia[9], where the disease is responsible for a high proportion of blindness[10–13]. Patients either present with acute primary angle closure (APAC) or have PACG upon presentation (**Supplementary Note**). We previously performed a GWAS of PACG susceptibility on 1,854 PACG cases and 9,608 controls with replication in 1,917 cases and 8,943 controls, identifying three susceptibility loci[1].

We now expand the study to perform a discovery-stage GWAS on a combined total of 6,525 PACG cases and 19,929 controls, which were enrolled from 15 countries spanning East Asia, South Asia, Europe, and South America (**Fig. 1** and **Supplementary Table 1**). We applied routine quality control checks for SNPs and samples as is usually done for GWAS analyses (Online Methods). SNPs at ten distinct loci surpassed $P < 1 \times 10^{-6}$ (**Supplementary Table 2**), a threshold we took to be indicative of suggestive evidence of association with disease[14]. Three of these loci have previously been reported (**Fig. 2** and **Supplementary Table 3**)[1]. We then subjected the ten sentinel SNPs representing each of the ten independent loci to replication genotyping in a further 3,978 cases and 9,638 controls from 14 countries (**Supplementary Table 1**). Significant replication was observed at eight distinct loci (**Table 1** and **Supplementary Table 2**; the initial associations observed at *FNDC3B* rs16856870 on chromosome 3 and *SLC38A6* rs10483730 on chromosome 14 did not replicate), and meta-analysis of all discovery and replication samples totaling 10,503 PACG cases and 29,567 controls showed genome-wide significant evidence of association for the eight loci with PACG (**Fig. 2** and **Table 1**). This two-stage study design is powered to detect effect sizes as low as 1.15 with minor allele frequencies (MAFs) as low as 0.15 at genome-wide significance (**Supplementary Table 4**).

We next asked whether heterogeneity in genetic effect sizes exists across ancestry groups and geographical locations and found that only *EPDR1* rs3816415 showed discernable evidence of heterogeneity in the overall meta-analysis ($P_{het} = 0.0072$, I^2 index = 43.0%). Closer scrutiny showed that effect sizes were consistently larger in Europeans (OR = 1.42) than in Asians (OR = 1.21) (**Fig. 3** and **Table 1**), despite similar risk allele frequencies across the ancestry groups (**Supplementary Table 5**). This discrepancy could be due either to more unreliable estimation in Europeans because of the smaller sample size in comparison to Asians (n = 1,105 European PACG cases versus 9,398 Asian PACG cases) or to a genuine difference in effect between Asians and Europeans[15–17]. We did not observe significant heterogeneity in effect sizes at the other four loci (**Fig. 3** and **Table 1**). Imputation-based fine-mapping and regional association analysis showed that each SNP locus mapped distinctly among its nearest genes, mostly framed by recombination events (**Supplementary Fig. 1**). However, as the GWAS approach assays mostly common, representative genetic variants across the human genome, we are unable to exclude the possibility that the identified SNPs at each locus could be tagging functional variants that are exerting control on distant gene targets in a position- and orientation-independent manner[18,19].

We next examined the ocular expression of genes located in the newly identified PACG loci by RT–PCR. We detected mRNA expression of *EPDR1*, *GLIS3*, *FERMT2*, *DPM2*, *PIP5KL1*, and *FAM102A* in human ocular anterior segment tissues such as the iris, ciliary body, and trabecular meshwork (**Supplementary Fig. 2a**). We also observed mRNA expression of all six genes in the cornea, lens, retina, choroid, optic nerve head, and optic nerve. We also investigated the distribution of the encoded proteins of these genes in ocular tissues by immunohistochemical labeling of sections of a normal human eye (**Supplementary Figs. 3–9**), testing for tissue specificity of expression through immunoblot analysis in ocular-tissue-derived cell lines

A full list of authors and affiliations appear at the end of the paper.

Received 7 November 2015; accepted 7 March 2016; published online 4 April 2016; doi:10.1038/ng.3540

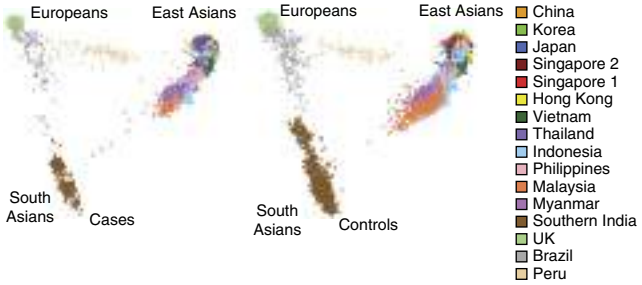

Figure 1 Distribution of PACG cases and controls from the GWAS discovery stage, which encompassed collections from 15 countries. Cases and controls are projected onto the top two principal components of genetic stratification, with cases on the left and controls on the right. Principal-component comparisons for each of the East Asian countries are shown in **Supplementary Figure 10**.

(**Supplementary Fig. 2b–h**). Overall, protein expression and localization corroborated the mRNA data, except in the case of GLIS3, where pronounced protein expression was seen in the iris, different to what was observed in mRNA expression analysis (**Supplementary Fig. 2a**). This difference may be attributed to the insensitivity of the RT–PCR technique for transcripts present at low levels.

EPDR1 encodes a glycosylated type II transmembrane protein known as ependymin-related 1. It potentially has a role in cell adhesion, as it is similar to protocadherins and ependymins[20]. SNP *EPDR1* rs16879765 has been shown to be significantly associated with Dupuytren's contracture, an inherited disorder of connective tissues[21]. Our genome-wide significant association at *EPDR1* for PACG is marked by the sentinel SNP rs3816415, which is very poorly correlated with rs16879765 despite being located less than 1 kb away. This pleiotropic association with *EPDR1* merits further study and highlights the relevance of cell adhesion molecules more broadly in PACG pathology.

SNP rs3739821 is located in an intergenic region between *DPM2* and *FAM102A*, a gene yet to be fully characterized. Mutations in *DPM2* have been linked to congenital defects in glycosylation[22], leading to severe neurological phenotypes. Although not much is known about *FAM102A* except that its expression is sensitive to the addition of β-estradiol[23], the nearby *PIP5KL1* gene (**Supplementary Fig. 1**) has been reported to be involved in cell proliferation[24] and potentially in tumorigenesis. Our expression analysis showed that all three genes (*FAM102A*, *DPM2*, and *PIP5KL1*) were expressed in all eye tissues tested, thus providing biological support for their involvement in PACG (**Supplementary Figs. 2** and **7–9**). Further fine-mapping work is needed to identify the causative gene in this locus.

CHAT on chromosome 10 encodes choline acetyltransferase. This is an enzyme responsible for synthesis of the neurotransmitter acetylcholine, which has a role in pupillary constriction. Anticholinergic medications can precipitate acute PACG via pupillary dilatation and subsequent pupillary block[25,26]. Therefore, it is plausible that natural genetic variation in a gene influencing acetylcholine metabolism could influence risk for PACG.

FERMT2 encodes a protein called pleckstrin-homology-domain-containing family C member 1 (PLEKHC1), a component of the extracellular matrix, and could thus have a role in cell adhesion[27]. PLEKHC1 belongs to the same pleckstrin family of proteins as PLEKHA7, and we previously showed that common SNPs mapping to *PLEKHA7* are significantly associated with susceptibility to PACG[1]. Our current observation of genome-wide significant associations at *FERMT2* and *EPDR1*, as well as the previous report of *PLEKHA7*, strongly implicates the cell–cell adhesion process as being important in the pathogenesis of PACG.

GLIS3 is a member of the GLI-similar subfamily of Krüppel-like zinc-finger proteins[28]. Earlier studies have shown that mutations in *GLIS3* cause neonatal diabetes and congenital hypothyroidism[29]. SNP markers mapping close to *GLIS3* have been observed to be significantly associated with type 1 diabetes in Europeans (rs7020673)[30], type 2 diabetes in East Asians (rs7041847)[31], and fasting plasma glucose levels in a large meta-analysis of European collections (rs7034200)[32]. These SNPs are independent from rs736893, which we observe here to be associated with PACG. These observations implicate yet unknown metabolic pathways that could contribute to PACG pathogenesis.

We next looked up reported loci showing genome-wide significant association with POAG[3,4,33,34] in our PACG discovery GWAS data set, as susceptibility variants for the two common forms of glaucoma could potentially be shared. We observed evidence of association at *ARHGEF12* rs2276035 and *GAS7* rs12150284. For both loci, the direction of effect was consistent in PACG and POAG (**Supplementary Table 6**). Reciprocally, we also assessed all eight genome-wide significant PACG loci in 968 POAG cases and 3,916 controls of Singaporean Chinese descent[35] but did not observe consistent evidence of association between the PACG loci and POAG (**Supplementary Table 7**).

Both ocular axial length and anterior chamber depth have previously been reported as anatomical risk factors for PACG, whereby individuals with eyes having less anterior chamber depth and shorter axial length are at increased risk of PACG[36]. We examined the six loci associated with axial length at

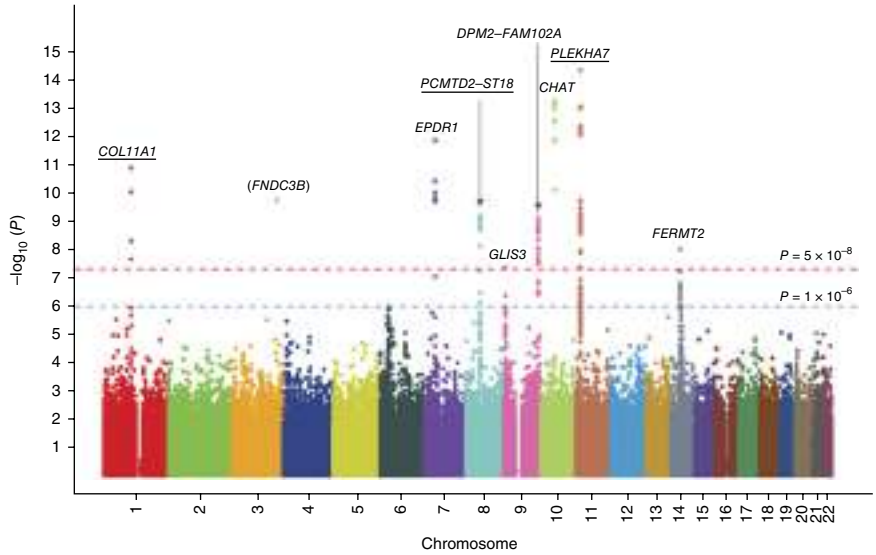

Figure 2 Results of the discovery GWAS meta-analysis. The three previously reported loci are underlined. *FNDC3B* did not replicate in the replication collections. SNPs at *EPDR1*, *GLIS3*, *DPM2–FAM102A*, *CHAT*, and *FERMT2* represent new genome-wide significant associations.

Table 1 Results for the eight genome-wide significant loci upon meta-analysis of all PACG case–control collections

SNP (risk/reference)	Chr.	Position (bp)	Gene locus	Stage	Per-allele OR	*P*	P_{het}	I^2 index (%)
New loci								
rs3816415 (A/G)	7	37,988,311	*EPDR1*	GWAS	1.28	1.28×10^{-12}	0.6	0
				Replication	1.17	0.00032	0.0013	60.4
				All-data meta-analysis	1.24	5.94×10^{-15}	0.0072	43.0
				Asian descent	1.21	7.49×10^{-11}	0.095	29.1
				European descent	1.42	1.86×10^{-6}	0.029	55.3
rs736893 (G/A)	9	4,217,028	*GLIS3*	GWAS	1.16	4.23×10^{-8}	0.85	0
				Replication	1.20	4.64×10^{-8}	0.48	0
				All-data meta-analysis	1.18	1.43×10^{-14}	0.78	0
				Asian descent	1.17	1.2×10^{-11}	0.57	0
				European descent	1.25	0.00015	0.94	0
rs3739821 (G/A)	9	130,702,477	*DPM2–FAM102A*	GWAS	1.17	7.08×10^{-10}	0.93	0
				Replication	1.11	0.0013	0.28	15.7
				All-data meta-analysis	1.15	8.32×10^{-12}	0.62	0
				Asian descent	1.15	4.5×10^{-11}	0.46	0
				European descent	1.12	0.06	0.79	0
rs1258267 (A/G)	10	50,895,770	*CHAT*	GWAS	1.25	5.06×10^{-14}	0.59	0
				Replication	1.16	0.00046	0.57	0
				All-data meta-analysis	1.22	2.85×10^{-16}	0.58	0
				Asian descent	1.22	4.99×10^{-16}	0.58	0
				European descent	1.43	0.24[a]	0.32	14.2
rs7494379 (G/A)	14	53,411,391	*FERMT2*	GWAS	1.15	9.26×10^{-9}	0.56	0
				Replication	1.11	0.00065	0.24	19.2
				All-data meta-analysis	1.14	3.43×10^{-11}	0.39	5.0
				Asian descent	1.13	5.42×10^{-9}	0.36	7.3
				European descent	1.22	0.00066	0.52	0
Previously reported loci								
rs3753841 (G/A)	1	103,379,918	*COL11A1*	GWAS	1.18	1.18×10^{-11}	0.32	11.4
				Replication	1.29	1.15×10^{-14}	0.47	0
				All-data meta-analysis	1.21	1.27×10^{-23}	0.21	16.8
				Asian descent	1.21	4×10^{-21}	0.35	8.1
				European descent	1.20	0.00076	0.099	42.0
rs1015213 (A/G)	8	52,887,541	*PCMTD1–ST18*	GWAS	1.44	1.75×10^{-9}	0.21	21.2
				Replication	1.40	5.47×10^{-8}	0.51	0
				All-data meta-analysis	1.42	5.42×10^{-16}	0.34	8.0
				Asian descent	1.44	1.68×10^{-13}	0.096	29
				European descent	1.35	0.0006	0.99	0
rs11024102 (G/A)	11	17,008,605	*PLEKHA7*	GWAS	1.20	4.1×10^{-15}	0.77	0
				Replication	1.15	5.51×10^{-5}	0.48	0
				All-data meta-analysis	1.18	1.93×10^{-18}	0.71	0
				Asian descent	1.20	8×10^{-19}	0.87	0
				European descent	1.05	0.38	0.54	0

All SNPs reported here were directly genotyped on the GWAS arrays. Chr., chromosome.
[a]The minor allele for *CHAT* rs1258267 is very rare in Europeans (**Supplementary Table 5**). Of the six European-ancestry populations (Australia, Brazil, Peru, Poland, UK, and United States), only those from Brazil, Peru, and Poland had MAF >1% and thus could be tested for genetic association.

genome-wide significance previously reported in a large meta-analysis of 12,531 Europeans and 8,216 Asians[37] in our discovery GWAS for PACG. None of the associations (**Supplementary Table 8**) survived correction for multiple comparisons. We note nominal evidence of association with PACG at the *ABCC5* locus, which we previously reported[38] as being associated with anterior chamber depth (for SNP rs4148579, pairwise $r^2 = 0.99$ with the previously reported rs1401999; OR = 1.07, $P = 0.017$).

We then checked whether any of the five newly associated PACG loci directly underlie functional genomic elements. We observed that almost all of the sentinel SNPs as well as SNPs in linkage disequilibrium (LD) are located within potential transcription factor binding sites (**Supplementary Table 9**)[39–41]. None of the sentinel SNPs tag ($r^2 > 0.8$) any exonic SNPs in genes within the respective loci. Examination of recently available large-scale expression quantitative trait locus (eQTL) mapping databases[42,43] indicated that only SNPs rs3739821 on chromosome 9 and rs7494379 on chromosome 14 are significant eQTLs in human tissues (**Supplementary Table 10**). However, the data may allow us to draw limited inferences, as rs3739821 has significant eQTL effects on *DPM2* ($P = 1.44 \times 10^{-12}$) and *FAM102A* ($P = 4.57 \times 10^{-6}$), as well as on the neighboring *ST6GALNAC6* ($P = 6.79 \times 10^{-20}$) and *ST6GALNAC4* ($P = 5.32 \times 10^{-6}$) genes[42]. Looking up our loci in a second eQTL database derived from gene expression analysis in blood cells[44], SNP rs3739821 has a significant

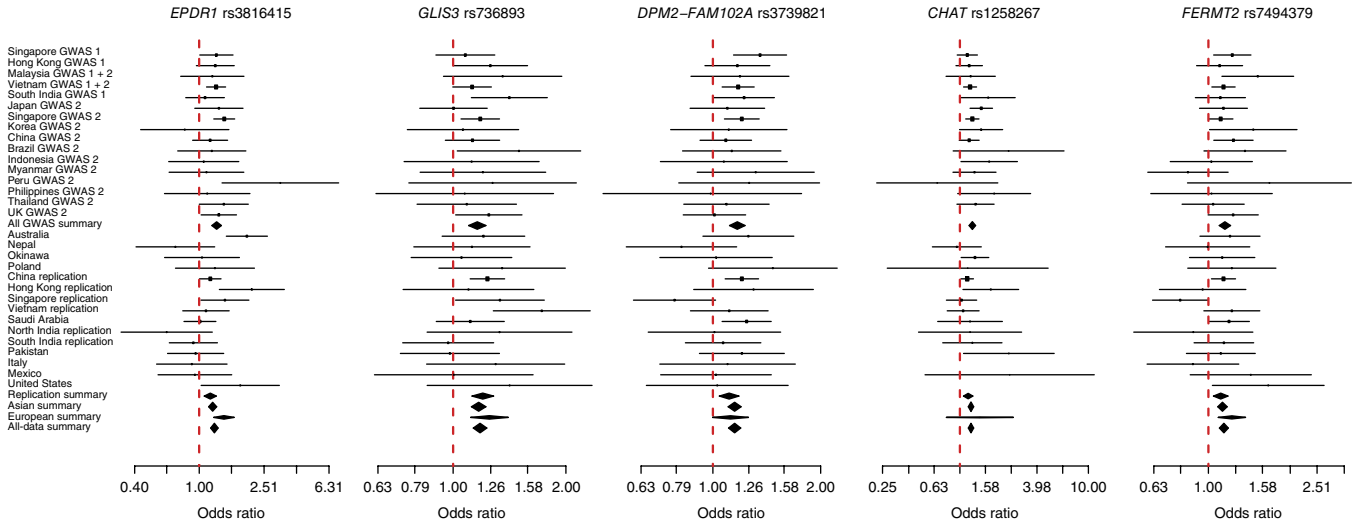

Figure 3 Forest plots for the five new genome-wide significant loci. Point estimates for each locus are denoted as risk allele odds ratios, accompanied by horizontal lines representing the 95% confidence interval for each point estimate. Diamonds represent meta-analyses for the GWAS discovery stage, replication stage, all Asians, and all Europeans, as well as for all samples. The vertical dashed red line represents an OR of 1.00, indicating no effect.

eQTL effect on *ST6GALNAC4* in monocytes, associated with lower expression ($\beta = -0.1$, $P = 2.4 \times 10^{-8}$). Further work is needed to determine the functional effects of these variants on PACG susceptibility.

In summary, our expanded GWAS and replication study of PACG has identified five new susceptibility loci, thus bringing the total number of replicated loci to eight. These eight loci explain up to 1.8% of the overall disease variance in PACG, in line with observations for many complex diseases[45,46]. These results further reinforce the potential importance of cell–cell adhesion and collagen metabolism in PACG pathogenesis. Furthermore, our observations newly implicate acetylcholine metabolism, yet uncharacterized metabolic pathways mediated through zinc-finger activation and repression of transcription, and changes in glycosylation as candidate pathways for future work aimed at identifying the mechanisms responsible for PACG susceptibility.

URLs. PLINK, http://pngu.mgh.harvard.edu/~purcell/plink/; R statistical package, https://www.r-project.org/; IMPUTE, https://mathgen.stats.ox.ac.uk/impute/impute_v2.html.

METHODS

Methods and any associated references are available in the online version of the paper.

Accession codes. The genome-wide association summary statistics for all SNP markers with direct microarray genotyping together with imputation fine-mapping of the significant loci are provided as the **Supplementary Data Set**.

Note: Any Supplementary Information and Source Data files are available in the online version of the paper.

ACKNOWLEDGMENTS

This research is supported by the Singapore Ministry of Health's National Medical Research Council under its Translational and Clinical Research (TCR) Flagship Programme Grant Stratified Medicine for Primary Angle Closure Glaucoma (NMRC/TCR/008-SERI/2013) and the Singapore Translational Research (STaR) Investigator Award Singapore Angle Closure Glaucoma Program Characterization, Prevention, and Management (NMRC/STAR/0023/2014), as well as the Biomedical Research Council, Agency for Science, Technology and Research (A-STAR), Singapore. A.T.L.-S. gratefully acknowledges support from grants RUI 1001/PPSP/812101 and RUI 1001/PPSP/812152 from the Universiti Sains Malaysia. H.J., C.Q., and N. Wang acknowledge support from the Program of Beijing Scholars (2013), Leading Talents–High-Level Talents of the Health System of Beijing (2009-1-05), and the National Major Scientific and Technological Special Project for 'Significant New Drugs Development' (2011ZX09302-007-05), as well as Project of the National Natural Science Foundation of China (81570837) grants.

AUTHOR CONTRIBUTIONS

T.A. and C.C. Khor conceived the project. T. Do., H.J., M.N., R.G., K.A.-A., R. Duvesh., L.J.C., Z.L., M.E.N., S.A.P., C.Q., H.-T.W., H. Sakai., M.B.d.M., Y.A., T.L.H.D., Y.I., R.A.P.-G., T.Z., A.C.D., J.B.J., P.O.S.T., T.A.T., H.A., F.A., S.M., P.T.K.C., L.A.A., T. Dada., T.T.L., M.S.A., N.K., B.W., Y.Y.A., J.M.-N., S.V., S.S., R.H., A.J., M.B., D.G., D.H.S., H.W., V.K.Y., L.W.Y., T.B.T., M.M., T.T.N., E.U.L., K.-H.P., W.A.W., R.S.K., C.T., Y.K., S.S.T., K.P., J.F.S., Y.H.S., A.F., M.O., J.S.M.L., V.T., C.C. Khaing., T.M., S.N., C.-Y.K., G.T., S.F., R.W., H.M., T.T.G.N., T.D.T., M.U., J.M.M., N.R., Y.M.A., R.D.R., S.A.V., S.K.F., Z.X., X.Y.C., J.N.F., K.S.S., T.T.W., D.T.Q., R.V., S. Kavitha., S.R.K., N. Soumittra., B.S., B.-A.L., J.O., J.P.C.d.V., V.P.C., R.Y.A., B.B.d.S., C.C.S., M.C.A., E.K.-J., G.B.F., V.C.T., R.F., Y.J., N. Waseem., S.L., H.N.P., S.A.-S., E.R.C., M.I.K., R. Dada., K. Mohanty., M.A.F., A.W.H., K.P.B., E.H.G., A.P., T.P., M.A.T.C., I.R.F., C.S.L., E.R., V.W.I., G.C., G.P., C.L., P.R., L.M., S.C., J.C.H.C., B.N.K.C., J.W.H.S., H.M.T., K.T.O., A.T.H., V.H.Y., X.-Y.N., F.P., D.P., P.F., J.J.W., P.M., J.H.F., R.R.A., M.A.H., R. Stead., R. Quino., S.N.Z., U.L., R. Shetty., M.Z., H.W.B., N.L.O., T.K., A.M., W.L.H., L.D., Y.H.H., C.A.K., M.K., Z.E.D., J.I.M.P., A.G., J.W.J., T.S.H., N. Srisamran, T.S., S.H.S., V.H.D., S.S.B., C.-L.H., D.T.T., R. Sihota., S.-C.L., K. Mori., S. Kinoshita., A.I.d.H., R. Qamar., Y.-X.W., Y.Y.T., E.-S.T., C.H.-M., D.L.-G., S.M.S., C.-Y.C., J.C.Z., C.P.P., H.T.T.B., O.H., J.E.C., D.P.E., M.Y., J.M.N., M.L.G.-F., L.X., R.R., A.T.L.-S., T.Y.W., S.A.-O., N.H.D., P.S., C.C.T., P.J.F., L.V., K.T., E.N.V., and N. Wang were responsible for sample collection, data analysis, and sample administration. M.L.H., M.S., E.P., S.J.D., N.V.V.C., J.B., Y.X.Z., A.K., S.T.L., S.H.C., R.P.E., A.S., K.H.P., J.A., G.B., H. Snippe., and B.B. contributed control data sets with genome-wide genotyping data. M.-C.L., A.S.C., S.R.G., Y.F.C., and E.N.V. were responsible for molecular biology work and pathological tissue staining and interpretation. The manuscript was written by C.C. Khor, with approval from all authors. All authors read and approved the final version of the manuscript for publication. T.A. was responsible for obtaining financial support for the study.

COMPETING FINANCIAL INTERESTS

The authors declare no competing financial interests.

1. Vithana, E.N. *et al.* Genome-wide association analyses identify three new susceptibility loci for primary angle closure glaucoma. *Nat. Genet.* **44**, 1142–1146 (2012).

2. Thylefors, B., Négrel, A.D., Pararajasegaram, R. & Dadzie, K.Y. Global data on blindness. *Bull. World Health Organ.* **73**, 115–121 (1995).
3. Hysi, P.G. *et al.* Genome-wide analysis of multi-ancestry cohorts identifies new loci influencing intraocular pressure and susceptibility to glaucoma. *Nat. Genet.* **46**, 1126–1130 (2014).
4. Gharahkhani, P. *et al.* Common variants near *ABCA1*, *AFAP1* and *GMDS* confer risk of primary open-angle glaucoma. *Nat. Genet.* **46**, 1120–1125 (2014).
5. Wiggs, J.L. *et al.* Common variants at 9p21 and 8q22 are associated with increased susceptibility to optic nerve degeneration in glaucoma. *PLoS Genet.* **8**, e1002654 (2012).
6. Aung, T. *et al.* A common variant mapping to *CACNA1A* is associated with susceptibility to exfoliation syndrome. *Nat. Genet.* **47**, 387–392 (2015).
7. Foster, P.J., Buhrmann, R., Quigley, H.A. & Johnson, G.J. The definition and classification of glaucoma in prevalence surveys. *Br. J. Ophthalmol.* **86**, 238–242 (2002).
8. Cheng, J.W., Zong, Y., Zeng, Y.Y. & Wei, R.L. The prevalence of primary angle closure glaucoma in adult Asians: a systematic review and meta-analysis. *PLoS One* **9**, e103222 (2014).
9. Quigley, H.A. & Broman, A.T. The number of people with glaucoma worldwide in 2010 and 2020. *Br. J. Ophthalmol.* **90**, 262–267 (2006).
10. Foster, P.J. & Johnson, G.J. Glaucoma in China: how big is the problem? *Br. J. Ophthalmol.* **85**, 1277–1282 (2001).
11. Foster, P.J. *et al.* The prevalence of glaucoma in Chinese residents of Singapore: a cross-sectional population survey of the Tanjong Pagar district. *Arch. Ophthalmol.* **118**, 1105–1111 (2000).
12. Dandona, L. *et al.* Angle-closure glaucoma in an urban population in southern India. The Andhra Pradesh eye disease study. *Ophthalmology* **107**, 1710–1716 (2000).
13. Quigley, H.A., Congdon, N.G. & Friedman, D.S. Glaucoma in China (and worldwide): changes in established thinking will decrease preventable blindness. *Br. J. Ophthalmol.* **85**, 1271–1272 (2001).
14. Purdue, M.P. *et al.* Genome-wide association study of renal cell carcinoma identifies two susceptibility loci on 2p21 and 11q13.3. *Nat. Genet.* **43**, 60–65 (2011).
15. International Parkinson Disease Genomics Consortium. Imputation of sequence variants for identification of genetic risks for Parkinson's disease: a meta-analysis of genome-wide association studies. *Lancet* **377**, 641–649 (2011).
16. Ellinor, P.T. *et al.* Meta-analysis identifies six new susceptibility loci for atrial fibrillation. *Nat. Genet.* **44**, 670–675 (2012).
17. Gudbjartsson, D.F. *et al.* A sequence variant in *ZFHX3* on 16q22 associates with atrial fibrillation and ischemic stroke. *Nat. Genet.* **41**, 876–878 (2009).
18. Pomerantz, M.M. *et al.* The 8q24 cancer risk variant rs6983267 shows long-range interaction with *MYC* in colorectal cancer. *Nat. Genet.* **41**, 882–884 (2009).
19. Tuupanen, S. *et al.* The common colorectal cancer predisposition SNP rs6983267 at chromosome 8q24 confers potential to enhanced Wnt signaling. *Nat. Genet.* **41**, 885–890 (2009).
20. Gregorio-King, C.C. *et al. MERP1*: a mammalian ependymin-related protein gene differentially expressed in hematopoietic cells. *Gene* **286**, 249–257 (2002).
21. Dolmans, G.H. *et al.* Wnt signaling and Dupuytren's disease. *N. Engl. J. Med.* **365**, 307–317 (2011).
22. Barone, R. *et al.* DPM2-CDG: a muscular dystrophy–dystroglycanopathy syndrome with severe epilepsy. *Ann. Neurol.* **72**, 550–558 (2012).
23. Wang, D.Y., Fulthorpe, R., Liss, S.N. & Edwards, E.A. Identification of estrogen-responsive genes by complementary deoxyribonucleic acid microarray and characterization of a novel early estrogen-induced gene: *EEIG1*. *Mol. Endocrinol.* **18**, 402–411 (2004).
24. Shi, L. *et al.* Overexpression of PIP5KL1 suppresses cell proliferation and migration in human gastric cancer cells. *Mol. Biol. Rep.* **37**, 2189–2198 (2010).
25. Lachkar, Y. & Bouassida, W. Drug-induced acute angle closure glaucoma. *Curr. Opin. Ophthalmol.* **18**, 129–133 (2007).
26. Mandak, J.S., Minerva, P., Wilson, T.W. & Smith, E.K. Angle closure glaucoma complicating systemic atropine use in the cardiac catheterization laboratory. *Cathet. Cardiovasc. Diagn.* **39**, 262–264 (1996).
27. Shen, Z. *et al.* Novel focal adhesion protein kindlin-2 promotes the invasion of gastric cancer cells through phosphorylation of integrin β1 and β3. *J. Surg. Oncol.* **108**, 106–112 (2013).
28. Kim, Y.S., Nakanishi, G., Lewandoski, M. & Jetten, A.M. GLIS3, a novel member of the GLIS subfamily of Krüppel-like zinc finger proteins with repressor and activation functions. *Nucleic Acids Res.* **31**, 5513–5525 (2003).
29. Senée, V. *et al.* Mutations in *GLIS3* are responsible for a rare syndrome with neonatal diabetes mellitus and congenital hypothyroidism. *Nat. Genet.* **38**, 682–687 (2006).
30. Barrett, J.C. *et al.* Genome-wide association study and meta-analysis find that over 40 loci affect risk of type 1 diabetes. *Nat. Genet.* **41**, 703–707 (2009).
31. Cho, Y.S. *et al.* Meta-analysis of genome-wide association studies identifies eight new loci for type 2 diabetes in east Asians. *Nat. Genet.* **44**, 67–72 (2012).
32. Dupuis, J. *et al.* New genetic loci implicated in fasting glucose homeostasis and their impact on type 2 diabetes risk. *Nat. Genet.* **42**, 105–116 (2010).
33. Burdon, K.P. *et al.* Genome-wide association study identifies susceptibility loci for open angle glaucoma at *TMCO1* and *CDKN2B-AS1*. *Nat. Genet.* **43**, 574–578 (2011).
34. Chen, Y. *et al.* Common variants near *ABCA1* and in *PMM2* are associated with primary open-angle glaucoma. *Nat. Genet.* **46**, 1115–1119 (2014).
35. Li, Z. *et al.* A common variant near *TGFBR3* is associated with primary open angle glaucoma. *Hum. Mol. Genet.* **24**, 3880–3892 (2015).
36. Nongpiur, M.E. *et al.* Lack of association between primary angle-closure glaucoma susceptibility loci and the ocular biometric parameters anterior chamber depth and axial length. *Invest. Ophthalmol. Vis. Sci.* **54**, 5824–5828 (2013).
37. Cheng, C.Y. *et al.* Nine loci for ocular axial length identified through genome-wide association studies, including shared loci with refractive error. *Am. J. Hum. Genet.* **93**, 264–277 (2013).
38. Nongpiur, M.E. *et al. ABCC5*, a gene that influences the anterior chamber depth, is associated with primary angle closure glaucoma. *PLoS Genet.* **10**, e1004089 (2014).
39. Boyle, A.P. *et al.* Annotation of functional variation in personal genomes using RegulomeDB. *Genome Res.* **22**, 1790–1797 (2012).
40. Ward, L.D. & Kellis, M. HaploReg: a resource for exploring chromatin states, conservation, and regulatory motif alterations within sets of genetically linked variants. *Nucleic Acids Res.* **40**, D930–D934 (2012).
41. ENCODE Project Consortium. An integrated encyclopedia of DNA elements in the human genome. *Nature* **489**, 57–74 (2012).
42. Westra, H.J. *et al.* Systematic identification of *trans* eQTLs as putative drivers of known disease associations. *Nat. Genet.* **45**, 1238–1243 (2013).
43. GTEx Consortium. The Genotype-Tissue Expression (GTEx) project. *Nat. Genet.* **45**, 580–585 (2013).
44. Fairfax, B.P. *et al.* Genetics of gene expression in primary immune cells identifies cell type–specific master regulators and roles of HLA alleles. *Nat. Genet.* **44**, 502–510 (2012).
45. Okada, Y. *et al.* Genetics of rheumatoid arthritis contributes to biology and drug discovery. *Nature* **506**, 376–381 (2014).
46. Speliotes, E.K. *et al.* Association analyses of 249,796 individuals reveal 18 new loci associated with body mass index. *Nat. Genet.* **42**, 937–948 (2010).

Chiea Chuen Khor[1–3,124], Tan Do[4,124], Hongyan Jia[5,124], Masakazu Nakano[6,124], Ronnie George[7,124], Khaled Abu-Amero[8,9,124], Roopam Duvesh[10,124], Li Jia Chen[11,124], Zheng Li[1], Monisha E Nongpiur[2], Shamira A Perera[2], Chunyan Qiao[5], Hon-Tym Wong[12], Hiroshi Sakai[13], Mônica Barbosa de Melo[14], Mei-Chin Lee[2], Anita S Chan[2], Yaakub Azhany[15], Thi Lam Huong Dao[4], Yoko Ikeda[16], Rodolfo A Perez-Grossmann[17], Tomasz Zarnowski[18], Alexander C Day[19–21], Jost B Jonas[22], Pancy O S Tam[11], Tuan Anh Tran[23], Humaira Ayub[24], Farah Akhtar[25], Shazia Micheal[26], Paul T K Chew[27], Leyla A Aljasim[28], Tanuj Dada[29], Tam Thi Luu[30], Mona S Awadalla[31], Naris Kitnarong[32], Boonsong Wanichwecharungruang[33,34], Yee Yee Aung[35], Jelinar Mohamed-Noor[36], Saravanan Vijayan[10], Sripriya Sarangapani[37], Rahat Husain[2,38], Aliza Jap[2,38], Mani Baskaran[2], David Goh[2], Daniel H Su[2], Huaizhou Wang[5], Vernon K Yong[12], Leonard W Yip[12], Tuyet Bach Trinh[23], Manchima Makornwattana[39], Thanh Thu Nguyen[40], Edgar U Leuenberger[41,42], Ki-Ho Park[43], Widya Artini Wiyogo[44,45], Rajesh S Kumar[46], Celso Tello[47], Yasuo Kurimoto[48], Suman S Thapa[49], Kessara Pathanapitoon[50], John F Salmon[51], Yong Ho Sohn[52], Antonio Fea[53], Mineo Ozaki[54,55], Jimmy S M Lai[56], Visanee Tantisevi[57], Chaw Chaw Khaing[58], Takanori Mizoguchi[59], Satoko Nakano[60], Chan-Yun Kim[61], Guangxian Tang[62], Sujie Fan[63], Renyi Wu[64], Hailin Meng[65], Thi Thuy Giang Nguyen[4], Tien Dat Tran[4], Morio Ueno[16], Jose Maria Martinez[66], Norlina Ramli[67,68], Yin Mon Aung[69,70], Rigo Daniel Reyes[71,72],

Stephen A Vernon[73,74], Seng Kheong Fang[75], Zhicheng Xie[1], Xiao Yin Chen[1], Jia Nee Foo[1], Kar Seng Sim[1], Tina T Wong[2], Desmond T Quek[2], Rengaraj Venkatesh[76], Srinivasan Kavitha[76], Subbiah R Krishnadas[77], Nagaswamy Soumittra[37], Balekudaru Shantha[7], Boon-Ang Lim[12], Jeanne Ogle[12], José P C de Vasconcellos[78], Vital P Costa[77], Ricardo Y Abe[77], Bruno B de Souza[14], Chelvin C Sng[27], Maria C Aquino[27], Ewa Kosior-Jarecka[18], Guillermo Barreto Fong[79], Vania Castro Tamanaja[80], Ricardo Fujita[81], Yuzhen Jiang[19–21], Naushin Waseem[19,21], Sancy Low[19–21], Huan Nguyen Pham[23], Sami Al-Shahwan[28], E Randy Craven[28,82], Muhammad Imran Khan[83], Rrima Dada[29], Kuldeep Mohanty[29], Muneeb A Faiq[29], Alex W Hewitt[84,85], Kathryn P Burdon[31,84], Eng Hui Gan[36], Anuwat Prutthipongsit[39], Thipnapa Patthanathamrongkasem[39], Mary Ann T Catacutan[41], Irene R Felarca[41], Chona S Liao[41], Emma Rusmayani[44], Vira Wardhana Istiantoro[44], Giulia Consolandi[53], Giulia Pignata[53], Carlo Lavia[53], Prin Rojanapongpun[57], Lerprat Mangkornkanokpong[86], Sunee Chansangpetch[86], Jonathan C H Chan[87], Bonnie N K Choy[56], Jennifer W H Shum[56], Hlaing May Than[88], Khin Thida Oo[69,70], Aye Thi Han[69,70], Victor H Yong[2], Xiao-Yu Ng[2], Shuang Ru Goh[2], Yaan Fun Chong[2], Martin L Hibberd[1], Mark Seielstad[89], Eileen Png[1], Sarah J Dunstan[90,91], Nguyen Van Vinh Chau[92], Jinxin Bei[93,94], Yi Xin Zeng[93–95], Abhilasha Karkey[96], Buddha Basnyat[96], Francesca Pasutto[97], Daniela Paoli[98], Paolo Frezzotti[99], Jie Jin Wang[100], Paul Mitchell[100], John H Fingert[101,102], R Rand Allingham[2,103], Michael A Hauser[2,103,104], Soon Thye Lim[105], Soo Hong Chew[106], Richard P Ebstein[107], Anavaj Sakuntabhai[108,109], Kyu Hyung Park[110], Jeeyun Ahn[111], Greet Boland[112], Harm Snippe[112], Richard Stead[73], Raquel Quino[71], Su Nyunt Zaw[69,70], Urszula Lukasik[18], Rohit Shetty[46], Mimiwati Zahari[67,68], Hyoung Won Bae[61], Nay Lin Oo[58], Toshiaki Kubota[60], Anita Manassakorn[57], Wing Lau Ho[86], Laura Dallorto[53], Young Hoon Hwang[52], Christine A Kiire[51], Masako Kuroda[48], Zeiras Eka Djamal[44], Jovell Ian M Peregrino[41], Arkasubhra Ghosh[46,113], Jin Wook Jeoung[43], Tung S Hoan[40], Nuttamon Srisamran[39], Thayanithi Sandragasu[36], Saw Htoo Set[35], Vi Huyen Doan[30], Shomi S Bhattacharya[21], Ching-Lin Ho[2], Donald T Tan[2], Ramanjit Sihota[29], Seng-Chee Loon[27], Kazuhiko Mori[16], Shigeru Kinoshita[16], Anneke I den Hollander[26,83], Raheel Qamar[24,114], Ya-Xing Wang[115], Yik Y Teo[1,116–119], E-Shyong Tai[116,120], Curt Hartleben-Matkin[121], David Lozano-Giral[122], Seang Mei Saw[2,116], Ching-Yu Cheng[2,27], Juan C Zenteno[122,123], Chi Pui Pang[11], Huong T T Bui[23], Owen Hee[12], Jamie E Craig[31], Deepak P Edward[28,82], Michiko Yonahara[13], Jamil Miguel Neto[78], Maria L Guevara-Fujita[81], Liang Xu[115], Robert Ritch[47], Ahmad Tajudin Liza-Sharmini[15], Tien Y Wong[2], Saleh Al-Obeidan[8], Nhu Hon Do[4,125], Periasamy Sundaresan[10,125], Clement C Tham[11,125], Paul J Foster[19–21,125], Lingam Vijaya[2,7,125], Kei Tashiro[6,125], Eranga N Vithana[2,125], Ningli Wang[5,115,125] & Tin Aung[2,27,125]

[1]Genome Institute of Singapore, A-STAR, Singapore. [2]Singapore Eye Research Institute, Singapore National Eye Centre and Eye ACP, Duke–National University of Singapore, Singapore. [3]Department of Biochemistry, National University of Singapore, Singapore. [4]Vietnam National Institute of Ophthalmology, Hanoi, Vietnam. [5]Beijing Tongren Eye Center, Beijing Tongren Hospital, Capital Medical University, Beijing Ophthalmology and Visual Science Key Laboratory, Beijing, China. [6]Department of Genomic Medical Sciences, Kyoto Prefectural University of Medicine, Kyoto, Japan. [7]Jadhavbhai Nathamal Singhvi Department of Glaucoma, Medical Research Foundation, Sankara Nethralaya, Chennai, India. [8]Department of Ophthalmology, College of Medicine, King Saud University, Riyadh, Saudi Arabia. [9]Department of Ophthalmology, College of Medicine, University of Florida, Jacksonville, Florida, USA. [10]Department of Genetics, Aravind Medical Research Foundation, Madurai, India. [11]Department of Ophthalmology and Visual Sciences, Chinese University of Hong Kong, Hong Kong, China. [12]Department of Ophthalmology, Tan Tock Seng Hospital, NHG Eye Institute, Singapore. [13]Department of Ophthalmology, University of the Ryukyus, Okinawa, Nishihara, Japan. [14]Center of Molecular Biology and Genetic Engineering, University of Campinas, Campinas, Brazil. [15]Department of Ophthalmology, School of Medical Sciences, Health Campus, Universiti Sains Malaysia and Hospital Universiti Sains Malaysia, Kelantan, Malaysia. [16]Department of Ophthalmology, Kyoto Prefectural University of Medicine, Kyoto, Japan. [17]Instituto de Glaucoma y Catarata, Lima, Peru. [18]Department of Diagnostics and Microsurgery of Glaucoma, Medical University, Lublin, Poland. [19]NIHR Biomedical Research Centre for Ophthalmology at Moorfields Eye Hospital and University College London Institute of Ophthalmology, London, UK. [20]Glaucoma Service, Moorfields Eye Hospital NHS Foundation Trust, London, UK. [21]Division of Genetics, UCL Institute of Ophthalmology, London, UK. [22]Department of Ophthalmology, Medical Faculty Mannheim of the Ruprecht Karls University Heidelberg, Heidelberg, Germany. [23]Ho Chi Minh City Eye Hospital, Ho Chi Minh City, Vietnam. [24]Department of Biosciences, COMSATS Institute of Information Technology, Islamabad, Pakistan. [25]Pakistan Institute of Ophthalmology, Al-Shifa Trust Eye Hospital, Rawalpindi, Pakistan. [26]Department of Ophthalmology, Radboud University Medical Centre, Nijmegen, the Netherlands. [27]Department of Ophthalmology, National University Health System, Yong Loo Lin School of Medicine, National University of Singapore, Singapore. [28]King Khaled Eye Specialist Hospital, Riyadh, Saudi Arabia. [29]All India Institute of Medical Sciences, New Delhi, India. [30]Department of Glaucoma, Da Nang Eye Hospital, Da Nang City, Vietnam. [31]Department of Ophthalmology, Flinders University, Flinders Medical Centre, Adelaide, South Australia, Australia. [32]Department of Ophthalmology, Faculty of Medicine Siriraj Hospital, Mahidol University, Bangkok, Thailand. [33]Glaucoma Services, Department of Ophthalmology, Rajavithi Hospital, Bangkok, Thailand. [34]College of Medicine, Rangsit University, Bangkok, Thailand. [35]Mandalay Eye Department, Mandalay Eye ENT Hospital, University of Medicine Mandalay, Mandalay, Myanmar. [36]Department of Ophthalmology, Hospital Kuala Lumpur, Kuala Lumpur, Malaysia. [37]Vision Research Foundation, Sankara Nethralaya, Chennai, India. [38]Division of Ophthalmology, Changi General Hospital, Singapore. [39]Department of Ophthalmology, Thammasat University Faculty of Medicine, Rangsit, Thailand. [40]Eye Department, Viet Tiep General Hospital, Hai Phong, Vietnam. [41]Asian Eye Institute, Manila, Philippines. [42]Division of Ophthalmology, University of the East, Manila, Philippines. [43]Department of Ophthalmology, Seoul National University College of Medicine, Seoul, Republic of Korea. [44]Glaucoma Service Jakarta Eye Center, Jakarta, Indonesia. [45]Faculty of Medicine, University of Indonesia, Jakarta, Indonesia. [46]Narayana Nethralaya Eye Hospital, Bangalore, India. [47]Einhorn Clinical Research Center, New York Eye and Ear Infirmary of Mount Sinai, New York, New York, USA. [48]Department of Ophthalmology, Kobe City Medical Center General Hospital, Kobe, Japan. [49]Nepal Glaucoma Eye Clinic, Tilganga Institute of Ophthalmology, Kathmandu, Nepal. [50]Department of Ophthalmology, Faculty of Medicine, Chiang Mai University, Chiang Mai, Thailand. [51]Oxford Eye Hospital, John Radcliffe Hospital, Oxford University Hospitals NHS Trust, Oxford, UK. [52]Department of Ophthalmology, Konyang University, Kim's Eye Hospital, Myung-Gok Eye Research Institute, Seoul, Republic of Korea. [53]Dipartimento di Scienze

Chirurgiche, Università di Torino, Turin, Italy. [54]Ozaki Eye Hospital, Hyuga, Japan. [55]Department of Ophthalmology, Faculty of Medicine, University of Miyazaki, Miyazaki, Japan. [56]Department of Ophthalmology, University of Hong Kong, Hong Kong, China. [57]Department of Ophthalmology, Faculty of Medicine, Chulalongkorn University, Bangkok, Thailand. [58]Department of Ophthalmology, No. 1 Defence Services General Hospital, Yangon, Myanmar. [59]Mizoguchi Eye Hospital, Sasebo, Japan. [60]Department of Ophthalmology, Oita University Faculty of Medicine, Oita, Japan. [61]Department of Ophthalmology, Yonsei University College of Medicine, Seoul, Republic of Korea. [62]Shijiazhuang First Eye Hospital, Shijiazhuang, China. [63]Handan Eye Hospital, Handan, China. [64]Eye Institute and Affiliated Xiamen Eye Center, Xiamen University, Fujian Provincial Key Laboratory of Ophthalmology and Visual Science, Xiamen, China. [65]Anyang Eye Hospital, Anyang, China. [66]Department of Ophthalmology, Pasig City General Hospital, Pasig City, Philippines. [67]University of Malaya, Eye Research Centre, Kuala Lumpur, Malaysia. [68]Department of Ophthalmology, Faculty of Medicine, University of Malaya, Kuala Lumpur, Malaysia. [69]Myanmar Eye Centre, Pun Hlaing Silom Hospital, Yangon, Myanmar. [70]Myanmar Eye Centre, Shwe La Min Hospital, Yangon, Myanmar. [71]Department of Ophthalmology/Glaucoma Section, Asian Hospital and Medical Center, Muntinlupa City, Philippines. [72]Binan Doctors Eye Center, Binan Doctors Hospital, Laguna, Philippines. [73]Department of Ophthalmology, University Hospital Nottingham, University of Nottingham, Nottingham, UK. [74]BMI Park Hospital Nottingham, Nottingham, UK. [75]International Specialist Eye Centre, Kuala Lumpur, Malaysia. [76]Glaucoma Clinic, Aravind Eye Hospital, Pondicherry, India. [77]Glaucoma Clinic, Aravind Eye Hospital, Madurai, India. [78]Department of Ophthalmology, Faculty of Medical Sciences, University of Campinas, Campinas, Brazil. [79]Instituto de Ciencias Médicas, Lima, Peru. [80]Hospital Nacional Arzobispo Loayza, Lima, Peru. [81]Centro de Genética y Biología Molecular, Universidad de San Martín de Porres, Lima, Peru. [82]Wilmer Eye Institute, Johns Hopkins Hospital School of Medicine, Baltimore, Maryland, USA. [83]Department of Human Genetics, Radboud University Medical Centre, Nijmegen, the Netherlands. [84]Menzies Institute for Medical Research, University of Tasmania, Hobart, Tasmania, Australia. [85]Centre for Eye Research Australia, University of Melbourne, Royal Victorian Eye and Ear Hospital, Melbourne, Victoria, Australia. [86]Department of Ophthalmology, King Chulalongkorn Memorial Hospital, Bangkok, Thailand. [87]Department of Ophthalmology, Queen Mary Hospital, Hong Kong, China. [88]Department of Ophthalmology, North Okkalarpa General Hospital, Yangon, Myanmar. [89]Institute for Human Genetics, University of California, San Francisco, San Francisco, California, USA. [90]Oxford University Clinical Research Unit, Ho Chi Minh City, Vietnam. [91]Peter Doherty Institute for Infection and Immunity, University of Melbourne, Melbourne, Victoria, Australia. [92]Hospital for Tropical Diseases, Ho Chi Minh City, Vietnam. [93]Sun Yat-Sen University Cancer Center, State Key Laboratory of Oncology in South China, Collaborative Innovation Center for Cancer Medicine, Guangzhou, China. [94]Department of Experimental Research, Sun Yat-sen University Cancer Center, Guangzhou, China. [95]Peking Union Medical College, Beijing, China. [96]Oxford University Clinical Research Unit–Nepal, Patan Academy of Health Sciences, Patan Hospital, Patan, Nepal. [97]Institute of Human Genetics, Friedrich Alexander Universität Erlangen-Nürnberg (FAU), Erlangen, Germany. [98]Department of Ophthalmology, Monfalcone Hospital, Gorizia, Italy. [99]Department of Surgery, Section of Ophthalmology, University of Siena, Siena, Italy. [100]Centre for Vision Research, Department of Ophthalmology, Westmead Institute for Medical Research, University of Sydney, Sydney, New South Wales, Australia. [101]Department of Ophthalmology and Visual Sciences, Carver College of Medicine, University of Iowa, Iowa City, Iowa, USA. [102]Wynn Institute for Vision Research, University of Iowa, Iowa City, Iowa, USA. [103]Department of Ophthalmology, Duke University Eye Center, Durham, North Carolina, USA. [104]Department of Medicine, Duke University Medical Center, Durham, North Carolina, USA. [105]Division of Medical Oncology, National Cancer Centre, Singapore. [106]Department of Economics, National University of Singapore, Singapore. [107]Department of Psychology, National University of Singapore, Singapore. [108]Institut Pasteur, Functional Genetics of Infectious Diseases Unit, Department of Genomes and Genetics, Paris, France. [109]Centre National de la Recherche Scientifique, Unité de Recherche Associée 3012, Paris, France. [110]Department of Ophthalmology, Seoul National University Bundang Hospital, Gyeonggi, Republic of Korea. [111]Department of Ophthalmology, Seoul Metropolitan Government Seoul National University Boramae Medical Center, Seoul, Republic of Korea. [112]Department of Medical Microbiology and Virology, University Medical Center Utrecht, Utrecht, the Netherlands. [113]GROW Research Laboratory, Narayana Nethralaya Foundation, Bangalore, India. [114]Department of Biochemistry, Al-Nafees Medical College and Hospital, Isra University, Islamabad, Pakistan. [115]Beijing Institute of Ophthalmology, Beijing Tongren Hospital, Capital Medical University, Beijing, China. [116]Saw Swee Hock School of Public Health, National University of Singapore, Singapore. [117]Life Sciences Institute, National University of Singapore, Singapore. [118]National University of Singapore Graduate School for Integrative Science and Engineering, National University of Singapore, Singapore. [119]Department of Statistics and Applied Probability, National University of Singapore, Singapore. [120]Department of Medicine, Yong Loo Lin School of Medicine, National University of Singapore, Singapore. [121]Department of Glaucoma, Institute of Ophthalmology 'Conde de Valenciana', Mexico City, Mexico. [122]Department of Genetics, Institute of Ophthalmology 'Conde de Valenciana', Mexico City, Mexico. [123]Department of Biochemistry, Faculty of Medicine, Universidad Nacional Autónoma de México, Mexico City, Mexico. [124]These authors contributed equally to this work. [125]These authors jointly directed this work. Correspondence should be addressed to C.C. Khor (khorcc@gis.a-star.edu.sg), N. Wang (wningli@vip.163.com) or T.A. (aung_tin@yahoo.co.uk).

ONLINE METHODS

Patient collections. DNA samples from all PACG cases and controls were collected after written informed consent was obtained from each participant, strictly in accordance with the tenets of the Declaration of Helsinki. Details for each case–control collection are provided in the **Supplementary Note**.

Genotyping. For the GWAS discovery stage, genome-wide genotyping was performed using the Illumina 610K/660W and OmniExpress BeadChips following the manufacturer's instructions and as previously described[1].

For the replication stage, the most significantly associated SNPs from the discovery stage were genotyped using Applied Biosystems TaqMan genotyping assays as well as the Sequenom MassARRAY system, as previously described[47]. We performed cross-platform concordance checks and verified > 99.9% concordance of genotypes for the SNP markers surpassing genome-wide significance reported here.

Statistical analysis. Stringent quality checks were performed on a per-SNP and per-sample basis, with removal of SNPs showing a genotyping success rate of <95% or a MAF of <1%, as well as deviation from Hardy–Weinberg equilibrium ($P < 1 \times 10^{-6}$ for deviation). Samples were similarly checked, and those with a genotyping success rate of <95% were removed, as were those showing excesses heterozygosity and outliers on principal-component analysis of genetic ancestry. PACG cases were contrasted to ancestry- and geographically matched controls for each country strata, as is now routinely done in GWAS[48–50]. PACG cases and controls appeared to be well matched in terms of ancestry for each stratum, as well as in overall assessment (**Fig. 1** and **Supplementary Figs. 10** and **11**). In the discovery stage, we analyzed a total of 745,080 SNPs with direct genotyping and > 4,500,000 SNPs with imputation. The relationship between each variable genetic SNP marker and PACG disease was measured using logistic regression with further adjustments for principal components of genetic stratification. We observed minimal overall genomic inflation in each of the discovery sample collections and in the discovery meta-analysis (overall λ_{GC} for the meta-analysis = 1.05; **Supplementary Fig. 12** and **Supplementary Table 1**). We then performed a meta-analysis of all the discovery-stage PACG collections, summarizing the data across the 16 case–control strata (**Supplementary Table 1**) using random-effects meta-analysis. We used the random-effects model to provide for more robust estimation of *P* values and odds ratios in the discovery stage because of the ancestrally and geographically diverse patient collections. Such an approach allows us the best chance of identifying PACG susceptibility variants shared by most of the ancestry groups.

The biological relationships of all remaining samples were then verified using the principle of variability in allele sharing. Identity-by-state information from comparisons of each sample pair was derived using PLINK software (see URLs). For each pair of individuals showing evidence of cryptic relatedness (possibly due either to inadvertent sample duplication or biologically related samples), we excluded the sample with the lower call rate from further analysis. Principal-component analysis was then undertaken to minimize spurious associations due to ancestry differences between PACG cases and controls. Plots of principal components were generated using the R statistical package (see URLs).

For both the GWAS discovery and replication stages, the association between SNP genotypes and PACG disease status was measured using score-based tests (1 degree of freedom). These general tests model additive effects of the minor allele on disease risk. They do not assume any mode of inheritance and are well described elsewhere. Each SNP genotype is coded according to allele dosage: 0 for individuals with the wild-type genotype for a given SNP, 1 for individuals heterozygous for the alternate allele, and 2 for individuals homozygous for the alternate allele.

In the GWAS discovery stage, the association analysis was also adjusted for the principal components of genetic stratification for sample collections where residual population stratification existed. Details on the overall genomic inflation factor and number of principal components used for adjustment in each of the GWAS discovery collections are provided in **Supplementary Table 1**. The genome-wide association summary statistics for all SNP markers with direct microarray genotyping together with imputation fine-mapping of the significant loci are provided as the **Supplementary Data Set**.

As the replication stage only tested a limited number of SNP markers, we were unable to adjust for population stratification in this stage. Nonetheless, association tests were performed for each stratum separately, and the cohorts were subsequently combined in meta-analysis. Meta-analysis was conducted using inverse-variance weights for each PACG case–control collection, which calculates an overall *z* statistic, its corresponding *P* value, and accompanying odds ratios for each SNP analyzed. All *P* values reported here are two-tailed.

At each locus, the sentinel SNP is defined as the most significant directly genotyped SNP within that locus. Independent loci are defined as loci with no LD between them (pairwise r^2 <0.01) and are located more than 1 Mb apart from one another.

Genotype imputation. To improve the genetic resolution beyond that provided by the directly genotyped SNPs present on standard-content GWAS arrays, we performed imputation for the GWAS discovery sample collections using samples and SNP markers passing standard GWAS quality control checks. The imputation and phasing of genotypes were carried out using IMPUTE2 software (see URLs) with a reference panel constructed from cosmopolitan population haplotypes based on data obtained for 2,535 individuals from 26 distinct populations around the world. These data are part of the 1000 Genomes Project Phase 3 (June 2014) release. Imputed genotypes were called with an IMPUTE probability threshold of 0.90, with all other genotypes classified as missing. We applied additional quality control filters to exclude SNP markers with a call rate of <99% should the SNP have a MAF of <5% in either cases or controls. For common SNPs with MAF > 5%, the filtering criterion was set to exclude SNPs with a call rate of <95%.

Power calculation. All statistical power calculations were performed as previously described for two-stage GWAS and replication studies[50]. We present these power calculations for each of the following conditions: (i) GWAS discovery stage only and (ii) GWAS discovery and replication stages (**Supplementary Table 4**).

Expression analysis. Expression of *EPDR1*, *GLIS3*, *DPM2*, *FAM102A*, *PIP5KL1*, and *FERMT2* was assessed by semiquantitative RT–PCR using gene-specific primers (**Supplementary Table 11**) on the following human ocular tissues: sclera, cornea, lens with lens capsule, iris, trabecular meshwork, ciliary body, retina, choroid, optic nerve head, and optic nerve. Human donor eyes were obtained from the Florida Lions Eye Banks and dissected into respective ocular regions for RNA extraction and semiquantitative RT–PCR expression analysis. Ethical approval for this section of the study was granted by the Institutional Review Board of the Singapore Eye Research Institute for donor eyes procured from the Florida Lions Eye Bank. All of the investigated genes produced multiple transcripts through alternative splicing that resulted in several protein isoforms. In this study, we investigated the mRNA expression of the full-length or leading transcript that produced the 'canonical' protein isoform (**Supplementary Table 11**). The NCBI reference sequence from which the primer sequences were derived is indicated for each gene. Primers were selected specifically to target the mRNA and not the genomic DNA of the genes examined. All gene-specific primers therefore spanned an intron, and the sizes of the PCR products obtained (*EPDR1*, 210 bp; *GLIS3*, 247 bp; *DPM2*, 218 bp; *FAM102A*, 155 bp; *PIP5KL1*, 189 bp; *FERMT2*, 159 bp) confirmed the amplification of mRNA. We were unable to successfully amplify a specific PCR product for the *CHAT* gene despite multiple attempts. The ocular expression of CHAT protein was therefore investigated through immunoblot and immunohistochemistry analyses in ocular tissues. Total RNA was extracted from a variety of ocular tissues (sclera, cornea, iris, trabecular meshwork, ciliary body, lens and capsule, retina, choroid, optic nerve head, and optic nerve) with TRIzol reagent (Invitrogen) in accordance with the manufacturer's protocol. First-strand cDNA synthesis was performed with the SuperScript First-Strand Synthesis System for RT–PCR (Invitrogen) using random primers. Semiquantitative RT–PCR was performed according to the manufacturer's protocol, with SYBR Green Mastermix (Invitrogen) using the specified gene primers and equal amounts of cDNA template. The resulting PCR products were separated on a 2%

agarose gel and visualized by ethidium bromide staining. The ubiquitously expressed β-actin (*ACTB*) gene (primers listed in **Supplementary Table 11**) was used as an amplification and normalizing control. All RT–PCR products were resequenced to confirm that the correct template was targeted by the primer pair selected for each gene. Semiquantitative RT–PCR was performed in triplicate to confirm the expression results, and a representative image of each agarose gel is shown.

Immunoblotting. A human non-pigmented ciliary epithelial (NPCE) cell line was provided by M. Coca-Prados (Yale School of Medicine); a human trabecular meshwork (HTM) cell line was purchased from PromoCell; and a human cervical adenocarcinoma cell line (HeLa S), a human breast adenocarcinoma cell line (MCF-7), and a human embryonic kidney epithelial cell line (HEK293) together with a human retinal pigment epithelial cell line (APRE-19) were obtained from the American Type Culture Collection. All cell lines were tested for mycoplasma and were found to be negative. Cell lysates were generated by lysing individual cell lines with lysis buffer (50 mM Tris-HCl, pH 8, 150 mM NaCl, 1.0% Nonidet P-40, 0.5% deoxycholate, 0.1% SDS, 0.2 mM sodium orthovanadate, 10 mM sodium fluoride, 0.4 mM EDTA, and 10% glycerol). Proteins were resolved by SDS–PAGE and transferred to HyBond-C Extra nitrocellulose membranes (Amersham Life Science). Membranes were blocked in 5% nonfat milk with 10% BSA and 0.1% Tween-20 in Tris-buffered saline (20 mM Tris-HCl, pH 7.6 and 150 mM NaCl) for 1 h before incubation with antibody to choline acetyltransferase (1:500 dilution) from Pierce (PA1-9027; RI); antibody to ependymin-related protein 1 (zebrafish) (EPDR1) (1:500 dilution) from antibodies-online (AA 38-225); antibody to GLIS3 (1:250 dilution) from Sigma-Aldrich (HPA056426); antibody to FERMT2 (1:250 dilution) from Sigma-Aldrich (HPA040505); antibody to DPM2 (1:250 dilution) from Sigma-Aldrich (SAB1104864); antibody to FAM102A (1:250 dilution) from Novus Biologicals (NBP1-88808); antibody to PIP5KL1 (1:250 dilution) from Novus Biologicals (NBP2-29992); and antibody to GAPDH (1:50,000 dilution) from Santa Cruz Biotechnology (sc-25778). Blocking and blotting with antibodies were performed in 5% nonfat milk with 10% BSA and 0.1% Tween-20 in PBS for 1 h each. Horseradish peroxidase (HRP)-conjugated secondary antibodies (GE Healthcare Biosciences) were applied to detect the bound primary antibodies, and signal was visualized with Luminata Forte Western HRP substrate (Millipore).

Immunofluorescence confocal microscopy of tissue sections. Three archival human enucleated eye globes from Singapore (Singapore General Hospital–SNEC Ophthalmic Pathology Service, SGH Department of Pathology) were retrieved for immunofluorescence analysis as normal controls. Ethical approval was provided by the Singapore Health Services Centralized Institutional Review Board. These globes were enucleated for other pathological diagnoses and did not have any intraocular disease. Immunofluorescence analysis was performed according to our previously published protocol[6]. Briefly, paraffin sections were cut at 4 μm and fished onto coated slides, before being dewaxed. Antigen retrieval was performed using Leica Bond ER2 solution for 20 min at 100 °C. Tissue sections were then blocked using 10% FBS and 0.1% Tween-20 in PBS with 1× penicillin-streptomycin for 1 h at room temperature. All primary antibodies were diluted by 1:100 with blocking buffer and incubated with sections overnight at 4 °C. Sections were subsequently labeled with FITC-conjugated (1:300 dilution) anti-mouse, anti-rabbit, or anti-goat secondary antibody (Jackson Laboratories), followed by application of Vectashield with DAPI (Vector Laboratories). Stained histology sections were then coverslipped and stored in the dark at 4 °C. Images were acquired with a Leica TCS SP8 confocal microscope (Leica Microsystems) at the Advanced Bioimaging Core at the Academia, Singapore Health Services.

47. Dunstan, S.J. *et al.* Variation at *HLA-DRB1* is associated with resistance to enteric fever. *Nat. Genet.* **46**, 1333–1336 (2014).
48. Verhoeven, V.J. *et al.* Genome-wide meta-analyses of multiancestry cohorts identify multiple new susceptibility loci for refractive error and myopia. *Nat. Genet.* **45**, 314–318 (2013).
49. Al Olama, A.A. *et al.* A meta-analysis of 87,040 individuals identifies 23 new susceptibility loci for prostate cancer. *Nat. Genet.* **46**, 1103–1109 (2014).
50. Kiryluk, K. *et al.* Discovery of new risk loci for IgA nephropathy implicates genes involved in immunity against intestinal pathogens. *Nat. Genet.* **46**, 1187–1196 (2014).

doi:10.1038/ng.3540

Stronger Association of *CDKN2B-AS1* Variants in Female Normal-Tension Glaucoma Patients in a Japanese Population

We read with great interest the article by Ng et al.[1] entitled "Genetic Association at the 9p21 Glaucoma Locus Contributes to Sex Bias in Normal-Tension Glaucoma," that was recently published in *Investigative Ophthalmology & Visual Science*. As the 9p21 locus was identified by a genome-wide association study (GWAS) to be associated with primary open-angle glaucoma (POAG), and the association was found to be significantly stronger among the normal-tension glaucoma (NTG) subgroup (for review see Ref. 2), Ng et al.[1] extended the analysis to investigate the influence of sex difference on the genetic association at the 9p21 locus. They carefully analyzed the genotype data of 13 variants linked with clinical information and clearly presented the results that: (1) the sex bias was present within advanced NTG cases, (2) the strongest associated variant in all POAG cases showed stronger association in females than in males with a statistically significant difference in female-to-male odds ratio (OR) comparison, and (3) the significant association was observed only in females under the NTG to high-tension glaucoma (HTG) subanalysis along with a significant difference in OR comparison. Although they used a large reliable number of samples and obtained robust results, they honestly pointed out the limitation of the study as the analyses were performed without replication using a cohort derived from a single ethnic background (i.e., Australian of European descent).

Therefore, we reanalyzed our two GWAS datasets[3,4] using our Japanese population in an attempt to assess their findings. We ended up with 975 healthy controls and 1244 POAG cases composed of 545 HTG and 699 NTG patients (HTG and NTG were denoted as HPG and NPG, respectively, in our previous article[4]) for the analysis (Table 1). Among the 13 variants at the 9p21 locus that Ng et al.[1] analyzed, we were able to directly compare the genotype data of three variants on *CDKN2B-AS1* from our previous datasets. With regard to the female-to-male analyses, we indeed observed a stronger association for all of the variants in the female patients (Table 2). Especially rs7049105, a variant in Japanese NTG patients considered to be influenced by sex, because the OR of NTG to control showed a significant heterogeneity ($P = 0.0427$) between the female and male groups (Table 2). Overall, these results suggested that although the allele frequencies of the variants slightly differs between the populations, the stronger association of the female NTG patients seen in the Australian population seemed to be replicated in our Japanese female NTG patients.

In the normal clinical setting, the female NTG patients who we encounter tend to be elderly and thin, and often possess other clinical features such as low blood pressure, myopia, migraine, neck stiffness, and so on. Not only identifying the genetic variants responsible for the disease onset by case-control association studies, but also carefully linking these phenotypes to each identified variant (as Ng et al.[1] performed for the sex difference), should greatly contribute to the elucidation of the complex etiology of glaucoma.

Kazuhiko Mori[1]
Masakazu Nakano[2]
Yuichi Tokuda[2]
Yoko Ikeda[1]
Morio Ueno[1]
Chie Sotozono[1]
Shigeru Kinoshita[1,3]
Kei Tashiro[2]

Table 1. Sample Data

Groups	*n* (mean age ± SD)		
	All	Female	Male
POAG	1244 (62.6 ± 13.6)	649 (62.9 ± 13.5)	595 (62.2 ± 13.8)
HTG	545 (64.1 ± 12.8)	255 (64.3 ± 12.9)	290 (63.9 ± 12.7)
NTG	699 (61.4 ± 14.2)	394 (62.0 ± 13.8)	305 (60.6 ± 14.6)
Control	975 (56.5 ± 14.0)	617 (57.2 ± 13.7)	358 (55.3 ± 14.4)

Table 2. Sex Comparison of CDKN2B-AS1 Variants in a Japanese Population

SNP	Female			Male			Het. *P*‡
	Allele Freq.*	*P* Value†	OR (95% CI)†	Allele Freq.*	*P* Value†	OR (95% CI)†	
POAG versus control							
rs7049105	0.692/0.615	5.38×10^{-5}	1.41 (1.19–1.66)	0.665/0.641	2.99×10^{-1}	1.11 (0.91–1.35)	0.0689
rs4977574	0.501/0.421	7.37×10^{-5}	1.37 (1.17–1.61)	0.485/0.439	4.96×10^{-2}	1.21 (1.00–1.45)	0.2705
rs1333049	0.518/0.444	2.54×10^{-4}	1.34 (1.15–1.57)	0.504/0.462	7.28×10^{-2}	1.19 (0.98–1.43)	0.3053
HTG versus control							
rs7049105	0.648/0.615	2.39×10^{-1}	1.14 (0.92–1.42)	0.649/0.641	7.86×10^{-1}	1.03 (0.82–1.30)	0.5116
rs4977574	0.478/0.421	3.92×10^{-2}	1.25 (1.01–1.53)	0.478/0.439	1.58×10^{-1}	1.17 (0.94–1.46)	0.6188
rs1333049	0.504/0.444	3.03×10^{-2}	1.26 (1.02–1.55)	0.495/0.462	2.50×10^{-1}	1.14 (0.91–1.42)	0.4782
NTG versus control							
rs7049105	0.721/0.615	1.34×10^{-6}	1.62 (1.33–1.97)	0.679/0.641	1.24×10^{-1}	1.20 (0.95–1.51)	0.0427
rs4977574	0.515/0.421	3.72×10^{-5}	1.46 (1.22–1.75)	0.492/0.439	5.10×10^{-2}	1.24 (1.00–1.54)	0.2449
rs1333049	0.527/0.444	3.05×10^{-4}	1.39 (1.16–1.67)	0.513/0.462	5.63×10^{-2}	1.24 (0.99–1.54)	0.3754

* Mean risk allele frequencies of case/control samples in each group.

† Each *P* value and Odds Ratio (OR) adjusted for our two datasets was calculated by using Cochran–Mantel–Haenszel test implemented in PLINK, version 1.07.

‡ The *P* value for OR heterogeneity between female and male in each study was calculated using the Breslow-Day test implemented in PLINK v1.07.

Investigative Ophthalmology & Visual Science

[1]Department of Ophthalmology; [2]Department of Genomic Medical Sciences; and the [3]Department of Frontier Medical Science and Technology for Ophthalmology, Kyoto Prefectural University of Medicine, Kyoto, Japan.
E-mail: shigeruk@koto.kpu-m.ac.jp or tashiro@koto.kpu-m.ac.jp

KM and MN contributed equally to the work presented here and should therefore be regarded as equivalent authors.

References

1. Ng SK, Burdon KP, Fitzgerald JT, et al. Genetic association at the 9p21 glaucoma locus contributes to sex bias in normal-tension glaucoma. *Invest Ophthalmol Vis Sci*. 2016;57:3416–3421.
2. Abu-Amero K, Kondkar AA, Chalam KV. An updated review on the genetics of primary open angle glaucoma. *Int J Mol Sci*. 2015;16:28886–28911.
3. Nakano M, Ikeda Y, Taniguchi T, et al. Three susceptible loci associated with primary open-angle glaucoma identified by genome-wide association study in Japanese population. *Proc Natl Acad Sci U S A*. 2009;106:12838–12842.
4. Nakano M, Ikeda Y, Tokuda Y, et al. Common variants in CDKN2B-AS1 associated with optic-nerve vulnerability of glaucoma identified by genome-wide association studies in Japanese. *PLoS One*. 2012;7:e33389.

Citation: *Invest Ophthalmol Vis Sci.* 2016;57:6416–6417.
doi:10.1167/iovs.16-20417

The effect of topical application of 0.15% ganciclovir gel on cytomegalovirus corneal endotheliitis

Noriko Koizumi,[1,2] Dai Miyazaki,[3] Tomoyuki Inoue,[4] Fumie Ohtani,[3] Michiko Kandori-Inoue,[3] Tsutomu Inatomi,[1] Chie Sotozono,[1] Hiroko Nakagawa,[1] Tomoko Horikiri,[1] Mayumi Ueta,[5] Takahiro Nakamura,[5] Yoshitsugu Inoue,[3] Yuichi Ohashi,[4] Shigeru Kinoshita[5]

▶ Additional material is published online only. To view please visit the journal online (http://dx.doi.org/10.1136/bjophthalmol-2015-308238).

[1]Department of Ophthalmology, Kyoto Prefectural University of Medicine, Kyoto, Japan
[2]Department of Biomedical Engineering, Faculty of Life and Medical Sciences, Doshisha University, Kyoto, Japan
[3]Division of Ophthalmology and Visual Science, Faculty of Medicine, Tottori University, Tottori, Japan
[4]Department of Ophthalmology, Ehime University School of Medicine, Ehime, Japan
[5]Department of Frontier Medical Science and Technology for Ophthalmology, Kyoto Prefectural University of Medicine, Kyoto, Japan

Correspondence to
Professor Noriko Koizumi, Department of Ophthalmology, Kyoto Prefectural University of Medicine, 465 Kajii-cho, Hirokoji-agaru, Kawaramachi-dori, Kamigyo-ku, Kyoto 602-0841, Japan; norikoiz@koto.kpu-m.ac.jp

Received 14 December 2015
Revised 13 March 2016
Accepted 10 April 2016
Published Online First 3 May 2016

To cite: Koizumi N, Miyazaki D, Inoue T, *et al*. *Br J Ophthalmol* 2017;**101**:114–119.

ABSTRACT

Background/aims The aim of this study was to evaluate the therapeutic efficacy and drug transfer of topical application of 0.15% ganciclovir (GCV) gel on cytomegalovirus (CMV) corneal endotheliitis.

Methods This study is a multicentre, prospective, interventional case series. Seven eyes of seven immunocompetent patients diagnosed with CMV corneal endotheliitis, based on clinical manifestations and qualitative PCR, were enrolled in this study. The patients were treated with topical applications of 0.15% GCV gel six times daily for 12 weeks without concomitant systemic GCV. Clinical evaluations and quantitative PCR of CMV were performed, and GCV concentrations in aqueous humour were measured by liquid chromatography/tandem mass spectrometry.

Results Clinical improvement of coin-shaped lesions, other types of keratic precipitates, corneal oedema, and anterior chamber inflammation was confirmed at the 4-week visit in all seven eyes. The GCV treatment significantly decreased the CMV copy numbers ($p<0.0001$). After 12 weeks of treatment, six eyes recovered clear corneas with good vision, and endothelial function was well maintained. Detectable levels of GCV were confirmed in the aqueous humour of all the eyes. The mean GCV concentration in the anterior chamber was 162.0±202.4 ng/mL. The re-emergence of CMV without symptoms was observed in one eye with lower drug transfer. No side effects were observed.

Conclusions Clinical improvement and reduced CMV copy numbers in the aqueous humour were confirmed in the CMV corneal endotheliitis cases. Although the case numbers are limited and long-term follow-up is necessary, the topical application of 0.15% GCV gel appears to be a useful treatment option for CMV endotheliitis.

Trial registration number UMIN000012435.

INTRODUCTION

Corneal endotheliitis, characterised by localised corneal oedema with keratic precipitates (KPs), often results in severe corneal endothelial dysfunction.[1 2] In 2006, we reported the first case of cytomegalovirus (CMV)-induced corneal endotheliitis in which CMV DNA was detected in aqueous humour by PCR and which showed a positive response to systemic ganciclovir (GCV) treatment.[3] Recently, attention has been focused on CMV as an aetiological factor of anterior segment inflammation in immunocompetent individuals suffering from anterior uveitis with ocular hypertension[4 5] and corneal endotheliitis.[3 6–8] Clinical evidence of CMV-related endotheliitis has accumulated,[6–11] and current emphasis is on the importance of early diagnosis and treatment.[12–14]

Several studies, including ours, have reported the usefulness of the systemic and topical application of anti-CMV medications, such as GCV and valganciclovir.[3 6 8 10–14] Our recent study of 106 eyes with CMV endotheliitis in Japan involved the systemic administration of anti-CMV drugs in 67.9% and topical administration of GCV prepared from intravenous infusion vials in 75.2% of the cases. Forty-eight per cent of the patients received both systemic and topical anti-CMV treatment; this combination resulted in improvement or complete remission of KPs and corneal oedema in the majority of cases.[14] Systemic GCV is recognised as an effective treatment for acute inflammation in CMV endotheliitis; however, the long-term use of systemic GCV is limited due to its systemic side effects. Topical GCV therapy has been considered as a combination therapy with systemic GCV or as a prophylactic therapy. The clinical effect of 0.15% GCV gel, approved for herpes simplex virus (HSV) keratitis, has been suggested in some cases.[13 15] However, because 0.15% GCV gel has not been approved and marketed in Japan, GCV eye drops prepared in hospital dispensaries from vials designed for intravenous infusion are often used instead, as clinical studies approved by local ethics committees.[8 10 14] Considering the heightened recognition of CMV endotheliitis and the increasing number of patients in university hospitals, extensive and long-term use of hospital-prepared eye drops might raise concerns regarding its chemical stability and safety.

The aim of this prospective study was to elucidate the effects of the topical use of commercially available 0.15% GCV gel on CMV endotheliitis without concomitant systemic GCV. Clinical evaluations and quantitative PCR of CMV were performed, and GCV concentrations in aqueous humour were measured by liquid chromatography/tandem mass spectrometry (LC-MS/MS).

METHODS

A prospective clinical study of 0.15% GCV gel treatment for CMV endotheliitis was conducted at

three university hospitals: Kyoto Prefectural University of Medicine, Tottori University, and Ehime University. The study protocol was approved by the institutional review boards of the three hospitals before beginning the study, which was conducted according to the tenets of the Declaration of Helsinki. The study subjects received complete information regarding the protocol, and written informed consent was obtained from each participant prior to entry into the study. This study is registered at http://www.umin.ac.jp as study no. UMIN000012435.

Inclusion and exclusion criteria

The patients in this study were diagnosed with CMV endotheliitis based on clinical manifestations and viral examination using qualitative PCR of their aqueous humour; all matched the diagnostic criteria of CMV endotheliitis.[14] Patients treated with any form of GCV therapy (topical or systemic) in the prior month were excluded.

Treatment protocol

The patients were treated with 0.15% GCV gel (Virgan, Laboratoires Théa, Clermont-Ferrand, France) six times a day in combination with 0.1% fluorometholone and antibiotic eye drops four times a day for 12 weeks. Anti-glaucoma medication was continued for patients under treatment. To eliminate the possible effect of steroids on the clinical evaluation, patients who had been treated with a stronger steroid, such as 0.1% betamethasone, had their medication changed to 0.1% fluorometholone for 4 weeks prior to being included in the study after obtaining informed consent.

Clinical evaluation

Slit-lamp examinations were performed, and best-corrected visual acuity (BCVA), intraocular pressure (IOP), endothelial cell density (ECD), and central corneal thickness (CCT) were measured before treatment and at 4 and 12 weeks during treatment.

Quantitative analysis of CMV DNA by real-time PCR

Before treatment and after four and 12 weeks of treatment, 120–150 µL of aqueous humour were collected using an anterior chamber tap, 0.5–3 h after the GCV gel application. CMV DNA copy numbers were measured at Tottori University by real-time PCR according to previously described methods.[16 17] Briefly, DNA was extracted using a QIAamp DNA mini kit (Qiagen, Hilden, Germany) and amplified for the glycoprotein B gene of CMV using a LightCycler (Roche, Basel, Switzerland).[17] The copy number was calculated based on known dilutions of cloned glycoprotein B DNA. The cut-off value of real-time PCR followed by DNA extraction was determined as 10 copies per 100 µL sample based on receiver operating characteristic analysis, using the WHO international standard for human CMV (data not shown); $<1.0\times10^2$ copies/mL of CMV DNA was considered negative.

LC-MS/MS measurement of GCV concentration in aqueous humour

Pharmacodynamic assessment was conducted by measuring GCV concentrations in aqueous humour using LC-MS/MS at JCL Bioassay Corporation (Osaka, Japan).

Statistical analysis

Data are presented as mean±SD. The significance of the treatment effect of GCV gel was determined using a paired t test, repeated-measures analysis of variance (ANOVA) and post hoc test. p Value <0.05 was considered significant. A minimum sample size of seven was estimated to be necessary, assuming a within-subject variance of 1, a correlation between repeated measures of 0.2, and error variance of 2. This sample size provided a power of 80% for repeated-measures ANOVA, with a 0.05 significance of error rate.

RESULTS

Clinical manifestations of patients with CMV endotheliitis

Seven eyes of seven patients were enrolled in this study from December 2013 to December 2014. Patient demographic data and clinical manifestations are summarised in table 1 and online supplementary table s-1. Qualitative PCR examination of the aqueous humour showed that all seven eyes were positive for CMV but negative for HSV and varicella zoster virus (VZV).

The patients were seven immunocompetent Japanese men, 39–74 years of age (63.4±10.7 years). Six of the seven eyes had previously been treated for anterior uveitis with ocular hypertension or Posner–Schlossman syndrome at other ophthalmology clinics, and corticosteroid eye drops had been applied routinely for more than 1 year. One case involved decompensation of a corneal graft after a second penetrating keratoplasty (PK) with recurrent inflammation, which was resistant to steroid and immunosuppressive treatment. Despite the topical steroid treatment, these seven cases exhibited progressive corneal endotheliitis with corneal endothelial cell loss, and they were referred to the university hospitals.

At the initiation of topical GCV therapy, coin-shaped lesions were detected in four eyes (57.1%), other forms of KPs were present in six eyes (85.7%), corneal oedema was observed in five eyes (71.4%) and mild anterior chamber inflammation was observed in five eyes (71.4%). Topical glaucoma medications were applied to five eyes (71.4%); acetazolamide tablets were used concurrently for four of those eyes (57.1%). Despite the use of glaucoma medications, two eyes showed elevated IOPs >21 mm Hg. The patients' BCVAs ranged from 0.03 to 1.5 (decimal fraction), and average visual acuity was 0.55. Specular microscopy images were obtained before treatment in four cases; ECD was significantly lower in the affected eyes than in the unaffected eyes of those four patients (1707±396 and 2830 ±297 cells/mm^2, respectively) (p=0.0008). The ECDs of the other three cases were not evaluated due to severe corneal oedema (table 1).

Clinical responses to 0.15% GCV gel treatment

After a 4-week administration of 0.15% GCV gel, the coin-shaped lesions disappeared from all four eyes in which they had been observed. Other forms of KPs, corneal oedema and anterior chamber inflammation improved in all cases. All seven eyes showed positive responses to treatment (table 2). Representative slit-lamp images are shown in figure 1 and online supplementary figures s-1 and s-2. A clear cornea was recovered in six eyes (85.7%) (except case 7). In case 7, the corneal epithelial oedema improved and the anterior chamber inflammation subsided, but corneal endothelial function did not recover due to irreversible corneal endothelial damage (see online supplementary figure s-3).

During the 12-week administration of 0.15% GCV gel, inflammation was well controlled and none of the seven cases showed clinical recurrence of corneal endotheliitis (table 3). However, re-emergence of CMV DNA was detected in aqueous humour by real-time PCR in one eye (case 6), without the patient's subjective complaint. After 12 weeks of treatment, corneal oedema diminished and clear specular microscope images were obtained in six cases. The average ECD of the six

Table 1 Clinical manifestations of CMV corneal endotheliitis before treatment

Case no.	Coin-shaped lesions	Other forms of KPs	Corneal oedema	AC cells	BCVA (decimal fraction)	IOP (mm Hg) (No. of glaucoma medications)	Endothelial cell density (cells/mm^2)		Central corneal thickness (μm)	CMV copy number in AH (copies/mL)
							Affected eye	Unaffected eye		
1	1+	2+	–	1+	1.2	28 (1+Tb)	2091	3178	563	4.0×10^3
2	–	2+	1+	1+	1.5	16 (3+Tb)	1303	2473	500	2.0×10^3
3	3+	3+	2+	–	0.4	16 (0)	ND	3121	763	2.0×10^4
4	3+	3+	2+	1+	0.8	11 (2+Tb)	ND	2621	722	2.9×10^4
5	–	2+	1+	1+	0.7	35 (3+Tb)	1436	2745	ND	7.8×10^3
6	1+	1+	–	–	1.2	14 (3)	2000	2924	593	1.0×10^7
7	–	–	3+	1+	0.03	15 (0)	ND	2129	648	5.0×10^2

Severity of oedema, KPs and AC cell were graded as no findings, 1+(mild), 2+(moderate) and 3+(severe).
AC, anterior chamber; AH, aqueous humour; BCVA, best-corrected visual acuity; CMV, cytomegalovirus; IOP, intraocular pressure; KPs, keratic precipitates; ND, not detectable; Tb, acetazolamide tablet.

eyes was 1343±365 cells/mm^2. The four eyes in which ECD data were compared before and after 12 weeks of treatment showed no significant changes in post-treatment versus pretreatment ECD (p=0.49).

CCT was measured in six eyes before treatment; average CCTs at the three time points (before and after four and 12 weeks of treatment) were 631±99, 550±70 and 561 ±75 μm, respectively. CCT decreased significantly during treatment (p=0.048). BCVA improved in three cases that showed visual disturbance due to corneal oedema (cases 3, 4 and 5). The average BCVA of all seven eyes increased from 0.55 before treatment to 0.63 and 0.62 at four and 12 weeks, respectively; these changes were not statistically significant. Decreased IOP and reduced use of anti-glaucoma medications were observed in some cases. However, most patients continued to use anti-glaucoma medications due to concerns regarding the progression of visual field loss caused by the long history of high IOP. No systemic or local side effects were observed in any of the patients.

Quantification of CMV DNA in aqueous humour

CMV DNA copy numbers in the patients' aqueous humour are shown in tables 1–3 and figure 2A. Before treatment, CMV DNA copy numbers in each eye ranged from 5.0×10^2/mL to 1.0×10^7/mL; following topical GCV therapy, the CMV copy numbers decreased significantly (p<0.0001). Although case 4 had a slight increase in viral copy numbers at week 4, the clinical features improved at week 4, and the viral copy numbers were below the cut-off value at week 12. Six of the seven eyes responded after 4 weeks, and all seven eyes responded within 12 weeks of treatment. The CMV copy numbers in six cases decreased to less than the cut-off level after 12 weeks of treatment. In case 6, a re-emergence of CMV DNA in aqueous humour was detected by real-time PCR after 12 weeks of treatment.

GCV concentration in aqueous humour

GCV concentrations in the aqueous humour of each patient are summarised in figure 2B; the range was 24.3–691.0 ng/mL and average GCV level was 162.0±202.4 ng/mL.

DISCUSSION

GCV, an antiviral agent developed in the 1980s, has a strong antiviral effect against HSV, VZV and CMV.[18] While a topical ophthalmic GCV gel has been approved for the treatment of HSV keratitis[19] in more than 30 countries, it has not been approved for CMV endotheliitis in any countries, as that is a newly recognised CMV infection. To the best of our knowledge, this is the first prospective study to evaluate the antiviral effect of 0.15% GCV gel on CMV endotheliitis using quantitative PCR combined with monitoring GCV concentration in aqueous humour.

In this study, seven eyes of seven patients diagnosed with CMV endotheliitis based on clinical manifestations and viral examinations using qualitative PCR of their aqueous humour were treated with 0.15% GCV gel. Coin-shaped lesions, a

Table 2 Treatment outcomes of clinical manifestations and CMV copy numbers after 4 weeks of administration of 0.15% ganciclovir gel

Case no.	Coin-shaped lesions	Other forms of KPs	Corneal oedema	AC cells	BCVA (decimal fraction)	IOP (mm Hg) (no. of glaucoma medications)	Endothelial cell density (cells/mm^2)	Central corneal thickness (μm)	CMV copy number in AH (copies/mL)	Clinical evaluation of treatment
1	–	–	–	–	1.2	14 (1)	2032	496	ND	Effective
2	–	1+	–	–	1.5	10 (3)	1484	496	ND	Effective
3	–	A few	–	–	0.6	–	652	543	9.8×10^2	Effective
4	–	1+	–	–	0.8	16 (2+ Tb)	652	595	6.0×10^4	Effective
5	–	–	–	–	1	23 (Tb)	1340	508	ND	Effective
6	–	1+	–	–	1.5	10 (3)	1672	500	ND	Effective
7	–	–	2+	–	0.03	14 (0)	ND	668	ND	Partially effective

Severity of oedema, KPs and AC cell were graded as no findings, 1+ (mild), 2+ (moderate) and 3+ (severe).
AC, anterior chamber; AH, aqueous humour; BCVA, best-corrected visual acuity; CMV, cytomegalovirus; IOP, intraocular pressure; KPs, keratic precipitates; ND, not detectable; Tb, tablet.

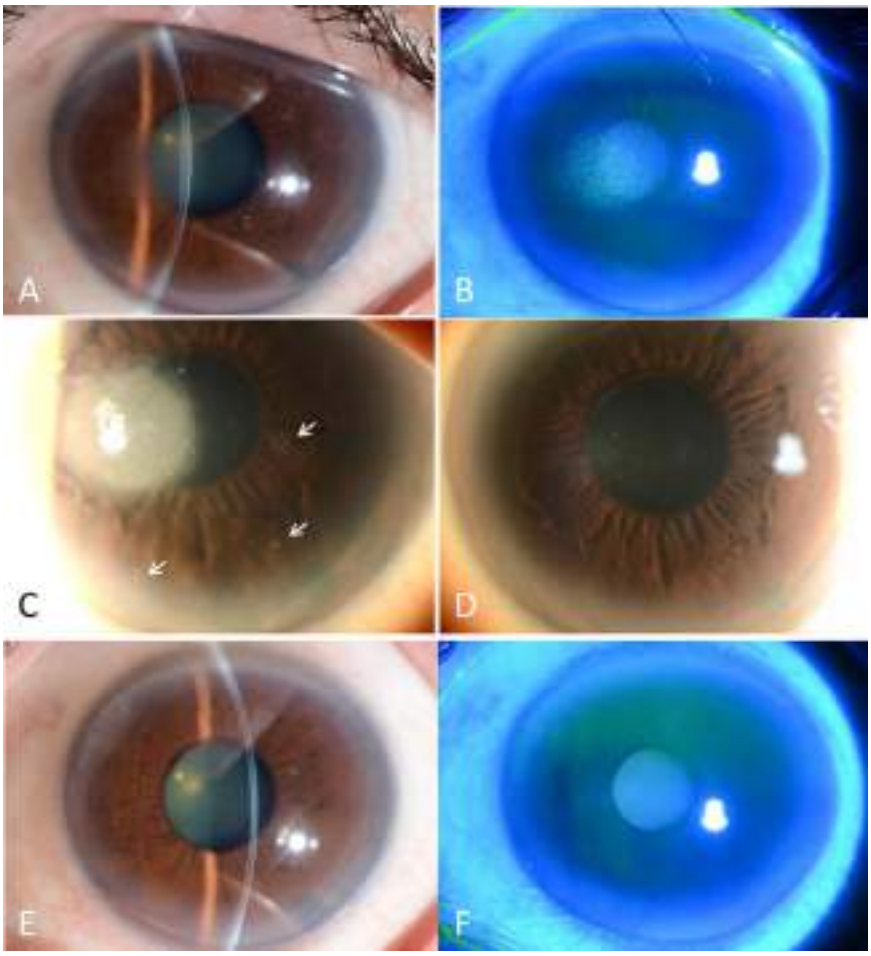

Figure 1 Representative anterior-segment photographs of cytomegalovirus corneal endotheliitis before and after topical application of 0.15% ganciclovir gel treatment (case 3). Before treatment, localised corneal oedema surrounded by keratic precipitates (KPs) was observed (A–C). Epithelial oedema was evident based on fluorescein staining (B). A scleral scattering photograph distinguished a stromal/epithelial oedema lesion and multiple coin-shaped lesions (C, arrows). After 4 weeks of treatment, the corneal oedema and coin-shaped lesions had disappeared, and several fine KPs were observed (D). After 12 weeks of treatment, this patient recovered a clear cornea without any signs of inflammation (E and F).

specific finding of CMV endotheliitis,[10 14 20] responded to the GCV gel very well and disappeared after 4 weeks of treatment. Accompanying findings, such as corneal oedema and anterior chamber reactions, were also controlled well with the GCV treatment. Real-time PCR showed a significant decrease in CMV DNA copy numbers in aqueous humour after treatment compared with pretreatment levels. After 12 weeks of treatment, six of the seven eyes recovered a completely clear cornea, and endothelial function was well maintained.

GCV concentrations were evaluated in the aqueous humour of the patients after administration of the gel. While GCV was detected in all of the samples, in some cases the concentrations were lower than in the reported ED50 (0.1–1.6 μg/mL).[18] Based on the pharmacological data (using rabbit eyes), GCV concentrations in corneal tissues are expected to be approximately 10 times higher than those found in aqueous humour after a single-dose instillation of GCV (Center for Drug Evaluation and Research. NDA Application 22–211. Available at: ⟨http://www.accessdata.fda.gov/drugsatfda_docs/nda/2009/022211_zirgan_toc.cfm⟩). Given the significant therapeutic efficacy of GCV observed in our study, we surmised that the therapeutic level of GCV concentration in the cornea was reached.

While there were large individual differences in GCV concentrations in aqueous humour, individual concentrations were well

Table 3 Treatment outcomes of clinical manifestations and CMV copy numbers after 12 weeks of administration of 0.15% ganciclovir gel

Case no.	Coin-shaped lesions	Other forms of KPs	Corneal oedema	AC cells	BCVA (decimal fraction)	IOP (mm Hg) (no. of glaucoma medications)	Endothelial cell density (cells/mm^2)	Central corneal thickness (μm)	CMV copy number in AH (copies/mL)	Clinical evaluation of treatment
1	–	–	–	–	1.2	13 (1)	1719	558	ND	Effective
2	–	–	–	–	1.5	12 (3)	1677	485	ND	Effective
3	–	–	–	–	0.8	–	1000	531	ND	Effective
4	–	A few	–	–	1.2	12 (2+ Tb)	826	580	ND	Effective
5	–	–	–	–	1.0	36	1324	491	ND	Effective
6	–	1+	–	–	0.7	11 (3)	1513	514	1.9×10^4	Mild reactivation
7	–	–	2+	–	0.03	10 (0)	ND	698	ND	Partially effective

Severity of oedema, KPs and AC cell were graded as no findings, 1+ (mild), 2+ (moderate) and 3+ (severe).
AC, anterior chamber; AH, aqueous humour; BCVA, best-corrected visual acuity; CMV, cytomegalovirus; IOP, intraocular pressure; KPs, keratic precipitates; ND, not detectable; Tb, tablet.

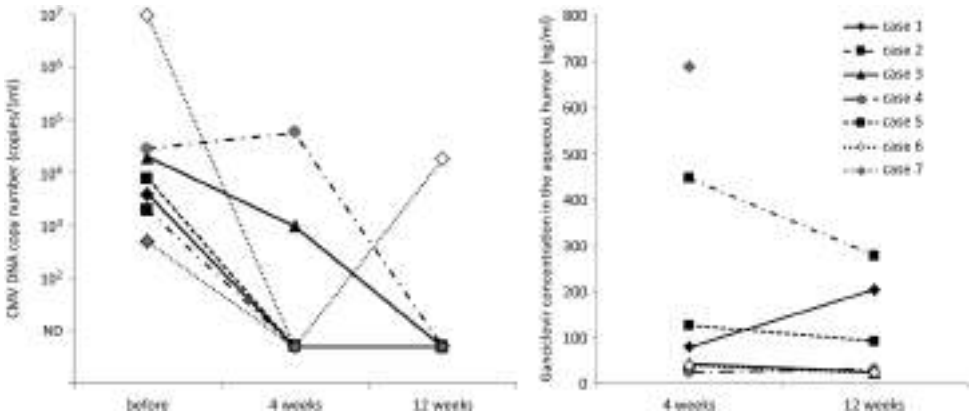

Figure 2 Changes in cytomegalovirus (CMV) DNA copy numbers and ganciclovir (GCV) concentration in the aqueous humour. (A) CMV copy numbers decreased significantly after treatment ($p<0.0001$). The CMV copy numbers decreased to less than the cut-off level (1×10^2 copies/mL) in six cases after 12 weeks of treatment. In case 6, a minor viral reactivation was detected by real-time PCR after 12 weeks of treatment. (B) GCV was detected in all collected samples by liquid chromatography/tandem mass spectrometry. GCV concentration ranged from 24.3 to 691.0 ng/mL; average GCV level was 162.0±202.4 ng/mL.

maintained throughout the treatment period. It is interesting that cases 3 and 4, which had low levels of aqueous GCV (<50 ng/mL), were more likely to have positive CMV DNA, even after treatment. Similarly, case 6, in which re-emergence of CMV DNA in the aqueous humour was observed at 12 weeks of treatment, also had low levels of aqueous GCV (24 and 39 ng/mL at 4 and 12 weeks, respectively). In contrast, the other four cases, with aqueous GCV concentrations >80 ng/mL, responded well to GCV treatment, and CMV copy numbers were maintained under the detection limit throughout the observation period. These results support the therapeutic and antiviral effects of 0.15% GCV gel for CMV endotheliitis. It is suggested that a combination therapy of 0.15% GCV gel with systemic GCV or valganciclovir might be a better initial treatment in patients with low GCV levels. Monitoring CMV DNA in aqueous humour might also be helpful in refractory cases.

Limitations of this study include (1) a small number of cases and short-term follow-up and (2) lack of a placebo-treated group for comparative study. The characteristic feature of CMV endotheliitis is that it is a progressive and recurrence-prone disease that often causes irreversible corneal endothelial dysfunction if not adequately treated with antiviral treatment. Thus, we considered it unethical to include a placebo-treated group. The long-term safety and efficacy of 0.15% GCV gel in the treatment of CMV endotheliitis remain to be determined, and there is an undeniable possibility of drug toxicity, such as toxic keratopathy, affecting the ocular surface. Prospective clinical trials to determine the local/systemic safety and efficacy of 0.15% GCV gel are needed.

In this study, progressive corneal endotheliitis and CMV DNA were detected by PCR prior to GCV treatment, even though the patients had been treated with corticosteroids for more than a year. After 0.15% GCV treatment, improvement of the clinical manifestations and lower CMV copy numbers were confirmed by real-time PCR, and therapeutic levels of aqueous humour GCV were detected. Thus, although there was no negative control group treated by placebo or corticosteroid only, the improved clinical findings are considered to be due to the antiviral effect of the 0.15% GCV gel.

The pathogenic mechanism of CMV endotheliitis has yet to be defined. CMV infection of corneal endothelial cells has been identified by confocal microscopy as 'owl's eye' cells in patients' corneal endothelia.[7 21] Recently, the replication ability of CMV in human corneal endothelial cells was reported in an in vitro study,[22] suggesting the possibility of corneal endothelial cell damage induced by CMV virions released into aqueous humour. CMV viral load is also known to be associated with corneal endothelial cell damage in CMV anterior uveitis and corneal endotheliitis.[17 23] Similar CMV genotypes have been detected in eyes with corneal endotheliitis and anterior uveitis;[24] therefore, sufficient and sustainable reductions of CMV in the corneal endothelium and aqueous humour might be beneficial for preventing irreversible corneal endothelial dysfunction in the long term in patients with primary CMV endotheliitis and post-keratoplasty patients with CMV endotheliitis.

The usefulness of the systemic and topical application of anti-CMV medications, such as GCV and valganciclovir, has been reported previously. However, most previous studies have demonstrated the efficacy of oral and hospital compounded topical GCV, but not the commercially available form. In particular, ours is the first study to evaluate the drug transfer of GCV applied topically to the anterior chamber in patients with CMV endotheliitis without concomitant systemic GCV or valganciclovir. Although this was a small case study, the possible relationship between GCV concentration in aqueous humour and CMV copy numbers might provide new and useful information for establishing future standard therapies for CMV endotheliitis.

Clinical improvements and lower CMV copy numbers in aqueous humour were confirmed in patients with CMV endotheliitis following topical application of 0.15% GCV gel without concomitant systemic GCV therapy. On another front, 0.15% GCV gel alone seemed to be insufficient in some cases, especially those whose aqueous GCV concentrations were low or in whom a high CMV copy number was detected in the aqueous humour. For those intractable cases, systemic GCV therapy, preferably a combination therapy of topical and systemic GCV, might be necessary to prevent irreversible corneal endothelial damage. We consider a combination therapy of systemic and topical GCV treatment to be ideal for CMV endotheliitis with clinically apparent corneal oedema or decreased endothelial cell count to prevent the progression of corneal endothelial damage. However, there are drawbacks associated with the long-term use of systemic GCV due to systemic side effects and the high cost of the medication. While those issues

should be considered in future prospective, randomised clinical trials, our current suggestion is to offer a combination therapy of systemic and topical GCV for 4–12 weeks as an initial treatment, followed by topical GCV treatment as a maintenance therapy. In cases with mild inflammation without apparent progress of corneal endothelial damage, topical GCV treatment might be the first treatment option. The case numbers are limited and long-term recurrence follow-up is necessary, but 0.15% GCV gel appears to be a useful treatment option for CMV endotheliitis.

Contributors NK, DM and TI: conception and design of the work, the acquisition, analysis and interpretation of data. Drafting the work. FO, MK-I, TI, CS, HN, TH, MU and TN: the acquisition, analysis of data. Drafting the work. YI, YO and SK: the analysis and interpretation of data. Revising the work critically for important intellectual content. Final approval of the version published was obtained by all authors. Agreement to be accountable for all aspects of the work in ensuring that questions related to the accuracy or integrity of any part of the work are appropriately investigated and resolved by all authors.

Funding This study was partially supported by M's Science Corporation, Kobe, Japan. M's science provided 0.15% GCV gel and research consumables for real-time PCR for this study.

Competing interests None declared.

Ethics approval Institutional Review Boards of Kyoto Prefectural University of Medicine, Tottori University, and Ehime University.

Provenance and peer review Not commissioned; externally peer reviewed.

REFERENCES

1 Khodadoust AA, Attarzadeh A. Presumed autoimmune corneal endotheliopathy. *Am J Ophthalmol* 1982;93:718–22.
2 Suzuki T, Ohashi Y. Corneal endotheliitis. *Semin Ophthalmol* 2008;23:235–40.
3 Koizumi N, Yamasaki K, Kawasaki S, *et al*. Cytomegalovirus in aqueous humor from an eye with corneal endotheliitis. *Am J Ophthalmol* 2006;141:564–5.
4 Chee SP, Bacsal K, Jap A, *et al*. Clinical features of cytomegalovirus anterior uveitis in immunocompetent patients. *Am J Ophthalmol* 2008;145:834–40.
5 van Boxtel LA, van der Lelij A, van der Meer J, *et al*. Cytomegalovirus as a cause of anterior uveitis in immunocompetent patients. *Ophthalmology* 2007;114:1358–62.
6 Chee SP, Bacsal K, Jap A, *et al*. Corneal endotheliitis associated with evidence of cytomegalovirus infection. *Ophthalmology* 2007;114:798–803.
7 Shiraishi A, Hara Y, Takahashi M, *et al*. Demonstration of "owl's eye" morphology by confocal microscopy in a patient with presumed cytomegalovirus corneal endotheliitis. *Am J Ophthalmol* 2007;143:715–17.
8 Suzuki T, Hara Y, Uno T, *et al*. DNA of cytomegalovirus detected by PCR in aqueous of patient with corneal endotheliitis after penetrating keratoplasty. *Cornea* 2007;26:370–2.
9 Yamauchi Y, Suzuki J, Sakai J, *et al*. A case of hypertensive keratouveitis with endotheliitis associated with cytomegalovirus. *Ocul Immunol Inflamm* 2007;15:399–401.
10 Koizumi N, Suzuki T, Uno T, *et al*. Cytomegalovirus as an etiologic factor in corneal endotheliitis. *Ophthalmology* 2008;115:292–97.e3.
11 Anshu A, Chee SP, Mehta JS, *et al*. Cytomegalovirus endotheliitis in Descemet's stripping endothelial keratoplasty. *Ophthalmology* 2009;116:624–30.
12 Chan AS, Mehta JS, Al Jajeh I, *et al*. Histological features of Cytomegalovirus-related corneal graft infections, its associated features and clinical significance. *Br J Ophthalmol* 2016;100:601–6.
13 Chee SP, Jap A. Treatment outcome and risk factors for visual loss in Cytomegalovirus endotheliitis. *Graefes Arch Clin Exp Ophthalmol* 2012;250:383–9.
14 Koizumi N, Inatomi T, Suzuki T, *et al*. Clinical features and management of cytomegalovirus corneal endotheliitis: analysis of 106 cases from the Japan corneal endotheliitis study. *Br J Ophthalmol* 2015;99:54–8.
15 Chee SP, Jap A. Immune ring formation associated with cytomegalovirus endotheliitis. *Am J Ophthalmol* 2011;152:449–53.e1.
16 Ikeda Y, Miyazaki D, Yakura K, *et al*. Assessment of real-time polymerase chain reaction detection of Acanthamoeba and prognosis determinants of Acanthamoeba keratitis. *Ophthalmology* 2012;119:1111–19.
17 Kandori M, Miyazaki D, Yakura K, *et al*. Relationship between the number of cytomegalovirus in anterior chamber and severity of anterior segment inflammation. *Jpn J Ophthalmol* 2013;57:497–502.
18 Field AK, Davies ME, DeWitt C, *et al*. 9-([2-hydroxy-1-(hydroxymethyl)ethoxy] methyl)guanine: a selective inhibitor of herpes group virus replication. *Proc Natl Acad Sci USA* 1983;80:4139–43.
19 Hoh HB, Hurley C, Claoue C, *et al*. Randomised trial of ganciclovir and acyclovir in the treatment of herpes simplex dendritic keratitis: a multicentre study. *Br J Ophthalmol* 1996;80:140–3.
20 Hwang YS, Shen CR, Chang SH, *et al*. The validity of clinical feature profiles for cytomegaloviral anterior segment infection. *Graefes Arch Clin Exp Ophthalmol* 2011;249:103–10.
21 Kobayashi A, Yokogawa H, Higashide T, *et al*. Clinical significance of owl eye morphologic features by in vivo laser confocal microscopy in patients with cytomegalovirus corneal endotheliitis. *Am J Ophthalmol* 2012;153:445–53.
22 Hosogai M, Shima N, Nakatani Y, *et al*. Analysis of human cytomegalovirus replication in primary cultured human corneal endothelial cells. *Br J Ophthalmol* 2015;99:1583–90.
23 Miyanaga M, Sugita S, Shimizu N, *et al*. A significant association of viral loads with corneal endothelial cell damage in cytomegalovirus anterior uveitis. *Br J Ophthalmol* 2010;94:336–40.
24 Oka N, Suzuki T, Inoue T, *et al*. Polymorphisms in cytomegalovirus genotype in immunocompetent patients with corneal endotheliitis or iridocyclitis. *J Med Virol* 2015;87:1441–5.

The effect of topical application of 0.15% ganciclovir gel on cytomegalovirus corneal endotheliitis

Noriko Koizumi, Dai Miyazaki, Tomoyuki Inoue, Fumie Ohtani, Michiko Kandori-Inoue, Tsutomu Inatomi, Chie Sotozono, Hiroko Nakagawa, Tomoko Horikiri, Mayumi Ueta, Takahiro Nakamura, Yoshitsugu Inoue, Yuichi Ohashi and Shigeru Kinoshita

Br J Ophthalmol 2017 101: 114-119 originally published online May 3, 2016
doi: 10.1136/bjophthalmol-2015-308238

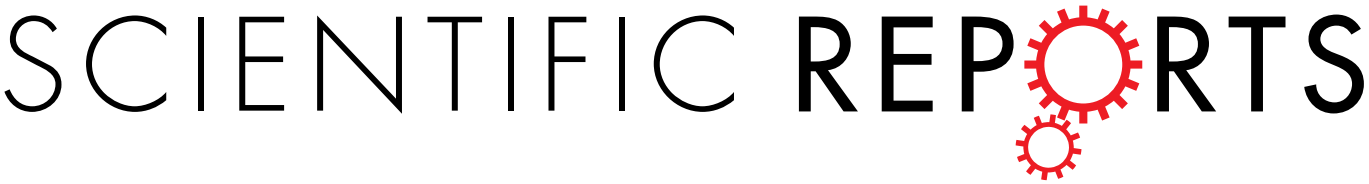

OPEN

Received: 15 September 2016
Accepted: 01 February 2017
Published: 08 March 2017

Efficient and reliable establishment of lymphoblastoid cell lines by Epstein-Barr virus transformation from a limited amount of peripheral blood

Natsue Omi[1], Yuichi Tokuda[1], Yoko Ikeda[2], Morio Ueno[2], Kazuhiko Mori[2], Chie Sotozono[2], Shigeru Kinoshita[2,3], Masakazu Nakano[1] & Kei Tashiro[1]

Lymphoblastoid cell lines (LCLs) transformed by Epstein-Barr virus (EBV) serve as an unlimited resource of human genomic DNA. The protocol that is widely used to establish LCLs involves peripheral blood mononuclear cell isolation by density gradient centrifugation, however, that method requires as much as 5 ml of peripheral blood. In this study, in order to provide a more simple and efficient method for the generation of LCLs, we developed a new protocol using hemolytic reaction to enrich white blood cells for EBV transformation and found that the hemolytic protocol successfully generated LCLs from a small volume (i.e., 0.1 ml) of peripheral blood. To assess the quality of genomic DNA extracted from LCLs established by the hemolytic protocol (LCL-hemolytic), we performed single nucleotide polymorphism (SNP) microarray genotyping using the GeneChip® 100 K Array Set (Affymetrix, Inc.). The concordances of the SNP genotyping resulting from genomic DNA from LCL-hemolytic (99.92%) were found to be as good as the technical replicate (99.90%), and Kappa statistics results confirmed the reliability. The findings of this study reveal that the hemolytic protocol is a simple and reliable method for the generation of LCLs, even from a small volume of peripheral blood.

The Epstein-Barr virus (EBV) is known to infect and transform human B cells into lymphoblastoid cell lines (LCLs) *in vitro*[1]. LCLs serve as an unlimited resource of human genomic DNA, as the established cell lines apparently maintain the genome intact through generations, regardless of the viral genome persisting intracellularly[2,3]. In fact, several non-profit depository facilities currently make a huge contribution to the scientific community by storing a number of LCLs and distributing genomic DNA derived from them to researchers upon request[4,5]. Moreover, our research group at Kyoto Prefectural University of Medicine (KPUM), Kyoto, Japan consistently collects thousands of blood samples from patients and healthy volunteers, and we have performed several genome-wide association studies (GWAS) using their genomic DNA[6–9]. With each sample that we obtain, we are also establishing LCLs to serve as a resource of future studies, such as for a resequencing analysis of the disease-associated regions identified by GWAS. However, the procedure for establishing LCLs is often time-consuming and labor-intensive, especially when numerous samples need to be simultaneously handled, due to the complex steps needed to generate LCLs. In addition, we occasionally encounter situations in which the amount of blood that can be collected from a subject is less than 5 ml, i.e., less than the amount needed to establish LCLs via the use of the conventional method involving density gradient centrifugation. Therefore, the aim of this present study was to develop a more simple and effective method for generating LCLs.

At present, the most widely accepted method for the establishment of LCLs utilizes the protocol of density gradient centrifugation in order to prepare peripheral blood mononuclear cells (PBMCs) from peripheral blood (hereafter referred to as the "gradient protocol") before EBV infection[10–13]. For the gradient protocol, there are

[1]Department of Genomic Medical Sciences, Kyoto Prefectural University of Medicine, Kyoto, Japan. [2]Department of Ophthalmology, Kyoto Prefectural University of Medicine, Kyoto, Japan. [3]Department of Frontier Medical Science and Technology for Ophthalmology, Kyoto Prefectural University of Medicine, Kyoto, Japan. Correspondence and requests for materials should be addressed to K.T. (email: tashiro@koto.kpu-m.ac.jp)

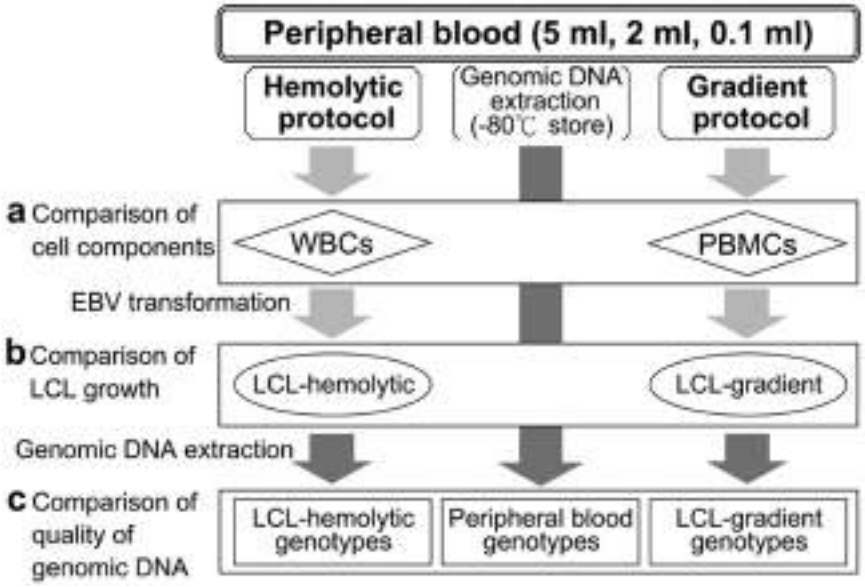

Figure 1. Study design for the comparative experiments. To evaluate the efficiency and reliability of the hemolytic protocol (flowchart, left side), a quantitative comparison was made with the gradient protocol (flowchart, right side) by changing the starting blood volume (5 ml, 2 ml, or 0.1 ml) with respect to the following three categories: (**a**) Comparison of the features of the cells (cell recovery, viability, and proportion of cell components) of the isolated WBCs prepared by the hemolytic protocol or PBMCs prepared by the gradient protocol, (**b**) Comparison of the growth curves of establishing LCLs (ellipse) from WBCs (LCL-hemolytic) or PBMCs (LCL-gradient), and (**c**) Comparison of the quality of genomic DNA (rectangle) based on the SNP genotype data (central arrow).

a wide variety of commercially available reagents that allow researchers to separate PBMCs from the different layers of the other components of blood based on each density[13–15]. The gradient protocol typically requires 5 ml or more of peripheral blood in order for it to be overlaid onto the gradient-making reagent[16–18]. Moreover, post centrifugation, the method required to collect the interface layer, which contains PBMCs, is complex. An alternative method to establish LCLs has been reported, which involves adding EBV-containing culture supernatant on white blood cells (WBCs) consisting of PBMCs and granulocytes, which are prepared by removing the lysed red blood cells from the peripheral blood by hemolytic reaction (hereafter referred to as the "hemolytic protocol")[19]. However, the initial volume of peripheral blood needed in that method is still 5 ml.

Thus, the aim of this present study was to develop a simple and efficient protocol for the establishment of LCLs, specifically focused on the generation LCLs from a limited amount of peripheral blood. In addition, in order to assess and confirm that the quality of the genomic DNA extracted from LCLs established by this novel method using hemolytic reaction (LCL-hemolytic) is as good as genomic DNA extracted from peripheral blood and genomic DNA extracted from LCLs established by the conventional method using density gradient centrifugation (LCL-gradient), we performed single nucleotide polymorphism (SNP) microarray genotyping using the GeneChip® 100 K Array Set (Affymetrix, Inc., Santa Clara, CA), and then compared the concordance of genotyping results using each of the genomic DNAs.

Results

Comparison of cell recovery, viability, and proportion of cell components. In this study, prior to initiating the comparison of cell recovery, cell viability, and the proportion of cell components, a preliminary test was performed to assess the effect of time during which peripheral blood samples were kept before being used as starting materials on the period of days required for successful LCL generation. In addition, the effect of temperature in which peripheral blood samples were kept before being used as starting materials on the period of days required for successful LCL establishment was also assessed (Supplementary Fig. S1). No significant difference was observed between peripheral blood samples stored at either 4 °C or 25 °C. In addition, no difference was observed between peripheral blood samples stored for 3 days and those used on day 0; i.e., the day the peripheral blood was obtained from the volunteer subjects (Supplementary Fig. S1a). After 7-days storage, the period of days required for successful LCL establishment was found to be prolonged (Supplementary Fig. S1b). Since up to 3-days storage produced no detrimental effect, we theorized that the storage time of within day 0 would also produce no detrimental effect. However, all experiments performed in this study were initiated on day 0.

As shown in Fig. 1a, we first examined the cell properties isolated by hemolytic or gradient protocols using a total of 120 samples from sample groups #1, #2, and #3 (Table 1a). Cell recovery via the gradient protocol was found to be significantly lower than that via the hemolytic protocol (Table 2). No significant difference in cell viability of the isolated cells was found between the two protocols, i.e., in regard to initiating with 5 ml or 2 ml of peripheral blood ($P > 0.05$). When starting with 0.1 ml of peripheral blood, the viability of the isolated cells via

Comparative experiment	Sample group	Blood volume (ml)	Participated volunteers (n)	Mean age at sampling (age range)	Sample number (n)		
					Peripheral blood	Hemolytic	Gradient
(a)	#1	5	20	64.3 (34–82) years	0	20	20
	#2	2	20	64.6 (30–86) years	0	20	20
	#3	0.1	20	69.7 (46–91) years	0	20	20
(b)	#4	5	10	61.7 (51–70) years	0	10	10
	#5	2	10	67.8 (57–76) years	0	10	10
	#6	0.1	10	67.3 (55–86) years	0	10	10
(c)	#7	5	3	52.0 (28–66) years	6*	3	3
	#8	2	3	72.0 (69–76) years	3	3	0
	#9	0.1	3	67.7 (65–69) years	3	3	0

Table 1. Sample information. *(3 blood samples from sample group #7) × (each technical replicate) = 6 microarray samples.

Sample group	Blood volume (ml)	Total WBC count in CBC ($10^3/\mu l$)*	Isolated WBCs by the hemolytic protocol		Isolated PBMCs by the gradient protocol		Viability comparison *P*-value***
			Recovery**	Viability**	Recovery**	Viability**	
#1	5	6.2 ± 1.2	47.4 ± 3.8	97.7 ± 1.3	18.4 ± 1.8	98.4 ± 1.7	0.1140
#2	2	5.6 ± 1.4	46.1 ± 4.1	97.1 ± 1.2	16.2 ± 2.1	98.1 ± 3.5	0.1925
#3	0.1	5.7 ± 1.3	41.6 ± 4.4	96.6 ± 1.5	14.6 ± 2.4	98.8 ± 5.6	0.0012

Table 2. Comparison of recovery and viability of isolated cells between the two protocols. *Values indicate the mean ± SD of total cell number of WBC in the CBC. **Values represented as the mean ± SD of the percentage. ***P-values indicate the comparison between the hemolytic and the gradient protocol by Wilcoxon signed-rank test.

the gradient protocol was slightly lower than that via the hemolytic protocol (Table 2; $P < 0.01$). The values of standard deviation (SD) for WBCs seemed to be relatively stable when compared with those of PBMCs, and this was confirmed by assessing the normality of the cell viabilities of WBCs ($P = 0.769$) and PBMCs ($P < 0.001$) by the Shapiro-Wilk test, thus suggesting that the hemolytic protocol is technically stable.

In order to determine which cell types were isolated, each cell fraction was stained and categorized, based on the morphology, as Neutrophils, Eosinophils, Basophils, Lymphocytes, and Monocytes. The major cell component populations isolated by the hemolytic protocol were neutrophils and lymphocytes, irrespective of the different starting volumes of peripheral blood (Table 3). As for the gradient protocol, the major cell component population was lymphocytes. However, the proportion of lymphocyte population decreased to less than 70% when started from 0.1 ml of peripheral blood (Table 3), probably due to the incorporation of neutrophils (~30%) while recovering a thin PBMC layer after density gradient centrifugation.

Comparison of LCL growth. The growth rate of LCLs established by each protocol (Fig. 1b) was compared. In total, 60 LCLs were generated by either hemolytic (LCL-hemolytic) or gradient (LCL-gradient) protocol using the samples from sample groups #4, #5, and #6 (Table 1b). When the initial volume of peripheral blood was sufficient (≥2 ml), both protocols effectively generated LCLs in 8 weeks (Fig. 2a,b). Cells prepared by each protocol showed unique growth curves. In LCL-gradient, rapid growth was observed during the initial 2 weeks, and a subsequent steady growth of LCLs was observed at close to 8 weeks, as is observed in a general LCL culture (Fig. 2a,b, solid gray square). In LCL-hemolytic, after continuous decrease of total cell number during the initial 2 weeks, rapid recovery of LCL growth was observed through 2 to 8 weeks (Fig. 2a,b, solid black circle). However, when starting with 0.1 ml of peripheral blood, the LCL-gradient failed to expand throughout the observation period, possibly due to the low number of initial viable PBMCs isolated by density gradient centrifugation (Fig. 2c, solid gray square). In contrast, LCL-hemolytic showed the above-described growth curve even when started from a small initial cell number (Fig. 2c, solid black circle), thus suggesting the usefulness of the hemolytic protocol for establishing LCLs from a limited amount of peripheral blood. It is important to note that although LCL-hemolytic initiated from 0.1 ml of peripheral blood required a somewhat longer culture period (i.e., 12 weeks, as opposed to 6 to 8 weeks), it was always possible to obtain a sufficient amount (i.e., a few micrograms) of genomic DNA.

Comparison of genotypes. In order to evaluate the influence of EBV infection and transformation to the genomic DNA of LCLs, SNP genotype data obtained from genomic DNA derived from peripheral blood and that obtained from genomic DNA derived from LCL-hemolytic were compared (Fig. 1c). For the evaluation, 24 samples were used from sample groups #7, #8, and #9 (Table 1c). The yield and the ratio of A260/280 absorbance of genomic DNAs from the 24 samples was found to be high enough for use in the microarray experiments (Table 4). The periods of each sample stored at −80 °C until isolation of DNA were as follows: #7: 136 weeks (peripheral blood) or 130 weeks (LCL), #8: 60 weeks (peripheral blood) or 52 weeks (LCL), and #9: 10 weeks (peripheral

Protocol	Sample group	Blood volume (ml)	WBCs				
			Granulocytes*			PBMCs*	
			Neutrophils	Eosinophils	Basophils	Lymphocytes	Monocytes
Hemolytic protocol	#1	5	52.8 ± 5.7	2.1 ± 1.3	0.4 ± 0.5	43.6 ± 5.3	1.2 ± 0.7
	#2	2	53.8 ± 6.9	1.5 ± 1.2	0.6 ± 0.5	43.1 ± 6.5	1.1 ± 0.8
	#3	0.1	52.3 ± 4.5	3.4 ± 1.7	0.6 ± 0.5	42.8 ± 4.7	1.1 ± 0.8
Gradient protocol	#1	5	8.2 ± 3.5	0.8 ± 0.7	0.2 ± 0.4	90.2 ± 4.3	0.9 ± 0.6
	#2	2	15.6 ± 5.0	0.8 ± 0.6	0.2 ± 0.4	82.6 ± 5.5	0.9 ± 0.7
	#3	0.1	30.2 ± 6.9	1.6 ± 0.8	0.3 ± 0.5	67.2 ± 7.1	0.8 ± 0.6

Table 3. Proportion of cell components of the isolated cells. *Values represent the mean ± SD of the percentage of the cells in each sample group.

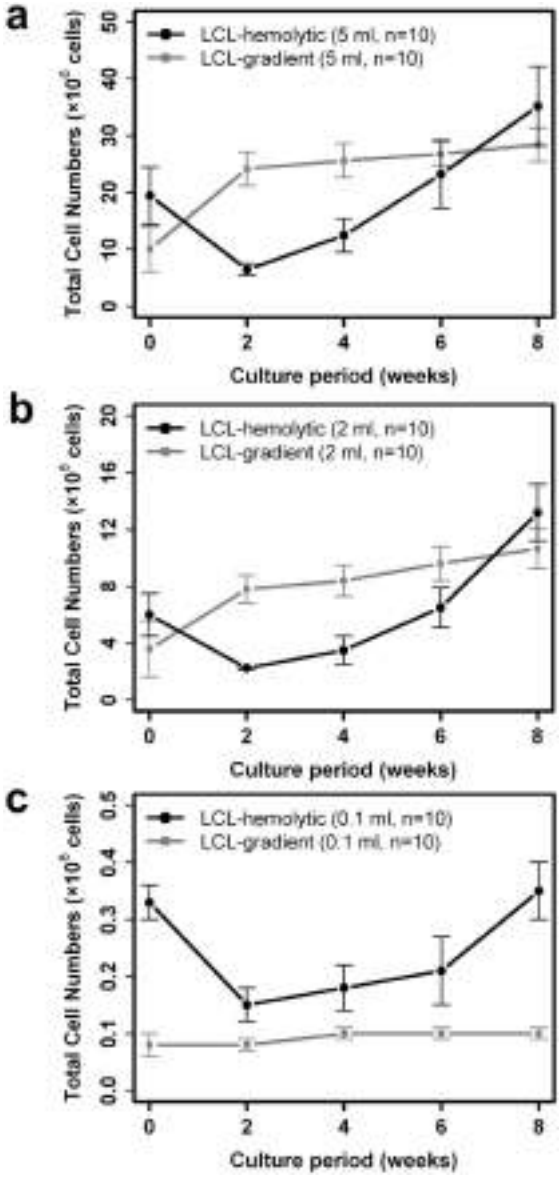

Figure 2. Growth curve of LCLs established from different blood volumes. The LCLs were established by either hemolytic (LCL-hemolytic, solid black circle) or gradient (LCL-gradient, solid gray square) protocol from the peripheral blood of 5 ml (**a**), 2 ml (**b**), or 0.1 ml (**c**). Each LCL was cultured until 8 weeks and observed at 2-week intervals. Each point indicates the average and standard error bar of 10 LCLs. The vertical axis indicates the total number of viable cells and the horizontal axis indicates the weeks post EBV infection.

Sample group	Blood volume (ml)	DNA source	−80 °C period (weeks)	Cell number when thawed ($\times 10^6$)	Viability when thawed (%)	Culture period (weeks)****	Final cell number ($\times 10^6$)	DNA yield (μg)	OD260/280
#7	5	Peripheral blood*	136**	—	—	—	—	4.2 ± 1.9	1.79 ± 0.09
		LCL-gradient	130***	1.2 ± 4.9	79.2 ± 4.7	6	2.3 ± 0.4	3.2 ± 0.7	1.96 ± 0.02
		LCL-hemolytic	130***	1.1 ± 2.2	80.2 ± 5.5	6	3.0 ± 0.4	3.8 ± 1.3	1.89 ± 0.01
#8	2	Peripheral blood*	60**	—	—	—	—	3.2 ± 2.2	1.82 ± 0.03
		LCL-hemolytic	52***	0.4 ± 0.4	78.9 ± 8.3	8	2.0 ± 1.0	2.6 ± 1.2	1.93 ± 0.04
#9	0.1	Peripheral blood*	10**	—	—	—	—	3.7 ± 3.5	1.82 ± 0.04
		LCL-hemolytic	0	—	—	12	0.7 ± 0.2	1.7 ± 0.6	1.88 ± 0.01

Table 4. Quality and quantity of genomic DNA for genotype concordance analyses. *350 ul of peripheral blood was used as a source of DNA. **Genomic DNA was stored at −80 °C. ***LCLs were stored at −80 °C after 2 weeks culture from EBV infection. ****Total cultivation time including 2 weeks culture before cryopreservation. Except for the "−80 °C period" and the "Cultivation period", the values represent the mean ± SD.

blood). As a result of quality control for SNP genotype data (see Supplementary Note and Supplementary Fig. S2), the concordance rate of technical replicates (Supplementary Fig. S3A) was 99.90% (Table 5), thus indicating that an error rate of approximately 0.1% spontaneously occurred during the 100K-microarray genotype experiments.

Given the above background technical replication data, the concordance rates between the data from genomic DNA from LCLs and that from peripheral blood DNA (Supplementary Fig. S3B) were extremely high (approximately 99.90%) in both the hemolytic and gradient protocols (Table 5). Moreover, when using the hemolytic protocol, the concordance rate remained constant when the starting volume of peripheral blood was reduced to 2 ml (99.90%), and remained high enough even when reduced down to 0.1 ml (99.82%) (Supplementary Fig. S3C and Supplementary Table S1). These results were also confirmed by the Kappa statistics (also known as "Cohen's kappa coefficient") (Table 5 and Supplementary Table S1).

Moreover, the genotype concordance was also analyzed by measuring a pairwise distance between the data derived from the LCL-hemolytic and its peripheral blood (Fig. 3). As a result, the distance obviously became closer to zero when the stringency of the SNP filter (call-rate per SNP) was increased up to >99%.

Taken together, these results suggest that the genomic DNA derived from LCLs established by the hemolytic protocol had a minimum effect of EBV transformation and was sustainable for practical use.

Discussion

The findings in this present study demonstrate that the hemolytic protocol is a reliable method for establishing LCLs, even when the initial amount of peripheral blood is limited, thus providing an advantage in terms of use for pediatric research and for patients in whom a sufficient amount of peripheral blood is difficult to obtain. Moreover, this method provides an advantage over the conventional gradient protocol, as it allows for an increased number of samples to be enrolled for genetic analysis.

It is important to note that when using the hemolytic protocol, the peripheral blood needs to be treated with a chilled hypotonic buffer for 15 minutes on ice in order to burst erythrocytes. As shown in Table 2, the viability of WBCs isolated by the hemolytic protocol was slightly lower than that of PBMCs isolated by the gradient protocol, although the difference, if any, was small enough not to influence on the following further analysis. In fact, the results showed that it was possible to establish LCLs efficiently via the hemolytic protocol (Fig. 2). In order to evaluate the influence of EBV infection and transformation to the genomic DNA of LCLs, the SNP genotype data obtained from genomic DNA derived from peripheral blood and that obtained from genomic DNA derived from LCL-hemolytic were compared (Table 5, Supplementary Table S1, Supplementary Note). Our findings showed that the concordance rate of the genotype data between the genomic DNA derived from LCLs and its peripheral blood turned out to be sufficiently high (>99.80%) in light of the concordance rate of the technical replicates (99.90%) (Table 5). Moreover, the obtained genotype data of LCLs appeared to be useful for practical use by applying appropriate QC filters (Fig. 3), which was comparable to the findings of the previous study[12], thus indicating that the hemolytic protocol is a rapid and practical method for establishing LCLs by EBV transformation.

It is also important to note that when using the hemolytic protocol, the PBMCs and granulocytes need to be co-cultivated during EBV transformation. Although that can be a concern, the findings of this study clearly shown that the hemolytic protocol is superior to the gradient protocol for establishing LCLs from 0.1 ml of peripheral blood. In this study, we found that the viability was significantly higher for WBCs than for PBMCs (Table 2), thus suggesting the effectiveness of the hemolytic protocol as a cell purification method for the generation of LCLs. When we examined the cell components of each fraction (Table 3), the content of PBMCs isolated by the gradient protocol was found to be greatly changed when the initial volume of peripheral blood was reduced down to 0.1 ml; i.e., the proportion of lymphocyte population decreased from 90% to less than 70% while the neutrophils increased to ~30%, probably due to the handling while collecting the PBMC layer. Putting the low recovery rate of the gradient protocol (~15%) together (Table 2), the inclusion of neutrophils may result in an insufficient number of B lymphocytes for EBV infection, and thus fail to expand as an LCL (Fig. 2c, solid-gray square). In contrast, since the procedure of the hemolytic protocol simply adopts the removal of erythrocytes, the cell density, as well as the content of enriched PBMCs, remained consistent without being affected by the initial volume of peripheral blood (Tables 2 and 3). Therefore, we feel that this simple and efficient procedure provides an advantage over the gradient protocol.

Compared sample		Peripheral blood from sample group #7 (All SNPs)					Concordance (%)	Kappa**
		AA	AB	BB	No call	Total		
Peripheral blood from sample group #7 (as technical replicate)	AA	127,257	57	0	626	127,940		
	AB	129	89,987	88	545	90,749		
	BB	0	61	126,041	622	126,724		
	No Call	936	509	859	895	3,199		
	Total	128,322	90,614	126,988	2,688	348,612*	99.90	0.9985
LCL-hemolytic from sample group #7	AA	127,613	68	0	647	128,328		
	AB	80	90,031	62	506	90,679		
	BB	0	78	126,305	644	127,027		
	No Call	629	437	621	891	2,578		
	Total	128,322	90,614	126,988	2,688	348,612*	99.92	0.9987
LCL-gradient from sample group #7	AA	127,139	52	0	568	127,759		
	AB	125	89,964	140	602	90,831		
	BB	0	77	125,774	548	126,399		
	No Call	1,058	521	1,074	970	3,623		
	Total	128,322	90,614	126,988	2,688	348,612*	99.89	0.9983

Table 5. Cross-classification of genotype calls for evaluating the protocols started from 5 ml of peripheral blood. *Affy100k Array (116,204 SNPs) × 3 samples = 348,612 SNPs. **Closer to 1.0 indicates higher reproducibility.

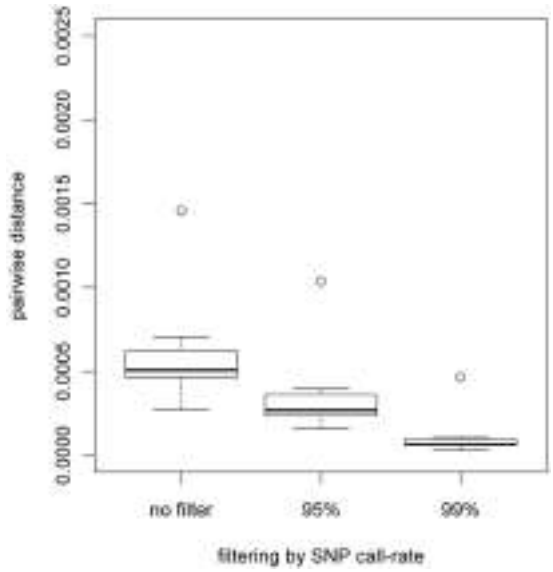

Figure 3. Genotype concordance by pairwise analysis. Genotype concordance between the genomic DNA from LCL-hemolytic and the peripheral blood, from which the LCLs were established, is shown as box plots with median values and interquartile range of pairwise distances. These box plots were generated using 9 samples from sample groups #7, #8, and #9 (Table 1). When the LCL-hemolytic samples maintain the genomic DNA intact, the pairwise distance should be close to 0. The vertical and horizontal axes indicate pairwise distance and the filtering conditions, respectively.

After infecting EBV to each isolated cell fraction, we observed distinct growth curves of LCLs based on the different protocols (Fig. 2). The LCLs established by the gradient protocol showed rapid growth for the first 2 weeks, as long as the initial cell number was sufficient (Fig. 2a,b), whereas the cell number drastically reduced in the first 2 weeks for LCLs established by the hemolytic protocol in all conditions (Fig. 2a–c). Since the initial pool of WBC fraction consisted of ~43% of lymphocytes together with ~52% of neutrophils (Table 3), this reduction appeared to be reflecting the cell number of more than 50% of the cell population that were not susceptible to EBV and eventually died within 2 weeks. On the other hand, the LCLs seemed to be consistently viable, which was apparent from the conversion into the growth phase of the LCLs after 2 weeks. Since the total cell number was approximately 0.3×10^6 cells at the time of EBV infection when starting with 0.1 ml of peripheral blood (Fig. 2c, solid-black circle), it indicated that the total number of lymphocytes should be less than 0.15×10^6 cells at that time, although the number was still approximately twice as many as the number of lymphocytes prepared by the

gradient protocol. This finding suggests that the limit of the total cell number for an efficient LCL generation was around 1×10^5 cells under our experimental conditions.

Although we are generally able to obtain a sufficient amount of blood necessary for any downstream experiments from each patient or volunteer, we sometimes encounter subjects in whom it is difficult to obtain a sufficient amount of peripheral blood. For example, in approximately 1% of the total number of volunteers in our cohort, including not only elderly but also young subjects, we had difficulty obtaining the biological samples needed for our experiments. In order to make good use of those samples, we therefore attempted to establish LCLs from the limited amount of peripheral blood, such as in the case of starting with 0.1 ml. As a result, our findings demonstrated that the LCLs were successfully established from this small amount of blood by the simple hemolytic protocol without affecting the quality (i.e., growth and quality of DNA) of LCLs as described above. Thus, those findings should be useful for the depository facilities worldwide and researchers who are performing large-scale population studies and genetics.

From another practical point of view, there are situations in which the blood samples are not be able to be processed immediately after collection. Chang *et al.* considered and examined the blood transporting time as one of the parameters that affects the efficiency and quality of LCL establishment[16] In this study, a total of 99 blood samples from sample groups #1 through #9 (Table 1) had a 100% success rate of LCL transformation by means of the hemolytic protocol, although these samples were collected, processed, and stored on the same day. We therefore examined the effect of keeping 5 ml or 0.1 ml of blood for 3 or 7 days at 4 °C or 25 °C prior to starting the establishment of LCLs by hemolytic protocol (Supplementary Fig. S1). As a result, we were able to establish LCLs from all of the samples. However, it took a longer period of time to transform into LCLs when the blood samples were kept for 7 days than those processed on the same day or kept for 3 days, especially when starting with a lesser volume of blood. For these reasons, we recommend to start the LCL establishment by hemolytic protocol within 3 days after receiving the blood.

In conclusion, the findings of this study demonstrated that the hemolytic protocol can serve as a reliable protocol in place of the gradient protocol for the establishment of LCLs. Of note, the hemolytic protocol enabled us to establish sufficient LCLs, even from a small amount of peripheral blood without affecting the quality of genomic DNA to be used for analysis. This simple, robust, and efficient protocol should prove to be practically useful, especially for the collection of tens of thousands of blood samples by a depository facility aimed at performing large-scale population studies.

Methods

Sample information. This study was approved by the Institutional Review Board of KPUM as part of ongoing studies, some of which have been published elsewhere[6–9,20–22]. All procedures were conducted in accordance with the tenets set forth in the Declaration of Helsinki, and written informed consent was obtained from all participating volunteers after receiving a detailed explanation of the procedures and possible consequences of being involved in the study. A total of 99 volunteers provided peripheral blood at the KPUM Hospital (Kyoto, Japan) for the present study (Table 1).

Study design. The design of this study is shown in Fig. 1, and the sample information is shown in Table 1. Comparisons of features of prepared cells by each protocol are shown in Tables 2 and 3, and comparison of LCL growth is shown in Fig. 2. Comparisons of the quality of the genomic DNA prepared from each material using each protocol are shown in Table 4. Comparison of the concordance of genotyping results using each genomic DNA is shown in Table 5, Fig. 3, and Supplementary Table S1.

Isolation of WBCs by the hemolytic protocol. Each volume of peripheral blood was centrifuged at $400 \times g$ for 10 minutes at room temperature (RT). After removal of the plasma fraction, the pellet was resuspended with a five-fold amount of hypotonic erythrocyte lysis buffer (Buffer EL; Qiagen, Valencia, CA, USA) against the initial blood volume, and then incubated for 15 minutes on ice in order to burst erythrocytes. After centrifugation at $400 \times g$ for 10 minutes at 4 °C, the supernatant containing the lysed erythrocytes was removed. The remaining pellet was then resuspended with a two-fold amount of Buffer EL against the initial blood volume, washed by centrifugation at $400 \times g$ for 10 minutes at 4 °C. After removing the supernatant, the pellet was promptly resuspended with standard B cell culture medium consisting of Gibco™ RPMI 1640 Medium (Life Technologies, Carlsbad, CA, USA) supplemented with 10% (v/v) fetal calf serum (FCS; Life Technologies), 1 mM MEM Non-Essential Amino Acid Solution (Life Technologies), 10 mM Sodium Pyruvate (Life Technologies), 1% (v/v) Penicillin-Streptomycin (Nacalai Tesque, Inc., Kyoto, Japan), and 50 μM 2-Mercaptoethanol (Nacalai Tesque). Finally, the cell number was counted by use of a hemocytometer in order to determine the appropriate cell density for EBV infection.

Isolation of PBMCs by the gradient protocol. Each volume of peripheral blood was diluted with an equal volume of phosphate buffered saline (PBS). The mixture was carefully layered onto an equal volume of Lymphocytes Separation Solution (Nacalai Tesque) to the initial blood volume for density gradient centrifugation. After centrifugation at $400 \times g$ for 30 minutes at RT, the upper layer was removed and the PBMC layer was then carefully transferred into a new tube by use of a sterile pipette. The isolated PBMC fraction was then washed twice with PBS by centrifugation at $250 \times g$ for 10 minutes at RT, and promptly resuspended with an equal volume of the standard culture medium to the initial blood volume. Finally, the cell number was then counted as described above.

Cell count, recovery rate, viability rate, and proportion of the cell components. Suspended cells were mixed with equal volume of Turk solution (Nacalai Tesque). Next, approximately 100 cells were set into

each of the four square corner areas of a glass covered Bürker-Türk hemocytometer cell counter plate, and then counted at approximately 400 cells per count. The complete blood count (CBC) of each sample was outsourced to an independent clinical laboratory (SRL, Inc., Tokyo, Japan) to be counted as described above. Based on the total number of WBC in the CBC and the isolated cells, the recovery rate (%) was calculated using the following formula:

$$recovery\ rate(\%) = \frac{total\ number\ of\ isolated\ cells}{total\ number\ of\ WBC\ in\ CBC} \times 100 \quad (1)$$

In addition, the dye exclusion test was performed using Trypan Blue Solution 0.4% (Life Technologies) stain in order to determine the number of viable cells present in the isolated cells. The viability rate (%) was calculated using the following formula:

$$viability\ rate(\%) = \frac{total\ number\ of\ unstained\ cells}{total\ cells(stained\ and\ unstained)count} \times 100 \quad (2)$$

Each isolated cell was smeared on a glass slide and stained with May-Grünwald and Giemsa Dye Solution (Wako Pure Chemicals, Osaka, Japan). The stained cells were classified into the following five components: neutrophils, eosinophils, basophils, lymphocytes, and monocytes based on the standard classification under a light microscope[23], and the percentage of each cell type included in 100 of the stained cells was then calculated.

Preparation of EBV supernatant from the B95-8 cell line. The EBV for LCL transformation was prepared and stocked as a culture supernatant of an EBV-producing marmoset cell line, B95-8[24], obtained from the Japan Health Sciences Foundation, Health Science Research Resources Bank (HSRRB, cell ID: JCRB9123). The maintenance of B95-8 cells and the viral supernatant were performed in accordance with the instructions from HSRRB. In brief, the B95-8 cells were cultured in Gibco™ RPMI 1640 with 10% FCS at 37 °C in 5% CO_2. Cultured conditioned medium was recovered, all debris was depleted by centrifugation at 400 × g for 10 minutes, and the recovered supernatant was then split into aliquots and stored at −80 °C until used for infection.

Establishment of LCL by EBV infection. LCLs were established from human peripheral blood cells or WBCs prepared by hemolytic protocol or PBMCs prepared by gradient protocol as follows. To the cells suspended in above-described standard B cell culture medium, a 50% volume of B95-8 supernatant was added to become 1.0×10^6 cells/ml as the final concentration. For establishing and maintaining LCLs, 1% (v/v) phytohemagglutinin (Life Technologies) was added[25]. Cells were then cultured at 37 °C in 5% CO_2, and one-third of the culture supernatant was replaced with fresh medium every 3-4 days. Phase-contrast microscopy revealed the transformation foci of LCLs typically at 4–7 days post infection. The success period of LCL establishment was defined as the day when the diameter of transformed cell clusters reached 50 μm. In order to evaluate the cell growth, the number of cells was counted at 2-week intervals until 8 weeks.

SNP genotyping and assessment of genotype concordance. Twenty-four samples were used from sample groups #7, #8, and #9 (Table 1c). Genomic DNA was extracted using the genomic BioRobot® EZ1™ Robotic Liquid Handler (Qiagen) in accordance with the manufacturer's instructions. The yield of DNA extraction and the ratio of A260/280 absorbance of genomic DNA was then measured and calculated (Table 4). The GeneChip® Mapping 100 K Array Set was used in accordance with the manufacturer's instructions, and genome-wide genotype data of 116,204 SNPs was then obtained for each sample. The SNP genotype data derived from each group was then compared and summarized as a cross-classification table (Table 5). The concordance rate of 348,612 (116,204 SNPs × 3 samples) SNP genotype calls was calculated using the following formula:

$$\text{concordance rate (\%)} = \frac{total\ number\ of\ identical\ calls\ at\ each\ genotype\ (AA,\ AB\ and\ BB)}{total\ number\ of\ genotype\ calls\ except\ for\ No\ Call} \quad (3)$$

Kappa statistics was applied to objectively assess the concordance rate. In addition, the pairwise distances between the SNP genotype data obtained from genomic DNA derived from peripheral blood and that obtained from genomic DNA derived from LCL-hemolytic was examined using PLINK open-source whole genome association analysis toolset software with the "–cluster" option (http://pngu.mgh.harvard.edu/~purcell/plink/), which is commonly used in genetics for calculating identity-by-state distances (Fig. 3). The value of pairwise distance indicates 0 if the pair is an identical twin (i.e., expected that all the genotypes to be fully matched). The number of SNPs to calculate pairwise distance was compared by the condition of SNP filtering based on the call rate as: no filter (i.e., all SNPs were applied), 95%, and 99% (i.e., the number of genotype with no call was less than 5% or 1% in each SNP, respectively; the regular filtering condition applied in GWAS). Additional information of the DNA microarray experiments and comparison processes are described in the Supplementary Note.

Statistical analysis. R software (http://www.r-project.org/) was used for all statistical analyses (i.e., Shapiro-Wilk test, Wilcoxon signed rank test, Wilcoxon rank sum test, and Kappa statistics) and for creating graphs. In addition, the

R package of "exactRankTests" was used for the Wilcoxon tests. To manage the genotype data, our in-house TG Server System based on the Labo Server Software System (World Fusion, Tokyo, Japan) was used as previously described[6–9]. Genotype concordance estimated by pairwise distance was analyzed by use of PLINK.

References

1. Kieff, E. & Rickinson, A. B. In *Fields Virology* Vol. 2 (eds. Knipe, D. M. & Howley, P. M.) 2511–2573 (Lippincott Williams & Wilkins, 2001).
2. Thorley-Lawson, D. A. & Gross, A. Persistence of the Epstein-Barr virus and the origins of associated lymphomas. *N. Engl. J. Med.* **350,** 1328–1337 (2004).
3. Sie, L., Loong, S. & Tan, E. K. Utility of lymphoblastoid cell lines. *J. Neurosci. Res.* **87,** 1953–1959 (2009).
4. Beck, J. C., Beiswanger, C. M., John, E. M., Satariano, E. & West, D. Successful transformation of cryopreserved lymphocytes: a resource for epidemiological studies. *Cancer Epidemiol. Biomarkers Prev*. **10,** 551–554 (2001).
5. Bass, H., Walters, R. & Darke, C. Provision of Epstein-Barr virus-transformed B-cell lines in a routine tissue typing laboratory: practicalities and applications. *Eur. J. Immunogenet.* **31,** 87–92 (2004).
6. Nakano, M. *et al.* Three susceptible loci associated with primary open-angle glaucoma identified by genome-wide association study in a Japanese population. *Proc. Natl. Acad. Sci. USA* **106,** 12838–12842 (2009).
7. Ueta, M. *et al.* Association between prostaglandin E receptor 3 polymorphisms and Stevens-Johnson syndrome identified by means of a genome-wide association study. *J. Allergy Clin. Immunol.* **126,** 1218–1225 (2010).
8. Nakano, M. *et al.* Common Variants in CDKN2B-AS1 Associated with Optic-Nerve Vulnerability of Glaucoma Identified by Genome-Wide Association Studies in Japanese. *PLoS One* **7,** e33389; 10.1371/journal.pone.0033389 (2012).
9. Nakano, M. *et al.* Novel common variants and susceptible haplotype for exfoliation glaucoma specific to Asian population. *Sci. Rep.* **4,** 5340; 10.1038/srep05340 (2014).
10. Neitzel, H. A routine method for the establishment of permanent growing lymphoblastoid cell lines. *Hum. Genet.* **73,** 320–326 (1986).
11. Lam, K. M. C. & Crawford, D. H. Method for generation of human B lymphoblastoid cell lines using Epstein-Barr virus. *Methods Cell Sci.* **17,** 67–74 (1995).
12. Herbeck, J. T. *et al.* Fidelity of SNP array genotyping using Epstein Barr virus-transformed B-lymphocyte cell lines: implications for genome-wide association studies. *PLoS One* **4,** e6915, 10.1371/journal.pone.0006915 (2009).
13. Frisan, T., Levitsky, V. & Masucci, M. Generation of lymphoblastoid cell lines (LCLs). *Methods Mol. Biol.* **174,** 125–127 (2001).
14. Bosslet, K., Ruffmann, R., Altevogt, P. & Schirrmacher, V. A rapid method for the isolation of metastasizing tumour cells from internal organs with the help of isopycnic density-gradient centrifugation in Percoll. *Br. J. Cancer* **44,** 356–362 (1981).
15. Ruitenberg, J. J., Mulder, C. B., Maino, V. C., Landay, A. L. & Ghanekar, S. A. VACUTAINER CPT and Ficoll density gradient separation perform equivalently in maintaining the quality and function of PBMC from HIV seropositive blood samples. *BMC Immunol.* **7,** 11, 10.1186/1471-2172-7-11 (2006).
16. Chang, I. C. *et al.* High-potentiality preliminary selection criteria and transformation time-dependent factors analysis for establishing Epstein-Barr virus transformed human lymphoblastoid cell lines. *Cell Prolif.* **39,** 457–469 (2006).
17. Kong, S. Y. & Kang, S. Epstein-Barr virus-transformation of B-cell lines in ovarian cancer patients: feasibility of genomic storage for unlimited use. *J. Gynecol. Oncol.* **20,** 243–245 (2009).
18. Hui-Yuen, J., McAllister, S., Koganti, S., Hill, E. & Bhaduri-McIntosh, S. Establishment of Epstein-Barr virus growth-transformed lymphoblastoid cell lines. *J. Vis. Exp.*; 10.3791/3321 (2011).
19. Fukushima, Y., Ohashi, H., Wakui, K., Nishida, T. & Oh-ishi, T. A rapid method for starting a culture for the establishment of Epstein-Barr virus-transformed human lymphoblastoid cell lines. *Jpn. J. Hum. Genet.* **37,** 149–150 (1992).
20. Mori, K. *et al.* LOXL1 genetic polymorphisms are associated with exfoliation glaucoma in the Japanese population. *Mol. Vis.* **14,** 1037–1040 (2008).
21. Tokuda, Y. *et al.* An approach to predict the risk of glaucoma development by integrating different attribute data. *SpringerPlus* **1,** 41 (2012).
22. Nakano, M. *et al.* Trinucleotide Repeat Expansion in the TCF4 Gene in Fuchs' Endothelial Corneal Dystrophy in Japanese. *Invest. Ophthalmol. Vis. Sci.* **56,** 4865–4869 (2015).
23. Platt, W. R. *Color atlas and textbook of hematology* SECOND EDITION (Lippincott, 1979).
24. Miller, G., Shope, T., Lisco, H., Stitt, D. & Lipman, M. Epstein-Barr virus: transformation, cytopathic changes, and viral antigens in squirrel monkey and marmoset leukocytes. *Proc. Natl. Acad. Sci. USA* **69,** 383–387 (1972).
25. Chang, I. C., Ko, H. W. & Hwang, S. M. Capacity of robot handling for Epstein-Barr virus transformation. *Cell Prolif.* **42,** 10–14 (2009).

Acknowledgements

The authors wish to thank all of the participants who were enrolled in the study. In addition, the authors wish to thank Sayaka Ohashi and Naoko Saito for processing blood samples and performing genotyping, Hiromi Yamada for her assistance in sample information analysis, Ryuichi Sato and Fumiko Sato for the management of the genotype data and construction of the analyzing system, John Bush for reviewing the manuscript, and Tomoko Ichikawa for excellent secretarial assistance. This study was supported by financial grants from Collaborative Development of Innovative Seeds of Japan Science and Technology Agency (JST) to K.T.; the Ministry of Health, Labor, and Welfare of Japan to K.M., S.K., M.N., and K.T.; and the Santen Pharmaceutical Co., Ltd. to S.K. and K.T.

Author Contributions

N.O. designed the concept and directed the research. N.O., Y.T. & M.N. contributed to the design of all experiments and to the analysis of the data. N.O., Y.T., M.N., Y.I., K.M., C.S., S.K., and K.T discussed the results and commented on the manuscript. All authors reviewed the manuscript.

Additional Information

Supplementary information accompanies this paper at http://www.nature.com/srep

Competing Interests: The authors declare no competing financial interests.

How to cite this article: Omi, N. *et al.* Efficient and reliable establishment of lymphoblastoid cell lines by Epstein-Barr virus transformation from a limited amount of peripheral blood. *Sci. Rep.* **7**, 43833; doi: 10.1038/srep43833 (2017).

Hindawi
Stem Cells International
Volume 2017, Article ID 9210494, 9 pages
https://doi.org/10.1155/2017/9210494

Research Article

Myogenic Differentiation from *MYOGENIN*-Mutated Human iPS Cells by CRISPR/Cas9

Koki Higashioka,[1,2] Noriko Koizumi,[2] Hidetoshi Sakurai,[3] Chie Sotozono,[1] and Takahiko Sato[1]

[1]*Department of Ophthalmology, Kyoto Prefectural University of Medicine, Kyoto, Japan*
[2]*Department of Biomedical Engineering, Faculty of Life and Medical Sciences, Doshisha University, Kyotanabe, Japan*
[3]*Department of Clinical Application, Center for iPS Cell Research and Application, Kyoto University, Kyoto, Japan*

Correspondence should be addressed to Takahiko Sato; takahiko@koto.kpu-m.ac.jp

Received 12 January 2017; Accepted 5 March 2017; Published 4 April 2017

Academic Editor: Yuko Miyagoe-Suzuki

It is well known that myogenic regulatory factors encoded by the *Myod1* family of genes have pivotal roles in myogenesis, with partially overlapping functions, as demonstrated for the mouse embryo. *Myogenin*-mutant mice, however, exhibit severe myogenic defects without compensation by other myogenic factors. MYOGENIN might be expected to have an analogous function in human myogenic cells. To verify this hypothesis, we generated *MYOGENIN*-mutated human iPS cells by using CRISPR/Cas9 genome-editing technology. Our results suggest that MYOD1-independent or MYOD1-dependent mechanisms can compensate for the loss of MYOGENIN and that these mechanisms are likely to be crucial for regulating skeletal muscle differentiation and formation.

1. Introduction

In vertebrate embryos, skeletal muscles of the trunk and limbs are derived from the somites, from the dermomyotome which gives rise to myogenic progenitor cells that are directed into the skeletal muscle programme by four myogenic bHLH transcription factors, Myf5, Myod1, Mrf4, and Myogenin (Myog) [1–3]. The myogenic differentiation process in vertebrate embryos is regulated by these factors leading to the formation of multinucleated myotubes and subsequently to the regeneration of skeletal muscle by a reserve of myogenic stem cells in adulthood [4, 5].

Single or compound knockout mice for the genes encoding these myogenic factors have been created to identify their function in myogenesis [3]. Single *Myf5*- or *Myod1*-deficient mice revealed no striking skeletal muscle phenotype [6–8], pointing to overlapping functions between these myogenic determination factors [9–11]. *Mrf4*, which is coexpressed with *Myf5* at the onset of myogenesis, also acts as an early myogenic determination factor [11]. Double and triple mutants for these genes demonstrate their role in determining muscle cell fate. The fourth member of this gene family, *Myog*, is expressed at the onset of muscle cell differentiation. Single *Myog*-deficient mice exhibit severe defects of skeletal muscle formation during development, at a stage when Myod1 and, in many muscles, Mrf4 are also present. This therefore demonstrates that Myog is required for embryonic muscle differentiation, and no redundant or compensatory mechanisms replace its function, unlike for the other myogenic regulatory factors [10, 12–15].

In this study, we have tackled the question of whether these myogenic factors have analogous interrelationships in human myogenesis and, in particular, whether human MYOGENIN (MYOG) is also essential for muscle cell differentiation and muscle fiber formation in myogenic cells derived from human induced pluripotent stem (hiPS) cells. To perform functional experiments, we have used versatile genome-editing technology, with the CRISPR/Cas9 system [16, 17].

Table 1: Candidates and oligos for *MYOGENIN* exon1 target positions for CRISPR/Cas9.

Position		Target sequence	Sequence information		Number of target sites		
Start–end	+/−	20 bp + **PAM**	GC (%)	Tm (°C)	20 bp	12 bp	8 bp
143–165	−	**cct**gcctgtccacctccagggct	70	84	1	61	5171
147–169	−	**cct**gtccacctccagggcttcga	65	80	1	38	92,481
152–174	−	**cca**cctccagggcttcgaaccac	65	79	1	89	10,513
155–177	−	**cct**ccagggcttcgaaccaccag	65	79	1	8	11,331
156–178	+	ctccagggcttcgaaccacc**agg**	65	79	1	1	4654
158–180	−	**cca**gggcttcgaaccaccaggct	65	81	1	7	21,861
166–188	+	tcgaaccaccaggctacgag**cgg**	60	77	1	10	12,349
170–192	**+**	accaccaggctacgagcgga**cgg**	65	82	1	1	3812
171–193	−	**cca**ccaggctacgagcggacgga	70	82	1	8	1537
174–196	−	**cca**ggctacgagcggacggagct	70	83	1	3	479
191–213	+	**gga**gctcaccctgagccccgagg	75	84	1	43	382

pX458-*hMYOG*+189_F primer: CACCaccaccaggctacgagcgga. pX458-*hMYOG*+189_R primer: AAACtccgctcgtagcctggtggt.

2. Materials and Methods

2.1. Gene Targeting with Human iPS Cells. The *hMYOG*-targeting plasmid vector, pX458-*hMYOG*+189, was constructed using the pX458 vector (Addgene #48138, Cambridge, USA) [17] with ligating oligos (Table 1) as described, and plasmid DNA was introduced into HEK293- or Hu5/KD3-immortalized human myogenic cells [18], with ViaFect reagent (Promega, Madison, USA). The electroporator NEPA21 (NEPA GENE, Chiba, Japan) was used for introducing plasmids into hiPS cells [19].

2.2. Cell Culture and Myogenic Differentiation. The hiPS cells were maintained on SNL feeder cells, treated with 10 μg/ml of mitomycin (Sigma, St. Louis, USA) in DMEM (Wako, Osaka, Japan) supplemented with 10% of fetal bovine serum (GIBCO, Grand Island, USA), or expanded in Primate ES cell medium (ReproCELL, Kanagawa, Japan) supplemented with 10 ng/ml of recombinant human FGF2 (bFGF; Wako, Osaka, Japan) and 100 μg/ml of G418 (Nacalai Tesque, Kyoto, Japan). *MYOG*-deficient iPS cells were maintained on SNL feeder cells or iMatrix-511 (Nippi, Tokyo, Japan)-coated plates with StemFit AK03N (Ajinomoto, Tokyo, Japan) under a feeder-free culture system [20].

For the derivation of myogenic cells from hiPS cells, the detailed protocol of Tanaka et al., based on MYOD1 induction [21], was followed. In brief, single iPS cells carrying an inducible MYOD1 activation system were expanded in Primate ES cell medium without bFGF and with 10 μM of Y-27632 (Nacalai Tesque, Kyoto, Japan) for 24 hours and then induced into myogenic cells by adding 500 ng/ml of doxycycline (Dox; Tocris, Bristol, UK). After 24 hours, culture medium was changed into myogenic differentiation medium composed of alpha-MEM (Nacalai Tesque, Kyoto, Japan) with 5% of KSR (GIBCO, Grand Island, USA) and 500 ng/ml of Dox. After 6 days, culture medium was changed into muscle maturation medium, DMEM/F12 (Nacalai Tesque, Kyoto, Japan), with 5% of horse serum (Sigma, St. Louis, USA), 10 ng/ml of recombinant human insulin-like growth factor 1 (IGF-1; PeproTech, Hartford County, USA), and 200 μM of 2-mercaptoethanol (2-ME; Sigma, St. Louis, USA).

To obtain myogenic cells derived from embryonic mesodermal cells, single iPS cells were expanded in StemFit AK03N supplemented with 10 μM of Y-27632. After 2 days, the culture medium was changed into modified mesodermal differentiation medium as described by Loh et al. [22]. Cultured cells were passaged 12 days later and cultured in mesoderm differentiation medium with 10 μM of Y-27632 for 2 days. To initiate myogenic differentiation, medium SF-O3 (EIDIA, Tokyo, Japan), supplemented with 10 ng/ml of bFGF, 10 ng/ml of IGF-1, 10 ng/ml of HGF (PeproTech, Hartford, USA), and 200 μM of 2-ME, was used and changed into myogenic differentiation medium with IGF-1 after 4 days and then with IGF-1 and HGF after 3 days [23]. To obtain more mature myogenic differentiation, culture medium was changed into DMEM/F12 supplemented with 2% of horse serum, 10 ng/ml of IGF-1, and 200 μM of 2-ME 2 weeks later and induced cells were harvested at day 60 [23].

2.3. Cell Sorting. Cultured cells transfected with pX458-*hMYOG*+189 were dissociated with TrypLE select (GIBCO, Grand Island, USA) at 37°C for 5 min for detecting transfected cells. Dissociated cells were resuspended with 1% bovine serum albumin in PBS. Cell debris were eliminated with a cell strainer (35 μm; BD, New Jersey, USA), and suspensions were stained with propidium iodide (Molecular Probes, Eugene, USA) to exclude dead cells. Cells were analyzed and collected by a cell sorter using FACSJazz (BD, New Jersey, USA).

2.4. Quantitative PCR Analyses. Total RNAs from sorted or cultured cells were extracted using the RNeasy micro kit (QIAGEN, Hilden, Germany). For quantitative PCR analyses, single strand cDNA was prepared using a SuperScript VILO kit (Invitrogen, Carlsbad, USA) as in the manufacturer's protocol. All RT-qPCR reactions were carried out in triplicate using THUNDERBIRD SYBR qPCR Mix (TOYOBO, Osaka, Japan), normalized to the mRNA expression level of

Table 2: Primer sequences for T7 endonuclease assay and quantitative RT-PCR.

Genes	Sequences	Amplicon size
Primer for T7 EI assay		
MYOG gDNA_F	5′-GGCCGCCCAGCTAGGAGTAATTGA-3′	786
MYOG exon1_R	5′-CGCTCGATGTACTGGATGGCACTG-3′	
Primer for RT-qPCR		
*RPL13A*_F	5′-CCCTGGAGGAGAAGAGGAAA-3′	91
*RPL13A*_R	5′-ACGTTCTTCTCGGCCTGTTT-3′	
*MYOG*_F	5′-GCTCAGCTCCCTCAACCA-3′	94
*MYOG*_R	5′-GCTGTGAGAGCTGCATTCG-3′	
*MYOD1*_F	5′-GCACTACAGCGGCGACTCC-3′	118
*MYOD1*_R	5′-GTAGGCGCCTTCGTAGCAG-3′	
Endo-*MYOD1*_F	5′-CACTCCGGTCCCAAATGTAG-3′	180
Endo-*MYOD1*_R	5′-TTCCCTGTAGCACCACACAC-3′	
*MRF4*_F	5′-GGCCAAGTGTTTCCGATCAT-3′	89
*MRF4*_R	5′-AAGGCTACTCGAGGCTGACG-3′	

ribosomal protein L13A (RPL13A). Primer sequences (5′ to 3′) are listed in Table 2.

2.5. Immunofluorescence Assay. Cultured cells were fixed in 4% paraformaldehyde for 10 min at 4°C, permeabilized with 0.2% Triton and 50 mM NH_4Cl. Fixed samples were pretreated with Blocking One (Nacalai Tesque, Kyoto, Japan) for 30 min at RT and incubated with anti-MYOGENIN (diluted 1 : 100, Santa Cruz Biotechnology, California, USA), anti-MYOSIN HEAVY CHAIN (MYHC, diluted 1 : 200, Santa Cruz Biotechnology, California, USA), anti-TRA-1-81 (diluted 1 : 200, Cell Signaling Technology, Massachusetts, USA), anti-SSEA4 (diluted 1 : 200, Cell Signaling Technology, Massachusetts, USA), anti-OCT4A (diluted 1 : 200, Cell Signaling Technology, Massachusetts, USA), and anti-NANOG (diluted 1 : 200, Cell Signaling Technology, Massachusetts, USA) antibodies in 5% of Blocking One in PBS with 0.1% Tween20 (PBST) overnight at 4°C. After three washes with PBST, cells were incubated with Alexa488-, Alexa594-, or Alexa647-conjugated secondary antibodies (diluted 1 : 500, Molecular Probes, Eugene, USA). Cells were washed with PBST three times and mounted in SlowFade Diamond antifade mountant with DAPI (Molecular Probes, Eugene, USA). Fluorescent images were collected on the software of BZ-X700 (Keyence, Osaka, Japan). Cultured cells were analyzed from triplicate experiments.

3. Results

3.1. Human MYOGENIN Genomic DNA Editing with the CRISPR/Cas9 System. To generate *MYOG*-mutated hiPS cells by double-strand break in *MYOG* exon1 which includes coding sequence (Figure 1(a)), we selected several sequences bound to single guide RNA for targeting by nuclease Cas9 from the CRISPRdirect website as candidates (http://crispr.dbcls.jp, Table 1) [24] and ligated them into the pX458 vector to create the pX458-*hMYOG*+189-editing vector, which targets a unique 20 bp sequence in *hMYOG* exon1 (position 170–192; accaccaggctacgagcgga, Figure 1(b)). The effect of a double-strand break in *hMYOG* genomic sequences was evaluated by heteroduplex PCR fragments, involving the sequences targeted by the pX458-*hMYOG*+189-editing vector, monitored in HEK293 cells and T7 endonuclease I (T7EI). Enzymatic digested PCR bands of 500 bp and 300 bp were observed in T7EI-treated genomic DNA (Figure 1(c)). The data suggested that nuclease Cas9 and single guide RNA target *hMYOG* genomic sequences of exon1. The expression of *MYOG* is initiated in differentiating myogenic cells. To check the amount of *MYOG* transcripts produced from this Cas9 construct, immortalized Hu5/KD3, human myoblasts, transfected with or without the pX458-*hMYOG*+189 vector were differentiated in medium with 2% horse serum for 48 hours. The transcriptional level of *MYOG* was attenuated in differentiated Hu5/KD3 cells (Figure 1(d)). This CRISPR/Cas9 construct for *hMYOG* sequences may not only be effective because of its genomic double-strand break which knocks out *MYOG* expression but may also affect the remaining *MYOG* transcription level.

3.2. Generation of MYOGENIN-Mutated hiPS Cells. In order to generate *MYOG*-mutated hiPS cells, we used hiPS cells carrying a *MYOD1* expression construct which is inducible with Dox to activate the myogenic programme (Figure 2(a)) [21]. The iPS cells were expanded on SNL feeder-coated plates after electroporation with pX458-*hMYOG*+189 vector for 48 hours, and GFP-positive cells were collected by cell sorting (Figures 2(b) and 2(c)). These cells were plated out to form colonies which were individually picked up. Each clone was screened for further analyses.

We were able to identify 25 clones, which were lacking the wild-type *MYOG* sequences (wild type: 19.4%, heterozygotes; 64.5%, homozygotes; and 16.1%, total screened clones $n = 31$) by checking genomic sequences around the targeted *MYOG* region. Selected clone number 28 or clone number C3 was confirmed to have biallelic on-target frameshift

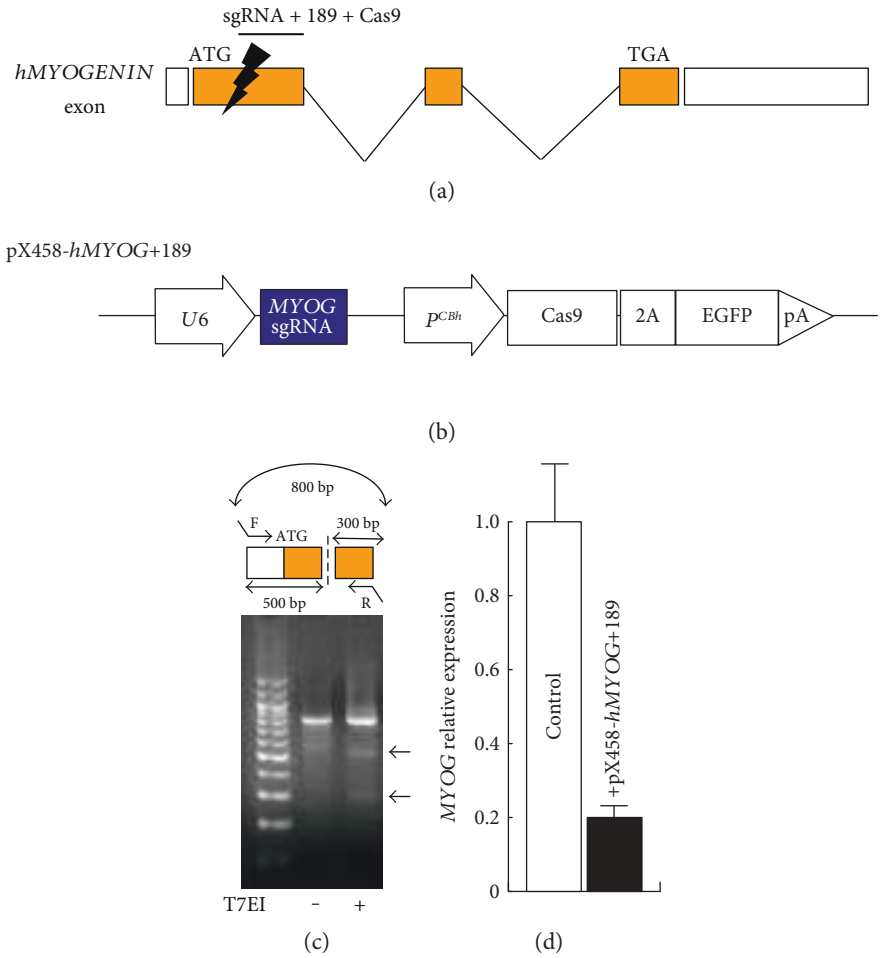

Figure 1: Effect of single guide sequence for *hMYOGENIN* by the CRISPR/Cas9 system. A schematic representation of *MYOG* exons and introns. A candidate position for Cas9 targeting of *MYOG* exon1 (a). pX458-*hMYOG*+189, a construct for driving single guide RNA bound to *MYOG* exon1 and bicistronic expression of both Cas9 and GFP (b). T7 endonuclease I assay for Cas9-mediated cleavage (arrows, 500 bp and 300 bp) on an agarose gel, showing comparable modification of the targeted human *MYOG* genomic fragment in HEK293T cells (c). Relative expression of *MYOG* in Hu5-immortalized human myoblast cells transfected with or without the pX458-*hMYOG*+189 vector. All error bars indicate ±SEM ($n = 3$).

mutations, 5 bp of deletion, and an extra 1 bp of integration in the *hMYOG*-sgRNA and Cas9-targeted region as shown in Figure 2(d). These data suggest that this targeting CRISPR/Cas9 system is sufficiently efficient to knockout both alleles of *MYOG* directly by introducing out-of-frame mutations (lower images in Figure 2(f)). *MYOG*-mutated hiPS cells (clone number 28) were immunostained with undifferentiated pluripotent markers, anti-SSEA4, anti-OCT3/4, anti-TRA1-80, and anti-NANOG antibodies, to evaluate the undifferentiated pluripotent state, and these markers were detected positively in *MYOG*-mutated hiPS cells (Figure 2(e)). To confirm the translation of truncated MYOG protein from these mutated sequences, myogenic cells differentiated from Dox-treated hiPS cells for 7 days were immunoreacted with antibodies against human MYOG N-terminus and C-terminus relatively because *MYOG* mRNAs are transcribed with the extra stop codon, which results from the *MYOG* gene targeting. Myogenic cells derived from wild-type hiPS cells were detected by both of these MYOG antibodies; however, the C-terminus of MYOG was not detected in *MYOG*-mutated hiPS cells (Figure 2(f)).

3.3. Skeletal Myogenic Differentiation by MYOD1 Induction. To investigate human MYOG function during myogenic differentiation, MYOD1 was overexpressed in hiPS cells by administrating Dox as shown in Figure 3(a). *MYOD1* expression mimics bicistronic mCherry fluorescence after Dox treatment (Figure 3(b)). Induced myogenic cells derived from hiPS cells were cultured in vitro under differentiation conditions and immunostained for MYHC expression as an indicator of their ability to differentiate into skeletal muscle fibers (Figure 3(c)). Although the rate of myoblast fusion in *MYOG*-mutated hiPS cell clone number 28 was slightly less than that of wild type (Figure 3(d)), terminal differentiation is similar.

To further characterize the differentiation of these myogenic cells, RNA expression of myogenic factors was analyzed by quantitative RT-PCR. The transcript for *MYOG* was downregulated as shown in Figure 1(d) with unknown mechanisms; however, other myogenic factors, notably

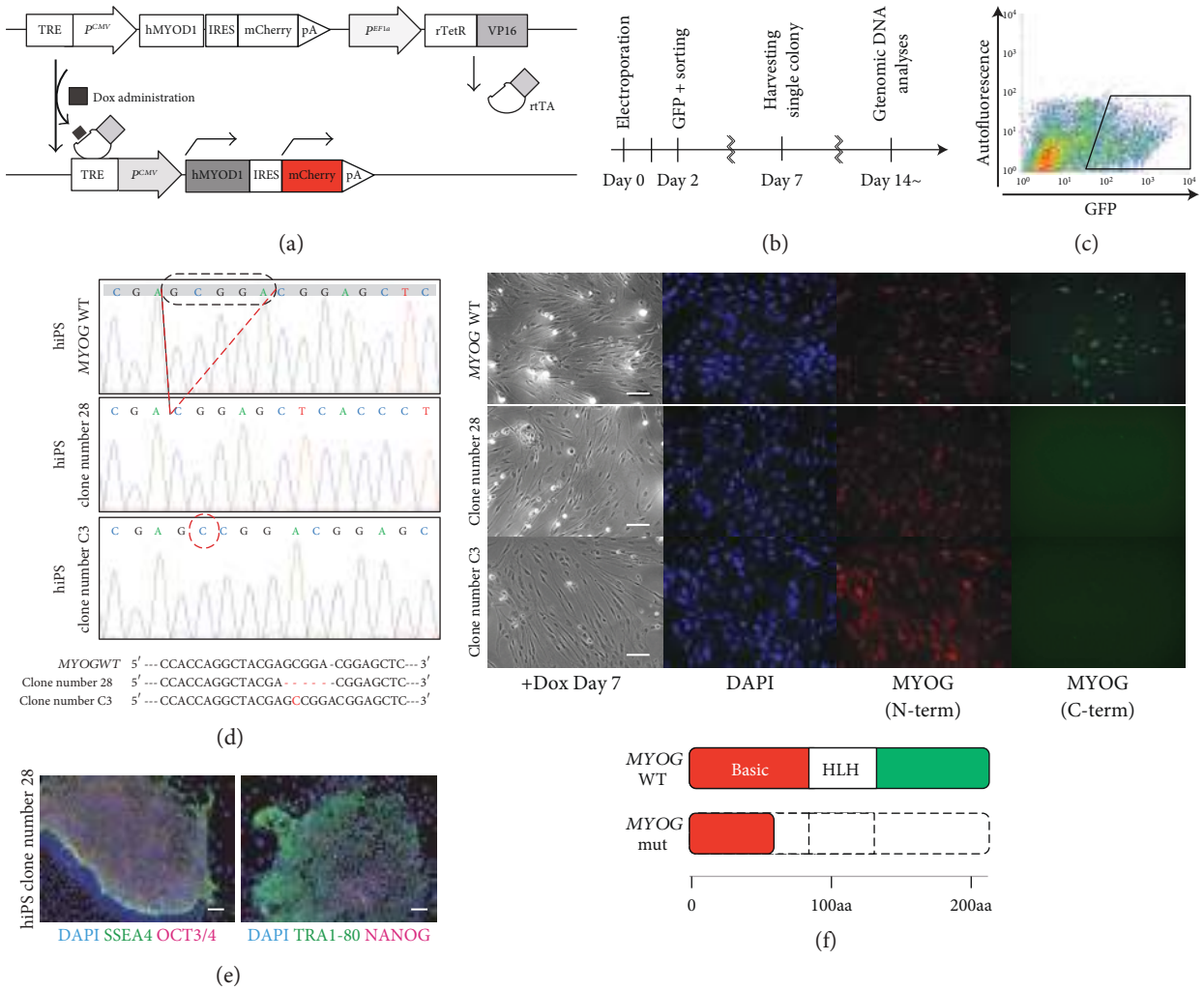

Figure 2: Generation of *hMYOGENIN*-mutated hiPS cells. A schematic model for the induction of myogenic cells derived from hiPS cells by overexpression of *MYOD1* marked with mCherry (red) after administrating Dox (a). A flowchart of the time course for the identification of *MYOG*-mutated hiPS cells (b). FACS analyses to isolate hiPS cells after the introduction of the pX458-*hMYOG*+189 vector (c). Genomic sequence data around the region targeted by pX458-*hMYOG*+189. 5 bp of deletion in clone number 28 and 1 bp of insertion in clone number C3 (dashed lines, (d)). Established hiPS cells were immunostained with undifferentiated pluripotent cell markers, anti-SSEA4 (green in left panel), anti-OCT3/4 (red in left panel), anti-TRA1-80 (green in right panel), and anti-NANOG (red in right panel) antibodies. Nuclei were stained with 4′6-diamidino-2-phenylindole (DAPI, blue). Scale bar, 100 μm (e). Differentiated myogenic cells after Dox treatment for 7 days were immunostained with anti-MYOG N-terminus (N-term, red) and C-terminus (C-term, green) antibodies. Nuclei were stained with 4′6-diamidino-2-phenylindole (DAPI, blue). Scale bar, 100 μm (upper in (f)). Putative MYOG protein structures both in wild-type (*MYOG* WT) and mutated cells (*MYOG* mut) (lower in (f)).

transcripts of *MYOD*1 or *MRF4*, were upregulated under conditions where *MYOG* is mutated in human myogenic cells (Figures 3(e)–3(g)).

3.4. Skeletal Muscle Differentiation via Mesodermal Differentiation In Vitro. Transient overexpression of *MYOD1* might have overcome the effect of MYOG deficiency because artificially high MYOD1 may compensate the inactivation of the *MYOG* gene in human myogenic cells. To avoid excessive MYOD1 levels, myogenic cells were induced from mesodermal precursors derived from hiPS cell clone number 28, without administration of Dox as shown in Figure 4(a).

The percentage of mesodermal induction marked by DLL1 [22] was shown by FACS analyses and was similar irrespective of *MYOG* mutation (Figure 4(b)). In myogenic cells derived from mesodermal precursors, total *MYOD1* transcripts did not accumulate, in contrast to Dox-treated hiPS cells, including lower level of endogenous *MYOD1* expression (Figure 4(c)). Under these conditions, MYHC-positive differentiated myofibers derived from both MYOG-positive and MYOG-negative hiPS cells were identified to a similar extent (Figure 4(d)). To analyze myogenic differentiation potential from mesodermal cells, transcripts of myogenic regulatory factors were monitored in these cells. The level of *MYOG* transcript was attenuated; however, *MYOD1* or *MRF4* transcripts were not much changed in wild-type and *MYOG*-mutated myogenic cells, as upregulated in *MYOG*-mutated cells during periods of cell culture (Figure 4(e)).

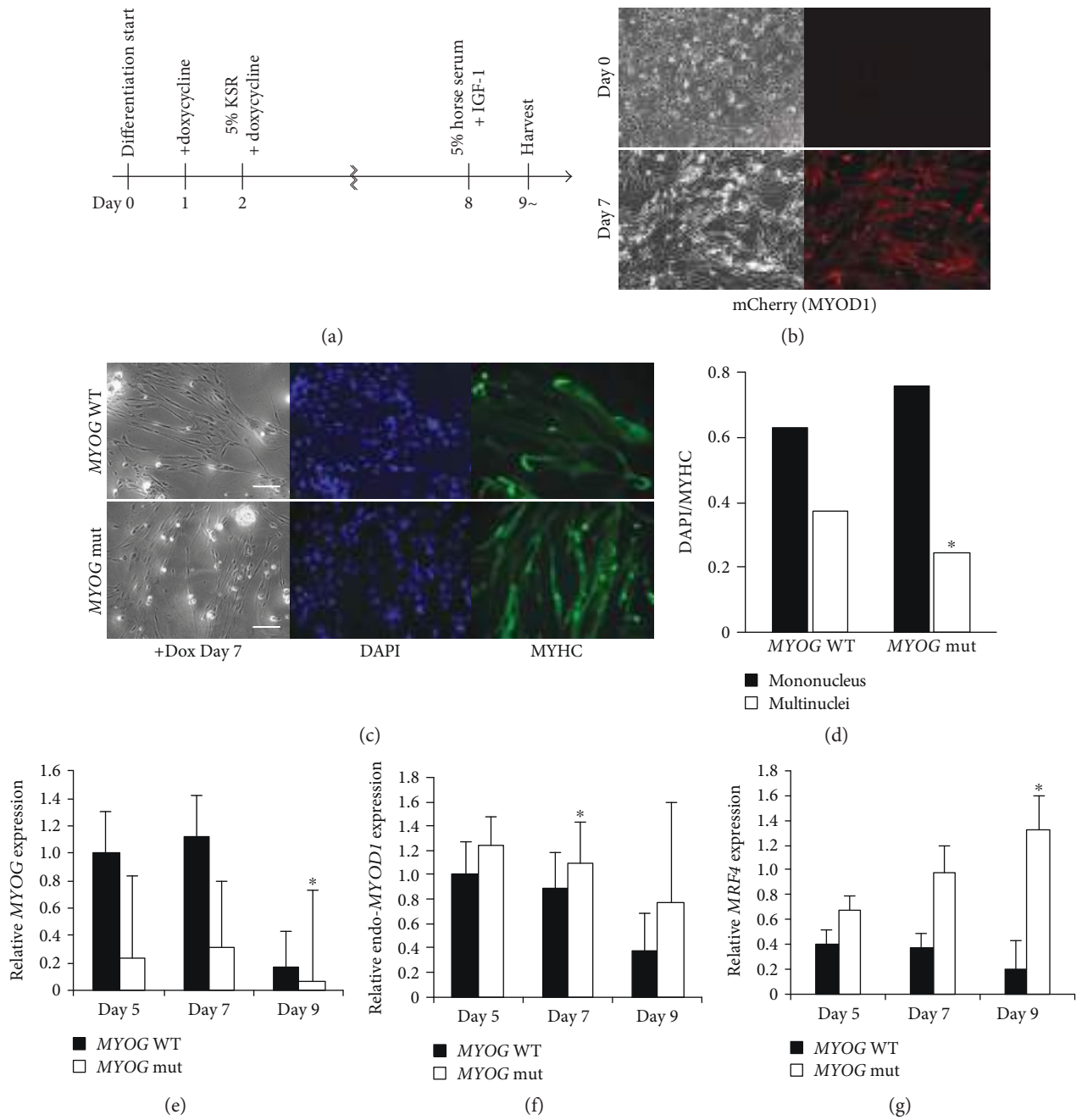

Figure 3: Myogenic differentiation in skeletal muscle cells derived from *MYOGENIN*-deficient hiPS clone number 28 cells. Myogenic differentiation flowchart of the time course (a). Morphological changes and mCherry fluorescent expression after treatment with Dox (b). Differentiated myogenic cells derived from hiPS cells with or without MYOG by Dox treatment for 7 days were immunostained with anti-MYOSIN HEAVY CHAIN (MYHC, green) antibody. Nuclei were stained with 4′6-diamidino-2-phenylindole (DAPI, blue). Scale bar, 100 μm (c). The ratio of DAPI-positive mono or multiple nuclei staining present in single MYHC-positive myofibers derived from wild-type or *MYOG*-mutated hiPS cells (d). Relative expression of transcripts for myogenic regulatory factors, *MYOG* (e), endogenous *MYOD1* (f), and *MRF4* (g), in differentiated myogenic cells treated with Dox for 5, 7, and 9 days. All error bars indicate ±SEM ($n = 3$). P values are determined by a t-test from a two-tailed distribution. $^*P < 0.05$.

4. Discussion

Here, we report the generation of *MYOGENIN*-deficient hiPS cells and the impact on human myogenic differentiation using CRISPR/Cas9 technology. This bacterial system has emerged as an effective tool for gene targeting through non-homologous end joining (NHEJ); however, it has been reported to be inefficient for precise editing of genomic sequences. In this study, we selected the sequence of *MYOG* exon1-targeted sgRNA with the Cas9 complex as a unique

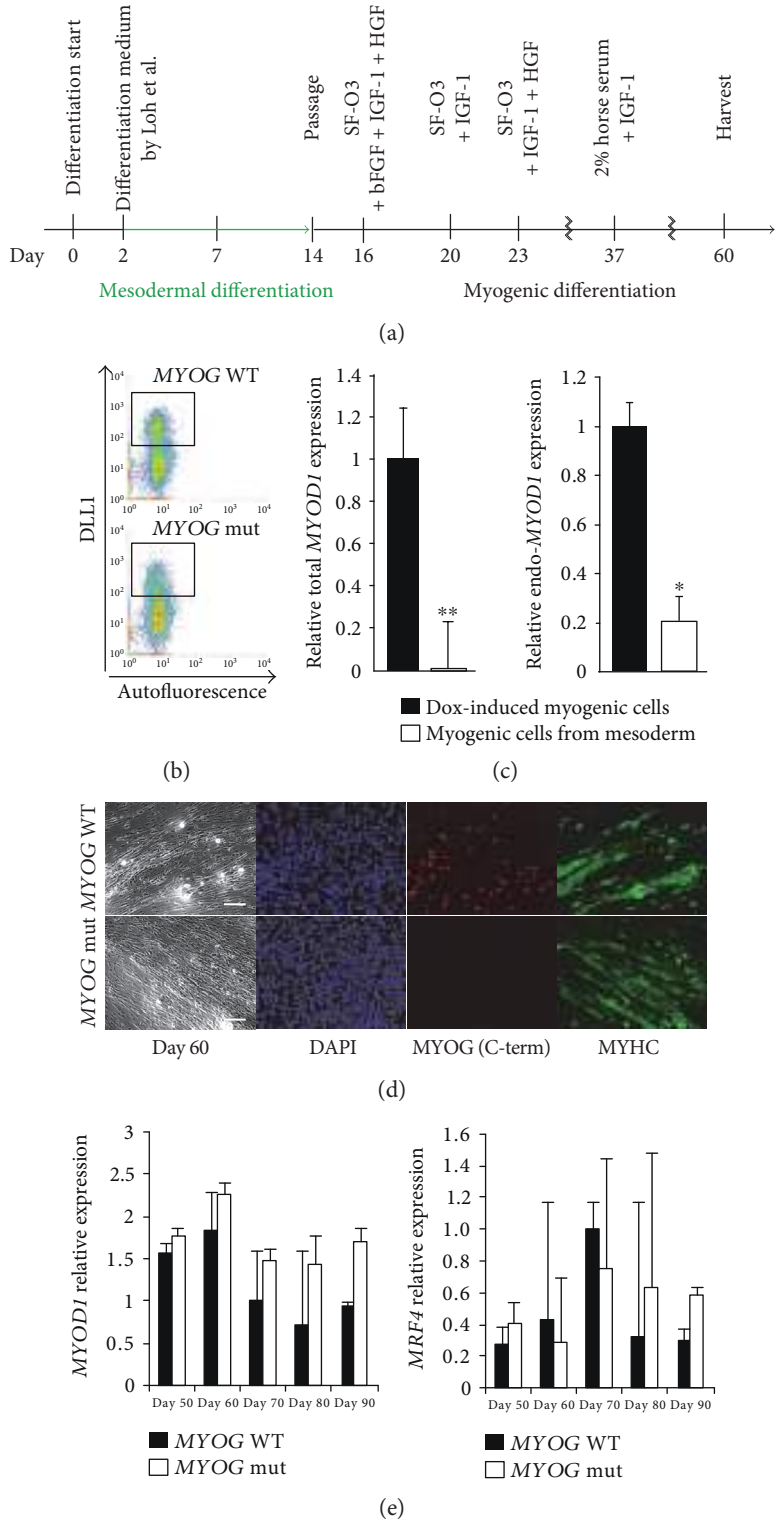

Figure 4: Myogenic differentiation from mesodermal precursors derived from *MYOGENIN*-deficient hiPS clone number 28 cells. Mesodermal and myogenic differentiation flowchart of the time course for muscle cells derived from hiPS cells (a). FACS analyses of DLL1-positive mesodermal cells derived from hiPS cells (b). Relative expression of total *MYOD1* and endogenous *MYOD1* (c). Differentiated myogenic cells derived from mesodermal cells with or without MYOG for 60 days were immunostained with anti-MYOSIN HEAVY CHAIN (MYHC, green) antibody. Nuclei were stained with 4′6-diamidino-2-phenylindole (DAPI, blue). Scale bar, 100 μm (d). Relative expressions of *MYOD1* and *MRF4* transcripts in wild-type or *MYOG*-mutated myogenic cells derived from mesodermal cells (e). All error bars indicate ±SEM ($n = 3$). P values are determined by a t-test from a two-tailed distribution. $^{*}P < 0.05$, $^{**}P < 0.01$.

in genomic sequence, which targeted *MYOG* by the T7EI assay not with high efficiency; however, the result of genomic editing in hiPS cells showed high efficiency for knocking out the *MYOG* gene, including in heterozygotes with an efficiency of over 80%. This was not changed with additional azidothymidine, which has been reported to increase the efficiency for NHEJ [25] (not shown).

While knockout mice of *Myog* exhibit a lethal deficiency of differentiated skeletal myofibers, there are nevertheless residual myofibers in *Myog* mutants [12, 13]. The possible differences between in vivo and in vitro situation of *Myog* mutants could be explained by the selection of a particular route to muscle cell differentiation from Myog-independent lineage in vitro, potentially controlled by MyoD1 and Mrf4 because Mrf4 can drive early myogenic differentiation in the myotome when Myog protein is not initially accumulated [10, 14]. Alternatively, there may be a threshold level of total myogenic regulatory factors required in myoblasts to trigger the terminal differentiation program. We have not observed any deficiencies of myogenic differentiation with *MYOG*-mutated cells under two different conditions, either with overexpression of MYOD1 or through medium conditions that promote mesodermal cell progression towards myogenesis. Mutated hiPS cells without not only *MYOG* but also other myogenic factors, *MYF5*, *MYOD1*, and *MRF4*, would be necessary for further analyses to identify the relationships of human myogenic regulatory factors because we observed the upregulation of other myogenic factors in *MYOG*-mutated cells which might compensate MYOG functions in vitro, and triple knockout of *Myog*, *Mrf4*, and *Myod1* or *Myf5*, *Myod1*, and *Mrf4* exhibited impaired ability to terminally differentiate into myofibers, not double knockout of *Myod1* and *Mrf4* [8, 10]. Moreover, there is also other possibility that Myog via skeletal muscle affects systemic factors in vivo [13] and that this feeds back on myofiber formation.

Taken together, these results demonstrate that *MYOG*-mutated human iPS cells have the capacity for myogenic differentiation and can form terminally differentiated myofibers, under differentiation conditions, in contrast to results on developing mouse *Myog* mutants.

Conflicts of Interest

No competing financial interests exist.

Acknowledgments

This research has been supported by grants-in-aid from the Japan Agency for Medical Research and Development, Projects for Technology Development, Development of Cell Transplantation Methods for Refractory Muscle Diseases, and AMED-CREST (AMED) and a grant from Nakatomi Memorial Foundation. The authors are grateful for Hu5/KD3-immortalized human myogenic cells provided by Dr. Naohiro Hashimoto (National Center for Geriatrics and Gerontology, Ōbu, Japan) and for the advice about the maintenance of cell culture from Tomoko Horikiri.

References

[1] J. Molkentin and E. Olson, "Defining the regulatory networks for muscle development," *Current Opinion in Genetics & Development*, vol. 6, no. 4, pp. 445–453, 1996.

[2] M. Buckingham, "Skeletal muscle formation in vertebrates," *Current Opinion in Genetics & Development*, vol. 11, no. 4, pp. 440–448, 2001.

[3] M. E. Pownall, M. K. Gustafsson, and C. P. Emerson Jr., "Myogenic regulatory factors and the specification of muscle progenitors in vertebrate embryos," *Annual Review of Cell and Developmental Biology*, vol. 18, pp. 747–783, 2002.

[4] M. Parker, P. Seale, and M. Rudnicki, "Looking back to the embryo: defining transcriptional networks in adult myogenesis," *Nature Reviews Genetics*, vol. 4, no. 7, pp. 497–507, 2003.

[5] R. Sambasivan and S. Tajbakhsh, "Skeletal muscle stem cell birth and properties," *Seminars in Cell & Developmental Biology*, vol. 18, no. 6, pp. 870–882, 2007.

[6] M. A. Rudnicki, T. Braun, S. Hinuma, and R. Jaenisch, "Inactivation of *MyoD* in mice leads to up-regulation of the myogenic HLH gene *Myf-5* and results in apparently normal muscle development," *Cell*, vol. 71, no. 3, pp. 383–390, 1992.

[7] T. Braun, M. A. Rudnicki, H. Arnold, and R. Jaenisch, "Targeted inactivation of the muscle regulatory gene *Myf-5* results in abnormal rib development and perinatal death," *Cell*, vol. 71, no. 3, pp. 369–382, 1992.

[8] B. Kablar, K. Krastel, S. Tajbakhsh, and M. A. Rudnicki, "*Myf5* and *MyoD* activation define independent myogenic compartments during embryonic development," *Developmental Biology*, vol. 258, no. 2, pp. 307–318, 2003.

[9] A. Rawls, J. Morris, M. Rudnicki et al., "Myogenin's functions do not overlap with those of MyoD or Myf-5 during mouse embryogenesis," *Developmental Biology*, vol. 172, no. 1, pp. 37–50, 1995.

[10] M. Valdez, J. Richardson, W. Klein, and E. Olson, "Failure of Myf5 to support myogenic differentiation without Myogenin, MyoD, and MRF4," *Developmental Biology*, vol. 219, no. 2, pp. 287–298, 2000.

[11] L. Kassar-Duchossoy, B. Gayraud-Morel, D. Gomes et al., "Mrf4 determines skeletal muscle identity in *Myf5*: *Myod* double-mutant mice," *Nature*, vol. 431, no. 7007, pp. 466–471, 2004.

[12] P. Hasty, A. Bradley, J. Morris et al., "Muscle deficiency and neonatal death in mice with a targeted mutation in the *myogenin* gene," *Nature*, vol. 364, no. 6437, pp. 501–506, 1993.

[13] Y. Nabeshima, K. Hanaoka, M. Hayasaka et al., "*Myogenin* gene disruption results in perinatal lethality because of severe muscle defect," *Nature*, vol. 364, no. 6437, pp. 532–535, 1993.

[14] J. Venuti, J. Morris, J. Vivian, E. Olson, and W. Klein, "Myogenin is required for late but not early aspects of myogenesis during mouse development," *Journal of Cell Biology*, vol. 128, no. 4, pp. 563–576, 1995.

[15] C. Berkes and S. Tapscott, "MyoD and the transcriptional control of myogenesis," *Seminars in Cell & Developmental Biology*, vol. 16, no. 4-5, pp. 585–595, 2005.

[16] M. Jinek, K. Chylinski, I. Fonfara, M. Hauer, J. Doudna, and E. Charpentier, "A programmable dual-RNA-guided DNA endonuclease in adaptive bacterial immunity," *Science*, vol. 337, no. 6096, pp. 816–821, 2012.

[17] L. Cong, F. Ran, D. Cox et al., "Multiplex genome engineering using CRISPR/Cas systems," *Science*, vol. 339, no. 6121, pp. 819–823, 2013.

[18] K. Shiomi, T. Kiyono, K. Okamura et al., "CDK4 and cyclin D1 allow human myogenic cells to recapture growth property without compromising differentiation potential," *Gene Therapy*, vol. 18, no. 9, pp. 857–866, 2011.

[19] H. Li, N. Fujimoto, N. Sasakawa et al., "Precise correction of the dystrophin gene in Duchenne muscular dystrophy patient induced pluripotent stem cells by TALEN and CRISPR-Cas9," *Stem Cell Reports*, vol. 4, no. 1, pp. 143–154, 2015.

[20] M. Nakagawa, Y. Taniguchi, S. Senda et al., "A novel efficient feeder-free culture system for the derivation of human induced pluripotent stem cells," *Scientific Reports*, vol. 4, p. 3594, 2014.

[21] A. Tanaka, K. Woltjen, K. Miyake et al., "Efficient and reproducible myogenic differentiation from human iPS cells: prospects for modeling Miyoshi myopathy in vitro," *PLoS One*, vol. 8, no. 4, article e61540, 2013.

[22] K. Loh, A. Chen, P. Koh et al., "Mapping the pairwise choices leading from pluripotency to human bone, heart, and other mesoderm cell types," *Cell*, vol. 166, no. 2, pp. 451–467, 2016.

[23] H. Sakurai, Y. Inami, Y. Tamamura, Y. Yoshikai, A. Sehara-Fujisawa, and K. Isobe, "Bidirectional induction toward paraxial mesodermal derivatives from mouse ES cells in chemically defined medium," *Stem Cell Research*, vol. 3, no. 2-3, pp. 157–169, 2009.

[24] Y. Naito, K. Hino, H. Bono, and K. Ui-Tei, "CRISPR-direct: software for designing CRISPR/Cas guide RNA with reduced off-target sites," *Bioinformatics*, vol. 31, no. 7, pp. 1120–1123, 2015.

[25] C. Yu, Y. Liu, T. Ma et al., "Small molecules enhance CRISPR genome editing in pluripotent stem cells," *Cell Stem Cell*, vol. 16, no. 2, pp. 142–147, 2015.

Sustained Activation of the Unfolded Protein Response Induces Cell Death in Fuchs' Endothelial Corneal Dystrophy

Naoki Okumura,[1] Miu Kitahara,[1] Hirokazu Okuda,[1] Keisuke Hashimoto,[1] Emi Ueda,[1] Makiko Nakahara,[1] Shigeru Kinoshita,[2] Robert D. Young,[3] Andrew J. Quantock,[3] Theofilos Tourtas,[4] Ursula Schlötzer-Schrehardt,[4] Friedrich Kruse,[4] and Noriko Koizumi[1]

[1]Department of Biomedical Engineering, Faculty of Life and Medical Sciences, Doshisha University, Kyotanabe, Japan
[2]Department of Frontier Medical Science and Technology for Ophthalmology, Kyoto Prefectural University of Medicine, Kyoto, Japan
[3]Structural Biophysics Group, School of Optometry and Vision Sciences, Cardiff University, Cardiff, United Kingdom
[4]Department of Ophthalmology, University of Erlangen-Nürnberg, Erlangen, Germany

Correspondence: Noriko Koizumi, Department of Biomedical Engineering, Faculty of Life and Medical Sciences, Doshisha University, Kyotanabe 610-0321, Japan; nkoizumi@mail.doshisha.ac.jp.

Submitted: October 31, 2016
Accepted: May 21, 2017

Citation: Okumura N, Kitahara M, Okuda H, et al. Sustained activation of the unfolded protein response induces cell death in Fuchs' endothelial corneal dystrophy. *Invest Ophthalmol Vis Sci*. 2017;58:3697–3707. DOI: 10.1167/iovs.16-21023

Purpose. The unfolded protein response (UPR) is believed to play a role in the pathogenesis of Fuchs' endothelial corneal dystrophy (FECD). The purpose of this study was to investigate whether unfolded proteins accumulate in the corneal endothelium in FECD and if they are involved in triggering cell death.

Methods. Descemet's membranes with corneal endothelial cells (CECs) were obtained during keratoplasty, and expression of aggresomes, type 1 collagen, fibronectin, and agrin was evaluated. Endoplasmic reticulum (ER) stress of immortalized human CECs from non-FECD subjects and from FECD patients (iHCEC and iFECD, respectively) were evaluated. The effect of MG132-mediated aggresome formation on the UPR and intrinsic pathway and the effect of mitochondrial damage on UPR were also examined. The effect of CHOP knockdown on the ER stress–mediated intrinsic pathway was also evaluated.

Results. Aggresome formation was higher in iFECD than in iHCEC and was colocalized with type 1 collagen, fibronectin, and agrin. GRP78, phosphorylated IRE1, PERK, and CHOP showed higher activation in iFECD than in iHCEC. MG132-mediated aggresome formation upregulated ER stress sensors, the mitochondrial membrane potential drop, cytochrome c release to the cytoplasm, and activation of caspase-9 and -3. By contrast, staurosporine-mediated mitochondrial damage did not induce ER stress. Knockdown of CHOP attenuated the ER stress-induced cleavage of caspase-9, which is caused by intrinsic pathway activation.

Conclusions. Excessive synthesis of extracellular matrix proteins induced unfolded protein accumulation in FECD. Prolonged ER stress–mediated cell death, occurring via the intrinsic apoptotic signaling pathway, therefore might be associated with the pathogenesis of FECD.

Keywords: Fuchs' endothelial corneal dystrophy, unfolded protein response, apoptosis, corneal endothelial cells

Fuchs' endothelial corneal dystrophy (FECD) is a bilateral and slowly progressive primary disease of the corneal endothelium. It is clinically categorized into three stages: (1) the presence of guttae without corneal edema, (2) the presence of guttae with stromal or epithelial edema, and (3) corneal scarring or neovascularization caused by long-standing corneal edema. The prevalence of FECD in the United States has been estimated to be as high as 4% of the population older than 40 years.[1] In agreement with this high prevalence, visual disturbance due to FECD is the leading cause of corneal transplantation. Recent data show that 15,707 (21.7%) of the 72,465 corneas provided by eye banks in the United States were used to treat FECD.[2]

Histological analysis has suggested that the corneal endothelial cell (CEC) loss occurring in FECD is due to apoptosis,[3–5] but the pathophysiologic cause of this apoptosis has not been identified. In 2010, Engler and colleagues[6] showed morphological alterations of the endoplasmic reticulum (ER), and upregulation of markers of the unfolded protein response (UPR), such as glucose-regulated protein (GRP78), α subunit of eukaryotic initiation factor 2 (eIF2α), and CCAAT-enhancer-binding protein homologous protein (CHOP) in the corneal endothelium of FECD patients. Hence, they postulated that the UPR plays an important role in the pathogenesis of FECD.[6] The same research group subsequently showed the involvement of the UPR in the CEC loss in an alpha 2 collagen VIII transgenic knock-in mouse, an animal model of early-onset FECD.[7]

The ER is the membranous tubular network that participates in cellular protein biosynthesis, lipid biosynthesis, and calcium homeostasis. Newly synthesized proteins mature and undergo proper folding in the ER.[8] A wide range of stresses, including increased secretory protein production, glucose deprivation, and hypoxia, induces the accumulation of unfolded or misfolded proteins in the ER lumen.[9,10] The conditions within

the ER are monitored by the UPR signaling pathway, and activation of the UPR restores protein folding homeostasis by reducing protein translation, increasing ER chaperone expression, and degrading misfolded proteins.[9–11] However, prolonged ER stress impairs protein homeostasis, which then triggers the UPR to induce apoptosis.[9,10,12] Consequently, targeting the UPR has emerged as a promising therapeutic modality for the treatment of diseases related to accumulation of unfolded or misfolded proteins in the ER.[13–15]

Our aim in the present study was to investigate the potential involvement of the UPR in FECD as a possible contributor to the underlying pathophysiological mechanism. Here, we have investigated the accumulation of unfolded or misfolded proteins in the corneal endothelium with the goal of detecting any functional links between the UPR and apoptosis of CECs in FECD.

Methods

Ethics Statement

The human tissue used in this study was handled under the guidelines based on the ethical principles of the Declaration of Helsinki. This study was performed according to a protocol approved by the ethical review committee of the Friedrich-Alexander University Erlangen-Nürnberg. Informed consent was acquired from the patients with FECD, and stripped Descemet's membranes with CECs were obtained during Descemet's membrane endothelial keratoplasty (DMEK). Normal human donor corneas were obtained from SightLife (Seattle, WA, USA; http://www.sightlife.org/). Informed written consent was obtained from the next of kin of all deceased donors with regard to eye donation for research. All tissue specimens were recovered under the tenets of the Uniform Anatomical Gift Act of the particular state in which the donor consent was obtained and the tissue recovered.

Cell Culture

The immortalized CECs from three patients with FECD were used as a cell model, and the immortalized CECs from three donor corneas were used as control (hereafter iFECD and iHCEC, respectively). Both iFECD and iHCEC were passaged from 30 to 40 times before use in these experiments. Descemet's membranes, including the CECs, were stripped from the corneas of patients with FECD during DMEK and used for cell cultivation. Three patients with FECD and the three donors of the non-FECD subject were older than 50 years.

The iFECD and iHCEC were cultured according to published protocols.[16,17] Briefly, the FECD-derived CECs and the control CEC were cultured for 14–21 days and then immortalized using SV40 and hTERT to produce iFECD and iHCEC cell lines, respectively. The coding sequences of the SV40 large T antigen and hTERT genes were amplified by PCR and were TA-cloned into a commercial lentiviral vector. The lentiviral vectors were transfected to human embryonic kidney 293T cells (RCB2202; Riken Bioresource Center, Ibaraki, Japan) along with three helper plasmids (pLP1, pLP2, and pLP/VSVG) using a transfection reagent. After 48 hours of transfection, the supernatant of the culture medium was harvested. For lentiviral transduction, the virus-containing supernatants of both genes were added to the cultures of HCECs in the presence of 5 μg/mL of polybrene. The immortalized cells were cultured in Dulbecco's modified Eagle's medium (DMEM; Life Technologies Corp., Carlsbad, CA, USA) containing 10% fetal bovine serum and 1% penicillin and streptomycin (Life Technologies Corp.). Once the cells were 80% confluent, the cells were trypsinized with 0.05% Trypsin-EDTA and passaged.

The iHCEC were cultured with DMEM supplemented with thapsigargin (10 μM; Wako Pure Chemical Industries, Ltd., Tokyo, Japan), and tunicamycin (30 μg/mL; Wako Pure Chemical Industries, Ltd.) to induce ER stress. The iHCEC were cultured with DMEM supplemented with staurosporine (0.5 μM; Sigma-Aldrich Corp., St. Louis, MO, USA) to induce apoptosis via the mitochondrial pathway. Unfolded protein aggregation was induced with MG132 (0.5 μM; Sigma-Aldrich Corp.).

Transmission Electron Microscopy (TEM)

Ultrastructural analysis of corneal specimens was performed on full-thickness corneas obtained during penetrating keratoplasty from patients with FECD ($n = 5$, mean age 63.3 ± 7.5 years) to assess whether the morphology of the ER and mitochondria was altered. Donor corneas from the non-FECD subjects were evaluated as a control. The central corneal endothelium was evaluated in FECD and in non-FECD subjects. Tissue specimens were fixed in 2.5% glutaraldehyde in 0.1 M phosphate buffer, postfixed in 2% buffered osmium tetroxide, dehydrated in graded alcohol concentrations, and embedded in epoxy resin, according to standard protocols. For analysis of cultured CECs, 1×10^5 cells were seeded onto Corning Transwell polyester membrane cell culture inserts (Corning, Inc., Corning, NY, USA) and grown until confluent. The entire Transwell inserts were fixed with 2.5% glutaraldehyde, 2% paraformaldehyde in 0.1 M Sorensen phosphate buffer. The Transwell membrane samples were washed in 0.1 M Sorensen phosphate buffer, processed through 0.5% uranyl acetate for en bloc staining, and subsequently dehydrated using an ascending ethanol series. The specimens were transferred to propylene oxide and then infiltrated and embedded in Araldite CY212 resin. Ultrathin sections were collected on uncoated G300 copper grids and stained with 1% aqueous phosphotungstic acid and uranyl acetate. Sections were examined with a transmission electron microscope (JEOL 1010; JEOL, Tokyo, Japan) equipped with a charge-coupled device camera (Orius SC1000; Gatan, Pleasanton, CA, USA).

Immunocytochemistry and Aggresome Staining

Descemet's membranes with CECs, obtained from 21 FECD patients during DMEK or from donor corneas from 20 non-FECD control subjects, and cultured CECs were fixed with 4% paraformaldehyde at room temperature for 10 minutes on glass slides. Excess paraformaldehyde was removed by washing with Dulbecco's PBS, and the samples were permeabilized with 0.5% Triton X-100 (Nacalai Tesque, Kyoto, Japan), and then incubated with 1% BSA to block nonspecific binding. The samples were incubated with primary antibodies against GRP78 (1:200; Santa Cruz Biotechnology, Santa Cruz, CA, USA), collagen I (1:200; Sigma-Aldrich Corp.), fibronectin (1:200; BD Biosciences, San Jose, CA, USA), agrin (1:200; Santa Cruz Biotechnology), and CHOP (1:200; Santa Cruz Biotechnology). Alexa Fluor 488-conjugated goat anti-mouse (Thermo Fisher Scientific, Waltham, MA, USA) antibodies were used as secondary antibodies at a 1:1000 dilution. For aggresome staining, samples were incubated with aggresome reagent (1:2000; Enzo Life Science Inc., Farmingdale, NY, USA) for 60 minutes. Nuclei were stained with 4′,6-diamidino-2-phenylindole (DAPI; Vector Laboratories, Burlingame, CA, USA). The slides were examined with a fluorescence microscope (DM 2500; Leica Microsystems, Wetzlar, Germany).

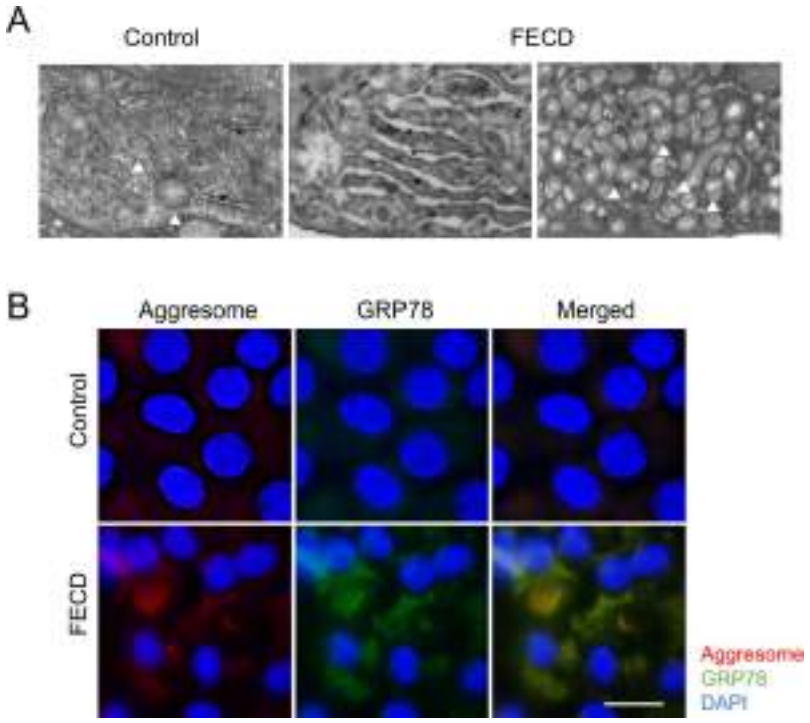

Figure 1. Accumulation of aggresomes in the corneal endothelium of FECD patients. (**A**) Corneal endothelium was evaluated by TEM. Representative TEM of non-FECD subject is shown as a control (*left*). Representative TEM of patients with FECD shows that ER is evident with morphological change with dilation in the corneal endothelium (*middle*). The morphology of the mitochondria is also altered and some mitochondria are dilated (*right*). *Asterisks* indicate ER, and *arrowheads* indicate mitochondria. (**B**) Descemet's membranes with corneal endothelium were obtained during DMEK, and stained for aggresomes and GRP78. Donor corneas were used as controls. A representative aggresome staining image shows diffuse staining and aggregations in the FECD but not in the control sample. Expression of GRP78 was higher in FECD samples and widely colocalized with aggresomes. Experimental findings were confirmed in at least 10 independent samples. Nuclei were stained with DAPI. *Scale bar*: 20 μm.

Quantitative Real-Time PCR

Gene expression levels were analyzed using TaqMan real-time PCR. Total RNA was extracted from the corneal endothelium from 10 patients with FECD and 10 donor corneas using the miRNeasy Mini Kit (Qiagen, Hilden, Germany). Then, cDNA was synthesized by SuperScript VILO MasterMix (Thermo Fisher Scientific). For quantification, standard curves using serial dilutions (10^2–10^7 copies) of plasmid-cloned amplicons were run in parallel. For normalization of gene expression levels, ratios relative to glyceraldehyde 3-phosphate dehydrogenase (GAPDH) were calculated.

The TaqMan primers used were for *COL1A1*, Hs00164004_ml; *FN1*, Hs00365052_ml; *AGRN*, Hs00394748_ml; and TaqMan predevelopment human GAPDH (Applied Biosystems, Foster City, CA, USA). The PCR was performed using the StepOne (Applied Biosystems) real-time PCR system. GAPDH was used as an internal standard.

Mitochondrial Membrane Potential

The iFECD and iHCEC were stained with 5,5′,6,6′-tetrachloro-1,1′,3,3′-tetraethylbenzimidazolylcarbocyanine iodide (JC-1) and the mitochondrial membrane potential was evaluated by fluorescence microscopy and flow cytometry, according to the manufacturer's protocol. Briefly, iFECD and iHCEC were cultured in medium supplemented with carbonyl cyanide-m-chlorophenylhydrazone (CCCP) (50 μM; Abcam, Cambridge, UK) for 9 hours as positive controls. For fluorescence microscopy analysis, the cells were incubated with MitoScreen (10 μM; BD Biosciences) for 15 minutes and fixed with 4% formaldehyde for 10 minutes, washed with PBS, and nuclei were stained with DAPI. The slides were examined with a fluorescence microscope (DMI 4000B; Leica Microsystems, Wetzlar, Germany). For flow cytometry, cells were washed twice with PBS and incubated with Accumax (Innovative Cell Technologies, San Diego, CA, USA) for 10 minutes at 37°C. The cells were recovered in Assay buffer supplemented with MitoScreen (10 μM; BD Biosciences), incubated for 15 minutes at 4°C, washed three times with PBS, and then resuspended in FACS buffer and analyzed by flow cytometry using CellQuest Pro software (BD Biosciences).

Immunoblotting

The cultured CECs were washed with ice-cold PBS and lysed with ice-cold RIPA buffer containing phosphatase inhibitor cocktail 2 (Sigma-Aldrich Corp.) and protease inhibitor cocktail (Roche Applied Science, Penzberg, Germany). Following centrifugation, the supernatant containing the total proteins was fractionated by SDS-PAGE. The separated proteins were transferred to polyvinylidene difluoride membranes, blocked with 3% nonfat dry milk, and incubated overnight at 4°C with the following primary antibodies: pancreatic ER kinase (PERK) (1:1000; Cell Signaling Technology, Inc., Danvers, MA, USA), phosphorylated PERK (1:1000; Cell Signaling Technology, Inc.), activating transcription factor 6α (ATF6α) (1:1000; Bio Academia, Inc., Osaka, Japan), inositol-requiring transmembrane kinase/endonuclease 1α (IRE1α) (1:1000; Cell Signaling Technology), phosphorylated IRE1α (1:1000; Novus Biologicals, Littleton, CO, USA), spliced active form of X-box binding protein 1 (XBP1s) (1:1000; BioLegend, San Diego, CA, USA), bcl2 (1:1000; Cell Signaling Technology), caspase-9 (1:1000;

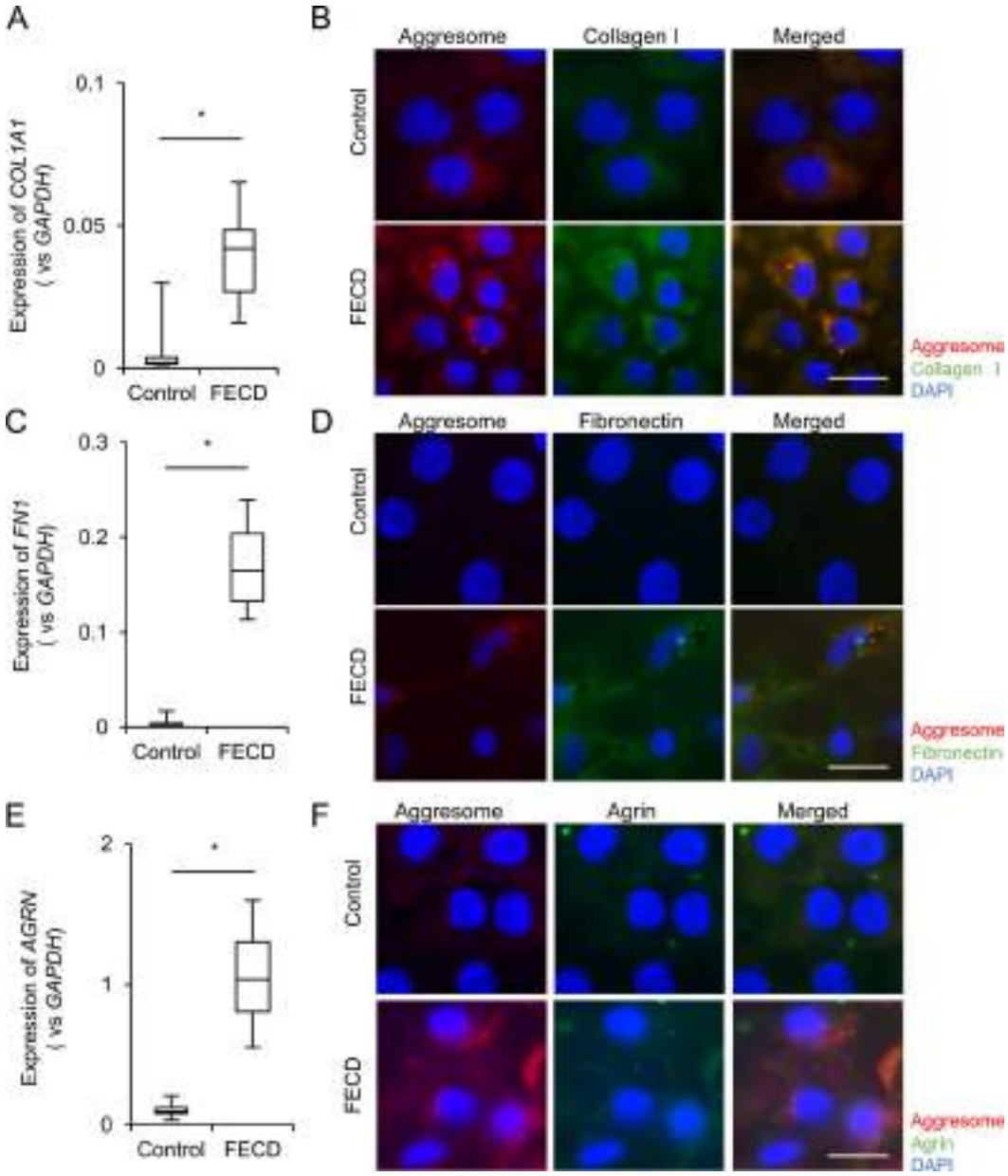

Figure 2. Involvement of ECM proteins and proteoglycan in the formation of aggresomes. (**A**, **C**, **E**) Total RNA was extracted from the corneal endothelium of the 30 patients with FECD and 30 donor corneas. Expression of type 1 collagen, fibronectin, and agrin in the corneal endothelium was determined by quantitative PCR. The mRNA expression of type 1 collagen, fibronectin, and agrin was significantly higher in FECD than in the control. $^*P < 0.01$. (**B**, **D**, **F**) Immunofluorescence staining showed that type 1 collagen, fibronectin, and agrin were more highly expressed in FECD than in control samples. Not all, but a certain amount of type 1 collagen, fibronectin, and agrin, was colocalized with aggresomes. Experimental findings were confirmed in at least 10 independent samples. Nuclei were stained with DAPI. *Scale bar*: 20 μm.

Cell Signaling Technology), caspase-3 (1:1000; Cell Signaling Technology), poly (ADP-ribose) polymerase (PARP) (1:2000; Cell Signaling Technology), CHOP (1:1000; Cell Signaling Technology), cytochrome c (BD Biosciences), voltage-dependent anion channel (VDAC; Cell Signaling Technology), and GAPDH (1:3000; Medical and Biological Laboratories Co., Ltd., Aichi, Japan). The blots were probed with horseradish peroxidase–conjugated secondary antibodies (1:5000; GE Healthcare, Piscataway, NJ, USA), developed with luminal for enhanced chemiluminescence using the ECL Advanced Western Blotting Detection Kit (Nacalai Tesque), and documented with an LAS4000S (Fuji Film, Tokyo, Japan) cooled charge-coupled-device camera gel documentation system. The relative density of immunoblot bands was determined using ImageJ software (http://imagej.nih.gov/ij/; provided in the public domain by the National Institutes of Health, Bethesda, MD, USA). Molecular weight markers (Bio-Rad, Hercules, CA, USA) were run alongside all samples.

For the assessment of release of cytochrome c from mitochondria to the cytoplasm, 5×10^5 iHCEC were seeded on a 10-cm culture dish, cultured for 24 hours, and then further incubated with fresh DMEM supplemented with thapsigargin (10 μM) tunicamycin (30 μg/mL), or MG132 for 24 hours. Cytoplasmic protein was isolated from mitochondrial protein by Mitochondria Isolation Kit (Thermo Fisher Scientific) according to manufacturer's protocol. Briefly, harvested cells were centrifuged at 800*g*, Mitochondria Isolation Reagent A was added to the tube, and the sample was stored on ice for

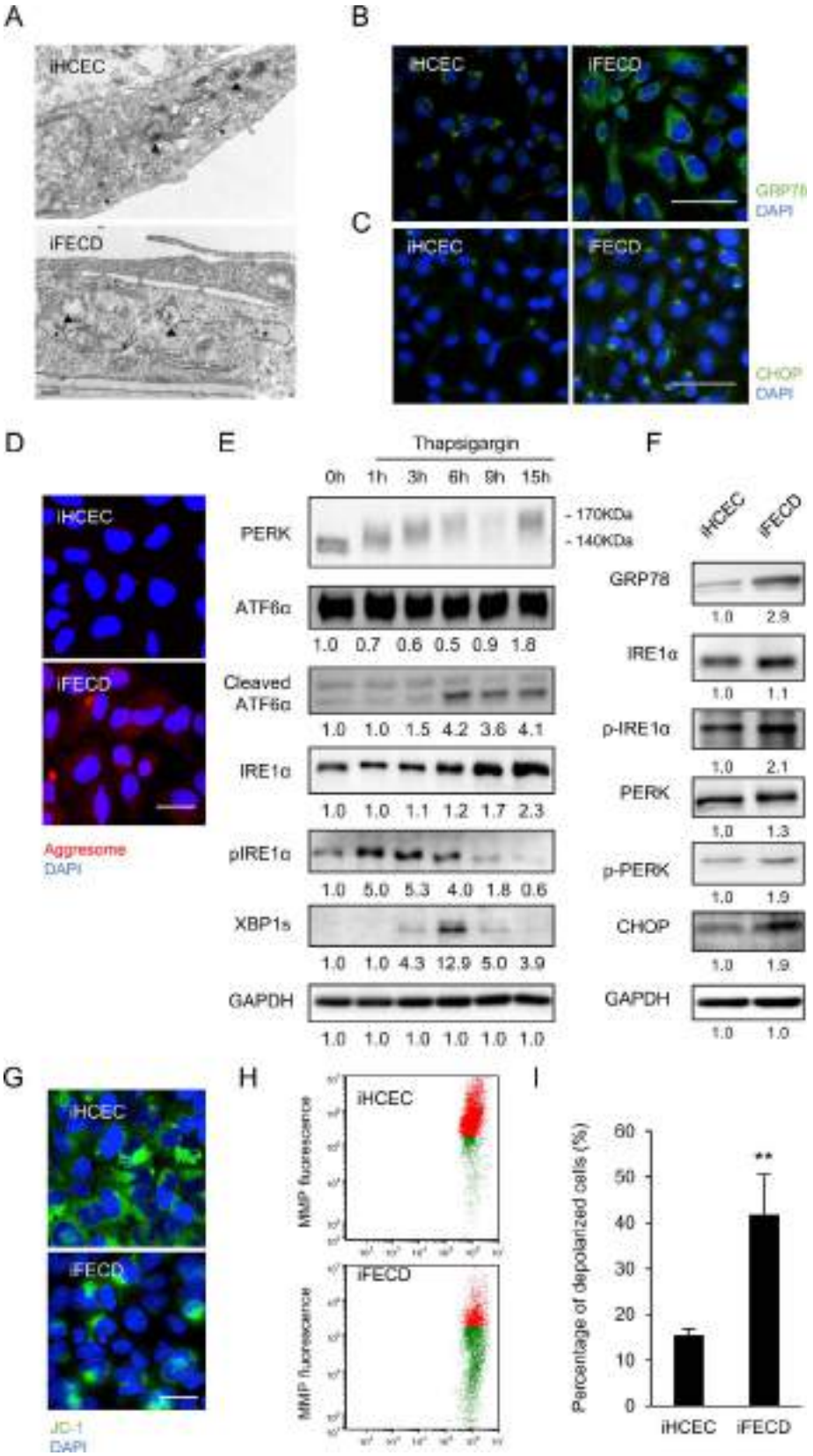

Figure 3. Accumulation of aggresomes and mitochondrial membrane depolarization in the FECD cell model. (**A**) The immortalized CECs from FECD patients (hereafter iFECD) were used as a cell model, and the immortalized CECs from donor corneas (hereafter, iHCEC) were used as controls. The iFECD and iHCEC cultured on Corning Transwell polyester membrane cell culture inserts were analyzed by TEM. ER was dilated, and mitochondria were dilated associated with altered inner structure morphology in iFECD, but not in iHCEC. *Asterisks* indicate ER, and *arrowheads* indicate mitochondria. (**B**, **C**) Immunofluorescence staining showed that strong expression of GRP78 and CHOP was observed in iFECD when compared with iHCEC. Nuclei were stained with DAPI. Experiments were performed on three independent samples. *Scale bar*: 40 μm. (**D**) iFECD

and iHCEC were cultured on culture plates and examined for formation of aggresomes. A high level of aggresome formation was observed in iFECD, but not in iHCEC. Nuclei were stained with DAPI. Experiments were performed on three independent samples. *Scale bar*: 50 μm. (**E**) The iHCEC established from donor corneas were cultured and stimulated with thapsigargin to induce ER stress. Western blotting showed that thapsigargin treatment induced the phosphorylation of PERK, cleavage of ATF6, and phosphorylation of IRE1 associated with XBP1 cleavage. The relative density of immunoblot bands in triplicate experiments was determined using ImageJ software. Relative fold differences were compared with the values at 0 hour. (**F**) Activation of ER stress–related proteins in iHCEC and iFECD was evaluated by Western blotting. Expression of GRP78, phosphorylated IRE1α and PERK, and CHOP was higher in iFECD than in iHCEC. The relative density of immunoblot bands was determined using ImageJ software. Experiments were performed using two iHCEC established from two independent non-FECD donor corneas and two iFECD established from two independent FECD donors. (**G**) JC-1 staining showed greater depolarization of the mitochondrial membrane potential in iFECD than in iHCEC. Nuclei were stained with DAPI. Experiments were performed on three independent samples. *Scale bar*: 50 μm. (**H**) Flow cytometry also showed greater depolarization of the mitochondrial membrane potential in iFECD than in iHCEC. *Red dots* indicate cells with normal mitochondrial membrane potential and *green dots* indicate cells with depolarized mitochondrial membrane potential. (**I**) Flow cytometry showed that 15.5% of iHCEC exhibited depolarization of mitochondrial membrane potential, but 41.7% of iFECD exhibited this depolarization ($n = 3$). Experiments were performed in triplicate. $^*P < 0.01$.

2 minutes. Then, Mitochondria Isolation Reagent B and Mitochondria Isolation Reagent C were added, and the tube was centrifuged at 700*g*. The supernatant was recovered, and centrifuged again. This final supernatant was recovered as cytoplasmic protein, and was used for Western blotting.

Knockdown of Genes by Small Interfering RNA (siRNA)

The iHCEC were seeded into a 24-well plate and cultured until they reached 50% to 70% confluence. The iHCEC were then incubated with RNAi duplex (DDIT3) and Lipofectamine RNAiMAX (Thermo Fisher Scientific), according to the manufacturer's protocol. Random RNAi low GC was used as a control and RT-PCR was performed to assess the knockdown of DDIT3.

Statistical Analysis

The statistical significance (*P* value) of differences between mean values of the two-sample comparison was determined with the Student's *t*-test. The comparison of multiple sample sets was analyzed using Dunnett's multiple-comparison test. The data represent the mean ± SEM.

Results

Accumulation of Unfolded Proteins in the Corneal Endothelium of Patients With FECD

Examination of the corneal endothelium of corneas obtained from FECD patients by TEM frequently showed ultrastructural alterations of the ER, mainly prominent and dilated ER cisternae (Fig. 1A; middle) in comparison with the non-FECD subject (Fig. 1A; left). Morphological alterations observed in the mitochondria included focal loss of cristae and distended shape (Fig. 1A; right). These morphological alterations in ER and mitochondria motivated us to determine the involvement of ER and mitochondria in the pathophysiology of FECD. We evaluated the extent of the accumulation of unfolded proteins in the FECD corneal endothelium. The CEC-Descemet's membrane whole mounts demonstrated higher levels of diffuse aggresome staining and perinuclear aggregations in the FECD specimens than in the control specimens (Fig. 1B). This increased expression of aggresomes in FECD samples was confirmed in all 21 individual Descemet's membranes. Double labeling of aggresomes and GRP78, which mediates the protein folding processes,[18] showed higher expression of GRP78 in FECD samples and a wide colocalization with aggresomes, suggesting the presence of increased amounts of unfolded or misfolded protein and subsequent UPR in the endothelial cells from patients with FECD (Fig. 1B).

We next evaluated the involvement of extracellular matrix (ECM) components, as these are produced by corneal endothelium in FECD and accumulate in guttae or thickened Descemet's membrane in the form of aggresomes. Similar to previous reports,[19,20] quantitative PCR showed that mRNA expression of type I collagen, fibronectin, and agrin was higher in patients with FECD than in controls (Figs. 2A, 2C, 2E; respectively). Correspondingly, immunofluorescence staining showed that protein expression of type I collagen, fibronectin, and agrin was higher in endothelial cells from FECD specimens than from control specimens. Interestingly, type I collagen, fibronectin, and agrin were found to partially colocalize with aggresomes, implying that excessive production of ECM components contributes to aggresome formation in the corneal endothelium in FECD (Figs. 2B, 2D, 2F).

Evaluation of the Involvement of the UPR in an FECD Cell Model

We previously established a cell model of FECD (iFECD) by culturing and immortalizing the CEC derived from FECD patients and control CEC derived from donor corneas (iHCEC).[16] Here, we used this model to evaluate the involvement of the UPR and its effects on mitochondria. Similar to the findings for surgical specimens, TEM observations revealed ultrastructural alterations, such as dilated ER cisternae and swollen mitochondria with partial loss of cristae, in iFECD but not in iHCEC (Fig. 3A). Asterisks indicate the ER, and arrowheads indicate mitochondria. Immunofluorescence microscopy showed higher expression levels of GRP78 and CHOP (an apoptosis inducer that is activated by ER stress) in iFECD than in iHCEC (Figs. 3B, 3C, respectively). Aggresome staining showed higher amounts of unfolded protein associated with aggregation in iFECD than in iHCEC (Fig. 3D).

These cells were then characterized for expression of three proximal sensors of the UPR: PERK, IRE1α, and ATF6α.[21] Treatment of iHCEC with thapsigargin, which acts as an ER stress inducer by specifically inhibiting the ER Ca^{2+}-ATPase,[22] increased the phosphorylation of PERK, the cleavage of ATF6, and the phosphorylation of IRE1. IRE1α is a protein kinase that initiates unconventional splicing of Xbp-1 mRNA to produce an active transcription factor,[21] and Western blotting showed that XBP1 expression was induced by thapsigargin stimulation (Fig. 3E; Supplementary Fig. S1). These results provide evidence that the UPR sensors, PERK, IRE1a, and ATF6a, are conserved in corneal endothelium to sense the ER stress. Consistent with the immunofluorescence images shown in Figures 3B and 3C, Western blotting showed that expression of GRP78 and CHOP was higher in iFECD than in iHCEC. We also evaluated the activation of IRE1α and PERK, which induces apoptosis due to ER stress, and showed that phosphorylation of PERK and of IRE1α was higher in iFECD than in iHCEC (Fig. 3F). Consistent

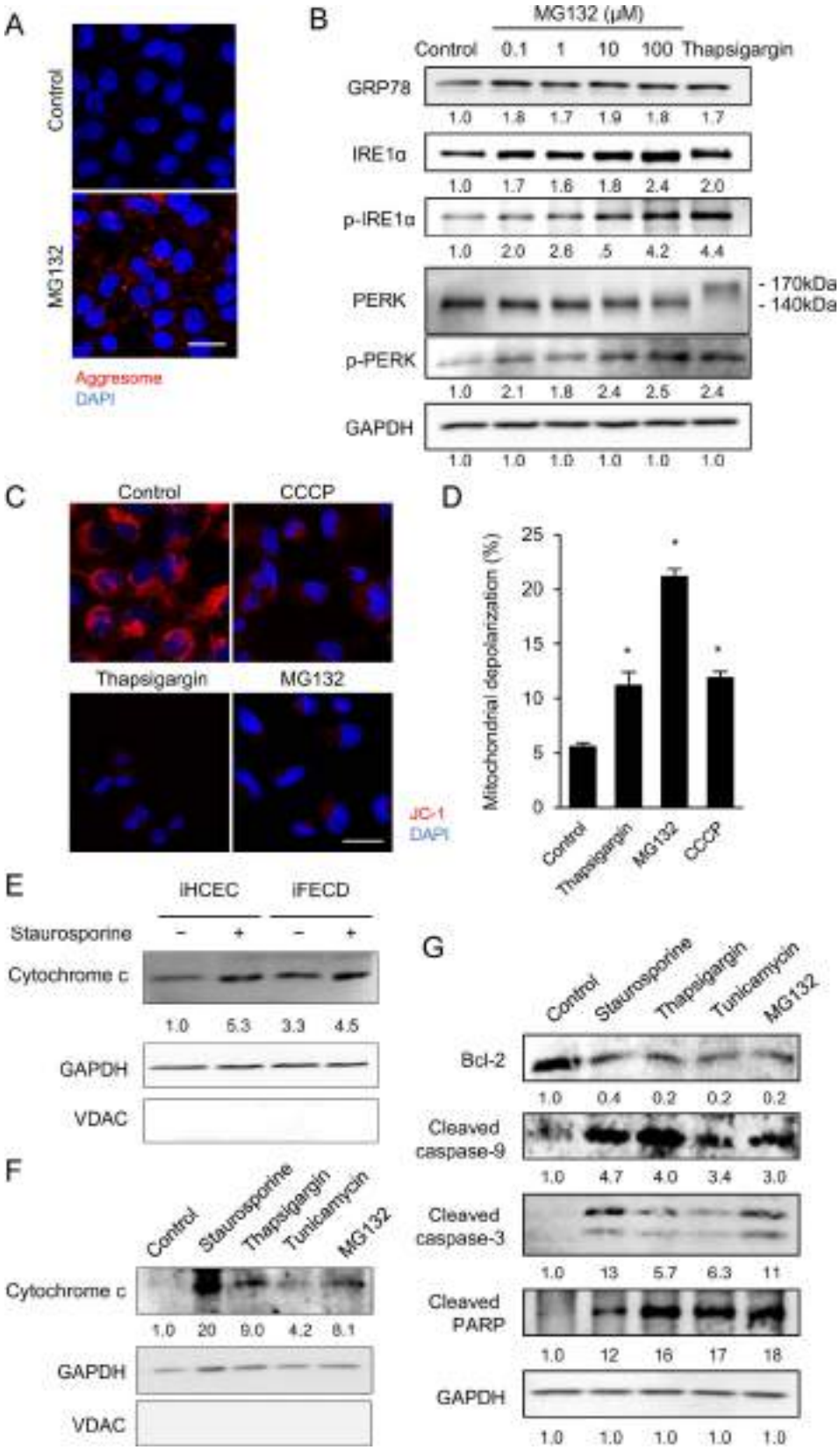

Figure 4. Involvement of aggresomes in mitochondrial pathway activation. (**A**) iHCEC were treated with 10 μM MG132 (a proteasome inhibitor), which reduces the degradation of ubiquitin-conjugated proteins to induce aggresome formation. *Scale bar*: 50 μm. (**B**) iHCEC were treated with MG132 or 10 μM thapsigargin as positive controls for 24 hours. Western blotting showed that MG132 treatment upregulated expression of GRP78, phosphorylation of IRE1α, and expression of PERK. The relative density of immunoblot bands in duplicate experiments was determined using ImageJ software. Relative fold differences were compared with the values of the control. (**C**) iHCEC were stimulated with CCCP, thapsigargin, and MG132, followed by evaluation of the mitochondrial membrane potential by JC-1 staining. Thapsigargin-mediated ER stress decreased mitochondrial

membrane potential, and MG132-mediated aggresome formation also decreased mitochondrial membrane potential. CCCP, a chemical inhibitor of oxidative phosphorylation, was used as a positive control for mitochondrial membrane potential depolarization. Experiments were performed in triplicate. Nuclei were stained with DAPI. *Scale bar*: 50 μm. (**D**) iHCEC were stimulated with CCCP, thapsigargin, and MG132, incubated in JC-1 staining reagent, and then evaluated for mitochondrial membrane potential by flow cytometry. Thapsigargin increased the depolarization of iHCEC mitochondria to 11.2% and MG132 increased this to 21.2%, whereas untreated control iHCEC depolarized at 5.6% ($n = 3$). Experiments were performed in triplicate. $^{*}P < 0.01$. (**E**) Release of cytochrome c from the mitochondria to the cytoplasm in iHCEC and iFECD was evaluated by Western blotting. Staurosporine was used as a positive control. Release of cytochrome c from the mitochondria to the cytoplasm was higher in iFECD than in iHCEC. The relative density of immunoblot bands was determined using ImageJ software. Experiments were performed by using two iHCEC established from two independent non-FECD donor corneas and two iFECD established from two independent FECD donors. (**F**) iHCEC were treated with staurosporine, thapsigargin, tunicamycin, and MG132. Staurosporine was used as a positive control, and it induced the release of cytochrome c from the mitochondria to the cytoplasm. Staurosporine, thapsigargin or tunicamycin caused ER stress and induced the release of cytochrome c. MG132-mediated aggresome formation also induced cytochrome c release. GAPDH was used as a cytoplasmic marker, and VDAC was used as a mitochondrial marker. The relative density of immunoblot bands in duplicate experiments was determined using ImageJ software. Relative fold differences were compared with the values of the control. (**G**) Western blotting showed that MG132 suppressed the expression of Bcl-2 and the cleavage of caspase-9, caspase-3, and PARP, as observed following thapsigargin- or tunicamycin-mediated ER stress. The relative density of immunoblot bands in triplicate experiments was determined using ImageJ software. Relative fold differences were compared with the values of control. Experiments were performed in triplicate.

with the morphological alterations of mitochondria observed with TEM, JC-1 staining showed greater depolarization of the mitochondrial membrane potential in iFECD than in iHCEC (Fig. 3G). Flow cytometry also showed significant greater depolarization of the mitochondrial membrane potential in iFECD than in iHCEC (Figs. 3H, 3I), suggesting that mitochondrial function is impaired in FECD.

Effect of Aggresome Formation on the UPR and Mitochondrial Function

We evaluated whether aggresome formation induces the UPR in CECs by treating iHCEC with the proteasome inhibitor MG132 in a similar manner to iFECD. Unfolded protein is degraded by the ubiquitin-proteasome system or folded properly by chaperone proteins, so even healthy cells will contain some amount of improperly folded protein. The MG132 treatment reduced the degradation of ubiquitin-conjugated proteins and induced aggresome formation in the iHCEC (Fig. 4A). MG132 treatment also upregulated the expression of GRP78 and the phosphorylation of IRE1α and PERK, indicating that MG132-mediated aggresome deposition induce ER stress (Fig. 4B). JC-1 staining showed that both thapsigargin-induced ER stress and MG132-mediated aggresome formation decreased the mitochondrial membrane potential. CCCP, a chemical inhibitor of oxidative phosphorylation, was used as a positive control (Figs. 4C, 4D). Cytochrome c is a component of the electron transport chain in mitochondria and is released from mitochondria into the cytoplasm during the initiation of apoptosis. Western blotting showed that the release of cytochrome c to the cytoplasm was higher in iFECD than in iHCEC (Fig. 4E). As was observed in iFECD, MG132 induced the release of cytochrome c to the cytoplasm in a similar manner to that observed with thapsigargin and tunicamycin, which both induce ER stress (Fig. 4F). Staurosporine was used as positive control (Fig. 4F). MG132 treatment suppressed the expression of Bcl-2, an integral outer mitochondrial membrane protein that blocks apoptotic cell death, and induced the cleavage of caspase-9, a proapoptotic protein activated by cytochrome c. In addition, MG132 treatment activated the execution caspase, caspase-3, as well as the downstream apoptosis-inducing molecule, PARP (Fig. 4G; Supplementary Fig. S2).

Mechanism of Mitochondrial Apoptotic Pathway Activation by ER Stress

Staurosporine-mediated mitochondrial damage induced the cleavage of caspase-9 and the subsequent activation of caspase-3 and PARP. This cascade of events is well recognized as the intrinsic apoptotic pathway in a wide range of cell types (Fig. 5A). We next examined CHOP, which is activated during chronic UPR by PERK and its downstream signal, and represents a transcription factor that regulates proapoptotic genes. Western blotting showed that treatment with thapsigargin, tunicamycin, and MG132 upregulated CHOP together with chaperone protein, but these responses were not observed following staurosporine treatment (Fig. 5B). Thapsigargin upregulated CHOP and activated caspase-9, whereas knockdown of CHOP by siRNA attenuated the downregulation of caspase-9 cleavage (Fig. 5C). The upregulation of GRP78 induced by thapsigargin was not altered by knockdown of CHOP.

Correspondingly, JC-1 staining showed that reduction of mitochondrial membrane potential by thapsigargin was prevented by siRNA-mediated knockdown of CHOP (Fig. 5D). These data suggest that activation of CHOP by the UPR triggers the intrinsic pathway associated with the alterations in both mitochondrial morphology and function. Based on these data, we proposed that excessive production of ECM proteins, including type I collagen and fibronectin, causes aggregation of unfolded or misfolded proteins and subsequent induction of the UPR. This UPR activation, in turn, triggers a cascade of molecular events that lead to apoptotic cell death by activation of the intrinsic apoptotic pathway (Fig. 5E).

Discussion

Prolonged UPR activation, caused by unmitigated ER stress and impaired homeostasis, induces cell death.[9,10,12] Following an impairment of homeostasis, the UPR serves as an apoptosis executor. This phenomenon has been accepted as indicating that the function of UPR-mediated apoptosis is to protect the organism from damaged cells that cannot ascertain the normal signaling components.[9] The "life or death" decision by the UPR serves as a universal underlying mechanism in the pathogenesis of various diseases, including neurodegenerative diseases, inflammation, metabolic disorders, liver dysfunction, and cancer.[9,10,13] For instance, accumulating evidence now supports a linkage of protein misfolding and inclusion body formation with neurodegenerative diseases, such as Alzheimer's disease, Parkinson's disease, and Huntington's disease.[23–26] In the field of eye disease, misfolded proteins and subsequent UPR signaling are related to pathogenesis in certain types of retinitis pigmentosa and Stargart-like macular degeneration.[27]

In the current study, we showed that excessive ECM proteins form aggregations of unfolded proteins in the corneal endothelium of FECD patients. The phenotypic clinical

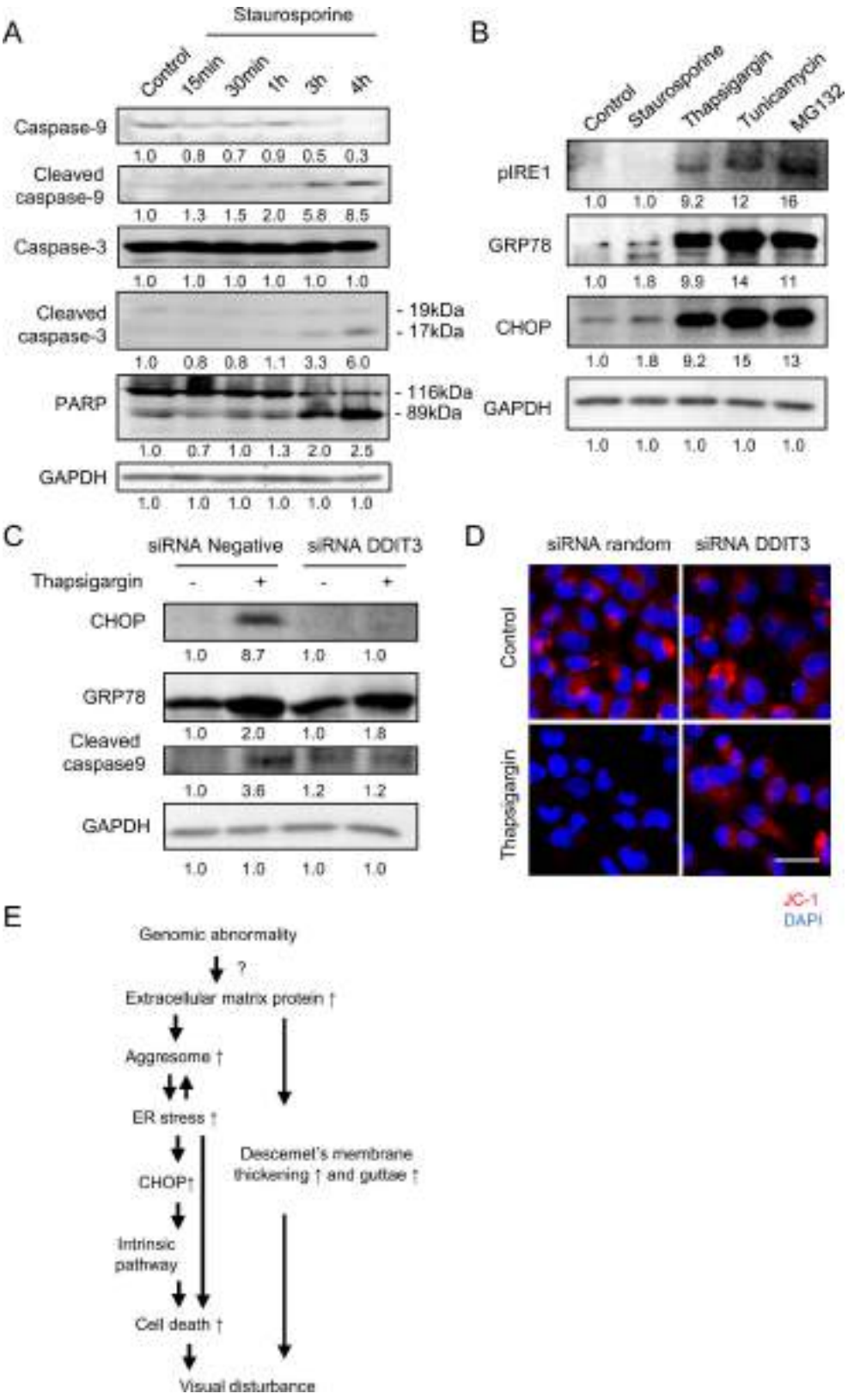

Figure 5. Involvement of CHOP as a "communicator" between the ER and the mitochondria during apoptosis. (**A**) iHCEC were cultured and then stimulated with staurosporine. Western blotting showed that staurosporine-mediated mitochondrial damage induces cleavage of caspase-9, caspase-3, and PARP. The relative density of immunoblot bands in duplicate experiments was determined using ImageJ software. Relative fold differences were compared with the values of the control. (**B**) iHCEC were treated with staurosporine, thapsigargin, tunicamycin, and MG132. Western blotting showed that thapsigargin, tunicamycin, and MG132 upregulated CHOP and GRP78. However, staurosporine did not upregulate CHOP. The relative density of immunoblot bands in duplicate experiments was determined using ImageJ software. Relative fold differences were compared with the values of the control. (**C**) iHCEC were incubated with RNAi duplex (DDIT3) and CHOP was knocked down. Thapsigargin increased CHOP and

activated caspase-9 in random siRNA controls. However, knockdown of CHOP by siRNA attenuated the caspase-9 cleavage. Induction of GRP78 by thapsigargin was not altered by knockdown of CHOP. The relative density of immunoblot bands in duplicate experiments was determined using ImageJ software. Relative fold differences were compared with the values of control. (**D**) Stimulation of iHCEC with knockdown of CHOP by siRNA and control iHCEC by thapsigargin. JC-1 staining shows depolarization of the mitochondrial membrane by thapsigargin in the control, but this was counteracted by knockdown of CHOP by siRNA. *Scale bar*: 50 μm. (**E**) Schematic image of our hypothetic pathophysiology was shown. Hyperproduction of ECM proteins and proteoglycans cause aggregation of unfolded or misfolded protein, and then induce unfolded protein response. A sustained unfolded protein response may at least partially activate the mitochondrial pathway through CHOP and induce apoptosis, as well as cause apoptosis through a mitochondria-independent pathway.

features of FECD are corneal guttae that are excrescences of the Descemet's membrane. Earlier studies demonstrated that certain types of ECM proteins and proteoglycans accumulate and form the guttae and thickening of Descemet's membrane.[19,20,28] Consistent with the general understanding that increased secretory protein production can trigger the formation of unfolded proteins in the ER lumen,[9] these accumulated proteins form aggregations of unfolded proteins in the FECD corneal endothelium. Although speculative, this idea may explain the clinical features, in which accumulation of ECM proteins is accompanied by a gradual loss of the corneal endothelium. We recently reported that high expression of genes inducing the epithelial mesenchymal transition (EMT) was involved in an excessive production of ECM proteins through the transforming growth factor (TGF)-β signaling pathway.[16] In addition, we postulated that the regulation of EMT-related genes, by counteracting this TGF-β signaling, may suppress the excessive production of ECM proteins.[16] Further study is required to determine whether suppression of excessive ECM production by inhibition of TGF-β signaling also represses the UPR; however, modulation of excessive protein production might be worth investigating as a therapeutic target for FECD treatment.

Three principal signal transducers (ATF6, PERK, and IRE1) that sense the protein folding conditions in the ER lumen have been identified.[9,29] Expression of these UPR transducers varies depending on tissues and cell types, but we have shown that all three signal transducers are conserved in the corneal endothelium and are activated by ER stress. ATF6 is expressed in the ER lumen, and unfolded protein accumulation causes delivery of ATF6 to the Golgi apparatus, whereas cleavage of the N-terminal cytosolic fragment results in activation of UPR target genes.[30] Consistently, we demonstrated that GRP78, a target gene of ATF6,[30] is highly expressed in FECD samples. When IRE1 senses unfolded protein, it cleaves the mRNA encoding X-box binding protein 1 (XBP1) and induces the spliced active form of XBP1. XBP1 regulates transcription of chaperones and ER-associated degradation components.[31]

PERK phosphorylates itself on sensing ER stress, and reduces mRNA translation by inactivating eIF2. Inactivation of eIF2 then increases ATF4, which in turn drives the expression of its target genes. One of the important target genes is CHOP, a transcription factor that regulates genes involved in apoptosis. PERK acts as protector of unfolded proteins, but it also contributes to cell death when the UPR reaches a critical level.[10,32] In the current study, we showed that a cell model derived from patients with FECD expressed higher levels of CHOP and this was associated with unfolded protein accumulation. In addition, knockdown of CHOP by siRNA suppressed the induction of the intrinsic apoptotic pathway by ER stress, indicating that CHOP activation due to ER stress triggers cell loss.

ER stress is transmitted to mitochondria by stress responsive signaling pathways or by altered transfer of metabolites such as Ca^{2+}.[10,33] Stress signaling from the ER to mitochondria results in prosurvival or proapoptotic responses in mitochondrial function, depending on the strength of the stress. Chronic exposure to ER stress reduces mitochondrial respiration and decreases cellular ATP levels, resulting in increases in Ca^{2+} in the mitochondria.[34] This subsequently induces mitochondrial fragmentation and elevation of mitochondrial permeability, which then initiates the intrinsic apoptotic signaling pathway.[10,35,36] We showed that the ultrastructure of mitochondria is altered in the corneal endothelium of patients with FECD. We also demonstrated that ER stress is transmitted to these mitochondria and initiates intrinsic apoptosis, whereas staurosporine-mediated apoptosis associated with dysfunction of mitochondria does not induce ER stress.

We postulate that the pathophysiology induced by apoptosis in response to chronic ER stress plays a central role in the progressive cell loss associated with FECD. In various cell types, ER stress affects mitochondrial DNA biogenesis and increases mitochondrially derived reactive oxygen species.[35–37] An involvement of mitochondrial dysfunction has consistently been suggested to play a role in FECD. For example, mitochondrial DNA damage repair was disturbed, mitochondrial DNA was degraded,[38] and antioxidant and oxidative stress–related gene expression were altered in FECD.[39]

In conclusion, the accumulation of excessive amounts of ECM proteins in FECD causes the accumulation of unfolded protein, and this might be associated with cell death through the intrinsic apoptotic signaling pathway. Further studies are needed, but inhibiting the intrinsic apoptotic pathway that arises as a UPR response might be a therapeutic target for FECD treatment.

Acknowledgments

Supported by the Program for the Strategic Research Foundation at Private Universities from MEXT (NK, NO).

Disclosure: **N. Okumura**, None; **M. Kitahara**, None; **H. Okuda**, None; **K. Hashimoto**, None; **E. Ueda**, None; **M. Nakahara**, None; **S. Kinoshita**, None; **R.D. Young**, None; **A.J. Quantock**, None; **T. Tourtas**, None; **U. Schlötzer-Schrehardt**, None; **F. Kruse**, None; **N. Koizumi**, None

References

1. Lorenzetti DW, Uotila MH, Parikh N, Kaufman HE. Central cornea guttata. Incidence in the general population. *Am J Ophthalmol*. 1967;64:1155–1158.
2. Eye Bank Association of America. Eye Banking Statistical Report. Washington, DC; 2014.
3. Borderie VM, Baudrimont M, Vallee A, Ereau TL, Gray F, Laroche L. Corneal endothelial cell apoptosis in patients with Fuchs' dystrophy. *Invest Ophthalmol Vis Sci*. 2000;41:2501–2505.
4. Li QJ, Ashraf MF, Shen DF, et al. The role of apoptosis in the pathogenesis of Fuchs endothelial dystrophy of the cornea. *Arch Ophthalmol*. 2001;119:1597–1604.
5. Szentmary N, Szende B, Suveges I. Epithelial cell, keratocyte, and endothelial cell apoptosis in Fuchs' dystrophy and in pseudophakic bullous keratopathy. *Eur J Ophthalmol*. 2005;15:17–22.

6. Engler C, Kelliher C, Spitze AR, Speck CL, Eberhart CG, Jun AS. Unfolded protein response in Fuchs endothelial corneal dystrophy: a unifying pathogenic pathway? *Am J Ophthalmol*. 2010;149:194–202.e2.
7. Jun AS, Meng H, Ramanan N, et al. An alpha 2 collagen VIII transgenic knock-in mouse model of Fuchs endothelial corneal dystrophy shows early endothelial cell unfolded protein response and apoptosis. *Hum Mol Genet*. 2012;21:384–393.
8. Ellgaard L, Helenius A. Quality control in the endoplasmic reticulum. *Nat Rev Mol Cell Biol*. 2003;4:181–191.
9. Walter P, Ron D. The unfolded protein response: from stress pathway to homeostatic regulation. *Science*. 2011;334:1081–1086.
10. Rainbolt TK, Saunders JM, Wiseman RL. Stress-responsive regulation of mitochondria through the ER unfolded protein response. *Trends Endocrinol Metab*. 2014;25:528–537.
11. Smith MH, Ploegh HL, Weissman JS. Road to ruin: targeting proteins for degradation in the endoplasmic reticulum. *Science*. 2011;334:1086–1090.
12. Tabas I, Ron D. Integrating the mechanisms of apoptosis induced by endoplasmic reticulum stress. *Nat Cell Biol*. 2011;13:184–190.
13. Jiang D, Niwa M, Koong AC. Targeting the IRE1alpha-XBP1 branch of the unfolded protein response in human diseases. *Semin Cancer Biol*. 2015;33:48–56.
14. Rozpedek W, Markiewicz L, Diehl JA, Pytel D, Majsterek I. Unfolded protein response and PERK kinase as a new therapeutic target in the pathogenesis of Alzheimer's disease. *Curr Med Chem*. 2015;22:3169–3184.
15. Hekmatimoghaddam S, Zare-Khormizi MR, Pourrajab F. Underlying mechanisms and chemical/biochemical therapeutic approaches to ameliorate protein misfolding neurodegenerative diseases [published online ahead of print February 22, 2016]. *Biofactors*. doi:10.1002/biof.1264.
16. Okumura N, Minamiyama R, Ho LT, et al. Involvement of ZEB1 and Snail1 in excessive production of extracellular matrix in Fuchs endothelial corneal dystrophy. *Lab Invest*. 2015;95:1291–1304.
17. Okumura N, Sakamoto Y, Fujii K, et al. Rho kinase inhibitor enables cell-based therapy for corneal endothelial dysfunction. *Sci Rep*. 2016;6:26113.
18. Mayer MP, Bukau B. Hsp70 chaperones: cellular functions and molecular mechanism. *Cell Mol Life Sci*. 2005;62:670–684.
19. Bourne WM, Johnson DH, Campbell RJ. The ultrastructure of Descemet's membrane. III. Fuchs' dystrophy. *Arch Ophthalmol*. 1982;100:1952–1955.
20. Weller JM, Zenkel M, Schlotzer-Schrehardt U, Bachmann BO, Tourtas T, Kruse FE. Extracellular matrix alterations in late-onset Fuchs' corneal dystrophy. *Invest Ophthalmol Vis Sci*. 2014;55:3700–3708.
21. Wu J, Kaufman RJ. From acute ER stress to physiological roles of the Unfolded Protein Response. *Cell Death Differ*. 2006;13:374–384.
22. Lytton J, Westlin M, Hanley MR. Thapsigargin inhibits the sarcoplasmic or endoplasmic reticulum Ca-ATPase family of calcium pumps. *J Biol Chem*. 1991;266:17067–17071.
23. Halliday M, Mallucci GR. Targeting the unfolded protein response in neurodegeneration: a new approach to therapy. *Neuropharmacology*. 2014;76:169–174.
24. Halliday M, Mallucci GR. Review: modulating the unfolded protein response to prevent neurodegeneration and enhance memory. *Neuropathol Appl Neurobiol*. 2015;41:414–427.
25. Huang HC, Tang D, Lu SY, Jiang ZF. Endoplasmic reticulum stress as a novel neuronal mediator in Alzheimer's disease. *Neurol Res*. 2015;37:366–374.
26. Scheper W, Hoozemans JJ. The unfolded protein response in neurodegenerative diseases: a neuropathological perspective. *Acta Neuropathol*. 2015;130:315–331.
27. Lin JH, Lavail MM. Misfolded proteins and retinal dystrophies. *Adv Exp Med Biol*. 2010;664:115–121.
28. Gottsch JD, Zhang C, Sundin OH, Bell WR, Stark WJ, Green WR. Fuchs corneal dystrophy: aberrant collagen distribution in an L450W mutant of the COL8A2 gene. *Invest Ophthalmol Vis Sci*. 2005;46:4504–4511.
29. Winnay JN, Kahn CR. PI 3-kinase regulatory subunits as regulators of the unfolded protein response. *Methods Enzymol*. 2011;490:147–158.
30. Haze K, Yoshida H, Yanagi H, Yura T, Mori K. Mammalian transcription factor ATF6 is synthesized as a transmembrane protein and activated by proteolysis in response to endoplasmic reticulum stress. *Mol Biol Cell*. 1999;10:3787–3799.
31. Reimold AM, Iwakoshi NN, Manis J, et al. Plasma cell differentiation requires the transcription factor XBP-1. *Nature*. 2001;412:300–307.
32. Tsaytler P, Harding HP, Ron D, Bertolotti A. Selective inhibition of a regulatory subunit of protein phosphatase 1 restores proteostasis. *Science*. 2011;332:91–94.
33. Bravo R, Vicencio JM, Parra V, et al. Increased ER-mitochondrial coupling promotes mitochondrial respiration and bioenergetics during early phases of ER stress. *J Cell Sci*. 2011;124:2143–2152.
34. Rizzuto R, De Stefani D, Raffaello A, Mammucari C. Mitochondria as sensors and regulators of calcium signalling. *Nat Rev Mol Cell Biol*. 2012;13:566–578.
35. Harding HP, Zhang Y, Zeng H, et al. An integrated stress response regulates amino acid metabolism and resistance to oxidative stress. *Mol Cell*. 2003;11:619–633.
36. Zheng M, Kim SK, Joe Y, et al. Sensing endoplasmic reticulum stress by protein kinase RNA-like endoplasmic reticulum kinase promotes adaptive mitochondrial DNA biogenesis and cell survival via heme oxygenase-1/carbon monoxide activity. *FASEB J*. 2012;26:2558–2568.
37. Cullinan SB, Diehl JA. PERK-dependent activation of Nrf2 contributes to redox homeostasis and cell survival following endoplasmic reticulum stress. *J Biol Chem*. 2004;279:20108–20117.
38. Czarny P, Seda A, Wielgorski M, et al. Mutagenesis of mitochondrial DNA in Fuchs endothelial corneal dystrophy. *Mutat Res*. 2014;760:42–47.
39. Jurkunas UV, Bitar MS, Funaki T, Azizi B. Evidence of oxidative stress in the pathogenesis of Fuchs endothelial corneal dystrophy. *Am J Pathol*. 2010;177:2278–2289.

Investigative Ophthalmology & Visual Science

SCIENTIFIC REPORTS

OPEN

Activation of TGF-β signaling induces cell death via the unfolded protein response in Fuchs endothelial corneal dystrophy

Received: 19 December 2016
Accepted: 21 June 2017
Published: 28 July 2017

Naoki Okumura[1], Keisuke Hashimoto[1], Miu Kitahara[1], Hirokazu Okuda[1], Emi Ueda[1], Kyoko Watanabe[1], Makiko Nakahara[1], Takahiko Sato[2], Shigeru Kinoshita[3], Theofilos Tourtas[4], Ursula Schlötzer-Schrehardt[4], Friedrich Kruse[4] & Noriko Koizumi[1]

Fuchs endothelial corneal dystrophy (FECD) is a slowly progressive bilateral disease of corneal endothelium in which accumulation of extracellular matrix (ECM) and loss of corneal endothelial cells (CECs) are phenotypic features. The corneal endothelium maintains corneal transparency by regulating water hydration; consequently, corneal endothelial dysfunction causes serious vision loss. The only therapy for corneal haziness due to corneal endothelial diseases, including FECD, is corneal transplantation using donor corneas, and no pharmaceutical treatment is available. We provide evidence that the expression levels of transforming growth factor-β (TGF-β) isoforms and TGF-β receptors are high in the corneal endothelium of patients with FECD. A cell model based on patients with FECD shows that TGF-β signaling induced a chronic overload of ECM proteins to the endoplasmic reticulum (ER), thereby enhancing the formation of unfolded protein and triggering the intrinsic apoptotic pathway through the unfolded protein response (UPR). We propose that inhibition of TGF-β signaling may represent a novel therapeutic target that suppresses cell loss as well as the accumulation of ECM in FECD.

Fuchs endothelial corneal dystrophy (FECD) is a slowly progressive bilateral disease of the corneal endothelium. The corneal endothelium maintains corneal transparency by regulating water hydration; consequently, severe damage to the corneal endothelium induces corneal haziness, resulting in critical vision loss. The only therapy for corneal haziness due to corneal endothelial diseases including FECD is corneal transplantation using donor corneas. The high prevalence of FECD (i.e., 4% of the population aged over 40 years in the United States[1]) makes FECD a leading cause of corneal transplantation[2]. However, the shortage of donor corneas, the difficulty of the surgical procedure, and the incidence of graft failure in both acute and chronic phases[3,4] encourages the development of pharmaceutical treatments.

The corneal endothelium in FECD shows features of apoptotic cells, such as positive TdT-mediated dUTP nick end labeling (TUNEL) staining, condensation of nuclei, and decreased cell size[5]. Apoptosis has been indicated to play an important role, but the pathophysiology of FECD remains unclear. Engler and colleagues reported morphological alterations of the endoplasmic reticulum (ER) in FECD and postulated that the unfolded protein response (UPR) plays an important role in inducing apoptosis[6]. Under normal conditions, secreted and membrane proteins are folded in the lumen of ER for delivery to membranes or extracellular secretion[7,8]. Properly folded proteins are packaged into ER exit vesicles, whereas improperly folded proteins are retained in the ER and are removed by proteasomal degradation, called ER-associated degradation (ERAD)[9]. This highly regulated system is monitored by a conserved signaling pathway, termed the UPR[10,11]. However, severe ER stress, with its associated impairment of homeostasis, induces chronic activation of the UPR, resulting in apoptosis to remove rogue cells[10,11]. Notably, increasing evidence now indicates that the UPR is involved in the pathogenesis

[1]Department of Biomedical Engineering, Faculty of Life and Medical Sciences, Doshisha University, Kyotanabe, Japan. [2]Department of Ophthalmology, Kyoto Prefectural University of Medicine, Kyoto, Japan. [3]Department of Frontier Medical Science and Technology for Ophthalmology, Kyoto Prefectural University of Medicine, Kyoto, Japan. [4]Department of Ophthalmology, University of Erlangen-Nürnberg, Erlangen, Germany. Correspondence and requests for materials should be addressed to N.K. (email: nkoizumi@mail.doshisha.ac.jp)

of various diseases, such as Alzheimer's disease, Parkinson's disease, diabetes mellitus, multiple myeloma, and retinitis pigmentosa[12–17].

The phenotypic features of FECD in the clinical setting are (1) formation of corneal guttae that are excrescences of the basement membrane (Descemet's membrane) and (2) endothelial cell loss[18]. Corneal guttae have been recognized as an abnormal accumulation of extracellular matrix (ECM) components, such as fibronectin and type 1 collagen, secreted by pathological corneal endothelium[19]. However, the mechanisms for upregulation of secretion of these ECM proteins and the association of the ECM accumulation with endothelial cell loss in FECD remain unclear. In the context of ECM production, we recently demonstrated in a cell model established from patients with FECD[20] that transforming growth factor-β (TGF-β) regulates excessive ECM protein production.

In the current study, the expression level of TGF-β isoforms and TGF-β receptors was examined in clinical samples of FECD patient corneal endothelium. We also examined the effect of TGF-β on the formation of unfolded protein and subsequent triggering of the UPR. Finally, we evaluated the feasibility of inhibiting TGF-β signaling as a possible therapeutic target for treatment of FECD.

Results

Expression levels of *TGF-β* isoforms and receptors in the corneal endothelium of Patients with FECD. We established a cell model from patients with FECD and showed that corneal endothelial cells (CECs) have a higher responsiveness to TGF-β when compared to control CECs, which results in excessive ECM production[20]. We therefore evaluated the expression levels of *TGF-β* isoforms and receptors in patient samples. Quantitative real-time polymerase chain reaction (PCR) assays showed that expression levels of *TGF-β1* and *TGF-β2* were significantly higher in Patients with FECD (n = 30) than in normal control subjects (n = 30) (2.76 and 4.36 fold, respectively) (Fig. 1a,b). Likewise, expression levels of *TGF-βR1* and *TGF-βR2* were significantly higher in FECD samples than in control samples (3.03 and 3.79 fold, respectively) (Fig. 1c,d).

Effect of TGF-β on ECM protein expression and unfolded protein formation. Descemet's membranes, including CECs, were obtained from patients with FECD who underwent Descemet's membrane endothelial keratoplasty (DMEK). The membranes were analyzed for the expression of ECM components by immunofluorescent staining. Expression of fibronectin, collagen type 1, collagen type 3, and transforming growth factor beta induced (TGFBI) was evident in the FECD specimens, especially in the cytoplasm of endothelial cells neighboring the guttae, but no or very faint expression of those components was observed in control specimens (Fig. 2a). We also evaluated the effect of TGF-β on ECM components and unfolded protein formation by using iFECD, which is a corneal endothelial cell model established from patients with FECD. Fibronectin and collagen type 1 were expressed in the cytoplasm in iFECD cells at levels similar to those observed in patient specimens. Aggresome staining showed that unfolded protein forms aggregates and fibronectin and collagen type 1 were at least partially colocalized to the aggresome. TGF-β treatment increased the expression of fibronectin and collagen type 1, as well as aggresome formation (Fig. 2b,c). Co-staining for the aggresome and protein disulfide isomerase (PDI, marker of ER) demonstrated that the aggresomes were localized to the ER (Fig. 2d). Flow cytometry showed that the intensity of aggresome staining was significantly higher in iFECD than in iHCEC; the latter is a cell model established from non-FECD human donor corneas. Notably, TGF-β stimulation caused an upregulation of the aggresome only in iFECD but not in iHCEC (Fig. 2e). Consistently, TGF-β induced a higher phosphorylation of PKR-like endoplasmic reticulum kinase (PERK), which is an ER sensor responsible for ER-mediated apoptosis, and increased expression of CCAAT-enhancer-binding protein homologous protein (CHOP), which is a transcription factor that transduces ER mediated apoptotic signals to the mitochondria, in iFECD than in iHCEC (Fig. 2f).

Activation of ER stress and the intrinsic apoptotic pathway by TGF-β. Phase contrast images showed that a greater number of cells was detached from the culture plate after 48 hours of TGF-β treatment in iFECD, whereas no cell detachment was evident in iHCEC after TGF-β treatment (Fig. 3a). These observations were consistent with the finding that TGF-β induced unfolded protein and subsequent ER stress only in iFECD (Fig. 2f). Western blotting showed that TGF-β induced expression of glucose-regulated protein78 (GRP78), phosphorylation of PERK and inositol-requiring enzyme 1α (IRE1α), and cleavage of activating transcription factor 6α (ATF6α) in iFECD, indicating that TGF-β induces unfolded protein and subsequent activation of all three ER sensors (Fig. 3b). Staining with 5, 5′, 6, 6′-tetrachloro-1, 1′, 3, 3′-tetraethylbenzimidazolylcarbocyanineiodide (JC-1) showed that the mitochondrial membrane potential (MMP) was depolarized by TGF-β treatment. Co-treatment with TGF-β and SB431542 suppressed the downregulation of MMP by TGF-β, suggesting that MMP depolarization was induced by activation of TGF-β signaling. Carbonylcyanide m-chlorophenylhydrazone (CCCP) was used as positive control to depolarize the MMP (Fig. 3c). Consistent with fluorescence microscopy, flow cytometry showed that TGF-β significantly upregulated the percentages of MMP depolarized iFECD when compared to the control iFECD (36.5 ± 2.1% and 22.9 ± 0.3%, respectively) (Fig. 3d). TGF-β also induced caspase 3/7 activation, which was repressed by the pan-caspase inhibitor, Z-VD-FMK (Fig. 3e). Taken together, these data suggest that TGF-β induces ER stress and activates the intrinsic apoptotic pathway in iFECD.

Effect of a chemical chaperone on ER stress and intrinsic apoptotic pathway. We also evaluated the effect of a chemical chaperone on ER stress and subsequent intrinsic apoptotic pathway activation. Aggresome staining showed that the chemical chaperone 4-phenylbutyric acid (4 PBA) repressed the formation of TGF-β mediated unfolded protein (Fig. 4a). Phase contrast microscopy showed that TGF-β induced cell detachment of iFECD, which was suppressed by 4 PBA (Fig. 4b). Consistently, TGF-β mediated phosphorylation of PERK, expression of CHOP, and cleavage of caspase 3 were suppressed by 4 PBA (Fig. 4c). Annexin V staining also

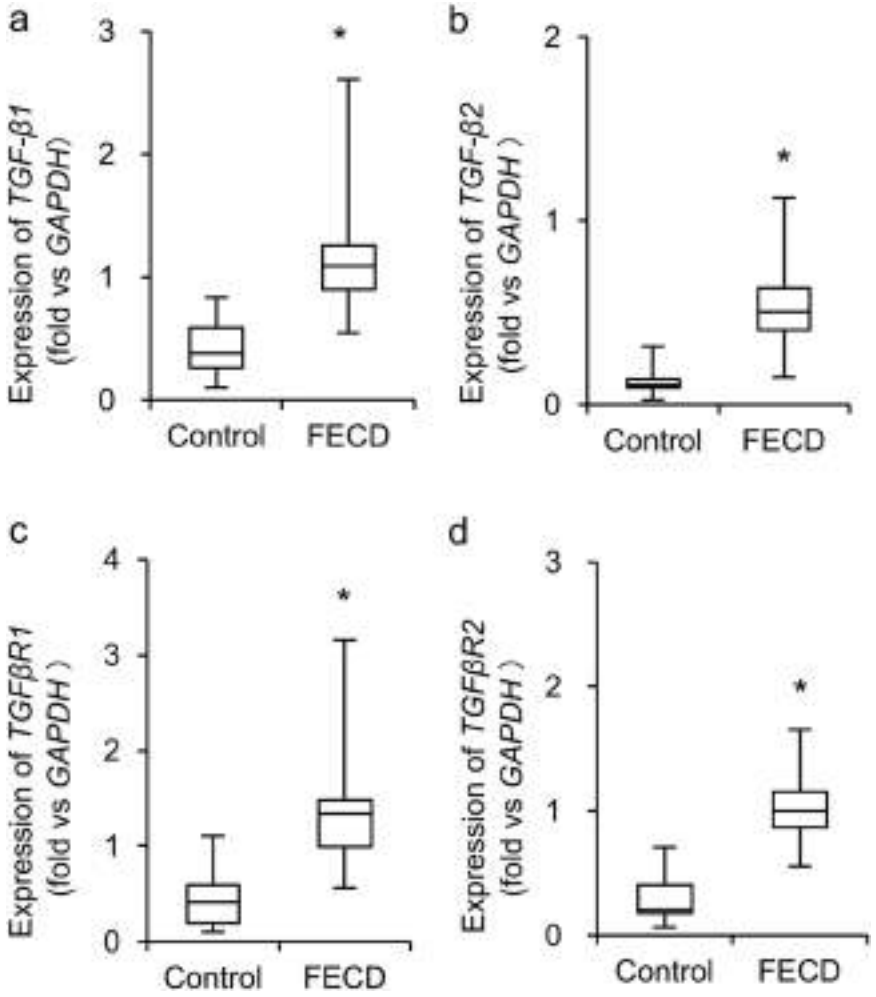

Figure 1. Expression of *TGF-β* isoforms and receptors in corneal endothelium of patients with FECD. (**a**–**d**) Descemet's membranes with CECs were obtained from 30 patients with FECD during Descemet's membrane endothelial keratoplasty (DMEK). Thirty human donor corneas from non-FECD subject were used as control. Expression levels of *TGF-β1*, *TGF-β2*, *TGFβR1*, and *TGFβR2* were evaluated by quantitative real-time PCR. GAPDH was used as an internal standard. The horizontal lines in the boxes indicate medians, the bottom of each box indicates the 25th percentile, and the top of each box indicates the 75th percentile. The horizontal lines outside the boxes indicate the range of mRNA level. The statistical analysis was performed by Mann–Whitney U test. *$P < 0.01$.

demonstrated the presence of apoptotic cells in TGF-β treated iFECD, but 4 PBA suppressed the occurrence of Annexin V positive cells (Fig. 4d). Flow cytometry also demonstrated that $29.8 \pm 0.6\%$ of the iFECD cells were Annexin V positive following TGF-β treatment, but 4 PBA significantly reduced the percentage of Annexin V positive cells to $26.9 \pm 0.2\%$ (Fig. 4e). These results suggest that suppression of unfolded protein formation or accumulation counteracted the UPR and subsequent intrinsic apoptotic pathway activation.

Feasibility of inhibiting TGF-β signaling pathway as therapeutic target for the treatment of FECD. We evaluated the effect of inhibiting the TGF-β signaling pathway on endothelial cell survival in iFECD. The iFECD was cultured with SB431542 (TGF-βR1 inhibitor) or a Smad inhibitor, or subjected to knockdown of TGF-βR1 by siRNA. Phosphorylation of Smad3 was suppressed by SB431542, knockdown of TGF-βR1, and the Smad inhibitor. The efficacy of knockdown of TGF-βR1 by siRNA was confirmed by western blotting. Western blotting also showed that fibronectin production was higher in iFECD than in iHCEC, as observed in the corneal endothelium of patients with FECD. On the other hand, inhibition of the TGF-β signaling pathway by all three independent methods suppressed the production of fibronectin in iFECD (Fig. 5a).

Aggresome staining demonstrated that the formation of unfolded protein was suppressed by SB431542, knockdown of TGF-βR1, and the Smad inhibitor (Fig. 5b). Expression of GRP78 was suppressed by SB431542, indicating the presence of unfolded protein in iFECD and its reduction by SB431542 treatment. Consistently, three ER sensors were downregulated by SB431542, which causes repression of CHOP (Fig. 5c). JC-1 staining showed that the MMP depolarization observed in iFECD was rescued by SB431542, knockdown of TGF-βR1, and the Smad inhibitor (Fig. 5d). Flow cytometry showed that the percentage of MMP depolarization in iFECD

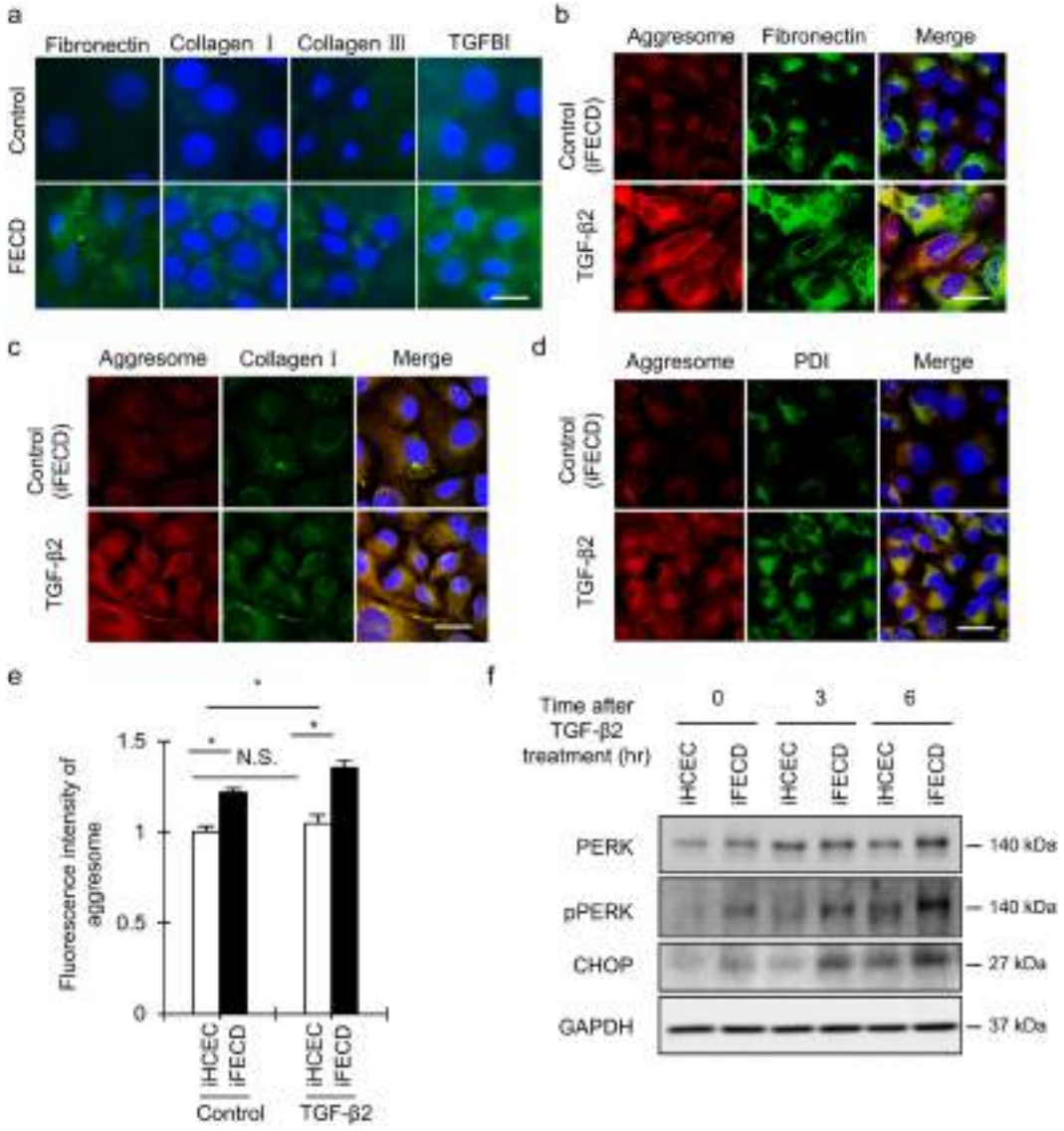

Figure 2. Effect of TGF-β on extracellular matrix (ECM) protein expression and unfolded protein formation. (**a**) Descemet's membranes including CECs were obtained from 22 patients with FECD during Descemet's membrane endothelial keratoplasty (DMEK) and were examined for the expression of ECM; fibronectin, collagen type 1, collagen type 3, and TGBI were evaluated by immunofluorescent staining. Human donor corneas from 19 non-FECD subject were used as control. Scale bar: 50 μm. (**b**,**c**) iFECD, which is a corneal endothelial cell model established from patients with FECD, were cultured and stimulated with TGF-β2 for 48 hours. The expression of fibronectin and collagen type 1 was evaluated by immunofluorescence staining. Unfolded protein was assessed by aggresome staining. Nuclei were stained with DAPI. Experiments were performed in triplicate. Scale bar: 50 μm. (**d**) Immunofluorescent staining of PDI and aggresome staining was performed to evaluate the codistribution of endoplasmic reticulum (ER) and unfolded protein. Nuclei were stained with DAPI. Experiments were performed in triplicate. Scale bar: 50 μm. (**e**) iFECD and iHCEC were cultured with or without TGF-β2 (10 ng/ml) for 48 hours. Cells were stained with aggresome and fluorescence intensity was evaluated by flow cytometry. Experiments were performed in triplicate. The statistical analysis was performed by Student's t-test. $^*P < 0.01$. (**f**) iFECD and iHCEC were cultured with or without TGF-β2 (10 ng/ml), and expression of PERK, phosphorylation of PERK, and expression of CHOP was evaluated by western blotting. Experiments were performed in triplicate. GAPDH was used as internal control.

was 10.9 ± 0.9%, but this was suppressed to 6.7 ± 0.8% by SB431542 (Fig. 5e). CCCP was used to depolarize MMP as positive control.

We also evaluated the effect of inhibition of TGF-β signaling on the apoptosis executor molecules. Western blotting showed that activation of caspase 3 and Poly (ADP-ribose) polymerase (PARP) by cleavage was counteracted by SB431542 (Fig. 5f). Densitometry analysis of western blotting also showed a significant downregulation of apoptosis executor molecules by SB431542 (Fig. 5g,h).

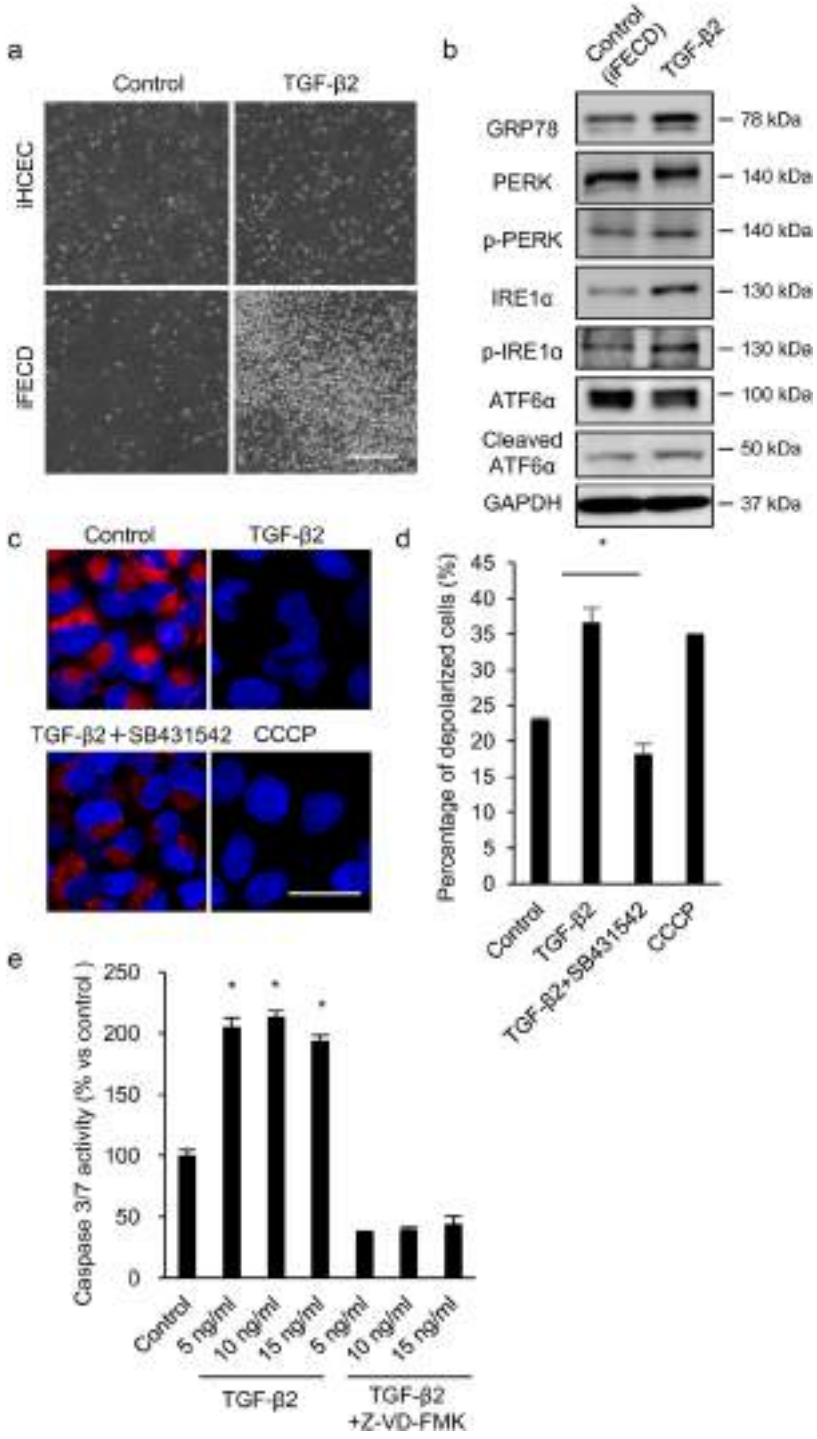

Figure 3. Activation of endoplasmic reticulum (ER) stress and subsequent intrinsic apoptotic pathway by TGF-β. (**a**) iFECD and iHCEC was cultured with or without TGF-β2 (10 ng/ml) for 48 hours. Representative phase contrast images are shown. Experiments were performed in triplicate. Scale bar: 200 μm. (**b**) iFECD was treated with TGF-β2 for 6 hours and expression of GRP78, PERK, IRE1α, and phosphorylation of PERK and IRE1α, and cleavage of ATF6α were evaluated by western blotting. Full-length blot of ATF6α is presented in Supplementary Fig. 1. GAPDH was used as internal control. Experiments were performed in triplicate. (**c**,**d**) iFECD was treated with TGF-β2, TGF-β2 + SB431542 for 6 hours. After JC-1 staining, mitochondrial membrane potential (MMP) depolarization was evaluated by fluorescence microscopy and flow cytometry. Nuclei were stained with DAPI for fluorescence microscopy analysis. CCCP was used as positive control to induce MMP depolarization. Experiments were performed in triplicate. Scale bar: 50 μm. The statistical analysis was performed by Student's t-test. *$P < 0.01$. (**e**) iFECD was treated with TGF-β2 (5, 10, or 15 ng/ml) for 6 hours with or without caspase inhibitor, Z-VD-FMK, then caspase 3/7 activity was determined by use of the Caspase 3/7 activity assay® Luminescent Assay. Experiments were performed in duplicate. The statistical analysis was performed by Dunnett's multiple comparisons test. *$P < 0.01$.

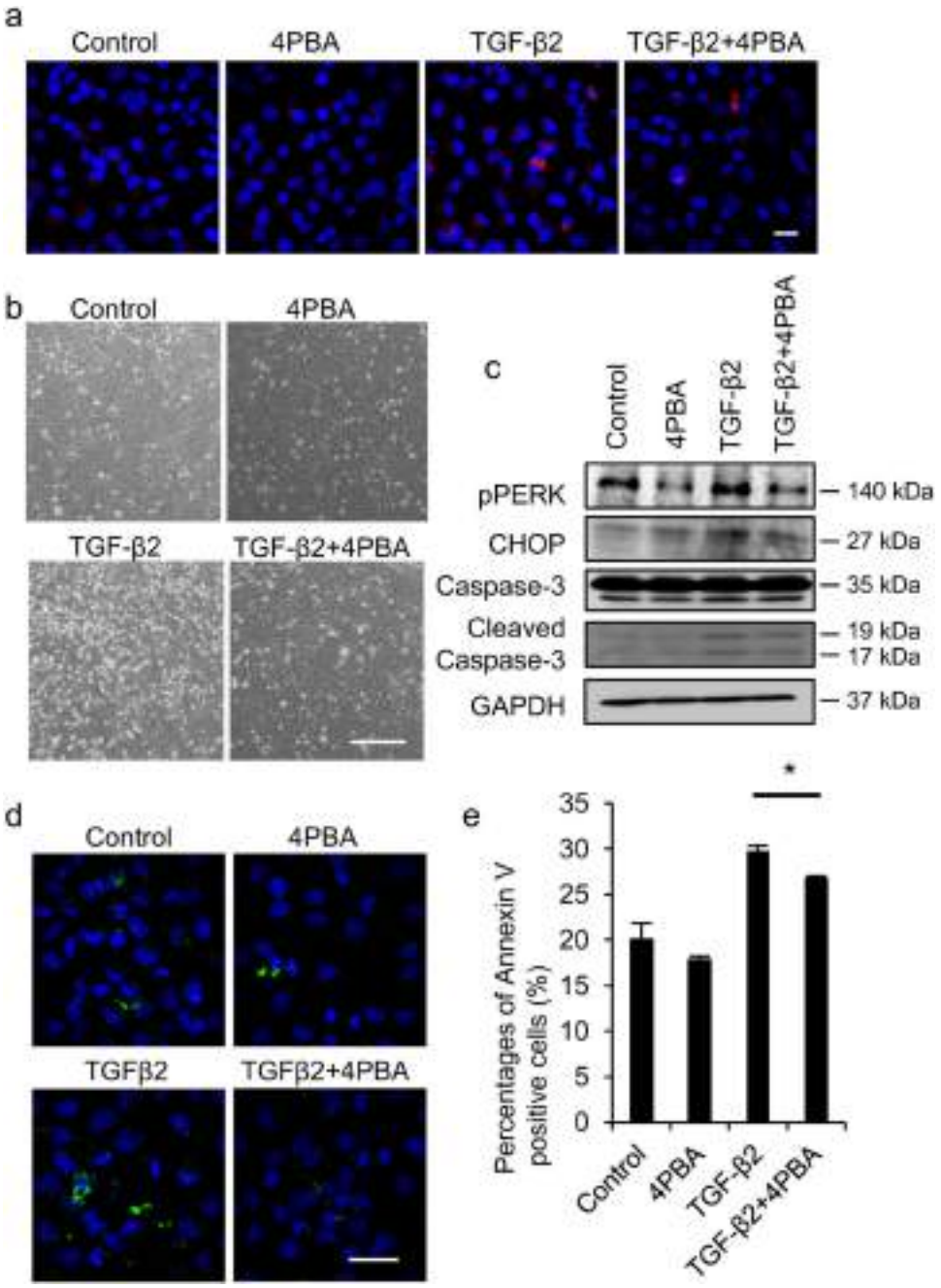

Figure 4. Effect of chemical chaperon on endoplasmic reticulum (ER) stress and intrinsic apoptotic pathway. (**a**) iFECD was treated with or without TGF-β2 (10 ng/ml) for 24 hours, and 4 PBA (5 mM) was added to the medium to evaluate the effect of a chemical chaperone on unfolded protein formation. Unfolded protein was evaluated by aggresome staining and nuclei were stained with DAPI. Experiments were performed in triplicate. Scale bar: 50 μm. (**b**) Representative phase contrast images are shown. TGF-β2 induces cell detachment of iFECD, but 4 PBA suppressed the cell detachment. Experiments were performed in triplicate. Scale bar: 200 μm. (**c**) Effect of chemical chaperon on ER stress and apoptosis was evaluated. TGF-β2 treated samples were recovered after coincubation with 4 PBA and phosphorylation of PERK, expression of CHOP, and cleavage of caspase 3 were examined by western blotting. Full-length blot of caspase 3 is presented in Supplementary Fig. 1. GAPDH was used as internal control. Experiments were performed in triplicate. (**d**,**e**) Apoptotic cell were evaluated by Annexin V staining and evaluated by fluorescent microscope and flow cytometry. Nuclei were stained with DAPI for fluorescence microscopy analysis. Experiments were performed in triplicate. Scale bar: 50 μm. The statistical analysis was performed by Student's t-test. *$P < 0.01$.

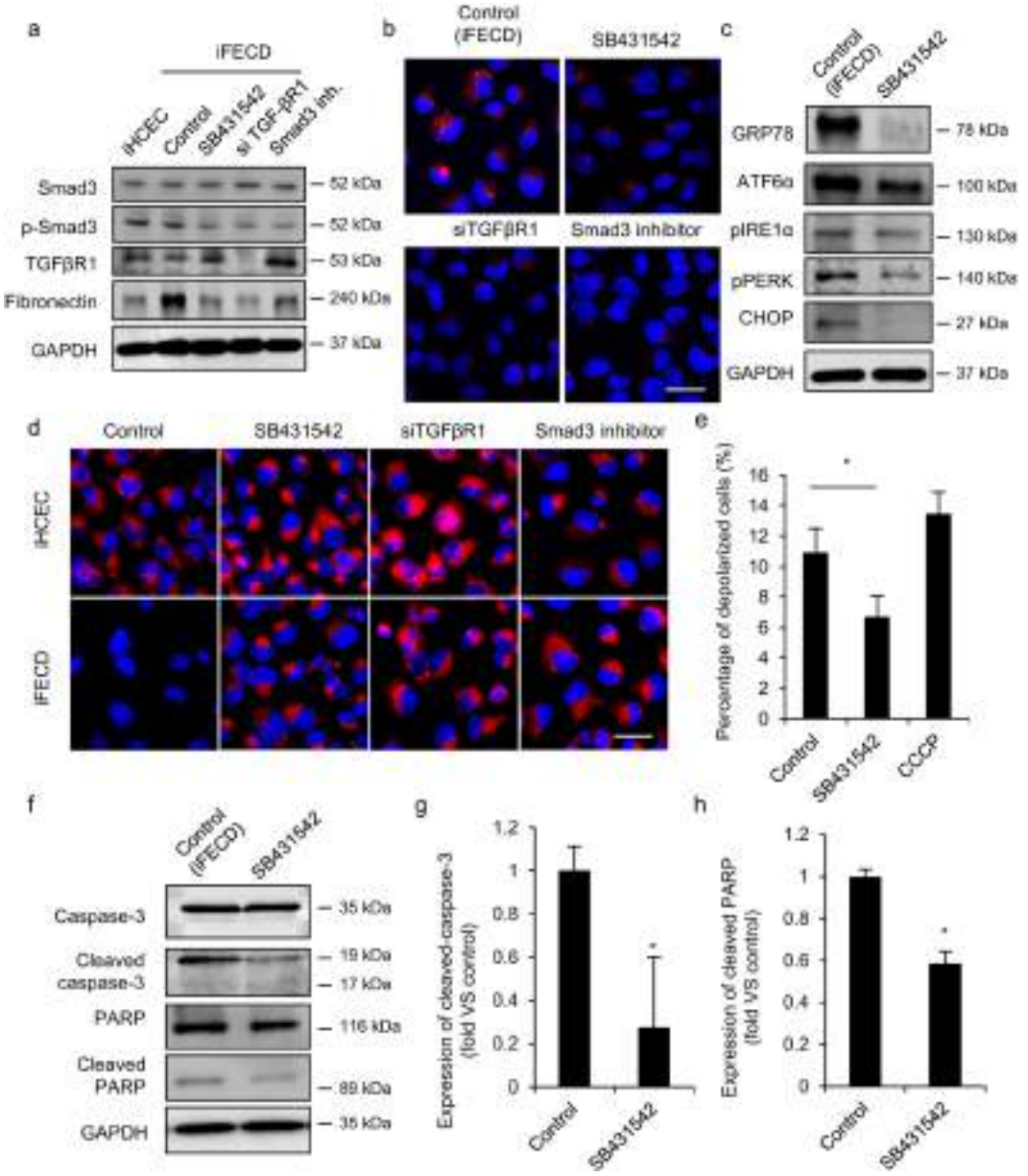

Figure 5. Effect of inhibiting TGF-β signaling pathway on endoplasmic reticulum (ER) stress mediated cell death. The effect of inhibiting TGF-β signaling pathway on extracellular matrix (ECM) production was evaluated. iFECD was cultured with SB431542 (TGF-βR1 inhibitor) or Smad inhibitor, or knockdown TGF-βR1 by siRNA. Phosphorylation of Smad3 was suppressed by SB431542, knockdown TGF-βR1, and Smad inhibitor. Production of fibronectin by iFECD was evaluated by western blotting. Experiments were performed in duplicate. (**b**) TGF-β signaling pathway was blocked by SB431542 (TGF-βR1 inhibitor) or Smad inhibitor, or knockdown TGF-βR1 by siRNA. The effect of TGF-β signaling pathway inhibition on unfolded protein was evaluated by aggresome staining. Experiments were performed in triplicate. Scale bar: 50 μm. (**c**) Effect of inhibition of the TGF-β signaling pathway on endoplasmic reticulum (ER) stress. Expression of GRP78, ATF6 pIRE1α, and CHOP, and phosphorylation of IRE1α and PERK was evaluated by western blotting. GAPDH was used as internal control. Experiments were performed in triplicate. (**d**,**e**) Effect of inhibiting TGF-β signaling pathway on mitochondrial membrane potential (MMP) depolarization was evaluated by fluorescent microscope after JC-1 staining and flow cytometry. Nuclei were stained with DAPI for fluorescence microscopy analysis. CCCP was used as positive control to induce MMP depolarization. Experiments were performed in duplicate. Scale bar: 50 μm. The statistical analysis was performed by Student's t-test. $^*P < 0.01$. (**f**–**h**) Western blotting was preformed to evaluate the effect of inhibiting TGF-β signaling pathway on cleavage caspase 3 and PARP. Full-length blots are presented in Supplementary Fig. 1. Densitometry analysis of three independent experiments was performed with ImageJ and plotted as graphs. The statistical analysis was performed with the Student's t-test. $^*P < 0.01$.

Discussion

TGF-β regulates a wide range of key events in cell proliferation, cell differentiation, wound healing, and immunity. Hence, it is also involved in different forms of pathogenesis, such as fibrosis, connective tissue disorders, and cancer[21–25]. Since the first report of a profibrotic effect of TGF-β, in which subcutaneous injection of TGF-β1 induce fibrotic lesions[26], many studies have confirmed TGF-β as an important modulator of fibrosis in many different cells and tissues[25]. TGF-β induces its profibrotic effect by promoting ECM synthesis, inhibiting collagenolysis, and enhancing the proliferation of fibroblasts during wound healing[26,27]. TGF-β is also recognized as one of the most important regulators of epithelial-mesenchymal transition (EMT) and the endothelial to mesenchymal transition (EndMT) in several models, such as tubulointerstitial renal fibrosis, pulmonary fibrosis, and heart fibrosis[28–30].

We reported that activation of TGF-β signaling augmented the accumulation of ECM components through activation of EMT inducer genes, such as *ZEB1* and *SNAI1*, in FECD[20]. In addition, a cell model derived from patients with FECD exhibited high responsiveness to TGF-β, as CECs established from patients with FECD produced higher amount of ECM following TGF-β treatment when compared with control CECs[20]. In the current study, we provided *in vivo* patient data showing that TGF-β isoforms; TGF-β1 and TGF-β2 and TGF-β receptors; TGF-βR1, and TGF-βR2 were highly expressed in patient corneal endothelium. To the best of our knowledge, this is the first data from patient tissue sample to show that the TGF-β signaling pathway is upregulated and may play an important role in FECD. The higher expression TGF-β receptors could also be a reasonable explanation for the strong responsiveness of FECD-CECs to TGF-β, as previously reported[20].

Unfolded protein accumulation in the ER lumen is triggered by several causes, such as nascent protein increases, mutations, shortages of chaperones, and oxidative stress[7,8,10,11]. We showed that TGF-β induced fibronectin and type 1 collagen synthesis associated with the formation of unfolded protein. Interestingly, TGF-β mediated UPR and intrinsic apoptotic-signaling activation was more evident in iFECD than in iHCEC. This finding is consistent with our previous findings, in which iFECD exhibited higher responsiveness to TGF-β[20], and with our current data in which TGF-β receptors were expressed at higher levels in patient samples. Further studies are needed to elucidate whether TGF-β induces the UPR by recruiting other proteins, such as type 3 collagen, clusterin, TGFBI, and proteoglycans, which are known to accumulate in FECD, similar to fibronectin and type 1 collagen[19,31,32]. Other possible combined mechanisms worth investigating in future research include the impairment of ERAD, which ubiquitinates and degrades unfolded proteins of the ER[9], in FECD, resulting in the formation of unfolded protein.

We also demonstrated that inhibition of the TGF-β signaling pathway suppressed aggresome accumulation and UPR, and subsequently repressed apoptotic signaling activation. The TGF-β signaling pathway has been an attractive therapeutic target in various diseases[21–25]. A possible side effect of TGF-β signaling inhibition is worsening of autoimmune disease due to the inhibition of regulatory T cells role; however, TGF-β inhibition has been generally considered to have limited adverse effects[24,33]. Several potential therapeutic strategies have been proposed to inhibit the TGF-β signaling pathway, such as (1) neutralizing antibodies or soluble receptors to TGF-β, (2) receptor kinase inhibitors, (3) Smad3 inhibitors, (4) Smad7 agonists, and (5) histone deacetylase inhibitors[24,33]. At present, clinical trials of anti-TGF-β antibodies and TGF-β receptor inhibitors have been performed for a numbers of cancers, such as renal cell carcinoma, melanoma, glioma, glioblastoma, hepatocellular carcinoma, pancreatic ductal carcinoma and ovarian cancers[24,33]. For targeting fibrotic disease, neutralizing antibodies for TGF-β were used for the treatment of primary focal segmental glomerulosclerosis and diabetic kidney disease[34–36].

In conclusion, we provided evidence that the expression level of TGF-β isoforms and TGF-β receptors are high in the corneal endothelium of patients with FECD. We propose that TGF-β signaling mediates a chronic overload of proteins to the ER, which enhances the formation of unfolded protein and activates the intrinsic apoptotic pathway through the UPR (Fig. 6). The inhibition of TGF-β signaling may therefore represent a therapeutic target for suppressing cell loss as well as for accumulation of ECM in FECD.

Methods

Ethics Statement. The human tissue used in this study was handled under the guidelines based on the ethical principles of the Declaration of Helsinki. This study was performed according to a protocol approved by the ethical review committee of the Friedrich-Alexander University Erlangen-Nürnberg. Informed consent was acquired from patients with FECD, then stripped Descemet's membranes with CECs were obtained during DMEK at University of Erlangen-Nürnberg. Normal human donor corneas were obtained from SightLife™ (http://www.sightlife.org/, Seattle, WA). No tissues were procured from prisoners.

Quantitative Real-Time PCR. Total RNA was extracted from the corneal endothelium of the FECD patient and donor corneas, and cDNA was synthesized by utilizing SuperScript™ VILO™ MasterMiX (Thermo Fisher Scientific Inc., Waltham, MA, USA). Quantitative real-time PCR was performed with a StepOnePlus™ Real-Time PCR System (Thermo Fisher Scientific Inc.). All samples were analyzed in duplicate with a program of 95 °C for 20 seconds and 40 cycles of 95 °C for 1 seconds and 60 °C for 20 seconds. For quantification, standard curves using serial dilutions (5–5^5 copies) of iHCEC cDNA were run in parallel. Ratios relative to GAPDH were calculated for normalization of gene expression levels.

Gene expression levels were analyzed using TaqMan® real-time PCR (Thermo Fisher Scientific Inc.). Taqman primers for *TGF-β1*, Hs00998133_ml; *TGF-β2*, Hs00234244_ml; *TGFβR1*, Hs00610320; *TGFβR2*, Hs00234253_ml; and TaqMan® pre-development human GAPDH (Thermo Fisher Scientific Inc.) were used.

Immortalization of CECs. The CECs from three patients with FECD and three donor corneas were cultured and immortalized as a cell model. Descemet's membranes, including the CECs, were stripped from three normal human donor corneas and from corneas of three patients with FECD during DMEK. The CECs were cultured and

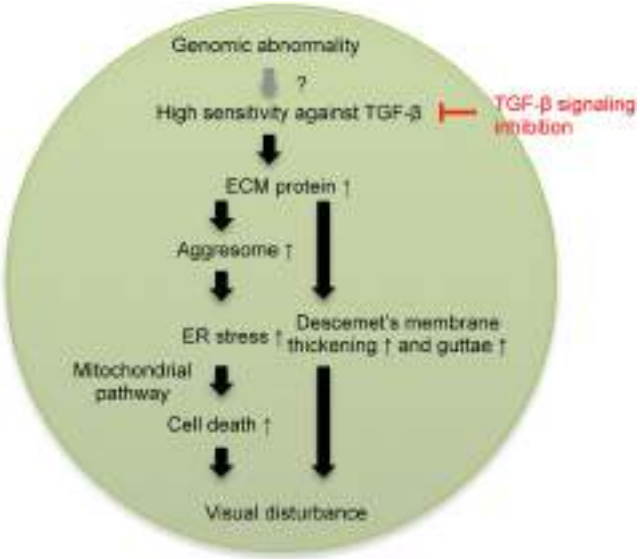

Figure 6. Schematic image shows possible pathophysiology of FECD. High sensitivity to TGF-β and activation of TGF-β signaling pathway induce excessive production of ECM components. ECM components form clinically phenotypic features, namely Descemet's membrane thickening and guttae formation. At the same time, the overload of ECM proteins will form unfolded protein and trigger the UPR, and the cells will undergo apoptosis through the intrinsic pathway. We also showed that TGF-β signaling pathway might be a possible therapeutic target for treatment of FECD.

immortalized according to modified published protocols. Briefly, Descemet's membranes containing the HCECs were digested with 1 mg/mL collagenase A (Roche Applied Science, Penzberg, Germany) at 37 °C for 12 hours. The CECs were seeded in one well of a 48-well plate coated with laminin E8 fragments (iMatrix-511; Nippi, Incorporated, Tokyo, Japan)[37] and were cultured by culture medium for CECs.

The culture medium was prepared according to published protocols[20,38]. First, human bone marrow mesenchymal stem cells (BM-MSCs) were plated at a density of 1.3×10^4 cells/cm^2 and cultured for 24 hours in Dulbecco's modified Eagle's medium (DMEM; Life Technologies Corp.) supplemented with 10% fetal bovine serum (FBS), 100 U/mL penicillin, and 100 μg/mL streptomycin. The culture medium was then replaced with the following: OptiMEM-I (Life Technologies Corp., Carlsbad, CA) containing 8% FBS, 5 ng/mL epidermal growth factor (Sigma-Aldrich Co., St. Louis, MO), 20 μg/mL ascorbic acid (Sigma-Aldrich Co.), 200 mg/L calcium chloride, 0.08% chondroitin sulfate (Wako Pure Chemical Industries, Ltd., Osaka, Japan), 50 μg/mL gentamicin, and conditioned by culturing BM-MSCs for 24 hours. Finally, the conditioned medium with BM-MSCs was collected for use as the culture medium for CECs.

CECs from patients with FECD and from donor corneas were cultured in the culture medium for CECs for 14–21 days and then immortalized using both SV40 and hTERT, according to published protocols. Immortalized CECs from patients with FECD and donor corneas were referred to as iFECD and iHCEC, respectively. The immortalized cells were cultured in DMEM containing 10% FBS and 1% penicillin and streptomycin (Life Technologies Corp.). Once the cells were 80% confluent, the cells were trypsinized with 0.05% Trypsin-EDTA and passaged.

The iFECD or iHCEC were cultured until confluent and further cultured with fresh DMEM supplemented with TGF-β2 for 24 hours for some experiments. The effect of a chemical chaperone was evaluated by culturing with DMEM supplemented with 4 PBA (5 mM, Merck Millipore, Billerica, Massachusetts, USA). To evaluate the effect of TGF-β signaling inhibition, the cells were incubated with 10 μM SB431542 (Merck Millipore) or 10 μM Smad 3 inhibitor (Santa Cruz Biotechnology, Santa Cruz, CA, USA). The siRNA for TGFβ R1 (Thermo Fisher Scientific Inc.) was also used to suppress TGF-β signaling. Briefly, cells were seeded into a 24-well plates and cultured until they reached 50–70% confluence. The cells were then incubated with RNAi duplex (TGFβR1) and Lipofectamine™RNAiMAX (Thermo Fisher Scientific).

Immunofluorescence staining. Descemet's membranes, including the CECs, derived from 22 patients with FECD and 19 donor corneas, and cultured iHCEC and iFECD underwent immunofluorescence and aggresome staining. Samples were fixed for 20 minutes with 4% paraformaldehyde, permeabilized with 0.5% Triton® X-100 (Nacalai Tesque, Kyoto, Japan), and then incubated with 1% bovine serum albumin (BSA) to block nonspecific binding. Samples were incubated with primary antibodies against fibronectin (1:200; Merck Millipore), collagen I (1:200; Merck Millipore), collagen III (1:100; abcam, Cambridge, UK), TGFBI (1:500; abcam), and PDI (1:200; Cell Signaling Technology, Danvers, Massachusetts, USA) overnight at 4 °C. Alexa Fluor® 488-conjugated goat anti-mouse (Life Technologies Corp.) antibodies were used as secondary antibodies at a 1:1000 dilution at room temperature for 1 hours. Nuclei were stained with DAPI (Vector Laboratories, Burlingame, CA, USA). The slides were examined with a fluorescence microscope (DM 2500; Leica Microsystems, Wetzlar, Germany).

Aggresome staining. Samples were stained with aggresome and aggregation of unfolded protein was evaluated by fluorescence microscope and flow cytometry according to the manufacturer's protocol. For fluorescence microscope analysis, samples were incubated with aggresome reagent (1:2000; Enzo Life Science Inc., Farmingdale, NY, USA) for 60 minutes and slides were examined with a fluorescence microscope (DM 2500). For flow cytometry, cells were washed twice with phosphate buffered saline (PBS) and incubated with Accumax™ (Innovative Cell Technologies, San Diego, CA, USA) for 10 minutes at 37 °C. Cells were recovered in fluorescence activated cell sorting (FACS) buffer composed of DMEM without Phenol Red (Nacalai Tesque) + 2%FBS, passed through a BD Falcon™ 70 μm cell strainer (BD Biosciences, Franklin Lakes, New Jersey, USA), and resuspended in FACS buffer. The cells were then incubated with aggresome reagent (1:2000) for 60 minutes at room, temperature, and washed three times with PBS. The cells were resuspended in FACS buffer and analyzed by flow cytometry using CellQuest Pro software (BD Biosciences).

Immunoblotting. The cells were washed with ice-cold PBS and lysed with ice-cold radio-immunopreci-pitation assay (RIPA) buffer containing phosphatase inhibitor cocktail 2 (Sigma-Aldrich Co.) and protease inhibitor cocktail (Roche Applied Science). Following centrifugation, the supernatant containing the total proteins was fractionated by sodium dodecyl sulfate (SDS)-poly-acrylamide gel electrophoresis (PAGE). The separated proteins were transferred to polyvinylidene difluoride (PVDF) membranes, blocked with 3% non-fat dry milk, and incubated overnight at 4 °C with the following primary antibodies: PERK (1:1000; Cell Signaling Technology), phosphorylated PERK (1:1000; Cell Signaling Technology), PERK (1:1000; Cell Signaling Technology), IRE1α (1:1000; Cell Signaling Technology, phosphorylated IRE1α (1:1000; Novus Biologicals, Colorado, USA), ATF6α (1:1000; Santa Cruz Biotechnology), CHOP (1:1000; Cell Signaling Technology), GRP78 (1:1000; Santa Cruz Biotechnology), Smad3 (1:1000; Cell Signaling Technology), phosphorylated Smad3 (1:1000; Cell Signaling Technology), TGFβR1 (1:1000; Santa Cruz Biotechnology), fibronectin(1:1000; BD Biosciences), caspase-3 (1:1000; Cell Signaling Technology), PARP (1:1000; Cell Signaling Technology), and GAPDH (1:2000; Medical & Biological Laboratories Co., Ltd., Aichi, Japan). The blots were probed with horseradish peroxidase-conjugated secondary antibodies (1:5000; GE Healthcare, Piscataway, NJ, USA) and developed with luminal for enhanced chemiluminescence using the ECL Advanced Western Blotting Detection Kit (Nacalai Tesque).

Mitochondrial membrane potential. The iFECD and iHCEC were stained with 5, 5′, 6, 6′-tetrachloro-1, 1′, 3, 3′-tetraethylbenzimidazolylcarbocyanine iodide (JC-1) and the mitochondrial membrane potential was evaluated by fluorescence microscopy and flow cytometry according to the manufacturer's protocol. For fluorescence microscopy analysis, the cells were incubated with MitoScreen (10 μM; Merck Millipore) for 15 minutes, fixed with 4% formaldehyde for 10 minutes, and the slides were examined with a fluorescence microscope (DM 2500; Leica Microsystems). For flow cytometry, cells were recovered in FACS buffer and incubated with MitoScreen (10 μM; Merck Millipore) for 15 minutes at 4 °C, washed three times with PBS, resuspended in FACS buffer, and analyzed by flow cytometry using CellQuest Pro software (BD Biosciences).

Caspase 3/7 activity assay. iFECD were seeded at a density of 5.0×10^3 cells/cm^2 per well on a 96-well plate for 24 hours, and were stimulated with TGF-β2 by culturing DMEM supplemented with TGF-β2 (5, 10, and 15 ng/ml) for 24 hours. As a control, iFECD were treated with a pan-caspase inhibitor, Z-VD-FMK (10 μM, Wako Pure Chemical Industries, Ltd.). The activity of caspase 3/7 was determined by the Caspase 3/7 activity assay® Luminescent Assay performed in accordance with the manufacturer's protocol using a Veritas™ Microplate Luminometer (Promega). Four samples were prepared for each group.

Annexin V assessment. Cell apoptosis was evaluated with Annexin V (Medical & Biological Laboratories Co., Ltd.) staining. For fluorescence microscopy analysis, the cells were incubated with DMEM supplemented with Annexin V for 30 minutes, followed by fixation with 4% paraformaldehyde for 10 minutes. The slides were examined with a fluorescence microscope (DM 2500; Leica Microsystems). For flow cytometry, cells were incubated with DMEM supplemented with Annexin V for 15 minutes, and harvested by digestion with Accumax™ (Innovative Cell Technologies). Recovered cells were then analyzed by flow cytometry using CellQuest Pro software (BD Biosciences).

Statistical Analysis. Statistical analysis was performed with the Excel software program (Microsoft Corporation, Redmond, Washington). The statistical significance (*P*-value) in mean values of the two-sample comparison was determined with the Student's t-test or Mann–Whitney U test. The statistical significance for the comparison of multiple sample sets was determined with Dunnett's multiple-comparisons test. A P-value of <0.05 was considered statistically significant. Values shown represent the mean ± standard error of the mean (SEM).

References

1. Lorenzetti, D. W., Uotila, M. H., Parikh, N. & Kaufman, H. E. Central cornea guttata. Incidence in the general population. *Am J Ophthalmol* **64**, 1155–1158 (1967).
2. Eye Bank Association of America. Eye Banking Statistical Report. Washington, DC (2014).
3. Tan, D. T., Dart, J. K., Holland, E. J. & Kinoshita, S. Corneal transplantation. *Lancet* **379**, 1749–1761, doi:10.1016/S0140-6736(12)60437-1 (2012).
4. Patel, S. V. Graft survival and endothelial outcomes in the new era of endothelial keratoplasty. *Exp Eye Res* **95**, 40–47, doi:10.1016/j.exer.2011.05.013 (2012).
5. Borderie, V. M. *et al*. Corneal endothelial cell apoptosis in patients with Fuchs' dystrophy. *Invest Ophthalmol Vis Sci* **41**, 2501–2505 (2000).
6. Engler, C. *et al*. Unfolded protein response in fuchs endothelial corneal dystrophy: a unifying pathogenic pathway? *Am J Ophthalmol* **149**, 194–202 e192, doi:10.1016/j.ajo.2009.09.009 (2010).

7. Hurtley, S. M., Bole, D. G., Hoover-Litty, H., Helenius, A. & Copeland, C. S. Interactions of misfolded influenza virus hemagglutinin with binding protein (BiP). *J Cell Biol* **108**, 2117–2126 (1989).
8. Ellgaard, L. & Helenius, A. Quality control in the endoplasmic reticulum. *Nat Rev Mol Cell Biol* **4**, 181–191, doi:10.1038/nrm1052 (2003).
9. Smith, M. H., Ploegh, H. L. & Weissman, J. S. Road to ruin: targeting proteins for degradation in the endoplasmic reticulum. *Science* **334**, 1086–1090, doi:10.1126/science.1209235 (2011).
10. Walter, P. & Ron, D. The unfolded protein response: from stress pathway to homeostatic regulation. *Science* **334**, 1081–1086, doi:10.1126/science.1209038 (2011).
11. Rainbolt, T. K., Saunders, J. M. & Wiseman, R. L. Stress-responsive regulation of mitochondria through the ER unfolded protein response. *Trends Endocrinol Metab* **25**, 528–537, doi:10.1016/j.tem.2014.06.007 (2014).
12. Lin, J. H. & Lavail, M. M. Misfolded proteins and retinal dystrophies. *Adv Exp Med Biol* **664**, 115–121, doi:10.1007/978-1-4419-1399-9_14 (2010).
13. Halliday, M. & Mallucci, G. R. Targeting the unfolded protein response in neurodegeneration: A new approach to therapy. *Neuropharmacology* **76**(Pt A), 169–174, doi:10.1016/j.neuropharm.2013.08.034 (2014).
14. Halliday, M. & Mallucci, G. R. Review: Modulating the unfolded protein response to prevent neurodegeneration and enhance memory. *Neuropathol Appl Neurobiol* **41**, 414–427, doi:10.1111/nan.12211 (2015).
15. Huang, H. C., Tang, D., Lu, S. Y. & Jiang, Z. F. Endoplasmic reticulum stress as a novel neuronal mediator in Alzheimer's disease. *Neurol Res* **37**, 366–374, doi:10.1179/1743132814Y.0000000448 (2015).
16. Scheper, W. & Hoozemans, J. J. The unfolded protein response in neurodegenerative diseases: a neuropathological perspective. *Acta Neuropathol* **130**, 315–331, doi:10.1007/s00401-015-1462-8 (2015).
17. Jiang, D., Niwa, M. & Koong, A. C. Targeting the IRE1 alpha-XBP1 branch of the unfolded protein response in human diseases. *Semin Cancer Biol* **33**, 48–56, doi:10.1016/j.semcancer.2015.04.010 (2015).
18. Vedana, G., Villarreal, G. Jr. & Jun, A. S. Fuchs endothelial corneal dystrophy: current perspectives. *Clin Ophthalmol* **10**, 321–330, doi:10.2147/OPTH.S83467 (2016).
19. Weller, J. M. *et al*. Extracellular matrix alterations in late-onset Fuchs' corneal dystrophy. *Invest Ophthalmol Vis Sci* **55**, 3700–3708, doi:10.1167/iovs.14-14154 (2014).
20. Okumura, N. *et al*. Involvement of ZEB1 and Snail1 in excessive production of extracellular matrix in Fuchs endothelial corneal dystrophy. *Lab Invest* **95**, 1291–1304, doi:10.1038/labinvest.2015.111 (2015).
21. Bierie, B. & Moses, H. L. Tumour microenvironment: TGFbeta: the molecular Jekyll and Hyde of cancer. *Nat Rev Cancer* **6**, 506–520, doi:10.1038/nrc1926 (2006).
22. Watabe, T. & Miyazono, K. Roles of TGF-beta family signaling in stem cell renewal and differentiation. *Cell Res* **19**, 103–115, doi:10.1038/cr.2008.323 (2009).
23. Wakefield, L. M. & Hill, C. S. Beyond TGFbeta: roles of other TGFbeta superfamily members in cancer. *Nat Rev Cancer* **13**, 328–341, doi:10.1038/nrc3500 (2013).
24. Neuzillet, C. *et al*. Targeting the TGFbeta pathway for cancer therapy. *Pharmacol Ther* **147**, 22–31, doi:10.1016/j.pharmthera.2014.11.001 (2015).
25. Morikawa, M., Derynck, R. & Miyazono, K. TGF-beta and the TGF-beta Family: Context-Dependent Roles in Cell and Tissue Physiology. *Cold Spring Harb Perspect Biol* **8**, doi:10.1101/cshperspect.a021873 (2016).
26. Roberts, A. B. *et al*. Transforming growth factor type beta: rapid induction of fibrosis and angiogenesis *in vivo* and stimulation of collagen formation *in vitro*. *Proc Natl Acad Sci USA* **83**, 4167–4171 (1986).
27. Ignotz, R. A. & Massague, J. Transforming growth factor-beta stimulates the expression of fibronectin and collagen and their incorporation into the extracellular matrix. *J Biol Chem* **261**, 4337–4345 (1986).
28. Zeisberg, M. *et al*. BMP-7 counteracts TGF-beta1-induced epithelial-to-mesenchymal transition and reverses chronic renal injury. *Nat Med* **9**, 964–968, doi:10.1038/nm888nm888 (2003).
29. Zavadil, J. & Bottinger, E. P. TGF-beta and epithelial-to-mesenchymal transitions. *Oncogene* **24**, 5764–5774, doi:10.1038/sj.onc.1208927 (2005).
30. Zeisberg, E. M. *et al*. Endothelial-to-mesenchymal transition contributes to cardiac fibrosis. *Nat Med* **13**, 952–961, doi:10.1038/nm1613 (2007).
31. Jurkunas, U. V. *et al*. Increased clusterin expression in Fuchs' endothelial dystrophy. *Invest Ophthalmol Vis Sci* **49**, 2946–2955, doi:10.1167/iovs.07-1405iovs.07-1405 (2008).
32. Jurkunas, U. V., Bitar, M. & Rawe, I. Colocalization of increased transforming growth factor-beta-induced protein (TGFBIp) and Clusterin in Fuchs endothelial corneal dystrophy. *Invest Ophthalmol Vis Sci* **50**, 1129–1136, doi:10.1167/iovs.08-2525iovs.08-2525 (2009).
33. Meng, X. M., Nikolic-Paterson, D. J. & Lan, H. Y. TGF-beta: the master regulator of fibrosis. *Nat Rev Nephrol* **12**, 325–338, doi:10.1038/nrneph.2016.48 (2016).
34. Cho, M. E., Smith, D. C., Branton, M. H., Penzak, S. R. & Kopp, J. B. Pirfenidone slows renal function decline in patients with focal segmental glomerulosclerosis. *Clin J Am Soc Nephrol* **2**, 906–913, doi:10.2215/CJN.01050207 (2007).
35. Trachtman, H. *et al*. A phase 1, single-dose study of fresolimumab, an anti-TGF-beta antibody, in treatment-resistant primary focal segmental glomerulosclerosis. *Kidney Int* **79**, 1236–1243, doi:10.1038/ki.2011.33 (2011).
36. Sharma, K. *et al*. Pirfenidone for diabetic nephropathy. *J Am Soc Nephrol* **22**, 1144–1151, doi:10.1681/ASN.2010101049 (2011).
37. Okumura, N. *et al*. Laminin-511 and -521 enable efficient *in vitro* expansion of human corneal endothelial cells. *Invest Ophthalmol Vis Sci* **56**, 2933–2942, doi:10.1167/iovs.14-15163 (2015).
38. Okumura, N. *et al*. Density-gradient centrifugation enables the purification of cultured corneal endothelial cells for cell therapy by eliminating senescent cells. *Sci Rep* **5**, 15005, doi:10.1038/srep15005 (2015).

Acknowledgements

This study was supported by the Program for the Strategic Research Foundation at Private Universities from MEXT (Koizumi, N. and Okumura, N.).

Author Contributions

N.O., S.K. and N.K. conceived and designed the study. K.H., M.K., H.O., E.U., K.W., M.N., T.S., T.T., U.S.S., and F.K. performed the experiments. N.O. drafted the article, and all authors revised the article and approved the final version to be published.

Additional Information

Supplementary information accompanies this paper at doi:10.1038/s41598-017-06924-3

Competing Interests: Noriko Koizumi, Naoki Okumura, and Shigeru Kinoshita are listed as inventors of the patent regarding the application of TGF-β signal inhibition for Fuchs endothelial corneal dystrophy.

Hindawi
Journal of Ophthalmology
Volume 2017, Article ID 9281745, 2 pages
https://doi.org/10.1155/2017/9281745

Editorial

Rho Kinase in Eye Disease

Naoki Okumura,[1] Shintaro Nakao,[2] Toshihiro Inoue,[3] and Padmanabhan Pattabiraman[4]

[1]*Department of Biomedical Engineering, Faculty of Life and Medical Sciences, Doshisha University, Kyotanabe, Japan*
[2]*Department of Ophthalmology, Graduate School of Medical Sciences, Kyushu University, Fukuoka, Japan*
[3]*Department of Ophthalmology, Kumamoto University, Kumamoto, Japan*
[4]*Department of Ophthalmology, Case Western Reserve University, Cleveland, OH, USA*

Correspondence should be addressed to Naoki Okumura; nokumura@mail.doshisha.ac.jp

Received 18 July 2017; Accepted 18 July 2017; Published 27 August 2017

Rho-associated protein kinase (ROCK) is a well-characterized effector of Rho GTPase, a small GTP-binding protein. The Rho/ROCK signaling pathways contribute to a wide range of fundamental cellular events, such as cell adhesion, motility, proliferation, differentiation, and apoptosis. The role of ROCK in the control of a wide spectrum of biological events has made it a subject of intensive investigation as an important therapeutic target in a wide range of diseases, including vascular disease, cancer, neuronal degenerative disease, asthma, and glaucoma.

The ROCK inhibitor, fasudil, was approved in 1995 for the prevention of cerebral vasospasm in patients with subarachnoid hemorrhage. In 2014, another ROCK inhibitor, ripasudil, was approved in Japan for the treatment of glaucoma and ocular hypertension. More importantly, the research supporting the involvement of ROCK signaling in glaucoma has now extended to other eye diseases, such as corneal endothelial disease, cataract, age-related macular degeneration, and proliferative vitreous retinopathy.

This special issue focuses on the involvement of ROCK signaling in the pathobiology of eye-related diseases and the possible applications of ROCK inhibitors as drugs for treating these disorders.

Numerous researchers have devoted their efforts toward the development of ROCK inhibitors that can target glaucoma. ROCK inhibitors alter the distribution of actin stress fibers and modulate the cell-matrix interactions of cultured trabecular meshwork and Schlemm's canal cells. In addition, topical administration of ROCK inhibitor eye drops reduces the intraocular pressure (IOP) in rabbit and monkey models by increasing the outflow capacity. Several ROCK inhibitors also reduced IOP in healthy human volunteers, as well as in patients with glaucoma and ocular hypertension in clinical studies. As mentioned above, ripasudil was approved in Japan as a first-in-class ROCK inhibitor ophthalmic agent for the treatment of glaucoma and ocular hypertension. Y. Kaneko et al. showed that a specific ROCK inhibitor, ripasudil hydrochloride hydrate, had an additional IOP-lowering effect in rabbit or monkey models when used in combined regimens that included β-blockers, $\alpha\beta$-blockers, α2-agonists, carbonic anhydrase inhibitors, and prostaglandin analogs. Their study indicated that ripasudil has a particular efficacy when used in combination with conventional eye drops. Ripasudil is a first-in-class ROCK inhibitor eye drop, so further basic and clinical data regarding its safety and effectiveness will be beneficial, especially for clinicians.

The use of ROCK inhibitors has been proposed for the treatment of corneal endothelial decompensation. N. Okumura et al. reviewed the usefulness of ROCK inhibitors both as eye drops and as adjunct drugs in cell-based therapies. They showed that ROCK inhibitors, supplied in the form of eye drops, promoted cell proliferation in animal models, and pilot clinical research suggests the occurrence of a similar response in humans as well. They have predicted the future use of topically applied ROCK inhibitors for the treatment of (1) Fuchs endothelial corneal dystrophy, combined with central corneal endothelial removal, and (2) acute corneal endothelial damage induced by cataract surgery. Along these

lines, A. Akhbanbetova et al. designed a cryoprobe for corneal endothelial removal prior to ROCK inhibitor administration as part of a treatment for Fuchs endothelial corneal dystrophy. They demonstrated that their cryoprobe destroys the corneal endothelium in a consistent manner, without altering the collagen fibril structure of the corneal stroma. N. Okumura et al. have also reviewed the accumulating evidence supporting the usefulness of ROCK inhibitors as adjunct drugs in a cell-based therapy. The first-in-man clinical trial of the cell-based therapy combined with a ROCK inhibitor as an adjunct drug for the treatment of corneal endothelial dysfunction was initiated in Japan in 2013. Future clinical assessments are necessary, but the potential for ROCK inhibitors to target the corneal endothelium is very promising.

ROCK inhibitors have also been researched as potent pharmaceutical agents for targeting retinal diseases, such as wet age-related macular degeneration, diabetic retinopathy, diabetic macular edema, and proliferative vitreoretinopathy. In addition to the preclinical data obtained using animal models, several clinical studies have now demonstrated a positive effect of ROCK inhibitors on retinal diseases. M. Yamaguchi et al. reviewed the recent progress on the mechanisms of ROCK signaling in vitreoretinal diseases and the potency of their clinical application. Vitreoretinal diseases are strongly modulated by vascular endothelial growth factor (VEGF), so intravitreous injection of anti-VEGF agents has been extensively used in the clinical setting. M. Yamaguchi et al. have reviewed the potent effects of ROCK inhibitor administration on each biological process involved in eye disease and have carefully compared ROCK inhibitor effects with those of anti-VEGF agents.

J. S. Moon et al. demonstrated in a rabbit model that intraoperative subconjunctival injection of ROCK inhibitor suppressed the inflammation and fibrosis that typically occur after extraocular muscle surgery. ROCK inhibitors are known to trigger an antifibrotic effect in several cell types in the eye, such as Tenon fibroblasts, the trabecular meshwork, retinal pigment epithelial cells, hyalocytes, and corneal stroma cells. Human clinical trials have not yet recapitulated this antifibrotic effect of ROCK inhibitors, but this phenomenon is worth further investigation.

Thus, growing evidence supports the usefulness of ROCK inhibitors as promising therapeutic modalities for the treatment of various ophthalmological disorders. We expect that this special issue will provide a cross-sectional platform for readers to discover the importance and possible future applications of ROCK inhibitors in the treatment of eye diseases.

Naoki Okumura
Shintaro Nakao
Toshihiro Inoue
Padmanabhan Pattabiraman

Send Orders for Reprints to reprints@benthamscience.ae

BENTHAM OPEN

CrossMark

The Open Ophthalmology Journal

Content list available at: www.benthamopen.com/TOOPHTJ/

DOI: 10.2174/1874364101812010154

REVIEW ARTICLE

Perspective of Future Potent Therapies for Fuchs Endothelial Corneal Dystrophy

Naoki Okumura, Ryousuke Hayashi and Noriko Koizumi*

Department of Biomedical Engineering, Faculty of Life and Medical Sciences, Doshisha University, Kyotanabe, Japan

Received: September 12, 2017 Revised: December 16, 2018 Accepted: January 30, 2018

Abstract:

Background:

Fuchs Endothelial Corneal Dystrophy (FECD) is a progressive disease that affects the corneal endothelium in both eyes. Recent studies have identified a novel genetic basis for FECD, and basic research findings have provided evidence for its underlying pathophysiology. Since its first description by Ernst Fuchs in 1910, the only therapeutic choice has been corneal transplantation using donor corneas. However, accumulating evidence suggests that a change in this "rule" may be imminent.

Conclusions:

This article reviews the current knowledge of the genetics and pathophysiology of FECD, and it introduces some potent therapeutic modalities that show promise as new treatments for this disorder.

Keywords: FECD, ECM, Endothelial Corneal Dystrophy, TCF4, SNP, ICD3.

1. INTRODUCTION

Fuchs Endothelial Corneal Dystrophy (FECD) is a progressive disease that affects the corneal endothelium in both eyes. The hallmarks of FECD in the clinical setting are the formation of excrescences, called guttae, on Descemet's membrane and the loss of corneal endothelial cells. FECD shows a gender dichotomy, with a female to male ratio of 2.5:1 to 3:1. FECD typically occurs at the age of 40–50, and it progresses to an advanced stage in some, but not all, patients. In the advanced stage, decompensation of the corneal epithelium disrupts the water balance in the corneal stroma, which induces edema of the corneal stroma and epithelium and causes severe vision loss [1]. Even in patients without corneal edema, the formation of guttae and the thickening of the Descemet's membrane due to accumulation of Extracellular Matrix (ECM) components results in forward light scatter and a loss of vision quality [2, 3].

Recent studies have indicated an association between a novel genetic pattern and the development of FECD. In addition, basic research studies are now beginning to reveal the underlying pathophysiology of this disease. Despite these advances in understanding the nature of FECD, the only therapeutic choice for its treatment remains corneal transplantation using donor corneas-the original treatment used when Ernst Fuchs first described this disease in 1910 [1]. However, accumulating evidence now indicates that important changes are imminent regarding the treatment of FECD. This article provides a review of the current knowledge of the genetics and pathophysiology of FECD, and it introduces some potent therapeutic modalities that show promise as new treatments for FECD.

2. METHODS

Literature searches were performed in PubMed (https:// www.ncbi.nlm.nih.gov/ pubmed) and ClinicalTrials.gov

* Address correspondence to this author at the Department of Biomedical Engineering, Faculty of Life and Medical Sciences, Doshisha University, 1-3 Tatara Miyokodani, Kyotanabe Kyoto, Japan, Tel: +81-774-65-6125; E-mail: nkoizumi@mail.doshisha.ac.jp

(https://clinicaltrials.gov/). Key search terms were the references cited in each eligible article that included "Fuchs endothelial corneal dystrophy," "TCF4," "single nucleotide polymorphism, SNPs, or polymorphism." This review is not a meta-analysis; therefore, we selected literature that allowed us to introduce future perspectives as well as to summarize the current status of this research topic.

3. GENETICS

Studies of familial FECD cases show that the disease has an autosomal dominant inheritance pattern [4]. However, a certain proportion of patients with FECD have sporadic disease, without a familial history. The ICD3 classification categorizes FECD patients as those with: 1) early-onset FECD, 2) identified genetic loci, and 3) disease without known inheritance [5].

Early-onset FECD is a rare form, and these patients exhibit corneal edema by the age of 30–40. Genetic screening of a family with early-onset FECD identified a missense mutation of the *COL8A2* gene that resulted in substitution of a lysine for a glutamine (Q455K) on chromosome 1 p34.3-p32. Analysis of large families with a common form of late-onset FECD also showed a significant linkage between the *FCD1*, *FCD2*, *FCD3*, and *FCD4* loci on chromosomes 13, 18, 5, and 9, respectively [6 - 9]. Four genes (*SLCA411*, *TCF8*, *LOXHD1*, and *AGBL1*) were reported as causal genetic mutations, although these genetic mutations were rarely identified in patients with FECD [9 - 14].

Researchers have since devoted their efforts to identify a genetic cause for the large proportion of patients with FECD. For example, a Genome-Wide Association Study (GWAS), conducted by Baratz and colleagues in 2010, identified a significant association between late-onset FECD and the intronic Single Nucleotide Polymorphism (SNPs) rs613872 in Transcription Factor 4 (*TCF4*) [15]. Similarly, replication studies have shown a strong association between rs613872 and FECD, mainly in Caucasian cohorts [16, 17]. Other SNPs in *TCF4,* apart from rs613872, were associated with FECD in populations from Singapore, Southern China, and India, suggesting the occurrence of ethnic variations in the SNPs in *TCF4* [18 - 20].

In 2012, Wieben and colleagues reported the discovery of an expanded CTG trinucleotide repeat in intron 3 of *TCF4* in patients with FECD [21]. Their investigation of 66 FECD cases and 63 unaffected controls demonstrated a sensitivity and specificity of 79% and 96%, respectively, for more than 50 repeats identifying FECD; this specificity was higher than that previously reported for the rs613872 SNP. The percentages of patients with FECD that harbored the CTG trinucleotide repeat expansion varied with their ethnicities; however, this strong association was replicated in multiple ethnic groups (Table **1**) [20, 22 - 27].

Table 1. Summary of previous reports of CTG trinucleotide repeat expansion in TCF4.

-	Wieben ED [21]	Mootha VV [22]	Xing C [23]	Nanda GG [20]	Vasanth S [24]	Nakano M [25]	Foja S [26]	Kuot A [27]
Population	Caucasian	Caucasian	Chinese	Indian	-	Japanese	German	Australian
Cases (FECD)	66	120	57	44	574	47	61	189
Controls	63	100	121	108	354	96	113	183
CTG≥40 or 50 (FECD)	79% (CTG≥50)	73% (CTG≥40)	44% (CTG≥40)	34% (CTG≥50)	62% (CTG≥40)	26% (CTG≥50)	77% (CTG>50)	51% (CTG≥40)
CTG≥40 or 50 (Control)	3% (CTG≥50)	7% (CTG≥40)	2% (CTG≥40)	5% (CTG≥50)	4% (CTG≥40)	0% (CTG≥50)	12% (CTG>50)	5% (CTG≥40)

4. PATHOPHISIOLOGY

4.1. The Unfolded Protein Response

Under normal conditions, proteins undergo folding in the lumen of the Endoplasmic Reticulum (ER), and correctly folded proteins are then packaged into ER exit vesicles for delivery to membranes for extracellular secretion. By contrast, improperly folded proteins are removed in the proteasome through the process known as ER-Associated Degradation (ERAD) [28 - 30]. However, impairment of homeostasis induces ER stress, which disrupts ERAD and triggers apoptosis to remove rogue cells that accumulate unfolded proteins [31, 32]. This highly regulated process is called the Unfolded Protein Response (UPR), and the UPR is involved in the pathogenesis of various diseases, including Alzheimer's disease, Parkinson's disease, diabetes mellitus, multiple myeloma, and retinitis pigmentosa [33 - 38].

In 2010, Engler and colleagues postulated that activation of the UPR plays a central role in the pathogenesis of FECD through the induction of apoptosis in corneal endothelial cells [39]. They showed an increased and dilated ER structure and upregulation of the markers of the UPR in the corneal endothelium of patients with FECD [39]. The same research group subsequently showed that homozygous knock-in of *Col8a2*$^{Q455K/Q455K}$, a causal gene for early-onset FECD, was sufficient to induce FECD-like ocular features in mice, and these changes were linked with UPR-associated apoptosis [40]. Recently, our group showed that ECM components, such as type I collagen and fibronectin, form aggregates of unfolded proteins in the corneal endothelium of FECD patients [41]. We also showed that activation of transforming growth factor-β (TGF-β) signaling causes a chronic overload of ECM proteins within the ER, which induces an accumulation of unfolded protein and activation of the intrinsic apoptotic pathway through the UPR [42]. The genetic background underlying the UPR induction is not yet elucidated; however, accumulating evidence supports a role for the UPR and associated apoptosis in FECD.

4.2. Oxidative Stress and Mitochondrial Dysfunction

Much research has confirmed an involvement of oxidative stress in the pathogenesis of FECD, and a linkage between mitochondrial dysfunction and the generation of oxidative stress is suggested [43 - 47]. For instance, an early study indicated that the numbers of mitochondria were decreased in parallel with downregulation of cytochrome oxidase [48]. Serial analysis of gene expression revealed that expression of mitochondrial antioxidant genes was diminished in the corneal endothelium of patients with FECD [49]. Jurkunas and colleagues demonstrated that an oxidant-antioxidant imbalance leads to oxidative DNA damage and apoptosis [44]. Very recently, Benischke and colleagues reported that constitutive activation of mitophagy causes a reduction in mitochondrial mass and depletion of the numbers of functional mitochondria [50]. Accumulating evidence suggests that oxidative stress, induced by mitochondrial dysfunction, damages corneal endothelial cells. Interestingly, ER stress activates the intrinsic apoptotic pathway (the mitochondrial pathway) in the corneal endothelium, as it does in other cell types [41]. Future studies will likely elucidate the nature of the involvement of both ER stress and oxidative stress in the pathogenesis of FECD.

4.3. RNA Foci

In 2015, Du and colleagues reported that the corneal endothelial cells of patients with FECD harbor poly$(CUG)_n$RNA, and this results in the formation of RNA foci. They also suggested that RNA toxicity and missplicing play an important role in the pathogenesis of FECD, similar to that played in myotonic dystrophy type 1, a trinucleotide repeat expansion disease [51]. Mootha and colleagues also identified RNA foci in the corneal endothelium of subjects with FECD who showed trinucleotide repeat expansion in TCF4, but these foci were absent from the corneal endothelium of subjects with FECD but without this trinucleotide repeat expansion [52].

5. FUTURE TREATMENTS

5.1. Current Therapy

Corneal transplantation using donor corneas is currently the only therapy for treating corneal endothelial decompensation diseases, including FECD. Penetrating keratoplasty, in which a full-thickness patient cornea is replaced with full-thickness donor cornea, has been performed since 1906. New surgical procedures, such as Descemet's Stripping Endothelial Keratoplasty (DSEK) and Descemet's Membrane Endothelial Keratoplasty (DMEK), selectively replace the diseased corneal endothelial layer with a lamellar donor graft that includes the corneal endothelium. These lamellar surgeries have advantages over penetrating keratoplasty, and their use has therefore spread explosively [53].

5.2. Tissue Engineering Therapy

The evolution of corneal transplantation procedures now enables less invasive treatment with better clinical outcomes, but problems remain. The most serious are the shortage of donor corneas, the difficulty of the surgical procedure, and the incidence of graft failure in acute and chronic phases. These issues have motivated researchers to devise tissue engineering treatments that can overcome the current transplantation limitations [53, 54].

Two strategies adopt the use of transplanted cultured corneal endothelial cells as regenerative medicine: 1) transplantation of a cultured corneal endothelial sheet by a procedure resembling DSEK or DMEK and 2) direct injection of cultured corneal endothelial cells, without a carrier, into the anterior chamber [55]. The sheets used in transplantation are produced by culturing corneal endothelial cells on a number of different substrates, such as collagen, amniotic membrane, and human corneal stroma, and animal experiments have confirmed that the transplantation of the

resulting sheet enables the regeneration of a transparent cornea [56 - 59]. However, to the best of our knowledge, the transplantation of cultivated corneal endothelial sheets has not yet been introduced into the clinical setting.

Some research groups, including ours, have attempted to regenerate corneal endothelium directly by injecting cultured corneal endothelial cells into the anterior chamber without a carrier [60 - 62]. However, animal experiments have revealed that an insufficient number of the injected cells adhere to the back side of the cornea, so that a corneal endothelium fails to regenerate in vivo. Our previous research indicated that cell adhesion is inhibited by the activation of Rho/ROCK signaling, and conversely, inhibition of this signaling pathway by a Rho kinase (ROCK) inhibitor enhances cell adhesion. Therefore, we applied a ROCK inhibitor to promote engraftment [63, 64]. We confirmed, using rabbit and monkey corneal endothelial dysfunction models, that coinjection of cultured corneal endothelial cells and a ROCK inhibitor into anterior chamber resulted in the regeneration of the corneal endothelium [64, 65].

In 2013, after obtaining the approval from the Japanese Ministry of Health, Labour, and Welfare, we initiated a clinical trial (Clinical trial registration: UMIN000012534) at the Kyoto Prefectural University of Medicine to evaluate this cell injection therapy as a treatment for corneal endothelial dysfunction [66]. Our preliminary clinical data have confirmed that coinjection of cultured corneal endothelial cells and a ROCK inhibitor regenerates the corneal endothelium and restores a transparent cornea in human subjects. Further clinical data are necessary, but cell-based therapy appears to be a potent future treatment for corneal endothelial decompensation diseases, including FECD.

5.3. ROCK Inhibitor Eye Drops

Rho is a small GTPase, and RhoA activates ROCK, a serine/threonine kinase that phosphorylates various substrates. ROCK signaling plays an essential role in several fundamental cellular events, such as cell adhesion, motility, proliferation, differentiation, and apoptosis [67 - 69]. In 2009, we reported that inhibition of ROCK signaling promotes the *in vitro* proliferation of corneal endothelial cells [63]. Subsequently, we found that administration of a ROCK inhibitor in eye drop form promotes wound healing in the corneal endothelium in rabbit and monkey models [70 - 72].

We have since conducted pilot clinical research to investigate the use of topically applied ROCK inhibitor eye drops in patients who have undergone central corneal endothelium removal by transcorneal freezing. Our findings suggested that the eye drop form of ROCK inhibitor is a potent therapeutic treatment choice for patients with early-stage FECD [71, 73]. Notably, one 52-year-old male patient diagnosed with late-onset FECD recovered full corneal transparency after transcorneal freezing and the use of ROCK inhibitor eye drops. His central corneal thickness was reduced from 703 μm to 568 μm and his visual acuity improved from 20/63 to 20/20. His corneal transparency was maintained for more than 6 years, and the original plans for an eventual corneal transplantation were canceled [73].

Recent investigations have examined the effect of surgical removal of the central Descemet's membrane, including pathological corneal endothelium [74 - 76], and one clinical study has indicated a positive effect of combining ROCK inhibitor eye drops with this procedure [77]. However, clinical data for the usefulness of ROCK inhibitors in FECD treatment remain limited, so randomized clinical trials are still needed before adoption of this eye drop as a routine therapeutic option.

5.4. Potent Pharmaceutical Agents

Stealth BioTherapeutics (Newton, MA) has been developing drug candidates for targeting diseases associated with mitochondrial dysfunction. They initiated a phase 2 clinical trial of elamipretide in eye drop form, with the expectation that this drug would target the inner mitochondrial membrane to help preserve mitochondrial energetics (http://www.stealthbt.com/). The results of this clinical trial have not yet been released, but elamipretide is currently the most advanced-stage pharmaceutical aimed at the treatment of FECD.

Kim and colleagues reported that N-Acetylcysteine (NAC), a thiol-containing antioxidant and radical scavenger, rescued cultured corneal endothelial cells from damage mediated by ER and oxidative stress [78]. They also demonstrated that systemic use of NAC suppressed the progression of FECD in early-onset FECD model mice ($Col8a2^{Q455K/Q455K}$), thereby providing an in vivo proof of concept of the use of NAC as a potent therapeutic candidate for treatment of FECD [78]. The same research group also showed that the addition of lithium further increased the survival of cultured corneal endothelial cells when ER and oxidative stresses were triggered [79]. A higher corneal endothelial cell density was also maintained in early-onset FECD model mice given a lithium treatment than in a non-treatment group [79]. The researchers suggested that lithium increases the survival of corneal endothelial cells by an upregulation of autophagy; therefore, lithium may represent a new therapeutic agent for the treatment of FECD [79].

More recently, the same group attempted a drug screening based on the postulated FECD pathophysiology involving ER and oxidative stresses and cell death [80]. They induced ER stress with thapsigargin and oxidative stress with hydrogen peroxide in cultured corneal endothelial cells, and then screened 640 compounds found in the Food and Drug Administration (FDA)-approved drug library. They reported that oxotremorine and mefenamic acid were potential survival factors that overcame stress-related cell death.

Our group has reported that activation of TGF-β signaling activates genes that induce the epithelial-mesenchymal transition (EMT). These include *ZEB1* and *SNAI1,* and their induction results in the accumulation of ECM components [81]. This production of ECM components was more strongly upregulated in cell models established from patients with FECD than in control corneal endothelial cells, following exposure of the cells to TGF-β. We recently reported high expression levels of TGF-β isoforms and TGF-β receptors in the corneal endothelium of patients with FECD, and we proposed that activation of TGF-β signaling induces a chronic overload of ECM components, resulting in apoptosis through the UPR [42]. We also showed that inhibition of TGF-β signaling suppressed this accumulation of ECM components and suppressed UPR-mediated apoptosis in cell models established from patients with FECD. These findings suggest that inhibition of TGF-β might be a potent therapeutic option [42]. A summary of the proposed drug candidates for treating FECD is shown in Table **2**.

Table 2. Proposed drug candidates for treating FECD.

Candidate Drugs	Status	Proposed Mechanism	Author or Company
Elamipretide	Phase 2 clinical study	Preserves mitochondrial energetics	Stealth BioTherapeutics
Rho kinase inhibitor	Pilot clinical research	Promotes cell proliferation	Okumura N, Koizumi N [71, 73]
N-acetylcysteine	Animal model	Increases cell survival	Kim EC [78]
Lithium	Animal model	Increases cell survival	Kim EC [79]
Oxotremorine	*in vitro*	Increases cell survival	Kim EC [80]
Mefenamic acid	*in vitro*	Increases cell survival	Kim EC [80]
TGF-β inhibitor	*in vitro*	Suppresses unfolded protein mediated cell death	Okumura N [42]

CONCLUSION

Corneal transplantation has been the only therapy available for treating FECD for many years. However, recent advancements in tissue engineering techniques may now provide innovative cell-based therapies. “Missing links” still necessitate further investigations, but new information regarding the genetic background and pathophysiology of FECD is rapidly accumulating. Importantly, the recent findings improve the understanding of FECD, but they also guide further investigations aimed at identifying future therapeutic modalities. Indeed, several drug candidates have recently been reported, although none of these drugs has yet been introduced into the market. Corneal transplantations using donor corneas continue to remain the standard treatment, but we believe that the new therapeutic options, such as cell-based therapy and the use of pharmaceutical agents, will provide less invasive and more effective therapies.

CONSENT FOR PUBLICATION

Not applicable.

CONFLICT OF INTEREST

Noriko Koizumi is listed as the inventor of the patent regarding the application of the ROCK inhibitor for corneal endothelium regeneration (registration number: 5657252). Noriko Koizumi and Naoki Okumura are listed as inventors of the patent regarding the application of TGF-β signal inhibition for treatment of Fuchs endothelial corneal dystrophy.

ACKNOWLEDGEMENT

This study was supported by the Program for the Strategic Research Foundation at Private Universities from MEXT (Koizumi, N. and Okumura, N.), JSPS KAKENHI Grant Numbers JP16K11307 (Koizumi, N) and JP 15K10885 (Okumura, N.).

REFERENCES

[1] Weisenthal R, Streeten B. Descemet's Membrane and Endothelial Dystrophies. Cornea 3rd edition. 2011;1:845-64.

[2] Wacker K, McLaren JW, Amin SR, Baratz KH, Patel SV. Corneal high-order aberrations and backscatter in fuchs' endothelial corneal dystrophy. Ophthalmology 2015; 122(8): 1645-52.
[http://dx.doi.org/10.1016/j.ophtha.2015.05.005] [PMID: 26050543]

[3] Watanabe S, Oie Y, Fujimoto H, *et al.* Relationship between corneal guttae and quality of vision in patients with mild fuchs' endothelial corneal dystrophy. Ophthalmology 2015; 122(10): 2103-9.
[http://dx.doi.org/10.1016/j.ophtha.2015.06.019] [PMID: 26189189]

[4] Eghrari AO, Riazuddin SA, Gottsch JD. Fuchs corneal dystrophy. Prog Mol Biol Transl Sci 2015; 134: 79-97.
[http://dx.doi.org/10.1016/bs.pmbts.2015.04.005] [PMID: 26310151]

[5] Weiss JS, Moller HU, Aldave AJ, *et al.* IC3D classification of corneal dystrophies-edition 2. Cornea. 2015; 34: pp. (2)117-59.

[6] Sundin OH, Jun AS, Broman KW, *et al.* Linkage of late-onset Fuchs corneal dystrophy to a novel locus at 13pTel-13q12.13. Invest Ophthalmol Vis Sci 2006; 47(1): 140-5.
[http://dx.doi.org/10.1167/iovs.05-0578] [PMID: 16384955]

[7] Sundin OH, Broman KW, Chang HH, Vito EC, Stark WJ, Gottsch JD. A common locus for late-onset Fuchs corneal dystrophy maps to 18q21.2-q21.32. Invest Ophthalmol Vis Sci 2006; 47(9): 3919-26.
[http://dx.doi.org/10.1167/iovs.05-1619] [PMID: 16936105]

[8] Riazuddin SA, Eghrari AO, Al-Saif A, *et al.* Linkage of a mild late-onset phenotype of Fuchs corneal dystrophy to a novel locus at 5q33.1-q35.2. Invest Ophthalmol Vis Sci 2009; 50(12): 5667-71.
[http://dx.doi.org/10.1167/iovs.09-3764] [PMID: 19608540]

[9] Riazuddin SA, Zaghloul NA, Al-Saif A, *et al.* Missense mutations in TCF8 cause late-onset Fuchs corneal dystrophy and interact with FCD4 on chromosome 9p. Am J Hum Genet 2010; 86(1): 45-53.
[http://dx.doi.org/10.1016/j.ajhg.2009.12.001] [PMID: 20036349]

[10] Vithana EN, Morgan PE, Ramprasad V, *et al.* SLC4A11 mutations in Fuchs endothelial corneal dystrophy. Hum Mol Genet 2008; 17(5): 656-66.
[http://dx.doi.org/10.1093/hmg/ddm337] [PMID: 18024964]

[11] Riazuddin SA, Vithana EN, Seet LF, *et al.* Missense mutations in the sodium borate cotransporter SLC4A11 cause late-onset Fuchs corneal dystrophy. Hum Mutat 2010; 31(11): 1261-8.
[http://dx.doi.org/10.1002/humu.21356] [PMID: 20848555]

[12] Mehta JS, Vithana EN, Tan DT, *et al.* Analysis of the posterior polymorphous corneal dystrophy 3 gene, TCF8, in late-onset Fuchs endothelial corneal dystrophy. Invest Ophthalmol Vis Sci 2008; 49(1): 184-8.
[http://dx.doi.org/10.1167/iovs.07-0847] [PMID: 18172091]

[13] Riazuddin SA, Parker DS, McGlumphy EJ, *et al.* Mutations in LOXHD1, a recessive-deafness locus, cause dominant late-onset Fuchs corneal dystrophy. Am J Hum Genet 2012; 90(3): 533-9.
[http://dx.doi.org/10.1016/j.ajhg.2012.01.013] [PMID: 22341973]

[14] Riazuddin SA, Vasanth S, Katsanis N, Gottsch JD. Mutations in AGBL1 cause dominant late-onset Fuchs corneal dystrophy and alter protein-protein interaction with TCF4. Am J Hum Genet 2013; 93(4): 758-64.
[http://dx.doi.org/10.1016/j.ajhg.2013.08.010] [PMID: 24094747]

[15] Baratz KH, Tosakulwong N, Ryu E, *et al.* E2-2 protein and Fuchs's corneal dystrophy. N Engl J Med 2010; 363(11): 1016-24.
[http://dx.doi.org/10.1056/NEJMoa1007064] [PMID: 20825314]

[16] Li YJ, Minear MA, Rimmler J, *et al.* Replication of TCF4 through association and linkage studies in late-onset Fuchs endothelial corneal dystrophy. PLoS One 2011; 6(4): e18044.
[http://dx.doi.org/10.1371/journal.pone.0018044] [PMID: 21533127]

[17] Ołdak M, Ruszkowska E, Udziela M, *et al.* Fuchs endothelial corneal dystrophy: Strong association with rs613872 not paralleled by changes in corneal endothelial TCF4 mRNA level. BioMed Res Int 2015; 2015: 640234.
[http://dx.doi.org/10.1155/2015/640234] [PMID: 26451375]

[18] Thalamuthu A, Khor CC, Venkataraman D, *et al.* Association of TCF4 gene polymorphisms with Fuchs' corneal dystrophy in the Chinese. Invest Ophthalmol Vis Sci 2011; 52(8): 5573-8.
[http://dx.doi.org/10.1167/iovs.11-7568] [PMID: 21659310]

[19] Wang KJ, Jhanji V, Chen J, *et al.* Association of transcription factor 4 (TCF4) and Protein Tyrosine Phosphatase, Receptor type G (PTPRG) with corneal dystrophies in southern Chinese. Ophthalmic Genet 2014; 35(3): 138-41.
[http://dx.doi.org/10.3109/13816810.2013.804098] [PMID: 23758498]

[20] Nanda GG, Padhy B, Samal S, Das S, Alone DP. Genetic association of TCF4 intronic polymorphisms, CTG18.1 and rs17089887, with Fuchs' endothelial corneal dystrophy in an Indian population. Invest Ophthalmol Vis Sci 2014; 55(11): 7674-80.
[http://dx.doi.org/10.1167/iovs.14-15297] [PMID: 25342617]

[21] Wieben ED, Aleff RA, Tosakulwong N, *et al.* A common trinucleotide repeat expansion within the transcription factor 4 (TCF4, E2-2) gene

predicts Fuchs corneal dystrophy. PLoS One 2012; 7(11): e49083.
[http://dx.doi.org/10.1371/journal.pone.0049083] [PMID: 23185296]

[22] Mootha VV, Gong X, Ku HC, Xing C. Association and familial segregation of CTG18.1 trinucleotide repeat expansion of TCF4 gene in Fuchs' endothelial corneal dystrophy. Invest Ophthalmol Vis Sci 2014; 55(1): 33-42.
[http://dx.doi.org/10.1167/iovs.13-12611] [PMID: 24255041]

[23] Xing C, Gong X, Hussain I, *et al.* Transethnic replication of association of CTG18.1 repeat expansion of TCF4 gene with Fuchs' corneal dystrophy in Chinese implies common causal variant. Invest Ophthalmol Vis Sci 2014; 55(11): 7073-8.
[http://dx.doi.org/10.1167/iovs.14-15390] [PMID: 25298419]

[24] Vasanth S, Eghrari AO, Gapsis BC, *et al.* Expansion of CTG18.1 trinucleotide repeat in TCF4 is a potent driver of fuchs' corneal dystrophy. Invest Ophthalmol Vis Sci 2015; 56(8): 4531-6.
[http://dx.doi.org/10.1167/iovs.14-16122] [PMID: 26200491]

[25] Nakano M, Okumura N, Nakagawa H, *et al.* Trinucleotide repeat expansion in the TCF4 gene in fuchs' endothelial corneal dystrophy in japanese. Invest Ophthalmol Vis Sci 2015; 56(8): 4865-9.
[http://dx.doi.org/10.1167/iovs.15-17082] [PMID: 26218914]

[26] Foja S, Luther M, Hoffmann K, Rupprecht A, Gruenauer-Kloevekorn C. CTG18.1 repeat expansion may reduce TCF4 gene expression in corneal endothelial cells of German patients with Fuchs' dystrophy. Graefes Arch Clin Exp Ophthalmol 2017; 255(8): 1621-31.
[http://dx.doi.org/10.1007/s00417-017-3697-7] [PMID: 28608272]

[27] Kuot A, Hewitt AW, Snibson GR, *et al.* TGC repeat expansion in the TCF4 gene increases the risk of Fuchs' endothelial corneal dystrophy in Australian cases. PLoS One 2017; 12(8): e0183719.
[http://dx.doi.org/10.1371/journal.pone.0183719] [PMID: 28832669]

[28] Hurtley SM, Bole DG, Hoover-Litty H, Helenius A, Copeland CS. Interactions of misfolded influenza virus hemagglutinin with Binding Protein (BiP). J Cell Biol 1989; 108(6): 2117-26.
[http://dx.doi.org/10.1083/jcb.108.6.2117] [PMID: 2738090]

[29] Ellgaard L, Helenius A. Quality control in the endoplasmic reticulum. Nat Rev Mol Cell Biol 2003; 4(3): 181-91.
[http://dx.doi.org/10.1038/nrm1052] [PMID: 12612637]

[30] Smith MH, Ploegh HL, Weissman JS. Road to ruin: Targeting proteins for degradation in the endoplasmic reticulum. Science 2011; 334(6059): 1086-90.
[http://dx.doi.org/10.1126/science.1209235] [PMID: 22116878]

[31] Walter P, Ron D. The unfolded protein response: From stress pathway to homeostatic regulation. Science 2011; 334(6059): 1081-6.
[http://dx.doi.org/10.1126/science.1209038] [PMID: 22116877]

[32] Rainbolt TK, Saunders JM, Wiseman RL. Stress-responsive regulation of mitochondria through the ER unfolded protein response. Trends Endocrinol Metab 2014; 25(10): 528-37.
[http://dx.doi.org/10.1016/j.tem.2014.06.007] [PMID: 25048297]

[33] Lin JH, Lavail MM. Misfolded proteins and retinal dystrophies. Adv Exp Med Biol 2010; 664: 115-21.
[http://dx.doi.org/10.1007/978-1-4419-1399-9_14] [PMID: 20238009]

[34] Halliday M, Mallucci GR. Targeting the unfolded protein response in neurodegeneration: A new approach to therapy. Neuropharmacology. 2014;76 Pt A:169-74.
[http://dx.doi.org/10.1016/j.neuropharm.2013.08.034]

[35] Halliday M, Mallucci GR. Review: Modulating the unfolded protein response to prevent neurodegeneration and enhance memory. Neuropathol Appl Neurobiol 2015; 41(4): 414-27.
[http://dx.doi.org/10.1111/nan.12211] [PMID: 25556298]

[36] Huang HC, Tang D, Lu SY, Jiang ZF. Endoplasmic reticulum stress as a novel neuronal mediator in Alzheimer's disease. Neurol Res 2015; 37(4): 366-74.
[http://dx.doi.org/10.1179/1743132814Y.0000000448] [PMID: 25310352]

[37] Scheper W, Hoozemans JJ. The unfolded protein response in neurodegenerative diseases: A neuropathological perspective. Acta Neuropathol 2015; 130(3): 315-31.
[http://dx.doi.org/10.1007/s00401-015-1462-8] [PMID: 26210990]

[38] Jiang D, Niwa M, Koong AC. Targeting the IRE1α-XBP1 branch of the unfolded protein response in human diseases. Semin Cancer Biol 2015; 33: 48-56.
[http://dx.doi.org/10.1016/j.semcancer.2015.04.010] [PMID: 25986851]

[39] Engler C, Kelliher C, Spitze AR, Speck CL, Eberhart CG, Jun AS. Unfolded protein response in fuchs endothelial corneal dystrophy: A unifying pathogenic pathway? Am J Ophthalmol. 2010;149(2):194-202 e2.
[http://dx.doi.org/10.1016/j.ajo.2009.09.009]

[40] Jun AS, Meng H, Ramanan N, *et al.* An alpha 2 collagen VIII transgenic knock-in mouse model of Fuchs endothelial corneal dystrophy shows early endothelial cell unfolded protein response and apoptosis. Hum Mol Genet 2012; 21(2): 384-93.
[http://dx.doi.org/10.1093/hmg/ddr473] [PMID: 22002996]

[41] Okumura N, Kitahara M, Okuda H, *et al.* Sustained activation of the unfolded protein response induces cell death in fuchs' endothelial corneal

dystrophy. Invest Ophthalmol Vis Sci 2017; 58(9): 3697-707.
[http://dx.doi.org/10.1167/iovs.16-21023] [PMID: 28727885]

[42] Okumura N, Hashimoto K, Kitahara M, *et al.* Activation of TGF-β signaling induces cell death *via* the unfolded protein response in Fuchs endothelial corneal dystrophy. Sci Rep 2017; 7(1): 6801.
[http://dx.doi.org/10.1038/s41598-017-06924-3] [PMID: 28754918]

[43] Jurkunas UV, Rawe I, Bitar MS, *et al.* Decreased expression of peroxiredoxins in Fuchs' endothelial dystrophy. Invest Ophthalmol Vis Sci 2008; 49(7): 2956-63.
[http://dx.doi.org/10.1167/iovs.07-1529] [PMID: 18378575]

[44] Jurkunas UV, Bitar MS, Funaki T, Azizi B. Evidence of oxidative stress in the pathogenesis of fuchs endothelial corneal dystrophy. Am J Pathol 2010; 177(5): 2278-89.
[http://dx.doi.org/10.2353/ajpath.2010.100279] [PMID: 20847286]

[45] Azizi B, Ziaei A, Fuchsluger T, Schmedt T, Chen Y, Jurkunas UV. p53-regulated increase in oxidative-stress-induced apoptosis in Fuchs endothelial corneal dystrophy: A native tissue model. Invest Ophthalmol Vis Sci 2011; 52(13): 9291-7.
[http://dx.doi.org/10.1167/iovs.11-8312] [PMID: 22064994]

[46] Bitar MS, Liu C, Ziaei A, Chen Y, Schmedt T, Jurkunas UV. Decline in DJ-1 and decreased nuclear translocation of Nrf2 in Fuchs endothelial corneal dystrophy. Invest Ophthalmol Vis Sci 2012; 53(9): 5806-13.
[http://dx.doi.org/10.1167/iovs.12-10119] [PMID: 22836768]

[47] Ziaei A, Schmedt T, Chen Y, Jurkunas UV. Sulforaphane decreases endothelial cell apoptosis in fuchs endothelial corneal dystrophy: A novel treatment. Invest Ophthalmol Vis Sci 2013; 54(10): 6724-34.
[http://dx.doi.org/10.1167/iovs.13-12699] [PMID: 24030461]

[48] Tuberville AW, Wood TO, McLaughlin BJ. Cytochrome oxidase activity of Fuchs' endothelial dystrophy. Curr Eye Res 1986; 5(12): 939-47.
[http://dx.doi.org/10.3109/02713688608995175] [PMID: 3026733]

[49] Gottsch JD, Bowers AL, Margulies EH, *et al.* Serial analysis of gene expression in the corneal endothelium of Fuchs' dystrophy. Invest Ophthalmol Vis Sci 2003; 44(2): 594-9.
[http://dx.doi.org/10.1167/iovs.02-0300] [PMID: 12556388]

[50] Benischke AS, Vasanth S, Miyai T, *et al.* Activation of mitophagy leads to decline in Mfn2 and loss of mitochondrial mass in Fuchs endothelial corneal dystrophy. Sci Rep 2017; 7(1): 6656.
[http://dx.doi.org/10.1038/s41598-017-06523-2] [PMID: 28751712]

[51] Du J, Aleff RA, Soragni E, *et al.* RNA toxicity and missplicing in the common eye disease fuchs endothelial corneal dystrophy. J Biol Chem 2015; 290(10): 5979-90.
[http://dx.doi.org/10.1074/jbc.M114.621607] [PMID: 25593321]

[52] Mootha VV, Hussain I, Cunnusamy K, *et al.* TCF4 Triplet repeat expansion and nuclear RNA foci in fuchs' endothelial corneal dystrophy. Invest Ophthalmol Vis Sci 2015; 56(3): 2003-11.
[http://dx.doi.org/10.1167/iovs.14-16222] [PMID: 25722209]

[53] Tan DT, Dart JK, Holland EJ, Kinoshita S. Corneal transplantation. Lancet 2012; 379(9827): 1749-61.
[http://dx.doi.org/10.1016/S0140-6736(12)60437-1] [PMID: 22559901]

[54] Patel SV. Graft survival and endothelial outcomes in the new era of endothelial keratoplasty. Exp Eye Res 2012; 95(1): 40-7.
[http://dx.doi.org/10.1016/j.exer.2011.05.013] [PMID: 21689649]

[55] Okumura N, Kinoshita S, Koizumi N. Cell-based approach for treatment of corneal endothelial dysfunction. Cornea 2014; 33(Suppl. 11): S37-41.
[http://dx.doi.org/10.1097/ICO.0000000000000229] [PMID: 25188790]

[56] Ishino Y, Sano Y, Nakamura T, *et al.* Amniotic membrane as a carrier for cultivated human corneal endothelial cell transplantation. Invest Ophthalmol Vis Sci 2004; 45(3): 800-6.
[http://dx.doi.org/10.1167/iovs.03-0016] [PMID: 14985293]

[57] Mimura T, Yamagami S, Yokoo S, *et al.* Cultured human corneal endothelial cell transplantation with a collagen sheet in a rabbit model. Invest Ophthalmol Vis Sci 2004; 45(9): 2992-7.
[http://dx.doi.org/10.1167/iovs.03-1174] [PMID: 15326112]

[58] Koizumi N, Sakamoto Y, Okumura N, *et al.* Cultivated corneal endothelial cell sheet transplantation in a primate model. Invest Ophthalmol Vis Sci 2007; 48(10): 4519-26.
[http://dx.doi.org/10.1167/iovs.07-0567] [PMID: 17898273]

[59] Koizumi N, Okumura N, Kinoshita S. Development of new therapeutic modalities for corneal endothelial disease focused on the proliferation of corneal endothelial cells using animal models. Exp Eye Res 2012; 95(1): 60-7.
[http://dx.doi.org/10.1016/j.exer.2011.10.014] [PMID: 22067130]

[60] Mimura T, Shimomura N, Usui T, *et al.* Magnetic attraction of iron-endocytosed corneal endothelial cells to Descemet's membrane. Exp Eye Res 2003; 76(6): 745-51.
[http://dx.doi.org/10.1016/S0014-4835(03)00057-5] [PMID: 12742357]

[61] Mimura T, Yamagami S, Usui T, *et al.* Long-term outcome of iron-endocytosing cultured corneal endothelial cell transplantation with

magnetic attraction. Exp Eye Res 2005; 80(2): 149-57.
[http://dx.doi.org/10.1016/j.exer.2004.08.021] [PMID: 15670793]

[62] Mimura T, Yamagami S, Yokoo S, *et al.* Sphere therapy for corneal endothelium deficiency in a rabbit model. Invest Ophthalmol Vis Sci 2005; 46(9): 3128-35.
[http://dx.doi.org/10.1167/iovs.05-0251] [PMID: 16123411]

[63] Okumura N, Ueno M, Koizumi N, *et al.* Enhancement on primate corneal endothelial cell survival *in vitro* by a ROCK inhibitor. Invest Ophthalmol Vis Sci 2009; 50(8): 3680-7.
[http://dx.doi.org/10.1167/iovs.08-2634] [PMID: 19387080]

[64] Okumura N, Sakamoto Y, Fujii K, *et al.* Rho kinase inhibitor enables cell-based therapy for corneal endothelial dysfunction. Sci Rep 2016; 6: 26113.
[http://dx.doi.org/10.1038/srep26113] [PMID: 27189516]

[65] Okumura N, Koizumi N, Ueno M, *et al.* ROCK inhibitor converts corneal endothelial cells into a phenotype capable of regenerating *in vivo* endothelial tissue. Am J Pathol 2012; 181(1): 268-77.
[http://dx.doi.org/10.1016/j.ajpath.2012.03.033] [PMID: 22704232]

[66] Okumura N, Kinoshita S, Koizumi N. Application of Rho kinase inhibitors for the treatment of corneal endothelial diseases. J Ophthalmol 2017; 2017: 2646904.
[http://dx.doi.org/10.1155/2017/2646904] [PMID: 28751979]

[67] Nakagawa O, Fujisawa K, Ishizaki T, Saito Y, Nakao K, Narumiya S. ROCK-I and ROCK-II, two isoforms of Rho-associated coiled-coil forming protein serine/threonine kinase in mice. FEBS Lett 1996; 392(2): 189-93.
[http://dx.doi.org/10.1016/0014-5793(96)00811-3] [PMID: 8772201]

[68] Riento K, Ridley AJ. Rocks: multifunctional kinases in cell behaviour. Nat Rev Mol Cell Biol 2003; 4(6): 446-56.
[http://dx.doi.org/10.1038/nrm1128] [PMID: 12778124]

[69] Narumiya S, Tanji M, Ishizaki T. Rho signaling, ROCK and mDia1, in transformation, metastasis and invasion. Cancer Metastasis Rev 2009; 28(1-2): 65-76.
[http://dx.doi.org/10.1007/s10555-008-9170-7] [PMID: 19160018]

[70] Okumura N, Koizumi N, Ueno M, *et al.* Enhancement of corneal endothelium wound healing by Rho-associated Kinase (ROCK) inhibitor eye drops. Br J Ophthalmol 2011; 95(7): 1006-9.
[http://dx.doi.org/10.1136/bjo.2010.194571] [PMID: 21398412]

[71] Okumura N, Koizumi N, Kay EP, *et al.* The ROCK inhibitor eye drop accelerates corneal endothelium wound healing. Invest Ophthalmol Vis Sci 2013; 54(4): 2493-502.
[http://dx.doi.org/10.1167/iovs.12-11320] [PMID: 23462749]

[72] Okumura N, Inoue R, Okazaki Y, *et al.* Effect of the Rho kinase inhibitor y-27632 on corneal endothelial wound healing. Invest Ophthalmol Vis Sci 2015; 56(10): 6067-74.
[http://dx.doi.org/10.1167/iovs.15-17595] [PMID: 26393474]

[73] Koizumi N, Okumura N, Ueno M, Nakagawa H, Hamuro J, Kinoshita S. Rho-associated kinase inhibitor eye drop treatment as a possible medical treatment for Fuchs corneal dystrophy. Cornea 2013; 32(8): 1167-70.
[http://dx.doi.org/10.1097/ICO.0b013e318285475d] [PMID: 23715376]

[74] Shah RD, Randleman JB, Grossniklaus HE. Spontaneous corneal clearing after Descemet's stripping without endothelial replacement. Ophthalmology 2012; 119(2): 256-60.
[http://dx.doi.org/10.1016/j.ophtha.2011.07.032] [PMID: 21982414]

[75] Galvis V, Tello A, Miotto G. Human corneal endothelium regeneration. Ophthalmology 2012; 119(8): 1714-5.
[http://dx.doi.org/10.1016/j.ophtha.2012.03.052] [PMID: 22858028]

[76] Bleyen I, Saelens IE, van Dooren BT, van Rij G. Spontaneous corneal clearing after Descemet's stripping. Ophthalmology 2013; 120(1): 215.
[http://dx.doi.org/10.1016/j.ophtha.2012.08.037] [PMID: 23283191]

[77] Moloney G, Petsoglou C, Ball M, *et al.* Descemetorhexis without grafting for fuchs endothelial dystrophy-supplementation with topical ripasudil. Cornea 2017; 36(6): 642-8.
[http://dx.doi.org/10.1097/ICO.0000000000001209] [PMID: 28476048]

[78] Kim EC, Meng H, Jun AS. N-Acetylcysteine increases corneal endothelial cell survival in a mouse model of Fuchs endothelial corneal dystrophy. Exp Eye Res 2014; 127: 20-5.
[http://dx.doi.org/10.1016/j.exer.2014.06.002] [PMID: 24952277]

[79] Kim EC, Meng H, Jun AS. Lithium treatment increases endothelial cell survival and autophagy in a mouse model of Fuchs endothelial corneal dystrophy. Br J Ophthalmol 2013; 97(8): 1068-73.
[http://dx.doi.org/10.1136/bjophthalmol-2012-302881] [PMID: 23759441]

[80] Kim EC, Toyono T, Berlinicke CA, *et al.* Screening and characterization of drugs that protect corneal endothelial cells against unfolded protein response and oxidative stress. Invest Ophthalmol Vis Sci 2017; 58(2): 892-900.
[http://dx.doi.org/10.1167/iovs.16-20147] [PMID: 28159976]

[81] Okumura N, Minamiyama R, Ho LT, *et al.* Involvement of ZEB1 and Snail1 in excessive production of extracellular matrix in Fuchs

endothelial corneal dystrophy. Lab Invest 2015; 95(11): 1291-304.
[http://dx.doi.org/10.1038/labinvest.2015.111] [PMID: 26302187]

BJO Online First, published on January 23, 2018 as 10.1136/bjophthalmol-2017-311145

Topical ganciclovir treatment post-Descemet's stripping automated endothelial keratoplasty for patients with bullous keratopathy induced by cytomegalovirus

Koji Kitazawa,[1,2] Passara Jongkhajornpong,[3] Tsutomu Inatomi,[4] Noriko Koizumi,[5] Kanae Kayukawa,[2] Koichi Wakimasu,[2] Chie Sotozono,[4] Shigeru Kinoshita[1,2]

[1]Department of Frontier Medical Science and Technology for Ophthalmology, Kyoto Prefectural University of Medicine, Kyoto, Japan
[2]Ophthalmology, Baptist Eye Institute, Kyoto, Japan
[3]Department of Ophthalmology, Ramathibodi Hospital, Mahidol University, Salaya, Thailand
[4]Department of Ophthalmology, Kyoto Prefectural University of Medicine, Kyoto, Japan
[5]Department of Biomedical Engineering, Faculty of Life and Medical Sciences, Doshisha University, Kyotanabe, Japan

Correspondence to
Dr Tsutomu Inatomi, Department of Ophthalmology, Kyoto Prefectural University of Medicine, Kyoto 602-0841, Japan; tinatomi@koto.kpu-m.ac.jp

Received 4 August 2017
Revised 13 October 2017
Accepted 25 November 2017

ABSTRACT

Background/aims To investigate the efficacy of topical ganciclovir (GCV) for preventing disease recurrence and improving the surgical outcome post-Descemet's stripping automated endothelial keratoplasty (DSAEK) in patients with cytomegalovirus (CMV) endotheliitis.

Methods This prospective, non-comparative case series study involved six eyes of six patients with endothelial decompensation due to CMV endotheliitis who underwent DSAEK, followed by a continuous, four to six times daily, topical administration of 0.5% GCV. Patient demographics, clinical history, and preoperative and postoperative examination (including any recurrence of CMV endotheliitis post-DSAEK), best corrected visual acuity (BCVA), intraocular pressure (IOP), graft survival rate and endothelial cell density (ECD) were examined.

Results No recurrence of CMV endotheliitis was detected post-DSAEK. The mean follow-up period was 40 months (range, 12–60 months). The mean preoperative BCVA was 1.52±0.68 LogMAR (range, 0.52–2.40 LogMAR), yet it had significantly improved to 0.15±0.16 LogMAR (range: −0.08 to 0.30 LogMAR) by 1 year postoperative ($P<0.01$). In all patients, IOP was well controlled (10–20 mm Hg) postsurgery. The mean preoperative donor ECD was 2692±177 cells/mm^2, and the mean postoperative ECD was 1974, 1771 and 1174 cells/mm^2 for the ECD loss of 26%, 33% and 54% at 6, 12 and 36 months, respectively. No adverse effects were observed associated with the long-term topical administration of GCV.

Conclusion The continuous topical application of 0.5% GCV was found to be effective for preventing the recurrence of CMV endotheliitis, and it provided the optimal mid-term clinical outcomes post-DSAEK in patients with CMV endotheliitis.

Trial registration number UMIN000026746

INTRODUCTION

Cytomegalovirus (CMV) endotheliitis is a unique type of CMV infection that was first described by Koizumi and associates[1] in 2006. The clinical characteristics of CMV endotheliitis include corneal endothelial cell (CEC) loss following focal corneal oedema, recurrent mild anterior uveitis, ocular hypertension and coin-shaped keratic precipitates (KP), which is the standard and most reliable clinical finding of CMV endotheliitis.[1 2] Typically, CMV endotheliitis often develops in men in their 60s and 70s, and in such cases, CMV-DNA from the aqueous humour is detected in an immune-competent patient with unilateral corneal endotheliitis. Previous studies have reported the detection of CMV-DNA in the corneal stroma of a patient with CMV endotheliitis, identified as 'owl's eye' morphology in the CECs and reduced endothelial cell associated with high CMV viral load,[3–5] and the pathogenesis of CMV endotheliitis has reportedly been considered to be a CMV infection directly related to CECs, and thus, systemic ganciclovir (GCV), topical 0.5% GCV eye drops, and 0.15% GCV gel has been used to treat patients suffering from CMV endotheliitis.[6 7]

CEC loss caused by CMV infection results in corneal decompensation, which ultimately requires corneal transplantation for treatment. The analysis of 106 CMV cases by the Japan Corneal Endotheliitis Study Group (JCESG) revealed that upon the diagnosis of CMV endotheliitis, corneal transplantation was performed in 29 eyes (25.7%).[2] Recently, Descemet's stripping automated endothelial keratoplasty (DSAEK) has become the standard procedure for treating corneal endothelial decompensation. However, it has been reported that in 57% of CMV endotheliitis eyes, persistent corneal oedema was observed after successful treatment.[8] In addition, high rates of graft failure after penetrating keratoplasty (PKP) and DSAEK have been reported in cases in which the recurrence of CMV occurred.[9–11] Moreover, Chan and associates[11] reported that CMV infection could cause graft failure in cases with a clinical diagnosis of allograft rejection.

To date, no standard protocol for the prevention of CMV endotheliitis recurrence post-DSAEK has been established. In this present case series study, we analysed six patients diagnosed with CMV endotheliitis with corneal endothelial decompensation who underwent DSAEK, and investigated the efficacy of the topical instillation of 0.5% GCV eye drops for the prevention of CMV endotheliitis recurrence, as well as the surgical outcomes post-DSAEK in terms of preserving the CEC count and maintaining good visual acuity.

To cite: Kitazawa K, Jongkhajornpong P, Inatomi T, *et al*. *Br J Ophthalmol* Epub ahead of print: [*please include* Day Month Year]. doi:10.1136/bjophthalmol-2017-311145

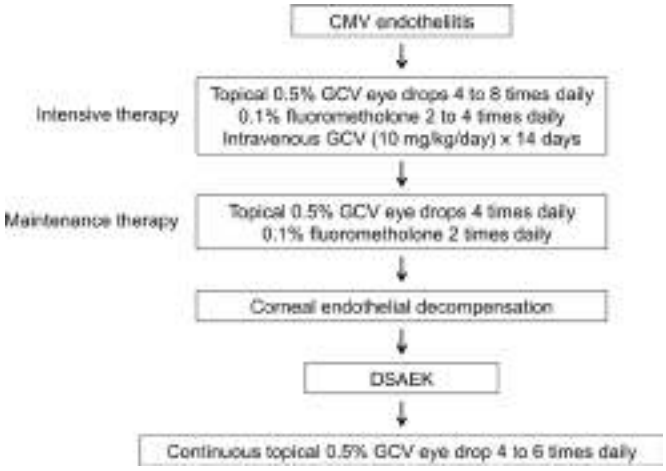

Figure 1 Standard protocol for the treatment of CMV endotheliitis, and for the treatment of bullous keratopathy induced by CMV post-DSAEK. CMV, cytomegalovirus; DSAEK, Descemet's stripping automated endothelial keratoplasty; GCV, ganciclovir.

METHODS

Study design

This prospective, non-comparative case series study was conducted at the Department of Ophthalmology, Kyoto Prefectural University of Medicine and the Baptist Eye Institute, Kyoto, Japan, from 1 June 2011 to 28 February 2017. This study was approved by the Kyoto Ethics Review Committee, Kyoto, Japan (Approval #1604) and was performed in accordance with the tenets set forth in the Declaration of Helsinki, and prior written informed consent was obtained from all patients. Clinical trial registration was obtained at UMIN (UMIN000026746) (http://www.umin.ac.jp/english/).

Preoperative evaluation

In this study, we recruited six patients with a previous definite diagnosis of CMV endotheliitis resulting in a severe irreversible endothelial dysfunction. The diagnostic criteria of CMV endotheliitis proposed by the JCESG were as follows: (1) viral examination by PCR of aqueous humour positive for CMV-DNA, yet negative for herpes simplex virus DNA and varicella-zoster virus DNA; (2) clinical manifestation of corneal endotheliitis with coin-shaped lesion/linear KPs or localised corneal oedema with KPs associated with two of the following three items, including recurrent/chronic uveitis, ocular hypertension/secondary glaucoma and CEC loss.[2] From each patient, aqueous humour was obtained using a 30-gauge needle integrated with a specially designed disposable pipette, as we previously reported.[12] Our standard treatment protocol for CMV endotheliitis is shown in figure 1. Patients with CMV endotheliitis received intensive treatment with systemic GCV (5 mg/kg, twice daily for 2 weeks) and the topical administration of 0.5% GCV eye drops, four to eight times daily, and continuous treatment with topical 0.5% GCV eye drops four times daily[6] (figure 1). In all patients, no active anterior chamber inflammation, in addition to well-controlled intraocular pressure (IOP), was confirmed prior to undergoing DSAEK surgery. In addition, the demographics and clinical history of all patients were obtained and recorded. Moreover, ocular examinations including BCVA, endothelial cell density (ECD), IOP and phakic status were performed and recorded. In all patients, anterior segment photographs were obtained presurgery and postsurgery.

Surgical procedure

All six patients underwent DSAEK under local or general anaesthesia. Phacoemulsification with intraocular lens insertion was performed on an individual basis depending on lens status and severity of cataract. The DSAEK procedure was performed using a Busin glide to carry the corneal graft into the anterior chamber.[13] Precut internationally shipped donor corneas obtained from SightLife Eye Bank (Seattle, WA) were surgically punched to a graft diameter of 8.0–8.5 mm depending on the diameter of the host cornea. Air injection into the anterior chamber was then performed to firmly attach the donor corneal graft to the host cornea, with a final adjustment of optimal IOP.

Postoperative management

As per the standard postoperative protocol reported in our previous study,[14] the medications consisted of systemic steroids (intravenous betamethasone 4 mg daily for 2 days), followed by oral betamethasone (1 mg daily for 5 days), and 0.3% gatifloxacin (four times daily) and 0.1% betamethasone (four times daily) for 6 months postoperatively. The topical medications were then gradually tapered depending on the severity of the patient's ocular inflammation and IOP. Topical 0.5% GCV was prescribed four to six times daily in accordance with the patient's previous activity of CMV endotheliitis and their response to the GCV treatment. The 0.5% GCV solution was prepared by dissolving GCV for use as an intravenous infusion drip.[6 15] All patients were then examined at 1 day, 7 days, 1 month, 3 months and then every 6 months after the operation.

Clinical outcomes

The primary outcome was the recurrence of CMV endotheliitis during the first postoperative year, with the recurrence being defined as focal corneal oedema following coin-shaped KPs or ocular hypertension. In suspicious cases, an aqueous tap was performed to confirm CMV-DNA. The secondary

Table 1 Patient demographics

Case number	Age/sex	Laterality	Operation	Previous ocular surgery	Systemic disease	Lens status
1	41/M	Left	DSAEK	None	None	Phakia
2	68/M	Left	DSAEK PE+IOL	TLE	HT, HL	Pseudophakia
3	75/M	Left	DSAEK PE+IOL	None	HL	Pseudophakia
4	82/M	Right	DSAEK	PE+IOL	Cerebral infarction, anaemia	Pseudophakia
5	68//F	Right	DSAEK	PE+IOL	DM, HT	Pseudophakia
6	49/M	Right	DSAEK PE+IOL	TLO	None	Pseudophakia

DM, diabetes mellitus; DSAEK, Descemet's stripping automated endothelial keratoplasty; F, female; HL, hyperlipidaemia; HT, hypertension; M, male; PE+IOL, phacoemulsification with intraocular lens implantation; TLE, trabeculectomy; TLO, trabeculotomy.

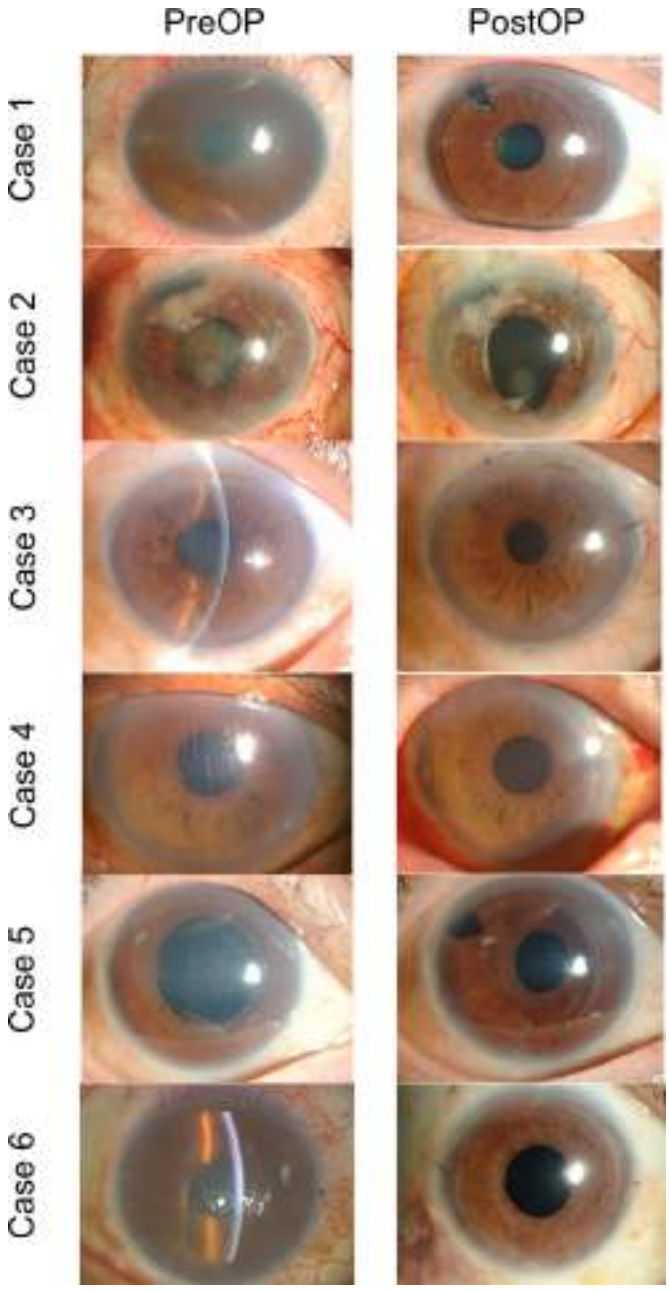

Figure 2 Preoperative and postoperative anterior segment photographs of six cases. Severe corneal oedema was observed in each case. After Descemet's stripping automated endothelial keratoplasty (DSAEK) surgery without complications, followed by continuous topical application of 0.5% ganciclovir, clear corneas were obtained, thus resulting in a significant improvement of visual function. A triple procedure was performed on cases 2, 3 and 6. Case 5 was the only eye with a phakic status, and no cases of cataract were observed after long-term ganciclovir application.

outcome was the examination of BCVA, IOP and ECD at 1 year post-DSAEK. BCVA, IOP, the anterior segment photograph and ECD measured by non-contact specular microscopy (EM-3000; TOMEY, Nagoya, Japan) were examined at each visit. The percentage of CEC loss was calculated by use of the following formula:

$$CEC\ loss\ (\%) = \frac{1-ECD\ at\ each\ time\ point}{post-cut\ \ ECD\ of\ donor\ graft} \times 100$$

Statistical analysis

A two-sample Wilcoxon signed-rank test was used to compare the differences between preoperative and postoperative BCVA. A P value of <0.05 was considered statistically significant.

RESULTS

This study included six patients with corneal endothelial decompensation caused by CMV endotheliitis.

Demographics and clinical findings

The patient demographics and clinical findings are summarised in table 1. The mean patient age was 63.8 years (range: 41–82 years), and five of the six cases (83.3%) were male. All patients were immunocompetent with unilateral CMV endotheliitis. The systemic conditions of the six patients included hypertension (n=2), diabetes mellitus (n=1), hyperlipidaemia (n=2) and anaemia (n=1). Four eyes (66.7%) were previously diagnosed as Posner-Schlossman syndrome (PSS), and the other two eyes were diagnosed as chronic anterior uveitis prior to the detection of CMV-DNA in the aqueous humour. In all patients, the anterior segment photographs revealed irreversible corneal decompensation (figure 2). In addition, secondary glaucoma was found in all patients, and two of those five eyes underwent glaucoma surgery; one of those two eyes underwent trabeculotomy while the other eye underwent trabeculectomy. The mean preoperative BCVA was 1.52±0.68 LogMAR (range: 0.52–2.40 LogMAR). In all cases, DSAEK was performed without any complications, followed by treatment with the standard post-DSAEK medical treatment protocol and the above-described continuous topical application of 0.5% GCV. Among the six treated eyes, three eyes underwent DSAEK combined with cataract surgery.

Clinical outcomes

In all patients, no obvious episode of recurrent CMV endotheliitis was observed postsurgery. However, one case (case 3) had mild anterior uveitis without coin-shaped KPs, and negative CMV-DNA detection from aqueous humour. The mean postoperative follow-up period was 40 months (range, 12–60 months), and the mean postoperative BCVA was 0.15±0.16 LogMAR (range, −0.08 to 0.30 LogMAR), thus illustrating significant improvement (P=0.03). Within the first 3 months postoperatively, all patients achieved the maximum visual recovery, and the BCVA was maintained until their final follow-up visit (figure 2). After surgery, IOP was normal in five eyes without the need of any antiglaucoma eye drop medication, yet one eye did require treatment with a topical administration of an antiglaucoma eye drop medication (0.005% latanoprost and 0.5% timolol). The mean preoperative ECD of the donor corneal grafts was 2692±177 cells/mm^2 (range: 2516–2869 cells/mm^2). At 12, 24 and 36 months postoperatively, the mean ECD was 1771, 1497 and 1174 cells/mm^2, respectively, and the mean ECD loss was 33%, 42% and 54%, respectively, and the mean ECD at final follow-up was 1304 cells/mm^2 (table 2). In all patients, no adverse drug reaction due to the long-term use of topical 0.5% GCV was observed.

DISCUSSION

The findings of this present study revealed that the topical administration of 0.5% GCV is an effective treatment to prevent the recurrence of CMV endotheliitis, and that it helped maintain the survival of the donor cornea graft up to 5 years postoperatively. It has previously been reported that GCV is effective in eliminating the CMV viral antigen, maintaining the control of

Table 2 Long-term clinical outcome post-Descemet's stripping automated endothelial keratoplasty using prophylactic 0.5% ganciclovir eye drops

			Preoperative		Postoperative (1 year)		Final visit		During follow-up time		Treatment
Case number	Operation	Follow-up (M)	BCVA	ECD (cells/mm^2)	BCVA	ECD (cells/mm^2)	BCVA	ECD (cells/mm^2)	Recurrence	IOP elevation	0.5% GCV eye drops
1	DSAEK	60	20/1000	2523	20/20	2613	20/20	1612	None	None	+
2	DSAEK PE+IOL	60	20/2000	2869	20/40	1111	20/40	461	None	None	+
3	DSAEK PE+IOL	54	20/2000	2552	20/30	1202	20/30	684	None	None	+
4	DSAEK	12	20/800	2855	20/40	1607	20/40	1607	None	None	+
5	DSAEK	30	20/63	2516	20/16	2146	20/16	2115	None	None	+
6	DSAEK PE+IOL	24	Counting fingers	2834	30/50	1949	30/50	1345	None	None	+

BCVA, best corrected visual acuity; DSAEK, Descemet's stripping automated endothelial keratoplasty; ECD, endothelial cell density; GCV, ganciclovir; IOP, intraocular pressure; PE+IOL, phacoemulsification with intraocular lens implantation; M, month

IOP and preventing CEC loss in cases of CMV-positive PSS.[16] It has also been reported that in patients with CMV endotheliitis who undergo corneal transplantation surgery, the postoperative recurrence of CMV is a serious complication that can lead to intractable graft failure.[9] For patients suffering from corneal endothelial disease, DSAEK has now become the 'treatment of choice' to reduce graft rejection and long-term postoperative PKP-related complications. To the best of our knowledge, there are no published studies regarding a preventive medicine protocol for improving the postoperative outcome of DSAEK in patients with CMV endotheliitis. In this present study, our findings demonstrated the efficacy of prophylactic topical GCV for the prevention of the recurrence CMV endotheliitis post-DSAEK, and in all six patients, no disease recurrence was observed throughout the 5-year follow-up period.

The findings of numerous studies have shown that several regimens of topical GCV combined with systemic treatment are effective for treating CMV endotheliitis.[1 4 6 15] However, the findings in previous reports have demonstrated that 25% of patients with CMV endotheliitis ultimately require corneal transplantation,[2] and that the prognosis is poor postcorneal transplantation for CMV endotheliitis-induced bullous keratopathy (BK).[8–10] Thus, it has been reported that CMV endotheliitis is one of possible causes of multiple graft failures.[6] Similar to the clinical findings in other reported DSAEK case series studies,[17–19] our findings revealed that ECD loss was approximately 33%, 42% and 54%, respectively, at 12, 24 and 36 months after surgery, possibly due to the fact that our six patients underwent continuous topical 0.5% GCV treatment throughout the postoperative follow-up period, or that the CMV endotheliitis had become inactive prior to DSAEK due to the intensive intravenous GCV treatment that the patients received for 2 weeks preoperatively. In fact, one case in this study without a history of ocular surgery (case 5) was found to have a CEC loss of only 6.0% at 3 years postoperatively, which is a favourable outcome post-DSAEK. However, we experienced two cases with an ECD of less than 1000 cells/mm^2 at 3 years postoperatively; one case was a patient with mild anterior uveitis in which the typical findings of CMV endotheliitis were not observed, while the other case was a patient who underwent trabeculectomy post-DSAEK. It has been reported that glaucoma and a history of glaucoma surgery are risk factors for early graft failure post-PKP and for the high level of CEC loss post-DSAEK.[20–22] Thus, eyes with a history of trabeculectomy might experience a rapid decrease in ECD even without a recurrence of CMV.

Serious side effects associated with local GCV administration have been reported, including severe neutropenia, cataract formation, retinal detachment and sterile endophthalmitis.[23 24] However, no adverse effects were observed in our case series as a result of the topical administration of 0.5% GCV. In addition, one case in this study with a phakic eye (case 1) was able to maintain BCVA without significant cataract formation throughout the 5-year follow-up period.

It should be noted that we experienced one case with mild anterior uveitis (case 3) without obvious recurrence of CMV endotheliitis post-DSAEK. However, at 4.5 years postoperatively, the ECD in that patient had decreased to less than 1000 cells/mm^2, thus suggesting that the response to 0.5% GCV eye drops might widely vary according to the severity of CMV reactivation, and that there might possibly be a different genotype of CMV.

It should also be noted that this current study did have some limitations, such as the small number of patients and that the study design was 'non-comparative'. However, the findings in the 2015 Japan Corneal Endotheliitis Study[2] showed that 25% of patients with CMV endotheliitis ultimately require corneal transplantation. The fact that there was no episode of recurrent CMV endotheliitis post-DSAEK in this present study suggests that continuous topical application of GCV may be effective for preventing the recurrence of CMV. Hence, a future large-scale study with a large number of control subjects is required to produce a definitive conclusion. Additionally, we postulated that topical GCV continuously should be prescribed as long as no complications are detected. However, GCV eye drops need to be prepared in hospital dispensaries from phials, and the use of GCV eye drops in clinical research currently requires approval by ethics committees. Thus, a clinical trial involving the topical use of commercially available 0.15% GCV gel on patients with CMV endotheliitis is currently being conducted by Koizumi and associates in Japan.[7]

In conclusion, the findings of this present study emphasise the importance of the continuous topical application of GCV for preventing the recurrence of CMV post-DSAEK, and that the treatment results in the preservation of ECD, the improvement of IOP control and maintaining the optimal visual outcome in patients with CMV endotheliitis. Moreover, our findings show that a strict and long-term follow-up is vital to prevent the recurrence of CMV endotheliitis.

Acknowledgements The authors wish to thank John Bush for editing the manuscript.

Contributors Conception and design of the study (TI, NK, CS, SK); collection of data (KK, PJ); management of data (KK, TI); analysis of data (KK, PJ, TI); interpretation of data (KK, PJ, TI); writing of the article (KK, PJ, TI); approval of the

manuscript (KK, PJ, TI, NK, KK, KW, CS, SK); obtaining of funding (SK); searching the literature (KK, PJ).

Funding This study was supported in part by a Grant-in-Aid for Scientific Research from the Ministry of Education, Science, Culture, and Sports of Japan.

Competing interests None declared.

Patient consent Obtained.

Ethics approval Ethics Review Board (ERB) of Kyoto Ethics Review Committee (ERB approval number 1604).

Provenance and peer review Not commissioned; externally peer reviewed.

REFERENCES

1 Koizumi N, Yamasaki K, Kawasaki S, *et al*. Cytomegalovirus in aqueous humor from an eye with corneal endotheliitis. *Am J Ophthalmol* 2006;141:564–5.
2 Koizumi N, Inatomi T, Suzuki T, *et al*. Clinical features and management of cytomegalovirus corneal endotheliitis: analysis of 106 cases from the Japan corneal endotheliitis study. *Br J Ophthalmol* 2015;99:54–8.
3 Shimazaki J, Harashima A, Tanaka Y. Corneal endotheliitis with cytomegalovirus infection of corneal stroma. *Eye* 2010;24:1105–7.
4 Shiraishi A, Hara Y, Takahashi M, *et al*. Demonstration of "owl's eye" morphology by confocal microscopy in a patient with presumed cytomegalovirus corneal endotheliitis. *Am J Ophthalmol* 2007;143:715–7.
5 Kandori M, Miyazaki D, Yakura K, *et al*. Relationship between the number of cytomegalovirus in anterior chamber and severity of anterior segment inflammation. *Jpn J Ophthalmol* 2013;57:497–502.
6 Koizumi N, Suzuki T, Uno T, *et al*. Cytomegalovirus as an etiologic factor in corneal endotheliitis. *Ophthalmology* 2008;115:292–7.
7 Koizumi N, Miyazaki D, Inoue T, *et al*. The effect of topical application of 0.15% ganciclovir gel on cytomegalovirus corneal endotheliitis. *Br J Ophthalmol* 2017;101:114–9.
8 Chee SP, Jap A. Treatment outcome and risk factors for visual loss in cytomegalovirus endotheliitis. *Graefes Arch Clin Exp Ophthalmol* 2012;250:383–9.
9 Su CC, Wang IJ, Chen WL, *et al*. Topical ganciclovir treatment in patients with cytomegalovirus endotheliitis receiving penetrating keratoplasty. *Clin Exp Ophthalmol* 2013;41:339–47.
10 Anshu A, Chee SP, Mehta JS, *et al*. Cytomegalovirus endotheliitis in descemet's stripping endothelial keratoplasty. *Ophthalmology* 2009;116:624–30.
11 Chan AS, Mehta JS, Al Jajeh I, *et al*. Histological features of cytomegalovirus-related corneal graft infections, its associated features and clinical significance. *Br J Ophthalmol* 2016;100:601–6.
12 Kitazawa K, Sotozono C, Koizumi N, *et al*. Safety of anterior chamber paracentesis using a 30-gauge needle integrated with a specially designed disposable pipette. *Br J Ophthalmol* 2017;101:548–50.
13 Busin M, Bhatt PR, Scorcia V. A modified technique for descemet membrane stripping automated endothelial keratoplasty to minimize endothelial cell loss. *Arch Ophthalmol* 2008;126:1133–7.
14 Kitazawa K, Kayukawa K, Wakimasu K, *et al*. Cystoid macular edema after descemet's stripping automated endothelial keratoplasty. *Ophthalmology* 2017;124:572–3.
15 Suzuki T, Hara Y, Uno T, *et al*. DNA of cytomegalovirus detected by PCR in aqueous of patient with corneal endotheliitis after penetrating keratoplasty. *Cornea* 2007;26:370–2.
16 Su CC, Hu FR, Wang TH, *et al*. Clinical outcomes in cytomegalovirus-positive posner-schlossman syndrome patients treated with topical ganciclovir therapy. *Am J Ophthalmol* 2014;158:1024–31.
17 Price MO, Gorovoy M, Benetz BA, *et al*. Descemet's stripping automated endothelial keratoplasty outcomes compared with penetrating keratoplasty from the cornea donor study. *Ophthalmology* 2010;117:438–44.
18 Price MO, Gorovoy M, Price FW, *et al*. Descemet's stripping automated endothelial keratoplasty: three-year graft and endothelial cell survival compared with penetrating keratoplasty. *Ophthalmology* 2013;120:246–51.
19 Price MO, Calhoun P, Kollman C, *et al*. Descemet stripping endothelial keratoplasty: ten-year endothelial cell loss compared with penetrating keratoplasty. *Ophthalmology* 2016;123:1421–7.
20 Aldave AJ, Chen JL, Zaman AS, *et al*. Outcomes after DSEK in 101 eyes with previous trabeculectomy and tube shunt implantation. *Cornea* 2014;33:223–9.
21 Ward MS, Goins KM, Greiner MA, *et al*. Graft survival versus glaucoma treatment after penetrating or descemet stripping automated endothelial keratoplasty. *Cornea* 2014;33:785–9.
22 Sugar A, Gal RL, Kollman C, *et al*. Factors associated with corneal graft survival in the cornea donor study. *JAMA Ophthalmol* 2015;133:246–54.
23 Arevalo JF, Garcia RA, Mendoza AJ. High-dose (5000-microg) intravitreal ganciclovir combined with highly active antiretroviral therapy for cytomegalovirus retinitis in HIV-infected patients in Venezuela. *Eur J Ophthalmol* 2005;15:610–8.
24 Oktavec KC, Nolan K, Brown DM, *et al*. Clinical outcomes in patients with cytomegalovirus retinitis treated with ganciclovir implant. *Am J Ophthalmol* 2012;153:728–33.

Topical ganciclovir treatment post-Descemet's stripping automated endothelial keratoplasty for patients with bullous keratopathy induced by cytomegalovirus

Koji Kitazawa, Passara Jongkhajornpong, Tsutomu Inatomi, Noriko Koizumi, Kanae Kayukawa, Koichi Wakimasu, Chie Sotozono and Shigeru Kinoshita

Br J Ophthalmol published online January 23, 2018

Effect of Trinucleotide Repeat Expansion on the Expression of *TCF4* mRNA in Fuchs' Endothelial Corneal Dystrophy

Naoki Okumura,[1] Ryosuke Hayashi,[1] Masakazu Nakano,[2] Kengo Yoshii,[3] Kei Tashiro,[2] Takahiko Sato,[4] Derek J. Blake,[5] Ross Aleff,[6] Malinda Butz,[7] Edward W. Highsmith,[7] Eric D. Wieben,[6] Michael P. Fautsch,[8] Keith H. Baratz,[8] Yuya Komori,[1] Makiko Nakahara,[1] Theofilos Tourtas,[9] Ursula Schlötzer-Schrehardt,[9] Friedrich Kruse,[9] and Noriko Koizumi[1]

[1]Department of Biomedical Engineering, Faculty of Life and Medical Sciences, Doshisha University, Kyotanabe, Japan
[2]Department of Genomic Medical Sciences, Kyoto Prefectural University of Medicine, Kyoto, Japan
[3]Department of Mathematics and Statistics in Medical Sciences, Kyoto Prefectural University of Medicine, Kyoto, Japan
[4]Department of Ophthalmology, Kyoto Prefectural University of Medicine, Kyoto, Japan
[5]Division of Psychological Medicine and Clinical Neurosciences, Cardiff University, United Kingdom
[6]Department of Biochemistry and Molecular Biology, Mayo Clinic, Rochester, Minnesota, United States
[7]Department of Laboratory Medicine and Pathology, Mayo Clinic, Rochester, Minnesota, United States
[8]Department of Ophthalmology, Mayo Clinic, Rochester, Minnesota, United States
[9]Department of Ophthalmology, University of Erlangen-Nürnberg, Erlangen, Germany

Correspondence: Noriko Koizumi, Department of Biomedical Engineering, Faculty of Life and Medical Sciences, Doshisha University, Kyotanabe 610-0321, Japan; nkoizumi@mail.doshisha.ac.jp.

Submitted: September 15, 2018
Accepted: December 10, 2018

Citation: Okumura N, Hayashi R, Nakano M, et al. Effect of trinucleotide repeat expansion on the expression of *TCF4* mRNA in Fuchs' endothelial corneal dystrophy. *Invest Ophthalmol Vis Sci*. 2019;60:779–786. https://doi.org/10.1167/iovs.18-25760

Purpose. CTG trinucleotide repeat (TNR) expansion is frequently found in *transcription factor 4* (*TCF4*) in Fuchs' endothelial corneal dystrophy (FECD), though the effect of TNR expansion on FECD pathophysiology remains unclear. The purpose of this study was to evaluate the effect of TNR expansion on *TCF4* expression in corneal endothelium of patients with FECD.

Methods. Peripheral blood DNA and Descemet membrane with corneal endothelium were obtained from 203 German patients with FECD. The CTG TNR repeat length in *TCF4* was determined by short tandem repeat (STR) assays and Southern blotting using genomic DNA. Genotyping of rs613872 in *TCF4* was performed by PCR. *TCF4* mRNA levels in corneal endothelium were evaluated by quantitative PCR using three different probes. Control corneal endothelial samples were obtained from 35 non-FECD subjects.

Results. The STR assay and Southern blotting showed that 162 of the 203 patients with FECD (80%) harbored CTG trinucleotide repeat lengths larger than 50. Quantitative PCR using all three probes demonstrated that *TCF4* mRNA is significantly upregulated in the corneal endothelium of patients with FECD, regardless of the presence of TNR expansion. However, the length of the TNR tended to show a positive correlation with *TCF4* expression level. No correlation was shown between the genotype of *TCF4* SNP, rs613872, and the level of *TCF4* expression.

Conclusions. Our findings showed that *TCF4* mRNA is upregulated in the corneal endothelium of patients with FECD. Further studies on the effects of *TCF4* upregulation on corneal endothelial cell function will aid in understanding the pathophysiology of FECD.

Keywords: Fuchs' endothelial corneal dystrophy, TCF4, trinucleotide repeat

Fuchs' endothelial corneal dystrophy (FECD) is characterized by a loss of corneal endothelial cells that is associated with a clinically phenotypical hallmark of guttae, which are excrescences of Descemet membrane formed by abnormal deposition of extracellular matrix. As the corneal endothelium maintains corneal transparency by regulating the degree of hydration in the corneal stroma, severe corneal endothelial cell loss due to FECD induces corneal haziness, resulting in vision loss.[1,2]

FECD is a hereditary disease with a typically autosomal dominant pattern of inheritance, though the genetic basis is not fully elucidated.[1,2] In 2012, Wieben and colleagues[3] reported that expansion of a trinucleotide repeat (TNR) in the third intron of *TCF4* was strongly associated with FECD, and the sensitivity and specificity for identifying FECD in their patient cohort was 79% and 96%, respectively.[3] They postulated that FECD is a TNR disorder within the non-coding region, with similarities to Friedreich's ataxia, myotonic dystrophy type 1, and fragile X syndrome.[3] Subsequently, other researchers have replicated this strong association in other independent cohorts such as Caucasian, Indian, Chinese, and Japanese.[4–9]

Simple sequence repeats exist throughout the human genome, but expansion of the TNR was discovered as causal genetic basis in patients with spinal and bulbar muscle atrophy in 1991.[10] Since the first discovery of TNR expansion disease,

more than 20 disorders have been identified, all of which are neurologic or neuromuscular degenerations.[11–13] TNR expansion disease can be categorized into two groups: TNR expansion disease occurring in coding regions or TNR expansion disease occurring in noncoding regions. Diseases with CAG repeat expansion in coding regions induce polyglutamine tracts, which generate toxic proteins. By contrast, TNR expansion in noncoding regions in triplet repeat disorders can suppress or enhance gene transcription of the surrounding gene, produce antisense RNA, alter the RNA splicing pattern by sequestration of splicing factors, result in intron retention, and/or have repeat-associated non-ATG (RAN) translation, and eventually play an essential role in pathophysiology.[13–19]

Elucidation of the effect of TNR expansion on expression of the gene harboring the expansion is beneficial for understanding the pathophysiology of triplet repeat diseases; however, the effect of TNR expansion on the transcription of TCF4 is not well elucidated in FECD. In the current study, we collected peripheral blood samples from 398 German patients with FECD, as well as the Descemet membrane and associated corneal endothelium when these patients underwent Descemet membrane endothelial keratoplasty (DMEK). We subsequently evaluated whether expression levels in the corneal endothelium were altered by TNR expansion in *TCF4* in samples derived from 203 of these FECD subjects.

Materials And Methods

Ethics Statement

Institutional review board approvals for research involving human subjects were obtained from the Friedrich-Alexander University Erlangen-Nürnberg, Doshisha University, Kyoto Prefectural University of Medicine, and the Mayo Clinic. The human tissue was handled under the guidelines based on the tenets of the Declaration of Helsinki. Non-FECD human donor corneas were obtained from SightLife (Seattle, WA, USA).

Study Participants

The 398 patients with FECD who were scheduled for DMEK were recruited between October 2013 and September 2015 at the Department of Ophthalmology, Friedrich-Alexander University Erlangen-Nürnberg. After informed consent, peripheral blood samples were collected and Descemet membranes with corneal endothelial cells (CECs) were obtained during DMEK. For samples utilized in this study, genomic DNA obtained from peripheral blood required a DNA concentration of $\geq$3.0 μg/mL and total RNA isolated from CEC's required an RNA integrity number (RIN) $\geq$5.2. Of the samples from the 398 patients, 203 fulfilled the quality criteria for genomic DNA and total RNA isolation. As controls, genomic DNA was isolated from donor corneas (corneal stroma) of 35 non-FECD subjects, and cDNA was synthesized from the CECs of the same 35 non-FECD subjects.

Preparation of Genomic DNA From Peripheral Blood and Donor Corneas

Genomic DNA was isolated from 200 μL of peripheral blood of FECD subjects or non-FECD donor corneal stromas with a commercial DNA kit (DNeasy Blood & Tissue Kit; Qiagen, Hilden, Germany). Briefly, peripheral blood and stromas were lysed with protease K, the lysate was applied to spin columns (DNeasy Mini Spin Columns; Qiagen), and the columns were washed with ethanol and then with buffer to elute the genomic DNA. The amount and quality of each isolated DNA sample were analyzed by UV spectrophotometry (NanoDrop; NanoDrop Technologies, Wilmington, DE, USA). As a control, genomic DNA was isolated from corneal stromas of the 35 non-FECD donor corneas.

Preparation of Total RNA and Synthesis of cDNA From Corneal Endothelium

An RNA extraction kit (RNeasy Mini Kit; Qiagen) was used to extract total RNA from the corneal endothelium obtained from the 203 FECD patients during DMEK. Briefly, Descemet membranes with corneal endothelium were lysed, and the lysate was applied to spin columns (Qiagen) with ethanol. The total RNA was eluted from columns, and cDNA was synthesized using a master mix (SuperScript VILO Master Mix; Thermo Fisher Scientific Inc., Waltham, MA, USA). As a control, Descemet membranes with corneal endothelium were peeled from the 35 non-FECD donor corneas, and cDNA was synthesized from the extracted total RNA.

Evaluation of CTG TNR Length

The CTG TNR length in *TCF4* was evaluated by a short tandem repeat (STR) assay, as described previously.[4] Briefly, PCR was performed for the CTG repeat region using one fluorescently labeled primer. The size of the products was determined by capillary electrophoresis on a DNA analyzer (ABI 3730xl; Applied Biosystems, Foster City, CA). Samples that showed a single signal by STR were further analyzed by Southern blotting (described previously)[3] using unamplified genomic DNA to determine if these samples carried a large repeat.

Quantitative Real-Time PCR

Quantitative real-time PCR (qPCR) was performed with a real-time PCR system (QuantStudio 3; Applied Biosystems). All samples were analyzed in duplicate with a program of 95°C for 20 seconds and 40 cycles of 95°C for 1 second and 60°C for 20 seconds. For quantification, standard curves were run in parallel using serial dilutions (5-5^{5}copies) of cDNA of cultured immortalized human CECs, as described previously.[20] Ratios relative to *GAPDH* were calculated for normalization of gene expression levels. In this study, qPCR was based on a hydrolysis probe system (TaqMan; Thermo Fisher Scientific, Inc.). The hydrolysis probes (Thermo Fisher Scientific, Inc.) were for *TCF4*, Hs 00971338_m1; Hs00162613_m1; Hs00972432_m1; and predevelopment human *GAPDH* (Thermo Fisher Scientific, Inc.).

Genotyping

Genotyping of rs613872 in *TCF4* was performed by PCR using the following primers: forward primer-5′-actgtcaagcactaagcaaa gagg-3′, reverse primer- 5′-cccagtagggttgtgatgatgatg-3′. PCR reactions were carried out with Ex Taq DNA polymerase (Takara Bio Inc., Otsu, Japan) under the following conditions: 1 cycle of denaturation at 94°C for 2 minutes followed by 35 cycles of denaturation at 94°C for 30 seconds, annealing at 55°C for 30 seconds, and elongation at 72°C for 30 seconds. Upon completion of the 35 cycles, a final elongation was performed at 72°C for 5 minutes. The PCR products were separated by electrophoresis on 2% agarose gels in Tris-acetate buffer, stained with ethidium bromide, imaged with a luminescence imager (LAS4000S; Fuji Film, Tokyo, Japan), and then extracted from the agarose gels using the a commercial gel and a PCR cleanup system (Wizard SV Gel; Promega, Madison, WI, USA). A terminator cycle sequencing

Investigative Ophthalmology & Visual Science

Table. Demographic Data of Patients With FECD and non-FECD Controls

	CTG Repeat			
	Control ($n = 35$)	No Expansion CTG < 50 ($n = 41$)	Expansion CTG ≥ 50 ($n = 162$)	*P* Value
Age, y	58.0 ± 13.1 (21, 92)	68.9 ± 10.2 (42, 90)	69.8 ± 9.4 (34, 87)	<0.01*
Sex				<0.01†
Male	28	11	74	
Female	7	30	88	

Data represent the mean ± SD (minimum, maximum).
* *P* value of Student's *t*-test for case and control age comparisons.
† *P* value of Fisher exact test for case and control sex comparisons.

kit and a DNA sequencer (Taq DyeDeoxy and 373A DNA sequencer; Applied Biosystems) were used for direct sequencing.

Statistical Analysis

Statistical analysis was performed with the R version 3.4.3 (R Foundation for Statistical Computing, Vienna, Austria). Possible confounding effects of sex and age of the subjects were assessed using the correlations between the case and control samples with the Student's *t* test or the Fisher exact test. Wilcoxon rank sum test was used to detect difference of expression of *TCF4* level between sexes. The statistical significance for the comparison of multiple sample sets was determined with the Steel-Dwass test. Spearman's rank correlation coefficient was used to determine any significant correlations between the CTG repeat length and expression of *TCF4* mRNA level. Results are expressed as mean ± SD. Statistical significance was defined as P value < 0.05.

Results

TNR Expansion in Patients With FECD

We first determined the lengths of the CTG TNR expansions in *TCF4* by analyzing genomic DNA from peripheral blood samples of 203 patients with FECD and from control corneal stromas from 35 non-FECD subjects. The STR assays and Southern blotting demonstrated that all 35 non-FECD control subjects had CTG TNR lengths <50, whereas 162 of 203 patients with FECD (80%) harbored CTG TNR lengths ≥50. The remaining 41 patients with FECD (20%) had TNR lengths <50 (Table). The mean subject age was 58.0 ± 13.3 (range, 21 to 92) years in the control group, 68.9 ± 10.3 (range, 42 to 90) in the FECD group without TNR expansion, and 69.8 ± 9.4 (range, 34 to 87) in the FECD group with TNR expansion. Consistent with previous reports,[2] the female ratio was higher in the FECD subjects (11 males and 30 females with CTG < 50, and 74 males and 88 females with CTG ≥ 50).

Expression Levels of *TCF4* in the Corneal Endothelium of Patients With FECD

We used qPCR to evaluate the expression level of *TCF4* in the corneal endothelium of patients with FECD. As TCF4 has multiple alternatively spliced isoforms, we used three probes (Thermo Fisher Scientific, Inc.) for qPCR that are all contained within the canonical TCF4 transcript (Refseq: NM_001083962) that encodes TCF4-B (Fig. 1). The expression level of *TCF4* determined by Hs00971338 was significantly higher in patients with FECD with or without CTG TNR expansion >50 than in non-FECD subjects (control: 7.2 ± 4.8; FECD without expansion: 22.3 ± 29.9; and FECD without expansion: 47.4 ± 46.3; $P < 0.01$). The *TCF4* level was also significantly higher in FECD with expansion than in FECD without expansion ($P < 0.01$; Fig. 2A). The expression level of *TCF4* determined by Hs00162613 was significantly higher in patients with FECD with or without CTG TNR expansion >50 than in non-FECD subjects (control: 2.2 ± 1.3, FECD without expansion: 4.5 ± 1.6, and FECD without expansion: 4.3 ± 1.3; $P < 0.01$); however, no statistically significant difference was observed in *TCF4* levels between FECD with expansion and FECD without expansion (Fig. 2B). The expression level of *TCF4* determined by Hs00972432 was higher in FECD with or without CTG TNR expansion >50 than in non-FECD subjects (control: 2.8 ± 3.1, FECD without expansion: 6.7 ± 4.9, and FECD without expansion: 10.8 ± 8.2), but only the *TCF4* level in FECD with expansion showed statistical significance when compared with the control subjects ($P < 0.01$). Consistent with the *TCF4* level determined by Hs00971338, the *TCF4* level determined by Hs00972432 was significantly higher in FECD with expansion than in FECD without expansion ($P < 0.01$; Fig. 2C).

Effect of CTG Repeat Length or Genotype on *TCF4* Expression Level

We evaluated whether the CTG TNR length or the genotype of the single nucleotide polymorphism (SNP) rs613872 in *TCF4* correlated with TCF4 expression levels in FECD. Spearman's correlation coefficient by rank test revealed a weak positive correlation between CTG TNR length in genomic DNA from peripheral blood and the expression level of *TCF4* in the corneal endothelium determined by Hs00971338 ($\rho = 0.24$, $P < 0.01$) and Hs00972432 ($\rho = 0.22$, $P < 0.01$; Figs. 3A, 3C). Conversely, the CTG TNR length did not show significant correlation with expression level of *TCF4* determined by Hs00162613 (Fig. 3B). We also evaluated the effect of other potent confounders, including sex and age, on the expression level of *TCF4*. The expression level of *TCF4* (normalized by expression level of *GAPDH*) in the corneal endothelium, determined by Hs00971338, was 39.1 ± 49.7 in males and

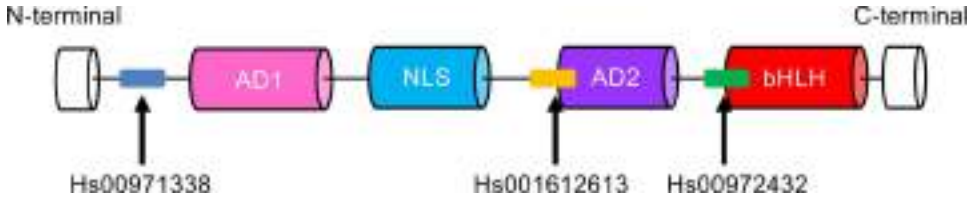

Figure 1. Schematic image of TCF4 and the genomic regions recognized by hydrolysis probes. Hs00971338 recognized the N-terminal side of active domain 1 (AD1), Hs00162613 recognized the N-terminal side of active domain 2 (AD2), and Hs00972432 recognized the N-terminal side of basic helix-loop-helix (bHLH) of *TCF4*.

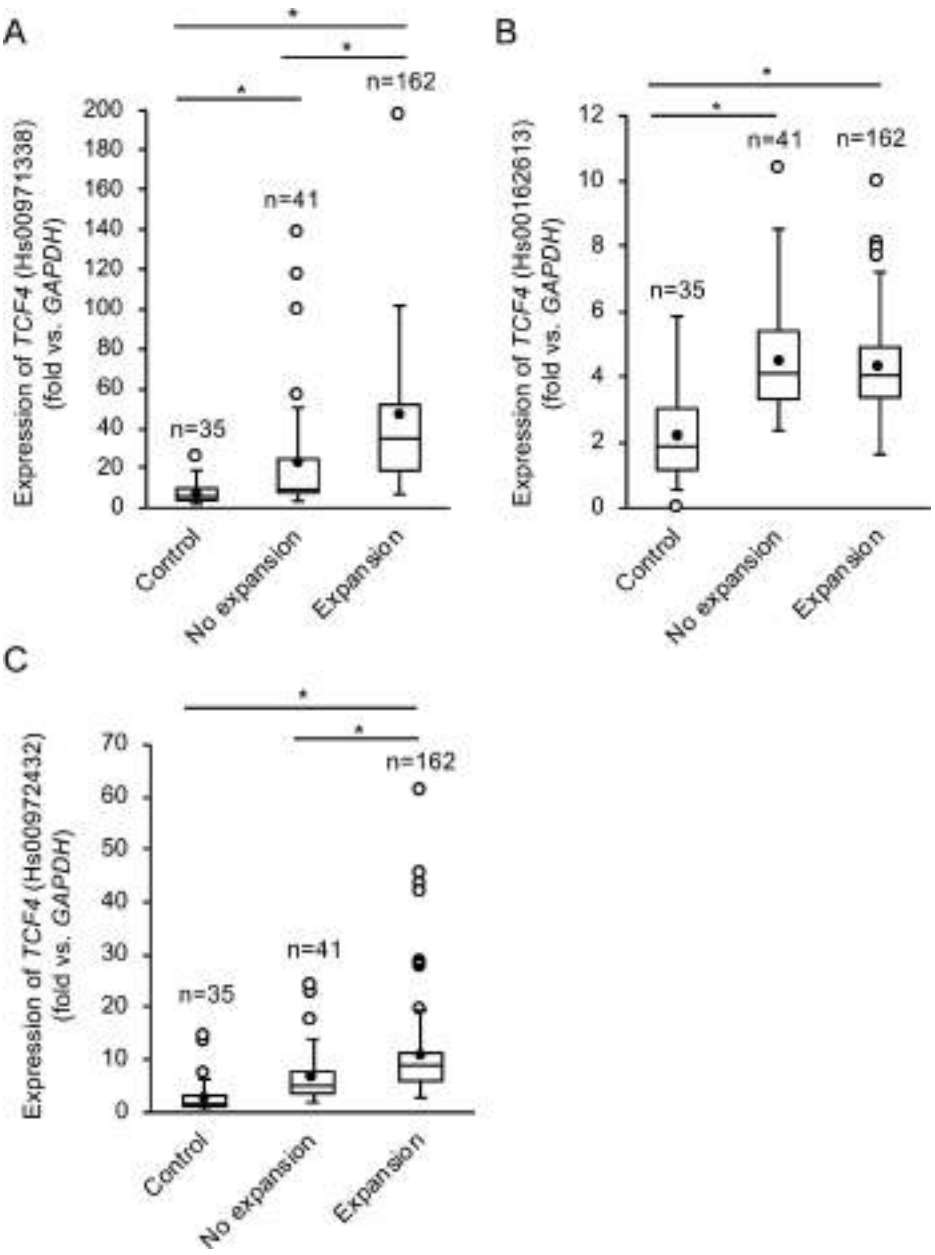

Figure 2. Expression of *TCF4* mRNA in corneal endothelium of patients with FECD. (**A**) Total RNA was extracted from the corneal endothelium of the 203 patients with FECD and 35 non-FECD subjects, and cDNA was synthesized. The expression level of *TCF4* determined by Hs00971338 was significantly higher in FECD with or without a CTG expansion of a trinucleotide repeat (TNR) expansion larger than 50 when compared with non-FECD subjects. In addition, *TCF4* level was significantly higher in FECD with expansion than in FECD without expansion. * $P < 0.01$. (**B**) Expression level of *TCF4* determined by Hs00162613 was significantly higher in FECD with or without a CTG TNR expansion larger than 50 than in non-FECD subjects. *$P < 0.01$. (**C**) Expression level of *TCF4* determined by Hs00972432 was higher in FECD with or without CTG-TNR expansion larger than 50 when compared to non-FECD subjects, but *TCF4* level showed a statistically significant difference only in FECD with expansion when compared to the control subjects. The *TCF4* level determined by Hs00972432 was significantly higher in FECD with expansion than in FECD without expansion. *$P < 0.01$. The statistical significance was determined with the Steel-Dwass test.

35.4 ± 36.2 in females ($P = 0.77$). Likewise, expression level of *TCF4* was similar level between sexes, at 3.9 ± 1.6 in males and 4.1 ± 1.4 in females, determined by Hs00162613 ($P = 0.29$), and 8.1 ± 6.7 in males and 9.7 ± 8.6 in females ($P = 0.10$), determined by Hs00972432. Since Wirgenes and colleagues previously reported that age showed a very weak positive correlation with *TCF4* mRNA levels in blood,[21] we also evaluated the correlation between age and the expression level of *TCF4* in the corneal endothelium. Spearman's correlation coefficient by rank test did not show a significant correlation with the expression level of *TCF4*, determined by Hs00162613 and Hs00972432, though the expression level determined by Hs00971338 revealed a weak positive correlation with marginal statistical significance (Supplementary Fig. S1).

Consistent with previous reports confirming the "G" risk allele in rs613872,[22] genotyping results showed that the genotype of this *TCF4* SNP was TT:30 (15%), TG:140 (69%), and GG:33 (16%) in German FECD cases, while it was TT:27 (77%), TG:7 (20%), and GG:1 (3%) in the control subjects ($P <$ 0.01). No correlation was found between the genotype of *TCF4*

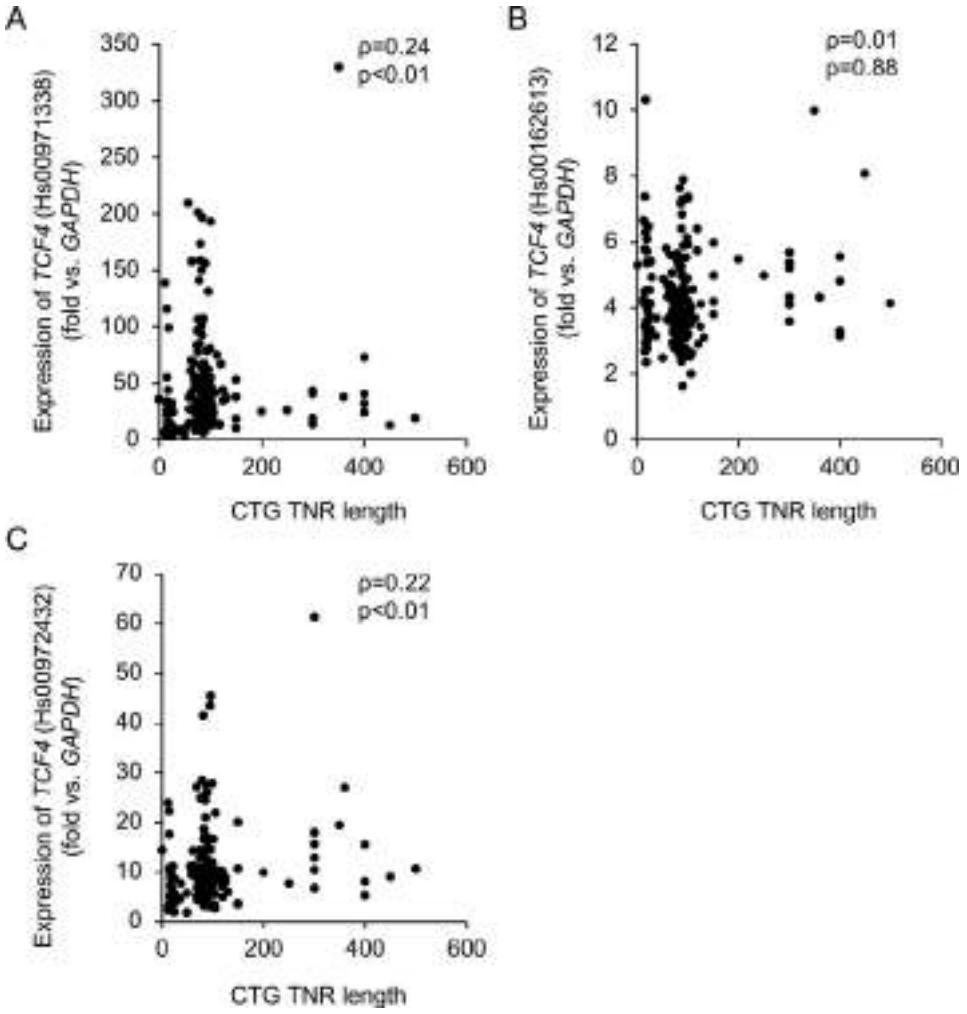

Figure 3. Correlation between CTG-TNR length and expression of *TCF4* mRNA. (**A**) CTG TNR length was evaluated by analyzing the genomic DNA from peripheral blood and expression levels were plotted for *TCF4* mRNA in the corneal endothelium of patients with FECD. Spearman's correlation coefficient by rank test revealed a weak positive correlation between CTG-TNR length and expression level of *TCF4* determined by Hs00971338 ($\rho = 0.24$, $P < 0.01$). (**B**) CTG-TNR length did not show a significant correlation with the expression level of TCF4 determined by Hs00162613 ($\rho = 0.01$, $P = 0.884$). (**C**) CTG-TNR length showed a weak positive correlation with the expression level of *TCF4* determined by Hs00972432 ($\rho = 0.22$, $P < 0.01$). Correlation was determined by a rank test using Spearman's correlation coefficient.

SNP rs613872 and expression level of *TCF4* determined by all three probes (Figs. 4A–C).

Discussion

Diseases with TNR expansion in non-coding regions typically cause a loss of gene function or toxic effects at the mRNA level, but their pathophysiology varies depending on the type and the location of the TNR.[12,13] For example, myotonic dystrophy 1 harbors CTG repeats within the 3′ UTR in the myotonic dystrophy protein kinase (*DMPK*) gene. These CTG repeats in *DMPK* gene lead to the formation of transcript aggregates in the nucleus (referred to as RNA foci) that sequester RNA-binding proteins, resulting in a spliceopathy of downstream effector genes.[23] In Friedreich's ataxia, a GAA repeat expansion in the first intron of the frataxin gene suppresses the frataxin mRNA and protein expression, leading to impaired mitochondrial iron transport.[24–26] Likewise, a CGG repeat expansion in the 5′UTR of the fragile X mental retardation gene (*FMR1*)[27] represses transcription by CpG hypermethylation of the FMR1 promoter.[28] However, suppression of gene expression by repeats is not always identified among triplet repeat expansion diseases. In spinocerebellar ataxia type 12, overexpression of the *PPP2R2B* gene[29] is linked to the length of a CAG TNR expansion, suggesting this is involved in the underlying pathophysiology.[30] These reports encouraged us to conduct the current study to answer the simple but fundamental question: "Does CTG repeat expansion in FECD alter the expression of *TCF4* mRNA level in the corneal endothelium?"

Studies reporting the expression of TCF4 in patients with FECD have resulted in contrasting conclusions. For example, Mootha and colleagues[31] reported no alterations in *TCF4* levels in the corneal endothelium of FECD patients when compared to control subjects. Likewise, Oldak and colleagues[32] analyzed the corneal endothelium from 40 FECD cases and 23 control subjects, and showed similar expression levels of *TCF4* in both groups and stable *TCF4* levels regardless of the risk allele of rs613872. By contrast, Foja and colleagues[9] reported decreased *TCF4* levels in the corneal endothelium of FECD patients in their examination of 6 FECD patients with TNR expansion >50 and 5 controls with TNR expansion <50.

In the current study, we demonstrated a significantly higher expression of *TCF4* at the mRNA level in the corneal endothelium of patients with FECD compared to normal

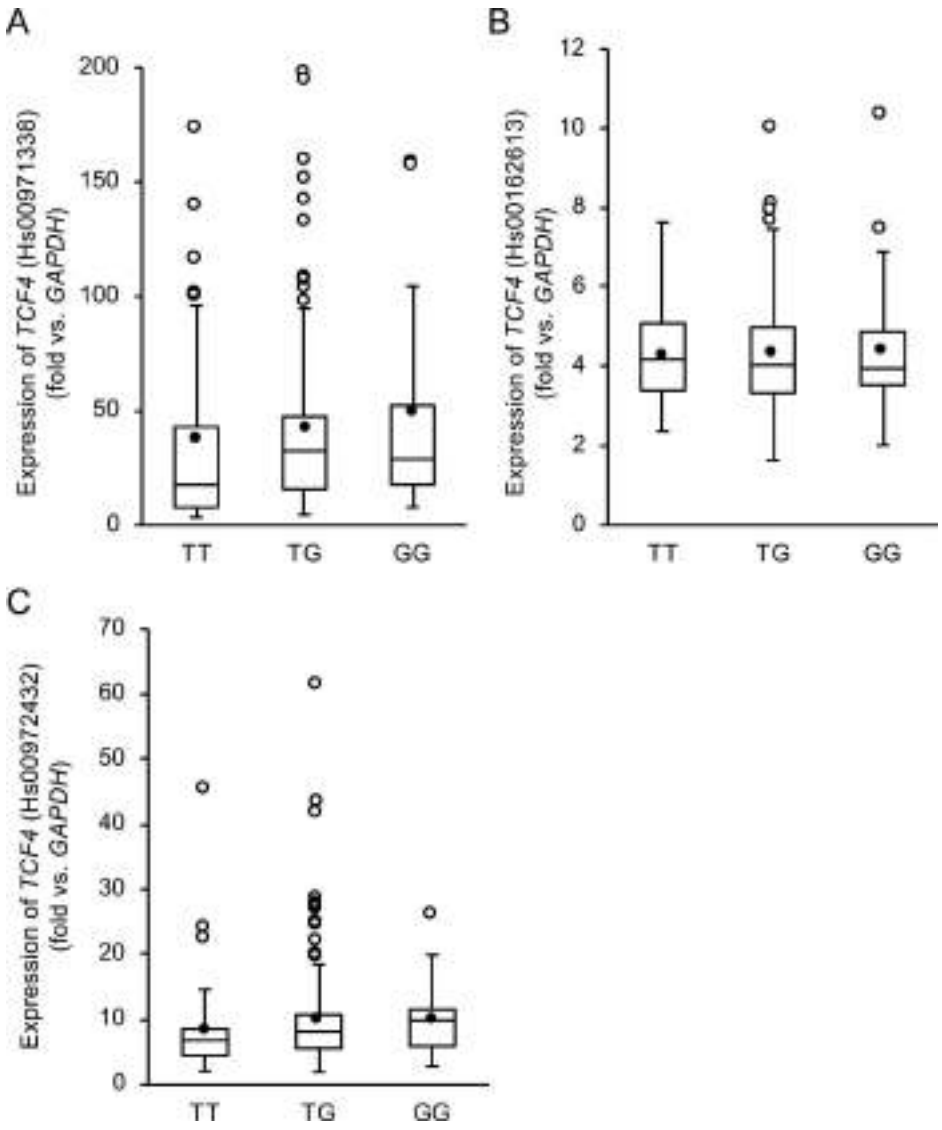

Figure 4. Correlation between the genotype of *TCF4* SNP, rs613872, and *TCF4* expression level. Genotyping of rs613872 in *TCF4* was performed by PCR. No statistically significant correlation was revealed by the Steel-Dwass test between the genotype of *TCF4* SNP rs613872 and the expression level of *TCF4* determined by three probes: (**A**) Hs00971338, (**B**) Hs001612613, and (**C**) Hs00972432.

controls. However, *TCF4* has multiple alternatively spliced variants and the variants expressed in corneal endothelium have not been elucidated. Therefore, we examined the splicing variants of *TCF4* at three different loci that correlated with conserved motifs in the TCF4 protein sequence, and we found upregulation of *TCF4* transcription in the patients with FECD, even in the patients without TNR expansion. Interestingly, the CTG repeat length, but not the presence of risk allele G in rs613872, tended to correlate with the TCF4 mRNA level. Further studies will be necessary to address whether expansion upregulates *TCF4* transcription and if the increase in TCF4 transcription has toxic effects in the corneal endothelium.

TCF4 encodes numerous transcripts, but the probeset Hs00971338, located proximally (5′) to the TNR, will only amplify the canonical TCF4 transcript encoding TCF4-B. Interestingly, the qPCR results showed that levels of the TCF4-B transcript are significantly elevated in FECD cases with repeat expansions when compared to cases without an expansion and controls. This finding may indicate a differential effect of the FECD-associated TNR in *TCF4* on the expression of the different TCF4 transcripts in CECs.

TCF4 is a basic helix-loop-helix (bHLH) transcription factor that plays an important role in various developmental processes.[33] One large-scale genome-wide association study (GWAS) identified *TCF4* as the first gene to show a strong association with schizophrenia.[34] *TCF4* variants have also shown associations with primary sclerosing cholangitis and Pitt-Hopkins syndrome, as well as with FECD.[33] The role of TCF4 in the context of disease pathogenesis still remains unclear, but involvement in the regulation of the epithelial-mesenchymal transition (EMT) was described in certain cell types. For instance, the overexpression of TCF4 in kidney cells induced EMT by upregulation of EMT-related markers.[35] In human neuroblastoma cells, genome-wide expression profiling showed that knockdown of TCF4 altered multiple signaling pathways related to the EMT and to transforming growth factor-β (TGF-β), an essential mediator of the EMT.[36] We established a cell model from patients with FECD and showed that TGF-β upregulates EMT-related genes, thereby inducing

excessive extracellular matrix (ECM) protein production, which is a hallmark of FECD.[20] More recently, we reported that upregulation of TGF-β signaling in FECD induces a chronic overload of ECM proteins to the endoplasmic reticulum in an immortalized cell model of FECD.[37,38] The overload of ECM protein results in accumulation of unfolded protein and triggers the intrinsic apoptotic pathway through the unfolded protein response.[37] These findings suggested that upregulation of *TCF4* can be linked to the underlying pathology of FECD, including upregulation of TGF-β signaling and chronic overloading of ECM proteins in the endoplasmic reticulum.

In conclusion, we have demonstrated that *TCF4* mRNA is upregulated in patients with FECD, regardless of the presence or absence of TNR expansion, but the length of the TNR in cases with expansion tended to correlate with the *TCF4* expression level. These findings suggest the possibility that upregulation of *TCF4* plays a central role in FECD. However, further studies are needed to identify the "missing link" between the increases in *TCF4* mRNA and the proposed pathophysiology that appears to involve upregulation of TGF-β signaling, disruption of protein loading in the endoplasmic reticulum.

Acknowledgments

The authors thank Seiichiro Sugita (Sugita Eye Hospital) for providing research materials, and Emi Ueda and Kyoko Watanabe for technical assistance.

Supported by the Program for the Strategic Research Foundation at Private Universities from MEXT (NK, NO), National Institutes of Health grant EY26490 (MPF) and the Robert Waller Career Development Award (KHB).

Disclosure: **N. Okumura**, None; **R. Hayashi**, None; **M. Nakano**, None; **K. Yoshii**, None; **K. Tashiro**, None; **T. Sato**, None; **D.J. Blake**, None; **R. Aleff**, None; **M. Butz**, None; **E.W. Highsmith**, None; **E.D. Wieben**, None; **M.P. Fautsch**, None; **K.H. Baratz**, None; **Y. Komori**, None; **M. Nakahara**, None; **T. Tourtas**, None; **U. Schlötzer-Schrehardt**, None; **F. Kruse**, None; **N. Koizumi**, None

References

1. Weisenthal R, Streeten B. Descemet's membrane and endothelial dystrophies. *Cornea Third edition* 2011;1:845–864.
2. Eghrari AO, Riazuddin SA, Gottsch JD. Fuchs corneal dystrophy. *Prog Mol Biol Transl Sci*. 2015;134:79–97.
3. Wieben ED, Aleff RA, Tosakulwong N, et al. A common trinucleotide repeat expansion within the transcription factor 4 (TCF4, E2-2) gene predicts Fuchs corneal dystrophy. *PLoS One*. 2012;7:e49083.
4. Mootha VV, Gong X, Ku HC, Xing C. Association and familial segregation of CTG18.1 trinucleotide repeat expansion of TCF4 gene in Fuchs' endothelial corneal dystrophy. *Invest Ophthalmol Vis Sci*. 2014;55:33–42.
5. Xing C, Gong X, Hussain I, et al. Transethnic replication of association of CTG18.1 repeat expansion of TCF4 gene with Fuchs' corneal dystrophy in Chinese implies common causal variant. *Invest Ophthalmol Vis Sci*. 2014;55:7073–7078.
6. Nanda GG, Padhy B, Samal S, Das S, Alone DP. Genetic association of TCF4 intronic polymorphisms, CTG18.1 and rs17089887, with Fuchs' endothelial corneal dystrophy in an Indian population. *Invest Ophthalmol Vis Sci*. 2014;55:7674–7680.
7. Vasanth S, Eghrari AO, Gapsis BC, et al. Expansion of CTG18.1 trinucleotide repeat in TCF4 is a potent driver of Fuchs' corneal dystrophy. *Invest Ophthalmol Vis Sci*. 2015;56:4531–4536.
8. Nakano M, Okumura N, Nakagawa H, et al. Trinucleotide Repeat Expansion in the TCF4 Gene in Fuchs' Endothelial Corneal Dystrophy in Japanese. *Invest Ophthalmol Vis Sci*. 2015;56:4865–4869.
9. Foja S, Luther M, Hoffmann K, Rupprecht A, Gruenauer-Kloevekorn C. CTG18.1 repeat expansion may reduce TCF4 gene expression in corneal endothelial cells of German patients with Fuchs' dystrophy. *Graefes Arch Clin Exp Ophthalmol*. 2017;255:1621–1631.
10. La Spada AR, Wilson EM, Lubahn DB, Harding AE, Fischbeck KH. Androgen receptor gene mutations in X-linked spinal and bulbar muscular atrophy. *Nature*. 1991;352:77–79.
11. Cummings CJ, Zoghbi HY. Fourteen and counting: unraveling trinucleotide repeat diseases. *Hum Mol Genet*. 2000;9:909–916.
12. Di Prospero NA, Fischbeck KH. Therapeutics development for triplet repeat expansion diseases. *Nat Rev Genet*. 2005;6:756–765.
13. Jones L, Houlden H, Tabrizi SJ. DNA repair in the trinucleotide repeat disorders. *Lancet Neurol*. 2017;16:88–96.
14. Zu T, Gibbens B, Doty NS, et al. Non-ATG-initiated translation directed by microsatellite expansions. *Proc Natl Acad Sci U S A*. 2011;108:260–265.
15. Sicot G, Gomes-Pereira M. RNA toxicity in human disease and animal models: from the uncovering of a new mechanism to the development of promising therapies. *Biochim Biophys Acta*. 2013;1832:1390–1409.
16. Cleary JD, Ranum LP. Repeat associated non-ATG (RAN) translation: new starts in microsatellite expansion disorders. *Curr Opin Genet Dev*. 2014;26:6–15.
17. Cleary JD, Ranum LP. New developments in RAN translation: insights from multiple diseases. *Curr Opin Genet Dev*. 2017;44:125–134.
18. Soragni E, Petrosyan L, Rinkoski TA, et al. Repeat-associated non-ATG (RAN) translation in Fuchs' endothelial corneal dystrophy. *Invest Ophthalmol Vis Sci*. 2018;59:1888–1896.
19. Sznajder LJ, Thomas JD, Carrell EM, et al. Intron retention induced by microsatellite expansions as a disease biomarker. *Proc Natl Acad Sci U S A*. 2018;115:4234–4239.
20. Okumura N, Minamiyama R, Ho LT, et al. Involvement of ZEB1 and Snail1 in excessive production of extracellular matrix in Fuchs endothelial corneal dystrophy. *Lab Invest*. 2015;95:1291–1304.
21. Wirgenes KV, Sonderby IE, Haukvik UK, et al. TCF4 sequence variants and mRNA levels are associated with neurodevelopmental characteristics in psychotic disorders. *Transl Psychiatry*. 2012;2:e112.
22. Baratz KH, Tosakulwong N, Ryu E, et al. E2-2 protein and Fuchs's corneal dystrophy. *N Engl J Med*. 2010;363:1016–1024.
23. Udd B, Krahe R. The myotonic dystrophies: molecular, clinical, and therapeutic challenges. *Lancet Neurol*. 2012;11:891–905.
24. Campuzano V, Montermini L, Lutz Y, et al. Frataxin is reduced in Friedreich ataxia patients and is associated with mitochondrial membranes. *Hum Mol Genet*. 1997;6:1771–1780.
25. Wilson RB. Frataxin and frataxin deficiency in Friedreich's ataxia. *J Neurol Sci* 2003;207:103–105.
26. Burk K. Friedreich ataxia: current status and future prospects. *Cerebellum Ataxias*. 2017;4:4.
27. Ciaccio C, Fontana L, Milani D, Tabano S, Miozzo M, Esposito S. Fragile X syndrome: a review of clinical and molecular diagnoses. *Ital J Pediatr*. 2017;43:39.
28. Pieretti M, Zhang FP, Fu YH, et al. Absence of expression of the FMR-1 gene in fragile X syndrome. *Cell*. 1991;66:817–822.
29. O'Hearn E, Holmes SE, Margolis RL. Spinocerebellar ataxia type 12. *Handb Clin Neurol*. 2012;103:535–547.

Investigative Ophthalmology & Visual Science

30. Swarup V, Srivastava AK, Rajeswari MR. Identification and quantification of differentially expressed proteins in plasma of spinocerebellar ataxia type 12. *Neurosci Res*. 2012;73:161–167.
31. Mootha VV, Hussain I, Cunnusamy K, et al. TCF4 triplet repeat expansion and nuclear RNA foci in Fuchs' endothelial corneal dystrophy. *Invest Ophthalmol Vis Sci*. 2015;56:2003–2011.
32. Oldak M, Ruszkowska E, Udziela M, et al. Fuchs endothelial corneal dystrophy: strong association with rs613872 not paralleled by changes in corneal endothelial TCF4 mRNA level. *Biomed Res Int*. 2015;2015:640234.
33. Forrest MP, Hill MJ, Quantock AJ, Martin-Rendon E, Blake DJ. The emerging roles of TCF4 in disease and development. *Trends Mol Med*. 2014;20:322–331.
34. Stefansson H, Ophoff RA, Steinberg S, et al. Common variants conferring risk of schizophrenia. *Nature*. 2009;460:744–747.
35. Sobrado VR, Moreno-Bueno G, Cubillo E, et al. The class I bHLH factors E2-2A and E2-2B regulate EMT. *J Cell Sci*. 2009; 122:1014–1024.
36. Forrest MP, Waite AJ, Martin-Rendon E, Blake DJ. Knockdown of human TCF4 affects multiple signaling pathways involved in cell survival, epithelial to mesenchymal transition and neuronal differentiation. *PLoS One*. 2013;8:e73169.
37. Okumura N, Kitahara M, Okuda H, et al. Sustained activation of the unfolded protein response induces cell death in Fuchs' endothelial corneal dystrophy. *Invest Ophthalmol Vis Sci*. 2017;58:3697–3707.
38. Okumura N, Hashimoto K, Kitahara M, et al. Activation of TGF-beta signaling induces cell death via the unfolded protein response in Fuchs endothelial corneal dystrophy. *Sci Rep*. 2017;7:6801.

Investigative Ophthalmology & Visual Science

Effect of Posterior Corneal Vesicles on Corneal Endothelial Cell Density and Anisometropic Amblyopia

Atsushi Noguchi, MD, Naoki Okumura, MD, PhD,*† Chie Sotozono, MD, PhD,* and Shigeru Kinoshita, MD, PhD*‡*

Purpose: To evaluate the effect of corneal vesicles in patients with posterior corneal vesicles (PCV) on corneal endothelial cell (CEC) density and the acquisition of amblyopia.

Methods: In this retrospective study of patients with PCV (18 eyes of 14 patients), CEC density was examined by noncontact specular microscopy during each follow-up examination. Best-corrected visual acuity and the objective refractive error were also examined.

Results: Of the 14 total patients, 10 were diagnosed with PCV and 4 were diagnosed with bilateral suspected PCV or posterior polymorphous corneal dystrophy (PPCD), and in all patients, no ocular abnormality other than corneal vesicles was observed. In patients with PCV and patients with bilateral suspected PCV or PPCD, mean CEC density was 1131 ± 338 and 1095 ± 492 cells/mm^2, respectively. In both PCV group and the bilateral suspected PCV or PPCD-group patients who were followed for 164.2 ± 25.4 months (range: 123–186 months), CEC density tended not to decrease. In patients with PCV, the mean best-corrected visual acuity of the unaffected eyes was significantly higher than that of the affected eyes with corneal vesicles (−0.10 ± 0.06 and 0.05 ± 0.13, respectively, $P = 0.012$). Four of 9 affected eyes (1 eye was excluded because of retinal atrophy) exhibited amblyopia, and all 4 eyes had astigmatism higher than 2 diopters.

Conclusions: Although CEC density of patients with PCV in this study was found to be stable over a long-term follow-up period, strict attention should be given to the possibility of amblyopia in eyes with PCV.

Received for publication October 24, 2017; revision received March 6, 2018; accepted March 12, 2018. Published online ahead of print May 1, 2018.

From the *Department of Ophthalmology, Kyoto Prefectural University of Medicine, Kyoto, Japan; †Department of Biomedical Engineering, Faculty of Life and Medical Sciences, Doshisha University, Kyotanabe, Japan; and ‡Department of Frontier Medical Science and Technology for Ophthalmology, Kyoto Prefectural University of Medicine, Kyoto, Japan.

Supported in part by Health and Labour Sciences Research Grants (Research on Intractable Diseases) from the Ministry of Health, Labour and Welfare of Japan.

The authors have no conflicts of interest to disclose.

Supplemental digital content is available for this article. Direct URL citations appear in the printed text and are provided in the HTML and PDF versions of this article on the journal's Web site (www.corneajrnl.com).

Correspondence: Shigeru Kinoshita, MD, PhD, Department of Frontier Medical Science and Technology for Ophthalmology, Kyoto Prefectural University of Medicine, 465 Kajii-cho, Hirokoji-agaru, Kawaramachi-dori, Kamigyo-ku, Kyoto 602-0841, Japan (e-mail: shigeruk@koto.kpu-m.ac.jp).

Key Words: posterior corneal vesicles, posterior polymorphous corneal dystrophy

(*Cornea* 2018;37:813–817)

Posterior polymorphous corneal dystrophy (PPCD) is a dominant inherited bilateral eye disease characterized by abnormalities of Descemet membrane and corneal endothelium.[1–3] Vesicle-like lesions, band lesions, and diffuse opacities are clinically observed in the posterior corneal layers in patients with PPCD. In addition, PPCD can exhibit various features such as peripheral synechiae, glaucoma, iris atrophy, corneal edema, and corneal steepening.[4–7] PPCD is genetically heterogeneous, and recent studies have reported that a mutation of the ovo-like zinc finger 2 gene (*OVOL2*) promoter was identified as the genetic basis of PPCD1[8] and that a mutation of the zinc finger E-box–binding homeobox 1 gene (*ZEB1*) was identified as the genetic basis of PPCD3.[9,10]

In 1981, Pardos et al proposed a new clinical entity termed "posterior corneal vesicles" (PCV).[11] In that study, the authors reported 6 patients with band-shaped vesicular lesions in a unilateral eye, yet without any other ocular abnormality, and showed that these lesions differed from those in PPCD, congenital glaucoma, and forceps-related injury. In addition, because 30 family members of the 6 patients with PCV in their study were not affected, they suggested that PCV is not an inherited disorder.[11]

To date, a few published reports on PCV describe it is asymptomatic and without visual impairment and that cases of PCV exhibit no ocular disorders other than band-shaped lesions.[11–14] However, the effect of the band-shaped lesions on visual acuity has yet to be fully elucidated.

In this study, we retrospectively reviewed 10 patients with PCV and 4 patients with bilateral suspected PCV or PPCD and evaluated the corneal endothelial cell (CEC) density during long-term follow-up. We also examined the effect of the existence of corneal vesicles on astigmatism and anisometropic amblyopia in patients with PCV.

MATERIALS AND METHODS

This study was conducted in accordance with a protocol approved by the Institutional Review Board of Kyoto Prefectural University of Medicine, Kyoto, Japan. In this retrospective study, we reviewed the medical records of patients who exhibited posterior corneal vesicular lesions

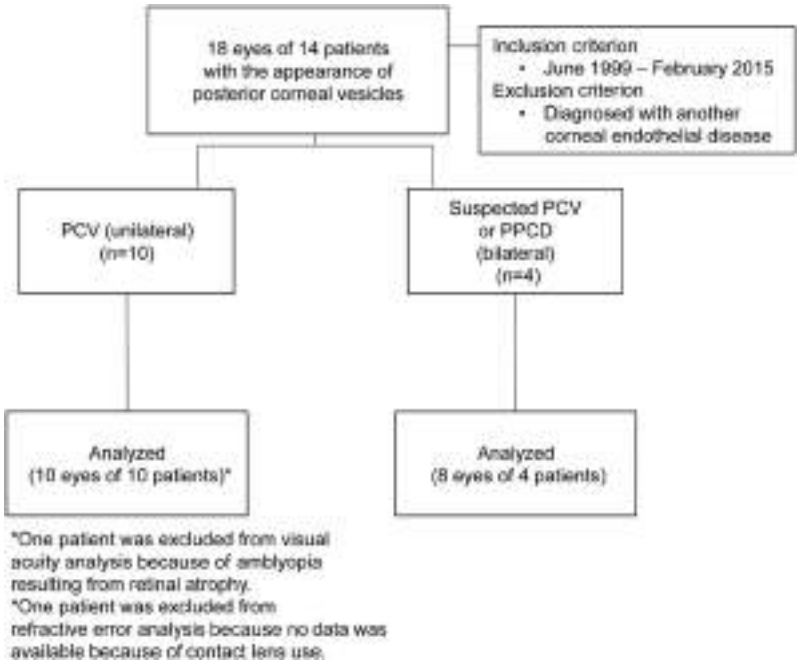

FIGURE 1. Flowchart of the patients included in the study.

and who were subsequently diagnosed with PCV or bilateral suspected PCV or PPCD between June 1999 and February 2015. Patients with unilateral vesicular lesions without any other ocular abnormality were diagnosed with PCV. Patients with bilateral vesicular lesions that could not be distinguished from PCV based on slit-lamp examination, and without PPCD-associated clinical features such as peripheral synechiae, glaucoma, iris atrophy, and corneal edema, were categorized as bilateral suspected PCV or PPCD. In each patient, the diagnosis was made by a single cornea specialist (S.K.) based on the assessment of slit-lamp microscopy and noncontact specular microscopy (FA-3809; Konan Medical Inc, Nishinomiya, Japan, EM-3000; Tomey Corporation, Nagoya, Japan) findings and a medical interview of the patient. Patients excluded from the study were those diagnosed with other corneal endothelial diseases such as congenital glaucoma, forceps-related injury, or Fuchs endothelial corneal dystrophy, as well as patients with bilateral vesicular lesions associated with other PPCD-associating features (Fig. 1). In each patient, the objective refractive error was evaluated using an auto refractometer/keratometer (RKT-7700; NIDEK Co Ltd, Gamagori, Japan), and best-corrected visual acuity (BCVA) was evaluated at each follow-up visit.

The data are presented as mean ± SD. The Student *t* test or the Mann–Whitney *U* test was used to determine statistical significance of the differences in the mean values of the 2-sample comparison. The Pearson χ^2 test was used to investigate the association between astigmatism and corneal vesicles.

RESULTS

This study involved 18 eyes of 14 patients that exhibited corneal vesicles without other pathological features. Ten patients (mean age: 19.7 ± 13.0 years, range: 6–51 years) exhibited unilateral band-like corneal vesicles and no other phenotypic features of PPCD, such as peripheral anterior synechiae, increased intraocular pressure, iris atrophy, or corneal edema, and were subsequently diagnosed with PCV (Fig. 2A). The other 4 patients (mean age: 31.8 ± 15.2 years, range: 15–49 years) exhibited bilateral corneal vesicles and were diagnosed with bilateral suspected PCV or PPCD. All 8 eyes of those 4 patients diagnosed with bilateral suspected PCV or PPCD only exhibited corneal vesicles that were similar to those in PCV cases and were difficult to distinguish from PCV based on slit-lamp microscopy and noncontact specular microscopy analysis, and no other ocular abnormality was observed (Fig. 2B). The baseline characteristics were similar between both groups. Horizontal vesicles were observed in 8 of the 10 eyes of the 10 patients in the PCV group and in 6 eyes

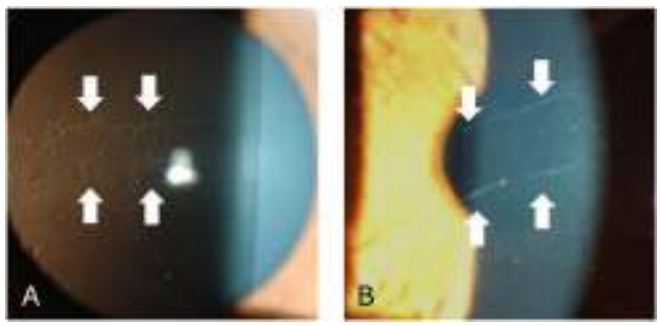

FIGURE 2. Representative slit-lamp microscopy images of a patient with unilateral PCV (A) and a patient with bilateral suspected PCV or PPCD (B). Both patients exhibited similar band-like corneal vesicles (arrows). In both patients, no other phenotypic features of PPCD, such as peripheral anterior synechiae, iris atrophy, or corneal edema, were observed.

TABLE 1. Characteristics of Patients With Unilateral PCV and Those With Bilateral Suspected PCV or PPCD

	PCV (10 Eyes of 10 Patients)	Bilateral Suspected PCV (8 Eyes of 4 Patients)	*P*
Age			
Mean ± SD, yrs	19.7 ± 13.0	31.8 ± 15.2	0.16
Range	6–51	15–49	
Sex, n (%)			
Male	4 (40.0)	2 (50.0)	
Female	6 (60.0)	2 (50.0)	
Direction of vesicles, n (%)			
Horizontal	8 (80.0)	6 (75.0)	
Horizontal + vertical	0 (0)	1 (12.5)	
Diagonal	2 (20.0)	0 (0)	
Small bullae-like vesicle	0 (0)	1 (12.5)	
Endothelial cell density*			
Mean ± SD, cells/mm^2	1131 ± 338	1095 ± 492	0.86
Range	482–1557	859–2272	

*Mean endothelial cell density of eyes with corneal vesicles.

of the 4 patients in the bilateral suspected PCV or PPCD group (Table 1). Keratometry values of the PCV-group patients and those of the bilateral suspected PCV or PPCD-group patients evaluated by the keratometer (RKT-7700) showed that no eyes exhibited corneal steepening (average keratometry values >48D) (see Supplemental Tables 1 and 2, Supplemental Digital Contents 1 and 2, http://links.lww.com/ICO/A668 and http://links.lww.com/ICO/A669), which is one of the clinical features of PPCD.[5–7]

Examination performed at the initial presentation revealed that mean CEC density of the 10 eyes of the 10 patients with PCV was 1131 ± 338 cells/mm^2, whereas that of the 8 eyes of the 4 patients with bilateral suspected PCV or PPCD was 1095 ± 492 cells/mm^2 (Table 1). In 2 patients with PCV and 3 patients with bilateral suspected PCV or PPCD, CEC density was evaluated longer than 10 years, and in both groups, CEC density tended to not decrease during the long-term follow-up period (Fig. 3A, B). CEC density of Japanese healthy individuals reported by Matsuda et al is shown in Supplemental Digital Content 3 (see Supplemental Table 3, http://links.lww.com/ICO/A670).[15]

Because we noticed that several patients in the PCV group exhibited unilateral amblyopia, we evaluated the visual acuity and objective refractive error in those patients. Our findings revealed that the mean BCVA of the unaffected eyes was significantly higher than that of the affected eyes with corneal vesicles (−0.10 ± 0.06 and 0.05 ± 0.13, respectively, P = 0.012). One patient (patient 9) was excluded from the BCVA analysis because of being afflicted with retinal atrophy. Four of 9 affected eyes exhibited a difference in BCVA higher than 0.20, and all 4 eyes were found to have astigmatism

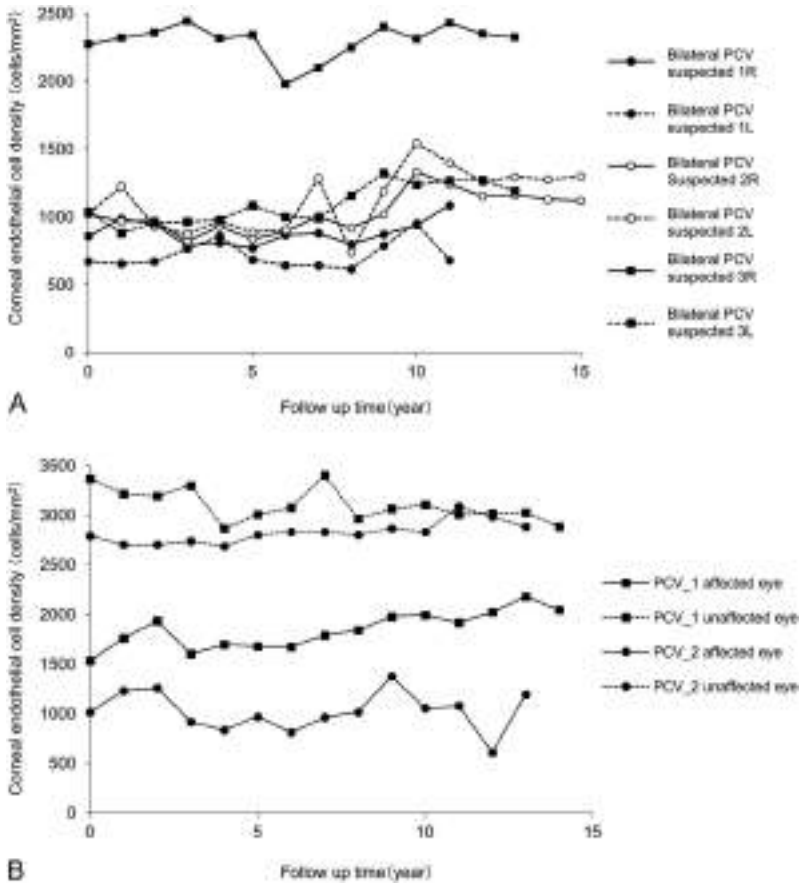

FIGURE 3. CEC density of patients with bilateral suspected PCV or PPCD and those with unilateral PCV. A, CEC density data of 3 patients with bilateral suspected PCV or PPCD obtained over a follow-up period of longer than 10 years are plotted. B, CEC density data of 2 patients with PCV are plotted.

TABLE 2. BCVA and Refractive Errors of Patients With Unilateral PCV

	BCVA (logMAR)			Sphere (D)		Cylinder (D)	
	Unaffected Eye	Affected Eye	Difference Between 2 Eyes	Unaffected Eye	Affected Eye	Unaffected Eye	Affected Eye
Patient 1	−0.08	−0.08	0	−2.50	−2.75	−0.75	−0.75
Patient 2	−0.08	−0.08	0	−2.50	−1.00	−0.50	−0.25
Patient 3	−0.08	0.22	0.30	−0.75	+1.00	−0.75	−2.25
Patient 4	−0.08	−0.08	0	−3.50	−2.25	−0.25	−0.75
Patient 5	−0.18	0.15	0.33	−0.25	+0.25	−0.25	−2.50
Patient 6	−0.18	0.15	0.33	−0.50	+0.50	−0.75	−2.75
Patient 7	−0.08	−0.08	0	−2.50	−1.75	−0.75	−1.50
Patient 8	0	0.15	0.15	−2.25	−2.00	−0.50	−1.25
Patient 9	−0.18	—	—	−0.25	0	0	−0.50
Patient 10	−0.18	0.10	0.28	No data	−0.50	No data	−2.50
Average	−0.10	0.05		−1.67	−0.89	−0.50	−1.39
SD	0.06	0.13		1.22	1.36	0.28	0.91
P	0.012*			0.22†		0.013†	

*Patient 9 was excluded because of amblyopia resulting from retinal atrophy.
†Patient 10 was excluded because no data were available because of contact lens use.

higher than 2 diopter (D). Mean astigmatism was significantly higher in the affected eyes than in the unaffected eyes (−1.39 ± 0.91 and −0.50 ± 0.28, respectively, $P = 0.013$). No significant difference in the spherical refractive error was observed between the affected and unaffected eyes (Table 2). One patient (patient 10) was excluded from the refractive error analysis because that patient used hard contact lenses and no refractive error data were obtained at her follow-up visits.

DISCUSSION

Because PPCD necessitates corneal transplantation in some cases because of corneal edema or diffuse corneal opacity,[4] various histological analyses are generally performed. In 1971, Boruchoff and Kuwabara[16] reported the presence of squamous epithelial-like cells in the vesicular lesions. Subsequently, researchers confirmed this by finding that epithelial-like cells exist in the PPCD cornea, using transmission and scanning electron microscopy.[17–19] However, no histological analysis of PCV corneas was performed because PCV does not induce corneal edema or opacity and corneal transplantation is not required. Such histological analysis might be crucial to answer whether PCV is a distinct clinical entity or whether unilateral PPCD was diagnosed with PCV, even if it is not a common form.

However, recent developments in in vivo confocal microscopy have enabled detailed evaluation of the vesicular lesions in patients with PCV. Watanabe et al reported that low density and various shapes of CECs were observed in the vesicular lesions of a 15-year-old girl with PCV.[13] Shiraishi et al[14] reported similar findings and showed that in 6 of 6 patients with PCV, density of CECs observed within the vesicular lesions ranged from 927 to 1593 cells/mm^2, whereas that of CECs observed in the nonvesicular lesion area ranged from 1095 to 1759 cells/mm^2, which is similar. Cell density in the fellow eyes, which were not affected by PCV, ranged from 2136 to 2723 cells/mm^2. In their study, the CECs observed in the vesicular lesions exhibited isoreflective nuclei and a low reflective cell membrane, a phenotypic pattern of normal CECs. Furthermore, they examined patients with PPCD using in vivo confocal microscopy and found that polymorphic cells exhibited hyperreflective nuclei (a characteristic of epithelial cells), consistent with the findings of histological analysis.[16–19] These findings may support the proposal of Pardos et al[11] that PCV is a clinical entity that is different from PPCD, although further study, especially genetic analysis and histological analysis of clinically diagnosed PCV, is necessary.

In this study, we found 4 patients who were affected bilaterally, and their pattern of corneal vesicles analyzed using slit-lamp microscopy and noncontact microscopy and their demographic background was similar to those of PCV. Therefore, we categorized the 4 patients who were affected bilaterally as PPCD or bilateral suspected PCV. However, PCV was originally proposed as a unilateral disease, and the existence of bilateral PCV may still be debatable. Further genomic analysis of the genetic basis of PPCD, which was not performed in this study, is necessary to determine a definitive diagnosis.

Unilateral amblyopia is conventionally defined as a difference in BCVA of 0.2 logMAR between 2 eyes.[20] To date, there have been only 4 reports describing PCV,[11–14] yet it is generally accepted that PCV is stable and asymptomatic. However, we showed that 4 of 9 patients with PCV (1 patient was excluded from analysis because of retinal atrophy) exhibited unilateral amblyopia, in which the difference in BCVA between the 2 eyes was higher than 0.2 logMAR. Moreover, all 4 patients with unilateral amblyopia had astigmatism higher than 2 D, and no other ocular abnormality such as corneal edema, glaucoma, and cataract was observed. Clinically, astigmatic anisometropia higher than 1 D is reportedly associated with the development of amblyopia.[21,22] This suggests that PCV can induce anisometropic amblyopia because of formation of astigmatism. Our findings suggest

that the onset of PCV might actually occur before the critical age for the acquisition of visual acuity.

It should be noted that this study does have some limitations, such as its retrospective design and the small number of patients. In addition, and although not performed in this study, genetic analysis for PPCD including ZEB1 and OVAL2 would help strengthen the diagnostic criteria for PCV and PPCD. Corneal topography imaging to evaluate corneal steepening and examination of the patient's relatives would also be beneficial.

In summary, in this study, we investigated 10 patients with PCV and 4 patients with bilateral suspected PCV or PPCD and examined the effect of posterior vesicles on the refractive error and BCVA. Although PCV is believed to be a nonprogressive and asymptomatic disorder, physicians should be aware that anisometropic amblyopia can be induced because of astigmatism.

ACKNOWLEDGMENT

The authors thank John Bush for editing the article.

REFERENCES

1. Cibis GW, Krachmer JA, Phelps CD, et al. The clinical spectrum of posterior polymorphous dystrophy. *Arch Ophthalmol.* 1977;95:1529–1537.
2. Waring GO III, Rodrigues MM, Laibson PR. Corneal dystrophies. II. Endothelial dystrophies. *Surv Ophthalmol.* 1978;23:147–168.
3. Laganowski HC, Sherrard ES, Muir MG. The posterior corneal surface in posterior polymorphous dystrophy: a specular microscopical study. *Cornea*. 1991;10:224–232.
4. Krachmer JH. Posterior polymorphous corneal dystrophy: a disease characterized by epithelial-like endothelial cells which influence management and prognosis. *Trans Am Ophthalmol Soc.* 1985;83:413–475.
5. Raber IM, Fintelmann R, Chhabra S, et al. Posterior polymorphous dystrophy associated with nonkeratoconic steep corneal curvatures. *Cornea*. 2011;30:1120–1124.
6. Aldave AJ, Ann LB, Frausto RF, et al. Classification of posterior polymorphous corneal dystrophy as a corneal ectatic disorder following confirmation of associated significant corneal steepening. *JAMA Ophthalmol.* 2013;131:1583–1590.
7. Liskova P, Palos M, Hardcastle AJ, et al. Further genetic and clinical insights of posterior polymorphous corneal dystrophy 3. *JAMA Ophthalmol.* 2013;131:1296–1303.
8. Davidson AE, Liskova P, Evans CJ, et al. Autosomal-dominant corneal endothelial dystrophies CHED1 and PPCD1 are allelic disorders caused by non-coding mutations in the promoter of OVOL2. *Am J Hum Genet.* 2016;98:75–89.
9. Krafchak CM, Pawar H, Moroi SE, et al. Mutations in TCF8 cause posterior polymorphous corneal dystrophy and ectopic expression of COL4A3 by corneal endothelial cells. *Am J Hum Genet.* 2005;77:694–708.
10. Liskova P, Evans CJ, Davidson AE, et al. Heterozygous deletions at the ZEB1 locus verify haploinsufficiency as the mechanism of disease for posterior polymorphous corneal dystrophy type 3. *Eur J Hum Genet.* 2016;24:985–991.
11. Pardos GJ, Krachmer JH, Mannis MJ. Posterior corneal vesicles. *Arch Ophthalmol.* 1981;99:1573–1577.
12. Harada T, Tanaka H, Ikema T, et al. Specular microscopic observation of posterior corneal vesicles. *Ophthalmologica*. 1990;201:122–127.
13. Watanabe R, Nakazawa T, Fuse N. Observation of posterior corneal vesicles with in vivo confocal microscopy and anterior segment OCT. *Clin Ophthalmol.* 2010;4:1243–1247.
14. Shiraishi A, Zheng X, Sakane Y, et al. In vivo confocal microscopic observations of eyes diagnosed with posterior corneal vesicles. *Jpn J Ophthalmol.* 2016;60:425–432.
15. Matsuda M, Yee RW, Edelhauser HF. Comparison of the corneal endothelium in an American and a Japanese population. *Arch Ophthalmol.* 1985;103:68–70.
16. Boruchoff SA, Kuwabara T. Electron microscopy of posterior polymorphous degeneration. *Am J Ophthalmol.* 1971;72:879–887.
17. Polack FM, Bourne WM, Forstot SL, et al. Scanning electron microscopy of posterior polymorphous corneal dystrophy. *Am J Ophthalmol.* 1980; 89:575–584.
18. Henriquez AS, Kenyon KR, Dohlman CH, et al. Morphologic characteristics of posterior polymorphous dystrophy. A study of nine corneas and review of the literature. *Surv Ophthalmol.* 1984;29:139–147.
19. Richardson WP, Hettinger ME. Endothelial and epithelial-like cell formations in a case of posterior polymorphous dystrophy. *Arch Ophthalmol.* 1985;103:1520–1524.
20. Norgett Y, Siderov J. Crowding in children's visual acuity tests–effect of test design and age. *Optom Vis Sci.* 2011;88:920–927.
21. Horwich H. Anisometropia amblyopia. *Am Orthopt J.* 1964;14:99–104.
22. Ingram RM. Refraction as a basis for screening children for squint and amblyopia. *Br J Ophthalmol.* 1977;61:8–15.

Association of rs613872 and Trinucleotide Repeat Expansion in the *TCF4* Gene of German Patients With Fuchs Endothelial Corneal Dystrophy

Naoki Okumura, MD, PhD, Ryousuke Hayashi, BS, MS,* Masakazu Nakano, PhD,† Kei Tashiro, MD, PhD,† Kengo Yoshii, PhD,‡ Ross Aleff, BS,§ Malinda Butz, BS,¶ Edward W. Highsmith, PhD,¶ Eric D. Wieben, PhD,§ Michael P. Fautsch, PhD,‖ Keith H. Baratz, MD,‖ Yuya Komori, BS,* Emi Ueda, BS,* Makiko Nakahara, PhD,* Julia Weller, MD,** Theofilos Tourtas, MD, PhD,** Ursula Schlötzer-Schrehardt, PhD,** Friedrich Kruse, MD, PhD,** and Noriko Koizumi, MD, PhD**

Purpose: To investigate single nucleotide polymorphisms (SNPs) and trinucleotide repeat (TNR) expansion in the transcription factor 4 (*TCF4*) gene in a large cohort of German patients with Fuchs endothelial corneal dystrophy (FECD).

Methods: Genomic DNA was obtained from 398 patients with FECD and from 58 non-FECD controls. Thirty-seven previously reported SNPs were evaluated by genotyping. The 398 FECD samples were analyzed for TNR expansions by short tandem repeat assays and Southern blotting. The possible associations between the TNR length and clinical parameters (age, sex, visual acuity, and central corneal thickness) were analyzed in 132 patients.

Results: The SNPs in *COL8A2*, *TCF8*, *LOXHD1,* and *AGBL1* showed no heterogeneity in 36 cases, although *SLCA411* showed 3 nonsense mutations. SNPs were detected for *TCF4* (rs613872, rs2123392, rs17089887, rs1452787, and rs1348047), but only rs613872 showed a significant association with FECD ($P = 9.93 \times 10^{-12}$). Overall, 315/398 (79%) patients harbored TNR lengths >50, whereas no non-FECD controls harbored TNR lengths >50. The *TCF4* SNP rs613872 genotype was TT: 39 (67%), TG: 18 (31%), and GG: 1 (2%) in non-FECD controls; TT: 39 (47%), TG: 38 (46%), and GG: 6 (7%) in FECD cases harboring TNR <50; and TT: 23 (8%), TG: 224 (79%), and GG: 38 (13%) in FECD cases harboring TNR >50 ($P = 2.93 \times 10^{-25}$). No significant association was detected between the TNR length and clinical parameters.

Conclusions: Our large German cohort demonstrated a significant association between the risk allele G in rs613872 and FECD, irrespective of TNR expansion, although this risk allele was more frequent in FECD cases with TNR expansion than without.

Key Words: Fuchs endothelial corneal dystrophy, TCF4, SNP

(*Cornea* 2019;00:1–7)

Received for publication September 7, 2018; revision received February 1, 2019; accepted February 20, 2019.
From the *Department of Biomedical Engineering, Faculty of Life and Medical Sciences, Doshisha University, Kyotanabe, Japan; †Department of Genomic Medical Sciences, Kyoto Prefectural University of Medicine, Kyoto, Japan; ‡Department of Mathematics and Statistics in Medical Sciences, Kyoto Prefectural University of Medicine, Kyoto, Japan; §Department of Biochemistry and Molecular Biology, Mayo Clinic, Rochester, MN; ¶Departments of Laboratory Medicine and Pathology, Mayo Clinic, Rochester, MN; ‖Ophthalmology, Mayo Clinic, Rochester, MN; and **Department of Ophthalmology, University of Erlangen-Nürnberg, Erlangen, Germany.
Supported by the Program for the Strategic Research Foundation at Private Universities from MEXT (N. Koizumi and N. Okumura); NEI grants EY25071 (K. H. Baratz and E. D. Wieben) and EY26490 (M. P. Fautsch); and the Mayo Foundation.
The authors have no conflicts of interest to disclose.
Supplemental digital content is available for this article. Direct URL citations appear in the printed text and are provided in the HTML and PDF versions of this article on the journal's Web site (www.corneajrnl.com).
Correspondence: Noriko Koizumi, MD, PhD, Department of Biomedical Engineering, Faculty of Life and Medical Sciences, Doshisha University, Kyotanabe 610-0321, Japan (e-mail: nkoizumi@mail.doshisha.ac.jp).

Fuchs endothelial corneal dystrophy (FECD) is a bilateral, progressive, and hereditary corneal disease. Hallmarks of FECD are formation of excrescences of Descemet membrane (basement membrane) due to excessive deposition of the extracellular matrix and loss of corneal endothelial cells. In its advanced stage, FECD is characterized by corneal stromal edema, which results in severe vision loss, and by eye pain due to epithelial edema.[1]

FECD is a genetically heterogeneous disease, typically exhibiting an autosomal dominant hereditary pattern with variations in penetrance and expressivity.[2] Linkage analysis in large families shows that FECD is associated with *FCD1*, *FCD2*, *FCD3*, and *FCD4* loci on chromosomes 13, 18, 5, and 9, respectively.[3–6] A missense mutation of *COL8A2,* which is a major component of Descemet membrane, is causative for the rare form of early-onset FECD but not for the common form of late-onset FECD.[7] Early genetic analyses of late-onset FECD revealed an association of 4 genes (*SLCA411*, *TCF8*, *LOXHD1*, and *AGBL1*) and the disease phenotype.[6,8–12] However, those genetic mutations were rarely identified in other cohorts of patients with FECD,[13] suggesting the existence of other causative genetic factors for most late-onset FECD cases.

In 2010, a genome-wide association study (GWAS) demonstrated a significant association between late-onset FECD and a single nucleotide polymorphism (SNP), rs613872, in the fourth intron of transcription factor 4 (*TCF4*) on chromosome 18.[14] Subsequent researchers replicated these findings, and several other SNPs in *TCF4* were also identified in other populations.[15–19] More recently, a strong association was found between FECD and expansion of a CTG trinucleotide repeat (TNR) in the third intron of *TCF4*,[20] and subsequent studies have replicated this association in other independent cohorts.[18,21–25]

These genetic analyses of causal genes in several cohorts and ethnicities have confirmed the presence of *TCF4* repeat expansion in most white populations studied thus far, but expansion occurs in a minority of Asian[18,26] and African American[27] patients with FECD. In the present study, we conducted a "semicomprehensive" analysis of the causal genetic mutations in a large German cohort of patients with FECD. We evaluated the 37 previously reported SNPs in *COL8A2*, *SLCA411, TCF8*, *LOXHD1, AGBL1*, and *TCF4*, as well as TNR expansion in 398 German patients with FECD who were scheduled for Descemet membrane endothelial keratoplasty. We also investigated the potential relationship between the TNR length and several clinical parameters related to the severity of FECD.

MATERIALS AND METHODS

Ethics Statement

The human tissue used in this study was handled under guidelines based on the ethical principles of the Declaration of Helsinki. This study was performed according to a protocol approved by the ethical review committee of the Friedrich–Alexander University Erlangen–Nürnberg, Doshisha University, Kyoto Prefectural University of Medicine, and the Mayo Clinic. Informed consent was acquired from all patients with FECD. Normal human donor corneas were obtained from SightLife (http://www.sightlife.org/, Seattle, WA).

Study Subjects

The 493 patients with late-onset FECD (German subjects of white descent) who were scheduled for Descemet membrane endothelial keratoplasty at the Friedrich–Alexander University Erlangen–Nürnberg were recruited between October 2013 and September 2015, and peripheral blood samples were obtained. Of the 493 patients, the peripheral blood leukocytes of 398 had the genomic DNA concentrations above 3.0 μg/mL required for this study and were used for subsequent genetic analyses. The samples were numerically coded at the Friedrich–Alexander University Erlangen–Nürnberg, and genomic DNA was analyzed at Doshisha University and Mayo Clinic in a pseudonymized fashion. As a control, genomic DNA was isolated from donor corneas (corneal stroma) of 58 non-FECD subjects of white descent. The potential effect of the TNR length on clinical parameters, such as age at the time of surgery, sex, visual acuity at the time of surgery, and central corneal thickness at the time of surgery, was evaluated in 132 patients with FECD.

Preparation of Genomic DNA

Genomic DNA was isolated from 200 μL of peripheral blood using the DNeasy Blood and Tissue Kit (Qiagen), according to the manufacturer's instructions. As a control, genomic DNA was similarly isolated from 58 residual corneal rims of non-FECD donor corneas used for corneal transplantation. The amount and quality of each isolated DNA sample were analyzed with a UV spectrophotometer (NanoDrop; NanoDrop Technologies, DE), and the samples were stored at −80°C until use.

Genotyping

The 37 previously reported SNPs in *COL8A2*, *SLCA411, TCF8*, *LOXHD1, AGBL1*, and *TCF4* in the 36 randomly selected FECD cases were genotyped by polymerase chain reaction (PCR) using the primers shown in Supplemental Table 1 (Supplemental Digital Content 1, http://links.lww.com/ICO/A778). In addition, rs613872 (SNPs in *TCF4*) was genotyped in all 398 FECD cases. The PCR reactions were performed with Ex Taq DNA polymerase (Takara Bio Inc, Otsu, Japan) under the following conditions: denaturation at 94°C for 30 seconds (1 cycle), annealing at 54 to 60°C for 30 seconds, and elongation at 72°C for 30 seconds (32–35 cycles). The PCR products were separated by electrophoresis on 2% agarose gels in Tris–-acetate buffer, stained with ethidium bromide, and analyzed with an LAS4000S luminescence imager (Fujifilm, Tokyo, Japan). The PCR products were extracted from the agarose gels using the Wizard SV Gel and PCR Clean-Up System (Promega, Madison, WI). Direct sequencing was performed with a Taq Dideoxy Terminator Cycle Sequencing Kit and a 373A DNA sequencer (Applied Biosystems, Foster City, CA), according to the manufacturer's instructions.

Evaluation of the CTG Repeat Length

The CTG repeat length in *TCF4* was determined by a short tandem repeat (STR) assay, as described previously.[20] Briefly, a fluorescently labeled primer was used for PCR of the CTG repeat region. The sizes of the PCR products were evaluated by capillary electrophoresis on an ABI 3730xl DNA Analyzer (Applied Biosystems, Foster City, CA). Samples demonstrating a single signal from the STR assay, which is too large for detection by the PCR-based STR assay, were subjected to Southern blotting on unamplified DNA, as described previously.[20]

Statistical Analysis

Statistical analysis was performed with the R statistical package (version 3.4.1 for Windows, Vienna, Austria). Differences between the 2 groups were detected with the Welch t test for age data and the χ^2 test for sex data. The differences among the 3 groups were statistically analyzed by the analysis of variance and the χ^2 test or Fisher exact test. Bonferroni correction was applied when the allele frequencies and genotype frequencies were compared between 1) control and FECD harboring TNR <50; 2) control and FECD

harboring TNR >50; and 3) FECD harboring TNR <50 and FECD harboring TNR >50 (significance threshold, $P = 0.05$ divided by the number of groups: $P = 0.017$). The Spearman rank correlation coefficient was used to determine any significant correlations between the TNR length and clinical parameters (age, visual acuity, and central corneal thickness at the time of surgery). Multivariate logistic regression analysis was applied to analyze the association between TNR >50 and several clinical parameters (age, sex, visual acuity, and central corneal thickness at the time of surgery). $P < 0.05$ was considered statistically significant. Results are expressed as mean ± SD.

RESULTS

The demographics of the subjects in this study are shown in Table 1. Consistent with previous reports,[28] the proportion of women (61%) was higher in the FECD group than in the non-FECD control group (38%). The mean age was 58.2 ± 11.9 (range, 18–92) years in the control group and 69.5 ± 9.6 (range, 32–92) years in the FECD group.

The SNPs in *COL8A2*, *TCF8*, *LOXHD1*, and *AGBL1* showed no heterogeneity in the 36 randomly selected FECD cases, but 3 nonsense mutations were detected in rs34460295, rs3827075, and rs3803956 of *SLCA411* (Table 2). Variations were also detected in several SNPs in *TCF4*, including rs613872, rs2123392, rs17089887, rs1452787, and rs1348047. However, only rs613872 showed a significant association with FECD compared with the non-FECD controls ($P = 9.93 \times 10^{-12}$). The mean age of the 36 FECD cases used for genotyping was 73.1 ± 6.4 (range, 60–86) years, and the sex distribution was 17 men and 19 women.

Given our finding that only rs613872 in *TCF4* was associated with FECD, we further evaluated the association between rs613872 and CTG repeat expansion in *TCF4* (Table 3). STR assay and Southern blotting results demonstrated that 315 of the 398 patients (79%) harbored CTG TNR lengths >50 (8 homozygous and 307 heterozygous patients), whereas 83 of the 398 patients (21%) did not harbor TNR lengths >50 (Table 1). The genotypes of rs613872 were TT:39 (67%), TG:18 (31%), and GG:1 (2%) in non-FECD controls; TT:39 (47%), TG: 38 (46%), and GG:6 (7%) in patients with FECD harboring TNR lengths <50; and TT:23 (8%), TG: 224 (79%), and GG:38 (13%) in patients with FECD harboring TNR lengths >50. The Fisher exact test showed a significant trend among the 3 groups: non-FECD control, FECD harboring TNR <50, and FECD harboring TNR >50 ($P = 2.93 \times 10^{-25}$). The difference between FECD harboring TNR <50 and FECD harboring TNR >50 was also statistically significant according to the Fisher exact test ($P = 9.88 \times 10^{-14}$). The allele of *TCF4* SNP rs613872 was T:96 (83%) and G:20 (17%) in the non-FECD controls; T:116 (70%) and G:50 (30%) in FECD harboring TNR lengths <50; and T:270 (43%) and G:360 (57%) in FECD harboring TNR lengths >50. The χ^2 test showed significance among all 3 groups—non-FECD control, FECD harboring TNR <50, and FECD harboring TNR >50 ($P = 1.91 \times 10^{-19}$)—and between the 2 groups—FECD harboring TNR <50 and FECD harboring TNR >50 ($P = 9.95 \times 10^{-10}$).

We also examined the potential correlation between the TNR length and the severity of FECD using the Spearman rank correlation coefficient to compare several clinical parameters defined at the time of surgery. The TNR length was not correlated with age ($P = 0.054$) (Fig. 1A), visual acuity ($P = 0.28$) (Fig. 1B), or central corneal thickness ($P = 0.63$) (Fig. 1C). In addition, none of these parameters showed any significant association with the CTG TNR length when analyzed by multivariate logistic regression (age: $P = 0.36$; sex: $P = 0.25$; visual acuity: $P = 0.51$; central corneal thickness; $P = 0.16$) (Table 4).

DISCUSSION

Linkage and mapping studies in FECD families have identified associations between coding mutations and FECD, including mutations in *COL8A2*, *SLCA411*, *TCF8*, *LOXHD1*, and *AGBL1*.[6,8–12] In the current study, none of the previously identified mutations in *COL8A2*, *TCF8*, *LOXHD1*, and *AGBL1* were found in a small subset of our cohort, although 3 nonsense mutations were identified in *SLCA411*. This latter gene is associated with congenital hereditary endothelial dystrophy and has been shown to be associated with FECD in Chinese, Indian, and white populations.[8,9] We found 3 SNPs (rs34460295, rs3827075, and rs3803956) in *SLCA411* in our cases, but these SNPs cause nonsense mutations and are not rare polymorphisms, according to the database of the 1000 Genomes Project. Accordingly, our results indicate that

TABLE 1. Demographic Data of Control and FECD Cases With and Without CTG TNR Expansion in *TCF4*

		No Expansion	Expansion	
	Control (n = 58)	CTG < 50 (n = 83)	CTG ≥ 50 (n = 315)	*P*
Age, yr	58.2 ± 11.9 (18, 92)	69.1 ± 10.2 (42, 92)	69.5 ± 9.4 (32, 90)	2.53×10^{-9}*
Sex				3.33×10^{-5}†
Male	36 (62%)	20 (24%)	135 (43%)	
Female	22 (38%)	63 (76%)	180 (57%)	

Data represent the mean ± SD (minimum, maximum).
*P value calculated using the analysis of variance.
†P value calculated using the χ^2 test.

TABLE 2. Genotyping of Reported SNPs in *COL8A2*, *SLCA411*, *TCF8*, *LOXHD1*, *AGBL1*, and *TCF4*

Gene	Chr Position	rs ID	Mutation	1000 Genomes (European)	Case
COL8A2				n = 2012	n = 36
	1:36099217	rs75864656	C>T	T = 0.0010	0/72
	1:36098770	rs369487110	C>T	T = 0.0000	0/72
	1:36098380	rs201235688	C>T	T = 0.0020	0/72
	1:36098332	rs80358192	A>C,G		0/72
SLC4A11					
	20:3237580–1		TCdel		0/72
	20:3234816	rs778688114	C>G,T		0/72
	20:3234760	rs200940928	A>G	C = 0.0000	0/72
	20:3234249	rs34460295	G>A	A = 0.0249	14/72
	20:3234173	rs3827075	T>A,G	G = 0.3956	22/72
	20:3233935	rs3803956	G>A	A = 0.1779	16/72
	20:3231375	rs193080010	G>A	A = 0.0000	0/72
	20:3231346	rs760889152	C>T		0/72
	20:3230970	rs139297339	C>A,T	T = 0.0010	0/72
	20:3230954	rs267607065	G>A		0/72
	20:3230934	rs78274653	C>T	T = 0.0000	0/72
	20:3229694	rs201595005	C>T	T = 0.0000	0/72
	20:3229632	rs755379986	C>G,T		0/72
	20:3229620	rs754745672	C>T		0/72
	20:3229410	rs201613216	C>T	T = 0.0010	0/72
	20:3229223	rs376848818	G>A		0/72
	20:3228952	rs267607064	G>A		0/72
	20:3228687	rs267607066	C>T		0/72
	20:3228366	rs58757394	G>A	A = 0.0089	0/72
TCF8					
	10:31461211	rs80194561	A>C	C = 0.00	0/72
	10:31521280	rs781750314	C>G		0/72
	10:31521764	rs19944415	A>C,G	C = 0.00, G = 0.00	0/72
	10:31521854	rs118020901	A>C	C = 0.0119	0/72
	10:31524042	rs78449005	C>G	G = 0.0010	0/72
LOXHD1					
	18:46591948	rs113444922	G>A		0/70
	18:46577732	rs141932807	C>T	T = 0.0000	0/72
	18:46521131	rs372241056	A>G		0/72
AGBL1					
	15:86674435	rs185919705	C>T	T = 0.0050	0/72
TCF4					
	18:55543071	rs613872	T>G	G = 0.1769	36/72
	18:55547934	rs2123392	T>C	C = 0.3588	9/72
	18:55541025	rs17089887	T>C	C = 0.0885	12/72
	18:55539976	rs1452787	A>G	G = 0.2972	5/72
	18:55382827	rs1348047	G>T	T = 0.2734	21/72

mutations in *COL8A2*, *SLCA411*, *TCF8*, *LOXHD1*, and *AGBL1* are very rare in German patients with FECD.

A previous GWAS and replication study by Baratz et al[14] that included 280 cases and 410 controls indicated a strong association between an intronic variant in *TCF4*, rs613872, and FECD. The minor allele (G) was present more frequently in FECD cases (G = 0.40) than in non-FECD controls (G = 0.15), and the odds ratio was 5.5 for 1 copy of the risk allele G (heterozygous) and 30 for 2 copies (homozygous).[14] Subsequent studies confirmed the association between rs613872 and FECD, but mainly in white cohorts.[15,19] In a previously reported German cohort, 33 (79%) of 42 unrelated patients with FECD had heterozygous TG, and 4 (10%) had homozygous GG. By contrast, 65 (70%) of 93 non-FECD controls had homozygous TT, and 21 (23%) had heterozygous TG.[24] These results were in agreement with the findings presented here for a larger cohort. However, rs613872 is monomorphic in several ethnic cohorts, such as Southern Chinese and Indian populations and populations of Chinese descent in Singapore. Instead, variations in *TCF4* SNPs other than rs613872 have been identified in Chinese and Indian FECD populations, suggesting the existence of

TABLE 3. CTG TNR Expansion and rs613872 Genotype of FECD Cases and Controls

		No Expansion	Expansion	
	Control (n = 58)	CTG < 50 (n = 83)	CTG > 50 (n = 315)	*P*
Genotype				2.93×10^{-25}*
TT	39 (67%)	39 (47%)	23 (8%)	
TG	18 (31%)	38 (46%)	224 (79%)	
GG	1 (2%)	6 (7%)	38 (13%)	
Allele				1.91×10^{-19}†
T	96 (83%)	116 (70%)	270 (43%)	
G	20 (17%)	50 (30%)	360 (57%)	

Data represent the number of samples (%).
*P value calculated using the Fisher exact test.
†P value calculated using the χ^2 test.

ethnic variations of SNPs in this gene.[16–18] In our analysis of rs613872 and 3 other SNPs identified in the Chinese and Indian studies, only rs613872 was associated with FECD in German patients. Although our control corneal tissues were obtained from white donors but were not limited to German subjects, our findings confirmed that the minor allele (G) was found frequently (G = 0.52) in German patients with FECD, in agreement with other studies on white cohorts.

Wieben et al[20] reported a strong association between expansion of CTG TNR in *TCF4* and FECD. Their evaluation of 66 FECD cases and 63 unaffected controls showed that a sensitivity and specificity of >50 repeats identifying FECD of 79% and 96%, respectively, with an even higher specificity than that reported previously for rs613872.[20] This strong association between *TCF4* TNR expansion and FECD was replicated in an independent white cohort, in which repeat expansion was found in 88 of 120 (73%) cases and in 7 of 100 (7%) control subjects.[21] This association has again been confirmed recently in another large cohort of 574 FECD cases and 354 controls, in which a repeat length >40 was identified in 62% of the FECD cases and 3.7% of the controls.[22] In a German cohort, 33 (79%) of 42 cases exhibited TNR expansion >50, whereas 10 (11%) of 93 cases exhibited an expanded allele.[24] The association of TNR expansion with FECD was replicated in other populations, although their reported frequencies of repeat expansion in FECD cases were lower than in white cohorts: 44% in Chinese, 34% in Indian, and 26% in Japanese.[18,21,23] This suggests that the frequency of harboring TNR expansion varies depending on ethnicity. Here, our results for this large German cohort showed that 79.4% of the FECD cases have TNR expansion >50, confirming that the frequency of German patients who harbor *TCF4* TNR expansion is strikingly similar to that of other white cohorts.

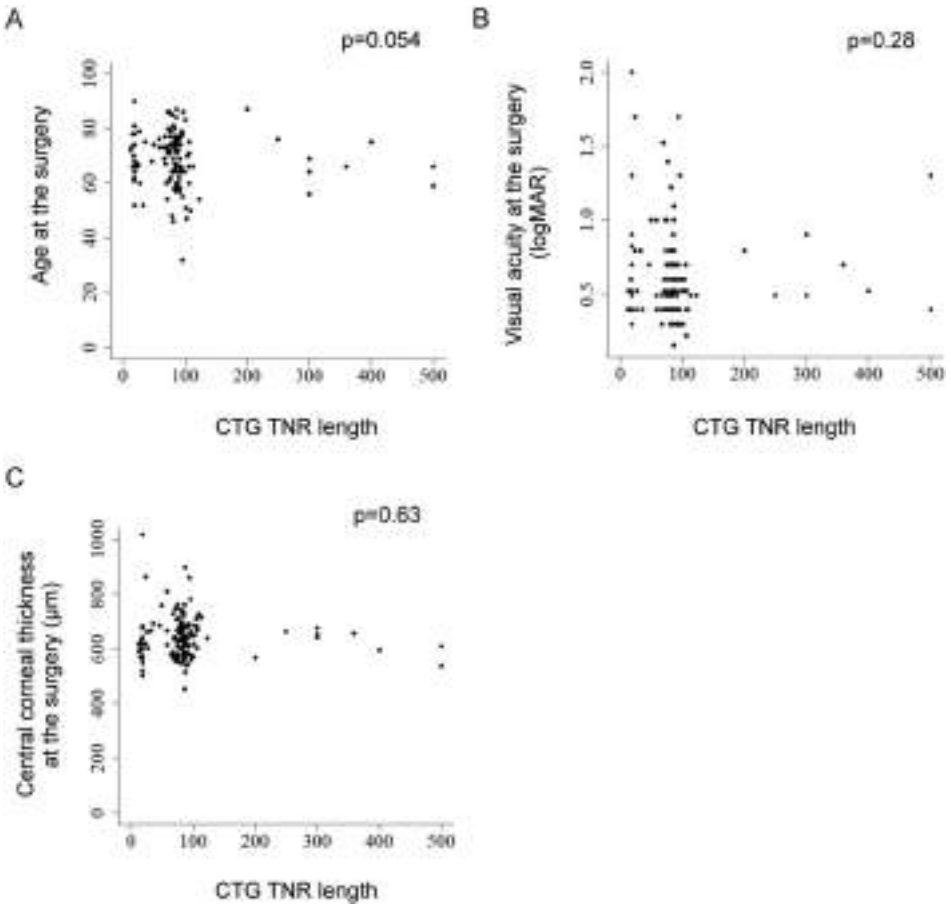

FIGURE 1. Correlation between the CTG TNR length and the severity of FECD. A, The CTG TNR length was evaluated by analyzing the genomic DNA from peripheral blood, and the patient age at the time of surgery was plotted. No significant correlation was noted between the CTG TNR length and the age at the time of surgery, based on the Spearman rank correlation coefficient (P = 0.054). B, No significant correlation was detected between the CTG TNR length and visual acuity at the time of surgery, based on the Spearman rank correlation coefficient (P = 0.28). C, No significant correlation was detected between the CTG TNR length and central corneal thickness at the time of surgery, based on the Spearman rank correlation coefficient (P = 0.63).

TABLE 4. Multivariate Analysis of the Associations Between CTG TNR Expansion and Patient Age, Sex, Visual Acuity, and Central Corneal Thickness at the Time of Surgery

Variables	Odds Ratio	95% Confidence Interval	*P*
Age, yr ≥71 (vs. <71)	1.55	0.61–3.91	0.36
Sex Female (vs. male)	0.57	0.22–1.48	0.25
Visual acuity (logMAR) ≥0.52 (vs. <0.52)	0.73	0.29–1.84	0.51
Central corneal thickness ≥635 (vs. <635)	1.97	0.76–5.10	0.16

logMAR, logarithm of the minimum angle of resolution.

Mootha et al[21] in their US cohort showed a more frequent occurrence of *TCF4* TNR expansion in cases with the G risk allele of rs613872. In the current study, we also showed a significant correlation between this G risk allele and *TCF4* CTG repeat expansion in our FECD cases. The likely explanation for the strong association of FECD with both rs613872 and TNR expansion is that only TNR expansion is causative for FECD, whereas the risk allele G of rs613872 is only in linkage disequilibrium. This hypothesis is supported by the observation that the association of TNR expansion with FECD is stronger than the association with SNPs demonstrated in other studies.[16–18,20–22] In addition, studies of ex vivo and cultured endothelial tissues have shown the occurrence of RNA toxicity, repeat-associated non-ATG translation, and altered TCF4 expression, which are mechanisms consistent with CTG repeat–induced disease.[29–31] In our current study, no significant association was detected between the CTG repeat length and several clinical parameters related to the severity of FECD. This suggests the existence of a threshold of the TNR length for disease induction, but the length is not related to disease severity. However, further studies on additional clinical parameters (eg, disease progression speed and guttae formation) are necessary to determine the threshold levels of the TNR length and the pathological phenotype.

Recently, Afshari et al[32] performed a GWAS on 1404 FECD cases and 2564 controls of European ancestry, followed by a replication study using independent data sets with 671 FECD cases and 778 controls. They showed that 3 novel SNPs in *KANK4* (rs79742895), *LAMC1* (rs3768617), and *LINC00970/ATP1B1* (rs1200114), in addition to *TCF4* (rs784257), are associated with FECD with genome-wide significance. Calculation of the genetic risk scores of these SNPs revealed a significant increase in the predictive value of *TCF4* SNP by adding the 3 novel SNPs, thereby supporting the concept of FECD as a multifactorial disease.[32] We have not performed confirmatory studies regarding those SNPs, but future subsequent replicate studies should further our understanding of the pathology of this disease.

In summary, we verified that potentially causative genetic mutations in *COL8A2*, *SLCA411*, *TCF8*, *LOXHD1*, and *AGBL1* are rare and that TNR expansion and SNP rs613872 in *TCF4* are strongly associated with FECD in the German population. In addition, TNR expansion is frequently identified in patients harboring the risk allele G of rs613872. Our findings further substantiate a significant role for TNR expansion in FECD and should encourage future research efforts to investigate the role of *TCF4* TNR expansion in the pathogenesis of FECD.

ACKNOWLEDGMENTS

The authors thank Dr. Seiichiro Sugita (Sugita Eye Hospital) for providing research materials.

REFERENCES

1. Weisenthal R, Streeten B. Descemet's membrane and endothelial dystrophies. *Cornea.* 2011;1:845–864.
2. Eghrari AO, Riazuddin SA, Gottsch JD. Fuchs corneal dystrophy. *Prog Mol Biol Transl Sci.* 2015;134:79–97.
3. Sundin OH, Jun AS, Broman KW, et al. Linkage of late-onset Fuchs corneal dystrophy to a novel locus at 13pTel-13q12.13. *Invest Ophthalmol Vis Sci.* 2006;47:140–145.
4. Sundin OH, Broman KW, Chang HH, et al. A common locus for late-onset Fuchs corneal dystrophy maps to 18q21.2-q21.32. *Invest Ophthalmol Vis Sci.* 2006;47:3919–3926.
5. Riazuddin SA, Eghrari AO, Al-Saif A, et al. Linkage of a mild late-onset phenotype of Fuchs corneal dystrophy to a novel locus at 5q33.1-q35.2. *Invest Ophthalmol Vis Sci.* 2009;50:5667–5671.
6. Riazuddin SA, Zaghloul NA, Al-Saif A, et al. Missense mutations in TCF8 cause late-onset Fuchs corneal dystrophy and interact with FCD4 on chromosome 9p. *Am J Hum Genet.* 2010;86:45–53.
7. Biswas S, Munier FL, Yardley J, et al. Missense mutations in COL8A2, the gene encoding the alpha2 chain of type VIII collagen, cause two forms of corneal endothelial dystrophy. *Hum Mol Genet.* 2001;10:2415–2423.
8. Vithana EN, Morgan PE, Ramprasad V, et al. SLC4A11 mutations in Fuchs endothelial corneal dystrophy. *Hum Mol Genet.* 2008;17:656–666.
9. Riazuddin SA, Vithana EN, Seet LF, et al. Missense mutations in the sodium borate cotransporter SLC4A11 cause late-onset Fuchs corneal dystrophy. *Hum Mutat.* 2010;31:1261–1268.
10. Mehta JS, Vithana EN, Tan DT, et al. Analysis of the posterior polymorphous corneal dystrophy 3 gene, TCF8, in late-onset Fuchs endothelial corneal dystrophy. *Invest Ophthalmol Vis Sci.* 2008;49:184–188.
11. Riazuddin SA, Parker DS, McGlumphy EJ, et al. Mutations in LOXHD1, a recessive-deafness locus, cause dominant late-onset Fuchs corneal dystrophy. *Am J Hum Genet.* 2012;90:533–539.
12. Riazuddin SA, Vasanth S, Katsanis N, et al. Mutations in AGBL1 cause dominant late-onset Fuchs corneal dystrophy and alter protein-protein interaction with TCF4. *Am J Hum Genet.* 2013;93:758–764.
13. Aldave AJ, Han J, Frausto RF. Genetics of the corneal endothelial dystrophies: an evidence-based review. *Clin Genet.* 2013;84:109–119.
14. Baratz KH, Tosakulwong N, Ryu E, et al. E2-2 protein and Fuchs's corneal dystrophy. *N Engl J Med.* 2010;363:1016–1024.
15. Li YJ, Minear MA, Rimmler J, et al. Replication of TCF4 through association and linkage studies in late-onset Fuchs endothelial corneal dystrophy. *PLoS One.* 2011;6:e18044.
16. Thalamuthu A, Khor CC, Venkataraman D, et al. Association of TCF4 gene polymorphisms with Fuchs' corneal dystrophy in the Chinese. *Invest Ophthalmol Vis Sci.* 2011;52:5573–5578.
17. Wang KJ, Jhanji V, Chen J, et al. Association of transcription factor 4 (TCF4) and protein tyrosine phosphatase, receptor type G (PTPRG) with corneal dystrophies in southern Chinese. *Ophthalmic Genet.* 2014;35:138–141.
18. Nanda GG, Padhy B, Samal S, et al. Genetic association of TCF4 intronic polymorphisms, CTG18.1 and rs17089887, with Fuchs' endothelial corneal dystrophy in an Indian population. *Invest Ophthalmol Vis Sci.* 2014;55:7674–7680.
19. Oldak M, Ruszkowska E, Udziela M, et al. Fuchs endothelial corneal dystrophy: strong association with rs613872 not paralleled by changes in

corneal endothelial TCF4 mRNA level. *Biomed Res Int.* 2015;2015: 640234.
20. Wieben ED, Aleff RA, Tosakulwong N, et al. A common trinucleotide repeat expansion within the transcription factor 4 (TCF4, E2-2) gene predicts Fuchs corneal dystrophy. *PLoS One* 2012;7:e49083.
21. Mootha VV, Gong X, Ku HC, et al. Association and familial segregation of CTG18.1 trinucleotide repeat expansion of TCF4 gene in Fuchs' endothelial corneal dystrophy. *Invest Ophthalmol Vis Sci.* 2014;55:33–42.
22. Vasanth S, Eghrari AO, Gapsis BC, et al. Expansion of CTG18.1 trinucleotide repeat in TCF4 is a potent driver of fuchs' corneal dystrophy. *Invest Ophthalmol Vis Sci.* 2015;56:4531–4536.
23. Nakano M, Okumura N, Nakagawa H, et al. Trinucleotide repeat expansion in the TCF4 gene in fuchs' endothelial corneal dystrophy in Japanese. *Invest Ophthalmol Vis Sci.* 2015;56:4865–4869.
24. Luther M, Grunauer-Kloevekorn C, Weidle E, et al. TGC repeats in intron 2 of the TCF4 gene have a good predictive power regarding to fuchs endothelial corneal dystrophy [in German]. *Klin Monbl Augenheilkd.* 2016;233:187–194.
25. Foja S, Luther M, Hoffmann K, et al. CTG18.1 repeat expansion may reduce TCF4 gene expression in corneal endothelial cells of German patients with Fuchs' dystrophy. *Graefes Arch Clin Exp Ophthalmol.* 2017;255:1621–1631.
26. Xing C, Gong X, Hussain I, et al. Transethnic replication of association of CTG18.1 repeat expansion of TCF4 gene with Fuchs' corneal dystrophy in Chinese implies common causal variant. *Invest Ophthalmol Vis Sci.* 2014;55:7073–7078.
27. Eghrari AO, Vahedi S, Afshari NA, et al. CTG18.1 expansion in TCF4 among African Americans with fuchs' corneal dystrophy. *Invest Ophthalmol Vis Sci.* 2017;58:6046–6049.
28. Krachmer JH, Purcell JJ, Jr, Young CW, et al. Corneal endothelial dystrophy: a study of 64 families. *Arch Ophthalmol.* 1978;96: 2036–2039.
29. Du J, Aleff RA, Soragni E, et al. RNA toxicity and missplicing in the common eye disease Fuchs endothelial corneal dystrophy. *J Biol Chem.* 2015;290:5979–5990.
30. Mootha VV, Hussain I, Cunnusamy K, et al. TCF4 triplet repeat expansion and nuclear RNA foci in fuchs' endothelial corneal dystrophy. *Invest Ophthalmol Vis Sci.* 2015;56:2003–2011.
31. Soragni E, Petrosyan L, Rinkoski TA, et al. Repeat-associated non-ATG (RAN) translation in Fuchs' endothelial corneal dystrophy. *Invest Ophthalmol Vis Sci.* 2018;59:1888–1896.
32. Afshari NA, Igo RP, Jr, Morris NJ, et al. Genome-wide association study identifies three novel loci in Fuchs endothelial corneal dystrophy. *Nat Commun.* 2017;8:14898.